PHOTOGRAPH THIS SHEET

AD-A212 786

DTIC ACCESSION NUMBER

LEVEL

INVENTORY 1

88CH2593-2 RID5993-MS-02

DOCUMENT IDENTIFICATION

1-3 Sept 1988

DAJA45-88-M-0150

This document has been approved for public release and sale; its distribution is unlimited.

DISTRIBUTION STATEMENT

ACCESSION FOR		
NTIS	GRA&I	X
DTIC	TAB	☐
UNANNOUNCED		☐
JUSTIFICATION	per form 50	
BY		
DISTRIBUTION /		
AVAILABILITY CODES		
DIST	AVAIL AND/OR SPECIAL	
A-1	21	

DISTRIBUTION STAMP

DTIC ELECTE SEP 20 1989 S E D

DATE ACCESSIONED

QUALITY INSPECTED 4

$ 70.00 6th International Symposium on Electrets (1SE 6) Proceedings Per Janet from the IEEE Service Center Single Publications sale Dept 445 Hoes Lane, Piscataway, N. J. 08854

9-15-89 hp

89. 9 12 078

DATE RECEIVED IN DTIC

DATE RETURNED

REGISTERED OR CERTIFIED NO.

PHOTOGRAPH THIS SHEET AND RETURN TO DTIC-FDAC

DTIC FORM 70A MAR 86

DOCUMENT PROCESSING SHEET

PREVIOUS EDITION MAY BE USED UNTIL STOCK IS EXHAUSTED.

AD-A212 786

88CH2593-2

6th International Symposium on Electrets (ISE 6)

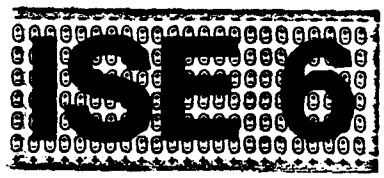

Proceedings

Edited by D.K. Das-Gupta and A.W. Pattullo

IEEE

US ARMY RESEARCH, DEVELOPMENT & STANDARDIZATION GROUP (UK)
BOX 65
FPO NY 09510-1500

FORWARDED ON LOAN.
PLEASE RETURN AS SOON
AS POSSIBLE.

88CH2593-2

6th International Symposium on Electrets (ISE 6)

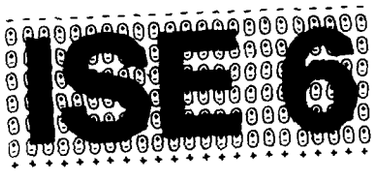

1-3 September 1988
The Queen's College, Oxford, England.

Proceedings

D.K. Das-Gupta and A.W. Pattullo
University of Wales, Bangor, U.K.

Sponsored by the IEEE Electrical Insulation Society

Library of Congress Catalog Number 88-81084

Available from the IEEE Service Center,
Single Publications Sales Department,
445 Hoes Lane, Piscataway, NJ 08854 USA

To be cited as:

Proceedings of the 6th International Symposium on Electrets, Oxford, England 1988. Edited by D.K. Das-Gupta and A.W. Pattullo (available from IEEE Service Centre ,445 Hoes Lane, Piscataway, N.J. 08854 USA).

Abstracting is permitted with credit to the source. Libraries are permitted to photocopy beyond the limits of U.S. copyright law for private use of patrons those articles in this volume which carry a code at the bottom of the first page, provided the per-copy fee indicated in the code is paid through the Copyright Clearance Center, 29 Congress Street, Salem, MA 01970, USA. Instructors are permitted to photocopy isolated articles for non-commercial classroom use without fee. For other copying, reprint or republication permission, write to Director, Publishing Services, IEEE, 345 East 47th Street, New York, NY 10017, USA. All rights reserved. Copyright © 1988 by The Institute of Electrical and Electronics Engineers, Inc.

Printed by: W.O. Jones (Printers) Ltd., Llangefni, Gwynedd, U.K.

PREFACE

ISE6 is a continuation of the series on "International Symposium on Electrets" which originated in Chicago in 1967. Further meetings followed at Miami (1972), São Carlos (1975), Kyoto (1978) and Heidleberg (1985). ISE5 was truly a great success and the delegates enjoyed the charming hospitality and the superb efficiency of the local symposium committee under the excellent chairmanship of Professor G.M. Sessler. Because of the tremendous interest in the science and applications of electrets it was felt that the ISE series should be held every three years.

ISE6 was originally scheduled to be held in New Delhi in December 1988 under the chairmanship of Professor P.K.C. Pillai, Indian Institute of Technology. Due to unforeseen problems the venue of ISE6 had to be changed in October 1987 to Queen's College, Oxford, England following a request from the local organising committee in New Delhi. The International Committee of the ISE series express their sympathy to Professor Pillai and his local committee for the serious difficulties which prevented them from holding the International Symposium on Electrets in charming and exotic India and hope that they may be more fortuitous in the future.

We are indeed grateful for the excellent response which we received from our colleagues in the five continents, in spite of such a late change in venue and time. For this, we express our appreciation of the efforts made by the members of the International Committee of the ISE series who encouraged their colleagues to make this meeting a success by active participation and worthy scientific contributions. We express our sincere thanks to the four eminent invited speakers Bob Fleming (Australia), Takeo Furukawa (Japan), Jim West (United States of America) and Gerhard Sessler (Federal Republic of Germany) for providing us with inspiration through their unique specialist knowledge and enthusiasm. We are also grateful to our session chairpersons and co-chairpersons who made each of the twelve sessions so succinctly enjoyable.

Finally my special thanks go to Professor G.M. Sessler who has provided me with unfailing support and advice and to Dr. Alistair Pattullo who carried so much burden of two jobs (secretary and treasurer) on his young shoulders with much enthusiasm which could not be faulted.

The scientific merit of this meeting may be judged by the wealth of knowledge implicit in the formal and poster contributions, collected in the conference proceedings. In just over one hundred years, much knowledge has been gained in the performance of electro- active properties of insulating

and semi-insulating materials and their use in industry, biology and other, diverse applications. For the future, electrets will make significant contributions in the fields of rapid storage and retrieval of information and also as sensors, enabling the measurement of minute changes in temperature, pressure etc. To sustain this progress, new improved materials must be disovered and better theoretical insights found. That is our pursuit.

Dilip K. Das-Gupta
Bangor, September 1988

Former Electret Symposia and their Proceedings

1) "Electrets and Related Electrostatic Charge Storage Phenomena" International Symposium held as part of the 132nd Meeting of the Electrochemical Society in Chicago, Illinois, U.S.A., 15-20 October 1967

   Published by the Electrochemical Society, Inc., 30 East Street, New York, New York 10017, U.S.A. (Edited by Lawrence M. Baxt and Martin M. Perlman), IV+150 pages, 1968.

2) "Electrets, Charge Storage and Transport in Dielectrics" International Symposium held as part of the 142nd Meeting of the Electrochemical Society in Miami Beach, Florida, U.S.A., 8-13 October 1972.

   Published by the Electrochemical Society, Inc., P.O. Box 2071, Princeton, New Jersey 08540, U.S.A. (Edited by Martin M. Perlman), XXIV+676 pages, 1973.

3) "International Symposium on Electrets and Dielectrics" Honoring the 70th Birthday of Prof. Bernhard Gross. Held in São Carlos, São Paulo, Brasil, 1-6 September 1975.

   Published by the Academia Brasileira de Ciências, Rio de Janeiro, Brasil (Edited by Milton Soares de Campos and organised by the Instituto de Fisica e Quimica de São Carlos, Universidade de São Paulo, Caixa Postal 369, 13560-São Carlos, São Paulo, Brasil), VI+448 pages, 1977.

4) "Charge Storage, Charge Transport, and Electrostatics with their Applications" International Workshop on Electric Charges in Dielectrics held in Kyoto, Japan, 9-12 October 1978.

   Copublished by Kodansha Ltd., 12-21 Otowa 2-chome, Bunkyo-ku, Tokyo 112, Japan and Elsevier Scientific Publishing Company, 335 Jan van Galenstraat, P.O. Box 211, NL-1000 AE Amsterdam, The Netherlands (Edited by Yasaku Wada, Martin M. Perlman and Hiroshi Kokaido), X+444 pages, 1979.

5) "International Symposium on Electrets" Honouring the 80th birthday of Prof. Bernard Gross. Held at the Castle of Heidelberg, West Germany, 4-6 September 1985.

   Available from IEEE Service Centre, 445 Hoes Lane, Piscataway, N.J. 08854 USA (Edited by G.M. Sessler and R. Gerhard-Multhaupt), XVI+980 pages.

Scientific Advisory Committee

Danz R. (GDR)
Davies D.K. (UK)
De Rossi D. (Italy)
Fukada E. (Japan)
Gerhard-Multhaupt R. (FRG)
Gromov V. (USSR)
Gunther P. (Switzerland)
Lang S.B. (Israel)
Lewiner J. (France)
Li Cong-Zhou (China)
Micheron F. (France)
Perlman M.M. (Canada)
Ruscher C. (GDR)
Soares de Campos M. (Brazil)
Sworakowski L. (Poland)
Van Roggen A. (USA)
Wada Y. (Japan)
Zhou Zhi-Gang (China)
Das-Gupta D.K. (UK)
Davis G.T. (USA)
Fleming R.J. (Australia)
Geiss D. (GDR)
Goodings A. (UK)
Gross B. (Brazil)
Ieda M. (Japan)
Leal Ferreira G.F. (Brazil)
Lewis T.J. (UK)
Mascarenhas S. (Brazil)
Murphy P.V. (Switzerland)
Pillai P.K.C. (India)
Sessler G.M. (FRG)
Sun Ximin (China)
Vandershueren J. (Belgium)
Van Turnout J. (Netherlands)
West J.E. (USA)

Symposium Organising Committee

D.K. Das-Gupta	Chairman
A.W. Pattullo	Secretary and Treasurer
G.M. Sessler	International Coordinator

Secretarial Services

The conference organisers are indebted to the staff of the School of Electronic Engineering Science at University College of North Wales, Bangor for assistance with the symposium organisation. In particular J. Ashe, S. Farrington, K. France and P. Jones together with J. Pattullo.

Acknowledgements

Gratidude is expressed to the IEEE, The Royal Society and to the European Research Office of the US Army in Great Britain for grants to help delegates requesting financial assistance.

CONTENTS

Preface iii

Former Electret Symposia and their Proceedings v

ISE6 Committees and Acknowledgements vi

SESSION 1 POLARIZATION DISTRIBUTION

1-1 **Determination of the Charge Distribution within an e-Irradiated Dielectric using the Pressure Wave Propagation Method** 1
M.P. Cals, J.P. Marque and C. Alquié

1-2 **Electrical Properties of Electrode-Polyethylene-Electrode Structures** 7
T. Ditchi, C. Alquié, J. Lewiner, R. Favrie and R. Jocteur

1-3 **Polarization Distributions in Isotropic, Stretched or Annealed PVDF Films** 13
E. Bihler, K. Holdik and W. Eisenmenger

1-4 **Determination of Temperature Distributions in Electret Foils** 18
R. Gerhard-Multhaupt, Z.F. Xia and A. Berraissoul

1-5 **The Thermal Step Technique Applied to the Study of Charge Decay in Polyethylene Thermoelectrets** 23
A. Toureille and J.P. Reboul

1-6 **Analysis of the Spatial Distribution of Polarization in PVDF Foils from the Frequency Spectra of the Pyroelectric Current** 28
S. Bauer and B. Ploss

SESSION 2 CHARGE STORAGE

2-7 **Charge Storage in Dielectrics (Invited)** 37
G.M. Sessler

2-8 **Effect of Crystallinity on Charge Storage in Polypropylene and Polyethylene** 47
R. Nath and M.M. Perlman

2-9 **The Trapping of Electrons in Polystyrene** 52
P.K. Watson

2-10 **Thermally Stimulated Depolarization Currents in a Polyzwitterion: An example of Chemical Relaxation** 57
E. Marchal

SESSION 3 CHARGE FORMATION

3-11 **Characterization of Polymers by Dielectric Spectroscopy (TSC)** 65
J.R. Saffell, J.P. Ibar, A. Bernes and T. Thomas

3-12 **Space Charge Investigation in β-PVDF by Thermally Stimulated Measurements** 70
R.M. Faria and A. Jorge

3-13 **Space-Charge Distributions in Electron-Beam Charged Mylar and Kapton Films** 75
J.E. West, H.J. Wintle, A. Berraissoul and G.M. Sessler

3-14 **Electron-Beam Poling of Very Thin PVDF and VDF-TrFE Copolymer Films** 80
D. Schilling, S. Schuler and K. Dransfeld

3-15 **A Summary of Corona Charging Methods** 87
J.A. Giacometti, G.F. Leal Ferreira and B. Gross

3-16 **Space Charge Formation Related to the Morphology of Polymers** 92
G. Krause, D. Meurer and D. Klee

SESSION 4 THEORETICAL CONCEPTS AND MODELS

4-17 **A Mathematical Model to Study the Influence of Space-Charges in a Needle-Plane-Arrangement in a Polymer** 98
H. Döpper

4-18 **Directional Trapping** 104
G.F. Leal Ferreira

4-19 **Hopping and Electron Glass Transport in CdF2:Y Crystals** 108
V. Dallacasa and C. Paracchini

4-20 **Effect of Inhomogeneity on the Determination of Density of States for Current Carriers in Insulators and Wide Band-Gap Semiconductors** 113
J. Sworakowski and S. Nešpurek

SESSION 6 ELECTRET 1

6-21 **Thermally Stimulated Processes in Organic Polymers (Invited)** 118
R.J. Fleming

6-22 **Effect of Mechanical Deformations on Thermally Stimulated Currents in Polymers I. Uniaxially *Cold-Drawn Polycarbonate*** 131
G. Yianakopoulos, J. Vanderschueren and J. Niezette

6-23 **Charging, Long-Term-Stability, and TSC-Measurements of SiO_2 - Electrets** 137
P. Günther

6-24 **Observation of UV Photo-Stimulated Currents of Teflon Electrets** 142
T. Oda, T. Utsumi and G. Matsubara

6-25 **Effect of Polymer Blending on the Dipoles of Constituent Polymers** 147
P.K.C. Pillai, A.K. Tripathi, R. Sekar, A. Tripathi and G.K. Narula

SESSION 7 ELECTRET 2

7-26 **Electromechanical Properties of Composite Electret Structures** 154
F. Micheron

7-27 **Bending Piezoelectricity of FEP-Teflon Electrets** 155
T. Takamatsu and H. Sasabe

7-28 **Defect Induced Mechanisms in the Ferroelectric to Paraelectric Phase Transition of Poly (Vinylidene Fluoride - Trifluorethylene) Copolymers** 160
R.L. Moreira, R. Almairac and M. Latour

7-29 **The Application of Silicon Dioxide as an Electret Material** 165
A.J. Sprenkels, W, Olthuis and P. Bergveld

7-30 **The Interaction of Fission Fragments with Electron Beam Charged Polyfluorethylene Propylene** 170
S.R. Berggren and G. John

7-31 **Anomalous Discharge Current in Copolymers of Vinylidene Fluoride and Trifluorethylene** 175
Y. Murata and N. Koizumi

SESSION 8 PIEZO- AND PYROELECTRICITY

8-32 **Piezoelectricity and Pyroelectricity in Polymers (Invited)** 182
T. Furukawa

8-33 **Investigation of Structural Changes in PVDF by Modified X-Ray Texture Methods** 194
D. Geiss

8-34 **Piezo- and Pyroelectricity and Structure of Doped Polymers** 199
R. Danz, B. Elling, W. Künstler, M. Pinnow, R. Schmolke, A. Wedel and D. Geiss.

8-35 **Nonlinear Piezoelectricity in Oriented Films of Poly Vinylidene Fluoride and its Copolymers** 204
M. Date, E. Fukada and J.H. Wendorff

SESSION 10 APPLICATIONS

10-36 **Modern Electret Applications - The First 20 Years (Invited)** 209
J.E. West

10-37 **Subminature Silicon Integrated Electret Condenser Microphone** 213
P. Murphy, K. Hübschi, N. De Rooij and G.A. Racine

10-38 **Market Situation of Piezo-, Pyro- and Dielectric Films: Latest Developments** 214
R.A. Betz

10-39 **PVDF Hydrophone for the Measurement of Shock Waves** 223
B. Granz

10-40 **Piezo-electric Film as a Sensor Element in Signature Verification** 229
P. de Bruyne

SESSION 11 APPLICATIONS 2

11-41 **Detection of Stress Field Shear Components by a Piezoelectric Polymer Tactile Sensor** 234
D. De Rossi, A. Nannini, C. Domenici and R. Francesconi

11-42 **Polarization Phenomena in Resinic Esters of Photothermoplastic Devices for Application to Holographic Optical Switching** 241
J. Dandurand, C. Lacabanne, J.Y. Moisan and C. Servens

11-43 **Normal and Anomalous Thermally Stimulated Currents and Space Charge in Polypropylene** 246
S.C. Datt, R.S. Baghel and R. Singh

11-44 **Pyroelectric Applications of Ferroelectric Polymers** 251
S.B. Lang and D.Q. Xiao

11-45 **Piezoelectricity in Nylon 5, 7** 256
P.E. Dunn and S.H. Carr

SESSION 5 POSTER PRESENTATION (1)

5-46 **Electro Active Properties of Ceramic-Polymer Composites** 261
M.J. Abdullah and D.K. Das-Gupta

5-47 **Dielectric Study of Al-Hydroxy-nontronite** 266
A. Anagnostopoulou-Konsta, N.H.J. Gangas, P. Pissis, L. Apekis and D. Petridis

5-48 **Dielectric Study of the Interaction of DNA and Water** 271
A. Anagnostopoulou-Konsta, D. Daoukaki-Diamanti, P. Pissis and E. Sideris

5-49 **Dielectric Study of Dry and Hydrated Microcrystalline Cellulose** 276
L. Apekis

5-50 **Dielectric Properties of Polyurethane Block Copolymers** 281
L. Apekis, P. Pissis, C. Christodoulides, G. Spathis, E. Kontou and V. Kefalas

5-52 **Concerning the ρ Relaxation During Amorphous Pet Crystallization by Thermally Stimulated Discharge** 286
J. Belana and P. Colomer

5-55 **Investigation of Crystalline Orientation, Thermodynamic Properties and Curie Transition on Ferroelectric VF_2/TrFE Copolymers** 291
A. Chalumeau

5-56	**On the Field Distribution and Effective Permittivity of Two-Layered Capacitors** R. Coelho and A. Cansell	292
5-57	**Opto-ferroelectric Memories using Vinylidene Fluoride Copolymers** M. Date, T. Furukawa and T. Yamaguchi	298
5-58	**Short-circuit Thermally Stimulated Currents in Polystyrene-Poly Methyl Methacrylate Blends** J.M. Keller, R.S. Baghel, R. Singh and S.C. Datt	303
5-59	**A Study of Absorption Currents in Acrylic Acid Doped Polystyrene** R. Singh, R.S. Baghel, J.M. Keller and S.C. Datt	308
5-60	**Thermally Stimulated and Isothermal Discharge of Corona Charged Polypropylene** R. Singh, J.M. Keller and S.C. Datt	313
5-61	**Polarization Behaviour of Iodine-Doped Polystyrene** R. Singh, S. Nayak, J.M. Keller and S.C. Datt	318
5-62	**Electrical Conduction in Acrylic Acid Doped Polystyrene** A.R.K. Murthy, R.S. Baghel, R. Singh and S.C. Datt	323
5-63	**Personnel Radiation Dosimetry using Electret Ionisation Chambers** K. Doughty and I. Fleming	328
5-64	**Electro-Optical Behaviour of Ferroelectric Liquid Crystal (FLC) Mixtures** H.R. Dübal, C. Escher and D. Ohlendorf	334
5-65	**Dielectric α Relaxation Study of Polyethylene by Thermally Stimulated Depolarization Currents and Thermal Sampling** J.M.M. Dueñas, R.D. Calleja and J.L.G. Ribelles	339
5-67	**Effect of Electrode Coating on Leakage Current and Surface Flashover Strength in Polymers** F.M.H. Youssef and T.D. Eish	344
5-68	**Surface Flashover and Surface Deterioration of Polymer Insulators in Vacuum** T.D. Eish and F.M.H. Youssef	349

5-69	**Factors Affecting Creepage and Clearance Distances of Polymer Insulators in Coastal and Marine Electrical Equipment** S.S. El-Dessouky and F.M.H. Youssef	354
5-70	**Dynamics of Polarization Growth and Polarisation Reversal in PVDF Films** M. Womes, E. Bihler and W. Eisenmenger	359
5-71	**Negative Charging and Secondary Emission of Teflon FEP under Electron Irradiation** A. Berraissoul and B. Gross	364
5-73	**TSDC Analysis of the Poly (Trans 1-Octenylene)** J. Fraile, A. Torres, J. Jiménez and J.A. de Saja	369
5-74	**PVDF Sensor array for Human Body Detection** R. Freitag and H. Meixner	374
5-76	**Ultrasonic Transducers using Piezoelectric PVDF Films** N. Kroemer, W. Manthey, W. Künstler, R. Danz and D. Geiss	379
5-77	**Piezoelectricity and Polarization of Acrylonitrile/ Methylacrylate Copolymer** W. Künstler, H.V. Berlepsch, A. Wedel, R. Danz and D. Geiss	384
5-78	**Influence and Implications of Surface Contaminations on the Charge Decay in Electrets** W. Stark, R. Danz, W. Künstler and D. Geiss	389
5-79	**Stochastic Hopping Transport in Disordered Polymers** I. Müller, L. Brehmer, D. Geiss, E. Platen, A. Liemant, and W. Wagner,	394
5-80	**Detection of Laser Radiation using PVDF Films** B. Elling, W. Künstler, R. Danz, D. Geiss, and W. Bohmeyer	399
5-81	**Constant Current Corona Triode with Bias Grid Voltage Control** J.A. Giacometti, and J.S. Campos	404
5-82	**Peak Shift due to the Electric Field on PETP Corona Charged Foils** J.A. Malmonge, G.F. Leal Ferreira, J.A. Giacometti and R.A. Moreno	409

5-83	**Some Studies on Glass Fibre Reinforced Polymer Composites** M. Goel	414
5-84	**Electric Polarization of Polymers in Metal-Dielectric-Metal Systems** V.A. Goldade, L.S. Pinchuk and Y.I. Voronezhtsev	419
5-85	**Charge Storage and Relaxation in $SrTiO_3$ and $KTaO_3$ Crystals** Y. Gorokhovatsky and Y. Sezonov	424
5-87	**TSD Currents in Thermally Aged and β-Irradiated Polyethyleneterephtalate (PET) Film** S.M. Gubanski, A. Gubanski and B. Macalik	425
5-89	**Application of a Second Order Response Theory to the Nonlinear Piezoelectricity of PVDF** P. Harnischfeger and B.J. Jungnickel	430
5-90	**A Method for Space Charge Distribution Determination in Thick Dielectric Samples** R. Kacprzyk	435
5-91	**Effect of Antistatic Agent on Electrical Conduction of Polypropylene Foil** R. Kacprzyk and E. Motyl	440
5-92	**A Surface T.S.C. Study of the Interaction Between a Gas and an Epoxy Resin** F. Kaouah, M. Bendaoud and N. Bouchtout	441
5-93	**The Formation of Deep Traps in the Near surface Layers of Fluoropolymer Corona Electrets** V.G. Boitsov, A.A. Rychkov and V.V Schvetz	446
5-94	**Time and Frequency Domain Performance of Ultrasonic Transducers** R. Lal and D.K. Das-Gupta	447
5-95	**Polarization Phenomena as a Characteristic of the "Structure" of the Polymeric Amorphous Phase** A. Bernes, D. Chatain and C. Lacabanne	452
5-96	**Characterization of the Microstructure of Latexes by Thermally Stimulated Currents** P. Cebeillac, C. Lacabanne and P. Dupuis	457

5-97 **Role of Interfaces on a Natural Composite Bioelectret: Bone** 462
A. Lamure, M.J. Fauran-Clavel, C. Lacabanne, M.F. Harmand, M. Vignoles and G. Bonel

5-98 **Phase Transition Investigation in Vinylidene Fluoride/Trifluorethylene Copolymers by Thermally Stimulated Conductivity Measurements** 467
M. Latour, R.M. Faria and R.L. Moreira

5-100 **Thermally Stimulated Current Study on Polyimide Film** 472
Q. Lei and F. Wang

5-103 **Method of Measurement of Space Charge Distribution in Double-Layer Composite Dielectrics** 477
Y. Zhang, D. Tu and Y. Liu

5-104 **Behaviour of Negatively Corona Charging Teflon-FEP at Elevated Temperature** 482
T.J. Lu, G.M. Yang and X.M. Sun

SESSION 9 POSTER PRESENTATION (2)

9-105 **Thermally Stimulated Currents of Corona Treated Teflon-FEP Electrets** 487
C.J. Dias, J.N. Marat-Mendes and J.A. Giacometti

9-106 **Isothermal Charge Decay of Teflon-FEP Electrets under a Corona Discharge** 493
C.J. Dias, J.N. Marat-Mendes and J.A. Giacometti

9-107 **Dosimetry at Interfaces: Measurements by Polypropylene Electrets at and Near Plane Interfaces Between Different Materials (C,Al,Cu,Sn,Pb) Irradiated with Cobalt 60 Gamma Rays** 499
P.N. Martin

9-108 **Calculations of the Ionization Distribution at, and Near, the Interfaces Between Two Media using P.N. Junction and Electret Detectors.** 504
P.N. Martin

9-111 **Kinetics of Radiation-Induced Dielectric Effect in Polymers** 509
V.I. Arkhipov, V.R. Nikitenko and A.I. Rudenko

9-113 **Electret State of Butadiene-Styrene Copolymers** 510
R. Capelletti and J. Pospisil

9-114 **Charging Characteristics of a Non-Woven Sheet Air Filter** 515
T. Oda, and J. Ochiai

9-119 **Polarization Phenomena of Biological Dielectric under the Influence of Electric and Magnetic Field** 520
J.C. Paul

9-120 **A.C. Poling of Solution Cast Films of Polyvinylidene Fluoride/Lead Zirconate Composites** 525
D. Sinha and P.K.C. Pillai

9-123 **Electret Formation and Charge Storage in Single Crystal Zirconia** 526
O.P. Puri, O. Sinha, K. Bota and T. Harrington

9-124 **Thermally Stimulated Current in Sodium Borosilicate Glass** 531
E. Rysiakiewicz-Pasek, V. Graveris and I. Krumins

9-125 **Mechanism of Charge Formation in the Irradiated Polyethylene** 536
V.V. Gromov, A.G. Rozno and O.V. Procopiev

9-126 **Increase of Refractive Indices in Liquid Dielectrics by Space Charge Accumulation** 537
T. Sato

9-127 **Investigation of Corona-Charging of Polypropylene at Elevated Temperatures** 538
H. Ding and Z.F. Xia

9-128 **Influence of Quenching on Charge Stability of Polymer Electrets** 543
Z.F. Xia

9-130 **Aluminium Porous Oxide for Electrets** 548
V.I. Shershulsky and D.V. Yakovlev

9-131 **Electret Air Filter used for Getting Rid of Bacteria** 549
L.S. Shi, B.J. Chen and Y.D. Wang

9-132 **TSC due to Polarization by Transference of Space Charge** 554
K. Shindo

9-134 **Thermally Stimulated Currents in Polymers and Dielectrics** 559
A. Mandowski and J. Swiatek

9-135 **Lateral Nonhomogeneous Decays of Surface Charge on Teflon-FEP Films** 560
X.M. Sun and D.G. Yang

9-136 **Electrification and Electret Effect in Polymer Friction** 565
A.I. Sviridyonok, A.F. Klimovich and S.I. Guzenkov

9-138 **Electrode Effect on Thermally Stimulated Discharge Current in Polystyrene Films** 570
A.R. Tiwari, K.K. Saraf and A.P. Srivastava

9-139 **Numerical Simulation of Non-Isothermal Dispersive Carrier Transport** 571
W. Tomaszewicz

9-140 **Experimental Determination of the Dispersion Spectrum of Zeolites** 576
M.H. Vélez and R. Roque-Malherbe

9-141 **Dielectric Effects of the Tunnel Mechanism of Relaxation** 581
V. Veksler and Y. Orlova

9-142 **Micromachining of Electret Materials, Advantages and Possibilities** 582
J.A. Voorthuyzen and P. Bergveld

9-143 **An Electret-Based Pressure Sensitive MOS Transistor** 587
J.A. Voorthuyzen and P. Bergveld

9-144 **Mica Electrets** 592
I.I. Inculet, R. M. Quigley and A. Garg

9-145 **The Use of Silicon Technology for an Electret Microphone Construction** 593
A.J. Sprenkels and P. Bergveld

9-146 **The Poling of Multiple-Layer Polyvinylidene Fluoride Films and their Piezoelectricities** 598
S. Wang, Y. Zhao and F. Yan

9-148 **Electret Radiation Dosimeter with Grid-Control** 603
Z.Z. Wang, C.Z. Xu and X.M. Sun

9-149	**Bulk and Interfacial Dielectric Response of Dysprosium and Ytterbium Oxide Thin Film Capacitors** T. Wiktorczyk	607
9-150	**Study on the Space Charge Peak of TSC in Pet Film** J. Wu and Q. He	612
9-151	**A New Composite Electret Film which is based on Polymer PVDF** D. Yang	617
9-152	**Temperature Dependence of -OH Band in Vinyl Chloride: Vinyl Acetate: Vinyl Alcohol Terpolymer** V.S. Panwar, R. Singh, N.P. Gupta and P.C. Mehendru	622
9-153	**AC Conductivity and Dielectric Constant Studies of Vinyl Chloride: Vinyl Acetate Copolymers** P.C. Mehendru, R. Singh, V.S. Panwar and N.P. Gupta	627
9-155	**The Experimental Study of the Electret Properties of Carp Scale** T. Zheng, Z. Wu and F. Xu	632
9-157	**The Analysis of Thermally Stimulated Current in Pork Bone** Y. Zhu, Z. Wu and F. Xu	637
9-159	**Effects of Plasma Treatment of Surfaces on Charge Storage in Polypropylene** H.J. Zhao, D.M. Tu, L.Y. Gao, Y.N. Liu and K.C. Kao	642
9-160	**Polymeric Materials with Enhanced Second Order Nonlinearities** H.E. Katz, M.L. Schilling, R.B. Comizzoli, K.D. Singer, J.E. Sohn, M.G. Kuzyk and W.R. Holland	647
9-163	**The Luminescence Stimulated by Temperature Change of Crystalline Films of N-Isopropylcarbazole** Z. Dreger, J. Kalinowski, R. Nowak and J. Sworakowski	652
9-164	**Touch Trigger Probe with PVDF Sensor** E. Haeusler and V. Rech	657

9-165 **Computerised Electret Dosimeter** 662
P.E. Cruvinel and S.Mascarenhas

9-166 **Vibetek 20® Piezoelectric Cable : A Continuous Process** 663
D.R. Fox

9-167 **Thermally Stimulated Current Studies of Corona Charged Tefzel** 668
E. Neagu and D.K. Das-Gupta

Author Index 673

Subject Index 680

DETERMINATION OF THE CHARGE DISTRIBUTION WITHIN AN e-IRRADIATED DIELECTRIC USING THE PRESSURE WAVE PROPAGATION METHOD

M.P. Cals, J.P. Marque and C. Alquié*

Office National d'Etudes et de Recherches Aérospatiales
BP 72, 92322 Châtillon Cedex, France
*Ecole Supérieure de Physique et Chimie Industrielles
de la Ville de Paris, 75005 Paris, France

ABSTRACT

The pressure wave propagation (PWP) method is used to investigate charge storage in Teflon FEP films irradiated with monoenergetic electron beam in a vacuum. Signals obtained at different time intervals during charging of the material up to - 7 kV will be presented and analysed.

INTRODUCTION

In the framework of a study of the discharge process occurring in a space environment, an experimental simulation of charging and discharging of polymer films, submitted to a e-irradiation, is conducted. The charge profiles in the irradiated films are measured using the laser induced PWP method [1-3]. As this method is non destructive, the evolution of the charge density can be recorded at various steps of the irradiation process, up to the occurrence of a discharge.

THE EXPERIMENT

The polymer samples used are 125 μm thick disks of FEP Teflon, 5 cm in diameter. No previous treatment is performed on these samples. One side of the sample is bonded to an electrode, which is also the absorbing target used to create the pressure pulse.

Very reproducible pressure waves are obtained by the impact of a 350 mJ, 3 ns, YAG/Nd laser pulse on a 500 μm thick aluminum target. The pressure pulses entering the

CH2593-2/ 88/ 0000-0001$01.00 Copyright 1988 IEEE

sample, measured using a piezoelectric quartz transducer, have an amplitude of about 30 bar in a vacuum, and a rise time of 4 ns.

The experimental simulation of dielectric discharge on satellites is carried out in a vacuum chamber, with an ambient pressure between 10^{-5} and 10^{-6} mbar. The sample is first irradiated with a 10^{-9} A.cm^{-2} monoenergetic electron beam in the range 5-50 keV. Then it is shifted under the detection electrode allowing the measurement of the charge distribution. During this displacement, the surface potential is measured. Finally, the short-circuit current induced by the pressure wave is amplified and recorded using a programmable digitizer. This sequence of irradiation and measurement is repeated several times until a discharge occurs.

RESULTS AND DISCUSSION

Positive charge injection at the target-FEP interface

Fig. 1 shows the evolution of current signals, representative of the charge distributions, during an irradiation. The sample is initially empty of charges (Fig. 1a). For each step in the irradiation process, the surface potential is indicated in Table 1.

Table 1: Experimental conditions relative to Fig. 1.

Figure	Irradiation duration (second)	Surface potential (kV)	Gap (μm)
1b	10	- 1.5	150
1c	55	- 4	150
1d	150	- 7	150
1e	after discharge	- 0.2	300

The first current pulse is observed when the pressure wave enters the sample (Fig. 1b to 1e) and shows a strong variation during irradiation. From eq (2) in [4], it is easily shown that if the electric field is uniform near

the target-insulator interface, corresponding to the absence of charges in this region, the first pulse represents the pressure pulse entering the sample. This situation corresponds to that observed in Fig. 1b. Conversely, a distortion of the first current pulse is characteristic of a non-uniform electric field at the interface, equivalent to the presence of charges in the insulator. Such a distortion, observed in figure 1c to 1e, strongly depends on the value of the gap g between the measuring electrode and the free surface of the sample, as shown in Fig. 2. This phenomenon can be interpreted by way of a numerical simulation (Fig. 3). This figure compares the electric field distributions corresponding to two different charge profiles, versus g. Positive charges at the interface (Fig. 3c) produce a non uniform electric field, and, for some value of g, the appearance of a zero-field plane. Consequently, the distortion of the first current pulse clearly proves the injection of positive charges.

Analysis of the near surface charges

The second negative pulse (Fig. 1b to 1d) corresponds to the electrons trapped close to the irradiated surface. The amplitude of this pulse is proportional to the density of the trapped electrons, in agreement with the value indicated by the surface potential. In figure 1e, a charge distribution measured after a discharge occurring for a surface potential larger than - 7 kV is presented. Almost all of the trapped electrons have disappeared. The maximum depth of penetration can be estimated from this signal if the transit time T of the pressure wave is known accurately, by measuring the pressure profile transmitted through the sample, at the end of the irradiation process. As an example, a current curve obtained for a beam energy of 20 keV and the corresponding pressure profile are show in Fig. 4. In this case, the time interval Δt between the onsets of the current and of the pressure is around 8 ns and corresponds to a depth of 10.4 μm.

Determination of the charge profile

If attenuation and dispersion of the elastic wave occurs during the propagation, the electric field distribution

can be deduced from eq (1) in [4] by a numerical deconvolution, if the pressure profile P is known. This profile is obtained by linear interpolation between pressure pulses measured by a quartz transducer behind the target and after propagation through 50 and 125 μm thick films. Beyond the transit time, the reflected wave at the sample-vacuum interface is taken into account by assuming a total reflexion. The solution D is obtained according to the method proposed by Phillips and adapted by Twomey [5]. The result of such a treatment is shown in Fig. 5, and applied to a signal current (Fig. 5a). The charge profile (Fig. 5b) is deduced from D by the Poisson's equation. The filtering parameter γ [5], chosen to minimize the deviation between the measured profile V and the calculated one P * D, is equal to 10^{-2} (Fig. 5c). The value of the mean depth is estimated between 1.4 and 1.7 μm. It is slightly less than previous measured values [6], particularly this obtained by Sessler [7] using the LIPP method and equal to 2 μm for E_B = 10 keV.

Next experiments now in progress will allow us to present charge profile and mean range variation as a function of the incident beam energy.

CONCLUSION

Evolution of the electric field distribution in e-irradiated polymer films are of interest for space industry to understand ESD on geostationnary satellites. The PWP method clearly puts in evidence the incident electrons trapped near the surface and positive charges injected at the opposite metal-polymer interface. These charges remain trapped after a surface discharge but buried electrons disappear. A numerical treatment leads to an improved determination of the charge distribution through the sample and gives the value of the mean depth of penetration versus the beam energy.

REFERENCES

[1] - P. Laurenceau, G. Dreyfus and J. Lewiner, Phys. Rev. Lett., 38, 46 (1977).

[2] - C. Alquié, G. Dreyfus and J. Lewiner, Phys. Rev. Lett., 47, 1483 (1981).

[3] - C. Alquié, J. Lewiner and G. Dreyfus, J. Phys. Lett., 44, L-171 (1983).
[4] - J. Lewiner, IEEE Trans. EI-21, 351 (1986).
[5] - S. Twomey, J. Assoc. Computer Mach., 10, 97 (1963).
[6] - B. Gross, G.M. Sessler, J.E. West, J. Appl. Phys., 48, 4303 (1977).
[7] - G.M. Sessler, J.E. West, R. Gerhard-Multhaupt, H. Von Seggern, IEEE Trans. NS29, 1644 (1982).

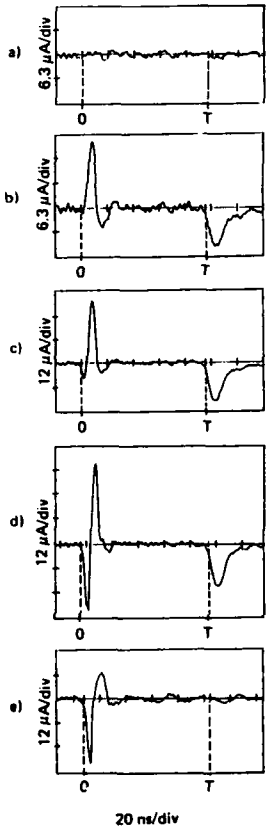

Fig. 1 – Evolution of current signals during an irradiation (E_B = 16 keV; I = 1 nA cm^{-2}).

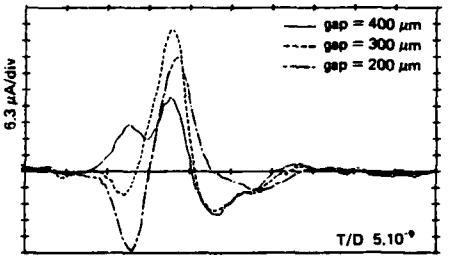

Fig. 2 – Evolution of the first current pulse for different values of the gap g.

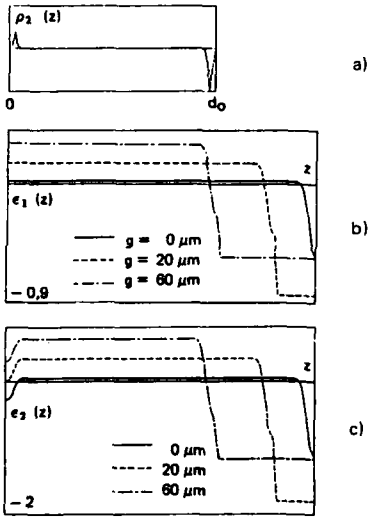

Fig. 3 – Spatial electric field distributions for different values of the FEP-electrode gap. b) $\rho(z) = \rho_1(z)$, c) $\rho(z) = \rho_1(z) + \rho_2(z)$ $(\rho_1/\rho_2 = 4)$.

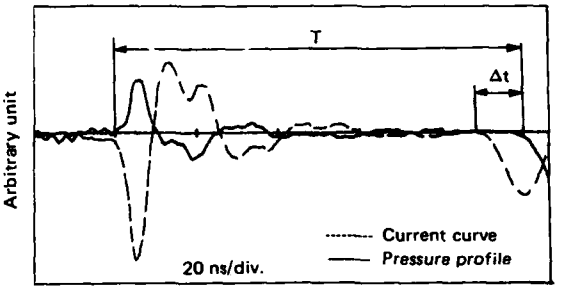

Fig. 4 – Determination of the transit time T and the maximum range $v\Delta t$. [$E_B = 20$ keV].

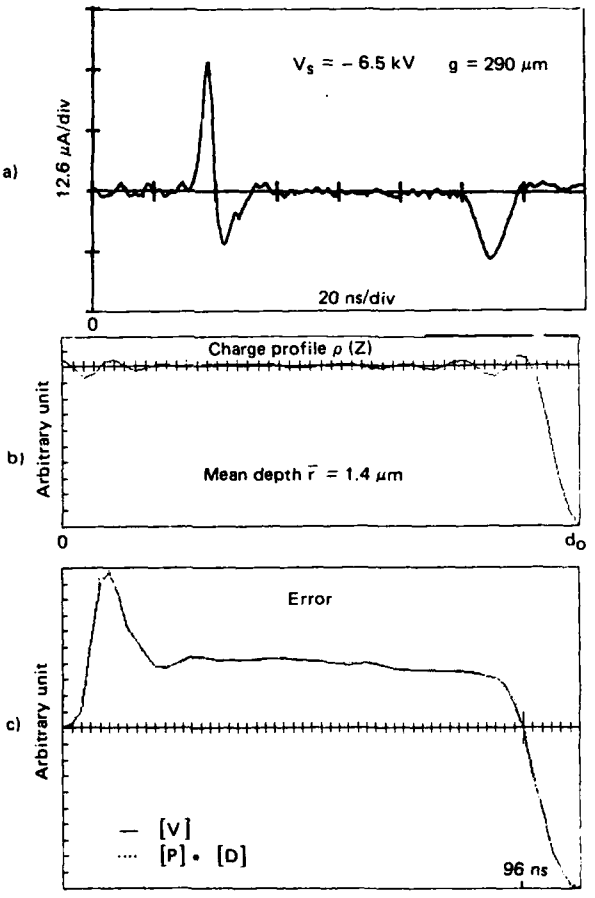

Fig. 5 – Charge profile (b) obtained by numerical deconvolution of a current signal (a) at $E_B = 16$ keV.

ELECTRICAL PROPERTIES OF ELECTRODE - POLYETHYLENE - ELECTRODE STRUCTURES

T. Ditchi, C. Alquié, J. Lewiner, R. Favrie* and R. Jocteur*

Ecole Supérieure de Physique et de Chimie Industrielles
10, rue Vauquelin, 75005 Paris, FRANCE

*SILEC, 77130 Montereau, FRANCE

ABSTRACT

The pressure wave propagation (PWP) method allows for the non destructive measurement of charge distributions in dielectric materials. This method has been used to study the electrical properties of electrode - polyethylene - electrode structures such as those involved in high voltage cables. In the work which is presented, we analyse in polyethylene samples, first the influence of the composition of the insulating resin itself, and second that of the electrodes. According to the chosen combination, charge transfer at the interfaces, migration of ionizable impurities or a strong decrease of both effects are observed. This application of the PWP method is of particular interest since it allows for a suitable choice of the materials and structure involved in insulator - conductor interfaces.

I - INTRODUCTION

High voltage power transmission cables using extruded synthetic insulation are already widely used in the world, essentially for alternative current links and, to a smaller extent, for direct current ones [1]. In both cases, a suitable choice of the materials constituting the cable structure is required in order to define equipments with increased performances.

One may distinguish between two parts in this structure : first the insulating material, generally made of low density polyethylene (LDPE), high density polyethylene (HDPE) or cross-linked polyethylene (XLPE), second the so-called "semiconducting" electrodes usually made of carbon loaded polyethylene. As to the insulator, although extra-clean polyethylene resins are used, impurities or residues resulting from the manufacturing process, such as compressor oil or lubricant, can be found in small quantities. As to the electrodes, they usually contain large amounts of additives, and impurities [2]. These impurities have a very large influence on the electrical properties of the structure, due to several phenomena. For instance, impurities contained in the insulating resin or diffusing from the electrodes into the insulator may

CH2593-2/ 88/ 0000-0007$01.00 Copyright 1988 IEEE

be at the origin of the build up, under electric stress, of a space charge or dipole distribution. Charge transfer may also occur at the interfaces. The local increase of the internal electric field which results from this non homogeneous charge distribution reduces the effective electric strength of the dielectric and may lead to disruptive phenomena.

In a recent past, only empirical methods of investigation of these processes were available. New perspectives are now opened by the pressure wave propagation (PWP) method [3-5] which allows for the direct, non destructive, measurement of the electric field distribution in the insulation. In this paper, the influence of the composition of the insulating resin and of the electrodes on the electrical properties of the electrode - insulator - electrode structure, is analysed, using the PWP method.

II - THE PRESSURE WAVE PROPAGATION METHOD

We will not describe in detail this method which has already been presented [3-5] but will simply recall its basic principle. A short rise time pressure wave, propagating at the sound velocity in a dielectric material, acts as a virtual probe sensitive to the electric field or to the charge density. It has been shown [3-5] that the variation in time of the charges induced on measuring electrodes, during the transit of the wave through the sample under test, is directly related to the field and charge spatial distributions.

Very reproducible pressure waves can be obtained by the impact of a short laser pulse on an absorbing target adjacent to the sample. The PWP method also allows to study the evolution of the charge distribution in a sample during a polarization process, while a high voltage is applied [6]. A complete measuring equipment is now commercially available [7].

In the experiments hereunder described, the samples are 2 mm thick LDPE plates, on which two semiconducting electrodes are hot-pressed. One of these electrodes is also used as a target for the laser beam. The samples are submitted to a 60 kV voltage at 50°C. During this polarization process, the evolution of the charge distribution is measured, untill a stabilization is reached.

III - INFLUENCE OF THE INSULATOR ITSELF

In order to evaluate the influence of impurities contained in the insulator itself, two different extra clean resins originating from two manufacturers are compared. In the following they are refered to as type A and type B resins. In this first step of the analysis, the electrodes have a standard composition already used for AC cables.

On Fig. 1, we compare the charge distributions obtained after stabilization for these two resins. For type A, under applied field charges of opposite polarity to that of the closest electrode gradually accumulate, and their maximum density reaches a few $\mu C/cm^3$. The electric field is maximum at the interfaces and is approximately twice the applied field. Conversely, for type B resin, a strong charge transfer occurs at both electrodes, leading to an increase of the electric field in the bulk of the sample. In this case, the maximum value of the internal field is equal to 110 % of the applied field in the bulk and reduces to 70 % of this field at the interfaces.

The difference between these two materials is striking and rather unexpected. In the next chapter we will also take into account the composition of the electrodes.

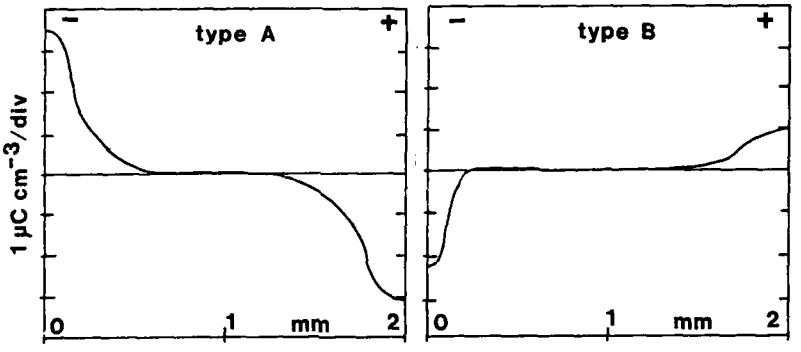

Fig. 1 : Stabilized charge densities in samples with standard electrodes, respectively for type A and type B resins.
Polarization conditions : 30 kV/mm, 50° C, 90 hours.

IV - INFLUENCE OF THE COMPOSITION OF THE ELECTRODES

The semiconducting electrodes which are used in high voltage cables contain several compounds, which may differ from a manufacturer to another, but generally include polyethylene, carbon black, plastifying agents and other additives in smaller quantities. In each of these constituants, impurities which vary with the origin of the product are always present [2]. For example "standard" electrodes considered in chapter III contain, among other chemical species, less than 1 % of zinc stearate, refered to as additive 1 (Ad 1) and a large amount (approximately 10 %) of an aromatic plastifying agent, noted additive 2 (Ad 2).

In order to determine the influence of these two additives on the electrical properties of the electrode - insulator - electrode structure, samples with electrodes without Ad 1 and others without Ad 2 were submitted to the polarization process previously described. The two insulating resins A and B were successively used in each case. The charge distributions measured after stabilization in these 4 sample configurations are presented on Fig. 2 and 3. Fig. 2 corresponds to electrodes without zinc stearate whereas Fig. 3 corresponds to electrodes without plastifying agent. On Fig. 4, we compare the distributions corresponding to standard electrodes to those obtained when zinc stearate is suppressed.

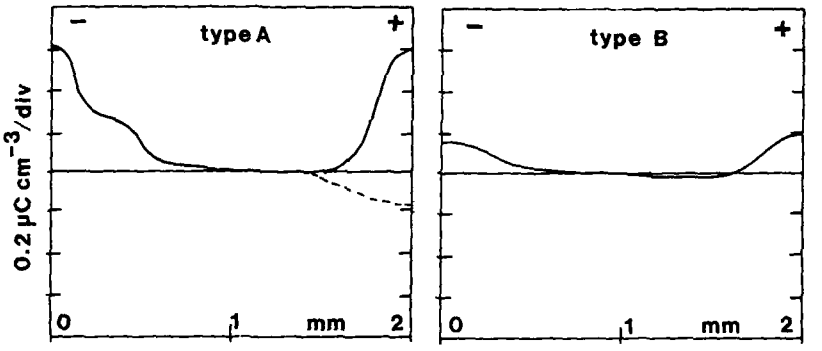

Fig. 2 : Same as Fig. 1, for electrodes without zinc stearate. The different distributions shown were obtained on different samples.

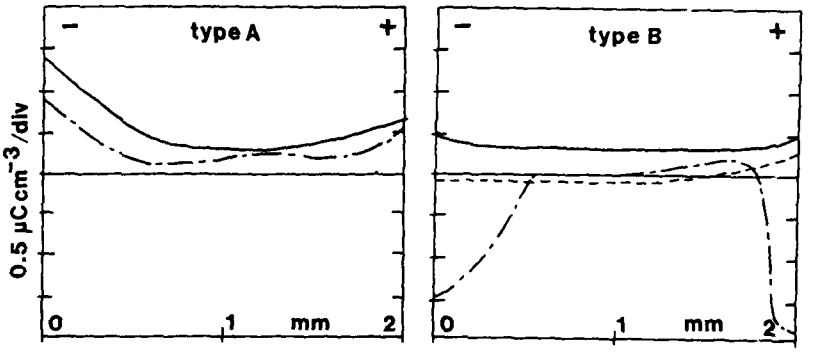

Fig. 3 : Same as Fig. 1, for electrodes without aromatic plastifying agent. The different distributions shown were obtained on different samples.

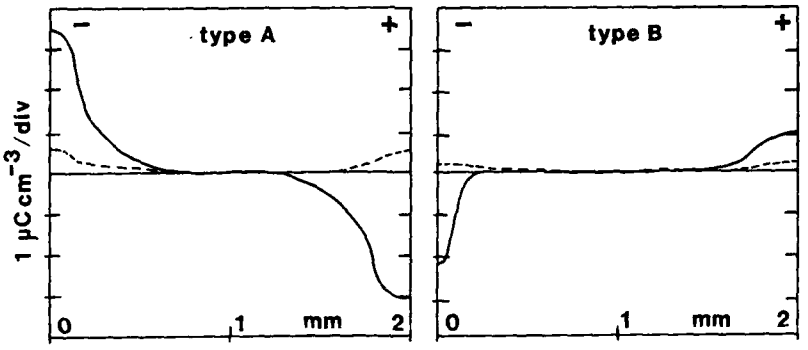

Fig. 4 : Comparison of the charge distributions corresponding to standard electrodes and to electrodes without zinc stearate.
Full line : standard electrodes.
Dotted line : electrodes without zinc stearate.

The most striking result is the large decrease of the charge densities measured in samples without Ad 1 (see Fig. 2 and 4). This decrease was observed on all samples, whatever the insulator used. The charge densities are reduced by a factor 5 in resin A. In resin B, the strong injection of negative charges at the cathode, which was observed with resin B and standard electrodes, has disappeared, and the density of the positive charges at the anode is reduced by a factor 5. With both insulating resins, positive charges are dominant, and in many samples, are spread throughout the insulator.

A possible interpretation is that zinc stearate diffuses in the insulator and is highly responsible for the development of space charges observed with the standard electrodes. As the interaction of this ionizable impurity with resins A and B leads in one case to heterocharges and in the other case to homocharges. it seems that these two resins contain also impurities which react differently with zinc stearate.

When the plastifying agent is suppressed from the composition of the electrodes, the behaviour of samples made with resin B is rather fluctuating, as can be seen on Fig. 3b. A possible explanation is that this plastifying agent controls the diffusion of Ad 1 in the insulator so that, when it is suppressed, the behaviour of the interfaces is not well controlled. Similarly, with resin A, when Ad 1 is present in the electrodes but Ad 2 is suppressed, we do not observe any more the large densities of heterocharges obtained with the standard electrodes.

In summary, it seems that the combination of Ad 1 and Ad 2 present in standard electrodes is largely responsible for the space charge distributions which develop, under electric stress, in the insulator. When Ad 1 is suppressed, the charge densities are greatly reduced, specially in resin B, and in this case the distortion of the field does not exceed 7 % of the applied one, at 50° C. Ad 2 seems to be responsible for the diffusion of zinc stearate in the insulator.

V - CONCLUSION

The PWP method was used to analyse the influence of the various chemical species present in the insulator and in the electrodes used in high voltage cables, on their electrical properties. Modifications of the composition of these materials have shown that the diffusion of zinc stearate in the insulator plays an important role in the build up of a space charge and that this diffusion is made easier by other additives contained in the electrodes.

This application of the PWP method provides a direct way to define materials for the electrode - insulator - electrode structures used in high voltage insulation.

REFERENCES

[1] Perret J., Fournié R., *IEEE 1975 Conference on Dielectric Materials* Measurements and Applications, Cambridge, 1975.

[2] Crine J.P., Pelisson S., St-Onge H., Conference JICABLE 87, Versailles, Sept. 87, pp. 206-213, edited by S.E.E., 48, rue de la Procession, 75015, Paris, France.

[3] Laurenceau P., Dreyfus G., Lewiner J., Phys Rev. Lett. 38, pp. 46-49, 1977.

[4] Alquié C., Dreyfus G., Lewiner J., Phys. Rev. Lett. 47, pp. 1483-1487, 1981.

[5] Lewinèr J., IEEE Trans. Elect. Ins., EI-21, pp. 351-360, 1986.

[6] Chapeau F., Ditchi T., Alquié C., Lewiner J., Perret J., Dalle B., Conference JICABLE 87, Versailles, Sept. 87, pp. 91-97.

[7] HLP Technologies, 14, rue de la Glacière, 75013 PARIS, FRANCE.

Polarization Distributions in Isotropic, Stretched or Annealed PVDF Films

E. Bihler, K. Holdik* and W. Eisenmenger
Physikalisches Institut, Universität Stuttgart,
Pfaffenwaldring 57, 7000 Stuttgart 80
*present address: SEL AG, ZT/FZWM, Lorenzstraße 10, 7000 Stuttgart 40

1.Introduction

The spatial distribution of the piezoelectric coefficient in polarized PVDF has been investigated by several authors using different methods /1-6/. In addition also the time development of the polarization distribution in PVDF under external electric fields was studied for a variety of commercially available PVDF films from different suppliers using the piezoelectric pressure step (PPS) technique /7/. For a field strength ranging from 0.5 to 1 MV/cm, samples from different suppliers developped either i) a central polarization zone with no piezoeffect in the boundary regions close to the film surface or ii) a polarization maximum close to the positive charging electrode (anode) without polarization from about the centre of the film to the negative electrode. Since sample inhomogeneities can be excluded, the development of polarization zones are to be explained by charge injection and trapping /3,9/.

The different behaviour i) and ii) in principle must be attributed either to possible differences in the general chemical composition of the films of different suppliers or to differences in the crystallite structure. So far it was found /11/ that the central polarization zone i) appeared in films with a finite content of β-form crystallites, whereas the polarization maximum at the positive electrode ii) appeared for pure α-material. In order to check the possible influence of the crystallite structure independently from the chemical sample composition, we investigated the polarization distributions for the same material as received first with dominant α-crystallite content, then after biaxially stretching in order to increase the β-crystallite content and finally after annealing again in order to reduce the β-crystallite content.

2. Experimental Technique

The spatial distribution of the polarization in PVDF films was measured at room temperature with the PPS-method /3,7/. In order to investigate the time development under external fields a thin insulating PET-film covering an evaporated aluminium electrode was inserted between sample and the measuring electrode. This additional polymer acts as a broadband coupling capacitor to the measured displacement current. It does not influence the shape of the signal.

The crystallite phase composition of the PVDF films was determined by IR absorption. The ratio between the relative absorption at 530 cm^{-1} (α-crystallites) and 510 cm^{-1} (β-crystallites) is taken as a standard for the α/β-phase content (according to /8/).

CH2593-2/ 88/ 0000-0013$01.00 Copyright 1988 IEEE

3.Results

A commercial PVDF film ("Dyflor 2000", Dynamit-Nobel, Troisdorf, FRG) with almost all crystallites of α type was poled at room temperature. The film was poled 1h at a field strength of 0.5 MV/cm and afterwards kept under zero voltage conditions for another hour. The piezo profile in Fig. 1 shows a sharp peak located closely to the anode.

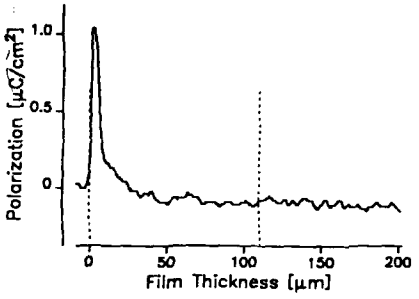

Fig. 1:
Isotropic PVDF film,
thickness 110 μm
poled 1 h at 0.5 MV/cm.

The same material then was stretched at a temperature of 150 °C with a thickness reduction to about 20% of its original value. The α/β phase ratio of the stretched film was 3.9. The time development of the polarization profiles of the stretched film is shown in Fig.2a for a field strength of 0.6 MV/cm. The development starts always with a homogeneous profile caused by the external field. The signal then begins to change its shape indicating homo charge injection from both electrodes, the build up of an almost central polarization zone with polarization free film boundaries and trapping of injected charges at the boundaries of the polarization zone. (The same polarization development was already observed in stretched films as received with finite β crystallite content /7/.)

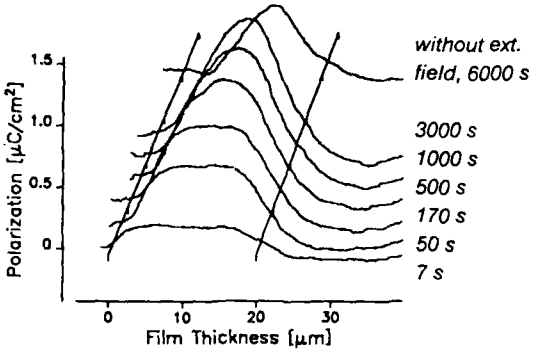

Fig. 2a:
Stretched film,
thickness 20 μm,
α/β phase ratio 3.9
field strength 0.6 MV/cm

At medium field strength (0.8 MV/cm), see Fig.2b, the profile shows a nearly rectangular shape. The zone near the cathode, which is free from polarization, is smaller than at lower field strength. At both electrodes again homo charge injection is observed.

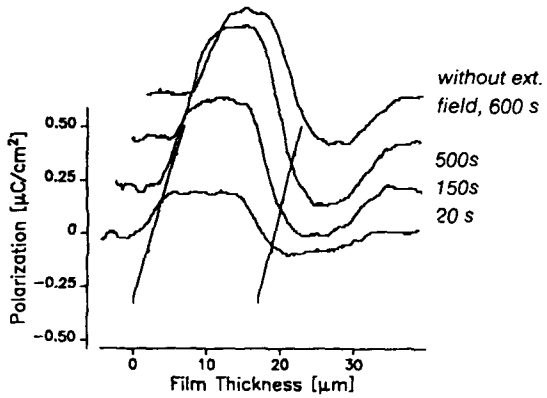

Fig. 2b:
Stretched film,
thickness 20 μm,
α/β phase ratio 3.9
field strength 0.8 MV/cm

For higher field strength (1.8 MV/cm) homogeneous profiles are observed as depicted in Fig. 2c. In this case the transition from zero to maximum polarization at the film boundaries is within the experimental resolution.

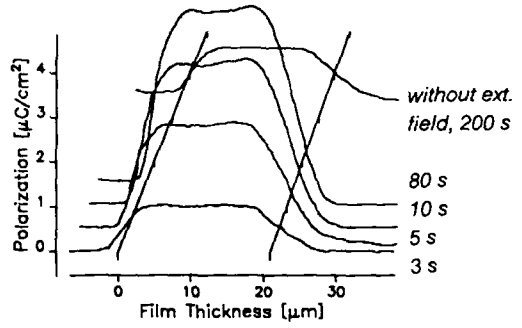

Fig. 2c:
Stretched film,
thickness 20 μm,
α/β phase ratio 3.9
field strength 1.8 MV/cm

Now the stretched films were finally annealed at 180 °C for 3 h. The film thickness increased by a factor of 2.5. The α/β phase ratio increased to 17. The polarization develops again only in a small region close to the anode. The polarization step at the

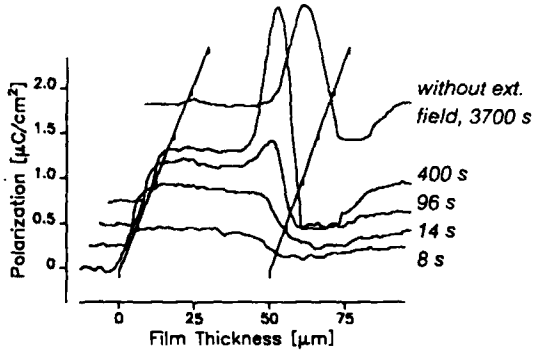

Fig. 3:
Annealed film,
thickness 55 μm,
α/β phase ratio 17
field strength 0.6 MV/cm

cathode gets smoothed out with time indicating homo charge injection. The plateau between the cathode and the anode polarization peak is decreasing with increasing polarization in the peak, indicating an increasing internal field in the polarization zone and charge trapping at the boundaries of this zone.

For comparison we investigated also a stretched material supplied from the Kureha company, Japan. The α/β ratio was determined to 1.25. Fig.4a shows the time evolution of the polarization for this sample under an external field of 0.6 MV/cm. Again a central polarization zone develops for this β-material.

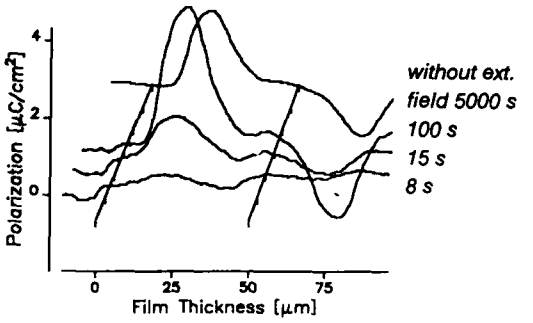

Fig. 4a:
Kureha, as received
thickness 50 μm,
α/β phase ratio 1.25
field strength 0.6 MV/cm

Now this film material was annealed at 160 °C for 3 h. The α/β ratio increased to only 1.5. The thickness increased by 10% to 55 μm. The polarization development in Fig.4b shows a polarization zone shifted towards the anode. First the step at the cathode becomes smoothed indicating charge injection. The same occurs later at the anode. The position of the resulting internal permanent polarization apparently is determined by the differences in the charge mobility and injection from the electrodes.

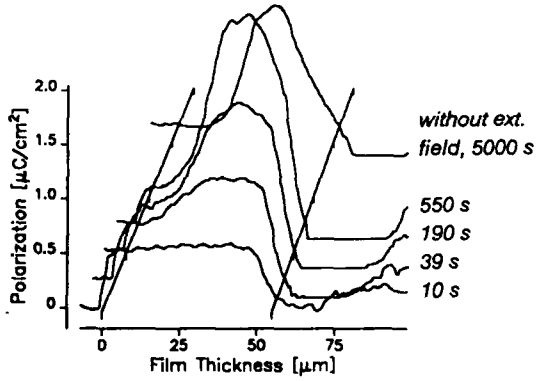

Fig. 4b:
Annealed Kureha film,
thickness 55 μm,
α/β phase ratio 1.5
field strength 0.6 MV/cm

4. Summary and Conclusions

The development of inhomogeneous and internal polarization zones can be attributed to charge injection and charge trapping at the polarization zone boundaries /3,9/. The polarization zone develops at a position where the critical field strength for dipole

orientation in the crystallites is exceeded by the approach of injected homo charges (or without injection by the depletion of internal homocharges and the excess of heterocharges). The critical field for α-crystallites corresponds to an electric field phase transition at 1.2 MV/cm /10/. (For β-material a thin film permanent polarization threshold of 0.5 MV/cm is reported /12/.)

Since we observe for α-material a polarization zone at the anode for a total field strength of 0.6 MV/cm, this indicates strong negative charge injection at the cathode with high charge mobility and little positive charge injection from the anode. There may be also an additional field enhancement in the anode regime by intrinsic positive charges in the film which are depleted at the anode by extraction to the cathode leaving excess heterocharges in the anode regime /11/.

The development of central polarization zones in PVDF containing β-crystallites indicates injection of charges with both signs and almost equal mobility. Since the difference in the position of the polarization zone between pure α-material and films containing β-crystallites evidently is caused by the β-crystallite content, the β-crystallites either determine the charge injection rate or the mobility or both. A strong reduction of the mobility of negative (and positive) charges can be explained by the model of polarized crystallites as traps /3,9/. The trap properties of β-crystallites can be explained by the same mechanism of charge trapping by oriented dipole ends at the crystallite surface. Thus the transition from the polarization zone at the anode in α-material to the central polarization in β-material can be explained by the reduction of the mobility of negative charges by β-crystallites. The influence on the mobility of positive charges is expected to be comparatively small, because this mobility appears to be already low in the pure α-material.

5. Acknowledgement

The authors are very grateful to A.Dörnen for the IR absorption measurements. Financial support by the Deutsche Forschungsgemeinschaft is gratefully acknowledged.

5. References

1. P.J.Phelan et al., Ferroelectrics 7,375 (1974);
2. H.Sussner, K.Dransfeld, J.Poly.Sci.: Polymc `hysics Ed.,16,529 (1978)
3. W.Eisenmenger , M.Haardt, Solid State Comm., 41, 917 (1982)
4. S.B.Lang et al., J.Appl.Phys., 54, 5598 (1983)
5. G.M.Sessler et al., IEEE 1987 Annual Report CEIDP, 319 (1987)
6. for a review see: G.M.Sessler (ed.): Electrets, Springer (1987)
7. K.Holdik,W.Eisenmenger, ISE5, Heidelberg, p. (1985)
8. N. Murayama, J.Poly.Sci.: Polymer Physics Ed., 13, 929 (1975)
9. W.Eisenmenger et al., IEEE 1982 Annual Report CEIDP, 52 (1982)
10. G.T.Davies et al., J.Appl.Phys., 49, 4998 (1978)
11. K.Holdik, Thesis, Universität Stuttgart, 1985
12. D.Nägele, D.Y.Yoon, Appl.Phys.Lett., 33, 132 (1978)

DETERMINATION OF TEMPERATURE DISTRIBUTIONS IN ELECTRET FOILS

R.Gerhard-Multhaupt,* Xia Zhong-fu,** and A.Berraissoul

Institute for Electroacoustics, Technical University of Darmstadt, Merckstrasse 25, D-6100 Darmstadt, F.R.G.

ABSTRACT

The well-known thermal-pulse technique is based on the temporal change of the temperature distribution in an electret sample; the resulting non-uniform thermal expansion in the sample volume leads to an electrical signal which contains information on the charge or polarization profile. Here, a new method is proposed in which known charge profiles (e.g. electron-beam-deposited charge layers) serve as probes for the temperature distribution as it develops after heat-pulse excitation of one of the sample electrodes. The principle of operation is discussed and first experiments are reported. From the results, heat-transport parameters of electret materials may be determined.

PRINCIPLE OF OPERATION

Several methods were suggested for the measurement of charge and polarization profiles in the thickness direction of electrets [1,2]; one of them is the thermal-pulse technique [3-5] whose principle is described by the following equation [4]:

$$\Delta V(t)=[(\alpha_x-\alpha_\varepsilon)/\varepsilon\varepsilon_0]\int_0^d \varrho(x)\,dx\int_0^x \Delta T(x',t)\,dx', \qquad (1)$$

where $\Delta V(t)$ is the voltage change across the sample, α_x and α_ε are the thermal-expansion coefficient and the temperature coefficient of the dielectric constant ε, respectively, $\varrho(x)$ is the space-charge density, and $\Delta T(x,t)$ is the temperature increase at depth x and time t after the thermal pulse. For the derivation of Eq.(1), space-dependent quantities are assumed to vary only in the thickness direction and the sample is supposed to contain no quasi-permanent polarization which would lead to an additional pyroelectric signal.

CH2593-2/ 88/ 0000-0018$01.00 Copyright 1988 IEEE

Instead of using Eq.(1) for the determination of an unknown charge distribution under the assumption of a calculated temperature profile [3-5], samples with known space-charge profiles are employed, and the temperature distribution is determined. In order to avoid a numerical deconvolution of the integral in Eq.(1), very thin charge layers should be assumed:

$$\varrho(x)=\sigma_n \delta(r_n-x), \tag{2}$$

where σ_n and r_n are the charge per unit area and the depth, respectively, of the n-th charge layer, and δ denotes the Dirac distribution. Insertion of this expression (2) into Eq.(1) leads to

$$\Delta V(r_n,t)=[(\alpha_\lambda-\alpha_\varepsilon)/\varepsilon\varepsilon_0]\sigma_n \int_0^{r_n} \Delta T(x',t)\,dx'. \tag{3}$$

By differentiating and rearranging this relation, the desired formula for the temperature increase at depth r_n and time t is obtained. If several samples with charge sheets at different positions are used the derivative can be approximated by the quotient of differences:

$$\Delta T(r_n,t)=[\varepsilon\varepsilon_0/|(\alpha_\lambda-\alpha_\varepsilon)\sigma_n|][\Delta V(r_n,t)-\Delta V(r_{n-1},t)]/\Delta r. \tag{4}$$

Thus, the temporal development of the temperature profile at the discrete positions given by the charge-layer depths in a series of otherwise identical electret samples may be determined.

EXPERIMENTAL PROCEDURE

Fluoroethylenepropylene (Teflon FEP) samples of 25μm thickness were evaporated with 40nm thick circular aluminium electrodes of 24mm diameter and guard rings. They were charged through their free surfaces by means of monoenergetic electron beams with energies of 9.5, 16.0, 21.5, 25.0, 30.0, 34.0, 38.0, 42.0, and 45.0keV; in addition to these samples with charge layers in different depths, surface-charged electrets were generated by use of a negative corona discharge with a grid. The charge-centroid positions were determined by thermal-pulse experiments [6]; for confirmation, split-Faraday-cup [7] and LIPP [8] measurements are performed and compared with previous results [1]. For all samples, the charge density was chosen as approximately 115μC/m².

The thermal-pulse experiments were carried out with an apparatus similar to that described in the literature [6]: Light pulses of about 50μs duration from an electronic flash (mecablitz 216) are used to heat the sample electrode. The resulting voltage change is amplified by a CA3130 BiMOS operational amplifier and recorded on a Sony/Tektronix 214 storage oscilloscope. Twenty discrete values at equally spaced (Δt=0.5ms) times between 0 and 9.5ms were taken from this record for further evaluation; since it is easy to determine, the time of the voltage maximum (at which the thermal pulse has just entered the sample) is chosen as t=0.

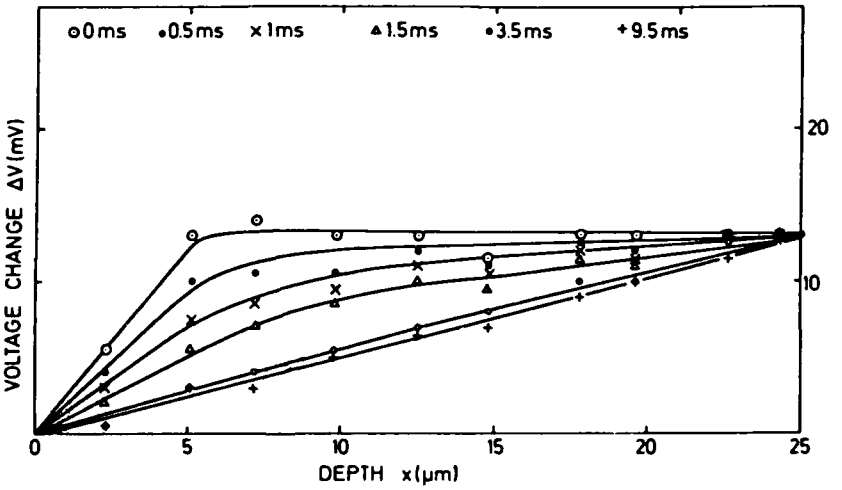

Fig.1. Thermal-pulse-induced voltage changes in electron-beam-charged Teflon FEP at selected times.

RESULTS AND DISCUSSION

Fig.1 shows the voltage change $\Delta V(x)$ for the charge-layer positions $x=r_n$ at selected times as indicated; in addition to the measured data, $\Delta V(x=0)=0$ was assumed. Experimental values taken at the same time are connected by approximative curves. Evaluation of the these data according to Eq.(4) leads to Fig.2 where again the values for the same time are joined by approximative curves. For obtaining the temperature increase in K, literature values [1,4] of 0.00008/K, -0.00025/K, 2.1, and 8.86pF/m were used for the parameters α_x, α_ε, ε, and ε_0, respectively, together with the above-mentioned charge density of 115μC/m².

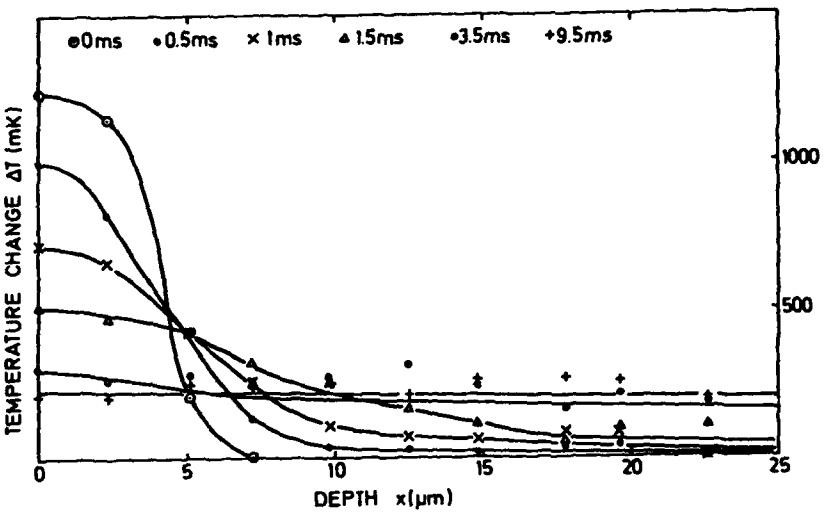

Fig.2. Temperature changes in Teflon FEP after thermal-pulse excitation as calculated from the data of Fig.1.

The temperature changes depicted in Fig.2 demonstrate the expected thermal equalization which takes about 10ms; by comparison with theoretical curves, the determination of heat-conduction and diffusion parameters would be possible. Since the largest changes are found in close proximity of the heated electrode, a much higher spatial resolution in this thickness range would be desirable. Electron-beam charging with relatively high energies through the opposite free sample surface, however, leads to charge layers of finite thickness and is difficult to control because of partial leakage to the electrode. Therefore, only very few charge-layer positions were used in this preliminary study. It is planned to vary the method by employing two-sided metallized samples so that electron-beam charging and thermal pulsing can be carried out from the same side.

If more complex charge or polarization profiles are employed, numerical deconvolution of the integral in Eq.(4) should still allow for a determination of temperature changes. The mathematical treatment [9] developed for the thermal-pulse technique can probably be adapted for this purpose, since the above integral is essentially symmetric with respect to $\varrho(x)$ and $\Delta T(x)$ (x=0 has to be replaced by x=s and vice versa, as the

convolution volumes of the two cases are complementary to each other); this can be shown by partial integration under the assumption of suitable boundary conditions. A further extension of the present idea is the analogous "reversal" of the laser-intensity modulation method [10] based on periodic heating instead of pulsing.

CONCLUSION

The proposed "reversal" of the thermal-pulse technique allows for the determination of temperature profiles in electret materials. The validity of the new method was demonstrated by preliminary experimental results for electron-beam-charged Teflon FEP samples.

ACKNOWLEDGEMENTS

The authors are indebted to Prof.Dr.G.M.Sessler for stimulating discussions, to Dr.T.Motz and Mr.Ding Hai for experimental advice, and to Mr.H.Eisenhauer for sample preparation. Thanks are also due to the Stiftung Volkswagenwerk for financial support to all authors.

REFERENCES AND FOOTNOTES

1. G.M.Sessler (Ed.), Electrets, Top.Appl.Phys. 33, 2nd Enlarged Ed. (Springer, Heidelberg & New York 1987).
2. R.Gerhard-Multhaupt, IEEE Trans.Electr.Insul. EI-22, 531-554, (1987).
3. R.E.Collins, Appl.Phys.Lett. 26, 675-677, (1975).
4. R.E.Collins, Rev.Sci.Instrum. 48, 83-91, (1977).
5. R.E.Collins, J.Appl.Phys. 51, 2973-2986, (1980).
6. H.von Seggern, J.E.West, R.A.Kubli, Rev.Sci. Instrum. 55, 964-967, (1984).
7. B.Gross, G.M.Sessler, J.E.West, J.Appl.Phys. 45, 2841-2851, (1974).
8. G.M.Sessler, J.E.West, R.Gerhard-Multhaupt, H.von Seggern, IEEE Trans.Nucl.Sci. NS-29, 1644-1649, (1982).
9. F.I.Mopsik, A.S.DeReggi, J.Appl.Phys. 53, 4333-4339, (1982).
10. S.B.Lang, D.K.Das-Gupta, J.Appl.Phys. 59, 2151-2160, (1986).

*Present address: Heinrich-Hertz-Institut Berlin GmbH, Einsteinufer 37, D-1000 Berlin 10, F.R.G.
**Permanent address: Pohl Institute, Tongji University, 1239 Siping Road, Shanghai 200092, China

THE THERMAL-STEP-TECHNIQUE APPLIED TO THE STUDY OF CHARGE DECAY IN POLYETHYLENE THERMOELECTRETS

A. TOUREILLE and J.P. REBOUL
Laboratoire d'Electricité
UNIVERSITE DES SCIENCES ET TECHNIQUES DU LANGUEDOC
34060 MONTPELLIER CEDEX FRANCE

ABSTRACT

A non-destructive method for locating the space charge and measuring the residual electric field, inside thick samples, is described. The technique consists in applying a thermal step on one or the other side of the sample.

The propagation of the thermal expansion and the relative shift of the charges induce currents in the external circuit which are computed. The method has been used to study the change of charge density and charge location, as a function of time, in several PE thermoelectrets formed under different charging conditions.

INTRODUCTION

Several methods are available for studying the space charge inside a poled insulating material. Someones, such as TSC methods, consist in discharging the sample by regular heating, but they are not suited to the watching over of the charge decay because, when studied only once, the sample gets discharged.

The determination of the density of space charge and its localization, without discharging the material, is not easy. The principle of most methods is to have the layers inside the material make small amplitude motion. If so, the motion of the resulting charge attached to each layer induces currents in the external circuit. A pulse of heat[1] or a pulse of pressure[2] applied to one side of the sample are the principal means to make the layers move.

On the same principle, we have set up a method already mentioned in another work[3] which consist in applying a step of temperature, that is a rapid and known increase of temperature, to one side of the sample. The purpose of the present paper is to describe the method and to give some distributions of space charge in PE thermoelectrets obtained with this method.

EXPERIMENTAL TECHNIQUE

The samples are in the form of square sheet 400 cm2 area and one or few millimeters thick. Two circular electrodes 50 mm in diameter are attached on each side of the sheet. These are made of either thin metal-deposited layers or of semiconductive polymer films The use of sheets much more larger than

CH2593-2/ 88/ 0000-0023$01.00 Copyright IEEE

electrodes is required by the flash-over prevention during the high voltage charging operation.

The sample with its electrodes is placed horizontally between two cylindrical brass pieces of the same diameter as the electrodes. The lower piece, in which the circulation of a warm liquid may be started, can play as a quick heater. The upper piece because of its weight acts as a press maintaining a constant pressure which improves the quality of contacts and facilitates the thermal exchanges. Because of its large thermal inertia it can also play as a cold source.

In order to prevent the material from being discharged by too high temperatures, the cell is previously cooled to - 10°C in a cooling cupboard and the step consists in a quick coming back to room temperature of the lower piece resulting from the circulation of the liquid.

The raise of temperature propagates through the sample up to the upper piece and is accompanied by a thermal expansion which affects the successive layers of the material. The charge exchange from one electrode to the other through the external circuit is measured with a 610 C Keithley electrometer and is recorded.

The method being non-destructive, the measurement may be repeated when desired provided that the cell has been previously cooled.Running two successive measurements with the step applied to one side, then to the other, is of interest. Indeed the concordance of the results confirms the validity of theory and calculations.

THEORY

When the temperature of an elementary layer increases from T to T+dT, its thickness dx increases to dx + d(dx) and its permittivity varies from ε to $\varepsilon+d\varepsilon$. In the own conditions of the experiment we can define a coefficient of thermal expansion in the x direction as $\alpha_x = \frac{d(dx)}{dx\ .dT}$, and a coefficient of thermal variation of ε as $\alpha_\varepsilon = \frac{d\varepsilon}{\varepsilon dT}$

In the assumption of a total charge density $\rho_{(x)} = \rho_{s(x)} - \frac{dP}{dx}$ with $\rho_{s(x)}$ the space charge density and P the permanent polarization, if any, the charge induced on the upper electrode per unit area is, according to Mopsik and al[4].

$$q_{(t)} = \frac{\alpha_x - \alpha_\varepsilon}{d} \left[\int_o^d \rho_{(x)} \left(\int_o^x T_{(x,t)} dx \right) dx - \int_o^d \frac{x}{d} \rho_{(x)} \left(\int_o^d T_{(x,t)} dx \right) \right] dx$$

with d the sample thickness

The current in the external circuit is : $I_{(t)} = - S \frac{dq_{(t)}}{dt}$, that is :

$$I_{(t)} = \frac{S(\alpha_x - \alpha_\varepsilon)}{d} \int_o^d x\rho_{(x)} \frac{d}{dt} (\bar{Td}_{(t)} - \bar{Tx}_{(x,t)})\, dx$$

with $\frac{1}{d} \int_o^d T_{(x,t)} dx = \bar{Td}_{(t)}$ the mean temperature in the sample

and $\frac{1}{x}\int_0^x T_{(x,t)}dx \approx \bar{T}x_{(t,x)}$ the mean temperature in the x thickness.

A condensed form may be written as $I_{(t)} \approx \frac{S(\alpha_x-\alpha_\varepsilon)}{d}\int_0^d F_{(x,t)}\,\rho_{(x)}dx$ (1)
with $F_{(x,t)} = 0$ for $x = 0$ and $x = d$.

The purpose is to find the distribution fonction of charge density $\rho(x)$ knowing $I(t)$ which has been recorded.

In the sample the temperature T(x, t) obeys the equation of heat $\frac{\partial^2 T}{\partial x^2}=w\frac{\partial T}{\partial t}$, where $W=\mu C \lambda$ with μ the volumic mass of the material, C, its massic heat and λ its coefficient of thermal conductivity. The boundary conditions taken into account to resolve the equation of heat are as follow :

1/ A perfect thermal pulse $\Delta T_0 = T_1 - T_0$ occurs at $x = -x_0$ for $t = 0$.
An equivalent thickness of material x_0 between the sample and the plane where the perfect temperature step occurs is needed.

2/ at $x = d+x'_0$, the temperature is T_0 and remains unchanged (cold source). Another equivalent thickness of material x'_0 between the sample and the plane of the cold source is also needed. In another treatment[3] we have replaced this last boundary condition by $T = T_0$ at $x = \infty$ which is an interesting approximation valid for small values of time t.

With the above boundary conditions, the solution of the equation of heat is : $T-T_0 = (T_1-T_0)(1-X/L - \frac{2}{\pi}\sum_1^\infty \frac{1}{n}\exp(-\pi^2n^2t/WL^2)\sin(n\pi X/L))$ (2)
with $X = x+x_0$ and $L = x_0+d+x'_0$.

Several parameters such as W, $\alpha_x-\alpha_\varepsilon$, x_0, x'_0 are unknown or known with unsufficient accuracy. So we have set up a calibrating measurement :

A constant dc voltage V = 1200 volts from a charged capacitor is appliedto the virgin sample (without space charge) with its electrodes acting as a capacitor in opposition. Then the step is applied as in the usual measurement and the current Io(t) restituted by the sample to the voltage source is recorded.

It may be shown that : $I_0(t) = -\frac{VC^2}{\varepsilon S^2}(\alpha_x-\alpha_\varepsilon)\int_0^d \frac{\partial T}{\partial t}dx$ with C the capacitance of the sample. Introducing $\bar{T}_d$, the mean temperature of the sample, leads to : $I_0(t) = -\frac{VC^2d}{\varepsilon S}(\alpha_x-\alpha_\varepsilon)\frac{\partial \bar{T}_d}{\partial t}$

The curve Io = f(t) may be computed and drawn for successive values of the parameters. The comparison of the computed curve to the experimental one leads to a good valuation of the parameters. In our case, we took :

$W = 4.10\ 10^6$, $\alpha_x-\alpha_\varepsilon = 5.0010^{-4}$, $x_0 = 1.6010^{-3}$, $x'_0 = 0.90\ 10^{-3}$

The temperature $T_{(x,t)}$ of the sample may be computed from eq.(2). The function $F_{(x,t)}$ of eq.(1) may also be computed ; $I_{(t)}$ is know from

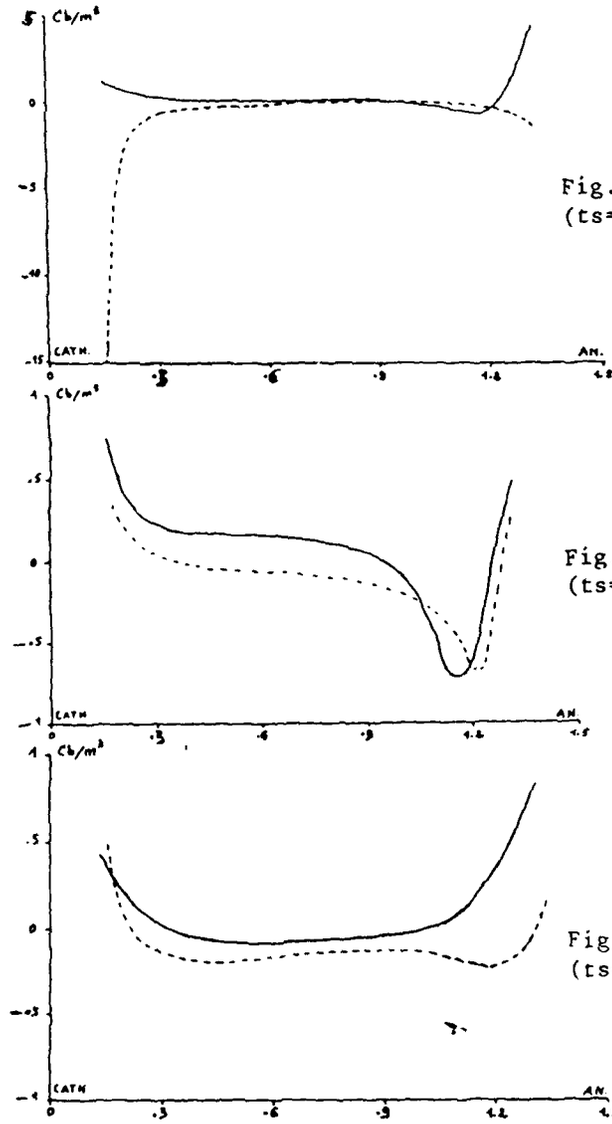

Fig.1
(ts=2hours)

Fig.2
(ts=1day)

Fig.3
(ts=45days)

Residual charge density from cathode to anode:
— semicond.electrodes; --- deposited Cu electrodes.

experiments. The determination of space charge density $\rho_{(x)}$ needs a deconvolution procedure. We used an analytic method consisting in replacing $F(x,t)$ by successive polynomials of x, for a serie of fixed and choosen values of t. The approximation was verified to remain valid for small enough values of t and, consequently, for values of x no much larger than d/2. Two-sided measurements were then needed for a complete determination of $\rho_{(x)}$

RESULTS AND DISCUSSION

We have studied HDPE samples, 1.5 mm thick, prepared by Treficable-Pirelli.

The samples are poled at 70°C, under 30 KV, during 24 hours. Then they are cooled to room temperature and the high voltage source is replaced by a short circuit. The measurement of charge density may be carried on after any desired values of storage time t_s. The curves in figs 1, 2 and 3 show the charge density as a function of x for respectively t_s = 2 hours, 1 day, 45 days and for the two kinds of electrodes.

For the earlier storage times the charge density strongly depends on the nature of electrode as shown in fig. 1. Homocharge near cathode seems specific of metal electrodes. Homocharge near anode seems specific of semiconducting electrodes.

For larger storage times the charge density tends to be identical with the two kinds of electrodes as shown in figs. 2 and 3. The nature and the distribution of charges would then be more specific of the sample material itself.

AKNOWLEDGEMENT

We are grateful to Treficable Pirelli for supporting this study and particularly to C. SIMON for helpfull discussions.

REFERENCES

1. COLLINS (R.E.) J. Appl. Phys., 47, 1976 p. 4804.

2. LAURENCEAU (P.), DREYFUS (G.), LEWINER (J.), Comptes rendus Acad. Sc. B 283, 1976 p. 135

3. TOUREILLE (A.), 2nd Int Conf. on polymer insulated power cables. Jicable 87 21-25 sept. 1987, Versailles p.98-103.

4. MOPSIK (F.I.), DE REGGI (A.S.), J. Appl. Phys., 53, 1982 p. 4333.

ANALYSIS OF THE SPATIAL DISTRIBUTION OF POLARIZATION IN PVDF-FOILS FROM THE FREQUENCY SPECTRA OF THE PYROELECTRIC CURRENT

S. Bauer, B. Ploss

Institut für angewandte Physik,
Universität Karlsruhe, Karlsruhe, West Germany

Intensity modulated radiation is absorbed at the surface of the PVDF-foil and generates a temperature wave. Its penetration depth decreases with increasing frequency of modulation. Pyroelectric currents are generated within the penetration depth of the temperature wave and contain, therefore, information on the spatial distribution of the polarization. The modulation frequency is varied over seven orders of magnitude. From the pyroelectric current the polarization distribution is deduced by a method of analysis which has been successfully used for the characterization of imperfections in semiconductors.

INTRODUCTION

A number of methods for analyzing charge and polarization distributions in pyroelectric polymers were developed during the last years. The methods which use propagating pressure pulses or pressure steps give direct images of either the piezoelectric distribution or of its gradient [1]. The methods using heat pulses or heat waves give the Fourier coefficients of the distribution, but the main difficulty is to deduce these Fourier coefficients from the experimental data [2-7]. In the present paper we develop a new deconvolution method. This method is tested experimentally with sandwiched PVDF-foils which are prepared with a priori known polarization distributions.

THEORETICAL BASIS

The sample is regarded as a infinite sheet of thickness d. The temperature increase in the sample after the absorption of an infinitely short heat pulse $q\delta(t)$ (q in J/m^2) and neglecting heat loss from the sample to the

CH2593-2/ 88/ 0000-0028$01.00 Copyright 1988 IEEE

surrounding is given by [2]:

$$\Delta T(x,t) = \Delta T_\infty + 2\Delta T_\infty \sum_{n=1}^{\infty} \cos\frac{n\pi x}{d}\, e^{-n^2 t/\tau} \qquad (1)$$

$\Delta T_\infty = \eta q/c\rho d$ with η the absorptivity of the metal electrode, $\tau = d^2/\pi^2 D$ with D the thermal diffusivity

If heat loss is taken into account, an approximate solution is:

$$\Delta T(x,t) = \Delta T_\infty e^{-t/\tau_{Th}} + 2\Delta T_\infty \sum_{n=1}^{\infty} \cos\frac{n\pi x}{d}\, e^{-n^2 t/\tau} \qquad (2)$$

$\tau_{Th} = c\rho d/2G$ with G the heat loss factor (in W/m^2K), $\tau_{Th} >> \tau$

For harmonic excitations $j(t) = j_0 + j_\omega e^{i\omega t}$ (in W/m^2) the solution of the heat conductivity equation can be found by convolution:

$$\Delta T_\omega(x,t) = \int_{-\infty}^{\infty} j(t')\Delta T(x,t-t')dt' \qquad (3)$$

$$\approx \frac{\eta j_0 \tau_{Th}}{c\rho d} + \frac{\eta j_\omega}{c\rho d}\left[\frac{\tau_{Th}}{1+i\omega\tau_{Th}} + 2\sum_{n=1}^{\infty} \cos\left(\frac{n\pi x}{d}\right) \frac{\tau/n^2}{1+i\omega\tau/n^2}\right] e^{i\omega t}$$

Assuming charge compensated polarization $\rho = dP/dx$ the pyroelectric current can be written as [6]:

$$I(\omega) = \frac{A}{d}\int_0^d p(x)\,\frac{\partial \Delta T_\omega(x,t)}{\partial t}\,dx\,, \qquad p(x): \text{ pyroelectric coefficient}$$

$$= \frac{\eta j_\omega A}{c\rho d}\left[\, p_0 \frac{i\omega\tau_{Th}}{1+i\omega\tau_{Th}} + \sum_{n=1}^{\infty} p_n \frac{i\omega\tau/n^2}{1+i\omega\tau/n^2}\,\right] e^{i\omega t} \qquad (4)$$

$$p_0 = \frac{1}{d}\int_0^d p(x)\,dx\,, \quad p_n = \frac{2}{d}\int_0^d p(x)\cos\frac{n\pi x}{d}\,dx$$

DECONVOLUTION METHOD

A measured spectrum of the pyroelectric current $I(\omega)$ is a function of the structure

$$f(\omega) = \sum_n \frac{i\ \omega/\omega_n}{1 + i\ \omega/\omega_n} C_n \tag{5}$$

or

$$\text{Re } f(\omega) = \sum_n \frac{(\omega/\omega_n)^2}{1 + (\omega/\omega_n)^2} C_n \tag{6}$$

$$\text{Im } f(\omega) = \sum_n \frac{\omega/\omega_n}{1 + (\omega/\omega_n)^2} C_n \tag{7}$$

The poles $i\omega_n$ and the respective residuals $\text{Res}_n = i\omega_n C_n$ contain the information of the order and of the amplitude of the Fourier coefficients of the polarization distribution. So these must be determined. With $x := \ln \omega$ and $x_n := \ln \omega_n$ results:

$$\text{Re } f(x) = \sum_n \frac{e^{2(x-x_n)}}{1 + e^{2(x-x_n)}} C_n \tag{8}$$

$$\text{Im } f(x) = \sum_n \frac{C_n}{e^{(x-x_n)} + e^{-(x-x_n)}} = \sum_n \frac{C_n}{2} \operatorname{sech}(x-x_n) \tag{9}$$

Im $f(x)$ is a sum of curves of the form $C_n/2\ \operatorname{sech}(x-x_n)$. These are relative broad structures, their half period corresponds to a relation $\Delta\omega/\omega \approx 14$. So only such structures can be directly dissolved, whose frequencies ω_n are separated relative far. The separability of different components can be improved with methods to increase the resolution. A method which has been successfully used for the separation of different relaxation processes in photoconductors is the convolution [8].

By means of the convolution theorem for the Fourier transformation

$$F\left[\, f(x) \,\right] = \int_{-\infty}^{\infty} f(x)\, e^{ikx}\, dx \tag{10}$$

the function

$$g(x) = \sum_{n} \frac{C_n}{2}\, e^{-\left[\frac{x-x_n}{\lambda}\right]^2} \tag{11}$$

can be computed of Re f(x) or of Im f(x). Using the functions

$$f_1(x) := e^{-\left[\frac{x}{\lambda}\right]^2}, \quad f_2(x) := \operatorname{sech}(x), \quad f_3(x) := \operatorname{sech}^2(x)$$

one gets

$$F\left[g(x)\right] = F\left[\frac{d}{dx}\, \mathrm{Re}\, f(x)\right] \frac{F\left[f_1(x)\right]}{F\left[f_3(x)\right]} \tag{12}$$

from Re f(x), or

$$F\left[g(x)\right] = F\left[\mathrm{Im}\, f(x)\,\right] \frac{F\left[f_1(x)\right]}{F\left[f_2(x)\right]} \tag{13}$$

from Im f(x).

In the limit $\lambda \to 0$ g(x) becomes a sum of delta distributions. Then the pyroelectric current is exactly deconvoluted and the distribution of polarization can be determined exactly. To do this deconvolution in fact, I(ω) must be known exactly, however. If I(ω) is a measured function and even if I(ω) is a numerically computed function with limited accuracy, then g(x) can only be computed with finite λ. This fact limits the separability of Fourier coefficients, which are too adjacent on a logarithmic scale.

The accuracy of the measured pyroelectric current I(ω) is the limiting factor for the possible value of λ for deconvolution. To test, if a chosen λ doesn't exceed the accuracy of the data, g(x) can be computed independently of Re I(ω) and of Im I(ω). If both provide the same

g(x), then the accuracy of the experimental data is sufficient for this λ.

In fact the deconvolution only can be done approximately with a finite λ. So a spectrum $I(\omega)$ is divided into two regions. In one part of the spectrum, the Fourier coefficients can be determined uniquely after deconvolution. These Fourier coefficients contain information on the polarization distribution of the whole sample, and they are used in this paper. In another part of the spectrum, the Fourier coefficients cannot be determined unique, e.g. it's impossible to distinguish the contribution of neighboured coefficients. This part of the spectrum only contains information on the polarization near the edge of the sample. The interpretation of these data will be the subject of a following paper.

EXPERIMENTAL

For the test of our deconvolution procedure we produced sandwiched PVDF samples with a priori known polarization distributions. Four 9 µm PVDF foils were glued together. On each side of the sample electrode structures were prepared by photolithographic technique. We choose an electrode structure with four contacts. This allowed the measurement of the pyroelectric current and additionally the measurement of the transient temperature on each side of the sample. The temperature was measured via the resistance of the metallization by a van der Pauw method [9].

The sample is heated with harmonically intensity modulated radiation by an IR laser diode. The modulation frequency is varied from 10^{-2} s^{-1} to 10^{5} s^{-1}. The pyroelectric current is amplified with a broadband current amplifier and measured with lock-in amplifiers. For the low frequency measurements a new type of digital working lock-in amplifier was developed [10]. The total arrangement was computer controlled.

MEASURING RESULTS

Figs. 1 and 2 show the transient temperature of the sample on each side. The measured points were fitted with literature data for the specific heat $c\rho$ and the

thermal diffusivity D. The absorbed power and the heat loss factor G were the only free parameters. The temperature data prove the thermal homogenity of the sample and are used to compute the absolute value of the pyroelectric coefficient.

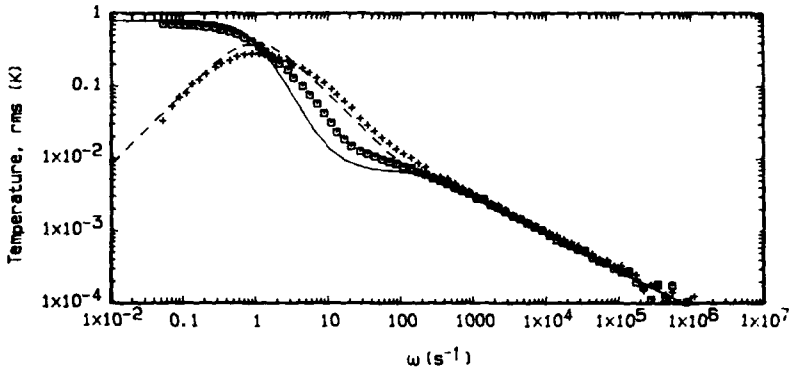

Fig. 1: The transient temperature measured on the front side of the sample depending of the frequency ω of the modulation. Real and imaginary part are marked by following symbols: Re>0:□, Re<0:△, Im>0:x, Im<0:+. The curves show the theoretical results: Re ——, Im ---, with absorbed power 250 µW and heat loss factor G=50 W/m^2K.

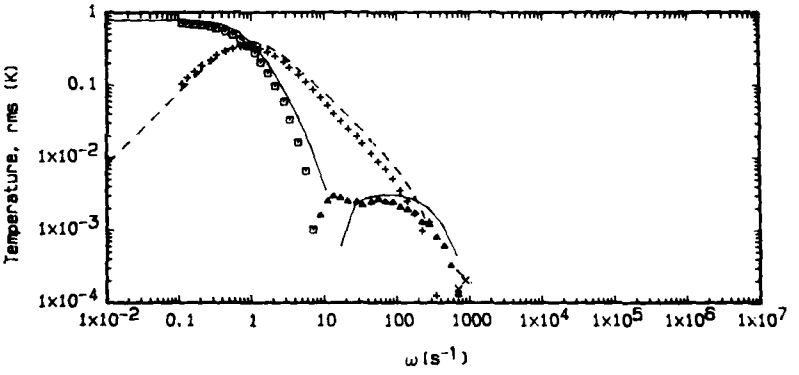

Fig. 2: The transient temperature measured on the back side of the sample. The symbols are the same as in Fig. 1. The theoretical curves are computed with the same parameters.

The measured pyroelectric current is shown in Fig.3. The imaginary part is a sum of sech functions (9). Each of them represents one Fourier coefficient. To show the broad structure of the sech function, one curve of this type is plotted at $\omega=1/\tau_{Th}$.

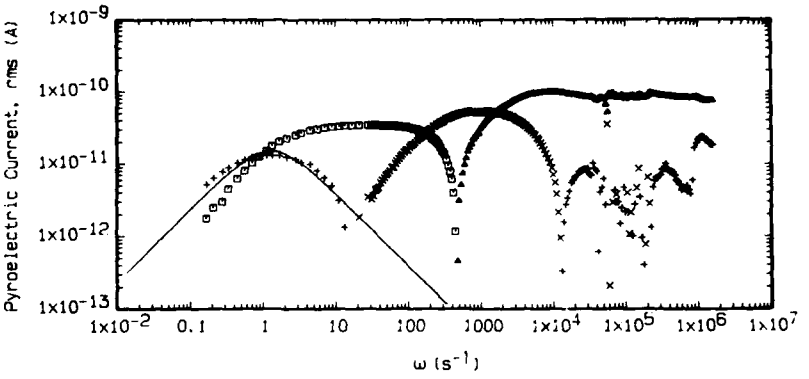

Fig. 3: Real and imaginary part of the pyroelectric current. A sech function is plotted at $\omega=1/\tau_{Th}$ to demonstrate this broad structure.

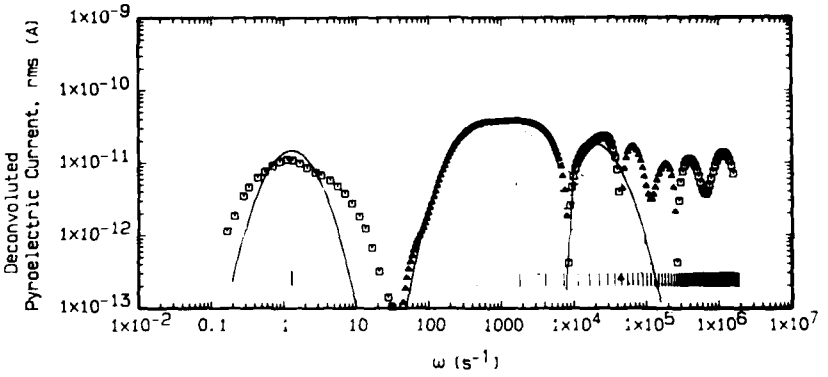

Fig. 4: The pyroelectric current of Fig. 3, deconvoluted with $\lambda=0.4\ln 10$. The frequencies $1/\tau_{Th}$ and n^2/τ are marked by vertical lines at the bottom. The experimental data are fitted with eight coefficients.

Real and imaginary part of the pyroelectric current are deconvoluted with $\lambda=0.4\ln 10$. The result of the deconvo-

lution is shown by the symbols in Fig. 4. This spectrum is a sum of Gaussian functions (11). The frequencies $\omega=1/\tau_{Th}$ and $\omega=n^2/\tau$ are marked at the bottom of the figure by vertical lines. For the fit we choose eight Fourier coefficients. The higher coefficients are too adjacent on the logarithmic scale, to be separated individually.

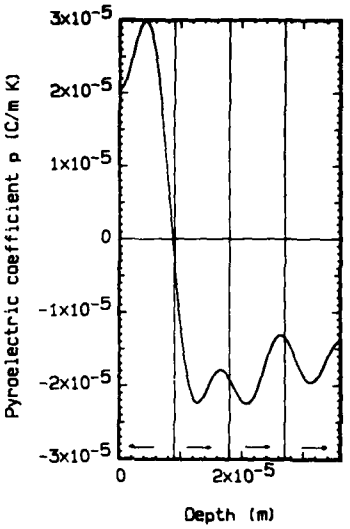

The distribution of the pyroelectric coefficient or equivalently the polarization distribution resulting from these eight coefficients is shown in Fig.5. It agrees well with the distribution expected from the prepared sample.

Fig. 5: The pyroelectric coefficient as a function of the depth of the sample, computed from the eight Fourier coefficients, which are used to fit the data in Fig. 4. The sample was prepared of four 9µm thick films. The polarization of these films is represented by arrows.

CONCLUSION

The experimental results show, that it is possible to determine about eight Fourier coefficients of the polarization distribution from a measured spectrum. Measuring the pyroelectric current with the modulation frequency varied over several orders of magnitude together with the use of the described deconvolution method allowed to characterize and to verify these coefficients individually in the spectrum.

ACKNOWLEDGEMENTS

Thanks are due to Prof. Dr. W. Ruppel and to Dr. habil. P. Würfel for helpful discussions. One of the authors (S.B.) thanks for financial support as a graduate stipendiat of the Land Baden-Württemberg.

REFERENCES

[1] R. Gerhard-Multhaupt, G. M. Sessler, J. E. West, K. Holdik, M. Haardt, and W. Eisenmenger, "Investigation of Piezoelectricity Distributions in Poly-(vinylidene fluoride) by Means of Quartz- or Laser-Generated Pressure Pulses", J. Appl. Phys. Vol 55, pp. 2769-2775, 1984

[2] A. S. DeReggi, C. M. Guttman, F. I. Mopsik, G. T. Davis, and M. G. Broadhurst, "Determination of Charge or Polarization Distribution across Polymer Electrets by the Thermal Pulse Method and Fourier Analysis", Phys. Rev. Lett. Vol 40, pp. 413-416, 1978

[3] F. I. Mopsik, and A. S. DeReggi, "Numerical Evaluation of the Dielectric Polarization Distribution from Thermal Pulse Data", J. Appl. Phys. Vol 53, pp. 4333-4339, 1982

[4] H. von Seggern, "Thermal-Pulse Technique for Determining Charge Distributions: Effect of Measurement Accuracy", Appl. Phys. Lett. Vol 33, pp. 134-137, 1978

[5] S. B. Lang, D. K. Das-Gupta, "A New Technique for Determination of the Spatial Distribution of Polarization in Polymer Electrets", Ferroelectrics Vol 60, pp. 23-36, 1984

[6] S. B. Lang, D. K. Das-Gupta, "Laser-Intensity-Modulation-Method: A Technique for determination of Spatial Distributions of Polarization and Space Charge in Polymer Electrets", J. Appl. Phys. Vol 59, pp. 2151-2160, 1986

[7] S. B. Lang, and Y. Qing-Rui, "Spatial Distributions of Polarization and Space Charge in Tin-Substituted Lead Zirconate Titanate Ceramics Using Laser Intensity Modulation Method (LIMM)", Ferroelectrics Vol 74, pp. 357-368, 1987

[8] B. Ploss, "Modulierte Photoleitung und modulierter Photo-Hall-Effekt an bipolarem CdTe zur Störtermanalyse", Dissertation Thesis, Karlsruhe 1987

[9] L. J. van der Pauw, "A Method of Measuring Specific Resistivity and Hall Effect of Discs of Arbitrary Shape", Philips Res. Repts. Vol 13, pp. 1-9, 1958

[10] S. Bauer, T. Lessle, and B. Ploss, "Concept for a Novel Type of Digital Working Lock-In Amplifier", to be published

CHARGE STORAGE IN DIELECTRICS

G. M. Sessler

Institute for Electroacoustics, Technical University of Darmstadt, Merckstrasse 25, D-6100 Darmstadt, F. R. G.

ABSTRACT

In this paper, some of the work on charge-storage processes in dielectrics performed over the past few years is reviewed. Results obtained on polymers with corona, electron-beam and pressure-pulse methods and pertaining to trap filling, spatial distribution of the charge, radiation-induced conductivity, and dynamics of the charge decay are discussed. Also, the generation of a variety of polarization distributions in PVDF with electron-beam and other methods is reviewed. Finally, some results on charge storage and transport in silicon dioxide are described.

1. INTRODUCTION

The status of the field of charge storage in dielectrics at the time of the 5th International Symposium on Electrets in 1985 (ISE-5) is documented in the Proceedings of this Symposium [1]. Since that time, advances in this area have been made in a number of aspects. This progress is in part due to the application of some recently-developed experimental techniques, such as pressure-pulse methods for measuring charge and polarization distributions, and electron-beam methods to charge, polarize, and study various insulators. With the availability of good experimental data, an appropriate analysis of charge-storage and charge-transport processes is now also possible.

In the present review, a few aspects of the work performed since 1985 are described. The discussion is limited to studies carried out in the authors or some associated laboratories and is restricted to material not covered in other review papers presented during ISE-6. More specifically, the scope of this paper includes work on charging, charge storage and charge transport in polymers, on partial polarization in PVDF, and on charge effects in

CH2593-2/ 88/ 0000-0037$01.00 Copyright 1988 IEEE

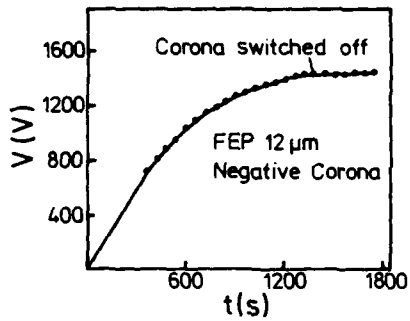

Fig. 1: Surface potential V as a function of time t for a 12 µm thick Teflon FEP sample negatively corona charged with a current of 3.0 *nA*. Line: experimental curve; dots: theoretical results; temperature 25 °C [4].

silicon dioxide. Progress in the study of thermally-stimulated processes, in the understanding of piezo-electric polymers and in applications is discussed in companion reviews.

2. CHARGE TRANSPORT IN POLYMERS

Charge transport in the low-mobility material Teflon FEP has previously been studied on samples first corona charged and then heated to a temperature where the potential decay is measurable [2]. The use of a constant-current corona made it recently possible to investigate hole and electron transport in highly-charged samples at room temperature [3,4]. In these experiments, the surface voltage is measured during and after charging with a constant corona current.

A typical result is depicted in Fig. 1. It shows initially a linear potential increase, followed by a sublinear region. After the corona is switched off, no discharge is observed. These results have been explained with a model assuming surface trapping during the linear voltage increase and bulk trapping thereafter, in both cases in deep traps. The free mobility in the bulk is found to be high ($> 10^{-8}$ cm^2/Vs) and guarantees the absence of space-charge accumulation.

The free electron mobility for FEP determined previously for temperatures between 145 and 250 °C is in the range of 10^{-11} to 10^{-12} cm^2/Vs [2,5] and thus comparable to the value found now at room temperature. These results show that, as expected, the free mobility is not a very strong function of temperature. The trap-modulated mobility was shown to be strongly temperature dependent and equal to

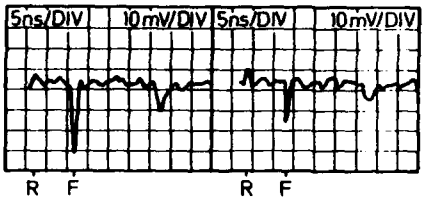

Fig. 2: LIPP responses of 22 µm Mylar PETP after corona charging (left) and after annealing 15 min at 85 °C (right). R corresponds to metalized rear side, F to charged front side [14].

about 10^{-11} cm^2/Vs at 180 °C [6].

Analyses of potential buildup and decay do not yield definite values of the carrier mobilities in the absence of more detailed knowledge about the dynamics of the carrier transport. Information of this kind can now be readily obtained with the new pressure-pulse techniques which allow one to determine the charge distributions in thin dielectrics [7-10]. Previous measurements with one such method indicated that retrapping in Teflon FEP is fast in the temperature range up to at least 120 °C [11].

New results, obtained with the laser-induced pressure pulse (LIPP) method [8,12], suggest slow retrapping or ohmic compensation for Mylar PETP up to 110 °C [13]. LIPP responses for negatively corona charged PETP before and after annealing are shown in Fig. 2 [14]. After heating to 85 °C, the negative charge peak is reduced in size but does not change its shape; this is primarily due to the alignment of dipoles in the field of the surface charges, an effect known to take place in Mylar at about 80 °C [15].

3. ELECTRON-BEAM CHARGING OF POLYMERS

3.1 Space charge and radiation-induced conductivity in FEP, PETP, and PI

According to recent LIPP studies, one-side metalized Mylar PETP and Kapton PI, charged with an electron beam through the nonmetalized surface, show charge distributions con-

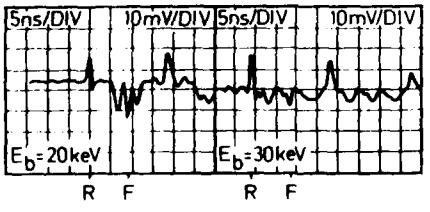

Fig. 3: LIPP responses of 22 µm Mylar PETP charged with electron beams of 20 keV (left) and 30 keV (right). F corresponds to irradiated front side [13].

sisting of a surface-charge layer and a volume-charge layer [13]. Typical LIPP responses for Mylar PETP charged with electrons of different energy are shown in Fig. 3.

The depth of the volume layers in Mylar PETP [13] and in Teflon FEP [12] is depicted in Fig. 4. The ratio of depths for the two materials corresponds nearly to the inverse density ratio of 1.5, as expected. However, agreement with the open-circuit charge centroids, determined previously from split-Faraday cup measurements [16-18], is only satisfactory for the PETP data: The depth of the charge centroid in PETP ist about 30 % smaller than the depth of the volume-charge layer, which can be explained by the presence of the above-described surface-charge. The charge centroid in FEP, however, is deeper in the material than the volume-charge layer; this deviation is presently not understood.

Storage of electron-beam deposited charge in polymers is affected by the long-term values of the delayed radiation-

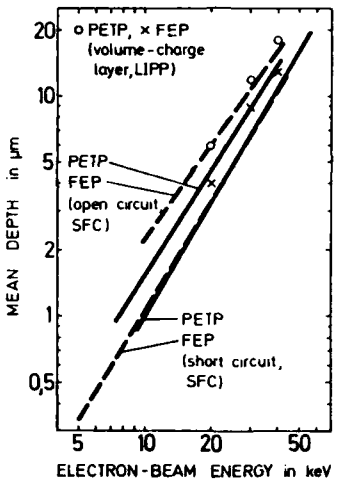

Fig. 4: Depth of volume-charge layers in PETP and in FEP, determined from LIPP experiments, and open-circuit and short-circuit charge centroids for these materials, determined with split-Faraday cup (SFC).

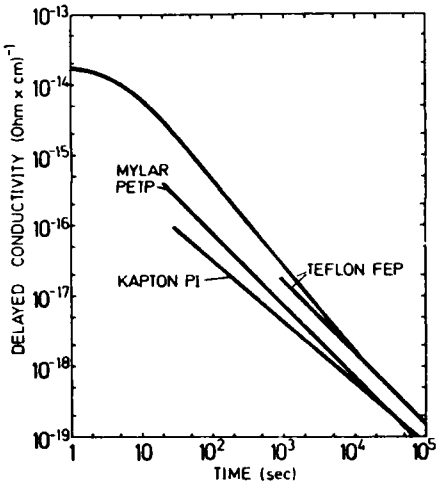

Fig. 5: Delayed radiation-induced conductivity of Mylar PETP and Kapton PI due to electron-beam pre-irradiation with dose of 0.2 Mrad [22]. Data for Teflon FEP from [19,20].

induced conductivity (DRIC) generated by the electron beam. Measurements of the DRIC for time periods much longer than 1 s have been performed on Teflon samples pre-irradiated with electron beam doses of 0.2 and 5 Mrad [19,20] and for Mylar and Kapton pre-irradiated with doses of about 10 Mrad [21].

New results for the DRIC of samples irradiated with low doses were obtained with two methods. One of these, described in detail before [19], is based on the measurement of the electrode charges of two-side metalized films charged with a partially penetrating electron beam. The other method utilizes one-side metalized samples which are electron beam charged through their metal layer. Immediately thereafter, the potential of the nonmetalized surface is monitored and the DRIC determined from the decay of this potential. Both methods gave comparable results for PETP, which has a small dark conductivity. For PI, with its larger dark conductivity, the results differ; therefore, only the PI-data obtained with the first method are used in the following, since this data reflects the DRIC which is generated in addition to the dark conductivity.

The results for Mylar PETP and Kapton PI [22] are compared in Fig. 5 with the older Teflon data. All results depicted in this Figure refer to samples irradiated only with the relatively small doses due to the electron beam charging process. As the Figure shows, the DRIC in Mylar and Kapton is considerably smaller than in Teflon; bimolecular recombination resulting in a 1/t-law [19] is approximately obeyed in all three materials. This is not the case for pre-irradiation in the Mrad range [19,20].

3.2 Polarization-Profiles in PVDF

The electron beam method has recently been used to polarize polyvinylidenefluoride (PVDF) selectively over part of its thickness [23]. Poling was accomplished by irradiating one-side metalized samples on their nonmetalized side with a partially-penetrating electron beam. An electric field is generated between the deposited charge and the rear electrode; it polarizes the nonirradiated part of the sample. A partial polarization can also be obtained on films charged through a floating metal electrode [24]. PVDF samples which are polarized over part of their thick-

ness show also piezoelectricity in that part of their volume and are called monomorphs.

Very recently, PVDF films were poled such that the polarization reverses sign in the midplane of the samples [25]. This kind of poling was performed on two-side metalized samples first irradiated on one and then on the other surface with an electron beam whose penetration depth equals half the sample thickness. During both irradiation periods, the irradiated surface remains in open circuit. The profile of the piezoelectric e_{33}-constant is equal to the polarization profile and the samples are called bimorphs.

The profiles of e_{33} in the thickness direction of PVDF films can also be determined with the LIPP method. After a time long compared to the ohmic relaxation time, the real charges either screen all or part of the polarization charges or dissipate by conduction [26]. The LIPP signal is now proportional to the unscreened part of the polarization gradient dP/dx and to de_{33}/dx. Since these two terms are proportional to each other, the LIPP response is altogether proportional to de_{33}/dx.

Examples of LIPP responses of a monomorph and a bimorph are shown in Fig. 6. While the polarization profile of the monomorph is almost rectangular, that of the bimorph is more rounded. PVDF films of this kind can be used as bending devices. These single-film benders have, compared to similar devices consisting of one poled and one unpoled film, or of two oppositely poled films cemented together, the advantages of smaller mechanical damping and simpler design.

Other techniques for poling PVDF do not show such flexibility in achieving different polarization distributions. This is obvious from Fig. 7 which depicts typical piezo-

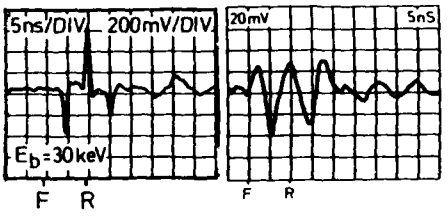

Fig. 6: LIPP responses showing de_{33}/dx of 22 µm PVDF after charging with 30 keV electron beams. Left: Monomorph charged through front surface F; Right: Bimorph charged first through front surface F, then through rear surface R.

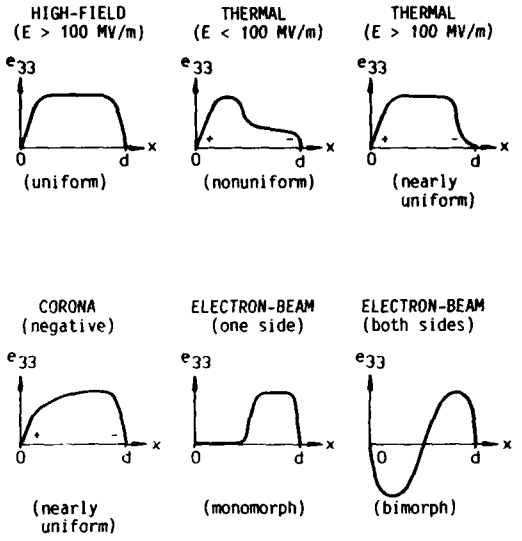

Fig. 7: Schematic representation of piezoelectric e_{33}-profiles in PVDF poled with different methods (E = poling field). These profiles correspond also to polarization.

electricity profiles obtained by LIPP experiments for PVDF samples poled by different methods. While the field-poled films have relatively uniform profiles [26], the thermally-poled samples exhibit nonuniformities which tend to disappear with increasing poling field [25]. The deficiencies of thermal poling have been attributed to the presence of space charge in the samples. Corona-poled PVDF shows also relatively uniform profiles with some deficiency in the vicinity of the metalized sample surface [25]. These results indicate that polarization and piezoelectricity distributions in PVDF depend critically on the poling method and often on the parameter values used in the application of these methods.

4. SILICON DIOXIDE ELECTRETS

While older data seemed to indicate that silicon dioxide (SiO_2) is not suitable for long-term charge retention [27], recent data shows this material to possess excellent storage capabilities for negative charge [28-30]. This is evident from Fig. 8, where isothermal potential-decay data for SiO_2 is compared with similar data for Teflon FEP [28]. The 1 μm SiO_2 layers were thermally grown and nega-

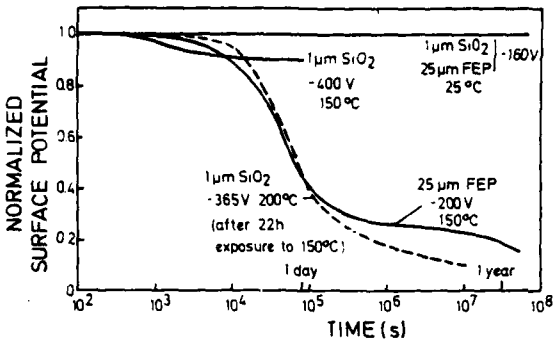

Fig. 8: Time dependence of surface potential of 1 μm corona-charged SiO_2 and 25 μm Teflon FEP electret at various temperatures [28]. The original potentials are indicated.

tively corona charged. According to the Figure, the surface potential for both materials is stable at room temperature. At higher temperatures, the SiO_2 electrets are more stable than the FEP electrets. Other experiments show that the TSD peak of these SiO_2 samples is located at about 300 °C but that considerably poorer charge retention is obtained for negatively corona-charged dry oxides and for CVD oxides as well as for all positively-corona-charged oxides [30].

Electron-beam irradiation can also be used to obtain positively and negatively charged dielectrics [31]. With SiO_2, positive charging by electron beams of about 1.5 keV, which have large secondary emission yields, is easily achieved; such samples show good charge retention properties with a TSD peak around 200 °C [30]. As opposed to this, negative electron beam charging is more difficult. This is probably due to a small capture cross section of the volume traps in SiO_2. Sizeable charging by direct irradiation with electron beams is therefore only possible for relatively thick samples, e. g. of 2.5 μm thickness. Even then, the charging is relatively inefficient as most of the beam electrons are not captured. Thinner layers can also be charged if the electron beam is slowed down by a polymer film before it hits the SiO_2 surface [29].

In Figure 9, the TSD curve for a negatively electron-beam charged 2.5 μm SiO_2 layer is compared with that for a negatively corona charged 1 μm layer. An electron beam of 8 keV, having a penetration depth of 1 μm, was used to

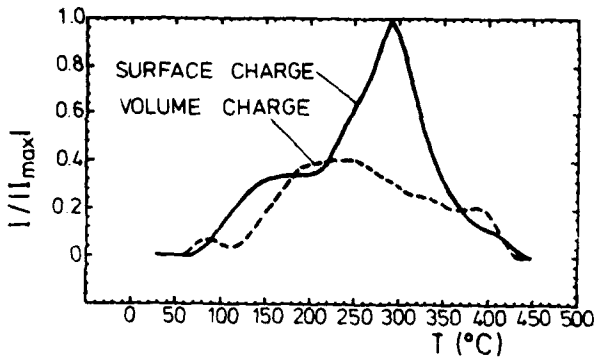

Fig. 9: Comparison of TSD curves for surface (corona) charged 1 μm SiO_2 and volume (electron beam) charged 2.5 μm SiO_2. Both samples are CVD oxides [29].

charge the 2.5 μm sample; the resulting charge is therefore a volume charge whereas the corona sample is surface charged. According to the Figure, the surface-charged sample shows a pronounced high-temperature peak; this is not the case for the volume-charged layer. These results indicate that the surface charges are immobilized in deep traps with a relatively narrow energy distribution while the volume charges are captured in more widely distributed, shallower traps [29].

Acknowledgments. The author is indebted to Prof. B. Gross for stimulating discussions on this paper, to Drs. A. Berraissoul and J. E. West for permission to show some data before publication, and to the Stiftung Volkswagenwerk for providing the laser used in the LIPP studies.

REFERENCES

[1] Proc. 5th Internat. Symposium on Electrets, Heidelberg 1985. Ed. by G. M. Sessler and R. Gerhard-Multhaupt (IEEE Service Center, Piscataway, N. J. USA).
[2] H.von Seggern, J. Appl. Phys. 50, 7039 (1979).
[3] B.Gross, J.A.Giacometti, G.F.Leal Ferreira, Appl. Phys. A37, 89 (1985).
[4] O.N.Oliveira, G.F.Leal Ferreira, Appl. Phys. A42, 213 (1987).
[5] H.von Seggern, 1980 Annual Report, CEIDP, pp. 345-352.
[6] G.M.Sessler, J.E.West, J. Appl. Phys. 47, 3480 (1976).
[7] C.Alquie, G.Dreyfus, J.Lewiner, Phys. Rev. Lett. 47, 1483 (1981).

[8] G.M.Sessler, J.E.West, R.Gerhard, Polym. Bulletin 6, 109 (1981); Phys. Rev. Lett. 48, 563 (1982).
[9] W.Eisenmenger,M.Haardt, Sol. St. Comm. 41, 917 (1982).
[10] R.Gerhard-Multhaupt, Phys. Rev. B27, 2494 (1983).
[11] C.Alquie, F.Chapeau, J.Lewiner, 1984 Annual Report, CEIDP, pp. 488 - 494.
[12] G.M.Sessler, J.E.West, R.Gerhard-Multhaupt, H.von Seggern, IEEE Trans. Nucl. Sci. NS-29, 1644 (1982).
[13] J.E.West, H.J.Wintle, A.Berraissoul, G.M.Sessler, companion paper in these Proceedings.
[14] J.E.West, unpublished
[15] W.A.Schneider, J.H.Wendorff, R.Gerhard-Multhaupt, 1983 Annual Report, CEIDP, pp. 441 - 446.
[16] B.Gross, G.M.Sessler, J.E.West, J. Appl. Phys. 48, 4303 (1977).
[17] G.M.Sessler, J.E.West, H.von Seggern, J. Appl. Phys. 53, 4320 (1982).
[18] A.Berraissoul, R.Gerhard-Multhaupt, B.Gross, Appl. Phys. A39, 203 (1986); A.Berraissoul, Dissertation (Fortschr. Ber. VDI, Reihe 21, Nr. 21).
[19] B.Gross, G.M.Sessler, J.E.West, J. Appl. Phys. 45, 2841 (1974).
[20] G.M.Sessler, Proc. Internat. Sympos. on Electrets and Dielectrics, Sao Carlos, 1975, pp. 321 - 335.
[21] R.Gregorio Filho, B.Gross, R.M.Faria, IEEE Trans. Electric. Insul. EI-21, 431 (1986).
[22] A.Berraissoul, unpublished
[23] B.Gross, R.Gerhard-Multhaupt, A.Berraissoul, G.M.Sessler, J. Appl. Phys. 62, 1429 (1987).
[24] E.Fukada, G.M.Sessler, J.E.West, A.Berraissoul, P.Günther, J. Appl. Phys. 62, 3643 (1987).
[25] G.M.Sessler, A.Berraissoul, Ferroel. 76, 489 (1987).
[26] G.M.Sessler, R.Gerhard-Multhaupt, H.von Seggern, J.E.West, IEEE Trans. Electric. Insulat. EI-21, 411 (1986).
[27] R.Williams, M.H.Woods, J. Appl. Phys. 44, 1026 (1973).
[28] D.Hohm, Fortschr. Ber. VDI, Reihe 10, Nr. 60.
[29] P.Günther, Diplomarbeit, T. H. Darmstadt, 1988.
[30] P.Günther, companion paper in these Proceedings.
[31] B. Gross, H.von Seggern, A.Berraissoul, IEEE Trans. Electric. Insulat. EI-22, 23 (1987).

EFFECT OF CRYSTALLINITY ON CHARGE STORAGE IN POLYPROPYLENE AND POLYETHYLENE*

R. Nath and M.M. Perlman

Dept. of Physics, Collège militaire royal de Saint-Jean
Québec, Canada J0J 1R0

ABSTRACT

Charge storage is greatly improved by annealing, different cooling rates, and stretching in polypropylene (PP) and polyethylene (PE). In annealed PP and PE storage increases linearly with both crystallinity and crystallite size. The half-value charge decay temperature can be used as a measure of the latter parameters. Annealing and cooling rate affect the rate of crystalline growth. Changes occur in both the physical and/or chemical nature and concentration of defects in the crystalline region, and traps at chain fold-amorphous interfaces. Annealing 4:1 stretched polypropylene film at 140°C gave a half-value charge decay temperature of 152°C, some 70°C higher than unannealed, unstretched film! Stretching increases amorphous content creating new boundaries, decreases crystallite size, and creates defect traps.

INTRODUCTION

We have shown [1] that control of morphological structure can greatly influence charge trapping, and hence storage lifetime, in PP and PE. Using nucleation and different molecular weights, the concentration and nature of deep traps at crystalline-amorphous boundaries and at defects was changed, and increases in lifetime observed. There is other qualitative [2], but little quantitative, information in the literature on the effects of crystallinity on charge storage. The same is true of structure-conductivity relations in polymers [3]. In view of the latter, we have carried out, for the first time, quantitative measurements to relate charge storage lifetime to percent crystallinity and crystallite size.

EXPERIMENT

Polymer films (50μ thick) were extruded from nominally pure PP and linear low density PE resins. The films were coated with vacuum evaporated aluminium on one side

CH2593-2/ 88/ 0000-0047$01.00 Copyright 1988 IEEE

for charge storage measurements (at 2°C/min), and were negatively corona charged (to -480 Volts) on the other side. Crystallinity was varied by annealing the films at different temperatures in the range 50 to 140°C for 2 hours, and then cooled slowly at 1°C/min. Isothermal crystallization was also followed by different cooling rates, i.e. fast quenching in a protective box placed in liquid N_2, 4°C/min and 1°C/min. PP films were also stretched 2, 3, 4 and 5.5:1 at R.T. Films stretched 4:1 were also annealed at a fixed temperature with the ends clamped. X-ray measurements were carried out to determine percent crystallinity and crystallite size. Charge storage was studied using thermally stimulated charge decay (TSCD).

RESULTS AND DISCUSSION

(1) Annealing PP and PE

Figure 1 shows three typical X-ray scans for unannealed and annealed PP films. For unannealed PP, one sees only a broad background centered around 15°. Samples annealed at 120 and 130°C show crystalline peaks typical of those found by others [4]. The sharpness and area under the peaks increases with annealing temperature. Percent crystallinity was calculated using Hinrichsen's method [5], where the true diffraction intensity is taken to be that above a curve drawn along the base of the peaks. The percent crystallinity is then the ratio of the area under the peaks to the total area. The results agreed with those from density measurements to within 5%. Crystallite size was calculated using Scherrer's method [6], i.e. from

$$t = (0.9\lambda)/\beta \, \mathrm{Cos}\theta_{hkl},$$

where t is the crystallite size perpendicular to the (hkl) plane, λ is the X-ray wavelength, β is the peak width in radians, and θ_{hkl} is the Bragg angle.

Figure 2 shows the TSCD half value temperatures ($T_{\frac{1}{2}}$) vs percent crystallinity for annealed PP and PE. In both plots, $T_{\frac{1}{2}}$ increases linearly with increase in percent crystallinity. Figure 3 shows increasing $T_{\frac{1}{2}}$ with crystallite size for the same samples, and one observes linearity again. Thus $T_{\frac{1}{2}}$ can be used as a measure of the latter parameters in PP and PE.

Traps at crystalline amorphous interfaces play a major

role in charge storage. The physical and chemical nature of these traps, and their concentration, changes with annealing.

Defects between the crystallites in fibrils, or in regions between the fibrils, and/or imperfections in the ordered phase, produce broadening of the crystalline peaks. The fibrils are composed of crystallites and twisting and branching that introduces amorphous regions. These fibrils are the subunits of the spherulite structure.

Charges get trapped at defects in the crystallites. The crystallites melt at higher temperatures as their size increases. Since the charge is not completely released until the melting point is reached, $T_{\frac{1}{2}}$ increases with crystallite size.

(2) Cooling Rate

$T_{\frac{1}{2}}$ increases from 97 to 106 to 116°C as the cooling rate decreases from quenching to 4 to 1°C/min. Percent crystallinity and crystallite size were calculated from X-ray scans (not shown) and are plotted as open circles on Figs. 2 and 3 for PP. The results are in good agreement with those previously obtained for annealing. As expected, $T_{\frac{1}{2}}$ increases as cooling rate decreases, since rapid cooling produces a smaller number of large crystallites, and slower cooling greater crystallinity, by allowing the crystallites more time to grow.

(3) Stretching PP

Figure 4 shows the TSCD $T_{\frac{1}{2}}$ for unannealed PP films vs stretching ratio at R.T. An optimum stretching ratio of 4:1 with a $T_{\frac{1}{2}}$ of 112°C was obtained. The latter ratio was chosen for further investigation. Stretching causes lamellae to slide over each other. The absolute concentration of the amorphous regions is also increased, as can be seen by comparing X-ray scans (not shown). New deep traps are created at chain-fold amorphous interfaces by stretching, as are defects within the crystallites by e.g. grain boundary motion. It has been previously shown that trap density increases with stretching [7].

Table I gives $T_{\frac{1}{2}}$, percent crystallinity, and crystallite size for stretched PP films, unannealed, and annealed for 2 hrs at 80, 100 and 140°C. The first row

of Table I and Figs. 2 and 3 show that for unannealed film, the percent crystallinity has decreased from 56 to 21% for the same $T_{\frac{1}{2}}$, due to the greater amorphous content, and the crystallite size has decreased from 136 to 25 Å due to lamellae separation. $T_{\frac{1}{2}}$ increases to 152°C for samples annealed at 140°C, some 70°C higher than for unstreteched, unannealed PP!

*Work supported by CRAD and NSERC, Canada, under grants 3610-402, and A-4930, respectively.

REFERENCES

[1] M.M. Perlman and S. Haridoss, Proc. of the 2nd International Conf. on Conduction and Breakdown in Solid Dielectrics, Ed. P. Fischer, p. 494-499, IEEE, CH2124-6, (1986).

[2] R.A. Creswell, M.M. Perlman and M.A. Kabayama in Dielectric Properties of Polymers, Ed. F. Karasz, p. 295-312, Plenum (1972).

[3] P.J. Phillips, IEEE Trans. Electr. Insul., EI-13, 69-81 (1978).

[4] K. Fujita, M. Daio, R. Okumura, S. Suchiro, S. Normura and H. Kawai, Polymer J. 15, 449-479, (1983).

[5] G. Hinrichsen, J. Polym. Sci. C, 38, 303-319 (1971).

[6] A.K. Gupta and R.P. Singhal, J. Polym. Sci., Polym. Phys. Ed., 21, 2243-2262 (1983).

[7] D.H. Park, J. Kyokame and K. Yoshino, Jpn. J. Appl. Phys., 26, L65-L67 (1987).

Table I

Stretched and Annealed PP films

Annealing conditions	Crystallinity (%)	Crystallite size (Å)	$T_{\frac{1}{2}}$ (°C)
unannealed	21	25	112
80°C	34.5	53.5	128
100°C	40	66.8	133
140°C	54.7	82.7	152

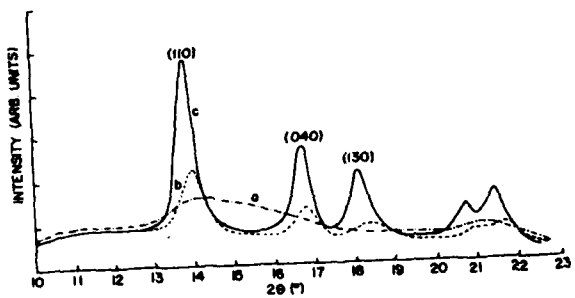

Fig. 1 - X-ray diffraction scans of PP (a) unannealed; annealed 2 hours at (b) 120°C, (c) 130°C.

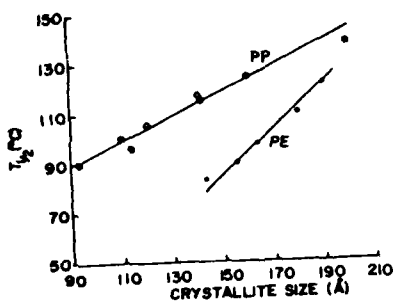

Fig. 3 - TSCD $T_{\frac{1}{2}}$ vs crystallite size in PP and PE (symbols as in Fig. 2).

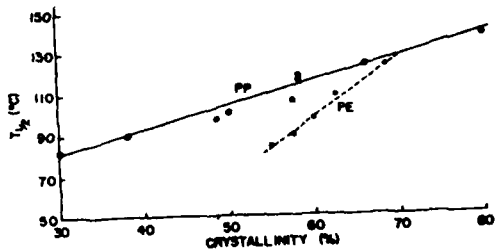

Fig. 2 - TSCD $T_{\frac{1}{2}}$ vs % crystallinity of PP and PE; ●, ●, - isothermal annealing of PP and PE respectively, 0 - different cooling rates for PP.

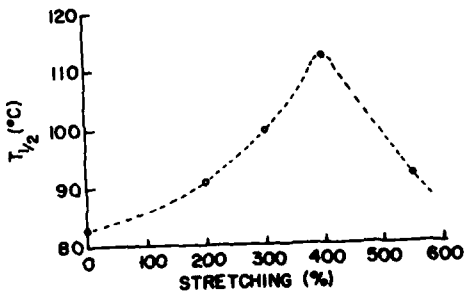

Fig. 4 - TSCD $T_{\frac{1}{2}}$ vs % stretching at R.T. of unannealed PP.

THE TRAPPING OF ELECTRONS IN POLYSTYRENE

P. Keith Watson

Xerox Corporation, 800 Phillips Road 0114-24D, Webster, NY 14580

ABSTRACT: A thin polystyrene film is charged with a short pulse of low energy electrons (2keV). Most of these electrons are deeply trapped in the polymer; the remaining electrons are excited from shallow traps into conduction levels and are swept out of the polymer. At short times, when most of these shallow-trapped electrons are excited into the conduction levels, the current approaches the space charge limit: hence we obtain a value for electron mobility. At long times (from about five seconds to thousands of seconds) the conduction process is dominated by the rate of excitation from deeper-lying trapping levels; the excitation of electrons from these traps can be analyzed in terms of a time-dependent demarcation energy E_m, related to elapsed time through the equation $E_m = kT\ell n(\nu_0 t)$. The time dependence of current is thus related to the distribution of electron traps in the polymer.

INTRODUCTION

In this paper we are concerned with the trapping and decay of electrons from polymer film electrets which have been charged with a low energy electron beam (1), We have applied the ideas on trap limited band motion and multiple trapping (2,3,4,5,6,7) which have been developed in the field of amorphous semiconductors, to describe the fate of these excess electrons. Thus we obtain information about shallow and intermediate traps in the electret that complements information obtained from TSD and other studies of deep traps.

When a pulse of electrons is injected into an insulating solid containing an arbitrary distribution of electron traps, there is a period of order 10^{-12} seconds during which time the electrons lose their excess energy and condense into the traps. If these traps have equal cross section, then the trapped electron distribution initially parallels the density distribution of the traps (2,4). If now we assume that electron transport is associated with conduction levels above E_o, then the leakage of electrons from the electret is determined by the rate of thermal excitation of electrons to $E \geq E_o$. Although initially the electron population will parallel the density of states, with the passage of time the shallow states will be preferentially depopulated and only those electrons which were initially in deep lying states will remain in the electret. Following Simmons and Tam (2) and others (3,4,5) we define a time-dependent thermalization energy, or demarcation energy, E_m such that traps located above E_m in energy have been emptied of electrons in

CH2593-2/ 88/ 0000-0052$01.00 Copyright 1988 IEEE

the interval from zero to time t, whereas electrons in traps below E_m remain frozen *in situ*. Thus, E_m moves away from the conduction levels with the passage of time, and the portion of the injected charge being excited into conduction levels must be excited from traps in the vicinity of E_m. Now trap release time is given by $t_r = v_o^{-1} \exp[(E_o - E_m)/kT]$ so the demarcation energy is $(E_o - E_m) = kT \ell n\, v_o t$, where the attempt frequency v_o is of order 10^{12}, and E_o defines the bottom of the conduction levels.

In general leakage current is proportional to the product of the number of electrons excited into the conduction levels and their drift velocity, so one cannot separate carrier density and mobility. However there are two important limiting cases which reduce the complexity of the problem and enable one to the separate the two variables. These are (a) the emission limit, in which the rate of excitation of carriers into the conduction levels is the rate limiting step, and the electrons excited above E_o are swept out of the sample as rapidly as they are excited into the conduction levels; (b) the space charge limit, in which the rate of excitation exceeds the rate at which the electrons drift in the field.

These two limiting cases represent the long-time and short-time asymptotes of current behaviour, and we define a time T which marks the transition between the two regimes. For $t<T$ we expect to observe case (b) space charge limited behaviour; For $t>T$ we should observe case (a), the emission limit. In the latter case current is proportional to the number of carriers excited from E_m into the conduction levels above E_o; now the numbers of carriers in this part of the Boltzman tail of the distribution is given by $n(t) = N_o \exp[-(E_o - E_m)/kT] \simeq N_o[v_o t]^{-1}$, and thus for a situation in which the density of states is uniformally distributed in energy, current should decay as t^{-1}. In the case of a non-uniform distribution of traps the product of current and time is linearly proportional to the occupied trap density at E_m, so that by plotting the product $I(t).t$ against $\ell n v_o t$ one obtains the distribution of electron emitting traps.

In case (b), space charge limited conduction, we are dealing with a situation in which there are so many carriers excited into the conduction levels that their drift velocity is rate limiting. Current should be proportional to V^2, and from this one may then define an effective carrier mobility. The activation energy of the electron mobility provides information about trapping states lying close to the conduction levels.

EXPERIMENTAL METHOD AND RESULTS

The technique used in these experiments is to measure the decay of surface potential of a polymer film electret following the injection of a pulse of electrons. This electron injection technique has been described previously (1) and is shown in Fig. 1. Two electron beams are used in these experiments; one beam injects electrons in to the free surface of the polymer film and the other beam monitors the surface potential.

Because of the very high effective impedance of the electron-beam electrometer we are able to monitor the surface potential for times as long as thousands of seconds after the charging pulse. A 2 keV electron beam is used to inject charge through the free surface of the polymer film; this beam scans a raster over a 4 x 4 cm^2 area of the sample surface and is automatically turned off when the required amount of charge has been deposited on the sample. Charging times typically range from 50 to 100 msec. The electrometer beam passes between the sample surface and a reference grid situated above the polymer film; this beam is collected on a split anode detector, connected via a differential electrometer to a high gain amplifier whose output is fed back to the reference grid. This feedback loop holds the read-out beam near its null position on the split anode and in so doing maintains the reference grid at the same potential as the sample surface. The grid potential is recorded and thus one obtains a direct reading of the surface potential of the sample and its variation with time.

The majority of our measurements have been made on a monodisperse polystyrene of 37,000 M.Wt, and a highly purified PS-2 (a polystyrene of broad molecular weight). The polymer films are cast from solution in benzene directly onto the surface of the metal substrate.

In these experiments we observe the surface potential of the polymer film electret vs. time following the charging pulse; typical results are shown in Fig. 2. The initial value of the surface potential is determined by the injected charge density and the effective capacitance of the sample. The rate of decay of this potential is dependent on both temperature and on initial charge density (i.e., on the field in the polymer). The rate of decay decreases with time and after about one thousand seconds the decay is too slow to measure, at which point the stable electret potential remains on the polymer surface, indicating that the electrons are frozen in deep traps within the polymer film. (The electrons can be released from these traps by heating above the glass transition temperature T_g).

In order to analyze these experimental results we need to calculate the sample current as a function of time, and this we obtain from the time derivative of the surface potential. The boundary conditions specified in our model are that the trapped electrons are located in a thin region near the polymer surface (2kV electron penetration depth $\simeq 0.2$ μm) and that electrons excited into the conduction levels are swept out of the sample with negligible re-trapping. Under the conditions of emission limited conduction (case (a) above) we can neglect any space charge in the polymer bulk, and the current flowing in the sample is exactly proportional to the rate of decay of surface potential. In case (b) (that of trap-modulated, space-charge-limited conduction) we derive the electron mobility from the initial value of dV/dt.

Extensive measurements of this type have been made on 37,000 M.Wt. polystyrene at temperatures from 30 to 140°C at various charging levels. In each experiment a pulse of 2 kV electrons was injected into the sample; the peak voltages ranged from 50 to 200 volts. The decay of surface potential was then monitored for about 2,000 seconds. After this the charge was erased by heating above T_g. The sample was then brought back to test temperature before recharging.

As already noted, at short times we expect the current to approach the space charge limit, and at longer times we should observe a transition to the emission limited case. To check this we have plotted log dV/dt vs. log V, for times of 0.1, 1.0, 10 and 100 seconds and find that for short times (less than 5 seconds or so) current is proportional to V^2, which is consistent with our SCL model. For longer times current is proportional to V^n where n is of order 1.3 to 1.5. (In the ideal case n should approach unity, but field-dependent emission leads to $n>1$).

From the space charge limited regime we can deduce the effective electron mobility, and from the temperature dependence of this mobility we can infer the activation energy of the mobility. In Fig. 3 we show μ vs 1/T for 37,000 M.Wt polystyrene, and note that the activation energy (0.7eV) indicates a dominant trapping level situated 0.7eV below the edge of the conduction level E_o. In contrast to this, our mobility measurements on highly purified PS-2 (a broad molecular weight polystyrene) indicates a trapping level about 0.15 eV below E_o.

The transition from SCL to emission limited current occurs at about 4 or 5 seconds for 37,000 M.Wt PS. For times longer than this the product I(t).t draws out the distribution of electron traps in the polymer. In Fig. 4 we show the product I(t).t for 37,000 M.Wt Polystyrene plotted against log t, and the appropriate energy scale. On this scale the lower limit of states that are accessible by this technique is set by the SCL transition; the upper time limit is about 2,000 seconds; thus, the upper and lower limits to (E_o-E_m) are 0.9 eV and 1.15 eV. The most notable feature of Fig. 4 is the broad peak in the trap density at 1.06 ± 0.1 eV. This distribution, and the trapping level at 0.7eV which modulates the carrier mobility, characterize the electron transport properties of the polymer.

REFERENCES

1. P.K. Watson, IEEE Transactions EI-22, 129 (1987).
2. J.G. Simmons and M.C. Tam, Phys. Rev. B 7, 3706 (1973).
3. A.I. Rudenko and V.I. Arkhjipov, J. Non-Cryst. Solids, 30, 163 (1978).
4. T. Tiedje and A. Rose, Solid State Comm. 37, 49 (1981).
5. J. Orenstein and M. Kastner, Phys Rev Lett. 46, 1421 (1981).
6. R.W. Schmidlin, Phys. Rev. B 16, 2362 (1977).
7. J. Noolandi, Phys. Rev. B 16, 4466, (1977).

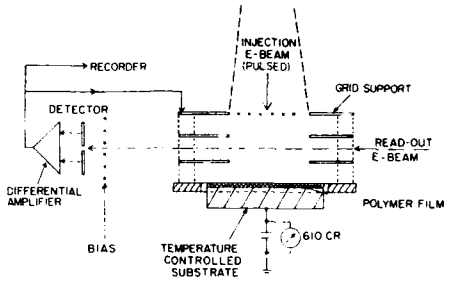

Fig 1. Electron beam apparatus. Beam energy 2 keV.

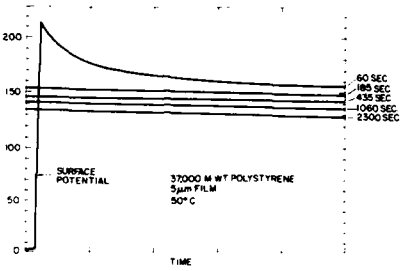

Fig 2. Typical decay characteristic of 37,000 M Wt polystyrene film.

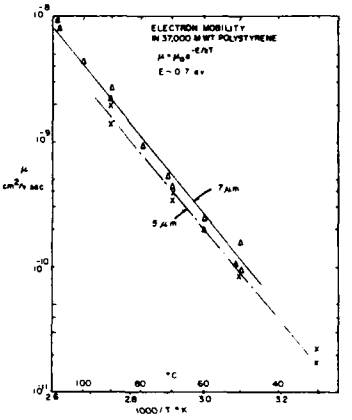

Fig 3. Electron mobility in 37,000 M Wt polystyrene. From initial slopes of decay characteristics.

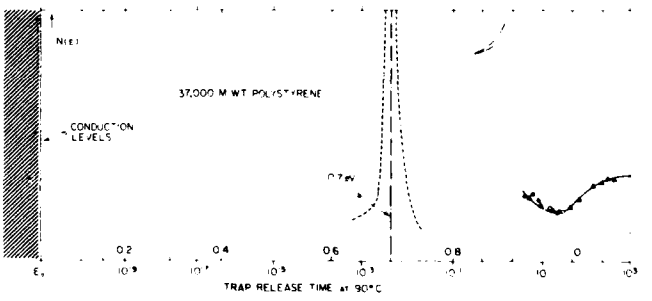

Fig 4. Trapping states active in electron transport in 37,000 M Wt polystyrene. The level at 0.7 eV is obtained from the activation energy of mobility (Fig 3). The structure from 0.9 to 1.1 eV is obtained from long time current decay.

THERMALLY STIMULATED DEPOLARIZATION CURRENTS IN A POLYZWITTERION : AN EXAMPLE OF CHEMICAL RELAXATION

Eve MARCHAL

Institut Charles Sadron (CRM-EAHP), 6 rue Boussingault, 67083 Strasbourg Cédex, France.

ABSTRACT.

The thermally stimulated depolarization current technique is used in the case where a temperature dependent equilibrium between two conformational isomers of different polarities can take place. If the relaxation times involved in this reaction are smaller than the orientational relaxation time, two positive and one negative peak may appear. Unlike classical TSD, the low temperature depolarization peak may become stronger at lower polarization temperatures. Equilibrium and rate constants of the reaction at various temperatures as well as dipole moment can be determined. An illustration of the theory is given for a polyzwitterion : μ = 25 Debyes for the extended sulphopropylbetaine group.

INTRODUCTION.

The thermally stimulated depolarization technique is widely used to study dipole and space charge relaxation as well as charge injection and detrapping. As will be shown below, it also proves to be a powerful technique to study a reversible reaction between a low dipole-moment-bearing species and its conformational isomer of high polarity. Such a chemical equilibrium reaction takes place in a small temperature range above room temperature in a polyzwitterion and its TSD diagram will be used to illustrate some theoretical considerations.

CH2593-2/ 88/ 0000-0057$01.00 Copyright 1988 IEEE

THEORETICAL.

Description.

Consider a closed constant volume system in which a reversible reaction takes place.

$$A \underset{k_r}{\overset{k_f}{\rightleftharpoons}} B \qquad (1)$$

The quantities k_f and k_r denote the rate constants for the forward and reverse reaction, respectively. Furthermore species B, the stable form at high T, has a strong permanent dipole moment (μ) while A has none (or only a relatively small one). The rates of most chemical reactions are very sensitive to temperature ; the law formulated by Arrhenius is still extensively used :

$$k = A \exp(-Ea/RT)$$

The constants A and Ea differ for k_f and k_r. In figure (1) the concentration C_B of B is shown by a dotted line as a function of temperature for a fictitious case. At any T, C_A and C_B are related through the equilibrium constant K

$$K = \frac{C_B}{C_A} = \frac{k_f}{k_r} \qquad (2)$$

Above T_c, $C_A \simeq 0$ and $C_B \simeq C_0$. We now apply a d.c. electrical field E_p at $T_p > T_c$ and make several hypothesis :

1) At any temperature in the range of interest, the dipole orientational relaxation time τ_0 of B is much higher than the chemical relaxation times related to the kinetics of reaction (1).

2) The direction of the molecular axis bearing the dipole moment of B is unchanged in the reaction $B \rightarrow A$.

3) The poling field is small enough so as to cause a negligible shift of the equilibrium constant: $\mu E_p \ll kT$. We also assume that T_p is high enough (or the poling time t_p long enough) so as to complete the

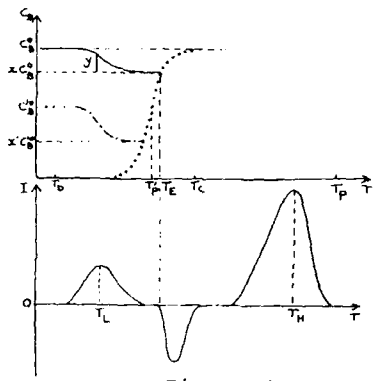

Figure 1

Upper diagram : concentration of polar species. (....) equilibrium curve ; (——) while heating, after poling at T_P and quenching ; (• — • —•) same as this last, after poling at T_P'. Lower diagram : current during heating, after poling at T_P.

orientational polarization of B, then proceed the experiment as usual by quenching, field on, to $T \ll T_D$, heating under short circuit while recording the current released. At low temperatures, the B species, concentration C_B, are oriented and stay so up to a stage, centered at T_L, where a certain amount, while still being oriented, will undergo the reaction B → A until they reach their equilibrium concentration (xC_B) at T_E. This is illustrated by the full curve in figure 1). Up to T_E, the sample has lost some polarization leading to a TSD peak proportional to $(1-x)C_B$. Between T_E and T_C, the equilibrium reaction (1) now favors the B species and the polarization increases until their concentration reaches again C_B, leading to a second (TSP) peak of opposite sign but of equal area. Upon further heating one will observe around T_H the classical peak due to disorientation of all the B species.

Quantitative.

Heating from T_D to T_E after poling at T_P.
The reaction under concern in this T range is

$$B \xrightarrow{k_r} A$$

The change in polarization P is due to a change in concentration of species B. We assume that there are no dipolar interactions between the species (Kirkwood factor g = 1). Their polarization is approximately

$$P = \epsilon_0 \mu^2 E_p N_A C_B / (3 kT) \qquad (3)$$

where $\epsilon_0 = 8.854 \times 10^{-12}$ f/m, N_A Avogadro number, k Boltzmann constant and C_B the concentration in molarities. Using the definition of a rate constant for the reaction of species whose concentration (y) decreases from $y = C_B - x\ C_B$ at t = 0 to $y = C_b - x\ C_B$ at t = t and finally to y = 0 at $t \to \infty$,

$$I = \frac{dP}{dt} = - G \frac{dy}{dt} = G k_r y^b$$

where $G = \epsilon_0 \mu^2 E_p N_A / (3 kT)$ and b is the order of the reaction. In the example given below B and A are conformational isomers, so that it is safe to assume a first order reaction (b = 1) for that case. Thus

$$I = G \frac{dy}{dt} = G A_r [\exp(-E_{ar}/kT)] y$$

A_r and E_{ar} being the preexponential factor and activation energy of k_r. The solution of this equation in the case of constant heating rate (h) ($T = T_0 + ht$), and neglecting the change of P due to T in expression (3) with respect to that due to C_B, is common to a variety of thermally stimulated phenomena.[1] It is the famous "first order kinetics" equation which applies to TSD.

In the present case, we note that k_r can be determined as a function of T through the ratio (dy/dt)/y which is the ordinate of the TSD curve divided by the area remaining under the peak above T.

Heating from T_E to T_c

The system now undergoes the equilibrium reaction (1).

$$I = G \frac{dC_B}{dt} = G(k_f C_A - k_r C_B)$$

with

$$C_0 = C_A + C_B$$

The resulting polarization curve has a different shape. Above T_C
The classical disorientation of the C_0 dipoles is observed in this region. The dipole moment of B can be determined from its area.

Comments.

Necessary conditions for the two low T peaks to occur are that 1) T_L be lower than the T range of the equilibrium curve . Using

$$kT^2 k_{rL} = A_r h \qquad \text{at peak maximum}$$

and relation (2), the condition is

$$A_r h \gg kT^2 k_{fL}$$

If T_L is very low, the 3 peaks are of equal area.
2) the cooling rate be faster than that needed for establishment of equilibrium.
If the last condition is not fulfilled, the resulting TSC curve consists of only two peaks of opposite sign and equal area : the sample is no longer an electret at low T.

At intermediate cooling rates, the peak at T_L is weaker than the one observed after quenching. If the rate of establishment of equilibrium concentration is close to the rate of change in C_B through heating the quantity x may depend on (h). If $T_H > T_E$ is lower than anticipated in figure (1) the two high T peaks superimpose and the resulting diagram consists of two positive peaks only. The sum of their areas is proportional to C_0. The quantity x is obtained from their ratio. This is the case in our experiments. By poling at various temperatures T_p' lower than T_C, and allowing t_p to be long enough so as to reach complete orientational polarization of the C'_0 species, the equilibrium concentration curve (dotted curve in figure (1) can be

determined from the area of the TSD curve. A remarkable situation arises when T_P (< T_c) is such that

$$y_{max} = C\beta(1-x) < C'\beta(1-x')$$

The variation of C_β in this case is illustrated in figure (1) by the dash-point curve. The area of the peak which appears at T_L is then higher than the corresponding one obtained when $T_P > T_c$. The variation of the low T peak strength with changing poling temperatures appears to be a good criterion for assessing the underlying mechanism of polarization, since lower peaks at higher poling temperatures cannot be observed for classical dipole disorientation processes.

Finally, we wish to mention that W. Scheider[2] and G. Schwarz[3] have predicted that, at constant temperature, two regions of dielectric dispersion can occur in the frequency domain when equilibrium chemical reactions occur under conditions similar to those stated above, mainly chemical relaxation time << τ_0. Experimental evidence is scarce for small molecules[4] and has led to a controversy in the case of a macromolecule in solution.[5] An advantage of the TSC technique is that is allows to determine $k_r(T)$, $K(T)$, and thus also $k_f(T)$.

EXPERIMENTAL.

The sample used, poly[4-vinyl-1-(3-sulphopropyl) pyridinium], was prepared by J.C. Galin in our Institute. Its synthesis is described in ref.6. The polymer is in a glassy state up to 220°C, above which it decomposes[7]. The powder is compressed into discs (ϕ = 1.2cm, e ≃ 1mm), both sides of which are coated with silver paint. Drying at 110°C, 12 hours under vacuum, is done in the TSD set-up before poling.

Figure 2 shows the TSD diagrams observed after poling at 140°C (full line) and 112°C (dashed line). Their origin is attributed to a reversible change of conformation of the $-\overset{+}{N}-(CH_2)_3-SO_3^-$ groups and to their disorientation. The less polar conformation (A) is the one in which the N^+ and SO_3^- atoms lie at closest approach; in the highly polar one (B) the sulphopropyl

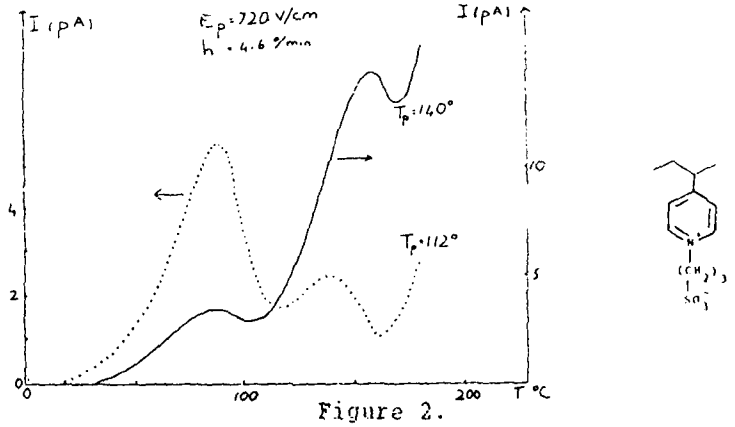

Figure 2.

TSD spectra of poly[4-vinyl-1-(3-sulphopropyl) pyridinium] (—— t_p = 15 min ; ..... t_p = 5 min) and chemical formula of one unit.

betaine group is extended. Using the above considerations and assuming $\mu_A = 0$ and density 1.2×10^{-3} Kg/m³, the equilibrium curve is found to lie in the range 90°-140°C, μ_B = 25 Debyes, in agreement with the estimated value of dipole moment for the fully extended form,

and $A_r = 9.3 \times 10^5$ sec^{-1}, $E_{ar} = 0.6$ eV; A_f, E_{af} } not yet determined

For undried samples, the apparent dipole moment μ_B is much higher.

CONCLUSION.

For a reversible reaction between a low dipole moment bearing species and its conformational isomer of high polarity, stable at high T, a theory is given to predict the TSC response after poling. The experimental diagram obtained for a particular polyampholyte could be interpreted using this theory, and dipole moment as well as the parameters governing the equilibrium reaction are determined. Depending on the experimental conditions and on the system, it is possible to obtain no electret formation. In the present sample, however, by poling above 140°C an electret bearing a dielectric constant increment of 140 is obtained.

ACKNOWLEDGMENTS.

The author wishes to thank Dr. H. Benoit and Dr. G. Weill for useful discussions.

REFERENCES.

[1] R. Chen and Y. Kirsch, "Analysis of Thermally Stimulated Processes", International Series on the Sciences of the Solid State Vol.15, 1981.

[2] W. Scheider, "Dielectric Relaxation of Molecules with Fluctuating Dipole Moment", Biophysical J. Vol.5, pp.617-628, 1965 ; and "On Modes of Dielectric Relaxation Due to Steady-State Chemical Processes" J. Phys. Chem. Vol.74, pp.4296-4298, 1970.

[3] G. Schwarz, "On Dielectric Relaxation Due to Chemical Processes", J. Phys. Chem. Vol.71, pp.4021-4030, 1967.

[4] G. Schwarz, "Acid-Base Catalysis of Dielectric Relaxation of Zwitterions", J. Phys. Chem. Vol.74, pp.654-658, 1970.

[5] E. Marchal, "Dielectric Relaxation Measurements as a Tool for Studying the Kinetics of the Helix-Coil Transition of Poly(γ-benzyl-L-Glutamate)", Biopolymers Vol.10, pp.417-419, 1971.

[6] V.M. Monroy Soto and J.C. Galin, "Poly(sulphopropylbetaines) : 1. Synthesis and Characterization", Polymer, Vol.25, pp.121-128, 1984.

[7] M. Galin, E. Marchal, A. Mathis, B. Meurer, Y.M. Monroy Soto and J.C. Galin, "Poly(sulphopropylbetaines) : 3. Bulk Properties", Polymer Vol.28, pp.1937-1944, 1987.

CHARACTERIZATION OF POLYMERS BY DIELECTRIC SPECTROSCOPY (TSC)

by J.R. Saffell, J.P. Ibar, A Bernes, T. Thomas

Solomat Partners L.P. Glenbrook Ind Park, Stamford CT 06906 USA. Solomat Mfg. Ltd. Ottery St Mary, Devon UK. Solomat France S.A. Ballainvilliers, 91160 FRANCE.

Thermally Stimulated Current (TSC) reveals the molecular mobility of the material's structure, with the rate of depolarization relating directly to the relaxation times of the internal motions.

The principle is to orient pendant polar groups of macromolecules, with a high voltage field at a high temperature - then to quench the material. On reheating, the polarized groups depolarize, creating a current.

In this paper, the TSC spectrum of amorphous and semi-crystalline polymers will be presented after a brief review of the principles of TSC. Then, the influence of chemical structure, and physical parameters will be presented. Finally, an automated technique for producing relaxation maps (RMA) will be demonstrated.

INTRODUCTION

Several techniques exist to analyze the molecular response of materials to physical or chemical inputs in order to determine their specific performances. Differential Scanning Calorimetry (DSC) and Dynamical Mechanical Analysis (DMA) are among the most popular in laboratories and on production sites. Other techniques include Thermal Mechanical Analyzers (TMA), stress relaxation or creep analyzers, thermal expansion coefficient devices, and dielectric constant analyzers.

Unique types of relaxation spectra can be obtained by recording the shortcircuit current during warming-up after a material sample has been polarized by a constant d.c. field above a transition temperature, then quenched. This technique was originally used to measure charge detrapping in low-molecularweight organic and inorganic compounds. This method is called Thermal Stimulated Current (TSC). Only since 1971 has this technique been applied to the study of structural transitions in polymers [1,2,3]. A thorough review the past twenty-five years is summarized in [3].

TECHNIQUE

In a typical Thermal Stimulated Current experiment a high-voltage stabilized d.c. supply is used for polarizing the sample above its main transition temperatures. The sample is heated to the polarization temperature under an electric field of about 4MeV/m. The sample is held for a certain time, then quenched. The external field is then removed and an electrometer is

CH2593-2/ 88/ 0000-0065$01.00 Copyright 1988 IEEE

connected to the sample to record the short-circuit current while reheating at a constant rate. A current is created as the material depolarizes, revealing the molecular mobility of the material's structure. The rate of depolarization is directly related to the relaxation times of the internal motions. The current peaks are found to correlate well with the transition temperatures measured by mechanical relaxation, DSC, and conventional (AC) dielectric spectroscopy.

RELAXATION MAP ANALYSIS (RMA): A NEW ANALYTICAL CONCEPT

In 1974, Professor C. Lacabanne [2] and her co-worker D. Chatain [2a], both of the laboratory of Physics of Solid in Toulouse, France, published the first of a series of innovative publications. Their work applied a new method of "windowing polarization" to study relaxation phenomena; this technique isolates elementary Debye type relaxations from the entire relaxation spectrum. In previous work, the TSC output consisted of unresolved broad peaks, the result of the interaction between several relaxation modes, which is typical of polymer transitions. Lacabanne submitted the polarized specimen to a windowing treatment (Fig 1). First, polarize the sample at temperature Tp for a limited time, tp, adjusted to prevent orientation of dipoles with long relaxation times. The sample is then quenched to a temperature Td, 5° to 10° below the polarization temperature Tp. Cut off the polarizing voltage and stay at Td for a time td, allowing depolarization of the oriented dipoles with shortest relaxation times. Finally, quench the sample to To << Td. Reheat at a constant rate and measure the current. When tp, td, and (Tp - Td) are correctly chosen, the spectrum of depolarization is "simple": the spectrum is described by several deconvoluted relaxation times, which are a function only of temperature. By varying the value of Tp, and repeating the above process, one can isolate the

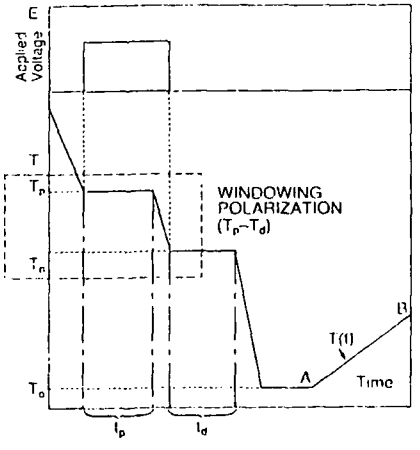

Figure 1

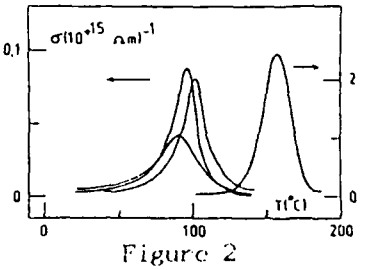

Figure 2

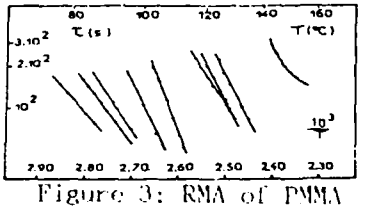

Figure 3: RMA of PMMA

elementary modes one by one (Fig 2), and construct the MATERIAL'S RELAXATION MAP (Fig 3).

PRINCIPLE OF TSC AND RELAXATION MAP ANALYSIS (TSC/RMA).

For observing the various thermally stimulated current peaks, the mobile units of the sample are orientated by a static electrostatic field (E) at a given polarization temperature, Tp. Additionally, the high static field is capable of injecting or stripping electrons from non-polar groups, effectively "tagging" the groups as they orient. When the polarization, P, has reached its equilibrium value the sample is quenched, and the field removed. The polarization recovery occurs on reheating at a constant rate. The depolarization current, I, flowing through the external circuit is measured by an electrometer, and allows measurement of the "dipolar conductivity" σ. If the isothermal polarization varies exponentially with time, then its relaxation time τ is deduced from the measure of σ:

$$\tau = P / \sigma E \qquad (1)$$

RMA:

When the polarization is due to a distribution of relaxation times, then the technique of windowing polarization (called "thermal cleaning") is used for deconvolution of the relaxation spectra [3], producing a Relaxation Map (Fig 3). For simple behaviour described by a Kelvin-Voigt model, the elementary relaxation time τi is given by:

$$\tau i(T) = P(T) / J(T); J(T) = \dot{P}(T). \qquad (2)$$

The analysis of each resolved spectrum gives a temperature dependent relaxation time $\tau i(T)$ which follows either an Arrhenius equation:

$$\tau i(T) = \tau oi^* \exp(\Delta H/kT) \qquad (3)$$

(where τoi^* is the pre-exponential factor, ΔH is the activation enthalpy, and k is the Boltzmann constant), or a Vogel equation:

$$\tau i(T) = \tau oi \exp[\alpha(T-T\infty)]^{-1} \qquad (4)$$

where τoi is the pre-exponential factor, α is the average thermal expansion coefficient of the free volume, and $T\infty$ is the critical temperature at which the relaxation time becomes infinite. Relaxation Map Analysis (RMA) determines the pre-exponential factor (related to the entropy of activation), and activation enthalpy, or the coefficient of free volume expansion, and temperature of frozen mobility ($T\infty$) for each elementary peak.

POLYCARBONATE

The application of the windowing polarization technology (RMA) to the study of amorphous polymer has revealed properties of the glassy state never observed before,

with investigations on polystyrene [4,5], PMMA [6,7], PVC [8], polycarbonate [9], and PET [10]. This new type of TSC analysis brings a new light to the following questions: Why is polycarbonate so tough ? Why are polystyrene and Plexiglas so brittle ? RMA shows that, in most amorphous polymers, the major motions responsible for internal flow decompose into a variety of elementary mechanisms well described by the activated state theories (Fig 4). However, in a few instances the molecular processes obey a WLF-type (Vogel-Fulcher) type of equation, which reveals the dominance of a free volume effect over an activated process for that relaxation mode. Such WLF activities observed for motions BELOW the glass transition seem to dominate only in tough polymers (Fig 5).

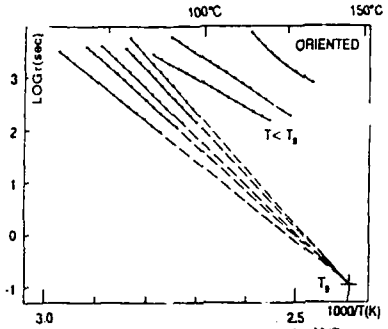

Figure 4: RMA of PS

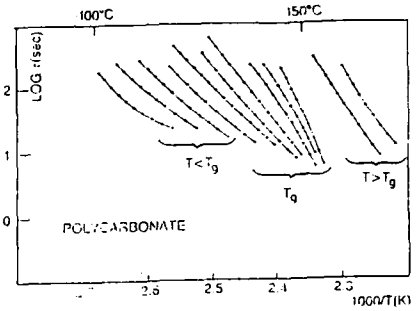

Figure 5: RMA of PC

POLYPROPYLENE

For semi-crystalline polymers, the power of resolution of RMA ascertains the difference between the macromolecules trapped in the interlamellar regions and those which belong to the true amorphous region; the reason is simple. In TSC, amorphous polyers display a very strong relaxation mode at the glass transition temperature, Tg. This mode is attributed to microbrownian motions of the amorphous chains. The understanding of the relative intensity of the interlamellar tissue versus the true amorphous component is crucial to determining the end user properties. In a semi-crystalline material, the window polarization analysis reveals two distinct

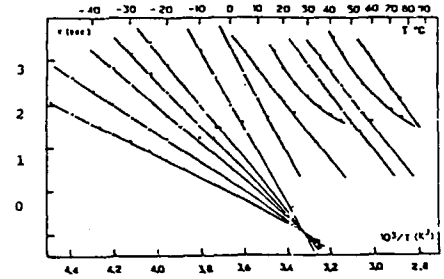

Figure 6: RMA of Polypropylene

relaxation modes at lower temperatures (Fig 6), clearly indicating the existence of a fine structure for the amorphous region. The relaxation component observed at lower temperatures is attributed to the regions free from constraint, i.e. to the interspherulitic region. This region of the polymer may be mechanically strained, as evidenced in Figure 6 (Polypropylene) by the presence of a law of compensation for the lower relaxation modes. TSC/RMA is therefore a unique technique to 'measure up' the extent of internal stress built up in a material, whether at the boundary between two phases, or the bulk.

INTERFACES

TSC/RMA is ideal for studying the quality of interfaces between the matrix and the fiber for a composite material, or to quantify the quality of the bonding phase for coatings and paints, using the same reasoning as applied to the amorphous phase in semicrystallite polymers. For semi-crystalline polymers, the component at higher temperatures corresponds to the amorphous chains under constraints from crystallites, i.e. intercrystallite regions. There is no compensation effect for these relaxations, since the effect of macroscopic stress will affect the inter-spherulitic tissue first. The free volume content in glassy thermoplastics and in the glassy phase of semi-crystalline polymers depends upon the rate of cooling through the glass transition and the processing conditions, strongly affecting certain mechanical properties. RMA easily identifies the relaxation modes which are free volume controlled: these relaxations are curved on a RMA plot (Fig 6). The dependence of processing variable on the free volume parameters for both the interspherulitic and the intraspherulitic amorphous phases can be separated and characterized.

REFERENCES

1) J. Vanderschueren,Ph. D Thesis, Univ Liege,Belgiun
1a) J. van Turnhout, "Thermally Stimulated Discharge of Polymer Electrets", Elsevier, New York, 1985
2) C.Lacabanne, Ph.D Thesis, Univ Toulouse, France,1974
2a) D. Chatain, Ph.D Thesis, Univ Toulouse, France, 1974
3) A. Bernes, C. Lacabanne et Al, in "Order in the Amorphous State of Polymers", p. 305-326, S.E. Keitnath Editor, Plenum Press (1987)
4) I. Diaconu and S.V. Dumitrescu, Eur.Polym. J., 14, 971-975 (1978)
5) S.K. Shrivastava, J.D. Randade, and A.P. Srivastava, Thin Solid Films, 67, 201-206 (1980)
6) J.K. Keszka, J Ulanski, I. Glowacki, and M. Kryszawski, J. Electrostatics, 16, 89-98 (1984)
7) K. Ohara and G. Rehage, Colloid Polym. Sci., 259, 318-325 (1981)
8) J.M. M. Barandiaran, J.J. Del Val, J. Colmenero, C. Lacabanne, D. Chatain, J. Millan, and G. Martinez, J. Macromol. Sci., Phys., B22, 645-663 (1984)
9) L. Guerdoux and E. Marchal, Polymer, 22, 1199-1204 (1981)
10) J.P. Ibar, Polym Plast Tech Eng, 17(1), 11 (1981)

SPACE CHARGE INVESTIGATION IN ß-PVDF BY THERMALLY STIMULATED MEASUREMENTS.

R. M. Faria and A. Jorge.

Instituto de Física e Química de São Carlos-USP
C.P. 369, 13560 São Carlos, Brasil.

ABSTRACT

Thermally Stimulated Current measurements in ß-PVDF films were carried out under an electric applied field. A strong peak was detected around 80°C for E = 100 kV/cm, and approximately at 110°C for E = 10 kV/cm. It was interpreted to be due to storage space charge thermally released since the peak always disappeared in a second measurement. However it was a ways present when consective measurements were carried out accompanied by an invertion of the applied field. We interpreted that the released charge was not swepted away the sample, but preferably remained trapped at surface traps. We found respectively 1.0 and 1.4 eV for the activation energies of the bulk and surface traps.

INTRODUCTION

Several papers had studied effects of polarization and storage space charge in PVDF of ß structural conformation [1-5]. In this work we present a new result joined with storage bulk charge in this material. Thermally Stimulated Conductivity (TSC) measurements showed a peak which was identified to be due to space charge release. However measurements of electric field invertion showed that this charge is not withdrawal by the field from the sample but remains trapped near the surface. The glow curve of the volume traps presents retrapping, while that of the surface traps presents a first-order kinetics. The activation energies of both traps

CH2593-2/ 88/ 0000-0070$01.00 Copyright 1988 IEEE

distributions were calculated.

EXPERIMENTAL PROCEDURE

The experiments were performed using stretched commercial PVDF films obtained from Bemberg. The ß conformation was obtained from stretched α samples of 50 μm, and confirmed by x-ray diffraction pattern. The samples had thickness of 12 μm and were metallised with a very thin layer of evaporated aluminium on both sides. The surface of the electrodes were of 7 cm^2.

In the TSC measurements the samples remained under a dc electric field E at a heating rate of 1.1 °C/min.

RESULTS

We carried out TSC measurements in ß-PVDF samples in the temperature range of 20 to 140 °C, with E either 10 kV/cm or 100 kV/cm. To be sure that carriers injection did no take place, we relized isothermal measurements of the stationary current for differents applied electrical fields.We conclude that at 135°C there is not injection below 200 kV/cm.

Figure 1 shows three consecutives TSC measurements with a field of 100 kV/cm. The first one presented a large peak at about 80 °C. After a cooling under the applied field, a new measurement was carried out , and it did not present any peak. The third measurement was recorded immediately the second cooling, which was recorded in short-circuit. In this last measurement a partial recovering of the peak was verified.

Similar results were obtained with measurements with an applied electric field of 10 kV/cm, however the maximum of the peak appeared at about 110 °C. In a second measurement realized with a field of inverted polarity, the amount of charge connected with the glow curve was

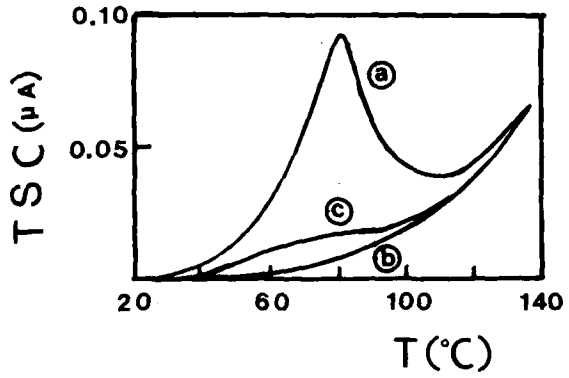

Fig. 1 - (a) First TSC measurement. (b) 2nd TSC, after cooling under applied field. (c) 3rd TSC, after cooling in short-circuit.

approximately twice that one presented in the first measurement. Figure 2 illustrates this phenomena showing two consecutives TSC cycles with the same intensity of the applied electric field (10 kV/cm), but with opposite polarities.

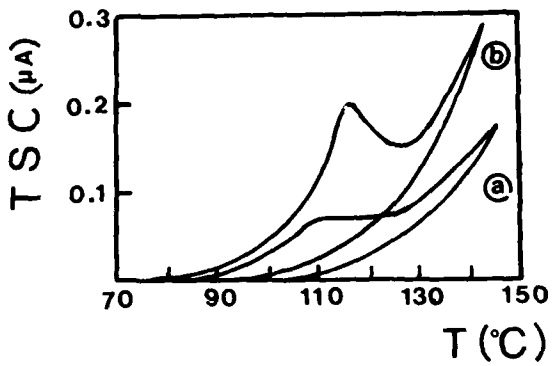

Fig. 2 - (a) First TSC cycle measurements. (b) Second cycle performed with field of inverted polarity.

The same charge presented by curve b is obtained whenever news measurements are carried out following the field inversion procedure. The glow curve of the cycle a of figure 2 (difference between the heating and the cooling), has a characteristic shape of a second order kinectics, while that of the curve b presents a characteristic of first order kinectics. So in the first case the retrapping takes place. The activation energy of the both curves were calculated by the initial rise method (figures 3a and 3b), giving 1.05 and 1.40 eV respectively for the a and the b curves.

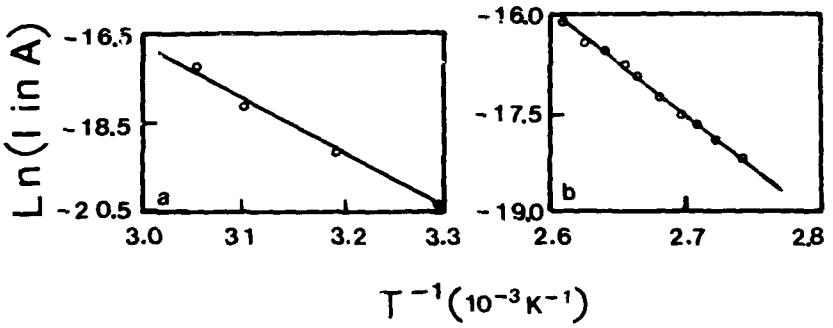

Fig. 3 - Activation energies determination by the initial rise method. (a) relative the glow curve of curve (a) of fig. 2. (b) relative to its curve (b).

DISCUSSION

Considering that a prominent peak appeared in the TSC thermogram, and that it did not is observed in a subsequent measurement, we suppose that it is due to space charge released by thermal effect. Since injection effect was already eliminated, the charge must be storaged probably into the bulk of the material. Based on the field inversion experiments (fig. 2), we also suppose that during the first TSC measurements the charge trapped in the volume of the

material were released, but they did not are withdrawal of the sample. They should be trapped in surface traps, and were again released in a next TSC measurements. This hypothese can explain the slightly recovery of the TSC presented in the figure 1 after a cooling in short-circuit. Finally the distinct values of the activation energies calculated from the A and the B curves of figure 2, reinforce this hypothese. It is well known that surface traps are deeper than that of volume.

Acknowledgements- The authors wish to thank Professor G F Leal Ferreira for many helpful discussions. They acknowledge the finantial support from TELEBRAS and CNPq.

REFERENCES

[1] N. Murayama, T. Oikawa, T. Kato, and K. Nakamura, J. Polym. Sci. Polym. Phys. Ed. 13, 1033 (1975).
[2] D. K. Das-Gupta and K. Doughty, J. Phys. D: Appl. Phys. 11, 2415 (1978).
[3] T. Mizutani, T. Nagata, and M. Ieda, J. Phys. D: Appl. Phys. 17, 1883 (1984).
[4] S. Eliasson, J. Phys. D: Appl. Phys., 19, 1965 (1986).
[5] S. T. Hughes and A. R. Piercy, J. Phys. D: Appl. Phys. 20, 1175 (1987).

SPACE-CHARGE DISTRIBUTIONS IN ELECTRON-BEAM CHARGED MYLAR AND KAPTON FILMS.

J.E.West,* H.J.Wintle,** A.Berraissoul, and G.M.Sessler

Institute for Electroacoustics, Technical University of Darmstadt, Merckstrasse 25, D-6100 Darmstadt, F.R.G.

ABSTRACT

The method of laser-induced pressure pulses (LIPP's) was used to determine space-charge distributions in 22 μm Mylar and Kapton films charged with 10 to 40 keV electron beams. For relatively low deposited-charge densities, corresponding to surface potentials below 300 V, two charge layers develop, one at the surface of the samples and one at a depth corresponding approximately to the electron range. For higher deposited-charge densities, when breakdown in the surrounding air occurs during pressurization, the surface-charge layer is positive. For deposited-charge densities in excess of 1 $\mu C/cm^2$, the space-charge layer is broader and, in the case of Kapton, is located deeper in the material than for smaller charge densities. Heating of the samples to 110 °C causes a decrease of the charge density without broadening of the charge layers.

1. INTRODUCTION

High-resolution pressure-pulse methods for measuring charge and polarization distributions [1-3] offer a valuable tool for the study of charging and discharging processes in dielectrics. So far, these methods have been most successfully applied to the polymer materials Teflon FEP and PVDF, although some measurements were also performed on Mylar PETP and on a few other polymers (for reviews, see [4,5]).

In the present paper, recent charge-distribution studies performed with one of the pressure pulse techniques, na-

* Permanent address: AT & T Bell Laboratories, Murray Hill, N. J. 07974, USA

** Permanent address: Queens University, Kingston, Ontario, K7L 3N6, Canada

CH2593-2/ 88/ 0000-0075$01.00 Copyright 1988 IEEE

mely the laser-induced pressure pulse (LIPP) method [6,7] will be discussed. In particular, new results obtained on Mylar and Kapton PI charged with monoenergetic electron beams of 10 to 40 keV energy are reported. Since the LIPP method and the procedure for charging polymers with electron beams have been described before [2,6-8], they will not be discussed in this paper. For the following it should be remembered that the LIPP responses correspond directly to charge density.

2. DEPENDENCE OF DISTRIBUTIONS ON ELECTRON-BEAM ENERGY

LIPP responses of 22 μm Mylar films metalized on one surface and charged through the nonmetalized surface with electron beams of various energies to low surface potentials are shown in Fig. 1. The pressure pulse enters the film through the metalized rear side at a time marked "R" in the figures, traverses the film in 9 to 10 ns, is reflected from the nonmetalized front side ("F"), traverses the film in opposite direction, is then reflected from the rear surface, etc. Thus, the time interval RF corresponds to the thickness of the film.

Figure 1 indicates that the space charge deposited by the 20, 30, and 40 keV electron beams accumulates in two layers, one at the nonmetalized surface (at F) and one in the volume. For the 10 keV electrons, only a single layer is found; this may be due to insufficient resolution (1 to 2 μm). Also visible in all responses are the positive induction charges on the rear electrode (at R) and the signals generated by the reflected pressure pulse and by later reflections (signals arriving later than F). The depth of the space-charge layer is 6 and 12 μm for the 20 and 30 keV electron beams, respectively. Assuming that 1/3 of the charge is located in the surface layer and 2/3 in the space-charge layer, the charge centroids correspond

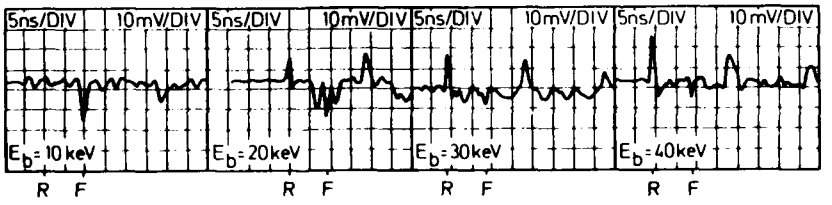

Fig. 1: LIPP responses corresponding to charge distributions of 22 μm Mylar charged to surface potentials of less than 300 V with electrons of energy E_b as indicated.

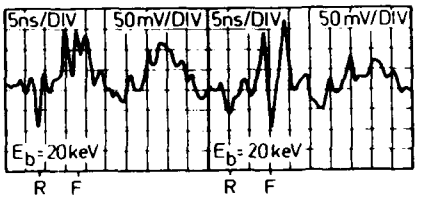

Fig. 2: LIPP responses of 22 μm Mylar charged with 20 keV electrons to 330 V (left) and 660 V before breakdown (right). Amplifier gain -10.

approximately to the centroid positions found by split-Faraday cup measurements [9-11] and by electron transmission measurements [10] on two-side metalized PETP.

Other charge-distribution studies in electron-beam charged polymer films were performed on two-side metalized samples and showed a single charge layer located close to a depth corresponding to the range of the electrons [6,7]. Smaller additional layers were occasionally found in FEP in the vicinity of the irradiated surface [6]. The origin of the large surface layer observed on Mylar and also on Kapton in the present study is not yet clear. It could be partially due to ohmic relaxation [12] or to dipole alignment in the electric fields of the deposited charge or it might originate from pre-existing charges in the polymer samples. These possibilities are presently under study.

3. INFLUENCE OF QUANTITY OF DEPOSITED CHARGE

LIPP responses of electron-beam charged, one-side metalized Mylar and Kapton samples do not always show two negative charge layers. If the surface potential is raised above 400 V, the surface layer reverses its sign. This is shown in Fig. 2, where LIPP responses of samples charged to different potentials are compared. The reversed surface peak in the right part of Fig. 2 at F (note that a negative-gain amplifier has been used) can be explained by breakdown during pressurization, when the Paschen limit is exceeded. The breakdown deposits a positive charge which overcompensates the negative surface charge but leaves the space-charge layer intact.

As long as the quantity of charge deposited in the film is below about 0.1 $\mu C/cm^2$, corresponding to surface potentials of about 800 V, the internal fields in the film are not so high as to cause significant charge drift or internal breakdown. This follows from a comparison of the two parts of Fig. 2: Both samples show a depth of the space-charge layer of about 6 μm.

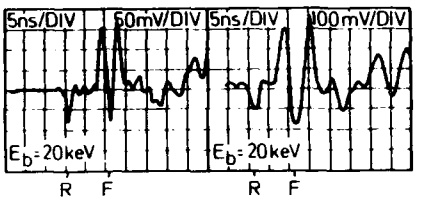

Fig. 3: LIPP responses of 22 μm Kapton charged with 20 keV electrons to integrated current densities of 25 nC/cm^2 (left) and 1.6 μC/cm^2 (right). Amplifier gain -10.

The situation changes for films with deposited charge densities well in excess of 0.1 μC/cm^2. Figure 3 depicts results for Kapton samples charged with very different integrated current densities. While the charge layer in the weakly-charged sample has a depth of 5 μm, the layer in the highly-charged sample is located at 9 μm depth and has broadened. This indicates that the high fields generated in the film during charging cause significant charge drift or even breakdown. In the Mylar samples, a broadening but no relocation of the charge layer is observed.

4. HEATING EFFECTS

Thermally-stimulated current experiments with Mylar and Hostaphan electrets charged with corona methods have shown peak regions at 80 and 110 °C [13,14]. These peaks were interpreted as being due to dipole alignment in the field of the space charge and to space-charge dissipation, respectively [13-15]. Heating to 110 °C should therefore significantly diminish the space charge.

LIPP responses obtained for electron-beam charged Mylar films before and after a linear temperature rise to 110 °C are shown in Fig. 4. As seen from the figure, the heating causes a decay, but no spreading of the surface-charge and volume-charge layers in the film. This indicates that charge release with slow retrapping and/or ohmic compensation is controlling the charge decay on the surface and in the volume at temperatures around 110 °C. Charge release with fast retrapping can be excluded.

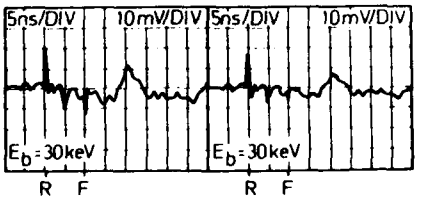

Fig. 4: LIPP responses of 22 μm Mylar charged with 30 keV electrons before (left) and after (right) linear heating (4 °C/min) from 25 to 110 °C.

5. CONCLUSIONS

The application of the LIPP method to electron-beam charged Mylar and Kapton films has provided new experimental results about space-charge distributions after charging and during charge decay. These results may be of value in future theories of charge transport in polymers.

Acknowledgments. The authors are indebted to the Stiftung Volkswagenwerk for providing the laser used in the experiments. One of the authors (H. J. W.) also acknowledges a research grant from the DAAD.

LITERATURE

[1] C. Alquié, G. Dreyfus, J. Lewiner, Phys. Rev. Lett. 47, 1483 (1981).
[2] G. M. Sessler, J. E. West, R. Gerhard, Polym. Bulletin 6, 109 (1981); Phys. Rev. Lett. 48, 563 (1982).
[3] W. Eisenmenger, M. Haardt, Solid State Communic. 41, 917 (1982).
[4] G. M. Sessler, Ed., "Electrets", Topics in Applied Physics Vol. 33, 2nd Edition, Springer Verlag, 1987.
[5] R. Gerhard-Multhaupt, IEEE Trans. Electric. Insulat. EI-22, 531 (1987).
[6] G. M. Sessler, J. E. West, R. Gerhard-Multhaupt, H. von Seggern, IEEE Trans. Nucl. Sci., NS-29, 1644 (1982).
[7] R. Gerhard-Multhaupt, M. Haardt, W. Eisenmenger, G. M. Sessler, J. Phys. D: Appl. Phys. 16, 2247 (1983).
[8] B. Gross, G. M. Sessler, J. E. West, J. Appl. Phys. 45, 2841 (1974).
[9] G. M. Sessler, J. E. West, H. von Seggern, J. Appl. Phys. 53, 4320 (1982).
[10] B. Gross, R. Gerhard-Multhaupt, K. Labonte, A. Berraissoul, Colloid & Polym. Sci. 262, 93 (1984).
[11] A. Berraissoul, R. Gerhard-Multhaupt, B. Gross, Appl. Phys. A39, 203 (1986); A. Berraissoul, Fortschritt Berichte VDI, Reihe 21, Nr. 21.
[12] B. L. Beers, V. W. Pine, Proceed. Spacecraft Charging Technology [illegible] 1980, pp. 17 - 32.
[13] H. von Seggern, J. Appl. Phys. 52, 4086 (1981).
[14] W. A. Schneider, J. H. [illegible]dorff, R. Gerhard-Multhaupt, 1983 Annual Report, CEIDP, pp. 441 - 446.
[15] H. von Seggern, 1984 Annual Report, CEIDP, pp. 468 - 473.

ELECTRON-BEAM POLING OF VERY THIN PVDF- AND VDF-TRFE COPOLYMER FILMS

Doris Schilling, Siegfried Schuler and Klaus Dransfeld;

Fakultät für Physik, Universität Konstanz, Postfach 5560, D-7750 Konstanz, FRG

A new method of electron-beam poling of very thin ($d \approx 100$ nm) Polyvinylidenefluoride (PVDF)- and Vinylidenefluoride-Trifluoroethylene copolymer (VDF-TrFE) films, cast from solution on a well polished metal-substrate, is presented. The penetrating electron beam passes through the thin polymer-film and its main energy dissipates inside the metal support. Due to the secondary electron emission from the film-surface a positive surface potential is left on the polymer producing the poling field towards the grounded metal-substrate. Using a chopped electron beam ($E_O = 5$ keV to 30 keV) poling-patterns have been created on the film. These polarized regions having a lateral resolution in the submicron-range are subsequently imaged in the scanning electron microscope at low beam intensity using the potential contrast method. The mechanism for the generation of contrast is discussed.

INTRODUCTION

In order to generate the well known piezo-, pyro- and ferroelectric properties of Polyvinylidenefluoride (PVDF), a novel poling method has recently been introduced by Sessler et al. [1] and Gross et al. [2]. These authors used an unfocussed monoenergetic electron beam to irradiate uniformly the sizeable area of the polymer. This technique is quite useful to generate piezoelectric monomorphs of large area [3].

In order to produce poling patterns of small lateral extension on PVDF and Vinylidenefluoride-Trifluoroethylene (VDF-TrFE) copolymer films, we used a focussed electron beam to be scanned across the sample for our poling experiments. The generated polarization profiles were examined lateron by the method of piezoelectrically generated pressure step (PPS) [4]. Polarized structures have been produced by chopping the electron beam during the poling process and afterwards were imaged in the scanning electron microscope (SEM) at low beam intensities using the method of potential contrast [5]. The horizontal resolution of the polarized

CH2593-2/ 88/ 0000-0080$01.00 Copyright 1988 IEEE

structures, however, is limited by the diffusion volume of the primary electrons inside the target reaching a diameter of the order of the penetration depth i.e. mostly above 1 μm.

As our aim is to produce poling patterns in the submicron range, we extended the experiments to the polarization of very thin (d $\approx$ 100 nm) VDF-TrFE copolymer films. This seems to be interesting for two reasons:
1) Decreasing the thickness of the polymer film is accompanied by a decrease in crystallite size as reported for 75/25 VDF-TrFE copolymer films by Kimura and Ohigashi [6].
2) We can apply a novel method of electron beam-poling, namely the "poling in the transmission mode" thereby avoiding the limitation in lateral resolution of the polarized structures mentioned above.

The characteristic feature of the new poling technique - schematically represented in Figure 1 - is the fact that the electron energy and charge are mainly deposited inside the metallic substrate. The poling field is created between the grounded metal plate supporting the PVDF- and VDF-TrFE copolymer film and the beam exposed polymer-surface which is positively charged due to secondary electron emission. We have found strong evidence (i.e. a "positive" polarization) for a successful application of the described poling technique [4,7]

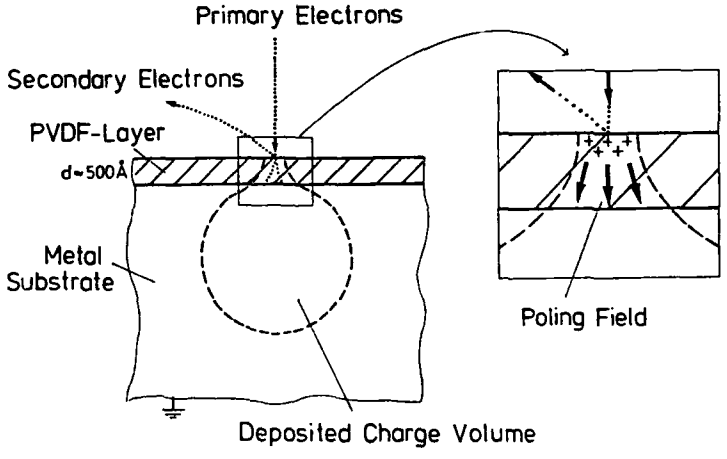

***Figure 1:** Schematic diagram showing the principle of poling very thin PVDF- and VDF-TrFE copolymer films using high energy electrons in the transmission mode.*

With regard to a possible application of PVDF and VDF-TrFE copolymers as a material for data storage, the described new poling method would be quite useful. Our main purpose here is to find out the minimum lateral resolution for the poling patterns and to understand the mechanism of creating such charged structures. First experimental results are reported here.

EXPERIMENTAL DETAILS

VDF-TrFE copolymer films of composition 50/50, 60/40 and 75/25 have been cast from a 1%-solution in Ethylmethylketone by spin-coating on a well polished copper substrate. The rotation frequency of 1250 rpm resulted in a film thickness of about 100 nm. Afterwards the samples have been irradiated with a focussed electron beam, whose energy was varied between 5 and 30 keV, and a beam-current in the order of 1 nA. The scanned area was changed between 15 x 15 μm^2 and 80 x 80 μm^2 with a scan lasting about 100 s. The electron beam was chopped with a different on- and off-time ratio thereby creating stripes of different width but for the same grating constant.

The polarization patterns created in this way were imaged lateron in the SEM by means of potential contrast in the secondary electron emission mode - a technique which is preferably used for imaging domain structures in ferroelectrics [8,9]. In order to avoid further charging of the polymer film the beam current was reduced to values below 1 pA. It must be emphasized that principally for thin polymer layers on a well conducting and grounded metal substrate there is no need to work at the "second crossover voltage" where (in the case of compact objects) the current of the incident electrons is balanced by the current of the secondary electrons leaving the surface, and where isolating materials can be examinated without charging. As in our case most of the primary electrons pass through the sample, charging is mainly due to secondary electron emission. Therefore it is quite useful to work at the highest energies possible in order to lower the secondary yield and to reduce the beam diameter and spot size leading to a higher lateral resolution.

RESULTS AND DISCUSSION

The SEM micrographs in Figures 2a) to 2d) show our first results of patterns generated by a chopped electron beam of 20 keV with a on/off ratio of 10/90 and 90/10 respectively on a 50/50 VDF-TrFE copolymerfilm of 100 nm in thickness. The photographs in Fig. 2a) and 2c) have been taken at 2 keV for a magnification-fac-

tor of 1200. Those in Fig. 2b) and 2d) represent the same samples at a magnification of 6000. Dark stripes on a light background are observed indicating that the contrast results from positive surface charges on the sample. It can be seen from the photographs 2a) and 2b) that the width of stripes does not exceed 500 nm whereas Figures 2c) and 2d) show the dark stripes are separated by less than 500 nm.

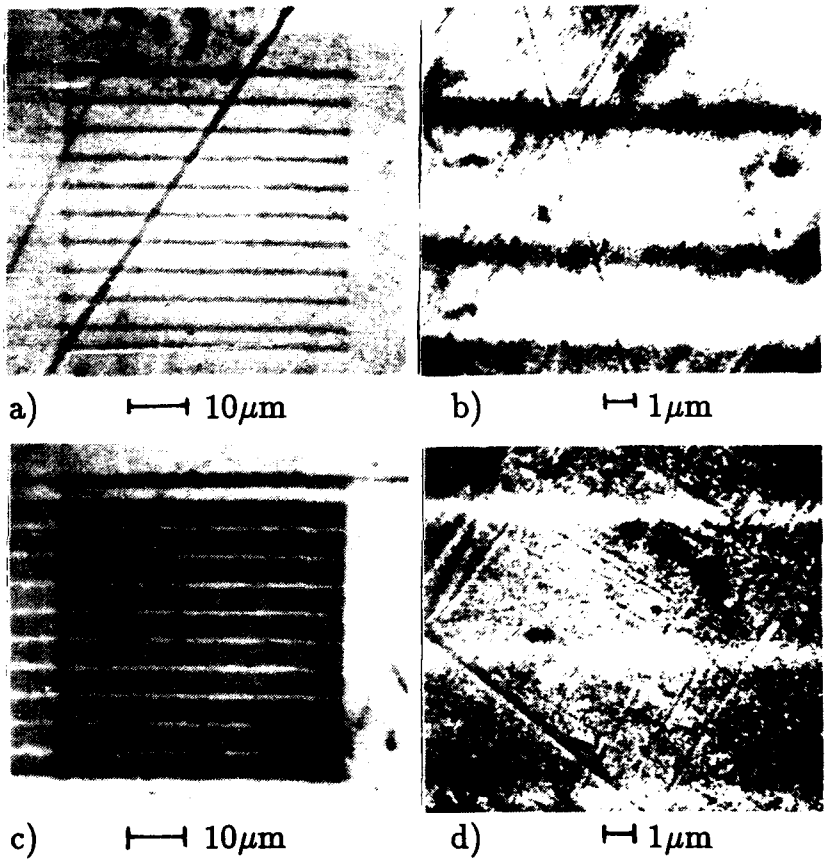

Figure 2: *Stripes polarized on a 100 nm thick layer of 50/50 VDF/TrFE-Copolymer in the transmission mode for a on-to-off ratio of 10/90 (a and b) and 90/10 (c and d) respectively. The photographs are taken for electrons of 2 keV at normal incidence and at magnifications of 1200 (a and c) and 6000 (b and d) respectively.*

From a comparison of micrographs taken in the secondary emission mode (see Fig. 3a)) with those generated by elastically backscattered electrons (see Fig. 3b)) for the same position on the thin copolymer samples we get a strong evidence that the observed contrast is due to surface potentials. As can be seen in Figures 3a) and 3b) both photographs show the same topographic structures but only in the secondary image (3a), which is mainly generated by low energy electrons the superimposed poling pattern is visible.

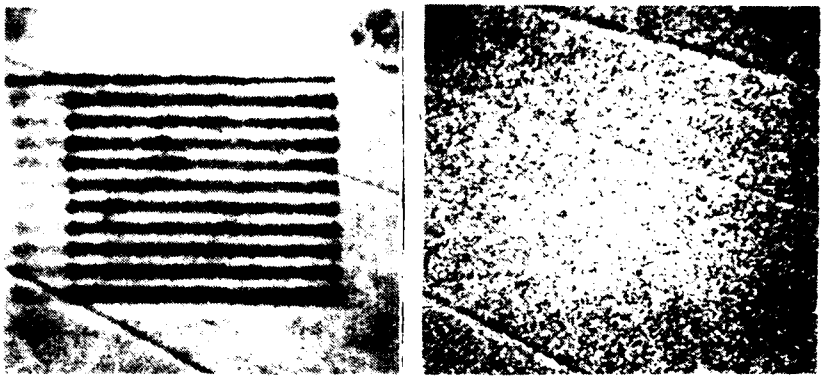

Figure 3: *Comparison between a SEM micrograph taken in the secondary-electron-mode (a) and in the backscattering-electron-mode (b) for exactly the same position on the sample. Only the secondary image shows the poling pattern.*

A destruction of the sample by heating effects, and probably also by chemical changes can be excluded as a possible origin of contrast because the main energy and charge of the electron beam is transferred to the substrate. Furthermore investigations with optical microscopy in the transmission and reflection mode as well as between crossed polarizers did not show any changes between irradiated and not-irradiated regions of the samples.

Concerning the origin of the observed contrast some questions still remain open, for example if the observed variation of the potential results from oriented ferroelectric dipoles or from fixed charges forming an electret. We observed a high thermal and a longtime stability of the polarization patterns on the copolymer films under investigation even some ten degrees above the Curie-temperature which is well known for thick copolymer foils from dielectric [10] or structural data [11,12] as well as from Brillouin Scattering experiments [13]. It is worth mentioning that for a somewhat

thicker sample (d ≈ 500 nm) we observed a typical pyroelectric activity [7] when heating during the SEM-observation, but for 100 nm copolymer films we did not yet succeed observing a pyroelectric response.

As for very thin (60 nm) VDF-TrFE copolymer layers a considerable increase of coercitive field is reported by Kimura and Ohigashi [6], we conclude that other ferroelectric properties may vary with thickness too, for example the Curie temperature may rise when lowering the film thickness. Furthermore the increasing influence of image charges in the metal substrate with dereasing film thickness may lead to the interesting stability of the poling patterns observed in our thin films even at elevated temperatures.

CONCLUSIONS

Irradiating thin films of ferroelectric polymers with a focussed electron beam in the transmission mode represents a novel technique for generating strong poling patterns in the submicron range.

The observation of the generated structures in scanning electron microscope strongly indicates that surface potentials on the samples are responsible for the contrast origin. Whether this potential contrast is due to fixed charges or to oriented dipoles in the polymer still remains an open question.

The charge patterns created in the thin films remain stable for a long time if the temperature is raised well above the bulk Curie-temperature of the material.

We are aware that for very thin polymer layers the physical and especially the electrical properties may differ from those of thick foils. Therefore it is necessary to further examinate, in the first place, the temperature dependent dielectric behaviour in order to study the Curie-temperature of very thin films.

In our view it is possible to optimize the irradiation conditions and thereby reduce the lateral width of polarized patterns by at least one order of magnitude. Using electrostatic beam blanking, experiments of very short poling time for very small polarized domains will be done.

REFERENCES

[1] G.M. Sessler, R. Gerhard-Multhaupt, J.E. West,
A. Berraissoul, "Nondestructive High-Resolution Measurement

of Charge, Polarization and Piezoelectricity Distribution in Thin Dielectric Films, *Proc. 2nd Intern. Symp. on Nondestr. Charact. of Mat.* II, 1387 (1986)

[2] B. Gross, R. Gerhard-Multhaupt, A. Berraissoul, G.M. Sessler; "Electron-Beam Poling of Piezoelectric Polymer Electrets", *J. Appl. Phys.* vol. 62, 1429 (1987)

[3] E Fukada, G.M. Sessler, J.E. West, A. Berraissoul, P.Günther, "Bending Piezoelectricity in Monomorph Polymer Films", *J. Appl. Phys.* vol 62, 3643 (1987)

[4] D. Schilling, K. Dransfeld, E. Bihler, K. Holdik, W. Eisenmenger, "Polarization Profiles of Electron-Beam Polarized Polyvinylidene Fluoride Films" submitted to *J. Appl. Phys.*

[5] D. Schilling, K. Dransfeld, "Imaging of Polarized Regions in Ferroelectric Polymers by Scanning Electron Microscopy", 6th Europ. Meeting on Ferroelectricity, Poznan, (1987), to be published in *Ferroelectrics*

[6] K. Kimura, H. Ohigashi, "Polarization Behaviour in Vinylidene Fluoride-Trifluoroethylene Copolymer Thin Films", *Jpn. J. Appl. Phys.* vol. 25, 383 (1986)

[7] D. Schilling, "Ferroelektrische Polymere als mögliche Datenspeicher", Ph. D. Thesis, University of Konstanz 1988

[8] R. Le Bihan, C. Sella, "Study of Domains of Ferroelectric Crystals with the Scanning Electron Microscope", *J. Phys. Soc. Jap.* vol. 28, 377 (1970)

[9] D.G. Coates, N. Shaw, "Direct Observation of Ferro-Electric *Domains* in Triglycine Sulphate Using the Scanning Electron Microscope", Sept. Congr. Intern. de Microscopie Électronique, Grenoble (1970)

[10] Y. Tajitsu, A. Chiba, T. Furukawa, M. Date, E. Fukada; "Crystalline Phase Transition in the Copolymer of Vinylidenefluoride and Trifluoroethylene", *Appl. Phys. Lett.* vol. 36, 286 (1980)

[11] A.J. Lovinger, T. Furukawa, G.T. Davis, M.G. Broadhurst, "Crystallographic Changes Characterizing the Curie Transition in Three Ferroelectric Copolymers of Vinylidene Fluoride and Trifluoroethylene: 1. As Crystallized Samples", *Polymer* vol. 24, 1225 (1983)

[12] A.J. Lovinger, T. Furukawa, G.T. Davis, M.G. Broadhurst, "Crystallographic Changes Characterizing the Curie Transition in Three Ferroelectric Copolymers of Vinylidene Fluoride and Trifluoroethylene: 2. Oriented or Poled Samples", *Polymer* vol. 24, 1233 (1983)

[13] D. Schilling, M. Lehndorff, K. Dransfeld, "Inelastische Lichtstreuung an VDF/TrFE-Copolymeren", DPG-Frühjahrstagung Sektion Polymerphysik, Kaiserslautern (1986)

A SUMMARY OF CORONA CHARGING METHODS

José A. Giacometti, G.F. Leal Ferreira and B. Gross

Instituto de Física e Química de São Carlos
Universidade de São Paulo - CP 369
13560 - São Carlos - Brasil

ABSTRACT

Corona charging is a powerful method for studying storage and electric charge transport in dielectric films. The development of this technique for the study of polymer foils is summarized. The improvement achieved with the use of a biased vibrating grid, allowing the measurement of the potential build-up is commented, as well as the latter one keeping constant the charging current. Other developments aimed to get more uniform charge deposition are also discussed.

INTRODUCTION

Since the fifties corona discharge is being used extensively in photocopyng machines to charge the photoconductors in order to achieve the image transference[1]. Later, it was sucessfully employed to charge dielectric foils aiming to the study of storage and charge transport in such materials and to large scale electret production[2].

This paper endeavors to briefly review the methods of corona charging, mainly the corona triode, directed to the investigation of transport properties. In this technique both the sample surface potential as well the sample current may be measured as function of time, during and after the charging. The analysis will be restricted to the the point to plane simmetry.

THE EARLIER PROCEDURES

The most simple way to achieve a charge deposition over a sample is to expose, for

CH2593-2/ 88/ 0000-0087$01.00 Copyright 1988 IEEE

short or long time, the dielectric surface directly to a corona point discharge, see the scheme of figure (1a). This procedure allows to reach high surface densities but the final sample voltage and the surface charge uniformity is not easily put under control. After the charging the sample surface potential V_S, can be monitored as function of time. A problem related with the V_S measurement is the time lost between the end of charging and the beginning of the decay, which may be important, at least, for samples exhibiting fast potential decay. A improved setup presented by Weinberg et al[3] in 1975, by means of which the steady state potential during charging can was obtained by a comparison method with a reference sample.

THE CORONA TRIODE

Later, an important improvement appeared[4], a metallic grid was inserted between the point and the sample to constitute the so called corona triode, as figure (1b) shows. Either the grid or the sample holder may be biased using a voltage supply. This setup allows to control the steady surface potential and the charging uniformity. However, the charging current, dependent on the voltage between the grid and sample surface, tends to decrease. The final sample voltage is equal to the grid bias voltage. By means of a vibrating grid it is possible to measure simultaneously with the current, the sample surface potential during as well after charging (with the requirement that the sample is charged uniformly). The potential decay may also be easily measured. The corona triode is very similar to the scorotrons[1] developped for use in photocopyng machines (using cylindrical geometry). Due its pratical interest several papers discussed its electrical characteristics[5].

THE CORONA TRIODE WITH CONSTANT CURRENT

The corona triode showed to be a very nice and inexpensive technique to produce charged surfaces with a high degree of lateral charge uniformity. On the other hand, since the

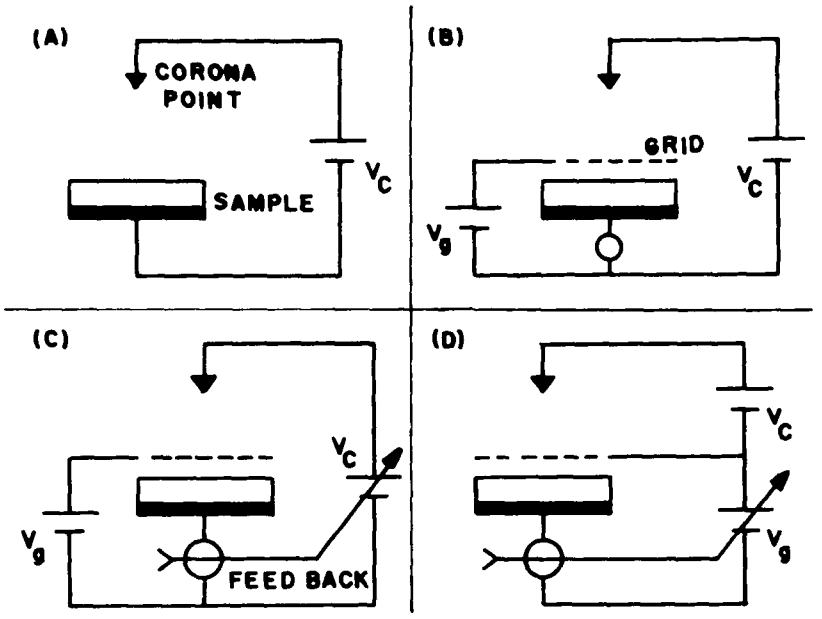

Figure (1). Schematics of setups for corona charging.

charging current decreases as function of the time, this makes the interpretation of the results difficult to be made. To overcame such a problem another improvement was added to the triode[6]. A feedback loop as figure (1c) shows, which detects the total current through the sample, acts on the corona point voltage allowing it to control the sample charging current, keeping it at a constant value I_o. This greatly eases the interpretation and allows to have a control during the charging process. From the total current equation we get

$$I_o = I_c(t) + C\ dV_s(t)/dt$$

were C is the sample capacity and $I_c(t)$ is mean conduction current. This equation shows that for the limiting case of a pure insulating foil the potential will increases linearly as function of time while for a leaky sample it will increase sublinearly. From the above equation we see that actually we have access to

$I_c(t)$, since I_o, C and $V_s(t)$ are known. Processes caracterized by a conductivity may easly be detected.

A new version of a corona triode with constant current where the sample current control is performed by controling the grid voltage, see figure (1d), is now under development[7]. The preliminary results shows that the operation of the triode can be extended over a large interval of charging currents and the sample charging uniformity may be further be improved.

It should be mentioned that at paralelling the increasing of the corona method a great advance in measuring devices were obtained: improved surface potential measurements, the widespread use of the open circuit thermal stimulation and charge profiles measurements, starting with the heat pulse technique[8] and even more involved ones (LIPP, LIMM)[9].

THEORETICAL DEVELOPMENTS - INFORMAL

The theoretical attempts to interpret the experimental results obtained under the corona charge method were responsible by the great of simplified models and exact calculations (Wintle, Perlman, Rudenko, Sessler, West, Batra, Seki, Reiser, our group and many others) appeared in the literature in the seventies involving space charge kinetics. In these first steps, models susceptible of analytic solution were integrated but many times the results did not duplicate the experimental ones, of course because they were oversimplified. The need for computer integration grew and, in this side, van Turnhout, von Seggern and Chudleygh were pioneers. Application of the transport equations to the new wave of dispersive transport of Scher and Montroll were accomplished (Carrano and Ferreira) but the results were never used seriously for interpretation of space charge motion. We apologized the missing of important researcher names in this informal and short appraisal (there is no space for references). Interesting phenomena, like the cross over effect by which the discharge is more effective

for higher initial charging, were discovered and discussed (Yeda, Perlman, etc..).

Before finishing, it should be mentioned that in most cases the corona charging method was used in polymer foils. The complex nature of these materials makes difficult to get a comprehensive set of data for them. It is not only the bulk that is complicate, but also the surface, that plays an active part in the trapping process. The pioneers thought that eliminating the injection electrode by using the corona charging technique, the bulk properties would appear clearly. But it proved not to be the case and more, it was found that the chemical products produced by the corona discharge may modify the surface or change the charge injection process.

ACKNOLEDGEMENTS: TELEBRAS, FAPESP, CNPQ and FINEP are thanked for affording improved structure to our Electret Group Prof. Bernhard Gross by their financial support.

REFERENCES:

1- R.M.Schaffert."Electrophtography". Focal 1975
2- G.M.Sessler, ed."Electrets". Springer-Verlag Berlin-1980
3- Z.A.Weinberg, D.L.Mathies, W.C. Johnson and M.A. Lampert. Rev. Sci. Instrum. vol46, pp201-203(1975)
4- R.A. Moreno and B. Gross. J.Appl.Phys., vol47, pp3397-3402(1976).
5- J. A. Giacometti. J. Phys. D: Appl. Phys., vol 20, pp675-682(1987).
6- B. Gross, J. A. Giacometti and G. F. Leal Ferreira. Ann. Rep. IEEE-CEIDP, pp39-44(1979).
7- J.A. Giacometti and J.S. Campos. see in this conference the paper "Constant current corona triode with bias grid voltage control"
8- R.E. Collins. Appl. Phys. Letts. vol.26, pp675-677(1975)
9- S.B. Lang and D.K. Das-Gupta. J. Appl.Phys., vol59, pp2151-2160(1986)
- P. Laurenceau, G. Dreyfus and J. Lewiner. Phys. Rev. Letts. vol38, pp46-49(1977)
- G.M. Sessler and R.Gerhard-Multhaupt. Radiat. Phys. Chem., vol23, pp363-380(1984)

SPACE CHARGE FORMATION RELATED TO THE MORPHOLOGY OF POLYMERS

Gregor Krause (*), Dietmar Meurer (*), Doris Klee (#)

(*) Institut für Allgemeine Elektrotechnik und Hochspannungstechnik der RWTH Aachen
Schinkelstr. 2, D-5100 Aachen, FRG

(#) Deutsches Wollforschungsinstitut
an der RWTH Aachen
Veltmanplatz 8, D-5100 Aachen, FRG

ABSTRACT

Thermally stimulated current measurements were carried out on polypropylene sheet samples to get information about temperature dependent space charge formation. The relaxation peak at crystallite melting temperature is related to the separation of stored charge carriers from helix-molecules in the crystalline region.
The method of thermally stimulated infrared spectroscopy reveales the space charge decay at lower temperatures being connected to the relaxation of helices embedded in the amorphous regions.
Observating the growth of electrical trees confirms the fact that charge carriers attach mainly to interfaces of the spherulites (amorphous regions) causing a privileged direction for an electrical breakdown.

1. INTRODUCTION

It is quite obvious that improving the electrical properties of polymers needs a better understanding of the processes occuring in the material under high electrical field stress.
Thermally stimulated depolarisation current measurements (TSD) are commonly used to investigate conduction properties and space charge phenomena in a wide range of temperature and field strength.
To find connections between electrical relaxations and structural or morphological changes of the polymer the technique of thermally stimulated fourier transformed infrared spectroscopy (TS-FTIR) is developed.

CH2593-2/ 88/ 0000-0092$01.00 Copyright 1988 IEEE

2. EXPERIMENTAL

TSD measurements are carried out on polypropylene sheets of 1.5mm thickness. Two manufacturing processes are applied forming different morphological properties: injection moulding and extrusion.
The electrodes of the TSD test cell are heated by a silicon oil circuit from room temperature up to the melting point with a linear heating rate of 0.6K/min. The loading voltage range is up to 100kV DC. Temperature programming and data aquisition is done by a microcomputer and an electrometer (Keithly 617).
To get information about thermally stimulated structural changes a special test cell with temperatur controller is applied to a conventional FTIR-spectrometer (Nicolet 20DX3). To compare data from TS-FTIR and TSD the same heating rate of 0.6K/min is used in both experiments. IR spectra are obtained automatically every 5K from a polypropylene foil sample of 150μm thickness. A microcomputer calculates the integral absorption of some special bands that can definitely be assigned to crystalline and non-crystalline structures.

3. RESULTS

The TSD spectrum of extruded polypropylene shows five distinct relaxation mechanisms (α_{1-5}). Each of the five peaks reacts sensitive to the polarisation parameters (Fig. 3b).

3.1 Melting of the crystalline regions

It is obvious that the α_5 peak at a temperature of about 150^{o}C indicates the melting point of the crystalline phase. At the same temperature a "rolling-up" process of the helical structure of the molecules occurs. For that reason the α_5 relaxation can be explained as a separation of charge carriers from the helix molecules in the crystalline structures of the polymer.
As a proof TSD spectra from samples with varing content of helix molecules meaning a variation of crystallinity are measured. Fig. 1 shows the rise of the α_5 current peak with increasing crystallinity.

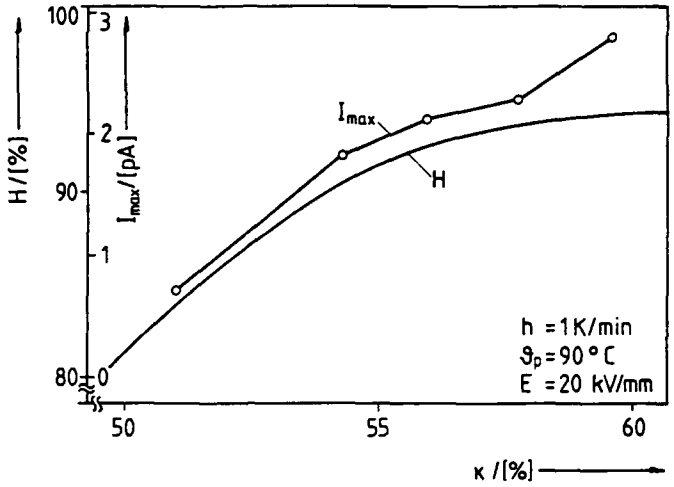

Fig. 1: Correlation of crystallinity and content of helix-molecules with the amplitude of the α_5 peak [1]

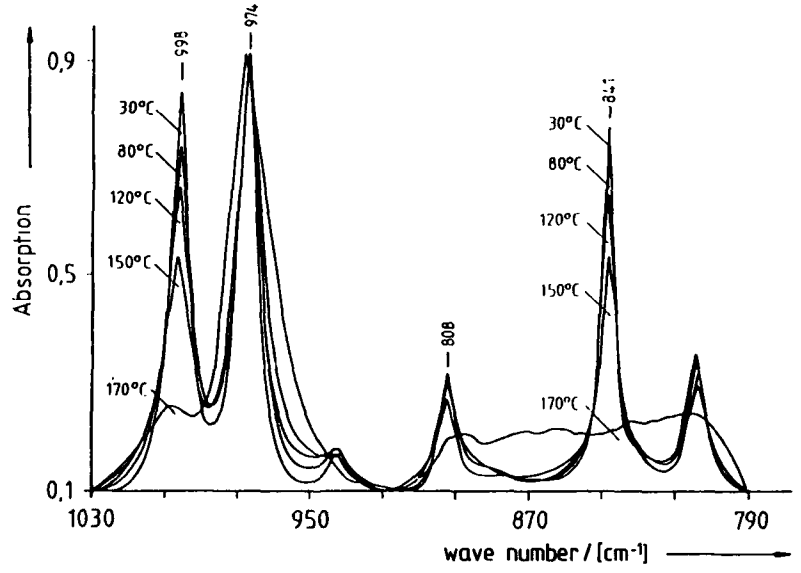

Fig. 2: TS-FTIR spectra of polypropylen

3.2 Space charge decay in the amorphous regions

The TS-FTIR spectra of polypropylene show significant changes of some absorption bands due to structural relaxation mechanisms (Fig. 2). The decrease of the absorption bands at wavenumber 998cm^{-1} and 841cm^{-1} represents the melting of the crystalline phase. The so called internal standard bands at 974cm^{-1} and 808cm^{-1} are responsable for structural relaxations in the amorphous phase [2].

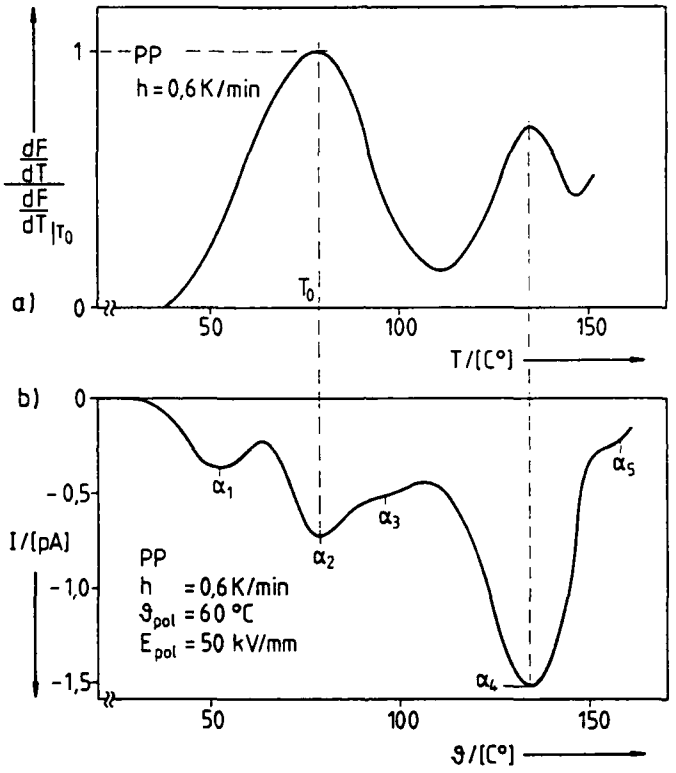

Fig. 3: Structural relaxation of the amorphous region correlated to space charge release

A comparison of the differentiation of the measured integral absorption of these bands versus temperature with the TSD current (representing the differentiation of the charge released from the volume) proves the

space charge decay at lower temperatures beeing connected with the relaxations in the amorphous phase (Fig. 3). It is to be supposed that charge carriers are separated from the intermediate areas by movement of the helices in the amorphous region even far below the temperatures where the helix molecules of the three-dimensional unit cells start to relax.
The influence of the non-crystalline regions is studied in (Fig. 4) by enlarging the fine spherolitic surface layer (enlarging the amount of the amorphous part) at injection moulded polypropylene samples: increasing the surface layer results in a larger α_4 peak and as well in a smaller α_5 relaxation.

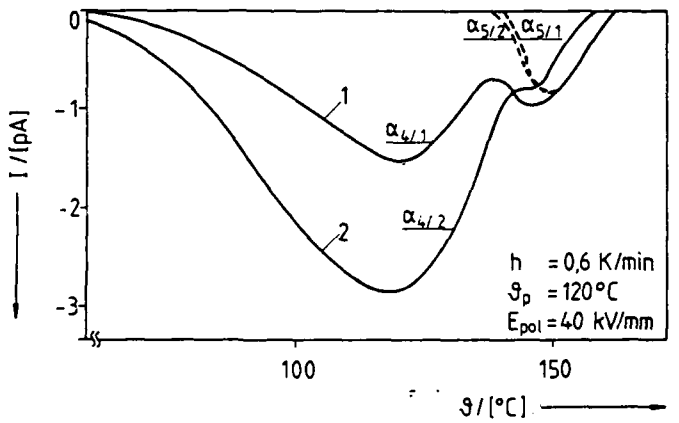

Fig. 4: TSD of injection moulded polypropylene with variing surface layers [3]

3.3 Electrical treeing in polypropylene

Depending on stressing parameters like temperature, field strength etc. stable space charges attach mainly to interfaces between the spherulites: the so called amorphous region. Monitoring the growth of electrical trees reveales that the branches prefer the direction of the structural boundaries where the charge is supposed to be fixed (Fig. 5).

Fig. 5: Initial state of an electrical tree in polypropylene

4. ACKNOWLEDGEMENT

This work has been financially supported by the Deutsche Forschungsgemeinschaft, Sonderforschungsbereich 106 : *Korrelation von* Fertigung und Bauteileigenschaften bei Kunststoffen.

REFERENCES

[1] B. Fruth
Über das Leitungsverhalten und den Raumladungsaufbau in teilkristallinen Kunstatoffen
Doct. Thesis, RWTH Aachen, 1986

[2] J.B. Luongo
Infrared study of polypropylene
Journ. of appl. Polymer Sience, No. 9, 1960

[3] B. Fruth, H.J. Richter, D. Meurer
Electrical conduction and space charge formation in semicrystalline polymers
IEEE Trans. o. El. Ins., Vol. EI-21, No. 3, 1986

A MATHEMATICAL MODEL TO STUDY THE INFLUENCE OF SPACE-CHARGES IN A NEEDLE-PLANE-ARRANGEMENT IN A POLYMER

Horst Döpper

Fachhochschule Giessen-Friedberg, FB E1
Wiesenstrasse 14, 6300 Giessen FRG

ABSTRACT

In polymeric insulating materials tree initiated breakdown is supported by space charges. A mathematical model is developed to study the influence of space charges on the field strength of a needle-plane-arrangement in polymeric materials. The model enables the consideration of the carrier injection at the metal-polymer contact. The movement of the charge carriers is dependant on field strength, temperature and carrier mobility. It is possible to regard the influences of electrons and holes, but in this paper the latter were neglected. The effectiveness of the method is shown by examples of thermal stimulated currents.

1. INTRODUCTION

Sometimes the high resistivities of high-grade polymeric insulating materials (for example polyethylene) are of disadvantage for the dielectric strength. If charge carriers are injected into the material, they form space charges with time constants in the order of months. These space charges cause extreme high field stresses, especially, when investigating an AC-stressed sample, the polarity of an electrode is contrary to the sign of the space charges. In this case the initiation of electrical treeing can be expected. The charge carriers will penetrate into the dielectric material at places, where the local field intensity caused by field inhomogenities is extremely high. In order to simulate realistic cases, experiments using inhomogeneous samples were carried out as needle tests.

The metal-polymer contact controls the injection of electrons into the polyethylene. Two effects are of importance, the Richardson-Schottky effect and the Fowler-Nordheim effect (tunnel effect). The latter is only of importance if the field strength exceeds 3 MV/cm. The conduction is of a hopping-type, the effective electron mobility is dependant on the temperature and on the kind of traps (deep or shallow). To reduce the number of unknown parameters, the influence of the

CH2593-2/ 88/ 0000-0098$01.00 Copyright 1988 IEEE

field intensity on the mobility (Poole-Frenkel effect) is neglected.

Tanaka [1] has proposed an energy spectrum of traps in polyethylene where the charge carriers are supposed to be electrons. Deep traps are placed around 1eV below the conduction band. They are responsible for the storage of charges for long times. Shallow traps up to 0.6eV below the conduction band are responsible for the conduction. If the injection current density has a value of $100pA/cm^2$, the filling up of the deep traps takes some hours [2]. The filling up times caused by the extremely high injection current densities, which are common in the needle-plane arrangement, are not known exactly, but one can assume that they must be shorter than 1 hour.

2. THE MATHEMATICAL MODEL

The mathematical model is based on Poisson's equation

$$\Delta \varphi = - \frac{\rho}{\varepsilon} \qquad (1)$$

Because of the complicated arrangement an analytical solution of the equation is not possible. A computer aided numerical method based on the charge simulation method will therefore be used. The simulating charges are point charges, line charges and circle charges. Fig. 1 shows the computation method of the charge injection: The surface of the needle is divided into discrete injecting areas A(j). The injected charges

$$Qs(0,j) = j_{inj}(j) * A(j) * \Delta t \qquad (2)$$

can be computed when the field intensities F(j) and the injection current densities j(j) are determined. The injected charge moves over the distance

$$s(0,j) = \mu(T) * F(0,j) * \Delta t \qquad (3)$$

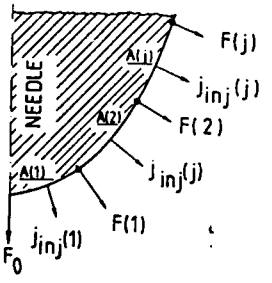

Fig. 1: Charge injection

A(j) = surface element
F(j) = field strength
$j_{inj}(j)$ = density of the injection current

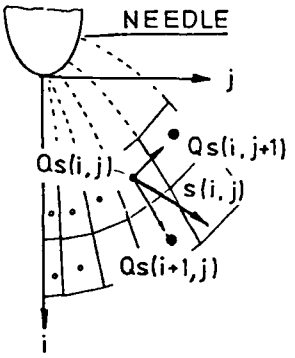

Fig. 2

The movement of a charge element across a grid of tori.
The charge Qs(i,j) moves over the distance s(i,j) and is distributed to the neighbouring charges.

deeper into the insulating material and is influenced by the field strength and by the mobility of the electrons. At the beginning of the following time interval Δt new charges are injected into the sample, the previous ones move ahead etc. After a time there are a lot of discrete charges in the sample. To reduce the computing time it will be necessary to limit the number of these charges.

The dynamic mathematical model satisfies this demand (Fig. 2).The interesting area of the sample is covered with a grid, which begins at the needle's surface. The elements of the grid are composed of tori, which can be filled up by space charges of different densities. The whole space charge is simulated by discrete circular charges which are situated in every torus of the grid. Influenced by the field strength in every torus, each discrete space charge element Qs(i,j) moves along a distance s(i,j) across the grid and its charge is distributed to the neighbouring elements Qs(i,j+1) and Qs(i+1,j). The distribution is controlled by the ratios s(i,j)/s(i,j+1) and s(i,j)/s(i+1,j). During every time interval Δt each charge element is treated in this manner.

3.STUDY OF PARAMETERS

The samples consist of needle electrodes embedded in a polyethylene bloc one side of which is covered with an evaporated chrome electrode. The diameter of the needles is 1mm and the tip radius is 5 µm. The distance between needle tip and ground is 2mm, the stressing voltage of the needle is -10 kV d.c. The calculations will be compared with experiments of G. Krause [3,4]. The electron mobility μ_0 is varied. If one assumes a dependence according to an Arrhenius plot the real mobility can be calculated as a function of the

temperature (k = Boltzmann's constant, W_{th} = thermal activation energy):

$$/u_T = /u_0 * \exp (- W_{th}/k * T) \quad (4)$$

Now some results of different test runs are presented:

3.1 The isothermal polarization (Fig. 3)

The dotted lines (70°C and 80°C) represent the measured values according to Krause [3]. They are approximated satisfactorily by the calculated curves.The mathematical model offers the advantage of studying the conditions within the space charge (for example field strength and the distribution of the charge carriers, Figures 4, 5).

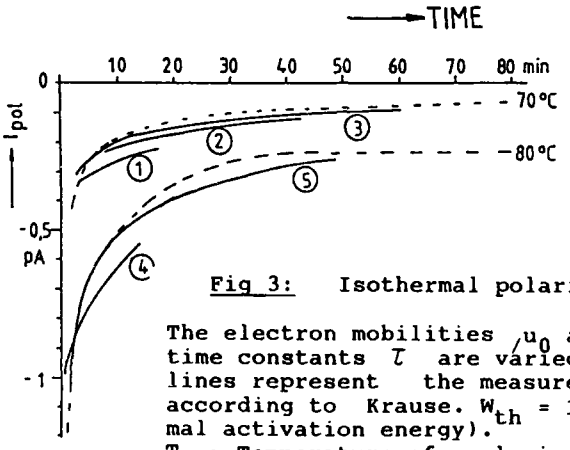

Fig 3: Isothermal polarization

The electron mobilities $/u_0$ and the storage time constants τ are varied. The dotted lines represent the measured values according to Krause. W_{th} = 1.2 eV (thermal activation energy).
T_p = Temperature of polarization.

line	$/u_0$ /(10^8 cm^2/Vs)	τ	T_p
1	11	1000 s	343 K
2	8.85	1000 s	343 K
3	8.85	800 s	343 K
4	8.85	800 s	353 K
5	7.2	800 s	353 K

3.2 The thermal stimulated polarization (Fig.6)

The thermal stimulated polarization can be computed from the parameters of the lines "3" and "5" (Fig.3) of the isothermal polarization.If need be the conditions within the sample (local electric field and charge density) can be studied.

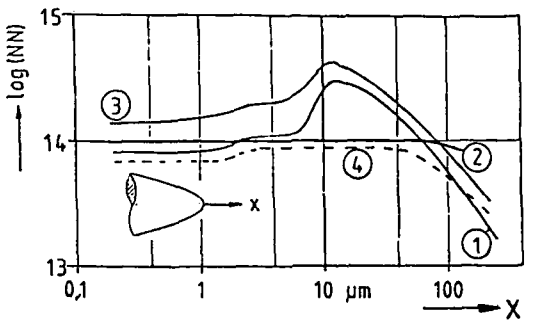

Fig 4: Isothermal polarization

Density of charge carriers at the axis of symmetry
Time of polarization = 50 minutes:
1.) Movable charges (shallow traps), 2.) fixed charges.
Time of polarization = 10 minutes:
3.) Movable charges (shallow traps), 4.) fixed charges.

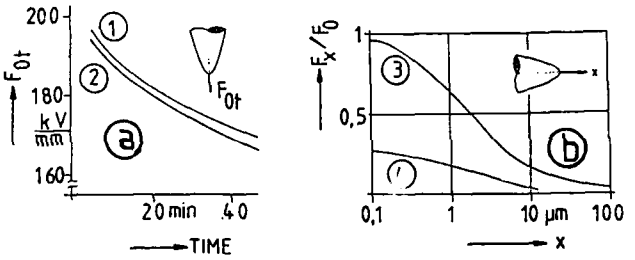

Fig. 5: Isothermal polarization

a) Field strength at the needle tip dependant on the time of polarization.
   1) Temperature of the polarization = 343 K.
   2) temperature of the polarization = 353 K.

b) Field strength at the axis of symmetry.
   3) Uninfluenced by space charges
   4) influenced by space charges, time of polarization 50 min, temperature of polarization 353 K.

3.3 The thermal stimulated depolarization

Fig. 7 shows in principle that the mathematical model enables the user to compute thermal stimulated depolarization currents. Here the isothermal polarization is

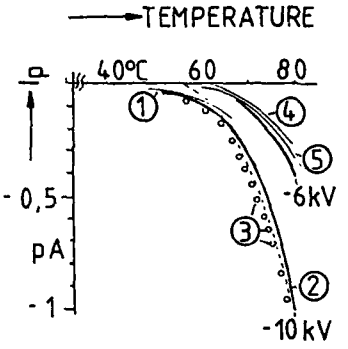

Fig. 6: Thermal stimulated polarization

W_{th} = 1.2eV, h = 1K/min.

The lines "-6kV" and "-10kV" are measured values of Krause.

$/u = /u_0/10^8 cm^2 Vs$

line	1	2	3	4	5
$/u$	11	6.6	8.3	6.6	8.3

followed by the thermal stimulated depolarization. In order to save computing time only the high stressed part of the dielectric material is modeled. The calculated depolarization current is too small, because the missing dielectric is not able to store charges which are not available when the sample is beeing discharged. A complete model of the sample is under consideration.

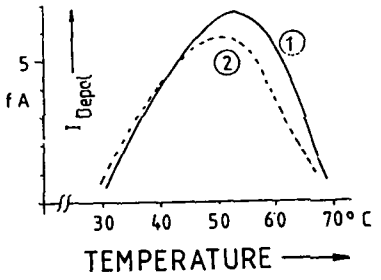

Fig.7: Thermal stimulated depolarization

The depolarization current depends on the length "l" of the grid at the axis of symmetry
line 1: l = 510 /um
line 2: l = 340 /um.

References

[1] Tanaka,T., Optical absorption and electrical conduction in polyethylene
J. Appl. Phys., Vol. 44, 3430 (1973)

[2] Patsch,R., Untersuchungen zum Leitungsverhalten technischen Polyaethylens bei hohen Feldstaerken
doctoral thesis Kassel 1980

[3] Krause, G., dissertation submitted for a diploma at the Rheinisch Westfaelische Technische Hochschule Aachen, Institut fuer Allgemeine Elektrotechnik und Hochspannungstechnik

[4] Döpper, H., Modellierung des Raumladungseinflusses auf die elektrische Feldstaerke innerhalb einer Nadel-Platte-Anordnung in festen Isolierstoffen
doctoral thesis Aachen 1988.

DIRECTIONAL TRAPPING

G.F.LEAL FERREIRA

INSTITUTO DE FISICA E QUIMICA DE SÃO CARLOS
UNIVERSIDADE DE SÃO PAULO
13.560 - SÃO CARLOS, SP, BRASIL

ABSTRACT

The concept of directional trapping, advanced by Adamec and Calderwood, is developped in a model allowing the (approximate) calculation of their effect on the current.

INTRODUCTION

Adamec and Calderwood [1] have put forward the hypothesis that charges in polymers may be immobilized simply because they have no way to follow moving in the field direction, as if they have reached an obstacle, and are ready to move again as soon as the field is reversed. They arrive to this conclusion experimenting with low density polyethylene. In the following we develop a simple model incorporating the main features of this kind of directional trapping and its effect on the electric current.

We assume that previously moving charges become progressively immobilized over a planar surface S of whatever shape (see fig.1). It is known [2] that for an uniform charge density σ over the surface, the component of the electric field normal to S is constant over S and equal to $\sigma/2\varepsilon$, ε being the permittivity of the medium. Therefore we infer that if the current density $\vec{j}$, defining the impinging carriers, is uniform, the actual charge density formed over S will also be uniform, whenever the

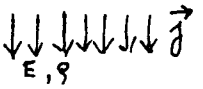

fig 1

CH2593-2/ 88/ 0000-0104$01.00 Copyright 1988 IEEE

deposited charges are not mobile over S. Calling E the electric field far from S, μ the mobility and ρ the charge density of the mobile carriers, the rate of increase of σ is:

$$\frac{d\sigma}{dt} = \mu\rho(E - \frac{\sigma}{2\varepsilon}) \qquad (1)$$

the quantity inside the brackets being the total electric field at any point over S. If S were inclined to $\vec{j}$, the normal component to S of E would enter Eq.(1). But, in what follows, only perpendicular obstacles will be assumed to exist.

S becomes completely charged for $\sigma = 2\varepsilon$. Then, the incoming current $\vec{j}$ does not reach it due to the formed tangential field.

S is our directional trap and the charge accumulated over it is supposed to be free when the field is reserved.

CURRENT KINETICS

Now, we want to calculate in a approximative way how the current will decrease after a field V/ℓ, ℓ being the thickness of the sample, is applied. Let the total area of the obstacles per unit volume be a; the density of charge in the traps will be a σ. This charge accumulation decreases the amount of free carriers, since we must have, approximately

$$V = E_o \ell + (\rho + a\sigma)\frac{\ell^2}{2} \qquad (2)$$

In (2), Eo is the field at the injecting contact, representing the contribution of charges at the electrode to the field inside the sample V. ρ and a σ were supposed to be uniformly distributed. The term $a\sigma\ell^2/2$ is equivalent to the polarization electromotive force of Joffé [3] in our case. We use as the boundary condition at the injecting electrode that the charge density there is a constant [4]

ρ_o. If the current density is j (time dependent), so $E_o = j/\mu\rho_o$. But, since $j = \mu\rho V/\ell$, (2) finally may be put so

$$V = \frac{\rho}{\rho_o} V + (\rho + a\sigma)\ell^2/2\varepsilon \qquad (3)$$

and from this ρ may be found and substituted in Eq.(1):

$$\frac{d\sigma}{dt} = \mu'\left(\frac{2\varepsilon V}{\ell^2} - a\sigma\right)\left(\frac{V}{\ell} - \frac{\sigma}{2\varepsilon V}\right) \qquad (4)$$

with $\mu = \mu'/\left(1 + \frac{2\varepsilon V}{\rho_o \ell^2}\right)$.

We call attention to the fact that if ρ_o is very large, the current will be space charge limited. On the other hand, if ρ_o is small the current is space charge free in the beginning, but the increasing charge accumulation decreases E_o and hencefort the current.

Eq. 4 may be integrated, thus resulting

$$\sigma = \frac{2\varepsilon V}{\ell}\,\frac{1-e^{-\alpha t}}{1-a\ell e^{-\alpha t}}\,, \quad \alpha = (1-a\ell)\frac{\mu' V}{\ell^2} \qquad (5)$$

and for the current density, finding ρ from (3) and using $j = \mu\rho V/\ell$:

$$j(t) = J(0)\cdot\frac{1 - a\ell}{1 - a\ell e^{-\alpha t}} \quad J(0) = \frac{2\varepsilon\mu V^2}{\ell^3\left(1+\frac{\varepsilon V}{\rho_o \ell^2}\right)} \qquad (6)$$

As asserted before, we see that for large ρ_o, $j \to \frac{V^2}{\ell^3}$, that is, space charge limited. In the other limit of small ρ_o, j is simply proportional to V/ℓ.

If the voltage is reversed after being applied for a time t_p in the forward direction the modulus of the initial current j_r is easily found to be

$$j_r = J(0)\left\{1 + \frac{2\varepsilon a}{\rho_o}\,\frac{V}{\ell}\,\frac{1-e^{-\alpha t_p}}{1-a\ell e^{-\alpha t_p}}\right\}$$

and is higher than the initial $j(\emptyset)$, the smaller the charge density ρ_o is , which means out of the space charge limited current regime.

CONCLUDING REMARKS

In the above model one important point was missed: the decrease of the mobility due to the decreasing avaiable space for the current. Each charged obstacle creates a kind of shadow behind it, which certainly will make the mobility lower. This effect awaits quantification.

ACKNOLEDGMENTS: TELEBRAS, FAPESP and FINEP are thanked for affording improved structure to our Electret Group Prof. Bernhard Gross by their finantial support.

REFERENCES

[1] V.Adamec and J.H.Calderwood "On the determination of electrical conductivity in Polyethylene". J.Phys.D:App.Phys., vol.14, pp.1487-94, 1981.

[2] E.Durand, Electrostatique, 3 Vol., Masson et Cia Editeurs, 1964, 1st vol. p.242.

[3] A.Joffé. The Physics of Crystals, Mc Graw-Hill Book Co. Inc., 1928, p.73.

[4] J.Mort, F.W.Schmidlin and A.I.Lakatos - "Transient internal photoemission of carriers in metal-insulators systems" - J.Applied Phys., vol.42, pp.5761-5769, 1971.

Hopping and electron glass transport in CdF2:Y crystals

V.Dallacasa and C.Paracchini
Dipartimento di Fisica. Universita' di Parma
Parma - Italy

Abstract

The models of electronic hopping conduction are summarized taking into consideration the effects of electron-electron interactions. The current- field-temperature characteristics in semiconducting CdF2:Y crystals at low temperatures are examined on the basis of such models, evidencing an electron hopping conduction, whit at electron correlations effects at low fields.

The electronic hopping transport has recently raised much interest [1]. This effect has been studied mainly in compounds with rather high conductivity at low applied electric fields and relatively little attention has been devoted to less conductive materials. In this work the electrical conductivity of semiconducting CdF2:Y crystals is examined in the temperature range 10 - 60 K by applying electric fields up to 50 KV/cm.

The electronic hopping conduction takes place when carriers, typically electrons, jump, with fixed or variable ranges, between the centers of a narrow impurity band energetically localized near the Fermi level. When fixed range jumps are involved, as usually happens in crystalline compounds, the dependence of the resistivity r on the temperature T is:

$$r = A \exp(w/kT) \qquad (1)$$

where the activation energy w is typically of about 0.01 eV and A from now forward means a generical proportionality factor. For variable ranges one has:

$$r = A \exp(To/T)^{(1/4)} \qquad (2)$$

where To is of the order of 10 K [2]. This last dependence is that usually observed in a wide variety of materials. At higher voltages the resistivity depends on the applied field E as:

CH2593-2/ 88/ 0000-0108$01.00 Copyright 1988 IEEE

$$r = A \exp(Eo/E)^{(1/4)} \qquad (3)$$

where Eo is about 10^6 V/cm. This field dependence arises from the fact that the thermal energy kT is substituted by that gained by the electric field eEl, where l is the carrier mean free path, that is the mean jump lenght. According to the previous formulas the study of the dependence of the resistivity on T and E may be examined considering two asymptotic trends: one at high temperatures following (2), the other at higher applied fields (3), that is when kT >> or << eEl respectively.

A more comprehensive theoretical analysis of this effect is due to Apsley and Hughes [3] who give a formula valid for the whole range of temperature and field of practical interest. These theories start from a single-electron model and do not consider the effect of the electronic correlation.

When the coulombic repulsion between electrons becomes comparable with the disorder energy (the energy for a jump) correlated hopping becomes possible [4,5]. Then many electrons may jump in a correlated way and this normally occurs when the carrier density n is sufficiently small (n<10^16 cm-3) as to reduce the screening effects, that is when the screening radius becomes of the order of the distance between carriers.

The theoretical treatment of the coulomb correlation [4,5] predicts the existence of a gap in the density of states at the Fermi level, known as "Coulomb gap". This gap arises from a rearrangement of the whole electron system during one jump and the energy required for the reassetment makes the transition energetically activated. As a consequence, the resistivity is predicted to depend on the temperature as:

$$r = A \exp(T1/T)^{(1/2)} \qquad (4)$$

as far as the temperature is low. A similar process, where the coulomb correlations are important, is known as "Coulomb ordering" and leads to a crystallization of the electrons into a Wigner-type glass [6,7]. Then the hopping distance R becomes fixed, but it varies with temperature as:

$$R = A \exp(T2/T)^{(1/4)} \qquad (5)$$

leading to a resistivity-temperature dependence similar to that indicated by equation (2), for non-correlated hopping. However T2>To indicating a higher activation energy. Both these effects of correlations lead to a reduction of mobility due to an increase of the binding energy for jumps and when the thermal or the field energy overcome such an increase, the effects of correlations disappear and the system returns to the non correlated hopping. Thus, low temperatures and/or low fields are needed to obtain these effects and experimentally one expects to observe them as a reduction of mobility in respect to the predictions of normal hopping.

Such situations are observed in CdF2:Y crystals, where the low carrier concentration makes it suitable for the formation of such electron-electron interactions, differently from what is observed in more conductive compounds [8]. The used samples are suitably heated in Cd vapour to reduce their resistivity [9,10] and the estimated electron density is 10^15-10^16 cm-3. After having evidenced a resistivity-temperature behaviuor indicated by equation (2), the I-V-T characteristics are fitted according to the Apsley-Hughes theory, obtaining a good agreement. Then an evaluation of the thermal activation energy of equation (1), of the density of states at the Fermi level N and of the inverse of the localization radius ϑ are obtained. The results are indicated in the following table.

---

sample	r	T3	N	ϑ
1	1.2	39	22	3.2
2	2.5	59	4.8	3.3
3	4.3	106	1.1	4.3

r = resistivity (ohmcm)
T3 = slope of r-T dependence (K)
N = density of states
at the Fermi level (10^17 cm^-3 eV^-1)
ϑ = inverse of the localization radius (10^6 cm^-1)

These values are similar to those obtained in other compounds [11-12] and assuming that the impurity band is about 10^-2-10^-3 eV wide, from the value of N one deduces a carrier density in agreement with that

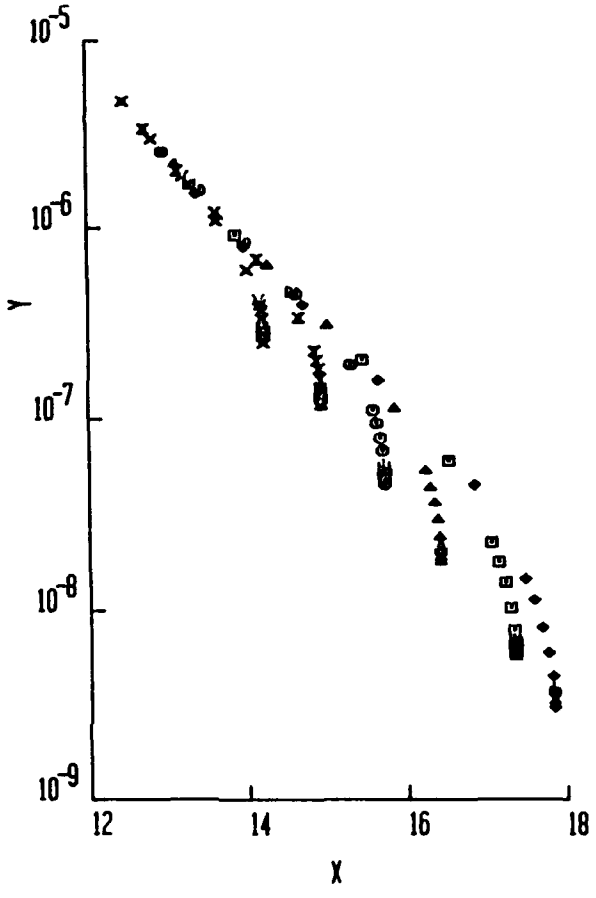

Fig.1 - Plot of the current-electric field-temperature for a CdF2:Y crystal. Current range: 7 10^-12 - 5 10^-5 A. Applied electric field range: 2.4 V/cm - 24 KV/cm. Temperature range: 12.8 - 31.8 K. The X and Y axis are chosen in order to distribute the experimental data on one single straight line when an hopping transport according to Apsley-Hughes theory takes place. The deviations from the linear trend observed at lower applied fields indicate a mobility reduction explainable with a Wigner-glass like correlated hopping transport.

previously indicated. The values of 1/a are slightly larger than the Bohr radius as found elsewhere [11].

At low fields abrupt deviations from the values expected for non correlated hopping are found as evidenced in Fig. 1. In such deviations the resistivity-temperature dependence is:

$$r = A \exp (T/T3)^{(1/4)} \qquad (6)$$

and they can be interpreted as due to the formation of electron correlated states and are examined according to the two forementioned models.

The choice between the two models is obtained considering that equation (6) suggests that a Wigner-glass state reproduces the behaviour of the anomalously low mobility values better than a coulomb gap state. Similar glass structures are found also in other compounds where the effects of coulomb repulsion occours on localized electron states [6,14]. By increasing the applied electric field and at high temperatures the correlated state is destroyed and the single electron conduction restored.

References

[1] N.F.Mott,E.A.Davies, Electronic processes in non crystalline solids. Pergamon press, Oxford (1971)
[2] N.F.Mott, Phil.Mag. 19 , 835-852 (1969)
[3] N.Apsley, H.P.Hughes, Phil.Mag. 31 , 1327 (1975)
[4] A.L.Efros, B.I.Shklovskii, J.Phys.C 8 ,L49 (1975)
[5] M.Pollak, Phil.Mag.B 42 , 781 (1980)
[6] M.Pepper, J.Phys.C 12 , L610 (1979)
[7] V.Dallacasa, J.Phys.C 19 , L485 (1986)
[8] M.Morgan, P.A.Walley, Phil.Mag. 23 , 661 (1971)
[9] J.D.Kingsley, J.S.Prener, Phys.Rev.Lett. 8 ,315(1962)
[10] V.Dallacasa, G.Frigerio, C.Paracchini, J.Phys.C, 18 , 2275 (1985)
[11] S.K.Evtimova, V.P.Dobrego, Semic.Sci.Techn, 1 , 161 (1986)
[12] A.G.Zabrodskii, A.I.Ionov, I.S.Shlimak, Sov.Phys.Semic, 8 , 322 (1974)
[13] M.Pollak, I.Riess, J.Phys.C, 9 , 2339 (1976)
[14] D.Monroe, A.C.Gossard, J.H.English, W.H.Haemmerle, M.A.Kastner, Phys.Rev.Lett. 59 , 1148 (1987)

Work supported by C.I.S.M. (M.P.I.).

EFFECT OF INHOMOGENEITY ON THE DETERMINATION OF DENSITY OF STATES FOR CURRENT CARRIERS IN INSULATORS AND WIDE BAND-GAP SEMICONDUCTORS

Juliusz Sworakowski[a] and Stanislav Nešpůrek[b]

(a) Institute of Organic and Physical Chemistry, Technical University of Wrocław, 50-370 Wrocław, Poland,
(b) Institute of Macromolecular Chemistry, Czechoslovak Academy of Sciences, 162 06 Prague, Czechoslovakia

ABSTRACT

The reliability of the determination of the density of local states in inhomogeneous samples from space-charge-limited currents is examined. It is shown that the densities of states may be determined with an error as large as several orders of magnitudes, depending on spatial distributions of the states. Energy scale may be determined to within a few kT.

INTRODUCTION

It has been recognized for several years (*cf.*, *e.g.* [1-3] for reviews of early work) that shapes of steady-stat space-charge-limited (SCL) current-voltage characteristics carry information about energetic distributions of local states influencing transport of charge carriers. Methods allowing for a direct determination of DOS functions from experimentally measured SCL characteristics were elaborated [4-8] and then successfully applied to several crystalline and amorphous samples. However, the results obtained from SCLC were found to substantially differ from those obtained using other methods (*e.g.*, field effect) [9,10]. One of the reasons for these discrepancies may lay in inhomogeneity of the samples. The aim of this note is to examine the effect of the inhomogeneity of samples on the accuracy of the determination of parameters of local states by the so-called "differential method" [5].

THE DIFFERENTIAL METHOD IN INHOMOGENEOUS SAMPLES

The differential method, as put forward by Nešpůrek and Sworakowski [5], allows one to determine an energetic distribution of local states in homogeneous samples. It should be stressed

CH2593-2/ 88/ 0000-0113$01.00 Copyright 1988 IEEE

that the derivation of the equations given in [5] is based on the assumption that both the field and the concentration of localized carriers at the collecting electrode are those characteristic of a uniform sample

$$F^h(D) = \frac{\varkappa_1 U}{D} , \qquad (1)$$

$$n_t^h(D) = \frac{\varkappa_1 \varkappa_2 \varepsilon U}{eD^2} . \qquad (2)$$

Here, the superscript "h" denotes parameters derived from the equations describing the situation in a homogeneous sample, U stands for the voltage applied, ε - for the electric permittivity, m is the slope of the current-voltage characteristic in the log-log scale ($m = d\ln j/d\ln U$), and $\varkappa_1$ and $\varkappa_2$ are factors given to within some 5% by the equations [6-8]

$$\varkappa_1 = \frac{2m-1}{m} ; \qquad \varkappa_2 = \frac{m-1}{m} = \varkappa_1 - 1 . \qquad (3)$$

Deviations from the above equations due to a non-uniformity of the spatial distribution of local states can be derived in a closed form assuming that the energetic profile of these states can be approximated by an exponential function

$$h(E,x) = h(E_0,x_0)f(E)g(x) \cong A\, g(x)\, exp\left(\frac{E}{kT_c}\right). \qquad (4)$$

Here f and g are functions describing energetic and spatial distributions of local states, respectively, A is a constant depending upon actual energetic profile, and $T_c = (m-1)T$.

Following the derivation employed by Sworakowski [11], one can demonstrate that the field and the density of localized charges at the collector are given by the equations

$$F^{inh}(D) = F^h(D)\, \Delta_1 , \qquad (5)$$

$$n_t^{inh}(D) = n_t^h(D)\, \Delta_2 , \qquad (6)$$

where the correction factors Δ_1 and Δ_2 are defined by the equations

$$\Delta_1 = \left(\frac{D}{L}\right)^{\alpha_1} \left(\frac{\int_0^D g(x)dx}{D}\right)^{\alpha_2} , \qquad (7)$$

$$\Delta_2 = \left(\frac{D}{L}\right)^{\alpha_1} \left(\frac{\int_0^D g(x)dx}{D}\right)^{\alpha_2 - 1} , \qquad (8)$$

the parameter L amounting to

$$L = \left\{\alpha_1 \int_0^D \left(\int_0^x g(z)dz\right)^{\alpha_2} dx\right\}^{1/\alpha_1} . \qquad (9)$$

After simple manipulations, one obtains the equations determining the position of the quasi-Fermi level at the collecting electrode of an inhomogeneous sample ($E_f(D)$) and the density of states at E_f ($h(E_f)$)

$$E_f^{inh}(D) = kT \ln\frac{D}{e\mu N \alpha_1 \Delta_1} + kT \ln\frac{U}{j} , \qquad (10)$$

$$h^{inh}(E_f) = \frac{\varepsilon \alpha_1 \alpha_2 \Delta_2}{eD^2 kT} \frac{U}{m-1} . \qquad (11)$$

Here, N is the effective density of extended states, μ - the mobility of charge carriers, and j stands for the current density.

We shall now put forward numerical estimates of the factors Δ_1 and Δ_2 for an exponential shape of $g(x)$

$$g(x) = exp\left(\frac{D-x}{r}\right) \qquad (12a)$$

$$g(x) = exp\left(\frac{x-D}{r}\right) \qquad (12b)$$

Errors made on neglecting the inhomogeneity of the samples are shown in Fig. 1. The results shown in the figure demonstrate that, while the uncertainty in the determination of the energy scale seldom exceeds a few kT, the error in the density of states may be as large as several orders of magnitude. It is also clearly seen from the figure that both Δ_1 and Δ_2 are only weak functions of m , hence our results hold for *any* distribution of local states.

Basing on the equations derived above, one can re-intrpret experimental results of measurements of SCL characteristics available in the

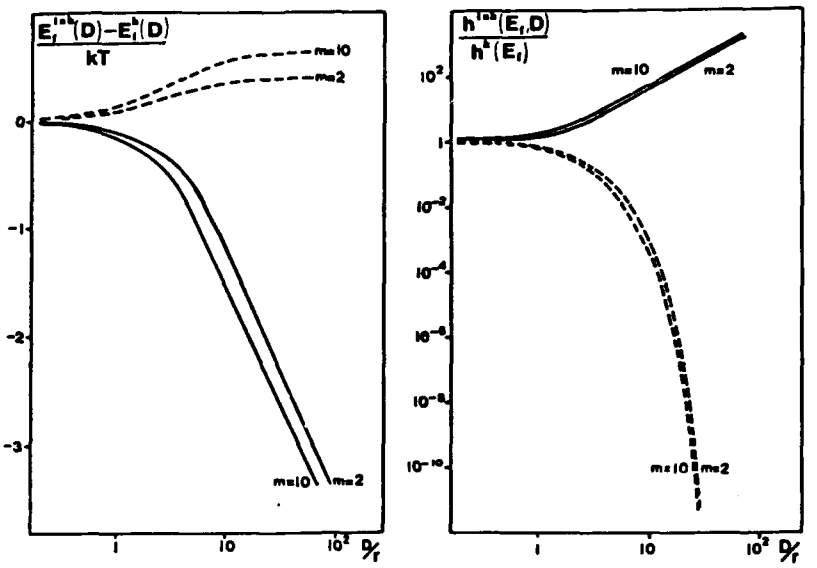

FIG.1. Position of the quasi-Fermi level and density of states in function of the spatial inhomogeneity. The parameter is the slope of the current-voltage characteristics, m. Solid lines - local states situated near the collecting electrode; dashed lines - states situated near the injecting electrode.

literature. We shall use the results of Solomon *et al.* [12], who reported on a thickness dependence of the density of states in amorphous Si, particularly pronounced in thin samples. The results, shown in Fig.2, demonstrate that the local states controlling the experimental SCL current-voltage characteristics are a superposition of bulk and surface states, located near the collecting electrode. The function describing the density of states at the Fermi level can be approximated by the function

$$h(E_f,x)=1.70\times10^{23}exp\left(\frac{x-D}{0.15}\right)+1.26\times10^{22}exp\left(\frac{x-D}{1.35}\right),$$

(x and D in μm, h in $m^{-3}eV^{-1}$).

ACKNOWLEDGEMENT

The research reported in this paper has been partly sponsored by the Polish Academy of Sciences within the Programme CPBP 01.12.

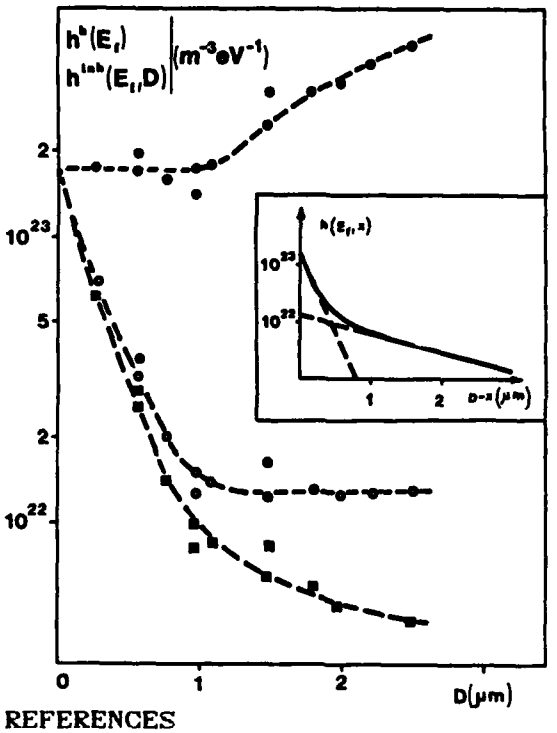

FIG. 2.
Thickness dependence of the densities of local states as reported by Solomon *et al.* [12] (squares) and the same dependence corrected for a gradient of density of states (assumed to be described by Eq. (16b)). Open circles - r=1.35μm, closed circles - r=0.15μm.

REFERENCES

[1] R.H. TREDGOLD, *Space Charge Conduction in Solids*, Elsevier, Amsterdam 1966

[2] M.A. LAMPERT and P. MARK, *Current Injection in Solids*, Academic Press, New York 1970

[3] K.C. KAO and W. HWANG, *Electrical Transport in Solids*, Pergamon Press, Oxford 1981

[4] J.C. PFISTER, *Phys. Stat. Sol. (a)*, **24**, K15 (1974)

[5] S. NEŠPŮREK and J. SWORAKOWSKI, *J. Appl. Phys.* **51**, 2098 (1980)

[6] F. STOCKMANN, *Phys. Stat. Sol. (a)*, **64**, 475 (1981)

[7] R.L. WEISFIELD, *J. Appl. Phys.*, **54**, 6401 (1983)

[8] O. ZMEŠKAL, F. SCHAUER and S. NEŠPŮREK, *J. Phys. C: Solid State Phys.*, **18**, 1873 (1985)

[9] K.D. MACKENZIE, P.G. LECOMBER and W.E. SPEAR, *Phil. Mag.*, **B46**, 377 (1982)

[10] P.G. LECOMBER and W.E. SPEAR, in: J.D. JOANNOPOULOS and G. LUCOVSKY (Eds.), *Physics of Hydrogenated Amorphous Silicon*, vol. 1, Springer, Berlin 1984

[11] J. SWORAKOWSKI, *J. Appl. Phys.* **41**, 292 (1970)

[12] I. SOLOMON, R. BENFERHAT and H. TRAN-QUOC, *Phys. Rev. B* **30**, 3442 (1984)

THERMALLY STIMULATED PROCESSES IN ORGANIC POLYMERS

R.J.Fleming

Department of Physics, Monash University
Clayton, Victoria 3168, Australia

ABSTRACT

Emerging trends in the interpretation of measurements of thermally stimulated conductivity, luminescence and depolarization in organic polymers are reviewed, in the context of charge trapping and transport. Particular attention is given to the following:
(1) the advantage of making simultaneous measurements (say TSC and TSL) on the same sample,
(2) the determination of the forms of quasicontinuous distributions of trap activation energies, and
(3) the use of thermally stimulated processes to monitor ageing (degradation) of polymeric insulants in power distribution cables, and hence estimate their economic service lifetimes.

INTRODUCTION

Quantitative analysis of thermally stimulated luminescence (TSL) and conductivity (TSC) to yield charge trapping parameters dates from 1945 [1] and 1951 [2] respectively. An analysis of thermally stimulated current originating in the relaxation of impurity-defect dipoles in an ionic solid was published in 1964 [3], and by 1975 TSD was firmly established as an alternative method of studying charge trapping and transport is non-metallic solids in general [4]. Many papers have been published reporting trap depths, frequency (or pre-exponential) factors, kinetic order of recombination leading

CH2593-2/ 88/ 0000-0118$01.00 Copyright 1988 IEEE

to TSL, and slow or fast retrapping associated with TSC; unfortunately, in most of them the single trap model [5] is assumed. Now it has been known since the early 1970s that a single TSL or TSC glow-curve can be satisfactorily fitted by a wide range of physically-realistic trapping parameters [6], and consequently very little significance can be attached to the results of an isolated curve-fitting exercise, no matter how sophisticated its algorithms. It is essential that the proposed trapping parameters be consistent with data gathered under widely varying heating programmes, e.g. different heating rates, varying delays between the end of irradiation and the commencement of heating, periods of isothermal decay during heating, and rapid cooling to the irradiation temperature followed by re-heating [7,8].

SIMULTANEOUS MEASUREMENT OF CORRELATED PHENOMENA

Most authors measure only one thermally stimulated process, e.g.TSL or TSD, and the information they gain is therefore of a very general nature and difficult to interpret unambiguously, particularly in polymers. The information harvest is much richer if two such correlated phenomena are measured simultaneously [9], and this can usually be achieved without unduly complex apparatus [10,11]. Separate measurements, even on the same sample, are less valuable because of the notorious marked dependence of polymer measurements on the detailed thermal history of the sample.

Consider the simultaneous measurement of TSL and TSC on a polymeric sample polarised by application of an external electric field at or above room temperature, cooled to liquid nitrogen temperature, exposed to ionizing radiation and heated with the field still applied. Both TSL and TSC require the release of charge carriers from traps; however, while geminate and non-geminate radiative

recombination will both generate a TSL signal, only non-geminate recombination will generate a TSC current, assuming a homogeneous distribution of the separations of trapped electrons and geminate luminescence centres with respect to distance and direction. Thus the presence of a TSL peak and the absence of a TSC peak in a given temperature range (typically 50K between the two half-maximum points of a glow curve in polymers) together indicate a trap density sufficiently high to ensure that the electron is trapped within the Onsager radius of its parent luminescence centre, and so a lower estimate of that density can be calculated. (One must bear in mind here that a photomultiplier with a cooled photocathode is usually a much more sensitive detector than even a high quality electrometer, and therefore a measurable TSC current may require a much larger radiation dose than a measurable TSL signal). The reverse situation indicates that (a) the escaping electrons were injected into traps during polarisation or cooling, with no associated activated luminescence centres, or (b) the radiative recombination probability is zero over the temperature range of the TSC peak (this can be fairly easily checked by searching for phosphorescence), or (c) there is an absence of luminescence centres near the emptying traps. The latter case can arise in polymers if electrons are trapped well within the crystalline regions, from which impurities (forming the luminescence centres) are usually excluded.

The interpretation of simultaneous TSL and TSD measurements is a little more complex. (In TSD measurements the sample is heated in short circuit, after polarisation and cooling, and usually after exposure to ionizing radiation when cooled). Comparison of the TSC and TSD glow curves, with and without exposure of the sample to ionizing radiation, will usually indicate whether a given peak in the TSD glow curve originates in the thermal disorientation

of dipoles oriented during polarisation, or in the movement of untrapped charge under its own electric field. In the latter case, comparison of the TSL and TSD glow curves leads to deductions similar to those outlined above for the TSL/TSC comparison. In the former case, the presence of a TSL and a TSD peak in a given temperature range in a semi-crystalline polymer strongly suggests that the electron traps are located very close to the disorienting dipoles on the polymer chains, the electron escape and the disorientation being driven by the same intra-chain molecular motion. (It is now accepted by many workers that the electron traps in semi-crystalline polymers are formed by the polymer chains themselves, at least in the amorphous regions, e.g. cavity traps [12]). Presence of a TSL peak and absence of a TSD peak therefore together indicate that no dipoles with significant dipole moment are located close to the sites of the appropriate molecular motion, while the reverse situation gives the same indication for electron traps.

TRAP ACTIVATION ENERGY AND FREQUENCY FACTOR DISTRIBUTION FUNCTIONS

Since the electron traps are formed by the polymer chains themselves, it is most unlikely that all traps will be identical, or that only a few discrete types of trap will exist; an immense variety of shape and size is to be expected, and with it a quasi-continuous distribution of activation energies, or frequency factors, or both. While the precise mathematical forms of these distributions in a given polymer is unlikely to affect seriously its practical performance as an insulator or electret, there is scientific value in attempting to document them.

The use of space-charge-limited currents (SCLC) to probe trap activation energy distributions is well established [13]. In the recently introduced temperature-modulated SCLC method [14] the temperature-dependence of the SCLC is

measured over a range of applied voltage ; experimental data for polycrystalline metal-free phthalocyanine, amorphous silicon and arsenic triselenide, and the deduced density of localised states (traps) plots, have been presented [15]. The experimental procedure is straight-forward and the analysis of the resulting data uncomplicated. However, it is essential that an efficient charge-injecting (ohmic) contact be made with the sample. This implies a minimum applied voltage given by [16]

$$V_{min} = el^2 (n_f + n_t)/\epsilon\epsilon_o$$

where l is the sample thickness, n_f and n_t are respectively the concentrations of free and trapped carriers at thermal equilibrium, and the other symbols have their usual meanings. Vmin could be as much as 100V for a 1μm thick polymer sample, and this perhaps explains why no report of the successful application of this technique to polymers has appeared in the literature.

Many authors have used TSC measurements to probe the energy distribution of traps in solid insulators, particularly semiconductors [17]. However, the analysis is complicated by the likely but unknown variation of the carrier mobility with temperature, and the possibility of extrinsic charge generation. To the best of my knowledge, the use of this technique to obtain the form of the distribution in a polymer has yet to be reported.

We have used TSL measurements to deduce the activation energy distribution for occupied traps in polystyrene [7,8], shown in Fig.1. We have also deduced the temperature dependence of the frequency factor, assumed the same for all traps. Since there is very little TSL emission from polymers above 0oC approximately, the method is limited to "shallow" traps. This limitation originates in the decreasing probability of radiative recombination of an electron with an activated luminescence centre

as the temperature increases, the luminescence centres in polymers frequently being aromatic impurity molecules ; attempts to dope the polymer with more efficient inorganic luminescence centres

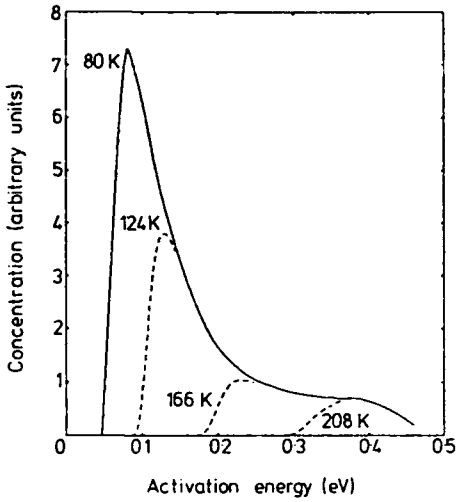

Fig.1. Trap depth distribution in polystyrene.

were unsuccessful. It should be pointed out that although first order kinetics was assumed in our earlier paper [7], i.e. every electronreleased from a trap recombines with a luminescence centre without first being retrapped, in agreement with the findings of most authors investigating TSL in polymers,this assumption is not necessary in our second method [8].

None of the methods mentioned above can distinguish between electron and hole traps, and it is always assumed that the traps are spatially homogeneously distributed (apart from the gross distinction between surface and bulk traps).However the recently developed pressure pulse methods of probing the spatial distribution of charge in insulators [18,19]

can distinguish between positive and negative carriers, within the appropriate resolution limits, assuming no complications due to polarisation. It might therefore be possible to combine pressure pulse and TSC data, collected before and after a small rise in sample temperature, to obtain more accurate information on the distributions of interest.

DEGRADATION OF POLYMER INSULANTS

The use of polymeric insulants in electrical power distribution systems is wide-spread, e.g. cross-linked polyethylene (XLPE), ethylene-propylene rubber, and ethylene-propylene-diene monomer [20]. Power utilities worldwide have underwritten an enormous research effort in attempting to extend the lifetime of their cabling, such failure frequently originating in the insulant. The importance of excluding moisture, and thereby preventing the formation of water (electrochemical)trees in the insulant, has been known for many years. Breakdown may also occur in dry field-stressed insulant following the formation of electrical trees, particularly along crystalline /amorphous interfaces.

A pressing problem is the estimation of the economic service life-time of a given cable in the absence of water [21]. (A figure of at least forty years is presently being targeted for XLPE cables rated 15-35 kV). Thermal endurance analysis [22] is well established, but since the laid-down procedures extend over at least 5000 hr, a reliable shorter method would be of great value.

TSD has been used to study electrical/thermal ageing in XLPE samples cut from commercially-produced cables [23]. The samples, 50-100μm thick, were aged by applying an ac voltage, typically 60-90kv, for 3-13 hours. The TSD glow-curves for a sample polarised for 1800s at 333K and 500V, before and after ageing, are shown in Fig.2. A doubling of the high

temperature peak height will be seen, with little change in the other two peaks. Other authors have reported a new TSD current peak around 340K in electrically stressed (ac and dc) XLPE [24]. A possible explanation of both results is that the applied field and

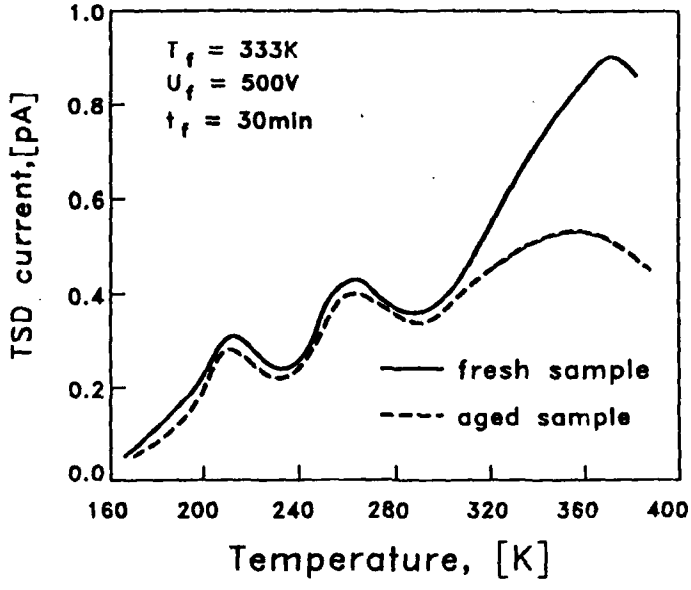

Fig.2. TSD of XLPE.

concomitant temperature increase induce a change in the supermolecular structure of the samples. (It was found that ageing also produced increases in the molecular weight, degree of cross-linking, and, surprisingly, breakdown ac field strength [23]). This suggestion is supported by a recent study [25] of the morphology of chemically crosslinked XLPE, which showed that after annealing within 5K of the melting point (~380K), two different crystallite thicknesses (11nm and 24nm) were produced. (It was also shown that, contrary to earlier reports, spherulites are not formed in XLPE). This difference arises from the fundamental incompatibility of the crosslinked

network and the low molecular weight sol (extractable) crystals. It was also found [26] that the concentration and maximum length of water trees almost doubled when the sample was annealed for 30 hours around 373K. The measurement and counting of such trees in a length of cable would be a time consuming and tedious business, and would preclude further measurements on the same cable at a later date. However, it may be that the growth of the high temperature TSD peak with time, as tabulated during an accelerated ageing programme, would provide a reliable and convenient yardstick with which to estimate the service lifetime of cable subsequently received from the manufacturers.

A study of ageing in polyethylene terephthalate (PET), also based on TSD measurements, has recently been reported [27]. Fig.3 shows the

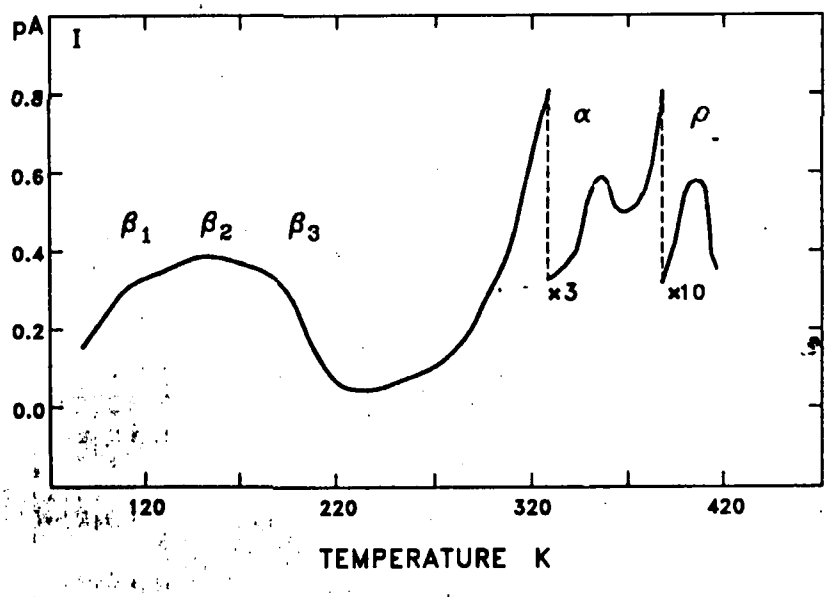

Fig.3. TSD of PET.

TSD glow-curve for a 36μm thick PET foil polarised for 1800s at 100V and 390K. It is believed [4] that the composite ß-peak covering the approximate range 80-220K is due to disorientation of polar side-groups below theglass transition, the α-peak at 360K to disorientation of (unidentified) main chain dipoles as a result of the glass transition, and the δ-peak around 410K to release of space charge from traps. Fig. 4 shows the variation of the α-peak and δ-peak heights with ageing time

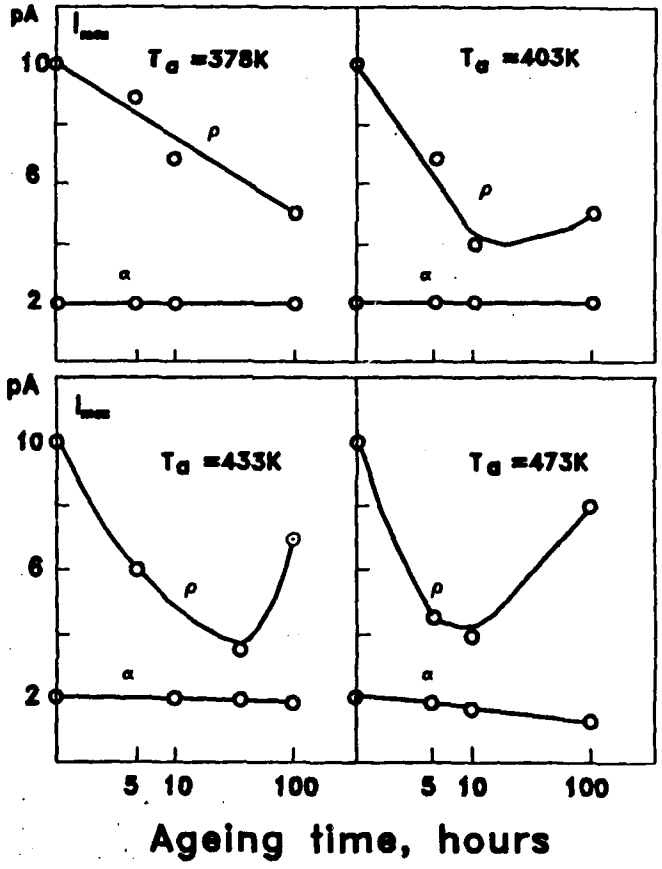

Fig. 4. TSD peak height variation in PET.

at four different temperatures. The authors attribute the variation in the δ-peak height to changes in trap concentration originating in spherulite size and density changes during ageing, and cite independent morphological data as support. They deduced the empirical equation

$$\log \tau = a - b\theta$$

relating life-time τ, as given by thermal endurance tensile strength measurements, and rate of increase θ of the δ-peak with ageing time between 10 and 100 hours (a and b are constants). Note that the dc conductivity, relative permittivity, loss factor and ac breakdown voltage of PET are not sensitive to short term (10-100 hours) ageing.

We have found that, when absorbed air is removed from chemically crosslinked XLPE, its TSL glow curve consists of a single peak around 108K (X-irradiation at liquid nitrogen temperature, heating rate 3K/minute). This contrasts markedly with the glow-curves of low and high density PE, which consist of three peaks at roughly 108, 153 and 243K. We have argued that the electron traps in low density PE are formed by the polymer chains themselves in the chain-fold regions of the samples [28], and thus the different result for XLPE is (a priori) consistent with a different morphology [25]. The glow curve of low density PE is sensitive to annealing close to the melting point [29], and we plan to study the effects of annealing and electrical stressing on the TSL, TSC and TSD glow curves of XLPE as part of a search for a reliable estimator of its service lifetime as a power cable insulant.

REFERENCES

[1] J.T.Randall and M.H.F.Wilkins, Proc.Roy.Soc.(London),A184,366(1945).
[2] R.H.Bube, Phys.Rev., 83,393(1951).
[3] C.Bucci,R.Fieschi and G.Guidi, Phys.Rev.,148,816(1966).

[4] J.van Turnhout, Thermally Stimulated Discharge of Polymer Electrets (Elsevier, Amsterdam 1975).
[5] R.Chen, J.Mat.Science,11,1521(1976).
[6] P.Kelly, M.Laubitz and P.Braunlich, Phys.Rev.,B4,1960(1971).
[7] L.F.Pender and R.J.Fleming, J.Phys.C:Solid State Phys.,10,1571(1977).
[8] R.J.Fleming and A.Markiewicz, IEEE Trans.Elec.Insulation,EI-22,29(1987).
[9] P.Braunlich, P.Kelly and J.-P.Fillard, Topics in Applied Physics,37,35(Springer-Verlag 1979).
[10] D.Ito and T.Nakakita, J.Appl.Phys., 51,3273(1980).
[11] A.Markiewicz and R.J.Fleming, J.Phys.D:Appl.Phys.,21,349(1988).
[12] R.H.Partridge, J.Poly.Sci.A3,2817(1965).
[13] K.C.Kao and W.Hwang, Electrical Transport in Solids (Oxford:Pergamon 1981).
[14] O.Zmeskal, F.Schauer and S.Nespurek, J.Phys.C:Solid State Phys.,18, 1873(1985).
[15] F.Schauer, S.Nespurek and O.Zmeskal, J.Phys.C:Solid State Phys.,19,7231(1986).
[16] S.Nespurek, O.Zmeskal and F.Schauer, phys.stat.sol.(a),85,619(1984).
[17] G.G.Roberts, N.Apsley and R.W.Munn, Phys.Rep.,60,59(1980).
[18] R.Gerhard-Multhaupt et al., J.Appl.Phys.,55,2769(1984).
[19] W.Eisenmenger and M.Haardt, Solid State Commun.,41,917(1982).
[20] Electrical Power Research Institute (EPRI) Report EL-4398 - Long-life Cable Development : Cable Materials Survey (March 1986).
[21] W.F.Horton, IEEE Trans.PAS-101,472(1982).
[22] IEC Standard Publications 216-1 (2nd Ed.) 1974 and 216-3 (2nd Ed.) 1980.
[23] S.M.Gubanski and B.Masurek, Eur.Symp. on Polymeric Materials (European Polymer Federation), Lyon-France, September 1987.
[24] K.Doughty, D.K.Das-Gupta and D.E.Cooper, IEEE Conf.Elec.Insul.and Dielectric Phenomena, 56 (1986).

[25] R.M.Gohil and P.J.Phillips, Polymer, 27,1687(1986).
[26] P.J.Phillips, IEE 4th Intern.Conf.on Dielectric Materials, Measurements and Applications, 1984, Conf.Publ.No.239, p.187.
[27] S.M.Gubanski, R.Kacprzyk and Z.Zubel, Fifth Int. Symp. on High Voltage Eng., Braunschweig, August 1987.
[28] A.Markiewicz and R.J.Fleming, J.Poly.Sci. Part B, Poly.Phys.,24,1713(1986).
[29] A.Markiewicz and R.J.Fleming, J.Poly.Sci. Part B, Poly.Phys.,25,1885(1987).

EFFECT OF MECHANICAL DEFORMATIONS ON THERMALLY STIMULATED CURRENTS IN POLYMERS I. UNIAXIALLY COLD-DRAWN POLYCARBONATE

G. YIANAKOPOULOS, J. VANDERSCHUEREN and J. NIEZETTE

Department of Macromolecular and Physical Chemistry, University of Liege, Belgium

ABSTRACT

The thermally stimulated depolarisation and polarisation current (TSDC and TSPC) methods have been used to study the intermediate relaxation induced in polycarbonate by uniaxial cold-drawing at various drawing ratios and rates. Since its characteristics differ markedly in TSPC and TSDC experiments, it is a non-equilibrium relaxation, presumably resulting from local orientation of chain segments made possible by the increase in free volume consecutive to the drawing process.

INTRODUCTION

There is still a great deal of controversy in the literature about the changes in structure and free volume as well as the orientation and internal stresses produced in polymers subjected to mechanical treatments such as cold and hot drawing or rolling [1]. From mechanical and dielectric measurements, in particular, it has been frequently observed that a nonequilibrium secondary relaxation could occur but so far, its origin has not been unequivocally determined because the reproducibility is generally poor and it sometimes also appears in "untreated samples" [2]. Elucidating the exact mechanism of such a relaxation could be important because its temperature range is generally in accord with the end-use range of the finished products. Such is especially the case in polycarbonate (PC) where the existence of a non-

CH2593-2/ 88/ 0000-0131$01.00 Copyright 1988 IEEE

equilibrium shoulder on the dissipation curve has been reported by several authors over the temperature range of 50 to 100°C. Little is known about the origin of this so-called α' intermediate relaxation (this designation steming from its location below the α relaxation due to the glass transition and above the local mode β relaxation). It has been sometimes associated with residual stress or aligned configuration of chain segments frozen in during the mechanical deformation. Details of its observation by different methods are given in reference 2.

In this paper, we report preliminary results about the appearance of the α' transition in TSPC and TSDC measurements obtained from uniaxially cold-drawn PC.

EXPERIMENTAL

Strips of Bayer Makrolon PC sheet 1 mm thick were stretched uniaxially beyond the yield point either in an Amsler tensor (at RT) or in an Instron tester provided with a conditioning oven (at 70-120°C) at various drawing rates (R_d = 0.5 to 25 cm/min). The drawing ratio λ (defined as the ratio of the initial/final cross-sectional area) varied from 1.6 to 2.1. After stretching, several square samples 2cmx2cm were cut starting from the middle of the "neck" formed and then metal coated. The TSPC and TSDC measurements were carried out with a three-terminal electrode system under a controlled nitrogen flow in the dielectric test cell of a relaxation spectrometer(Unirelax, Tetrahedron).

RESULTS AND DISCUSSION

For low to moderate drawing rates (0.5 to 5 cm/min) and whatever the final drawing ratio, no current peak was observed up to temperatures higher than Tg in samples without any external voltage being applied, showing that no spontaneous polarisation was present in the stretched material, eventhough the existence of molecular

alignment could be evidenced by birefringence measurements. This is in sharp contrast with results obtained in cold-rolled specimens where a well-defined α' transition occurs near 70°C [2]. The lack of any dipolar polarisation in drawn samples could result from the increase in segmental mobility avoiding any particular orientation of local chain segments during elongation. This increased mobility can be unambiguously demonstrated by the fact that cold-drawing of thermoelectrets (i.e. initially polarized materials) induces a substantial loss of charge, a process which would otherwise had occured only if the samples had been heated to above Tg [3]. Only for high drawing rates, one or two peaks can appear in materials heated under zero bias voltage (Fig.1). They are no more visible on a second TSDC run, indicating the nonreversible nature of the underlying process. They must be probably related to the important and hardly reliable thermal effects taking place at such rates of strain (the heat generated can produce inhomogeneous deformation with plastic instabilities and internal stresses [1] and the unavoidable existence of thermal gradients can induce a migration of charge carriers and thus a space charge polarisation).

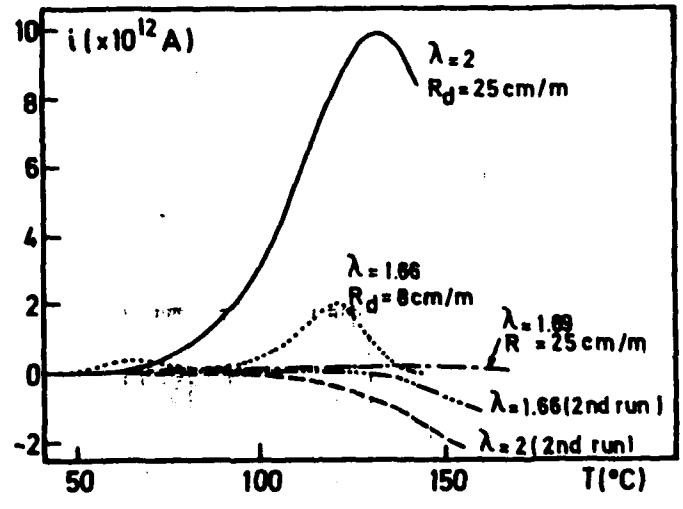

Fig.1. TSDC of nonpolarised cold-drawn PC.

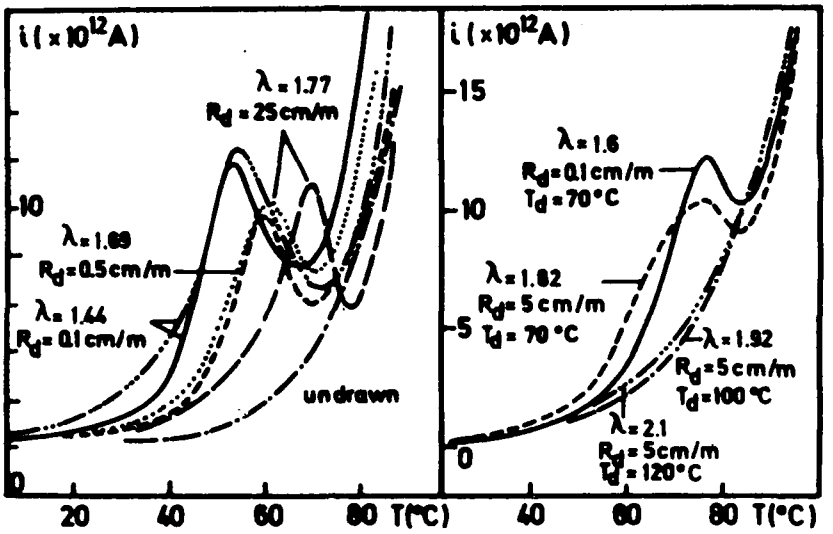

Fig.2. TSPC of undrawn and cold-drawn PC in the α' range.

Fig.3. TSPC of PC drawn at various temperatures Td.

Fig.2 shows the TSPC measured during heating of samples undrawn and drawn at RT at various drawing ratios and rates. In undrawn specimens, only a monotonous current increase can be observed, obviously corresponding to the material inherent conductivity. In cold-drawn samples, on the other hand, a well-defined α' peak always occurs in the 55-70°C range. Its position and amplitude depend on λ, R_d and the cutting place of the specimen but no direct relation between these parameters has been yet found. In samples drawn at higher temperatures (T < 80°C i.e. in the temperature domain of the α' relaxation), the peak still appears with similar properties (only a slight shift towards the 75-80°C range can be noted) while it is no more apparent for higher stretching temperatures (Fig.3). It has also been found that the peak characteristics are not significantly affected neither by the configuration of the specimen relative to the electrodes nor by a change in polarity of the applied field (the α' peak always occurs in the same direction than the con-

duction current). The α' relaxation is thus most probably of dipolar origin and could be related to a field-induced local orientation of chain segments as a result of the increase in free volume (and thus in chain mobility) occuring in cold-drawn materials [1]. The fact that the relaxation is no more observed in materials stretched at higher temperatures (100-120°C) is in support of this hypothesis.

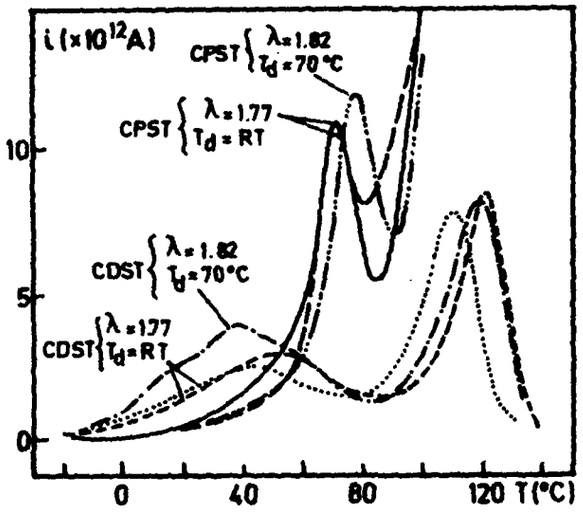

Fig.4. TSPC and subsequent TSDC of cold-drawn PC. The 2 curves refering to λ = 1.77 correspond to 2 different cutting places of the same drawn sample.

The α' process can also be evidenced in TSDC obtained after quenching under field of cold-drawn samples first submitted to a TSPC run up to 100°C (Fig.4) but in this case, the relaxation characteristics appear to be drastically modified : the peak is broadened (and occasionally structured), shifted towards the 40-60°C range and its amplitude is markedly lowered. Such a behaviour is in contrast with the results generally observed in undrawn polymers where the TSDC and TSPC peaks corresponding to a given relaxation are characterized by similar positions, heights and shapes and proves that

structural variations have occured during the polarisation step. In fact, the TSPC run is equivalent to anneal the drawn sample up to 100°C, a procedure which is known to induce physical property changes in the material, possibly via a reduction in free volume [2]. It follows that a progressive change in dipolar environment occurs during the heating-cooling TSPC cycle, which probably explains the shift and widening of the relaxation in subsequent TSDC measurements (as a result of widening of the distribution function of relaxation times).

CONCLUSION

In uniaxially cold-drawn polycarbonate, no spontaneous polarisation resulting from molecular orientation or internal stress can be evidenced by current measurements under zero bias voltage. The intermediate α' relaxation is generated only in TSPC and subsequent TSDC experiments but its properties are markedly different in the two types of spectra. In TSPC measurements, the molecular mechanism responsible for the α' peak is probably a field-induced local orientation of chain segments made possible by the increase in free volume consecutive to the drawing process. During this polarisation step, which involves a thermal treatment of the drawn material up to 100°C, a progressive change in structure and dipolar environment occurs and this tends to shift and broaden the relaxation as seen in subsequent TSDC cycles.

REFERENCES

[1] R.N.Haward, Ed., *The Physics of Glassy Polymers*, Appl. Sci. Publ., London, 1973.
[2] J.Hong and J.Brittain, "Thermally Stimulated Depolarization Current Studies on Strain-Induced Relaxations in Polymers," J. Appl. Polym. Sci., vol.26, pp. 2459-2469, 1981.
[3] J. van Turnhout, P. Klaase, P. Ong and L. Struik, "Physical Aging and Electrical Properties of Polymers," J. Electrostatics, vol.3, pp. 171-179, 1977.

CHARGING, LONG-TERM-STABILITY, AND TSC-MEASUREMENTS OF SiO_2-ELECTRETS

P. GÜNTHER

Institute for Electroacoustics, Technical University of Darmstadt, Merckstrasse 25, D-6100 Darmstadt, F.R.G.

ABSTRACT

SiO_2 layers of different thicknesses were either thermally grown or made by chemical vapour deposition on 2 inch, p-type silicon wafers. The samples were positively and negatively charged by means of liquid-contact, corona, and electron-beam methods. The surface potential decay was observed at room temperature over a period of more than one year. The positively charged SiO_2 showed a somewhat faster decay than the negatively charged material. This corresponded to open-circuit TSC-measurements, where negatively charged samples showed a higher peak temperature than positively charged samples. Also, positive electron-beam charging yields a higher peak temperature than positive corona charging. Activation energies of 1.0 eV and 1.4 eV were found for positively charged oxides, whereas for negatively charged samples activation energies of about 1.9 eV were calculated.

1. INTRODUCTION

In electret research and electret applications polymers are the most commonly used materials. However, in some applications problems might occur with compatibility to semiconductor materials, with stability of charges at high temperatures and with the relatively large thickness of polymer materials. The most widely used insulating material in semiconductor applications is SiO_2. Its ability to store charges at the Si-SiO_2 interface is well known [1]. Only a few papers deal with the charge storage behaviour of the non-metalized surface or the bulk of SiO_2 [2,3]. In these papers, the authors observed a relatively fast decay of the surface potential; thus SiO_2 seemed to be not as good an electret material as polymers. However, recently Hohm charged thermally-grown SiO_2 samples with the corona method and found a good stability of negative surface charges [4].

CH2593-2/ 88/ 0000-0137$01.00 Copyright 1988 IEEE

In the present paper three methods of charging are applied to SiO_2 samples. The results of observing the surface potential stability at room temperature over a period of more than one year are given, whereby different production methods of the SiO_2 are choosen as a parameter. Furthermore open-circuit TSC-measurements are carried out, activation energies are calculated and the results are compared to the decay curves.

2. SAMPLE PREPARATION

The samples consisted of 2 inch, 4 Ωcm, p-doped silicon wafers, which served as substrates. The wafers were oxidized either by thermal methods or by chemical vapour deposition. After removal of the unwanted oxide at the back surface, a 500 nm aluminium layer was evaporated. For practical reasons each wafer was cut into 4 pieces which had an area of about 5 cm^2. To distinguish between samples made by different oxidation processes they are designated as type A to type D as is shown in table 1.

TABLE 1: Samples prepared with different methods

type	oxidation parameters	thickness
A	dry oxygen, t_{ox}=80min, T=1100°C	150nm
B	H_2 and O_2, t_{ox}=220min, T=1100°C	1µm
C	O_2 + H_2O, t_{ox}=180min	1µm
D	doped CVD, T=450°C	1µm, 2.5µm

3. METHODS OF CHARGING

All types of samples could be either positively or negatively charged with the liquid-contact and corona methods in the same way as one charges polymer electrets [5]. Charging with an electron-beam requires knowledge of penetration depth and secondary emission yield at a certain energy of the beam-electrons [6,7]. According to a method of Gross et al. the samples could be positively charged by irradiation with electrons [8]. Negatively electron-beam charged SiO_2-electrets were prepared in two ways. The simplest way, namely irradiation with non-penetrating electrons, was only successful with 2.5 µm thick samples of type D. The reason for the fact that other samples with thinner oxides could not be charged in this manner is not known. The second way is to irradiate the samples through a thin polymer foil. In

doing so the penetration depth had to be of the order of the foil thickness.

4. STABILITY AT ROOM-TEMPERATURE

Samples of all types were charged with the corona method to a charge density of about 1 μC/cm². This corresponded to an electrical field of about 3 MV/cm, which was below the breakdown field in SiO_2. To observe the charge decay over a long time period, the samples were taken out of their storage box from time to time, and the surface potential V was measured with a Monroe probe. The results for negatively and positively charged samples can be seen in FIG. 1 and FIG. 2 respectively. The oxide thickness and the initial surface potential V_{max} are given in brackets. It can be seen that negatively charged samples showed a better stability of the surface potential than positively charged samples. Especially the negatively charged sample of type B showed no decay in a time period of one year.

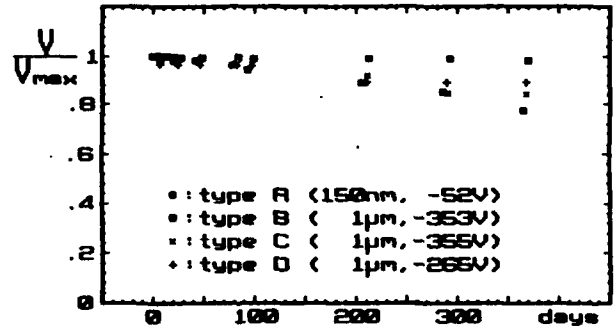

FIG. 1: Decay of negatively charged samples

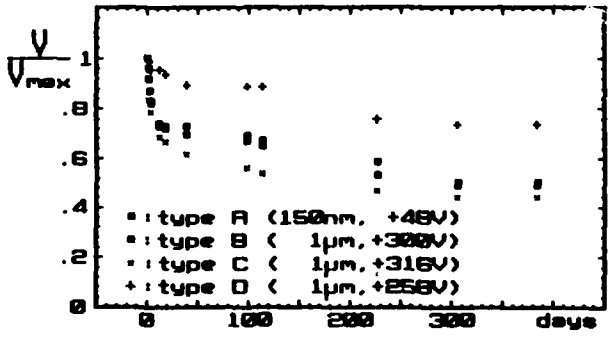

FIG. 2: Decay of positively charged samples

5. OPEN-CIRCUIT TSC-MEASUREMENTS

The experimental parameters of the open-circuit TSC-measurement were an airgap of about 1.5 mm and a linear temperature increase of 2 °C/min, which gave a maximum current of about 0.5 pA. The TSC-spectrum of negatively charged samples as well as of positively charged samples showed only one ore two relatively sharp peaks. As can be seen in figures 3 and 4, negatively charged samples showed the main peak at a temperature of about 300 °C, whereas positively charged samples exhibited the main peak at temperatures of less than 200 °C. In analysing the effects of different charging methods and different types of samples it was found that for negatively charged samples the charging method played a minor role with respect to the shape of the TSC-curve. But if one compares different types of samples some differences occur (FIG. 3). The oxides made with the CVD-process showed some discharge current at low temperatures before the maximum, which is not the case for wet grown oxides.

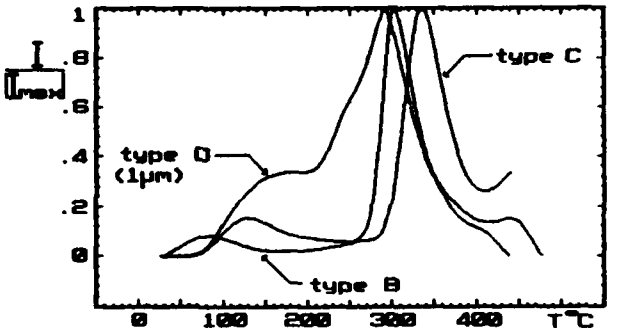

FIG. 3: TSC-curves of negatively charged SiO_2-electrets

FIG. 4: TSC-curves of positively charged SiO_2-electrets

For positively charged samples the shape of the discharge current depended rather on charging method than on the type of oxide. Electron beam charged samples showed a peak temperature of obout 200 °C, wheras samples charged with other methods had peak temperatures of less than 120 °C (FIG. 4). Because of the relatively sharp peaks, which could be found in most cases, activation energies were calculated with the 'Initial Rise' method of Garlick and Gibson [9]. An activation energy of about 1.9 eV was calculated for negatively charged samples. Positively electron beam charged samples gave an activation energy of 1.4 eV. Otherwise positively charged samples had activation energies of about 1.0 eV.

6. CONCLUSIONS

SiO_2, thermally grown as well as made by chemical vapour deposition, was charged with different methods. Results of charge decay at room temperature and open circuit TSC-experiments indicate good electret characteristics. Especially negatively charged samples and samples positively charged with electron beams showed high peak temperatures. Therefore one can expect a good charge stability even at temperatures where polymer-electrets already decay. Although some more experiments have to be carried out, SiO_2 seems to be an interesting electret material for many future applications.

ACKNOWLEDGMENTS

The author is indebted to Prof. G. M. Sessler for stimulating discussions and to the Institute Of Semiconductor Technology in Darmstadt for sample preparation.

REFERENCES

[1]A.Goetzberger,Archiv d. elektr. Übertr.,20,241 (1966)
[2]G.M.Sessler,J.E.West,Electrets,Charge Stor.,292(1973)
[3]R.Williams, M.H.Woods, J.Appl.Phys., 44, 1026, (1973)
[4]D.Hohm, VDI-Fortschrittsber., Reihe 10, Nr.60, (1986)
[5]G.M.Sessler,Electrets (2.Ed.), Springer Verlag (1987)
[6]T.E.Everhart,P.H.Hoff,J.Appl.Phys.,42(13),5837,(1971)
[7]H.Seiler, J. Appl. Phys. 54 (11), R1 - R17, (1983)
[8]B.Gross,H.von Seggern,J.West, J.A.P., 56, 2333,(1984)
[9]G.F.Garlick,A.F.Gibson, Proc.Phys.Soc. 60,574, (1948)

OBSERVATION OF UV PHOTO-STIMULATED CURRENTS OF TEFLON ELECTRETS

Tetsuji Oda, Tomoaki Utsumi* and Genso Matsubara

Department of Electrical Engineering, University of Tokyo
7-3-1 Hongo, Bunkyo-ku, Tokyo 113, Japan

Photo-Stimulated Currents (PSC) of corona-charged FEP and PTFE teflon electrets were observed to understand the charging mechanism of dielectric films. Very weak current of the order of 10 or 100 fA was found when monochromated UV photon of the D_2 lamp was irradiated to the film through the semi-transparent electrode. The current value and polarity are dependent on the thickness of the semi-transparent electrode. The current is mostly due to the charge injection from the electrode by the photo-irradiation.

INTRODUCTION

Photo-Stimulated Currents (PSCs) from polymers have been studied to understand the trap mechanism and so on by many researchers. The authors have also observed photo-stimulated currents of teflon materials[1] indicating that the critical energy of photon to generate PSC was 4.9 eV. However, the reproducibility of the PSC itself was not so well before. The light transmission factor of each sample was monitored to improve the reproducibility and some relation between the transmission factor and the PSC was found. Such test results are reported here.

EXPERIMENTAL

The sample film (PTFE or FEP teflon) of 100 μm thickness is metalized by the evaporation of thin gold as a semi-transparent electrode on one side. The other surface is charged by corona ions produced by 15 needles (typically ±22.5 kV) arrayed 11 cm over the film at 150°C for 30 min. The surface potential of the film is controlled by inserting the mesh grid electrode of V_g which is located 2 cm above the sample surface.

*He is now at Hitachi Research Laboratory, Hitachi Ltd.

CH2593-2/ 88/ 0000-0142$01.00 Copyright 1988 IEEE

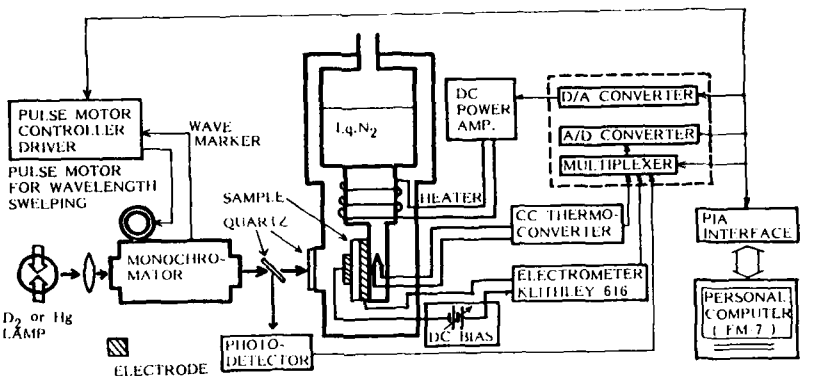

Fig.1 Schematic block diagram of PSC measuring system.

A Photo-Stimulated Currents (PSCs) measuring system is greatly improved by using the personal computer (Fujitsu FM-7 with six 6821PIA interface chips). The whole system is shown in Fig.1. The sample is installed in a cryostat where the charged surface is attached to a metal electrode and the light is irradiated to the back surface through the semi-transparent gold electrode. Scanning speed and range of photon energy are changed by the computer and,PSCs measured by an electrometer (Keithley 616) are digitalized and processed to increase the SN ratio by the hand-made AD converter system and the computer. The sensitivity of the PSC is fA range. A typical output example of test results for a negatively charged FEP teflon electret is Fig. 2 where a scanning wave-length, a sample temperature, a photo-intensity monitored in-situ

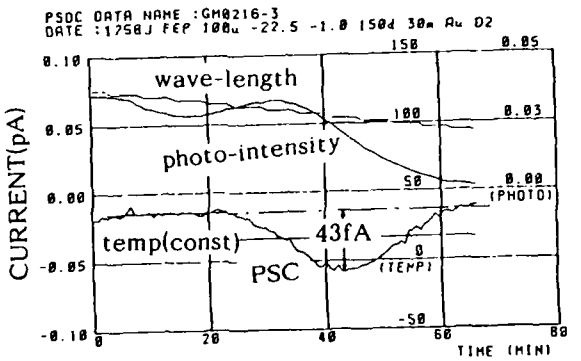

Fig.2 An example of PSC computer output of negatively corona charged FEP teflon where horizontal axis is time.

and PSC are shown. The transmission factor of the semi-transparent electrode is checked simply by using the commercial W-lamp and a photo-diode.

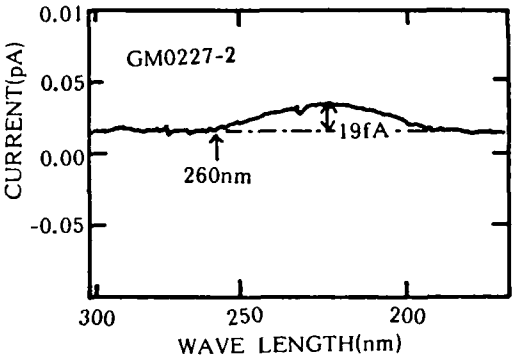

Fig.3 PSC of positively charged FEP.

RESULTS

PSCs of negatively and positively charged FEP teflon electrets are demonstrated in Figs. 2 and 3 respectively. In both cases, homo-currents are observed and the maximum values of TSCs are -43 fA or +19 fA. Those values are found to be strongly dependent on the transmission factor of the semi-transparent electrode which will be discussed later. The critical photon energy (minimum energy to generate PSC) was found to be 4.8 eV in every case.

Figure 4 is a light wave-length dependence of the transmission factor of the FEP film itself. One example of the light transmission factor of the FEP film coated by gold evaporated as the semi-transparent electrode is also included. The decrease of the transmission factor at short wave-length range is observed which is due to the absorption effect of the FEP teflon sheet itself.

In order to understand the photo-stimulation mechanism, surface potential profiles of charged films were observed by an automatic measuring system composed with a Monroe 244, a digital X-Y stage and so on. Figures 5 and 6 show examples of such profile-changes by the irradiation of ultra-violet light which was scanned by the Nikon mono-

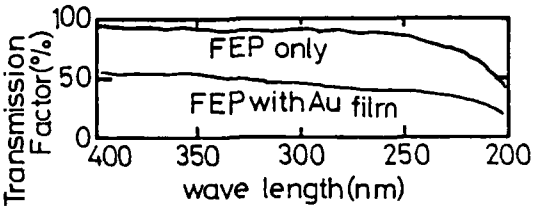

Fig. 4 The wave-length dependence of the transmission factor of FEP teflon sheets with and without gold film.

chrometer (P-250) from 300 nm to 200 nm for about 1 hour where a light source was a 30 W D_2 lamp. The average surface potential of negatively corona charged film was stable and about -800 V. The average potential was decreased to be about - 600 V after the irradiation. That is, the irradiation causes potential-change of about 200 V. In the case of positive charging, the original surface potential was about + 480 V indicating the unstableness of the positive charge. The UV irradiation also causes the surface potential decrease of about 160 V. This irradiation effect is convinced, for the same handling of the sample where the lamp power was off causes no such change of the surface potential.

Peak values of PSCs of various samples are plotted as a function of film's transmission factor in Fig. 7. In the case of negative charging, the peak is homo-current and increases in proportion to the transmission factor when the factor is less than 25%. When the film is positively charged, the polarity of the PSC depends on the transmission factor. That is, the PSC is hetero-current when the factor is small. The homo-current becomes dominant according to the increase of the transmission factor.

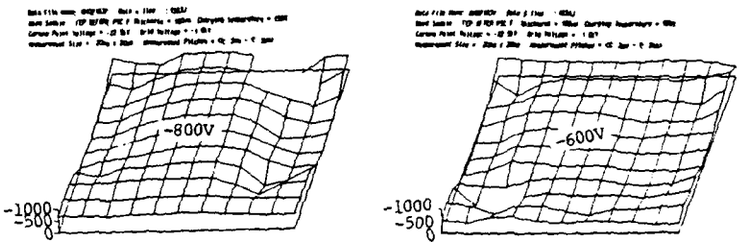

(a) Before PSC measurement (b) After PSC measurement
Fig.5 Surface potential profile of negatively charged FEP.

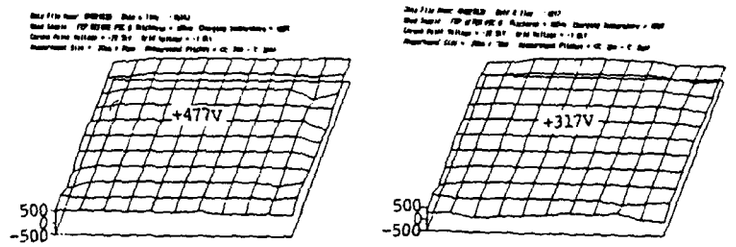

(a) Before PSC measurement (b) After PSC measurement
Fig.6 Surface potential profile of positively charged FEP.

DISCUSSION

To explain the experimental results, one model composed of two basic mechanisms is proposed where one is the electron discharge from the trap by the irradiation of photon energy, and the other is the photo-electron injection from the electrode metal. This model is shown in Fig.8. The supporting result to show the injection mechanism is the constant critical energy of 4.8 eV to generate the PSC for any material. The surface potential decrease of negatively charged film shown in Fig.5 explains the existing the discharge from the trap. The polarity change of PSC in Fig.7 is assumed that the charge injection from the semi-transparent electrode is larger than that from the left electrode when the semi-transparent gold electrode is thick and the factor is small.

REFERENCES

1] T.Oda and T.Utsumi:
Proc.ISE5 pp288-293
(1985)

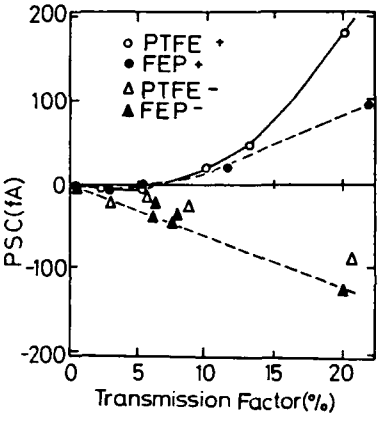

Fig. 7
Peaks of PSCs for different FEP or PTFE sheets versus the transmission factor.

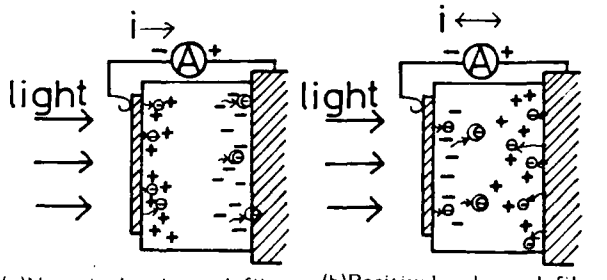

(a)Negatively charged film (b)Positively charged film

⊖ Injected electron from electrode

◎ Movable detrapped electron

Fig. 8 Model explaining the PSCs of teflon.

EFFECT OF POLYMER BLENDING ON THE DIPOLES OF CONSTITUENT POLYMERS

P.K.C. Pillai, A.K. Tripathi, R. Sekar, Anita Tripathi and G.K. Narula

Electrets & Optoelectronics Group, Physics Department
Indian Institute of Technology,New Delhi-110016, India

ABSTRACT

The films of polyblends of polymethyl-methacrylate:polyvinyl Acetate; polyethylene:PVC and polycarbonate:polypropylene were prepared either by solution cast technique or by compression moulding. The thermally stimulated discharge current studies on the thermoelectrets of these blends were carried out at different fields and temperatures. The results indicate that the polarization state in these blends is mainly due to charge carrier trapping that leads to induce dipole formation. Moreover, it has been found that the dipoles in the polyblends are so constrained that their contributioin to the total polarization of the blend is negligible.

INTRODUCTION

Lot of work is being done on polymerblends these days because of the possibility of tailoring economically the end product to suit the specific requirement. Good amount of literature is available on the mechanical properties of polyblends but no systematic study has been done on their electrical properties. In the present paper, an attempt has been made to investigate the effect of blending two polymers on their respective dipoles, using thermally stimulated discharge current (TSDC) method. This technique has shown that the characteristics of electrets are very sensitive to the structure of electret forming material [1]. Therefore, the TSDC study of polymer blends is likely to

CH2593-2/ 88/ 0000-0147$01.00 Copyright 1988 IEEE

give valuable informations about the molecular interaction and the extent of mixing between the two individual components. Polymer blends are heterogeneous mixtures and the possibility of charge carriers trapping at the trapping sites created by the grain boundaries of individual polymers will be higher in such blends.

The blends used in the present study are polymethylmethacrylate:polyvinyl-Acetate (PMMA:PVA_c, both polar and forms compatible blend) [2], polyethylene:polyvinylchloride (only PVC polar, noncompatible) and polycarbonate:polypropylene (PC:PP, only PC is polar, noncompatible blend).

EXPERIMENTAL

PMMA and PVC were obtained from BDH (India); PC from Bayer's (Germany); PP from Sri Ram Institute of Industrial Research (New Delhi) and PE and PVAC from Poly Sciences Inc. (USA). The blends and samples of PP:PC were made by melt extrusion and compression molding respectively. PVC:PE blend sample were prepared by solution cast method using cyclohexanon as solvant on Al substrate, PMMA:PVAC blend sample were coated on glass substrate using chloroform as solvant. These blends were made by taking the constituent polymers in 50:50 weight ratio. Vacuum deposited electrodes were used in case of PP:PC and PMMA:PVAC polyblends; while hot pressed Al foil electrodes were used in case of PVC:PE polyblend. Electrets of these samples were prepared at different poling temperatures and fields (as indicated in figures). The depolarization current was measured on a Keithley 610C electrometer.

RESULTS AND DISCUSSIONS

Typical TSDC spectra for PVC and PE are shown in Figs.1 and 2 respectively. The 86°C peak in PVC sample as expected is dipolar in nature, as the peak position is independent of both poling temperature (T_p) and poling field (E_p). The activation energy determined by initial rise method is found to be about 0.5 eV. The peak observed at about 105°C (Fig.2) in the TSDC thermogram of PE may be assigned to space charge as the peak current decreases with higher poling temperature. Moreover, the crystallite melting temperature for PE is also about 100°C. The TSDC thermograms of PP, PVAC and PMMA, PC were also recorded at different field and temperatures. These thermograms show usual dipolar or space charge peak [3,4].

The peak position in case of dipolar relaxation shifts toward higher temperature with increase in T_p as more and more dipoles are activated but above certain T_p value (where all the dipoles are activated) this becomes independent of T_p and the peak current (I_m) shows saturation with T_p. The dependence of I_m on E_p for a dipolar peak is linear. In case of space charge polarization I_m increases with T_p for T_p values less than peak temperature, thereafter it decreases. Moreover, it shows nonlinear dependence on E_p and its position is dependent on both E_p and T_p [1,5].

The effect of poling temperature (T_p) and poling field (E_p) on the TSDC spectrum of 50:50 polyblends are shown in Figs.3-5 and Figs.7,8 respectively. In PE:PVC polyblend (Fig.3) a peak at about 115°C is observed. As

is obvious from the figure the peak position is independent of both T_p and E_p indicating that it is dipolar in nature. At the same time the increase in peak current and the observed saturation effect at higher fields (inset) is the characteristic of a space-charge polarization.

Similar contradictory results are observed in case of polyblends PMMA:PVAC (Figs.4 & 6) and PP:PC (Figs.5 & 7). In Figures 4 & 6 the apparent independence of I_m on E_p is suggestive of dipolar polarization while the decrease in I_m at higher T_p and saturation with E_p is indicative of space-charge polarization. In PP:PC blend also we found that peak temperature shifts with T_p (Fig.5) indicating that the peak is due to space charge polarization but the linear dependence of I_m on E_p (not shown in Figure) is suggestive of dipolar relaxation. However, the variation of the peak temperature with E_p is characteristic of space charge polarization.

A possible explanation for this apparent contradiction in the result can be explained on the basis of induced dipole formation. It seems that during polarization the charge carriers both injected from electrodes as well as present in the sample are trapped in such a way as to form dipoles. Latter these dipoles are aligned in the presence of field to give rise to polarization state in polyblends. These results are also confirmed on the basis of activation energy values calculated from initial rise method for individual polymers and their blend [6]. Here it is pertinent to note that no characteristic dipolar peak of constituent polymer

was obtained in the depolarization spectro of polyblends. This clearly indicates that the contribution of dipoles in the total polarization of polyblends are either insignificant or is getting masked by the space charge polarization.

REFERENCES

1. J. Van Turhout, 'Thermally Stimulated Discharge of Polymer Electrets' (Elsevier, Amsterdam, 1975).

2. B. Schneier, J. Polym. Sci. 18 (1974) 1987.

3. P.K.C. Pillai, G.K. Narula, A.K. Tripathi and R.G. Mendiratta, Phys. Rev. B26 (1982) 2508.

4. R. Sekar, Anita Tripathi, T.C. Goel and P.K.C. Pillai, J. Mater. Sci. 22 (1987) 3353.

5. J. Van Turnhout, in Electrets, Vol.33, Topics of Appl. Phys. (Sringer, N.Y. 1980).

6. Anita Tripathi, A.K. Tripathi and P.K.C. Pillai, J. Appl. Phys. (In Press).

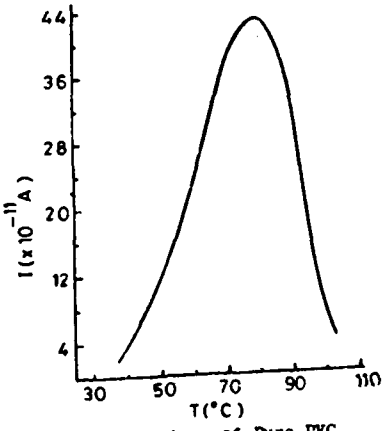

Fig.1. TSC Spectrum of Pure PVC Tp-80°C / Pol. Vol. 500V.

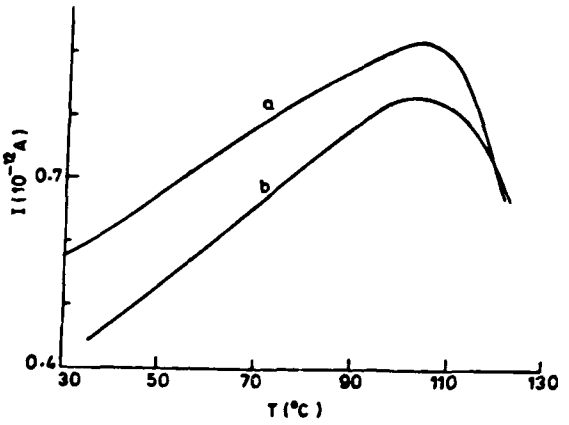

Fig.2 TSD spectra of PE sample. V_p=500 V: T_p, a,100° C; b, 110° C.

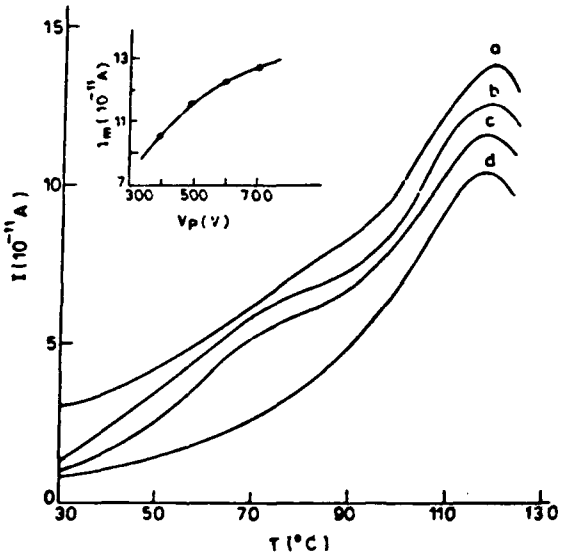

Fig.3 TSD spectra of PVC:PE polyblend. a, T_p 100° C, V_p 500 V; b, T_p 80 C, V_p 700 V; c, T_p 80 C, V_p 500 V; d, T_p 80 C, V_p 400 V.

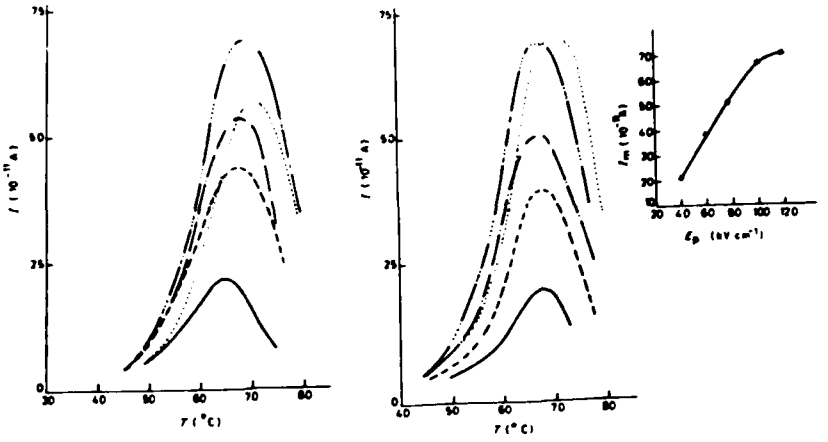

Fig. 6

Fig.4 Effect of T_p on TSD spectra of PMMA:PVAc at E_p=100kV/cm:(——)50°C, (—·—) 60°C, (—···· —) 80°C, (····) 100°C.

Fig.6 Effect of E_p on TSD spectra of PMMA:PVAc. at T_p=80°C: (——) 40 kV/cm, (— —) 60 kV/cm, (—·—) 80 kV/cm, (—···—) 100 kV/cm, (····) 120 kV/cm.

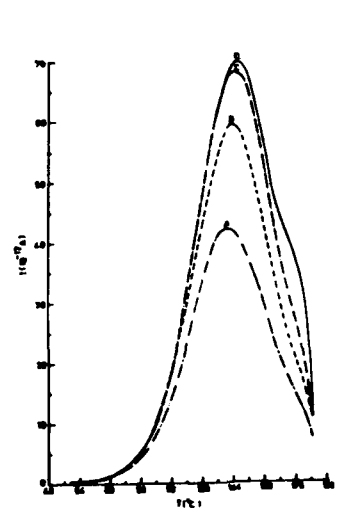

FIG. 5. Effect of T_p on TSD thermograms of PP:PC E_p = 50 kV/cm: *A*, 100°C; *B*, 120°C *C*, 140°C; *D*, 150°C; t_p = 1 h.

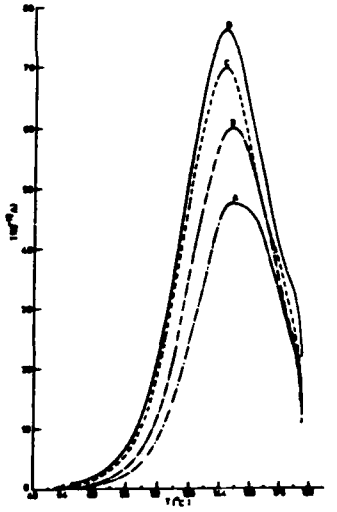

FIG. 7 Effect of E_p on TSD thermograms of PP:PC T_p = 150°C: *A*, 30 kV/cm; *B*, 40 kV/cm; *C*, 50 kV/cm; *D*, 60 kV/cm; t_p = 1h.

ELECTROMECHANICAL PROPERTIES OF COMPOSITE ELECTRET STRUCTURES

F. Micheron

Thomson-CSF/LCR, Orsay, France

ABSTRACT

A generalized thermodynamical model of composite electret structures is presented; in the case of excess charge electrets in serieswith linear dielectrics, it allows to compute the composite dielectric and mechanical properties, as well as the linear piezoelectric and pyroelectric effects. The electromechanical coupling coefficient and different figures of merit are computed for sensors and actuators, versus parameters defining the two dielectrics, and the geometry of the structure.

Since this model allows to define the equilibrium states of the composite structure, the conditions for electromechanical bistability are easily deduced.

BENDING PIEZOELECTRICITY OF FEP-TEFLON ELECTRETS

Toshiaki TAKAMATSU and Hiroyuki SASABE

The Institute of Physical and Chemical Research, 2-1 Hirosawa, Wako-shi, Saitama 351-01, JAPAN

Abstract

Bending piezoelectricity of unpoled and/or poled films of FEP-Teflon was investigated. Commercial films whose thickness ranges from 25 to 500 μm were used. The bending piezoelectric coefficient, β_{331}, for unpoled films or poled by applying an electric field E_p=1x10^{7}C/m at 130°C were estimated as (0.14-1.0)x10^{-9}C/m. The polarity of β_{331} changed when E_p was larger than 5x10^{7}V/m. Both surfaces of the unpoled film were negatively charged while the surface charge of the poled film were homocharges. Based on these results, mechanisms for the generation of bending piezoelectricity in the films were discussed.

1. Introduction

In the previous paper, we have reported that polypropylene (PP) and FEP-Teflon films showed the bending piezoelectric properties[1]. In case of FEP-Teflon electrets, the value of bending piezoelectric coefficient, β_{331}, was much larger than that of PP electrets. Especially, an unpoled FEP-Teflon showed the bending piezoelectricity. This paper represents some results on the bending piezoelectricity in the unpoled or poled films of FEP-Teflon.

2. Experimental

Commercial films of FEP-Teflon whose thickness ranges from 25 to 500 μm were supplied from Toray Co. Ltd. Both surfaces of the film were metallized with gold by the vacuum deposition as electrodes. The film was clamped at one end and the other end was bent by a moving driver perpendicular to the plane of the film. The tin foils were put on the electrodes as lead wires with a small amount of silver paste. The film was poled by

CH2593-2/ 88/ 0000-0155$01.00 Copyright 1988 IEEE

applying various electric field (E_p) for 30 minute at 130°C. The electric potential (ΔV) between the elect rode was directly measured with a vibrating reed electrometer as a function of bending deformation (Δx).

The bending piezoelectric coefficient (β_{331}) is defined by the following equation[2)]

$$\beta_{331} = V_3 l^2 \varepsilon_0 \varepsilon / (6\pi d \Delta x) \qquad (1)$$

and $$V_3 = \Delta V[C+C_0]/C \qquad (2)$$

Where C_0 is the input capacitance of measuring circuit, C the capacitance of the sample, l and d the length and the thickness of the sample, ε_0 and ε the dielectric constant in vacuum and of the sample, respectively. Therefore, the value of β_{331} is related to the ratio $V_3/\Delta x$. Two polarized films was piled each other with the same polarity of surface charge (defined as bimorph) and the β_{331} for the bimorph was also measured.

Surface charge (σ) of the unpoled or poled samples was measured by an induction method. Thermally stimulated current (TSC) of the samples was also measured at a heating rate of 2.6°C/min.

3. Results

Figure 1 shows the relationship between ΔV and Δx for the unpoled films. The value of ΔV increased with increasing Δx. The value of β_{331} strongly depends on the thickness of the unpoled film as shown in Fig. 2. That is, β_{331} decreased sharply with increasing thickness and reached a constant value. For the poled samples, on the

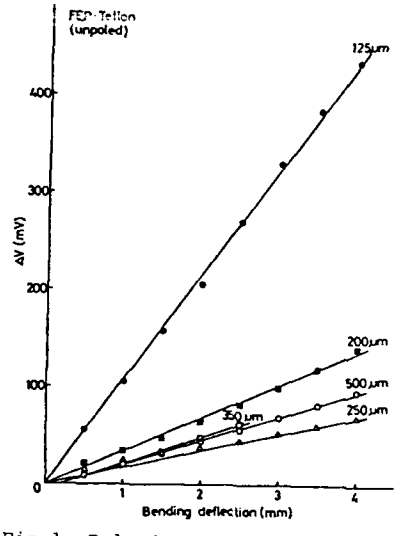

Fig.1. Relationship between ΔX and ΔV for the unpoled FEP-Teflon films.

Curve:	●	■	△	□	○
Thickness (μm):	125	200	250	350	500

other hand, the value of β_{331} seems to be independent of the film thickness as shown in Fig.3. Here the film was poled at $E_p = 1 \times 10^7$ V/m at $T_p = 130°C$.

Figure 4 shows the relationship between β_{331} and E_p for the bimorph. The value of β_{331} gradually decreased with increasing E_p and changed the polarity when E_p was above 5×10^7 V/m.

The relationship between σ and E_p for the films poled at 130°C is shown in Fig.5. When E_p was larger than 3×10^7 V/m, σ increased with increasing E_p and the polarity indicated homocharge.

Figure 6 shows TSC curves for the films poled under various E_p at 190°C. A broad peak appeared at about 170°C for all samples. When E_p was larger than 3×10^7 V/m, the second peak appeared at about 80°C.

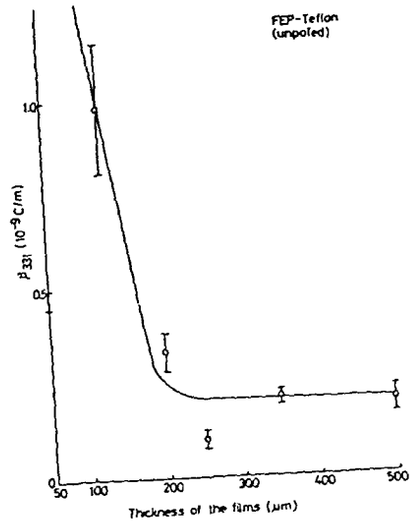

Fig.2. Relationship between thickness of the films, d, and β_{331} for the unpoled FEP-Teflon.

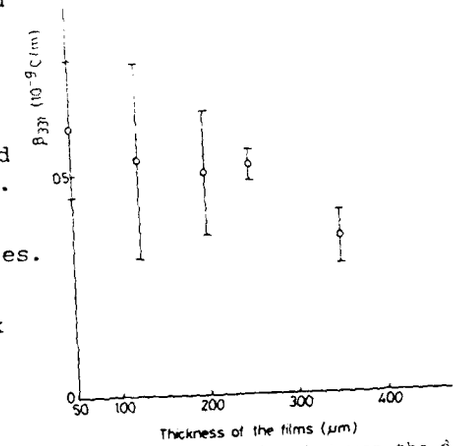

Fig.3. Relationship between the d and the β_{331} for a poled FEP-Teflon films. $E_p = 1 \times 10^7$ V/m and $T_p = 130°C$.

4. Discussion

As shown in Fig.1, the bending piezoelectricity appeared even in the unpoled films. This may be produced by the change of inhomogenous distribution

Of space charges which generated in the films during the industrial processes of the film formation. Both surfaces of the unpoled film showed negative polarity and the amount of charges was estimated as $(0.2\text{-}0.5)\times 10^{-5}\,C/m^2$. Distribution of charges was very inhomogenous. When the thickness of the film was within a range from 125 to 250 μm, charges with opposite polarities appeared on both surfaces, respectively. It means that a mechano-electret was formed. As the sample is nonpolar and the electric conductivity is very small ($\sim 10^{-17}$ S/cm), the space charge polarization due to macroscopic displacement of impurity ions can not be produced by the poling when E_p was 1×10^7 V/m at 130°C as shown in Fig.3. Therefore, the value of β_{331} may not be changed. When E_p was larger than 5×10^7 V/m at 130°C the homocharge can easily be produced. The homocharge increased with increasing E_p. A part of homocharges may be diffused and compensated with space charges existed in the films. As the result the value of β_{331} would decrease and

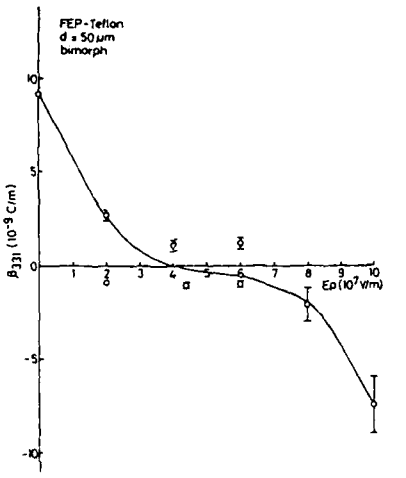

Fig.4. Relationship between the poling field E_p and β_{331} for the poled bimorph.

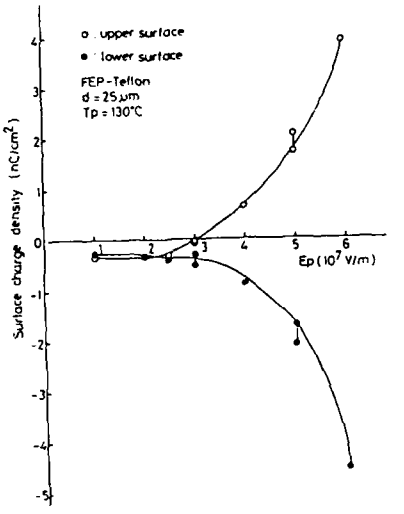

Fig.5. Relationship between surface charge and E_p.

change its polarity when E_p was larger than 5×10^{7} V/m.

The value of β_{331} for a corona charged bimorph was estimated as $(17-50)\times10^{-9}$ C/m and much larger than the others. The amount of surface charges by the corona poling is estimated as $(1-2)\times10^{-4}$ C/m^2 and much larger than that of the unpoled films, $(0.2-0.5)\times10^{-5}$ C/m^2. The homocharge is more stable and may effectively contribute to the bending piezoelectricity.

As shown in Fig.6, the TSC peak appeared at about 170°C. The peak temperature corresponds to crystalline dispersion of FEP-Teflon. The mechanism of TSC peak appeared at about 80°C is not clear yet. The analysis of the bending piezoelectricity in the polymer electrets are now in progress.

Reference

1. T.Takamatsu and H.Sasabe: Kobunshi Ronbunshu., 44 (7) 531 (1987)

2. H.Kawai: Jpn. J. Appl. Phys., 8 975 (1969)

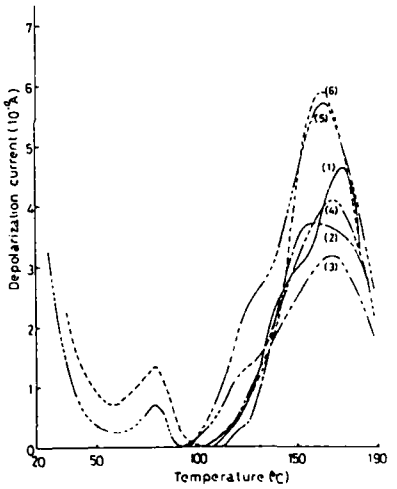

Fig.6. TSC curves for the poled films. T_p=190°C.

Curve	(1)	(2)	(3)	(4)	(5)	(6)
E_p (10^6 V/m)	4	8	16	24	32	35

DEFECT INDUCED MECHANISMS IN THE FERROELECTRIC-TO-PARAELECTRIC PHASE TRANSITION OF POLY(VINYLIDENE FLUORIDE - TRIFLUOROETHYLENE) COPOLYMERS.

R. L. Moreira, R. Almairac, and M. Latour

Groupe de Dynamique des Phases Condensées (LA233), Université des Sciences et Techniques du Languedoc, 34060 - Montpellier - Cedex - FRANCE.

ABSTRACT

X-ray techniques have been used to study the ferroelectric-to-paraelectric phase transition in poly(vinylidene fluoride-trifluoroethylene) copolymers. Thermal cycles for copolymers with 20 to 40 mol% trifluoroethylene are presented. Partial hysteresis cycle has been obtained for the 25 mol% trifluoroethylene sample. Clear evidence of anchoring and memory effects has been demonstrated. It appears that defects play a very important role on the mechanism of the transition. At least a part of them are mobile and can relax.

INTRODUCTION

Poly(vinylidene fluoride - trifluoroethylene) - P(VDF-TrFE) - copolymers are ferroelectric at room temperature, for TrFE contents ranging from 18 to 48 mol%. These materials present a first order phase transition (PT) to a disordered high temperature hexagonal phase. [1-3] Some important works have been carried out about these copolymers in the last years. [3,4] The results presented in the ref.4 have shown that, certainly, the defects present in the material play an important role on the PT behavior.

The purpose of the present work is to report on X-ray investigations about the influence of defects on the PT in 20 to 40 mol% TrFE copolymers. The results show some new effects, which can be understood by the interaction between defects and the order parameter.

CH2593-2/ 88/ 0000-0160$01.00 Copyright 1988 IEEE

EXPERIMENTAL

Resins of P(VDF-TrFE) copolymers were provided by Atochem (France). References are: P 988, P 989, P 997 and P 990, respectively for the samples with 20, 25, 30 and 40 mol% TrFE. The samples were melted, pressed at 200 □C, and then air-quenched to room temperature. The obtained films were about 250 μm thick.

X-ray transmission scans (2θ) were realized with a computer controlled apparatus, using monochromatic MoKα radiation. The samples were heated or cooled with ± 2□C/min rates. Each scan was performed isothermally during about 30 min. Measurements were taken for the first thermal runs. This procedure give us the so-called "normal" curves.

RESULTS AND DISCUSSION

Thermal hysteresis for the different copolymers are presented in Fig. 1. This figure shows the proportion of the ferroelectric phase, as obtained after numerical treatment of the intensities of the X-ray 2θ scans.[5] Increasing the defect rate (*) clearly favors the hexagonal phase: T_c decreases as the TrFE content increases from 20 to 40 mol%. Moreover, the thermal hysteresis is itself strongly defect dependent: it becomes narrower when the TrFE content increases. We can also observe a clear change of the shape of the hysteresis cycles. The slope of the heating curves strongly decreases when the TrFE content rises from 20 to 30 mol%. This indicates a strong coupling between the defects and the order parameter of the transition. [5]

The latest remark is confirmed by the result shown in Fig. 2, which presents an example of partial hysteresis cycle, obtained for the [illegible] mol% TrFE sample. At the (A) point on the heating curve, the temperature change is reversed. First, the evolution

(*) defects: (1) intra-chain defects, directly linked to the TrFE contents; and (2) intrinsic defects of the material.

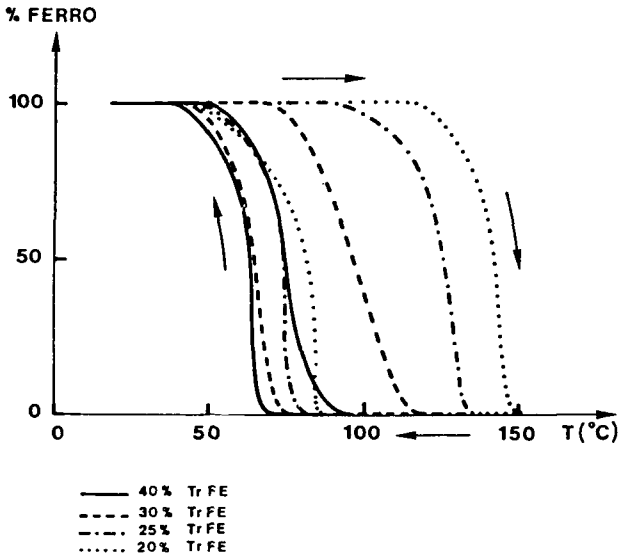

FIGURE 1. Temperature dependence of the % of the ferroelectric phase, for the P(VDF-TrFE) copolymers.

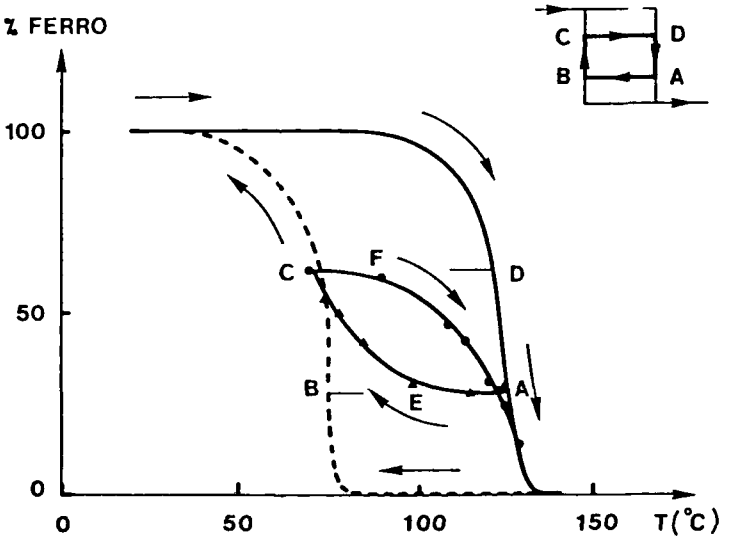

FIGURE 2. Partial hysteresis cycle for the 25 mol% TrFE copolymer. In the upper right hand side we show, schematically, the corresponding hysteresis (ABCDA) for a system without defects.

is that of a system without defect: AE segment. The influence of defects no longer becomes negligible around (E) point: along the EC line they favor the transition, which is then anticipated. The same process is observed for the reheating curve (starting from the (C) point): weak influence of defects from (C) to (F) and defect anticipated transition along the part FA.

Anchoring effect

The previous data have shown that the influence of defects is fundamental in the description of the transition. We will see now that this description must take into account all the thermal history of the sample. In Fig. 3 the heating run has been stopped at point (A). After 19 hours, the system have shown a slight evolution depicted by the AA' segment. Next, we restart the heating process. The system does not present any evolution until the (B) point, where it suddenly jumps to recover the "normal" heating curve at point (C). During all the time the sample was hold at constant temperature ((A) point), defects relax such that the whole system gets a more stable configuration. Restarting the heating process, this

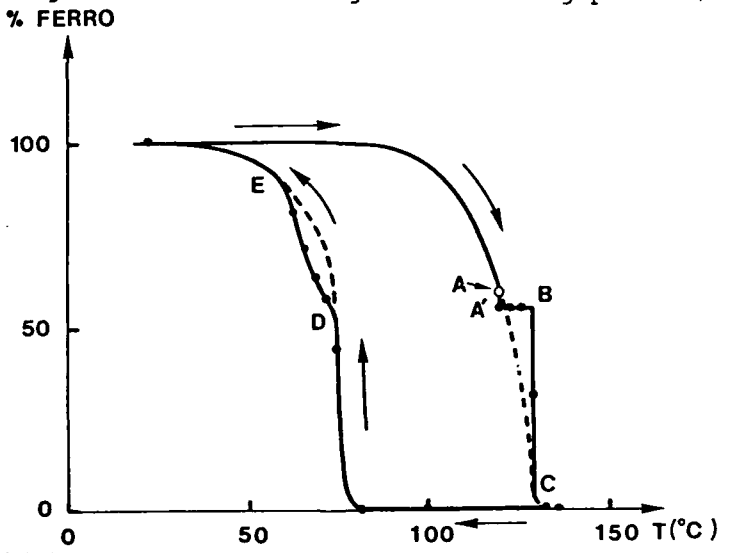

FIGURE 3. Anchoring and memory effects in a 25 mol% T-FE copolymer.

more stable configuration is then anchored by defects (AB), until the moment when a jump to the "normal" curve occurs (point (C)).

Memory effect

Now, the sample is cooled from the paraelectric phase. The defects which have relaxed along the AA' segment take time to adapt themselves to all the configurations followed by the system. A part of them stays in the state corresponding to the (A') point. Indeed, a clear anomaly is observed at the (D) point on the cooling curve, showing that the system kept a memory of the previous thermal history. Analogous effects, which are characteristic of systems containing mobile defects, have been observed in the case of incommensurate phases. [6,7]

In conclusion, defects play an essential role on the mechanism of the phase transition of P(VDF-TrFE) copolymers. We have demonstrated that at least a part of these defects are mobile and can relax, with relaxation times of the order of some hours.

Acknowledgements: One of us (R.L.M.) wishes to thank the Brazilian agency CNPq for fellowship support towards this work.

REFERENCES

[1] Y. Tajitsu, A. Chiba, T. Furukawa, M. Date and E. Fukada, *Appl. Phys. Lett.* 36, 286 (1980).
[2] A. J. Lovinger, T. Furukawa, G. T. Davis and M. G. Broadhurst, *Polymer* 24, 1233 (1983).
[3] K. Tashiro and M. Kobayashi, *Polymer* 27, 667 (1986).
[4] R. L. Moreira, P. Saint-Grégoire, M. Lopez and M. Latour, to appear in *J. Polym. Sci.: Part B*.
[5] R. L. Moreira, R. Almairac and M. Latour, to be published.
[6] P. Saint-Grégoire, F. J. Schäfer, W. Kleemann, J. Durand and A. Goiffon, *J. Phys. C: Solid State Phys.*, vol. 17, pp. 1375, (1984).
[7] P. Lederer, J. P. Jamet and G. Montambaux, *Ferroelectrics*, vol. 66, pp. 25-56, (1986).

THE APPLICATION OF SILICON DIOXIDE AS AN ELECTRET MATERIAL

A.J. Sprenkels*, W. Olthuis+ and P. Bergveld*

*Twente University, P.O.Box 217, 7500 AE, Enschede, The Netherlands
+CME Twente, P.O.Box 545, 7500 AM, Enschede, The Netherlands

ABSTRACT

We have investigated silicon dioxide for its electret properties. It appears that thermally grown silicon dioxide has a large lateral surface conductivity, resulting in a rather poor electret behaviour. This can be adequately reduced by a chemical surface modification resulting in an excellent silicon dioxide electret.

Our experiments have shown that corona-charged SiO_2 layers are much better resistant to high temperatures than Teflon-FEP electrets. A 1.1 μm thick SiO_2 layer, charged up to 150 V, yields a time constant of the charge decay in excess of 400 years at ambient laboratory conditions.

INTRODUCTION

Up to now mainly fluor carbon polymers, such as Teflon-FEP and Teflon-PTFE have been used as the electret material in microphones. Although Teflon is an excellent electret material its application techniques are hardly compatible with the use of new technologies, such as chemical etching techniques in the construction of a silicon subminiature electret microphone. For that reason it is worthwhile to investigate other materials employed in integrated circuit technology for their electret properties.

Preliminary measurements have been carried out on SiO_2 and Al_2O_3 samples. Based on these results and those reported in literature [1] as well as the fact that SiO_2 is a standard material in our laboratory, we have further investigated the electret properties of SiO_2 only.

In this paper it will be assumed that the *lifetime* of an electret is equal to the *time constant* of the charge decay, i.e. the period in which the electret charge has decayed to 63% of its initial value.

CH2593-2/ 88/ 0000-0165$01.00 Copyright 1988 IEEE

EXPERIMENTAL

All SiO_2 samples have been prepared by wet-thermal oxidation of 2-inch (100) 5-10 Ω cm p-Si wafers. In the first experiments we have charged 1.1 μm thick SiO_2 samples. These samples showed a charge decay, measured by the Monroe Isoprobe 244 electrostatic voltmeter, in the order of days which is unacceptable for microphone applications. In order to investigate the observed charge decay a steep charge profile has been created on a SiO_2 sample. The measured decay is shown in figure 1. The left side has been charged up to 150V, while the right side remained uncharged. As is clear from the figure, the charge is spreading relatively fast and evenly over the surface. This can be understood by assuming a relatively large lateral surface conduction. This lateral surface conductivity is mainly determined by a physical adsorption of polar groups (mainly water) to .he silanol groups at the interface [2]. These physically adsorbed OH-groups may be removed by a chemical surface modification, in which the polar silanol groups are substituted by apolar groups, which do not adsorb polar H_2O-groups [3]. This modification may be accomplished by treatment of the SiO_2 surface with Hexamethyldisilazane (HMDS). By this treatment the oxide surface is completely covered with a mono-layer of chemically bonded apolar CH_3-groups. Due to this treatment the adsorption of polar H_2O-groups has become very unlikely which

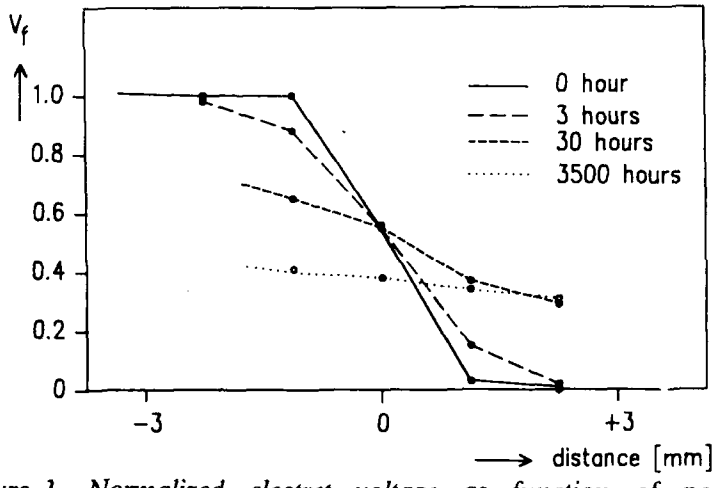

Figure 1 Normalized electret voltage as function of position and time showing the effect of the lateral surface conduction on a virgin 1.1 μm thick SiO_2 electret.

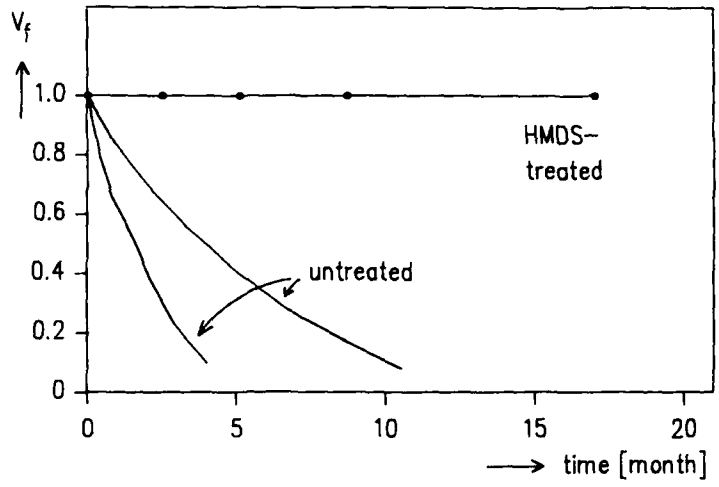

Figure 2 The normalized measured electret voltage decay at ambient laboratory conditions of some SiO_2 electrets with and without a HMDS treatment.

results in a very low surface conductivity. The results of this treatment are shown in figure 2. The lower curves represent the charge decay of a number of untreated SiO_2 electrets, which have been charged up to 150 V. The upper line represents the decay of a 150V-HMDS-treated SiO_2 electret.

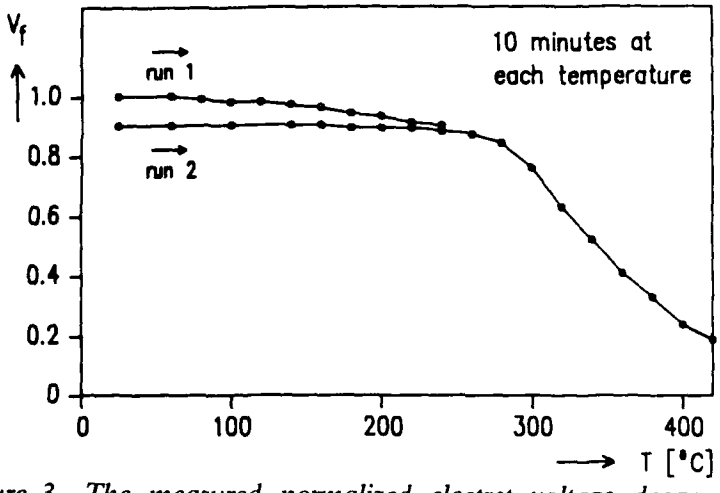

Figure 3 The measured normalized electret voltage decay of a 1.1 μm thick HMDS treated SiO_2 electret as a function of temperature.

In order to examine the temperature dependence, a HMDS-treated SiO_2 electret has been measured; the results are given in figure 3. The temperature has been increased in 20°C steps of 10 minutes each, from 20°C up to 240°C in the first run and from 20°C up to 400°C in the second run.

After each temperature step the sample was cooled down to room temperature and measured. Considering figure 3, some charge has been released in the first run at temperatures up to 240°C. During the second run hardly any charge has been released at temperatures below 240°C. It is concluded that the traps with a low activation energy had been released already in the first run and thus these traps were not active anymore during the second run. In the range from 240°C - 420°C the charge decay becomes significant again, which is due do the release of traps with a higher activation energy.

The *tendency* of the charge decay of the HMDS-treated SiO_2 electret appears to be comparable to that of Teflon [4]. However a higher temperature is needed for this type of electret to show the same charge decay as a Teflon electret. This suggests that the charges in a SiO_2 electret are more stable than in a Teflon electret. This is even more clear from figure 4, where the electret charge decay (trace 1) of a HMDS-treated SiO_2 electret is shown at a constant temperature

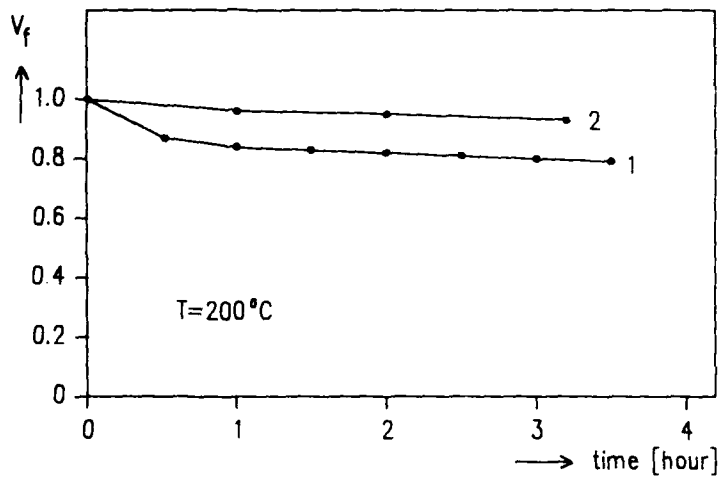

Figure 4 The normalized measured isothermal electret voltage decay of a 1.1 μm HMDS-treated SiO_2 electret at 200 °C (trace 1). If this electret is subsequently charged to its initial charge level, it has become better resistant to temperature (trace 2).

of 200°C. During the first hour the charge decays rapidly, while thereafter the decay is more or less stabilized. First the traps with a relatively low activation energy release their charges. After one hour these traps are empty and a second kind of deeper traps determines the charge decay. If this sample is charged again up to 150 V, and heated in the same way, trace 2 is found. The same phenomenon has been observed for Teflon electrets [5].

CONCLUSIONS

It has been demonstrated that an untreated SiO_2 layer is a poor electret mainly due to a large lateral surface conduction.

However a 1.1 μm thick SiO_2 layer turns into an excellent electret if the surface conductivity has been reduced by an appropriate chemical surface modification. This surface modification is adequately accomplished by a hydrophobic conversion using HMDS.

We have not measured any charge decay at room temperature for a period of 17 months of well-prepared SiO_2 electrets charged up to 150 V. This results in a lifetime (time constant) of more than 400 years.

It is adequate to age SiO_2 electrets by a two or three charge-discharge cycles prior to use. By this treatment, which is known as artificial ageing, the traps which cause an initial charge decay are discharged. It may be concluded that the charge decay mechanisms of Teflon and SiO_2 electrets are very much alike, occurring however at different temperatures.

REFERENCES

[1] D. Hohm and R.Gerhard-Mulhaupt, "Silicon-dioxide electret transducer", J. Acoust. Soc. Am., vol.75, no.4, pp. 1297-1298, April 1984.

[2] J.A Voorth[illegible], K. Keskin and P. Bergveld, "Investigations of the surface conductivity of silicon dioxide and methods to reduce it", Surface Science, vol.187, pp.201-211, 1987.

[3] A.van den Berg, P. Bergveld , D.N. Reinhoudt and E.J.R. Sudhölter, "Sensitivity control of ISFETs by chemical surface modification", S. and A., vol.8, pp.129-148, 1985

[4] A.J. Sprenkels, A silicon subminiature electret microphone", Thesis, Twente University, 1988.

[5] G.M Sessler, ed., "Topics in applied physics", vol.33, "Electrets", Springer-Verlag, Berlin, 1980.

THE INTERACTION OF FISSION FRAGMENTS WITH ELECTRON BEAM CHARGED POLYFLUOROETHYLENE PROPYLENE

Stephen R. Berggren and George John

Air Force Institute of Technology, Mail Stop AFIT/ENP
Wright-Patterson Air Force Base, Ohio, 45433

ABSTRACT

Interactions of fission fragments with charged polyfluoroethylene propylene (FEP) create detectable electrical signals characteristic of the event. FEP charged with 30-50 keV electrons can attain internal electrostatic fields that approach the dielectric strength. Fission of ^{235}U by thermal neutrons produce fission fragments with energies of 60-100 MeV that deposit their energy in 20-40 μm of FEP. This induces charge-pair production and a temporary radiation-induced conduction path detectable with conventional radiation detection electronics. The exact mechanisms and characteristics of this phenomena are being investigated for possible use in small, simple, self-powered thermal neutron detectors.

INTRODUCTION

Most applications of electrets for monitoring radiation have depended on the gross discharge of the electret. In this work electrets have been used to detect individual interactions from fragments resulting from the fission of ^{235}U by thermal neutrons. This is possible because the high energy of the fragments, 60-100 MeV, and their short range, 20-40 μm produce detectable pulses. Determining the characteristics of this signal and the mechanisms that produce it are the objects of our studies. The signal may be applicable to the design of small, simple, self-powered thermal neutron detectors.

FISSION FRAGMENTS

When a ^{235}U nucleus absorbs a neutron, it fissions into two smaller nuclei with a total kinetic energy of $\approx$ 167 MeV. The masses of these nuclei are bimodally distributed about 95 and 140 AMU. In addition there is a distribution in the kinetic energies of the fragments and in the direction of emission of the oppositely directed pairs. The fragments are positive ions with charges of +16 to +20 that heavily ionize any medium they traverse. A semi-empirical formula[1] was used to calculate the

stopping power (i.e., -dE/dx) for various fission fragments in FEP. The results are shown in Figure 1. The track length corresponds to the end point of each curve.

THEORY

A signal can occur from a fission track if mobile charge carriers exist in a conductive path across the field region. The charges may be those trapped in the charge region or charge pairs produced by ionization. The two sources may be distinguished by the effect of charge density on the signal.

Along a fission fragment track, gross ionization occurs by inelastic collisions between the heavily charged fragment and the valence electrons of the media. This should almost instantaneously create a conduction path across the field region of the electret. A rough estimate of its conductance is possible using a semi-empirical equation for radiation induced conductivity (RIC):[2]

$$g = 1.9 \times 10^{-16} \Phi^{\delta} \qquad (1)$$

where g is the conductivity in $(\text{ohms-cm})^{-1}$ and Φ is the dose rate in rads/sec with $\delta = 1.0$ for pulsed irradiation.[3] Although this equation is for relatively low dose rates from an electron beam, it will establish a lower limit to the conductance, C, of

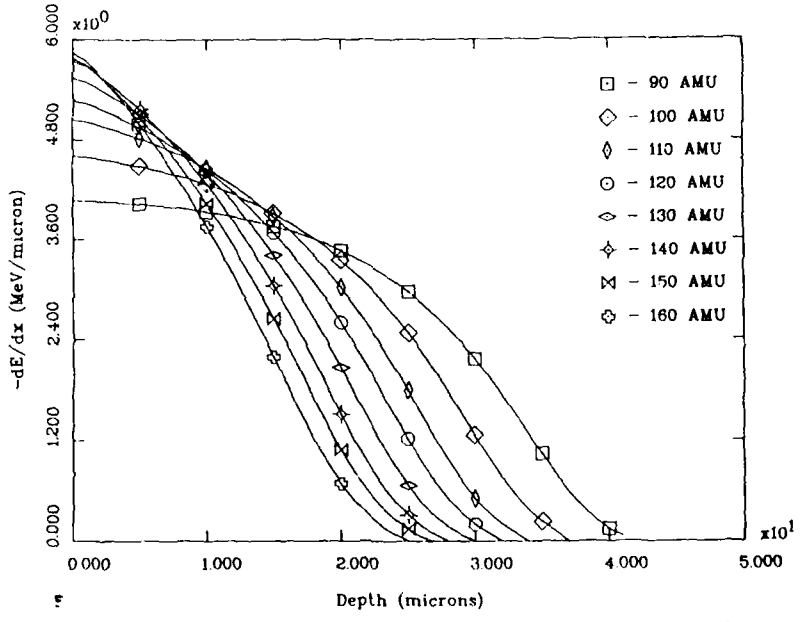

Figure 1: Fission Fragment Stopping Power in FEP.

the path, viz.,

$$C = \frac{3.04\ x\ 10^{-24}\ E_d(MeV)}{\rho(gm/cm^3)\ [T(cm)]^2\ t(sec)} \tag{2}$$

where E_d = the energy deposited by the fission fragment, ρ = density , T = track length and t = irradiation time. Note that the conductance is not a function of the radius of conductive effect. An 80 MeV fission fragment deposits its energy in $\approx$ 2 x 10^{-12} seconds and its track length is 30 μm to produce a C of $\approx$ 10^{-5} ohms^{-1}. Ionization and thermal effects, not considered in equation 1, should make the conductance significantly larger, if only for a few microseconds.

In an electric field the charge-carrier pairs in a conductor migrate to produce an electric signal. Charge-pair collection in various plastics was shown to go as:

$$Q_c\ \alpha\ F^{1.5} \tag{3}$$

where Q_c is the collected charge and F is the field strength.[4] The effective charge, Q_e, (that seen by the preamplifier) resulting from charge carrier pair production in the fission fragment path is:

$$Q_e = \frac{L\ e\ E_d}{D\ W} \tag{4}$$

where e = electronic charge, W is the energy needed to produce a charge-carrier pair, L is the charge layer depth and D is the electret thickness. A typical value for Q_e from charge pair collection is $\approx$ 2 x 10^{-15} coulombs.

A fission fragment track intersecting the charge region of the electret also provides a conductive path for trapped charges to reach the front surface. The charge released from a cylinder about the track may be estimated by assuming that the track is at surface potential, causing local breakdown conductivity. The effective charge is:

$$Q_e = \frac{\sigma^3\ L^3\ \pi}{D} \left[\frac{(1 - L/D)}{F_b\ \epsilon_0\ \kappa}\right]^2 \tag{5}$$

where σ is the charge density, ϵ_0 is the dielectric constant, κ is the dielectric coefficient and F_b is the dielectric breakdown strength of FEP. For an electret charged to 10^{-7} coul/cm^2 at 50 kV, Q_e by trapped charge collection is 5 x 10^{-15} coulombs. Note the cubic dependance of Q_e on σ. Note also that equation 5 is not dependant on fission fragment energy but requires only that the fission fragment penetrate to the charge region.

EXPERIMENTAL SETUP

The electret material used in the experiments is 25.4 μm Teflon FEP film coated on one side with 1000 angstroms of aluminum. The aluminized side is attached to a 3-cm diameter stainless steel carrier disk. On most samples, a 2.5-cm diameter central spot on the front surface is covered with 1000 angstroms of aluminum. The samples are charged using an electron beam system at energies from 10 to 50 keV.

Once charged and annealed, the samples are tested for their electronic response to fission fragment interaction. The test device and electronics are shown in Figure 2. As currently configured, the system is capable of reliably detecting effective charge events greater than 3×10^{-16} coulombs. The fission fragment source is a 2.5-cm diameter spot of 97 percent enriched ^{235}U electroplated onto a copper disk and installed in a thermal neutron pile.

RESULTS

Electron-beam charged electrets, exposed to fission fragments, yield a pulsed electrical signal. Figure 3 is a typical example of the charge distribution of the signal. Background noise is less than 3×10^{-16} coul.

Study of this signal is ongoing, but the following characteristics are noted:

1. The number of pulses seen does not correspond directly to the number of fission events. Only about one pulse appears per 100 fissions.
2. The pulse response of the electrets appears to decay with time.
3. Thermally annealed electrets produce significantly fewer pulses than unannealed electrets.
4. When first installed, freshly charged electrets produce spontaneous signals of similar characteristics. These signals disappear after $\approx$ 1 hr.

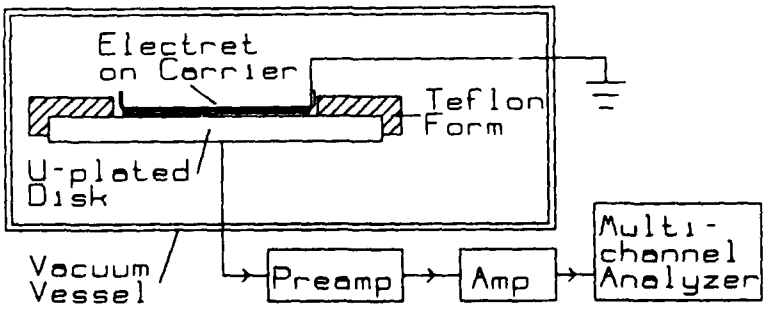

Figure 2: Electret Test Device and Electronics

DISCUSSION

The detection of only one percent of the fission events suggests that most of the signals are too small to be detected. This means that, despite the theoretical determination of signal size, the signal is less than 3 x 10^{-16} coulombs. An unexplained mechanism is responsible for an order of magnitude reduction in effective charge collection. It is possible that the very high dose rate along the fission fragment track creates additional trap sites that more than compensate for the added charge carriers. The resulting radiation hardening would produce a lower track conductance than calculated from equation 2. Research into this phenomena continues.

REFERENCES

1. E. C. Montenegro, S. A. Cruz, and C. Vargas-Aburto, Phys. Lett., 92A , 195, (1982).

2. B. Gross, G. M. Sessler and J. E. West, 1973 Annual Report: Conference on Electrical insulation and Dielectric Phenomena, 465, (1973).

3. B. Hilczer, and J. Malecki, Electrets, Studies in Electrical and Electronic Engineering, 14 , (1986).

4. E. H. Martin and J. Hirsch, J. Appl. Phys. 43 , 1001, (1977).

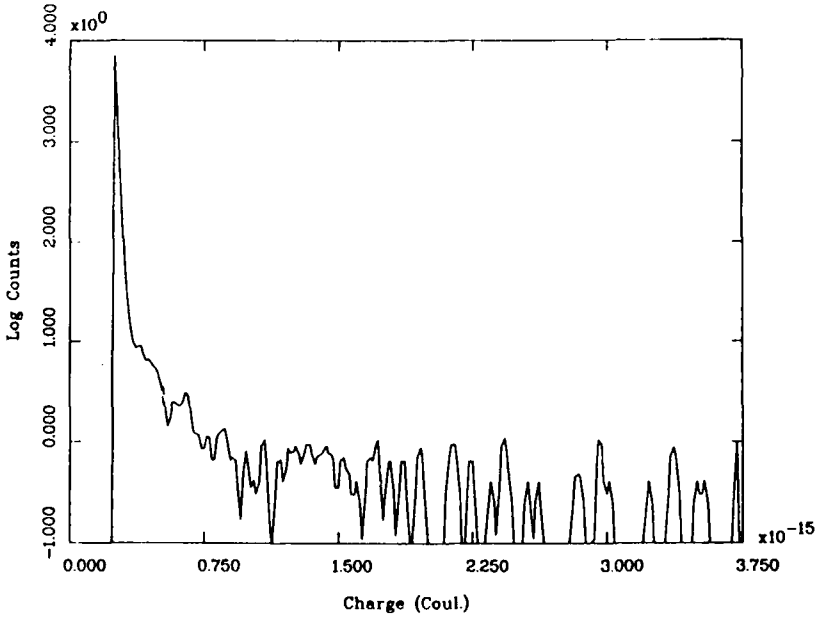

Figure 3: Charge Distribution of Fission Fragment Signal

ANOMALOUS DISCHARGE CURRENT IN COPOLYMERS OF VINYLIDENE FLUORIDE AND TRIFLUOROETHYLENE

Yukinobu Murata and Naokazu Koizumi*

Osaka Prefectural Technical College 26-12 Saiwaicho, Neyagawa 572 Japan and *Institute for Chemical Research, Kyoto University Uji, Kyoto-fu 611 Japan

When a steady or step voltage is applied to a dielectric material, the transient charge current decreases with time from the initial value to a leveled-off value or the leakage current arising from the conductivity of material The transient discharge current is the same as the charge current remaining after subtracting the leakage current. Unlike the ordinary charging and discharging processes, anomalous behavior was observed for copolymers of vinylidene fluoride and trifluoroethylene with varied comonomer content in which a current peak took place in a discharge process. The time taken for the current peak to appear the shorter, the higher the temperature. This unusual discharging occurred at higher temperatures above the ferroelectric transition, being much suppressed in electrodialyzed samples with less ionic impurity. Thus the anomalous discharge process is likely connected with a retarded discharge of ionic charge bound in the paraelectric phase

INTRODUCTION

Charge and discharge current transients using a relatively low electric field have been employed to study the relaxation process in insulating polymers as characterized by long relaxation times. In the course of study of the relaxation process as well as the dc conductivity in copolymers of vinylidene fluoride and trifluoroethylene, a conspicuous current peak was observed in discharge transients at high temperatures. A peak in current transients has been reported for a number of polymer insulators mainly in a charging process at more or less high electric field [1-3] The current peak found in discharging transients in this work was large in size and considerably dependent on temperature. We examined how the current peak was influenced by conditions such as the type of polymer, temperature, electric field in charging, etc. Although the mechanism of the current peak in discharging has not been made clear yet, this paper deals with [illegible] of the results and some discussion about this anomalous transient process in comparison with those reported for other mat[illegible]

CH2593-2/ 88/ 0000-0175$01.00 Copyright 1988 IEEE

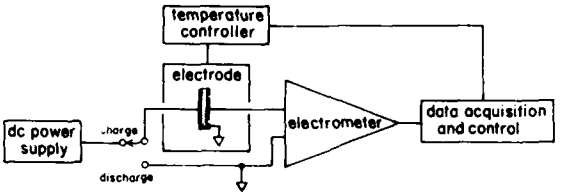

Figure 1. Experimental setup for measurements of transient current in charge and discharge processes for polymers.

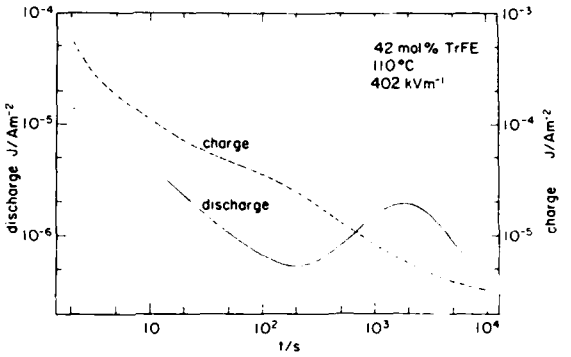

Figure 2. Comparison of charge and discharge transient currents for 42 mol% TrFE copolymer at 110 °C.

EXPERIMENTAL

The experimental setup for measurements of transient currents is illustrated in Fig. 1. A specimen mounted on a three terminal electrode was charged by a dc voltage of 1 to 100 V and the charging current was recorded by use of a Keithley Model 610C Electrometer a minor modification of which was made to be capable of automatic selection of the current range. The discharge current was observed by short-circuiting the charged electrode. Charge and discharge transient processes were recorded at the same temperature for 10 ks. In this work the apparent conductivity κ_{app}, that is, the current density J / the electric field E, as well as the current density J was plotted against time in some figures, since it is not necessarily appropriate to use the current density to discriminate the current level in different samples because of the difference in thickness among specimens. Polymer samples used were vinylidene fluoride (VDF) - trifluoroethylene (TrFE) copolymers with 63, 42, and 27 mol% TrFE and VDF - tetrafluoroethylene (TeFE) copolymer with 19.3 mol% TeFE which were provided by Daikin Industries Ltd. Electrodialyzed

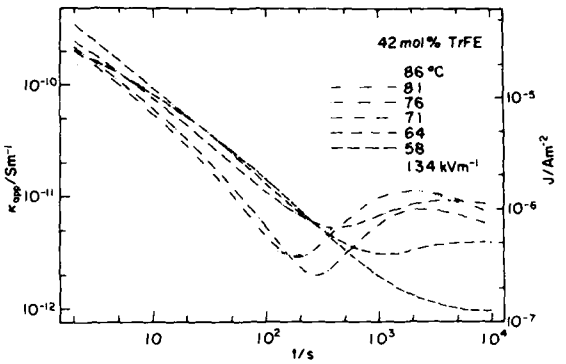

Figure 3. Variation of log κ_{app} - log t curves in discharge transient for 42 mol% TrFE copolymer with temperature between 58 and 86 °C.

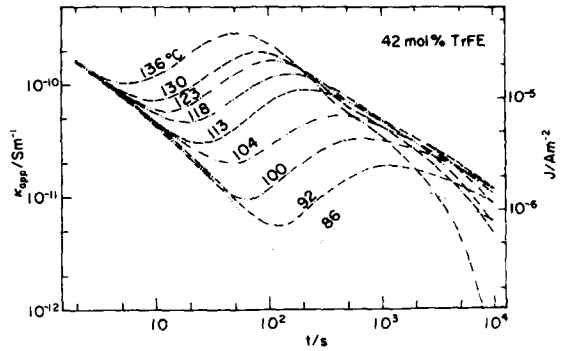

Figure 4. The same as Figure 3 in temperature range of 86 to 136 °C.

VDF-TrFE copolymer with 42 mol% TrFE was used as a sample with a low dc conductivity [4].

RESULTS AND DISCUSSION

Logarithmic plots of κ_{app} vs time t in charge and discharge processes for VDF-TrFE copolymers with 42 and 63 mol% TrFE near room temperature RT indicated ordinary dielectric behavior characteristic of polymer solids. Figure 2 shows log κ_{app} - log t curves for 42 mol% TrFE copolymer at 110 °C. In a striking contrast with the discharge transient at low temperature a conspicuous peak appears in the discharge curve, while no such a peak occurs in the charge curve. Since this copolymer exhibits the ferroelectric to paraelectric transition or the Curie transition around 340 K [5] and since the anomalous discharge transient is possibly related to the

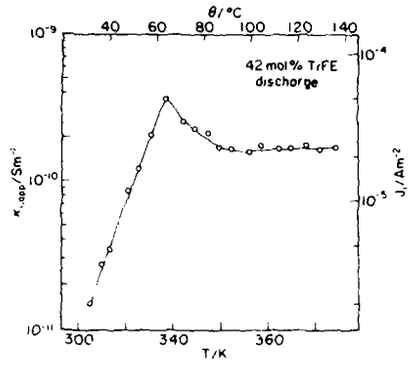

Figure 5 Variation of J_i and $\kappa_{i,app}$ with temperature for 42 mol% TrFE copolymer.

difference in structure between the ferroelectric and paraelectric phases, the discharge process was examined over a temperature range of RT to 136 °C. The discharge transient was traced in increasing order of temperature and log κ_{app} - log t curves are illustrated in two temperature regions as indicated in Figs. 3 and 4. In Fig. 3 the curves are considerably different between temperatures above 76 °C and below 71 °C. A marked current peak occurs at 76 °C and about 2 ks after the start of discharge, shifting to shorter times with increasing temperature, as seen in Figs. 3 and 4. A very dull peak is seen on the curves at 71 and 64 °C. These results mean that different mechanisms are involved in the discharge process between temperature regions or the phases above and below the Curie transition. The value of discharge current at 2 s after the start of discharge was taken as the initial current I_i, since it was hard to observe the true value of initial current. Variation of the initial current density J_i and initial apparent conductivity $\kappa_{i,app}$ with temperature T is depicted in Fig. 5 where a pointed peak takes place near the Curie temperature of 340 K [5]. Since the charging field was 134 kVm^{-1}, being much less than the coercive field of about 50 MVm^{-1} for this copolymer [6], the dielectric polarization at a low electric field contributes mostly to the initial current density in the discharge transient. Thus the peak or cusp of the J_i - T curve corresponds to the anomalous peak of permittivity at the ferroelectric transition [5]. Although no significant thermal hysteresis of the Curie transition was observed for 42 mol% TrFE copolymer in heating and cooling runs, copolymers with lower TrFE content show so large a thermal hysteresis that the Curie temperature is found at considerably different temperatures between

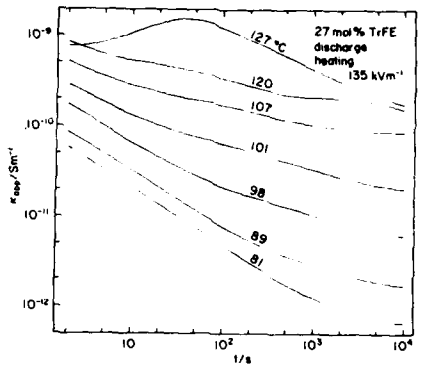

Figure 6. Variation of log κ_{app} - log t curves with temperature 27 mol% TrFE copolymer in a heating run.

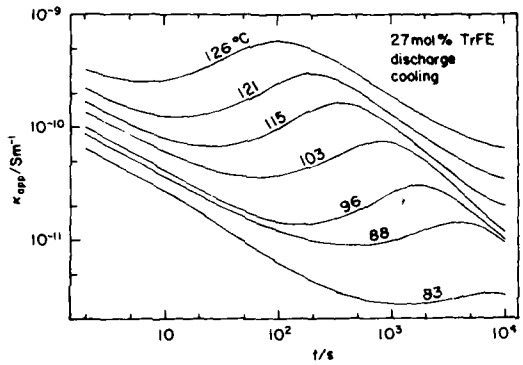

Figure 7. The same as Figure 6 in a cooling run.

heating and cooling runs. To examine the relation between the transient current process and the ferroelectric or paraelectric phase, the discharge transients for the copolymer with 27 mol% TrFE were traced in heating and cooling runs. Fig. 6 shows log κ_{app} - log t curves in discharging for 27 mol% TrFE copolymer in a heating run where a current peak appears at 127 °C. In a cooling run, however, the peak at 126 °C and 100 s moves down to longer time with decreasing temperature, occurring at temperature as low as 83 °C, as illustrated in Fig. 7. Considering that the Curie transition of 27 mol% TrFE copolymer by DSC method is 389 K in heating and 348 K in cooling [5], the peak in a cooling run is connected with structure in the paraelectric phase. Our attention has been directed to contribution of ionic impurities to this anomalous behavior in the

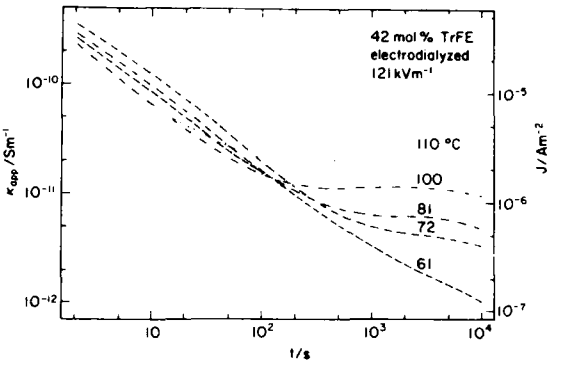

Figure 8. Discharge transients for electrodialyzed 42 mol% TrFE copolymer.

discharge process. The discharge transients were investigated for electrodialyzed copolymer with 42 mol% TrFE which had a lower dc conductivity [4]. It is evident that the peak in discharge transient is much depressed in electrodialyzed sample, as seen from Fig. 8. Increasing the charging field not only shifted the peak to longer time, but also made it sharper. Discharge transients were traced for VDF-TeFE copolymer with 19.3 mol% TeFE around 120 °C, but no peak was found for this copolymer.

In contrast with the cases in which the transient current peak takes place in a charging process at more or less high field [1-3], the current peak appears in the discharge process under certain conditions such as the paraelectric phase of VDF-TrFE copolymers. The current peak in charge processes has been discussed in terms of the theory of space charge limited current in insulators incorporated with injected charge [7]. In the present case the current peak is not due to the charge injected from electrodes [1-3], but rather connected with impurity ionic charge present in polymer samples, as much smaller peaks were observed in less conductive electrodialyzed copolymer with 42 mol% TrFE. It is another feature that the peak takes place only in the paraelectric phase of VDF-TrFE copolymer. This is supported also by results on VDF-TeFE copolymer with 19.3 mol% TeFE that did not show the peak in the ferroelectric phase at 128 °C [8]. It was considered that the charge loosely bound with dipoles in paraelectric crystalline regions migrates and forms polarization in charging and that the release of polarization or the retarded migration of charge contributes to a current peak in the discharge process. In the ferroelectric phase the charge is bound with dipoles and hindered from migration. The time at which the peak is observed in discharge process was considerably dependent on

temperature and logarithm of the time varied linearly with reciprocal of temperature K. Thus the enthalpy of activation estimated for the process was about 85 $kJmol^{-1}$. Further work is now in progress to elucidate the mechanism of peak in discharge transients.

REFERENCES

1. T. Mizutani, M. Ieda, and I. B. Jordan, "Anomalous Transient Currents in High-Density Polyethylene around 50-70 °C", Jpn. J. Appl. Phys. Vol. 18, pp. 65-70, 1979.
2. M. Onoda, H. Nakayama, and K. Amakawa, "Transient Current Peak on Plasticized Polyvinylchloride Containing Absorbed Water", Jpn. J Appl. Phys. Vol. 20, pp. 861-866, 1981.
3. R. Nath and A. Kumar, "Polarity-Reversal Current Transients in Cellulose Acetate Films", IEEE Trans. Electr. Insul. Vol. EI-21, pp. 333-337, 1986.
4. N. Koizumi and Y. Murata, "Electrodialysis of Vinylidene Fluoride-Trifluoroethylene Copolymer", Rep. Prog. Polym. Phys. Jpn. Vol. 24, pp. 435-436, 1986.
5. N. Koizumi, N. Haikawa, and H. Habuka, "Dielectric Behavior and Ferroelectric Transition of Copolymers of Vinylidene Fluoride and Trifluoroethylene", Ferroelectrics, Vol. 57, pp. 99-119, 1984.
6. N. Koizumi, Y. Murata, and H. Tsunashima, "Polarization Reversal and Double Hysteresis Loop in Copolymers of Vinylidene Fluoride and Trifluoroethylene", IEEE Trans. Electr. Insul. Vol. EI-21, pp. 543-548, 1986.
7 A. Many and G. Rakavy, "Theory of Transient Space-Charge-Limited Currents in Solids in the Presence of Trapping", Phys. Rev. Vol. 126, pp. 1980-1988, 1962.
8. Y. Murata and N. Koizumi, to be published.

Piezoelectricity and Pyroelectricity in Polymers

Takeo Furukawa

The Institute of Physical and Chemical Research
Wako, Saitama 351-01, Japan

Abstract

Piezoelectric activities of polymers arise from poling-induced orientation of dipoles (class 1) and uniaxial orientation of chiral molecules (class 2). The former accompanies pyroelectricity while the latter gains pyroelectricity if the spontaneous shear strain is incorporated. Strong activities have been found in class 1; ferroelectric polymers, polar polymers having large dielectric relaxations and composites containing a large amount of PZT. Poling conditions, factors that determine piezoelectric and pyroelectric activities and their basic mechanisms are discussed.

1. Introduction

Piezoelectric and pyroelectric polymers have attracted much interest these years as they revealed a new aspect of polymers as functional materials. The pioneering work by Fukada on piezoelectric biopolymers[1] lead to findings of large piezoelectric and pyroelectric activities in polyvinylidene fluoride (PVDF)[2,3] about 20 years ago. Early arguments on the origin of these activities in PVDF[4] seem to have reached the conclusion that they primarily arise from ferroelectric dipole orientation rather than trapped space charges[5]. Recent investigations in this field have been directed to understanding the ferroelectricity brought about by chain molecules[6]. In this paper, we review various aspects of piezoelectric and pyroelectric polymers with special emphasis on their relation to ferroelectricity.

2. Piezoelectric and pyroelectric Polymers

Production of an electrical response due to a mechanical excitation (piezoelectricity) or a thermal excitation (pyroelectricity) and vice versa requires a materials to have some asymmetric structure. Synthetic polymers, which are originally a random mixture of crystalline and noncrystalline molecules, must be subjected to special treatments to meet this requirement. Two types of treatments have been successfully employed. One applies a high dc electric field to induce orientation of dipoles. This treatment, called poling, creates polar orientation $P_1=\langle\cos\theta\rangle$ (first order Legendre polynomial) to impart both piezoelectric and pyroelectric properties associated with $C_{\infty v}$ symmetry. The other

CH2593-2/ 88/ 0000-0182$01.00 Copyright 1988 IEEE

adopts a mechanical drawing to induce uniaxial orientation $P_2=\langle 3\cos^2\theta-1\rangle/2$ (second order Legendre polynomial) of chain molecules. In combination with the chiral structure of constituent molecules, drawn polymers show piezoelectricity associated with D_∞ symmetry. Figure 1 depicts molecules (dipoles) in P_1 and P_2 orientations.

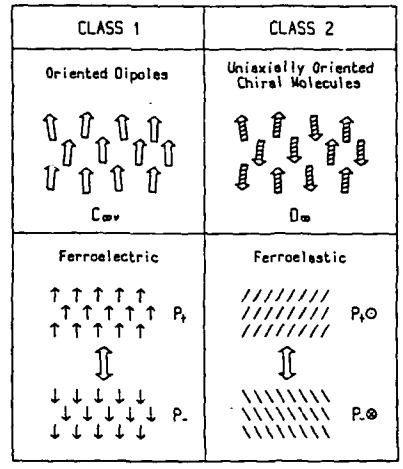

Fig.1 Orientation of molecules of class 1 and 2 polymers.

On the basis of these treatments, piezoelectric and pyro electric polymers are divided into two classes. Class 1 is represented by ferroelectric polymers such as PVDF and its copolymers with trifluoroethylene (TrFE) or tetrafluoroethylene (TeFE). Since they have switchable spontaneous polarization[7-9], we can achieve nearly perfect orientation of crystalline dipoles and strong activities by merely applying a sufficiently high field. The P_1 orientation can be achieved in most polar polymers by the thermal poling that induces frozen-in orientation of molecular dipoles. However, resulting P_1 value is usually insufficient to produce usable activities. Exceptions are an alternating copolymer of vinylidene cyanide (VDCN) with vinyl acetate (VAc)[10] and nylon 11 [11] which are suggested to be more or less ferroelectric-like. The composites of ferroelectric PZT ceramics with polar polymers[12,13] such as PVDF and polyoxymethylene have been developed along this line and have found use as flexible transducers.

Class 2 is represented by various biopolymers such as synthetic polypeptides, cellulose derivatives and DNA[14]. Isotactic polypropylene oxide and poly-β-hydroxybutylate also belong to this class. The P_2 symmetry is originally nonpolar and, therefore, non-pyroelectric. The shear strain in the plane containing the orientation axis generates the piezoelectric polarization in the direction perpendicular to the shear plane. The piezoelectric constant have been shown to be proportional to P_2[15]. It has been of recent interest that several chiral liquid crystals represented by DOBAMBC show ferroelectricity in their tilted smectic phase called a chiral smectic C phase (S_C^*)[16]. This phase has

a spontaneous polarization in the direction perpendicular to the tilt plane. Since the tilted structure is equivalent to being subjected to a spontaneous shear strain, we may regard that the spontaneous polarization of S_c^* is generated by the shear-induced piezoelectric polarization. It is known that the polarization reversal in ferroelectric liquid crystals accompanies inversion of the tilt angle as shown in Fig. 1. In this context, S_c^* liquid crystals are ferroelastic rather than ferroelectric. Synthesis of ferroelectric liquid crystalline polymers have been reported. They may be both piezoelectric and pyroelectric.

3. Measurements of piezoelectric and pyroelectric constants

Piezoelectricity is a cross coupling effect between elastic variables (stress:X, strain:x) and dielectric variables (displacement:D, field:E). Combinations of these variables give rise to four constants d, e, g, and h as shown in Fig. 2. The d-constant, for example, is defined by;

$$d=\frac{\partial D}{\partial X}=\frac{\partial x}{\partial E} \qquad (1)$$

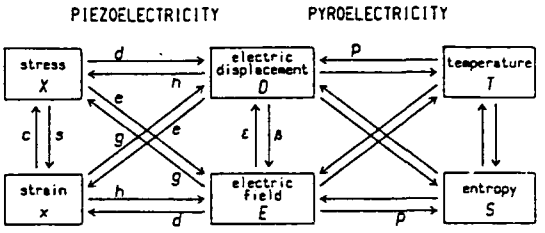

Fig.2 Definition of piezoelectric and pyroelectric constants.

The first definition refers to the direct effect and the second one the converse effect. The piezoelectric effect is alternatively described in terms of a rate of energy conversion from mechanical to electrical and vice versa. This gives rise to the electromechanical coupling coefficient,

$$k^2=\frac{d^2}{\varepsilon^{X}s^{E}}=\frac{e^2}{\varepsilon^{x}c^{E}} \qquad (2)$$

Combinations of dielectric variables and thermal variables (temperature:T, entropy:S) give rise to four pyroelectric constants. The most frequently used is the p constant defined by a change in D caused by a change in T.

The piezoelectric and pyroelectric constants are expressed in terms of the 3x6 and 3x1 matrices respectively. The $C_{\infty v}$ symmetry of class 1 yields,

$$d_{ij}=\begin{pmatrix} 0 & 0 & 0 & 0 & d_{15} & 0 \\ 0 & 0 & 0 & d_{15} & 0 & 0 \\ d_{31} & d_{31} & d_{33} & 0 & 0 & 0 \end{pmatrix} \qquad (3) \qquad p_i=\begin{pmatrix} 0 \\ 0 \\ p_3 \end{pmatrix} \qquad (4)$$

Here the 3-axis is taken in the poling direction which is along

the thickness of polymer films. In the following, we focus our interest on the piezoelectric 31 and 33 components and p_3.

A variety of techniques have been developed to determine these components of class 1 polymers (chapter 4 in ref. 5). They are summarized as follows.

(1) Direct effect : d_{31} (e_{31}^a), d_{33}^a, $d_p=2d_{31}+d_{33}$
(2) Converse effect : e_{31}^a, $g_{33}(d_{33})$
(3) Combination of direct and converse effects : $k_{31}(d_{31})$
(4) Resonance method : $k_{31}(d_{31})$, $k_{33}(e_{33})$

It is noted that e_{31}^a is not true e_{31} but an apparent one defined by d_{31}/s_{11} and d_{33}^a is also apparent d_{33} defined by e_{33}/c_{33}.

4. Poling conditions

The conventional poling procedure consists of applying a field E_p at a temperature T_p for a period t_p. These three parameters define the poling conditions. They should be chosen properly according to the mechanisms of the poling processes of respective materials. Poling at elevated temperatures for longer times does not necessarily provide higher activities.

4.1 Ferroelectric polymers

The poling process in ferroelectric polymers is basically the switching process. The switching characteristics of a 65/35mol% copolymer of VDF and TrFE at 20°C are shown in Fig. 4 where changes in D and its derivative $\partial D/\partial \log t$ are plotted against the logarithm of time t elapsed after the application of a step field. The sharp rise of D and the peak of $\partial D/\log t$ indicate the occurrence of the switching process. We find that the amount of reversed polarization is ca. 160 mC/m^2 being independent of applied field strength. As the field is increased, the switching time becomes much shorter to reach 100ns at 400MV/m [8]. These results indicate that we can pole ferroelectric polymers in a very short time, if

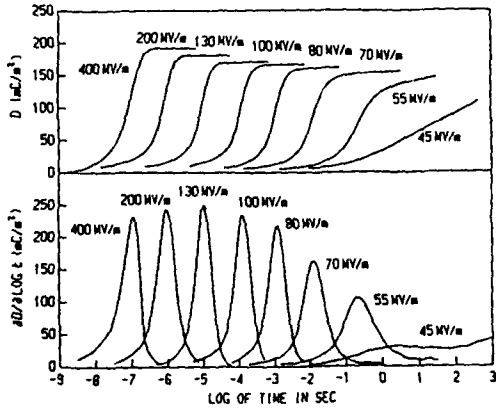

Fig. 3 Switching characteristics of VDF(65)/TrFE(35) copolymer at 20°C.

we apply a sufficiently high field. It is not necessary to elevate temperature, and apply the field for a long time. Poling at elevated temperatures sometimes results in smaller remnant polarization because of an increase in dipole fluctuations.

4.2 Highly polar polymers

If a polymer has a dielectric relaxation due to dipole motions at elevated temperatures, we can create P_1 symmetry by using a conventional thermal poling. That is, we apply a field at an elevated temperature where the dipoles undergo thermal motions and then cool to room temperature without removing the field to freeze-in the oriented dipoles. As a result, we obtain the remnant polarization which is proportional to the relaxation strength $\Delta\varepsilon$.

$$P_r=\Delta\varepsilon E_p \qquad (5)$$

In this case, it is essential to apply E_p as high as possible. The E_p is normally limited to ca. 100MV/m at elevated temperatures due to inevitable electrical breakdown. The t_p should be of the order of the relaxation time at T_p. Since $\Delta\varepsilon/\varepsilon_0$ is normally 5~10, we obtain small P_r of 4~8mC/m^2 leading to weak activities.

Exceptionally strong activities have been found for a noncrystalline copolymer of VDCN and VAc [10] which has a $\Delta\varepsilon/\varepsilon_0$ of ca. 125 above its T_g~170°C [17]. If we apply 50MV/m, we obtain a P_r of 55mC/m^2 which is comparable to that of PVDF. In addition to unusually large $\Delta\varepsilon$, this copolymer shows ferroelectric-like behavior below Tg. As shown in Fig. 4, we find reversal of a considerable amount of polarization (e_{31}^a) at a temperature 20°C below T_g. The switching time is much shorter than the extrapolated relaxation time, but is much longer compared to normal ferroelectric polymers.

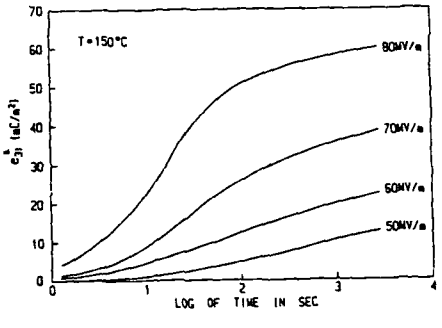

Fig. 4 Switching characteristics of VDCN/VAc copolymer at 150°C.

4.3 Composites of polymers with ferroelectric ceramics

The poling process in a polymer/ceramics composite is rather complex. Since ferroelectric ceramics have much larger permittivities than polymers, the poling field is greatly reduced in the ceramics phase. When the spontaneous polarization of the

ceramics tends align toward the applied field, severe discontinuity of the electric displacement takes place at the interface of polymer and ceramics. It seems impossible to pole the composite dielectrically. However, we know that we can pole it by using the conventional thermal poling. We have shown [18] that during poling at elevated temperatures, space charges in the polymer phase are accumulated near the interface to increase the internal field in the ceramics phase and remove the discontinuity of the electric displacement at the interface. Figure 6 shows the switching process of a composite of PZT ceramics and VDF/TrFE copolymer at 100°C and 12.5MV/m. Here a change in polarization is again monitored by the piezoelectric constant. We find that it takes long time (>1000s) to reverse the polarization, but PZT in the composite is fully poled toward reverse direction. In this case, t_p is given by the relaxation time inherent to the Maxwell -Wagner effect.

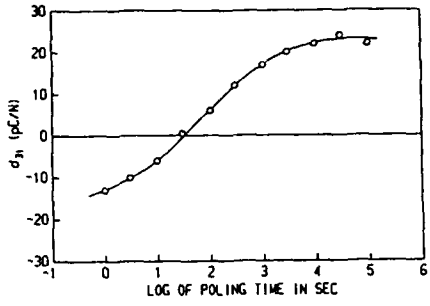

Fig. 5 Polarization reversal in PVDF/PZT composite.

Table 1 lists recommended poling conditions of three kinds of class 1 polymers.

Table 1 Typical Poling Conditions

Polymer	T_p	E_p(MV/m)	t_p(sec)
VDF/TrFE	RT	~100	<1
VDCN/VAc	T_g	50	100
PZT/PVDF	100°C	10	1000

5. Characterization of piezoelectric and pyroelectric constants

The piezoelectric and pyroelectric activities associated with P_1 symmetry of class 1 polymers are, in principle, proportional to the remnant polarization created in the sample because P_r is proportional to P_1. This is confirmed by the linear relation between e_{31}^a and P_r (Fig. 6) and p_3 and P_r (Fig. 7). It is interesting to note that all e_{31}^a data from undrawn samples lie on a single line of a gradient ca. 0.4 [19]. Drawing causes in-plane anisotropy that e_{31}^a is about ten times larger than e_{32}^a[20]. Koga and Ohigashi [21] have found that k_{33} is also proportional to P_r for VDF/TrFE copolymers irrespective of their compositions.

Characterizing piezoelectric and pyroelect constants in terms of their P_r dependences is particularly usei in predicting their

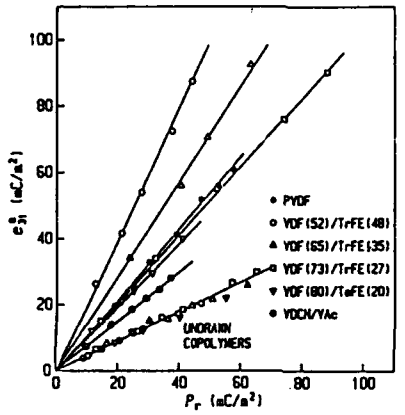

Fig. 6 Dependence of e_{31}^a on P_r for ferroelectric polymers.

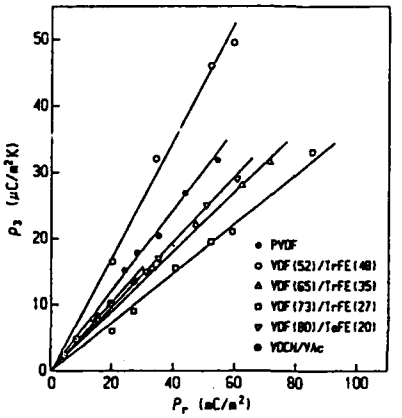

Fig. 7 Dependence of p_3 on P_r for ferroelectric polymers.

ultimate values, because P_r is predictable from the structure of a material. The maximum value of P_r of ferroelectric polymers can be calculated from their crystalline polarization, if the delicate problem about the local field is solved. Recently Al-Jishi and Taylor [22] reported that the local field in PVDF is nearly zero. This leads to the maximum P_r of 130mC/m² which is consistent with the calculation from a rigid dipole model and is much smaller than the early prediction [23] based on a Lorentz factor of 1/3. Ogura and Chiba [24] found slight enhancement of the local field in VDF/TrFE copolymers and obtained the crystalline polarizations nearly independent of the composition. We have experimentally reached a P_r of 100mC/m² in VDF-rich copolymers. This means that we are already near the goal for the ultimate activities of VDF copolymers.

The P_r due to frozen-in dipoles is proportional to $\Delta\varepsilon$ (eq.(5)). VDCN copolymerizes [25] with not only VAc but also with vinyl propionate (VPr), vinyl pivalate (VPr), vinyl benzoate (VBz), styrene (St) and methylmethacrylate (MMA). Figure 8 shows plots of e_{31}^a against $\Delta\varepsilon$ for various VDCN copolymers

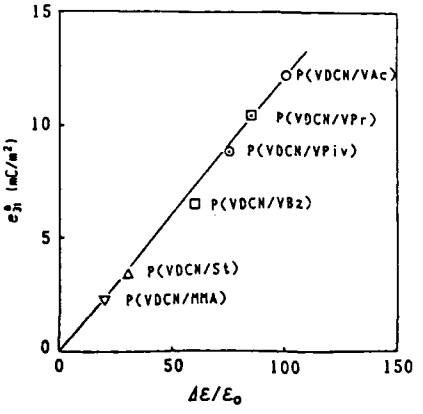

Fig. 8 Dependence of e_{31}^a on $\Delta\varepsilon$ in VDCN copolymers.

poled at a field of 20MV/m. Linear relationship implies that $\Delta\varepsilon$ is the most effective parameter in designing polymers having higher activities arising from frozen-in dipoles..

The P_r of polymer/ceramics composites depends upon the volume fraction of the ceramics phase. The volume fraction is limited by the closest packing of spherical particles, if the ceramics powder is dispersed in polymer matrix. Figure 9 shows the dependence of d_{31} on the volume fraction for the composite of PVDF and PZT [12]. The maximum d_{31} is about 1/10 that of PZT even though 60% volume fraction is achieved. This is primarily due to the substantial difference in permittivities of PZT and PVDF. Skinner et al. suggested [13] that the composites in that both ceramics and polymer are continuous are favored for higher activities, although they require elaborate processings.

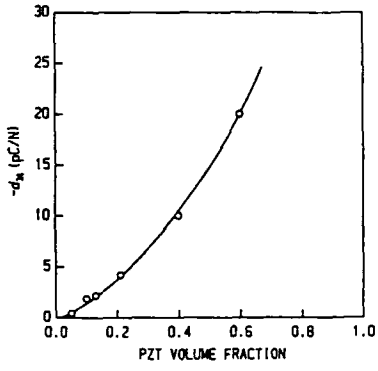

Fig.9 Dependence of d_{31} on PZT fraction in composite.

6. Mechanisms of piezoelectricity and pyroelectricity

There have been various mechanisms proposed to explain the piezoelectric and pyroelectric activities of poled polymers. Since most of them appeared before full recognition of ferroelectricity in polymers, they did not include the mechanisms inherent to ferroelectrics. We discuss here the mechanisms of piezoelectricity of ferroelectric polymers according to the conventional phenomenological theory. We start with the free energy expanded in terms of the electric displacement D and the strain x,

$$G = G_0 + \frac{1}{2}\chi D^2 + \frac{1}{4}\xi D^4 + \frac{1}{6}\zeta D^6 + \frac{1}{2}cx^2 - \frac{1}{2}\gamma xD^2 \qquad (6)$$

where G_0 is the free energy in the paraelectric phase, χ, ξ and ζ are the linear and nonlinear reciprocal permittivities and c is the elastic stiffness constant. We incorporated in the last term the electrostrictive nonlinear coupling γ between x and D^2. Differentiating G with respect to D and x generates nonlinear electromechanical equations from which we obtain at a condition of zero-stress (X=0),

$$x = \kappa D^2 \qquad (7)$$

where κ is another electrostriction constant defined by $\gamma/2c$. This equation implies that ferroelectric polarization accompanies strain through electrostriction. We also obtain,

$$E = \chi D + (\xi - \gamma^2/2c) D^3 + \zeta D^5 \qquad (8)$$

predicting a ferroelectric D-E hysteresis loop. Solving this equation for D at a condition of zero-field (E=0), we obtain expressions for the remnant polarization P_r and the remnant strain x_r.

Taking small deviations of related variables from the natural state (E=0, X=0), we also obtain expressions for the piezoelectric constants d, e, g, and h in terms of the products of the electrostriction constants and the remnant polarization.

$$h = \gamma P_r \qquad (9)$$

$$e = (\gamma/\varepsilon) P_r \qquad (10)$$

$$g = 2\kappa P_r \qquad (11)$$

$$d = (2\kappa/\varepsilon) P_r \qquad (12)$$

We have experimentally examined these phenomenological predictions with respect to a VDF(65)/TrFE(35) copolymer. Upon the application of a sinusoidal field E, D and x draw hysteresis loops as shown in Fig. 10. Here x is the strain along the thickness measured interferometrically [26]. The D-E loop gives a P_r of 86mC/m^2. It is seen that the copolymer is thickest when the polarization is zero and becomes thinner with increasing polarization. Replotting the results in terms of x vs. D (Fig. 11), we find a quad-

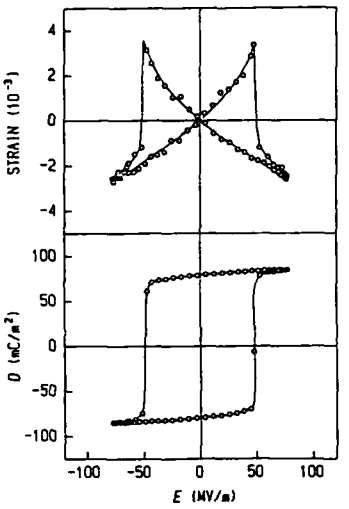

Fig.10 D-E and x-E loops for VDF/TrFE.

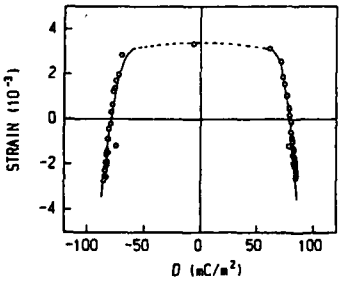

Fig. 11 Quadratic relation between x and D in VDF/TrFE.

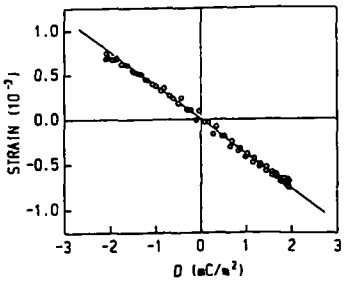

Fig. 12 Linear x-D relation at low fields in VDF/TrFE.

ratic relation as predicted from eq.(7) except for the flat region and obtain $\kappa_{33}=-2.1 m^4/C^2$. Low-field experiments have yielded a linear relationship between x and D as shown in Fig.12. We then have $g_{33}=-0.37 m^2/C$ in good agreement with prediction $2\kappa_{33}P_r$ (eq.(11)). This means that the piezoelectric activities of ferroelectric polymers are attributable to the electrostrictive coupling which has been accepted in genaral ferroelectrics.

We then discuss the molecular mechanisms of the electrostrictive coupling in VDF/TrFE copolymers. In their ferroelectric phase, copolymers adopt an all-trans conformation and a parallel packing of molecules. Transformation into the paraelectric phase is achieved by conformational changes into a random mixture of TT, TG and TG' bonds. The intermolecular distance thereby contracts while the fiber period expands as shown in Fig. 14 [27]. In other words, the ferroelectric phase has remnant strains x_{1r} and x_{3r} which are positive and negative respectively measured from the paraelectric phase. Using changes in lattice constants at the Curie point, we have[20],

$$x_{1r}= 0.113 \quad (13)$$
$$x_{3r}=-0.059 \quad (14)$$

Assuming that these strains totally arise from the electrostriction, we obtain via. eq (7).

$$\kappa_{31}=x_{1r}/P_r^2= 5.8 C^2/m^4 \quad (15)$$
$$\kappa_{33}=x_{3r}/P_r^2=-3.0 C^2/m^4 \quad (16)$$

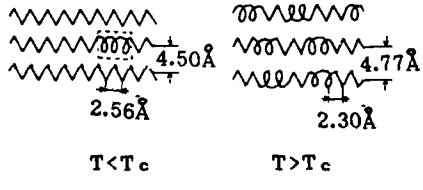

Fig.13 Structures of VDF/TrFE below and above T_c.

Here we used $P_r=140 mC/m^2$ based on the calculations by Ogura and Chiba [24]. We find that calculated κ_{33} is largely consistent with the observed. Disagreement may be mostly attributed to the situation that calculation was made with respect to the crystalline regions and experiments were made for a sample which is a mixture of crystalline and noncrystalline regions.

Figure 15 represents a model of poled polar polymer sample. It consists of N dipoles with effective moment μ and orientation coefficient $\langle\cos\theta\rangle$. Its remnant polarization in given by,

$$P_r=N\mu\langle\cos\theta\rangle/Al \quad (17)$$

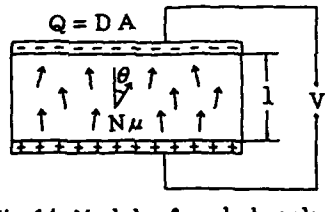

Fig.14 Model of poled polymer.

where l is the thickness and A is the area of electrodes.

Mechanisms of piezoelectricity have been discussed in terms of changes in the quantities comprised in P_r[23]. Actually, we measure the piezoelectric constants using charge Q, voltage V, deformation l and force F in place of D, E, x and X respectively. The experimental e-constant, for example, is given by,

$$e = \frac{l}{A}\left(\frac{\partial Q}{\partial l}\right)_{V=0} = \frac{l}{A}\left(\frac{\partial F}{\partial V}\right)_{\Delta l=0} \qquad (18)$$

There is charge Q on the electrodes of the sample and the sample receives force F from electrodes (C : capacitance).

$$Q=N\mu\langle\cos\theta\rangle/l+CV \qquad (19) \qquad F=Q^2/2Cl \qquad (20)$$

In this situation, the piezoelectric activity can arise from macroscopic dimensional changes, even if other quantities such as N, μ and $\langle\cos\theta\rangle$ remain unchanged when the sample is subjected to either mechanical or electrical excitation. This mechanism is commonly referred as "dimensional effect". Differentiating Q in eq.(19) with respect to l at V=0 (direct effect), we find,

$$e_{33}=-P_r \qquad (21)$$

Differentiating F in eq.(20) with respect to V (converse effect), we obtain the same relation. We also obtain,

$$e_{31}=0 \qquad (22) \qquad e_{31}^{a} = \nu_{31}P_r \qquad (23)$$

because the dimensional effect arises from a change in thickness only. Here ν_{31} is Poisson's ratio.

We have shown in Fig. 6 that e_{31}^{a} of undrawn copolymers is proportional to P_r with coefficient 0.4, which is a value of Poisson's ratio common to undrawn polymers. This implies that the dimensional effect dominates e_{31}^{a} in undrawn copolymers. However, this is not the case for drawn copolymers because of the substantial contribution from the electrostrictive coupling. Since κ_{31} and κ_{32} are opposite in sign, their contributions might have canceled each other in undrawn copolymers.

We have shown that g_{33} obtained from Fig. 12 totally arises from electrostriction. This does not exclude the contribution from the dimensional effect because it is included in κ_{33} (see eq.(20)).

A variety of mechanisms have been proposed so far to explain piezoelectric and pyroelectric activities of polymers. They are essentially attributed to changes in N, μ and $\langle\cos\theta\rangle$ caused by mechanical and thermal excitations. "N" changes if crystallinity changes[28,29]. "μ" depends upon the local electric field coupled with electronic polarizability[22] and the internal dis-

placement of constituent ions[30]. "$\langle\cos\theta\rangle$" is subject to changes in librational amplitude of dipoles[23] and the order parameter through electrostriction. These mechanisms together with the dimensional effect might have contributed to total activities[31]. There still remains uncertainty in determining their contributions quantitatively due to the complex problems arising from higher order structures of semicrystalline polymers.

References

[1] E.Fukada, J.Phys.Soc.Jpn., 10,149(1956).
[2] H.Kawai, Jpn.J.Appl.Phys., 8,975(1969).
[3] J.G.Bergman,J.H.McFee and G.R.Crane, Appl.Phys.Lett., 18,203(1971).
[4] Y.Wada, Jpn.J.Appl.Phys., 15,2041(1976).
[5] "The Applications of Ferroelectric Polymers", ed. T.T.Wang, J.M.Herbert and A.M.Glass, Blackie, U.K. (1987).
[6] Final Report of Special Project Research on "Organic Thin Films for Information Conversion" Supported by Ministry of Education, Science and Culture, Japan (1987).
[7] T.Furukawa and G.E.Johnson, Appl.Phys.Lett., 38,1027(1981).
[8] T.Furukawa, H.Matsuzaki, M.Shiina and Y.Tajitsu, Jpn.J.Appl.Phys., 26,554(1987).
[9] Y.Takahashi, Y.Nakagawa, H.Miyaji and K.Asai, J.Polym.Sci.part-C, 25,153(1987).
[10] S.Tasaka, K.Miyasato, M.Yoshikawa, S.Miyata and M.Ko, Ferroelectrics, 57,267(1984).
[11] S.C.Mathur, J.I.Scheinbeim and B.A.Newman,J.Appl.Phys.,56,2419(1984)
[12] T.Furukawa, K.Ishida and E.Fukada, J.Appl.Phys., 50,4904(1979).
[13] D.P.Skinner, R.E.Newnham and L.E.Cross, Mat.Res.Bull., 13,509(1978).
[14] E.Fukada, Adv.Biophys., 6,121(1974).
[15] T.Furukawa and E.Fukada, J.Polym.Sci.-Phys., 14,1979(1976).
[16] R.B.Meyer, L.Liebert, L.Strxelecki, and P.Keller, J.Phys., 36,L69(1975).
[17] T.Furukawa, M.Date, K.Nakajima and I.Seo, Jpn.J.Appl.Phys., 25,1178 (1986).
[18] T.Furukawa, K.Suzuki and M.Date, Ferroelectrics, 68,33(1986).
[19] T.Furukawa, J.X.Wen, K.Suzuki, Y.Takashina and M.Date, J.Appl.Phys., 56,829(1984).
[20] T.Furukawa and J.X.Wen, Jpn.J.Appl.Phys., 23,L677(1984).
[21] K.Koga and H.Ohigashi, J.Appl.Phys., 59,2142(1986).
[22] R.Al-Jishi and P.L.Taylor, J.Appl.Phys., 57,902(1985).
[23] M.G.Broadhurst, G.T.Davis, J.E.McKinney and R.E.Collins, J.Appl.Phys., 49,4992(1978).
[24] H.Ogura and A.Chiba, Ferroelectrics, 74,347(1987).
[25] A.b.Conciatori, L.E.Trapasso, and R.W.Stackman, "Encyclopedia of Polym. Sci. Tech" ed. H.F.Mark, John Wiley & Sons, NY, 14 (1971).
[26] D.M.Gookin, E.W.Jacobs and J.C.Hicks, Ferroelectrics, 57,89(1984).
[27] A.J.Lovinger, T.Furukawa, G.T.Davis and M.G.Broadhurst, Polymer, 24,1225(1983).
[28] H. Dvey-Aharon, T.J.Sluckin and P.L.Taylor, Ferroelectrics, 32,25(1981).
[29] R.E.Kepler, R.A.Anderson, and R.R.Lagasse, Ferroelectrics, 57,151(1984).
[30] K.Tashiro, M.Kobayashi, H.Tadokoro and E.Fukada, Macromolecules, 13,691(1980).
[31] Y.Wada, Ferroelectrics, 57,343(1984).

INVESTIGATIONS OF STRUCTURAL CHANGES IN PVDF BY MODIFIED X-RAY TEXTURE METHODS

D. Geiss

Institute of Polymer Chemistry "Erich Correns" Academy of Science of the GDR, Kantstr. 55, 1530 Teltow-Seehof, German Democratic Republic

ABSTRACT

Structural changes in the α-phase of poly-(vinylidenefluoride) (PVDF) due to poling have been investigated by means of a modified x-ray-texture method. Besides the conversion of the nonpolar α-phase into the polar α_p-phase a change of the orientation state is observed. Both effects can be separated from each other. Conclusions can be drawn about the molecular mechanism of polarization.

INTRODUCTION

The α-phase of PVDF is nonpolar due to the antiparallel alignment of the molecular dipoles of the tgtg' conformation in its monoclinic unit cell [1]. After poling (>50 MV/m) this material shows several conversions of the chain conformation as well as of the crystalline modifications [2-5]. Up to field strenghts of 200 MV/m a conversion into the polar α_p-phase is preferred [4]. We found this transition to be closly connected with a change of the orientation state [6]. Some of the published results differ concerning the the orientation of the crystallites involved in the transition α into α_p [5-7].

EXPERIMENTAL

This paper presents a further study of the structure conversion in the oriented α-phase occuring under field influence (150 MV/m). The results were obtained by means of polefigures

CH2593-2/ 88/ 0000-0194$01.00 Copyright 1988 IEEE

as well as the continuosly recorded impulse density $I(\alpha,\varphi)$ following the spiral of registration of the texture goniometer (Schulz reflection mode [8]). It has been shown in another paper [9] that the scan of the impulse density $I(\alpha,\varphi)$ often provides more evidence concerning changes of the orientation state than the polefigures themselves. That is true especially in such cases where conversions among crystalline modifications take place besides the changes in the orientation state.

From both the polefigures and the impulse density itis possible to separate the orientation distribution of the lattice planes (120) and (021) along the sample direction N-T (perpendicular to the draw direction M, poling field direction parallel to N), because the (021)- and the (120)-lattice planes have nearly the same scattering angle (ϑ_{021} = 13.35°, ϑ_{120} = 12.98°) but different positions in the polefigure. The distribution of the (021)-lattice plane was projected on N-T using the symmetry relations of the crystal lattice.

RESULTS AND DISCUSSION

The values obtained for the distributions of of the normals of the (021)- and (120)- planes as a function of the sample deflection angle α along N-T are shown in the figures 1. and 2. respectively.

According to the calculated x-ray intensity form factors [4] for the α- and the α_p-phase the intensity of the (120)-lattice plane becomes zero whereas the intensity of the (021)-lattice plane remains unchanged during the transition α into α_p. Therefore the separated (021)-distribution represents the transition of the crystalline structure whereas the (120)-distribution corresponds to the contribution to the whole structure conversion caused by the change of the orientation state only.

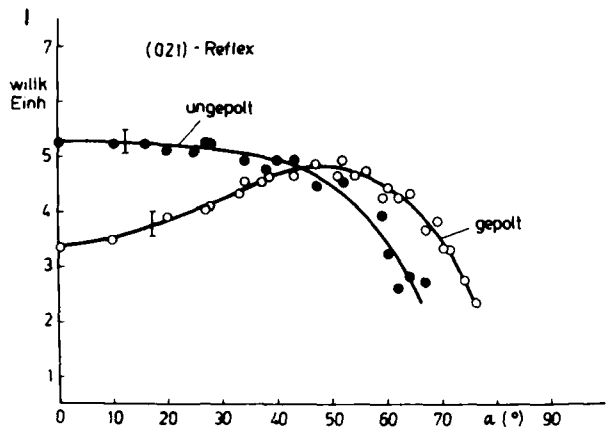

Fig. 1. Distribution of the normals of the (021)-lattice plane along N-T as a function of the sample deflecting angle α

The normals of the (021)-lattice plane in their projection on N-T are at a distance of 90° to the dipole direction provided [001] and draw direction coincide. Therefore the distribution of the unpoled sample in figure 1. confirms that the orientation of the dipoles in the T-direction is sligthly preferred before poling [10].

There is a significant shifting of intensity towards T after poling, which is equivalent to a improved alignment of the dipoles towards the field direction N.
Already the observed distinctions in the intensities at the sample deflection angle α=0° give evidence that those crystallites have changed their positions whose dipole directions were in the film plane before poling.

Figure 2. shows the distribution of the normals of the (120)-lattice planes obtained from the same scan of the impulse density as the (021)-distribution. There is a considerable difference in the intensity level between the unpoled and the poled samples as compared to

figure 1. This gives evidence that crystallites having a broad spectrum of orientations were converted.

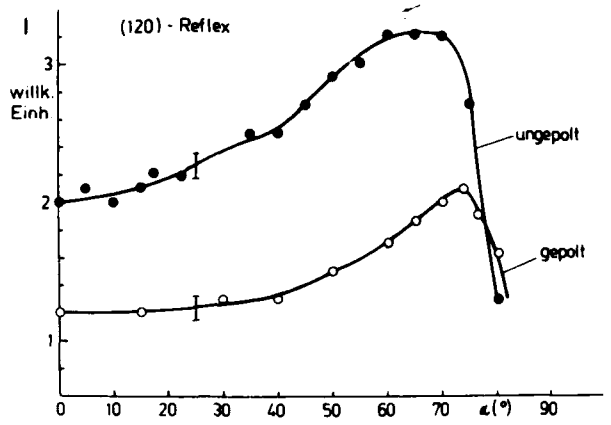

Fig. 2. Distribution of the normals of the (120)-lattice plane along N-T as a function of the sample deflecting angle α

Summarizing it can be concluded that the structure conversion of the α-phase due to poling consists at least of two different components.

1. Crystallites of the α_p-phase have been formed from crystallites of the α-phase with a broad orientation distribution of the crystallograpic dipole direction (crystallographic a-axis) to the poling field before poling. Especially those crystallites are involved which before poling were oriented with their dipole axes along the sample plane.

2. The dipole axes of the crystallites of the new α_p-phase exhibit a changed orientation distribution after poling in comparison to the orientation state of the crystallites of the α-phase before poling. The dipole directions in the α-phase have a slightly preferred orientation parallel to the sample direction T before poling. After poling the equivalent

dipole directions in the α_p-phase show a significantly preferred orientation parallel to the sample direction N (field direction).

There is no evidence in terms of the presented results that crystallites directed with their a-axes in the film plane before poling are converted in amorphous material, as suggested by Weinhold [7]. A conversion of these crystallites into a crystalline modification unknown till now seems to be rather likely. As Weinhold [7] and Newman [5] we found WAXS-intensities at scattering angles after poling which did not belong to any of the known modifications of PVDF.

On the basis of the presented experimental results and their interpretation we developed a concept published elsewhere [9] explaining the conversion of the α-phase into the α_p-phase on a molecular level.

REFERENCES

[1] Hasegawa,R., Takahashi,Y., Chatani,Y., Tadokoro,H.: Polym.J. 3(1972)600
[2] Southgate,P.D.: Appl.Phys.Lett. 28(1976)250
[3] Das Gupta,D.K., Dougthy,K.: Appl.Phys.Lett. 31(1977)585
[4] Davis,G.T., McKinney,J.E., Broadhurst,M.G., Roth,S.C.: J.Appl.Phys. 49(1978)4998
[5] Newman,B.A., Yoon,C.H., Pae,K.D., Scheinbeim,J.I.: J.Appl.Phys. 50(1979)6095
[6] Geiss,D., Danz,R., Janke,A., Kuenstler,W.: Proc.5th Intern. Symp. Electrets, Heidelberg 1985
[7] Weinhold,R.: Dissertation, Case Western Reserve Univ., Cleveland, Ohio, USA, 1982
[8] Schulz, L.G.: J.Appl.Phys. 20(1949)1030
[9] Geiss,D., Hofmann,D.: Progress in Polymer Science, submitted
[10] Geiss,D., Ruscher,Ch., Kofer,U.: Acta Polym. 34(1983)12

PIEZO- AND PYROELECTRICITY AND STRUCTURE OF DOPED POLYMERS

Rudi Danz, Burkhard Elling,Wolfgang Kuenstler, Manfred Pinnow, Rudolf Schmolke, Armin Wedel and Detlev Geiss

Institute of Polymer Chemistry "Erich Correns" Academy of Sciences of the GDR, Kantstr. 55 1530 Teltow, German Democratic Republic

ABSTRACT

We have doped poly(vinylidene fluoride) (PVDF) and poly(methylmethacrylate) (PMMA) with crystal violett and disperse red. Doping of PVDF with crystal violett has a great influence on the structure formation of the polymer. Resulting piezo- and pyroelectric properties of the doped films are presented.

1. INTRODUCTION

The introduction of optically active dopants into polymer films induces new useful electrical and optical properties of these materials. Polymer glasses doped with optically nonlinear organic dye molecules posses reasonable large second order nonlinear optical susceptibilities [1] . This concept involves electric field poling above the glass transition temperature of the sample resulting in an alignment of the dipolar dye molecules and yielding a noncentrosymmetric structure. We could show that field-induced alignment of the azo dye disperse red soluted in PMMA results in piezo- and pyroelectric activity. Field poling of PVDF films doped with crystal violett produces piezo- and pyroelectric polymer films with high absorbance in the visible spectral range.

CH2593-2/ 88/ 0000-0199$01.00 Copyright 1988 IEEE

2. PREPARATION TECHNIQUE

PMMA and PVDF were soluted in cloroform and dimethyl sulfoxide with dopants. This solution was cast onto glass forming doped PMMA and PVDF films. Doped PVDF films were four times stretched at about 170 °C by a hot-zone drawing process. The structure of stretched PVDF films was only β-modification. The electric contacts of the prepared films were evaporated aluminium electrodes. Doped PVDF films were poled at room temperature (poling time 10 s). Doped PMMA films were prepared by heating the films 10 K above the glass transition temperature of PMMA ($T_g \approx 370K$) applying a strong electric field and cooling down the sample with applied field below T_g .

3. STRUCTURE FORMATION IN PVDF BY DOPING

We have found that crystal violett (CV) has a great influence on the structure formation of PVDF. The structure of the doped unoriented

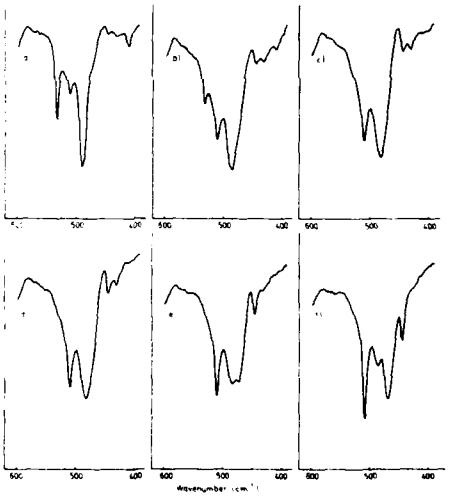

Fig. 1 Infrared spectra of PVDF as a function of the CV/polymer ratio in DMSO. m_{CV}/m_P=0(a);0.002(b); 0.01(c);0.02(d);0.08(e);0.40(f). c,d,e,f - extracted films

films was investigated by IR-spectroscopy. Infrared spectra were measured with a SPECORD M 80 (VEB Carl Zeiss Jena).
Fig. 1 shows the infrared spectra of doped PVDF in the structure-sensitive region from 600 to 400 cm^{-1}. The absorption bands at 410 and 530 cm^{-1} are assignable to the α-modification (TGT$\bar{G}$-conformation). The bands at 446 and 470 cm^{-1} are characteristic for β-modification (TT-conformation) while the bands at 430 cm^{-1} is assignable to γ-modification (T_3GT_3G-conformation). The 510 cm^{-1} (CF_2)-vibration band represents the amount of trans sequences in either the β- or γ-modification . Depending on the CV concentration PVDF films with α-, β- or γ-modification are obtained. Without any additive mainly α-structure is found (Fig. 1a). When large amounts of CV were added the βmodification predominates, which is indicated especially by a new strong band at 470 cm^{-1} (Fig. 1 e,f). In this case the dye was extracted by acetone.Infrared bands at 446 cm^{-1} (β), 430 cm^{-1} (γ) and 410 cm^{-1} (α) were used for quantitative analysis [2] . The results presented in Fig. 2 show that we can influence the structure formation of PVDF systematically by doping with crystal violett. In this way unoriented PVDF films of β-modification can be produced.

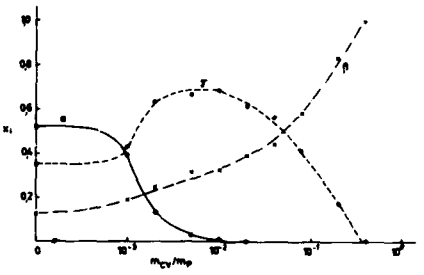

Fig. 2 Volume fractions x_i (α,β,γ) in PVDF films as a function of CV/polymer ratio

4. PIEZO- AND PYROELECTRICITY

We have measured the electrical polarization process in PMMA films doped with disperse red by pyro- and piezoelectric measurements in order to give evidence that there is a special dopant molecule orientation beside the orientation of the polar side groups of the PMMA molecules. The pyroelectric coefficient is a sublinear function of the poling field strength (Fig. 3). The incorporation of the dye results in a remarkable rise of the pyroelectric coefficient. The highest coefficients are reached at a dye concentration of 0,40 mass per cent. The d_{31}-piezoelectric coefficient amounts to 0.15 pCN^{-1} at 0.40% dye content at poling field strength of $5 \times 10^{7} Vm^{-1}$. Fig. 4 shows the piezoelectricity of the doped PVDF films (doped with 1% CV) in comparison to undoped PVDF films cast from DMSO solution and commercial films. The poling-field dependence is strongly shifted to lower field strengths, and relatively high piezoelectric coefficients are obtained. The shifting is also indicated in pyroelectric and polarization measurements. The doped PVDF films (thickness 10 um) have an absorbance of 90% at 632 nm.

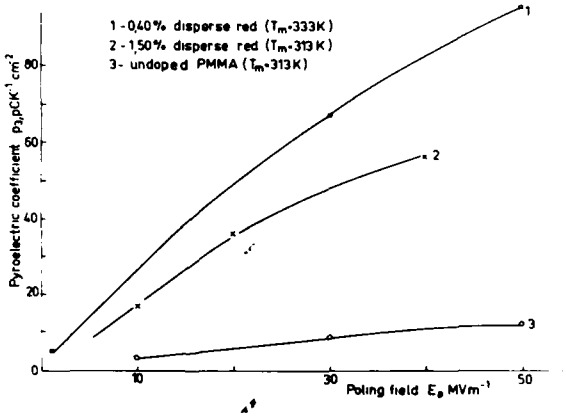

Fig. 3 Pyroelectricity of doped PMMA

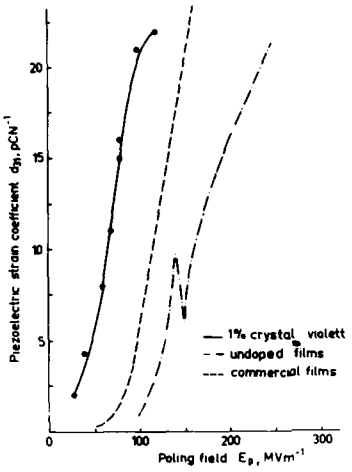

Fig.4 Piezoelectricity of doped and undoped PVDF

5. CONCLUSIONS

Doping of PVDF with crystal violett results in the formation of β - and γ-modifications. Ionic species have a significant effect on crystal growth [3]. The presence of dye ions reduces the electrostatic energy and therefore favours the formation of polar crystals. The strong shifting in the field dependence of the piezo- and pyroelectricity of doped PVDF may be due to the increasing mobility in the structure of PVDF caused by the incorporation of dyes.

6. REFERENCES

[1]K.D.Singer, S.J.Lalama and J.E.Sohn,"Organic Nonlinear Optical Materials", SPIE Integrated Optical Circ. Eng., Vol.578,pp. 130-136,1985.

[2]R.Schmolke,B.Elling,W.Kuenstler,R.Danz and D.Geiss,"Zum Einfluss von Kristallviolett auf die Strukturbildung von PVDF",Acta Polymerica,Vol.39,pp.164-168,1988.

[3]D.T.Grubb,P.Cebe and K.W.Choi,"Solution Grown Crystal of PVDF:the Effect of Ionic on Growth",Ferroelectrics,Vol.57,pp.121-138,1984.

NONLINEAR PIEZOELECTRICITY IN ORIENTED FILMS OF POLY VINYLIDENE FLUORIDE AND ITS COPOLYMERS

M. Date, E. Fukada and J. H. Wendorff*

The Institute of Physical and Chemical Research, Wako, Saitama 351-01, Japan
* Deutsches Kunststoff-Institute, 6100 Darmstadt, W.-Germany

ABSTRACT

The dynamic piezoelectric strain constant d_{32} of uniaxially stretched and poled poly(vinylidene fluoride) was reported to depend on the statically applied stress. In agreement with the phenomenological theory, the occurrence of the second harmonic component (2f) of the polarization for a sinusoidal stress (frequency f) was experimentally determined. The nonlinear piezoelectric constant showed relaxation in the glass transition temperature range.

1.Introduction

Piezoelectricity is usually treated as a linear phenomenon. Linear equations relate the polarization P and the strain S to the applied stress T and the applied electric field E :

$$P = d\,T + \eta^{T} E \qquad (1)$$
$$S = s^{E}T + dE \qquad (2)$$

where d is piezoelectric strain constant, s^{E} mechanical compliance and η^{T} dielectric susceptibility.

Most of the studies of piezoelectric polymers were concerned with the piezoelectric strain constant d_{31} defined as

$$d_{31} = \partial P_3 / \partial T_1 \qquad (3)$$

where P_3 is the polarization normal to the plane of the film (axis 3) and T_1 the mechanical stress applied along the draw direction (axis 1). This linear relation

CH2593-2/ 88/ 0000-0204$01.00 Copyright 1988 IEEE

dose not hold, however, for the piezoelectric strain constant d_{32}.

Recently B.R.Hahn [1,2] reported that d_{32} depends on stress T_2. Hahn found that d_{32} observed dynamically decreases and reverses its sign with increasing static stress T_2. This dependence of d_{32} on T_2 suggests that the expressions (1) and (2) given above are not sufficient.

The present paper is mainly concerned with experiments on nonlinear piezoelectric properties of PVDF and it's copolymers in the absence of an electrical field E.

2.Theoretical considerations

We define the following nonlinear equations:

$$P_3=d_{32}\,T_2+\beta_{322}\,T_2^2 \qquad (4)$$

under the condition $E_3=0$.

The nonlinear piezoelectric constant is defined as

$$\beta_{322}=(1/2)(\partial d_{32}/\partial T_2) \qquad (5)$$

When a static stress T_s and a sinusoidal stress with an amplitude T_0 are applied along the 2-direction (omitting the indices in the following):

$$T=T_s+T_0\sin(2\pi ft) \qquad (6)$$

The polarization may be expressed as

$$P=d(T_0\sin(2\pi ft)+T_s)+\beta(T_0\sin(2\pi ft)+T_s)^2 \qquad (7)$$

which can be recast in the following equations:

$$P=P(0)+P(f)+P(2f) \qquad (8)$$

$$P(0)=(dT_s+\beta T_s^2+(1/2)\beta T_0^2) \qquad (9)$$

$$P(f)=T_0(d+2\beta T_s)\sin(2\pi ft) \qquad (10)$$

$$P(2f)=-(\beta/2)T_0^2\cos(2\pi(2f)t) \qquad (11)$$

3.Experimental

The material used for our studies was PVDF provided by the Solvay Co. and VDF/TrFE (75/25) copolymer provided by the Daikin Kogyo Co.. PVDF sample was characterized by a number average molecular weight of Mn=38,000 g/mole, a draw ratio of 4 at 85°C , a thickness of 23 μ m, and a poling field of 1.5 MV/m. Copolymer sample a draw ratio of 2.5 at 70°C , a thickness of 20 μ m, and a poling field of 100MV/m.

4.Experimental results and discussions

At first, the dependence of the piezoelectric strain constant d_{32} on the static tension T_2 was observed with a small sinusoidal stress at a frequency of 0.8 Hz. The result is shown in Figure 1. These results agree with those published by B.R.Hahn[1,2]. From the data in Figure 1, the nonlinear piezoelectric constant β 322 was calculated as,

$$\beta_{322} = -4.1 \times 10^{-20}\ Cm^2/N^2$$

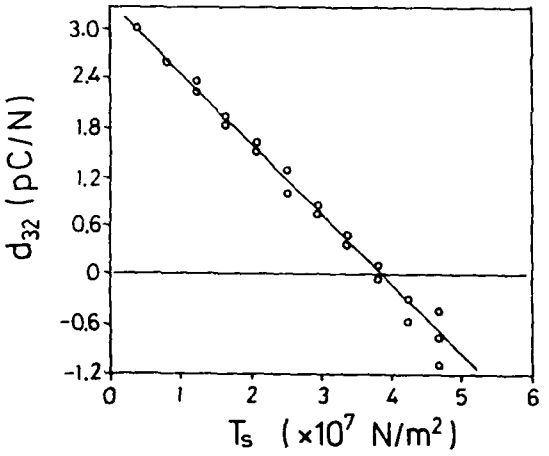

Fig.1 The dependence of the piezoelectric strain constant d_{32} at f=0.8Hz on the static stress T_2 for PVDF

In a second set of experiments we maintained a small static tension of 8.5×10^6 N/m^2 and subjected the sample to a sinusoidal strain at a frequency of 0.8 Hz. The strain amplitude was varied between 0.03 and 0.8% and the f=0.8 Hz as well as the f=1.6 Hz components of the polarization were investigated. The second harmonic component of the polarization P(2f) could clearly be detected. Figure 2 shows the results obtained at room temperature.

The absolute value of the nonlinear piezoelectric constant β_{322} as obtained from P(2f) and T_0 using expression (11) turned out to be:

$$\beta_{322} = -2P(2f)/T_0^2 = -3.6 \times 10^{-20}\ Cm^2/N^2$$

at a strain of 0.5%. This value is close to the one obtained on the basis of the stress dependence of the piezoelectric constant d_{32}.

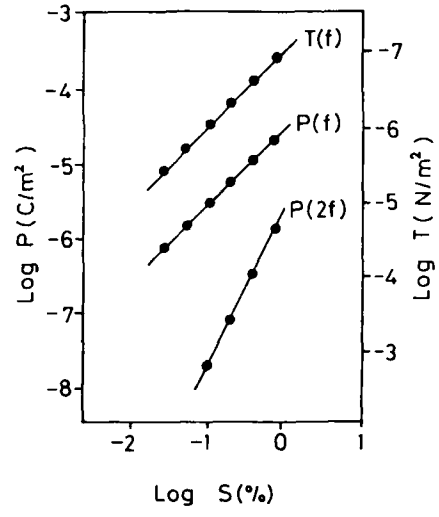

Fig.2 The components of sinusoidal polarization $P_3(f)$ and $P_3(2f)$, and the sinusoidal stress $T_2(f)$ at f=0.8Hz plotted against the sinusoidal strain $S_2(f)$ for PVDF

The effect of the static stress T_2 on the temperature dependence on the piezoelectric stress constant e_{32} for a copolymer film is shown in Figure 3. Below the glass transition temperature, no stress dependence is detected.

A nonlinear behavior occurs if the static stress is applied perpendicular to the chain orientation above the glass transition temperature. This suggests that the nonlinear properties are related to the thermal activation of molecular motions, which take place within the noncrystalline regions as well as interface regions. The transverse deformation induced by the stress T_2 leads to an increase or decrease of the average distance between the parallel chain molecules and thus to a reduction of the dipolar orientation.

References
[1] B.R.Hahn, Thesis., Technical University of Darmstadt, West-Germany
[2] B.R.Hahn, J. Appl. Phys. 57 1294 (1985)

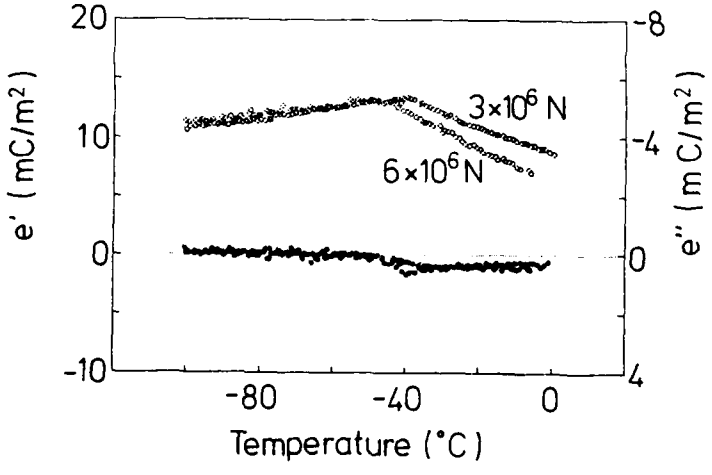

Fig.3 The temperature dependence of the complex piezoelectric stress constant e_{32} at 10Hz under different static tension for VDF/TrFE(75/25) copolymer

MODERN ELECTRET APPLICATIONS — THE FIRST 20 YEARS

J. E. West

AT&T Bell Laboratories
Acoustics Research Department
Murray Hill, New Jersey 07974

We are celebrating the Twentieth Anniversary of the commercialization of the modern foil electret microphone [1]. Foil electret microphones are electrostatic transducers with a permanently charged Teflon (Polytetrafluoroethylene PTFE) solid dielectric which generates an electric field in an airgap separating a diaphragm and backelectrode [2]. Four years after the first commercial appearance of these microphones, it was estimated that Japanese production alone exceeded 10 million units per year [3]. Today, at least 60 percent of the worlds production of microphones is done by robotic machines that produce and sort electret microphones for applications ranging from telephony to high fidelity reproduction. The success of foil electret microphones is attributed to their excellent acoustic properties, low cost, mechanical simplicity, and above all the stability of the charge in Teflon even under extreme environmental conditions. In addition to transducers, the application of electrets as a filter material greatly improved the capturing efficiency of both charged and neutral micro-particles as they pass through the filter [4]. These filters are commercially available and are used to maintain clean room environments. Bru es combining a ceramic magnet with electret fibers are being utilized for micro-contamination control in the semiconductor disc drive industry [5]. A comprehensive review [6], of the early developments in charging methods, environmental studies and many novel transducer applications, shows how foil electrets had began to change the course of microphone history.

This was not the first time in the twentieth century that electret devices, especially microphones and receivers had been offered for commercial use. The Bogen catalogues [7] of 1939 to 1940 offered several thick wax electret microphones based on patents issued to W. A. Bruno [8] under the name "No-Voltage Velotron." The large scale application of thick wax electret microphones came during World War II in Japanese field equipment [9]. Thick wax electrets had very poor electrical stability under nonshorted conditions,

CH2593-2/ 88/ 0000-0209$01.00 Copyright 1988 IEEE

therefore transducers made on this principle were subjected to large scale sensitivity fluctuations or even failure depending on environmental conditions. Thermoplastics such as acrylics, ethyl cellulose, polystyrene and vinyl polymers have the ability to store charge, and were suggested for applications as telephone transmitters in about 1948 [10]. In the early 1950's plate electret microphones were extensively studied, [11] however, they were not widely accepted because of charge instability and the rather large capacitance of the microphone.

A second and nearly parallel development of thin piezo or pyroelectric polymer electrets began in about 1968 when PVDF (polyvinylidene fluoride) was first reported to have a very strong permanent dipole moment [12]. The commercial application of thin piezo polymer foils also began in electroacoustics when transducers operating in transverse or longitudinal modes were fashioned into earphones and high frequency loudspeakers [13].

Since the commercial success of electroacoustic transducers in the audio frequency range, microphones using thin polymer electrets have been proposed that extend the frequency range from 10^{-3} Hz [14] to more than 2×10^{8} Hz [15] for use in solids, liquids, and gasses. The physical size of microphones based on both of the above principles have been reduced to micrometer dimensions [16,17]. Many other promising research activities continue to flourish in areas such as biomedicine, dosimeters, electrophotography [18], electrostatic recording [19-23], motors and generators, and photoelectrets [24] and have been comprehensively reviewed in the literature [18-23]. A review of applications of modern electrets utilizing the piezo, pyro, and ferroelectric properties of polar polymers have been exclusively treated in several books and conference proceedings [24-26].

REFERENCES

[1] Sony Corporation; see Electronics, Vol. 41, No. 26, p. 133 (23 Dec. 1968).

[2] G. M. Sessler and J. E. West, J. Acoust. Soc. Am. **40**, 1433 (1966).

[3] Jap. Elect. Ind. **19**, No. 11, p. 14 (Nov. 1972); **19**, No. 11, p. 22 (Nov. 1972).

[4] P. H. de Hann, J. van Turnhout, and K. E. D. Wapenaar, in Proc. 5th Int. Symp. on Electrets (ISE5), ed. by G. M. Sessler and R. Gerhaad-Multaupt, IEEE Library of Cong. No. 85-60544, pp. 789-794 (1985).

[5] S. A. Hoenig, The Univ. of Arizona, personal communications.

[6] G. M. Sessler and J. E. West, J. Acoust. Soc. Am. **53**, 1589-1600 (1973).

[7] Bogen Catalogue (1939), p. 16.

[8] W. A. Bruno, W. S. Patent 2,284,039 (26 May 1942; filed 16 July 1940).

[9] F. Gutmann, Rev. Mod. Phys. **20**, 457 (1948).

[10] T. A. Dickenson, Electrical Manufacturing, p. 101 (Aug. 1948).

[11] G. G. Wiseman and E. G. Linden, Electr. Eng. (Am. Inst. Electr. Eng.) **72**, 869 (1953).

[12] H. Kawai, Japn. J. Appl. Phys. **8**, 975 (1969).

[13] E. Fukada, Ultrason. **6**, 229 (1968); M. Tamura, T. Yamaguchi, T. Oyaba, and T. Yoshimi, J. Audio Eng. Soc. **23**, 21 (1975).

[14] G. M. Sessler and J. E. West, Proc. Seventh Int. Congr. Acoust., Budapest (1971), Paper 23E1.

[15] C. Becker and D. Lenz, in Proc. 5th Int. Symp. on Electrets (ISE5), ed. by G. M. Sessler and R. Gerhaad-Multaupt, IEEE Library of Cong. No. 85-60544, pp. 789-794 (1985).

[16] D. Hohn, Proc. 12th Intern. Congr. Acoust., Toronto (1986), Paper L3-3.

[17] J. Franz, Proc. 12th Intern. Congr. Acoust., Toronto (1986), Paper L3-2.

[18] R. M. Schaffert, "Electrophotography," J. Wiley and Sons (1975) p. 601-641.

[19] G. M. Sessler and J. E. West, in "Electrets" ed. by G. M. Sessler (Springer, Berlin 1980-1987) pp. 346-381.

[20] R. Gerhard-Multhaupt, B. Gross and G. M. Sessler, in "Electrets" ed. by G. M. Sessler (Springer, Berlin 1987) pp. 383-431.

[21] R. Gerhard-Multhaupt, IEEE Trans. on El. Insul., Vol. EI-22, No. 5, 531-547 (1987).

[22] G. M. Sessler and R. Gerhard-Multhaupt, ed. Proc. 5th Int. Symp. on Electrets (ISE 5), IEEE Library of Cong. No. 85-60544, pp. 711-818 (1985).

[23] B. Hilczer and J. Malecki, "Electrets" Elseiver (1986), pp. 314-342.

[24] V. M. Fridkin and I. S. Zheludev, "Photoelectrets and the Electrophotographic Process," Consultants Bureau (1960).

[25] P. M. Galletti, M. G. Broadhurst and D. DeRossi ed. Ferroelectrics, **60**, NO. 1/2/3/4 (1984), "Proc. of the First Int. Symp. on Piezoelectricity in Biomaterials and Biomedical Devices," Pisa, Italy, 1983.

[26] T. T. Wang and J. M. Herbet, ed., "The Applications of Ferroelectric Polymers," Blackie, London (1988).

SUBMINIATURE SILICON INTEGRATED ELECTRET CONDENSER MICROPHONE

P. Murphy and K. Hubschi

Lectret, S.A., Geneva, Switzerland

and

N. De Rooij and G.A. Racine

Universite de Neuchatel, Neuchatel, Switzerland

ABSTRACT

Silicon micromachining provides better precision for controlling diaphragm - backplate spacing in electret microphones than more classical techniques. The silicon support members can also be used to carry the integrated circuit amplifier which is usually required for impedance matching. We have prepared microphones which use one silicon wafer to support a thin polyester diaphragm and a second to carry a Teflon electret. Sub assemblies are diced from the wafer and bonded together to form complete microphones. The preamplifier circuit can be carried on either sub assembly. Microphones with reasonable signal to noise ratio can be obtained with edge dimensions of 3 mm or less. The electroacoustic properties of prototype units will be described.

MARKET SITUATION OF PIEZO-, PYRO- AND DIELECTRIC FILMS - LATEST DEVELOPMENTS.

R. A. BETZ

SOLVAY & Cie, Brussels, Belgium

ABSTRACT

Piezo- and pyroelectric films have gained more and more interest since their commercial introduction in 1981. A very extensive information campaign has led researchers to develop applications with piezo films in the field of large surface sensors, such as SIDS mattrass, road detectors, cable wrapping etc. The versatility of PVDF films has also been used in the manufacture of very small and sensitive detectors or detector arrays in very diversified fields : ultrasound sensors for non-destructive testing or medical imaging, infra-red array sensors for movement and heat sensing, force or acceleration detectors. Bimorphs have gained a special interest more recently since the publication of a description of a flat display panel (a giant television screen) using mono-oriented piezo films. Dielectric PVDF films are now a reality in Europe : several qualities that can be used in the capacitor industry are available; properties and industrial targets will be described.

1. PIEZOELECTRIC FILMS - RANGE AND PROPERTIES.

Polyvinylidene fluoride (PVDF) piezoelectric films, known since the beginning of the seventies [1], have gained lately more and more interest in the sensor industry due to their unique properties. The products can be divided roughly into two categories with different applications in mind : bioriented films and

CH2593-2/ 88/ 0000-0214$01.00 Copyright 1988 IEEE

monoaxial films. The first commercial quantities of these products have begun to appear on the western market in 1981. Today the range of thicknesses of the films (and sheets) goes from 6 μ to 2 mm. The market demand gives a repartition of approximately 95 % for biaxial films and 5 % for monaxial films, based on the number of applications. In biaxial films, the piezo-electric coefficients d31 and d32 are each equal to about 10 pC/N resp. 20pC/N for d_t. In monoaxial films, d31 and d_t equal 20-22 pC/N, d32 being practically zero (fig.1). Sheets in the thicknesses of 0,2 to 2 mm have been produced by a special process [2] limited to mono-oriented sheets.

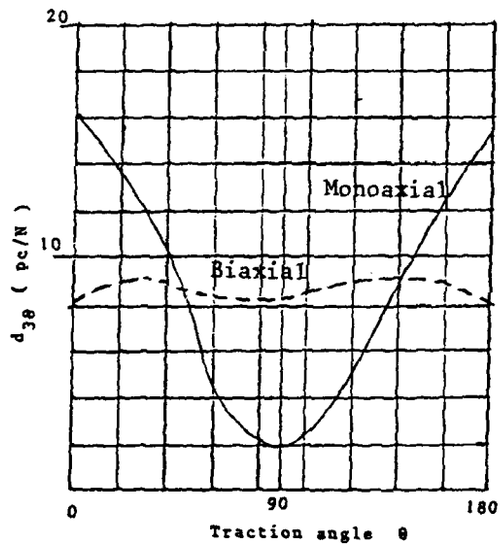

Fig.1.
Angle dependence of piezo constants.

LARGE SURFACE SENSORS

One of the main advantages of piezoelectric films vs PZT ceramics is the possibility to obtain sensors with large surface areas : poled films are now produced continously in widths up to 25 cm. One can therefore design a sensor of half a square meter without difficulty! This property has quickly been used to develop very sophisticated sensors for the detection of the

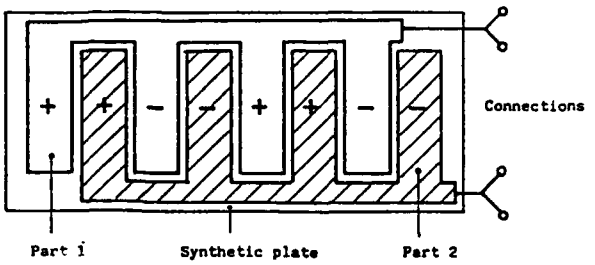

Fig. 2. Sensor electrodes for SIDS mattrass.

Sudden Infant Death Syndrom (SIDS), which is probably one of the most important disorders in babies of 1 year and less : more than 20.000 deaths are recorded each year in Europe alone! A piezo film of 0,15 sq.m is embedded between protective PVC [3] layers and continuously monitors the breathing of sleeping babies (fig.2). Because of insufficient oxygen content of the blood, certain babies can stop breathing : an alarm must warn the parents within 20 seconds. Road sensors have also called for long strips of sensitive film or cables to measure not only the presence of vehicles [4], but also their number or their weight on each axle. This is now commercialy done with 2 cm wide piezo films or piezo wrapped cables of a new design embedded in the roadway. Field tests are underway now. Another very interesting application using large surfaces of film still requires a sponsor : why not use a piezo film under the base line of a tennis court as an accurate sensor for "out" balls?

ULTRASONIC SENSORS AND ACCELEROMETERS.

The precrding applications may not appear to be very scientific : for the sake of conciseness, we did not mention all theoretical studies and calculations which underline the final sensors. Very accurate ultrasonic sensors are now produced by several companies in Great-Britain

[5], Germany [6] and Italy. They present numerous advantages over their ceramic counterparts : purity of signal, wide bandwidth, ease of manufacture. Accelerometers are also under study in France; in the USA, a newly developed instrument [7] used in an ultrasonic pulse-echo mode, can detect small cracks in composites : this sensor which is entirely portable (and named PARIS for Portable Automated Remote Inspection System), should be of great use to the aircraft and aerospace industries[8] and with some adaptation also in the chemical process industries for NDT testing of vessels and pipe lines. Medical instrumentation requires ultrasonic sensors of high signal-to-noise ratio. Apart from blood pressure devices, catheters and ultrasonic detectors measuring the water content of the skin[9], we want to mention the regular use of ultrasonic receivers in lithotripsy (extra-corporeal shock machine to smash kidney stones with acoustic waves). A presentation of this subject is given during this Symposium [9].

INFRA-RED DETECTORS

Much progress has been made during the last year or two in this field : the detectors based on PVDF piezo film are now used in great quantities for portable alarms, sensitive lamps and detectors [10]. The possibility of making arrays of sensitive elements has led to developments in two different directions : 1) with a fixed detector to record a movement; this is already realized with InAs or PbSe detectors. 2) with a mobile detector which focuses onto a fixed point. This last possibility is now intensively studied in the USA, in England and in France for military applications such as for so called smart munitions (Fig.3) [11].

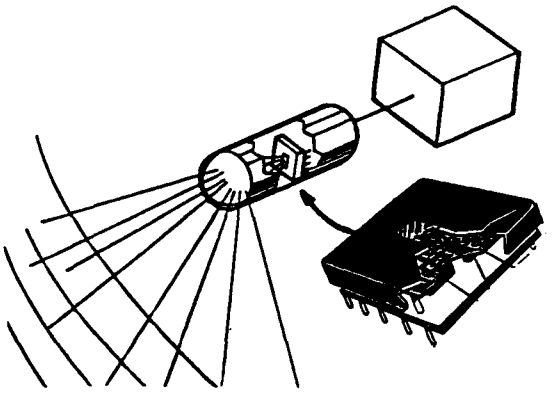

Fig.3. Infra-red detector for smart munitions.

BIMORPHS AND OTHER MONOAXIAL APPLICATIONS.

Laminates of thin ceramic pieces are commonly used in transducers for accentuating piezoelectric action. The same structure (Fig.4) can be easily constructed with PVDF piezo films or sheets; due to the low price of these films the process can be fully automated : presently three such laminating machines are operating or being developed for full production. Monoaxial film is preferred for these applications because of its high d31 coefficient. Applications range from movement or optical switches to robotic tactile sensors [12] or even to vibration control of a cantilever beam using PVDF in a space environment [13]. However the most striking idea has evolved lately [14] into a prototype of a large-area flat-panel television screen (or display), using piezofilm bimorphs as shutters to monitor hundreds of thousands of individual lights spots or pixels. This new display, currently under development, should replace existing technology that is much more expensive. In addition, these panels will have a resolution that is at least 4 times better than existing panels.

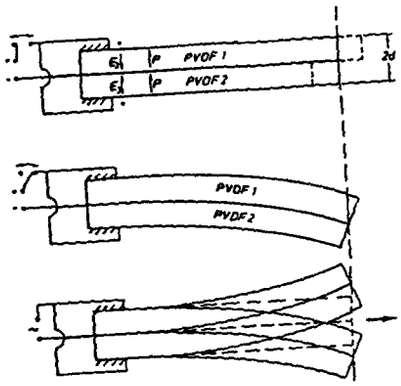

Fig.4.

Bimorphs

OTHER DEVELOPMENTS

We have listed more than ninety different applications of piezo films and sheets : the number of developments presently under way in the western sphere is growing rapidly; it is also known that these developments are slow and take several years to materialize. Knowing that the above presented applications are not complete, we nevertheless would like to set forth these last examples : matrix recognition sensor, sole for pedobaro-graphy, energy generation from water or wind, variable focus mirrors, air flow monitors, singning balloons or menus (!), ultrasonic graphic input tables etc.. One very interesting application is the use of piezo foils to determine the steady and unsteady surface forces called boundary layers around surfaces like airplane wings. The University of Berlin [15] has made considerable developments in this direction.

DIELECTRIC PVDF FILMS

Polyester, polypropylene and polycarbonate are the most widely used resins for manufacturing capacitor films in extreme dimensions : down to 1.1 µ in thickness, 3 mm in width and several hundreds of meters long. The industry has been searching and is still looking for better capacitance films; Up to now, PVDF is the polymer with the highest relative dielectric constant (ε = 12). Other major advantages of

PVDF biaxial capacitor films are their high breakdown strength, particularly in the DC area, excellent mechanical properties, non-flammability and very good chemical resistance e.g. against insulating oils. Several variations of the basic PVDF film for capacitors are now proposed : one type is a special version thermally stabilized (00651), another one has a lower dissipation factor (00652) as well as a higher dielectric breakdown voltage (see table 1).
A last quality (00654) has a dielectric constant which is pratically stable from -20°C to 80°C (fig.5).

Table 1. Property comparison of ALKORFOL-KF capacitor films.

	00650	00651	00652	00654
Tensile str. MD kg/mm2	15-20	15-20	10-15	15-20
Tensile str. TD kg/mm2	20-25	20-25	10-15	5-10
Diel. Const. 60Hz	11,0			
@ 22°C 10 Hz	10,7	10,5	9,0	12,0
10 Hz	7,0			
Dissipation factor @ 22°C, 10 Hz	0,012	0,015	0,009	0,008
Breakdown V. 22°C, V/µm	360	-	540	350

Other developments are awaited in this field. Several papers [15][16][17] have already dealt with the dielectric behaviour of copolymers of vinylidene fluoride and trifluoroethylene. Intensive studies are under way with these polymers.

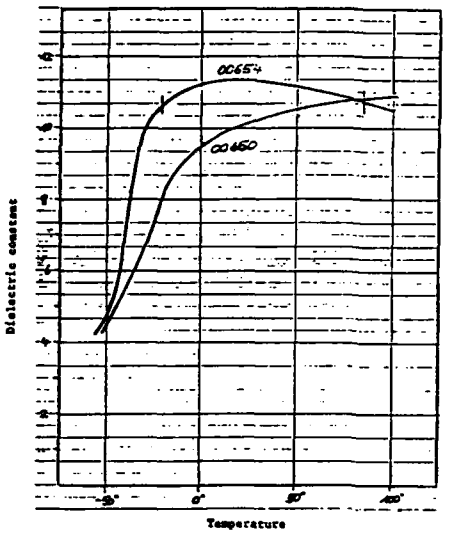

Fig.5.

Dielectric constant of ALKORFOL-KF capacitor films.

REFERENCES

[1] H. Kawai, Japan J. Appl. Phys. 8,975 (1969)
[2] D. Broussoux, H. Faccetti and F. Micheron, Eur. Patent Appl. 0048642
[3] Dr. von Nettelhorst, to be published.
[4] Federal Highway Admin., Seismic Detection of Motor Vehicles, FHWA-RD-76-161, May 1976.
[5] *Fulmer Research Inst., Cogent.* Ltd, England
[6] Imotec GmbH, Krautkramer GmbH.
[7] P. L. Squire, Sensors, 12, July 1986.
[8] G. Gerliczy and R.Betz, ISAF 86, Proc. 6th IEEE Intern. Symp. Applic. Ferroel., Bethlehem, PA, June 8-11, 1986.
[9] Personal communication
[10] Elektor, 74, Oct. 1986.
[11] A.P. Doctor and M. Rost, Sensors, 26, April 88
[12] J.D. Abramowitz et al., Computers in Eng., ASME Conf., 103 (1983).
[13] J.E. Hubbard, Jr. and C.W. Lowe, Report of the Charles Stark Draper Lab., Cambridge, Mass., Dec. 1985
[14] Patent to be published.
[15] Conf. Proc. of the Sensor 88 exhib.,

Nuremberg, May 3-5 (1988).
[16] K.J. Humphrey et al., ISE 5, Intern. Symp. on Electrets, 4-6 Sept. (1985).
[17] T. Yagi et al., Polymer J.(Japan), 12, No 4, 209 (1980)
[18] I.S. Suzuki et al., Polymer J.(Japan), 19, No 6, 681 (1987)

- - -

PVDF HYDROPHONE FOR THE MEASUREMENT OF SHOCK WAVES

B. Granz

Forschungslaboratorien der Siemens AG,
Erlangen

ABSTRACT

Focused fields of finite amplitude ultrasonic pulses as they can occur in lithotripsy can be measured with hydrophones made of the piezoelectric polymer PVDF. Extreme pretensions to the hydrophones - peak pressure of more than 20 MPa with a rise time of less than 50 nsec (shock pulses) - lead to a special construction of the hydrophone where sensitive area and metal electrodes are well separated spatially. With a 25 µm thin PVDF foil, a non metalized sensitive area of 3 mm diameter, a hydrophone of $2 \cdot 10^{-2}$ V/MPa with a bandwidth near 20 MHz is achieved. More than 10^5 focused shock pulses of about 20 MPa have been measured without a remarkable decrease in sensitivity of the hydrophone.

INTRODUCTION

Since ultrasonic shock waves have been used in the field of medical therapy e.g. for the desintegration of kidney stones (lithotripsy), increased attention is now turned to methods for the reliable measurement of high amplitude ultrasonic pressure fields. In lithotripsy the pressure pulse amplitude can rise to 100 MPa within a time shorter than 1 µs. One can imagine that pressure pulses able to desintegrate kidney stones are also able to destroy hydrophones. On the other hand, hydrophones made of the piezoelectric polymer PVDF have been widely used because of

CH2593-2/ 88/ 0000-0223$01.00 Copyright 1988 IEEE

their large bandwidth and their ease of construction /1/, /2/, /3/. The good dynamic response to pressure pulses higher than 70 MPa /4/ suggests the construction of PVDF hydrophones even for extreme requirements /5/.

The poor adhesion of metal contacts to the surface of the polymer PVDF is the main reason for the decrease in sensitivity of PVDF hydrophones in shock wave measurement. To overcome this disadvantage a totally new way of construction had to be developed.

CONSTRUCTION

The basic idea of our construction is not to use any metal contacts on the PVDF in the sensitive region. The pressure pulse produces alternating charges on the surface of the PVDF foil in a region where the foil is polarized and therefore piezoelectric. These alternating charges occur also if the foil is not metallized. The signal of these alternating charges is then capacitively coupled to metal electrodes away from the sensitive area. This spatial separation of the sensitive area and the electrodes allows a stable construction of the elctrodes without disturbing the pressure field.

The construction details of our hydrophone is shown in figure 1. This hydrophone will be referred to as the "contactless hydrophone".

A non metallized 25 µm thin PVDF foil is fixed by two clamp rings. This foil is polarized only in the center. This polarized spot of 3 mm diameter is the sensitive area. The signal from the alternating charges on both sides of the sensitive area is coupled through the deionized water to the signal ring and to the grounded ring which are both connected to a high impedance preamplifier.

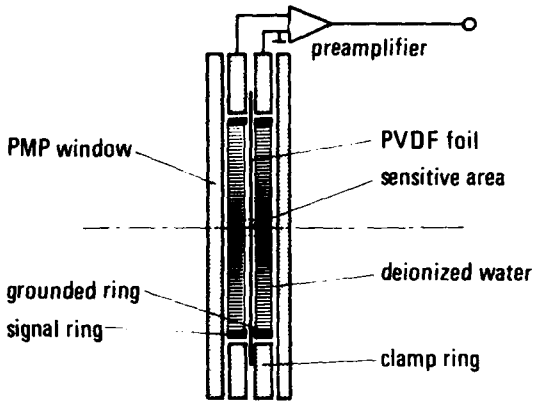

Fig. 1: Construction of the contactless PVDF hydrophone for shock waves

The windows to this chamber hydrophone are made of the highly transparent polymer polymethylpentene (PMP). To conserve the purity of the water all metal parts inside the chamber have to be of stainless steel. If the conductance of the water is below 10 uS/cm then the equivalent circuit of the hydrophone can be made up only by capacitors.

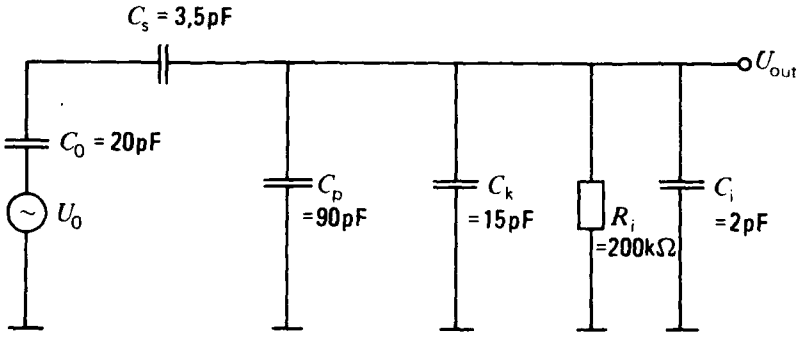

Fig. 2: Equivalent circuit for the contactless PVDF hydrophone for shock waves

The capacitor C_o of the sensitive area is coupled by C_s to the signalring and to the

grounded ring respectively. Both rings are short cut by the water (C_p) and by the cable capacitance (C_K). Additionally the signal line is loaded by the input resistance and capacitance R_i and C_i of the preamplifier. By neglecting R_i this circuit leads to a reduction of the original voltage of

$$\frac{U_{out}}{U_0} = \frac{C_0 \cdot C_s}{(C_0 \cdot C_s) + (C_0 + C_s) \cdot (C_p + C_k + C_i)}$$

For the numbers used in figure 2 one gets

$$\frac{U_{out}}{U_0} = 0.027$$

for frequencies higher than 100 kHz, where R_i is neglected.

RESULTS

All experiments are done with an elctromagnetic acoustic source /6/ which produces together with a polystyrene lens a pressure pulse of 20 MPa at a distance of 200 mm. The experimental set-up is shown in figure 3.

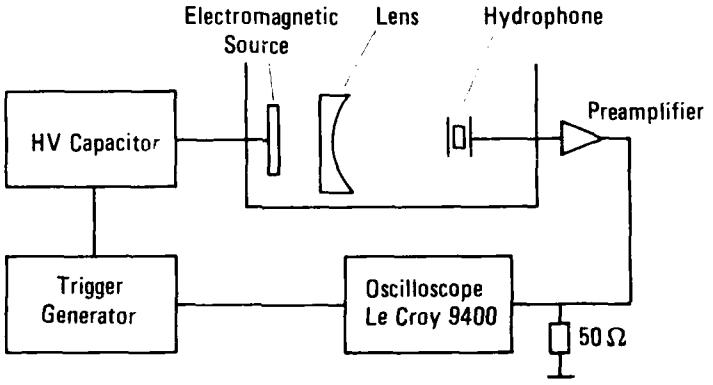

Fig. 3: Experimental set-up for the measurement of shock waves

The pressure pulses measured by the hydrophone in the focus of the lens is digitized to 8 bit with a sample rate of 100 Msamples/sec. A typical shock pulse is shown in figure 4.

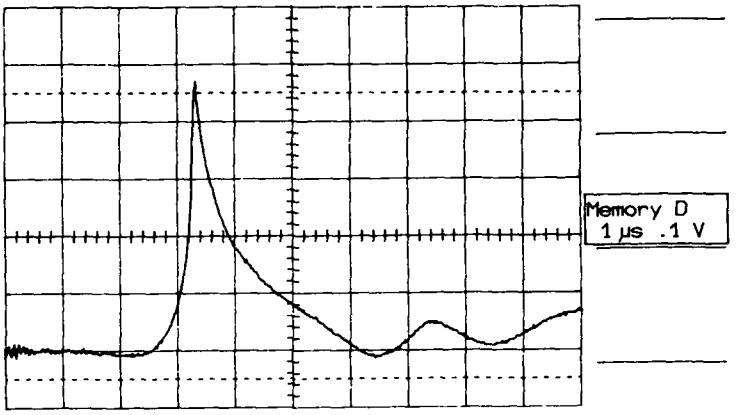

Fig. 4: Shock pulse in the focus of the acoustic lens. The peak pressure is 20 MPa

In figure 4 one can see the steeply rising slope, the needle-like top, and the smooth slope of the trailing edge. Rise times near 40 nsec have been measured. The later part of the trailing edge is affected by pulse portions diffracted by the metal rings outside the sensitive area. These diffraction effects increase in the measurement of plane waves. More than 10^5 pulses in the focus of the lens have been measured without any decrease in the sensitivity of the hydropone. The sensitivity at the amplifier output is approximately 20 mV/MPa, the -3dB bandwidth of the hydrophone with preamplifier is near 20 MHz.

CONCLUSION

The basic idea of separating the sensitive area and the metal electrodes leads to the

construction of a new type of hydrophone. With the piezoelectric foil PVDF as sensor material reliable measurements in the focus of a shock pulse generator can be made. These measurements can be made over a large bandwidth without there being any remarkable decrease of sensitivity. The sensitivity is high enough, to reduce the sensitive area to even 1 mm diameter for more accurate measurements.

REFERENCES

/1/ A.S. De Reggi, S.C. Roth, J.M. Kenney, S. Edelmann and G.R. Harris, "Piezoelectric polymer probe for ultrasonic applications", J. Acoust. Soc. Am. 69, 853-859, 1981

/2/ R.C. Shotton, D.R. Bacon and R.M. Quilliam, "A pvdf membrane hydrophone for the operation in the range 0.5 MHz to 15 MHz", Ultrasonics, pp. 123-126, may 1980

/3/ P.A. Lewin, "Miniature piezoelectric polymer ultrasonic hydrophone probes", Ultrasonics, pp. 213-216, september 1981

/4/ St.W. Meeks and R.Y. Ting, "Effects of static and dynamic stress on the piezoelectric and dielectric properties of PVDF", J. Acoust. Soc. Am., 74, pp. 1681-1686, 1983

/5/ M. Platte, "A polyvinylidene fluoride needle hydrophone for ultrasonic applications", Ultrasonics, pp. 113-118, may 1985

/6/ H. Reichenberger and G. Naser, "Electromagnetic Acoustic Source for the Extracorporal Generation of Shock Waves in Lithotripsy", Siemens Forsch. und Entw. Ber. 15, pp. 187-194, 1986

PIEZO-ELECTRIC FILM AS A SENSOR ELEMENT IN SIGNATURE VERIFICATION

P. de Bruyne

Institute for Communication Technology
ETH Zentrum-KT
CH-8092 Zurich, Switzerland

ABSTRACT.

The fraud protection currently provided by the Personal IdentificationNumber (PIN) is not always sufficient. Automatic verification of signatures at Point-Of-Sales, or bank terminals can improve this protection. Dynamic characteristics involved in writing a signature are difficult to forge but usually require specially wired pens, not suitable for hard day-to-day use. A low-cost Piezo-electric film underneath a writing surface can detect stylus position and velocity profiles, thus permitting verification of the signature using both static and dynamic features. Arrays of parallel electrodes detect pen velocity profiles without being affected by touching fingers or by noise.

INTRODUCTION.

Automatic verification of handwritten signatures has not found large scale application because the hardware has been expensive, unreliable and difficult to use. A wired stylus is usually required, causing problems of replacement when the wire becomes damaged. The use of PVDF piezo-electric membranes offer new possibilities in this field because the signature can be written with any ballpoint pen. Signals from the piezo-electric membrane containing information on the time profile of stylus pressure versus time, have been used in signature verification [1]. Such devices, however, are rather sensitive to accoustic noise and to pressure changes caused by the hand touching the tablet. The latter occurs often when left-handed persons write their signature.

BACKGROUND.

Static and dynamic characteristics of signatures which might be suitable for reliable signature verification have been investigated [2]. An error rate below 4% in detecting good forgeries, was easily achieved. This was accomplished by combining several testing criteria, each of which having an individual errorrate of

CH2593-2/ 88/ 0000-0229$01.00 Copyright 1988 IEEE

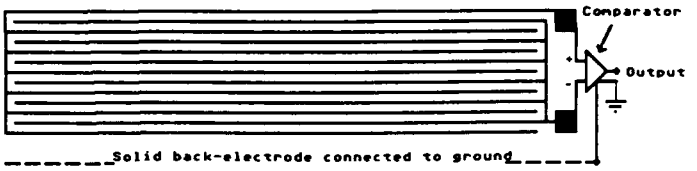

Fig. 1. Sensor with two sets of interleaving electrodes

as much as 20%. An errorrate of less than 0.1% against accepting signatures which are obviously different, may be obtained by elastic matching [3]. The required computation time, however, is very long and such performance is usually not necessary. The optical principle of frustrated total internal reflection, suitable for signature verification using static and dynamic feature extraction, has recently been investigated [4]. A normal ballpoint pen may be used with this device.However, piezo-electric methods appear to be much lower in cost (Patent applied for). These are the subject of this paper.

PRINCIPLE OF OPERATION.

A membrane with two sets of interleaving electrodes for detecting pen motion in a vertical direction is shown in Figure 1. The voltage difference output between these sets is insensitive to common mode noise such as caused by sound and by pressure of a finger. The solid electrode which is present on the reverse side, is grounded. A similar membrane with electrodes at right-angles to the first membrane, is used to detect pen motion in the horizontal direction. These membranes were mounted with their grounded electrodes facing each other.

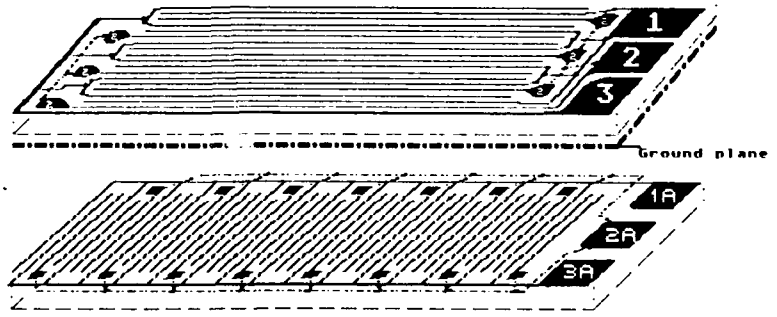

Fig. 2. Arrangement with 3 sets of electrodes for detection of pen motion in up/down and left/right directions

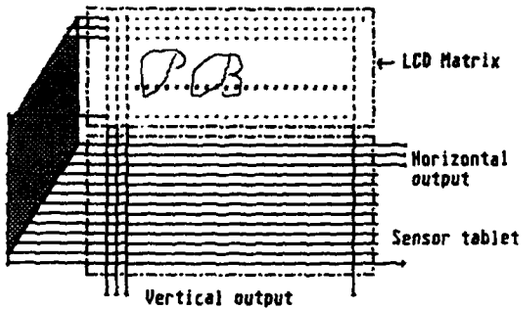

Fig. 3. Concept of a direcly connected matrix LCD

Velocity profiles.

With only 2 sets of interleaved electrodes as shown in Fig. 1, it is not possible to sense of direction of the pen motion. In Fig. 2 an arrangement with 3 sets of electrodes is shown, which can discern the motions up, down, left and right. When the pen is moving upwards, the electrode sets will be crossed in a 1, 2, 3, 1 . . sequence. When moving down the sequence will be 3, 2, 1 ,3 . . This arrangement will thus be able to record not only the the pen velocity, but also the true direction and distance from a starting point, assuming the pen is not lifted during the writing phase. When the pen is lifted and returned to the tablet, there is no way of knowing at which position it has landed. Changes of velocity in time are characteristic to the writer writing his signature and are difficult to forge. This arrangement hence is useful for verifying signatures by their dynamic features. It can not be used for recording the complete shape of a signature, because position information is lost when the pen is lifted at the end of each writing phase.

Position Tracing.

Figure 3 shows an arrangement of the tablet where each line-electrode is connected separately, assuring that absolute position, rather then relative motion, is sensed. A liquid crystal matrix display may be connected to the tablet to help the person writing his signature, without having to write on paper. An stylus can be used, which does not leave a mark on the actual tablet. A Matrix LCD may probably be directly connected to the array of electrodes via clamped diode sample and hold elements. This arrangement has not been tried out, as it involves integrating the diode connections of each line with

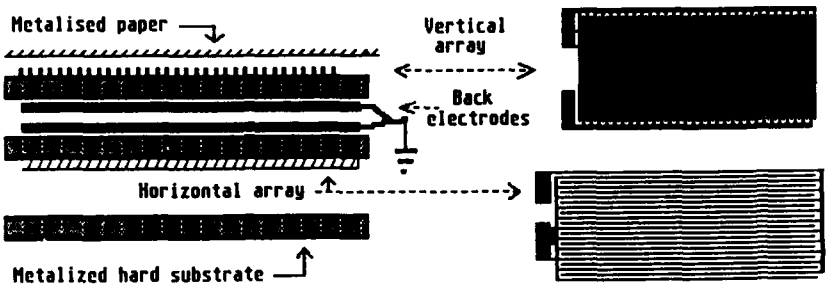

Fig. 4. Experimental tablet with 2 sets of electrodes

the LCD Matrix. It should provide a simple positional display, but it will need additional logic to extract the dynamic features required for signature verification.

Practical details.

A simple 3 mm thick tablet with an active area of 75 x 40 mm was assembled and is shown in Figure 4. Two electrode sets for each direction, of the type shown in Figure 1, were used. This permits the extraction of speed profiles in both the horizontal and vertical directions and is suitable for many applications of signature verification. The membrane material was made by Solvay & Cie of Brussels, Belgium and was coated with 800 nm of Aluminum. The material was first cleaned with alcohol, then dip-coated with a standard photolaquer, exposed, developed in an alkaline developer and then etched in a Ferric Chloride solution. The thin Aluminum coating required a carefully controlled developing and etching procedure. With further improvements a much finer structure than shown in Figure 2, should be practical. A PC board is used for the top and bottem cover and clamps the sensor sandwich. Contacting the electrodes was achieved with contact rubber from the watch industry. A sheet of metallized paper provides an electrostatic shield for the outer surfaces. The paper surface has a slight conductivity, which slowly discharges any voltage between the sets of electrodes when the tablet is not used. With a normal writing pressure on 1 mil membranes used in the model shown in Figure 4, signals of 50 mV p.t.p. were produced. This corresponds to a charge of 150 pC for a transition from one set of electrodes to another set. The actual contact area for a ballpoint pen pressing with

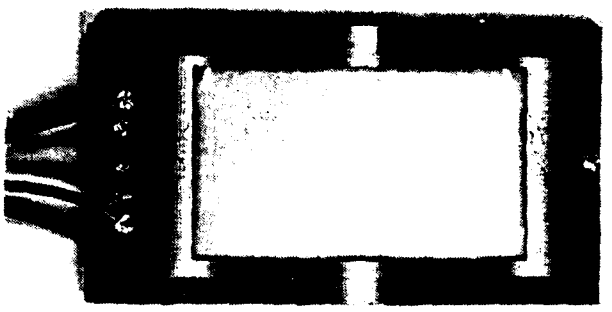

Fig. 5. Double membrane test assembly (120 x 65 x 3 mm)

0.5 N, is about 0.3 mm^2 and would provide about 150 V across the 1 pF capacity of this small membrane area. When single electrodes, such as shown in Figure 3 are used, each of length 60 mm and width 0.3 mm, a distribution of the charge takes place. The resulting signal of 0.7 V should be sufficient to drive one line of a LCD matrix display shown in Figure 3.

APPLICATION.

A high input impedance comparator circuit forms the connection to the digital interface with a personal computer, programmed for the desired verification and processing algorithms. Fraudulent use of the new smart cards could be reduced by requiring the user to write his signature instead of, or in addition to, giving his PIN number. The small amount of data required to store the dynamic features of the signature, can easily be accomodated in the card memory. The costs of such a system are probably small and are mainly in the hardware, as the terminal has computing facilities. The cost of the PVDF film amounted to less than $ 2.- for this tablet size.

REFERENCES.

1] Radice, P.F. **Personal verification device**, *U.S. Patent* 4,234,868

2] de Bruyne, P. **Signature verification using holistic measures** *Computers & Security* 4, (1985), pp. 309-315

3] de Bruyne, P., Forré, J. **Signature verification with elastic image matching**, *Proceedings of the 1986 Intern. Carnahan Conference on Crime Countermeasures*, Gotheborg, (1986), pp. 113-118

4] de Bruyne, P. , Meyer, U. **Vorrichtung und Verfahren zur Bestimmung der Echtheit einer Unterschrift,** *Swiss Patent Appl.* 683/87-9 (Filed February 24, 1987)

DETECTION OF STRESS FIELD SHEAR COMPONENTS BY A PIEZOELECTRIC POLYMER TACTILE SENSOR

D.De Rossi*°, A.Nannini*^, C.Domenici*° and R.Francesconi°

* Centro "E. Piaggio", University of Pisa
° C.N.R. Institute of Clinical Physiology, Pisa
^ S.S.S.U.P. "S. Anna", Pisa, Italy

ABSTRACT

A partial implementation of a multielement tactile sensor based on piezoelectric polymer technology is presented. The sensor ability to resolve the shear stress component acting on it under axisymmetric, normal loading at its boundary is demonstrated. This feature is thought to be instrumental in revealing incipient slippage detection during object grasping and manipulation.

INTRODUCTION

In the search for optimum materials and transduction phenomena to develop truly skin-like tactile sensors for prosthetics and advanced robotics, piezoelectric polymers have already originated widespread interest [1].
A common limitation of presently available sensors, however, resides in their lack of discrimination capability in respect to the stress field tensorial components, which virtually frustrates any effort to infer the vectorial force field distribution at the boundary generated by the sensor-object contact.
Recently, a biomimetic tactile sensor with stress-component discrimination capability has been proposed, a possible methodology for its dimensioning has been given and its ability to measure stress field normal components has been demonstrated [2].

CH2593-2/ 88/ 0000-0234$01.00 Copyright 1988 IEEE

In this paper we report a further implementation, specifically addressing the sensor ability to resolve shear stress components acting on it under a plane-stress loading condition. Detection of shear stress components is thought to be of paramount importance in revealing incipient object slippage during grasping and manipulation.

SENSOR DIMENSIONING

The proposed multicomponent transducer is composed of six piezoelectric polymer sensors, whose surfaces normal to the z-axis are covered with thin metal electrodes, respectively made of: two uniaxially oriented polyvinylidene fluoride (PVDF) elements, having orthogonal draw directions; a biaxially oriented PVDF element; two PVDF element obtained by cutting a uniaxially oriented PVDF thick slab along its thickness, one in a direction parallel to the draw direction and the other in a direction perpendicular to the draw direction; an uniaxially oriented polyhydroxybutirate (PHB) element. The polymer elements, all of thickness t equal to 100 μm, are inscribed in a circle of diameter b = 2 mm and embedded into a rubber pad.

The depth location of the sensor inside the elastic pad can be calculated by resorting to a combined engineering reasoning and the analytical solution of a classic problem of elastic contact [2].

To determine the upper z_M and lower z_m bounds for optimum depth location a set of variables should be specified, either of instrinsic (sensor material properties, geometry and characteristics of the electronic chain) and extrinsic nature (amplitude and minimum spatial wavelength λ_m of the load acting on the sensor surface). Having defined a set of input design parameters and material constants, as reported in Table 1 (the notation adopted in Ref.[2] is used), the range of optimum depth location can be determined by solving the following equations [2]:

$$z_M = \left\{ \frac{P\, d_6\, y\, t}{V_n^{(4)}\, \pi \epsilon_3^{(4)}} - y^2 + \left[\frac{(d_6\, y\, P\, t)^2}{(V_n^{(4)}\, \pi \epsilon_3^{(4)})^2} - \frac{2 d_6 y^3 P\, t}{V_n^{(4)}\, \pi\, \epsilon_3^{(4)}} \right]^{\frac{1}{2}} \right\}^{\frac{1}{2}} \qquad (1)$$

$$C\, b = \lambda_m(z,D) \qquad C = 2$$

$$z \exp\left(-\frac{2\pi}{\lambda_m} z\right)\left(\frac{2\pi}{\lambda_m}(d_3+d_1) + \frac{1}{z}(d_3-d_1)\right) = \frac{1}{D}(d_3+d_1) \cdot \exp\left(-\frac{2\, d_1}{d_3+d_1}\right) \qquad (2)$$

Table 1

PARAMETER	VALUE	REFERENCE
Stress piez. coeff. $d_6=d_{24}^{(4)}$	$-23\text{x}10^{-12}$ C/N	[3]
Rel. permittivity $\varepsilon_3^{(4)}/\varepsilon_o$	12	[2]
Stress piez. coeff $d_1=d_{31}^{(1)}$	$22\text{x}10^{-12}$ C/N	[2]
Stress piez. coeff. $d_3=d_{33}^{(1)}$	$-31\text{x}10^{-12}$ C/N	[2]
Sensor dynamic range D	2^{10}	[4]
Minimum detect. load P	$5\text{x}10^{-2}$ N	[5]
Minimum detect. volt. $V_n^{(4)}$	$1\text{x}10^{-6}$ V	-

In Fig. 1 the calculated range for optimum depth location of the sensor is shown.

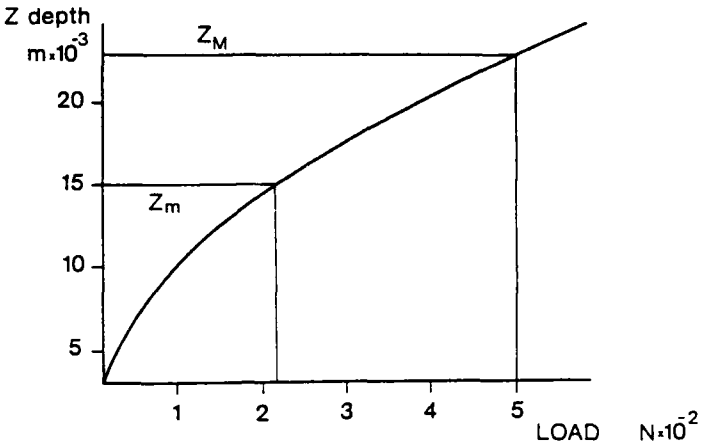

Fig. 1 Calculated optimum depth location for the multicomponent sensor. In the abscissa the corresponding theoretical values of minimum detectable loads at the boundary are indicated.

LOADING CONDITIONS AND SENSOR RESPONSE TO SHEAR

A 100 μm thick, 1 mm x 1 mm PVDF element obtained by cutting an uniaxially oriented thick slab (1 mm thick, courtesy of F. Micheron, Thomson-CSF) along its thickness, in a direction parallel to the draw direction has been metallized by silver paint and incorporated between two rubber sheets placed on a rigid foundation.
The load was exerted normally to the plane of the rubber sheets through a circular steel indenter, having a radius a = 0.75 mm, with round edges; the central axis of the sensor was displaced, during successive loadings, with respect to the longitudinal axis of the indenter and the charge outputs of the load cell and the sensor were simultaneously recorded.
The stress shear component for this plane stress problem has been calculated [6] and the sensor output transfer function is:

$$V = \frac{t}{\epsilon_3} d_6 \frac{P}{\pi a^2} \frac{4 z^2 y}{(z^2+(y-a)^2)(z^2+(y+a)^2)} \qquad (3)$$

In Fig. 2 the calculated charge response of the shear stress sensor in its different locations with respect to the indenter position is reported for different values of the load at the boundary.

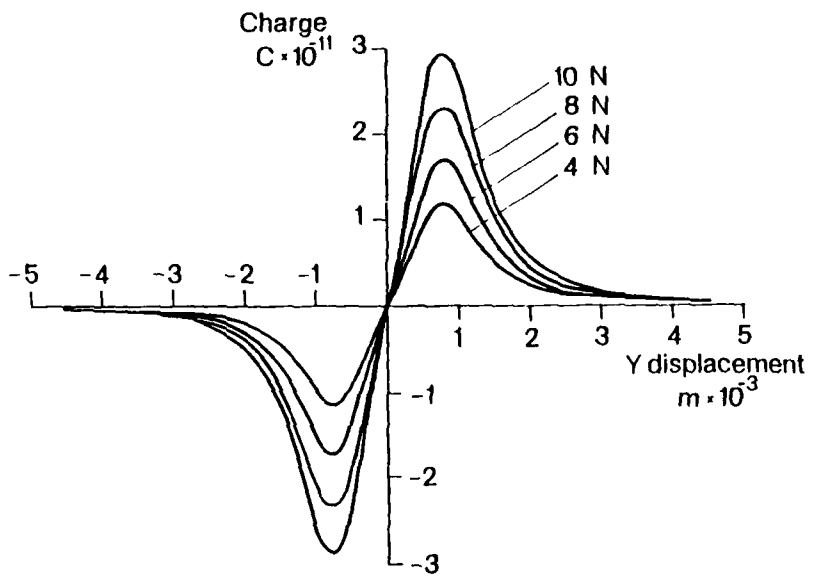

Fig. 2 Calculated spatial dependence of the charge response of the shear component sensor at different loads.

In Fig. 3 some experimental results are reported. The calculated and measured responses show a good qualitative agreement, but the measured charge response per unitary load has been found to be higher (from 30% to 100% using various rubbers) than the calculated one. Softer rubbers gave higher charge response per unitary load and higher "spatial spreading" of the signal (see Fig. 3).

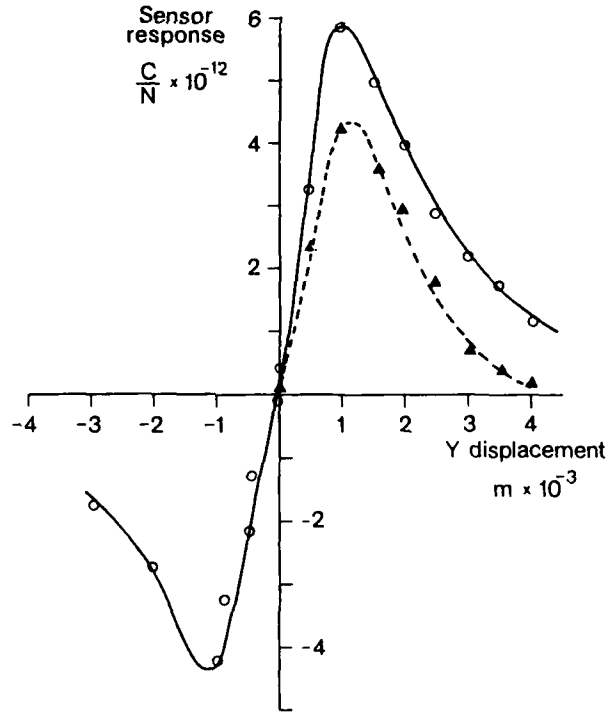

Fig. 3 Experimental data obtained applying the load at different lateral distances between the sensor and the indenter longitudinal axis. The curves refer to data obtained with a softer (solid curve) and harder (dashed curve) rubbers.

Work is continuing to provide a more quantitative description of the phenomenon by using more appropriate solid mechanics treatments [7] for the dimensioning of the sensor, seen as a layered medium.

REFERENCES

[1] P. Dario, "Transducers for advanced robotics", in The application of ferroelectric polymers, T.T. Wang, J.M. Herbert, A.M. Glass (Eds.), Blackie, Glasgow, 1988.

[2] D. De Rossi, A. Nannini and C. Domenici, "Biomimetic tactile sensor with stress-component discrimination capability", J. Molec. Electr., vol. 3 (4), pp. 173-181, 1987.

[3] E.L. Nix and I.M. Ward, "The measurement of the shear piezoelectric coefficients of polyvinylidene fluoride", Ferroelectrics, vol. 67, pp. 137-141, 1986.

[4] P. Dario, D. De Rossi, C. Domenici, R. Francesconi, "Ferroelectric polymer tactile sensors with anthropomorphic features", in Proc. 1st IEEE Int. Conf. on Robotics, pp. 332-340, IEEE Comp. Soc. Press, Silver Spring, 1984.

[5] L.D. Harmon, "Automated tactile sensing", Int. J. Robotic Res., vol. 1 (2), pp. 3-32, 1982.

[6] G.M. Gladwell, "Contact problems in the classical theory of elasticity, pp. 151-154, Sijthoff and Noordhoff, Alphen aan den Rijn, 1980.

[7] N.N. Lebedev and I.A. Ufliand, "Axisymmetric contact problem for an elastic layer", PMM, vol. 22, pp. 442-450, 1958.

POLARIZATION PHENOMENA IN RESINIC ESTERS OF PHOTOTHERMOPLASTIC DEVICES FOR APPLICATIONS TO HOLOGRAPHIC OPTICAL SWITCHING

J. DANDURAND, C. LACABANNE,

Laboratoire de Physique des Solides Associé au CNRS
Université Paul Sabatier
31062 Toulouse Cédex (France)

J.Y. MOISAN,

Centre National d'Etudes des Télécommunications
Département ROC/TAC -22301 Lannion Cédex (France)

C. SERVENS,

Institut du Pin, Université de Bordeaux I
33405 Talence Cédex (France)

ABSTRACT

Polarization phenomena in resinic esters for photothermoplastic devices have been investigated ty Thermally Stimulated Current spectroscopy. The relaxation mode observed below room temperature with the same characteristics in the three investigated resinic esters, has been assigned to localized movements of four to six bonds. The relaxation mode appearing above room temperature has been associated to the dielectric manifestation of the glass transition. It involves cooperative movements of main chains. The analysis of the corresponding relaxation map shows that the "structure" of Foral 85 is the most disordered.
Consequently, it allows delocalized movements of the largest sequences.

INTRODUCTION

The purpose of this work is to investigate polarization phenomena in resinic esters used in photothermoplastic devices for application to holographic optical switching [1]. A comparative study of three abietic esters -Staybelite Ester (SE10), Foral 85, Foral 105-

CH2593-2/ 88/ 0000-0241$01.00 Copyright 1988 IEEE

has been performed by Thermally Stimulated Current (TSC) spectroscopy. Differential Scanning Calorimetry (DSC) has been used for facilitating the interpretation of data.

RELAXATION AND TRANSITION SPECTRA

For Thermally Stimulated Current experiments, disk shaped samples -1 cm in diameter, 2 mm in width- have been used. They have been polarized by 500 V at 25°C for 3 mn, and cooled at LNT. The used set up has been previously described [2].

For differential Scanning Calorimetry, 10 mg of resin have been placed in the Aluminium pans of a Perkin Elmer DSC2.

In all abietic esters, two relaxation modes can be distinguished :
- below room temperature, the secondary relaxation mode has the lower intensity (~ 10^{-14} A),

- above room temperature, the primary relaxation mode is characterized by the higher intensity (~ 10^{-12} A).

Secondary Relaxation

In the three resinic esters, the secondary relaxation mode is characterized by two components respectively located at -150°C and -90°C. It has been associated to localized movements involving four to six bonds. At this scale, the "structure" of the three abietic esters is identical.

Primary relaxation and glass transition

The primary relaxation is characteristic of the studied resinic ester as shown by the temperature of the TSC maximum (Tm) -cf. Table 1-. The glass transition temperature (Tg) deduced from the DSC thermograms has also been reported on Table 1 for comparison.

Because of the proximity of Tm and Tg, the primary relaxation has been attributed to the dielectric

manifestation of the glass transition. So, it involves cooperative movements of main chains.

Table 1.- Primary relaxation and glass transition temperature.

SAMPLES	Tm (°C)	Tg (°C)
SE 10	50.5	35.5
Foral 85	48	37.9
Foral 105	57	47.4

It is interesting to note that the intensity of this relaxation is higher in Foral 85 than in SE 10 and Foral 105. This result can be explained by hydrogenation degree (SE 10) and steric hundrance (Foral 105).

RELAXATION MAP

The primary relaxation is complex. It has been resolved by the technique of fractional polarizations, into "elementary" TSC peaks. By elementary we mean well described by a single relaxation time τ. The temperature variations of τ have been plotted on Arrhenius diagrams. Figure 1 shows as example the relaxation map of Foral 85.

Figure 1.- Relaxation map of Foral 85

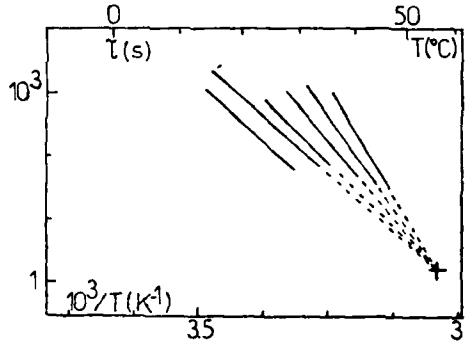

It illustrates the behavior observed in the three resinic esters ; the relaxation times observed around Tm obeys a compensation law :

$$\tau(T) = \tau_c \exp \{ \Delta H/k \, (T^{-1} - T_c^{-1}) \} \qquad [1]$$

where ΔH is the activation enthalpy, τ_c the compensation time, T_c the compensation temperature and k is the Boltzmann constant.

The values of τ_c, T_c and ΔH have been listed in Table 2.

It is interesting to note that τ_c remains of the order of magnitude of a few seconds, i.e. the characteristic value of the relaxation associated with the glass transition. The difference Tc - Tg is also practically constant while the activation enthalpies vary significantly. According to the model of Hoffman -Williams- Passaglia, the higher values of ΔH in Foral 85 may indicate the existence of movements of longer sequences revealing a more disordered structure.

TABLE 2.- Activation and compensation parameters in resine esters.

SAMPLES	ΔH (eV)	τ_c (sec)	T_c (°C)
SE 10	0.9 to 2	4.6	54.5
Foral 85	1.3 to 2.8	1.8	56
Foral 105	0.9 to 2	1.3	67

CONCLUSION

The Thermally Stimulated Current spectroscopy has been applied to the characterization of polarization phenomena in resinic esters. Foral 85 has the most intense polarization because of its specific molecular mobility due to the most disordered structure.

Acknowledgment

The financial support of the Centre National des Télécommunications is acknowledged.

REFERENCES

[1] J.Y. Moisan, P. Gravey, R. Lever, L. Bonnel, *Optical Engineering* **25**, 151 (1986).
[2] A. Bernes, *Thesis*, Toulouse (1985).

NORMAL AND ANOMALOUS THERMALLY STIMULATED CURRENTS AND SPACE CHARGE IN POLYPROPYLENE

S.C. Datt, R.S. Baghel and Ranjit Singh

Department of Postgraduate Studies and Research in Physics, Rani Durgavati Vishwavidyalaya, Jabalpur -482 001 (MP), India.

ABSTRACT

The short-circuit thermally stimulated discharge (TSD) currents for isotactic commercial grade polypropylene (PP) foils thermoelectrets, poled under different field and temperature conditions, have been found to indicate the distribution of traps in energy. Anomalous TSDCs flowing in the same direction as the charging current, observed for electrets poled above 100°C, have been considered to be due to injected space charge and the blocking condition of the electrodes.

INTRODUCTION

The understanding of the nature of polarization in most of the organic polymers, including polypropylene (PP), can not be considered to be complete [1]. The present work has been undertaken to investigate the nature of polarization in terms of the material parameters in commercial grade isotactic PP, using TSC technique.

EXPERIMENTAL

The measurements were made on isotactic 50 μm thick commercial grade PP for general use. After cleaning with ethanol, the samples were heated in air at 145°C for 6 h and then were subjected to room-temperature outgassing at 10^{-5} Torr for further period of 8 h. These samples were then vacuum aluminized on both sides over a central circular area of 10.2 cm^2.

The matallized samples were thermally polarized under different field and temperature conditions, ranging from 20-250 kV/cm and

CH2593-2/ 88/ 0000-0246$01.00 Copyright 1988 IEEE

20-145°C, respectively. The samples were polarized for 1 h at polarizing temperature and then were cooled to room-temperature (20°C) under the application of field. Total time of polarization in each case was 3 h. TSDCs were recorded by short-circuiting the samples through a 610C Keithley electrometer and heating them at a rate of 3°C/min.

RESULTS AND DISCUSSION

The characteristic thermograms (Figs.1-3) show that the electrets, generally, give three peaks located around 60, 100 and 120°C. Various features of these thermograms indicate the existence of surface and bulk traps with distribution in energy.

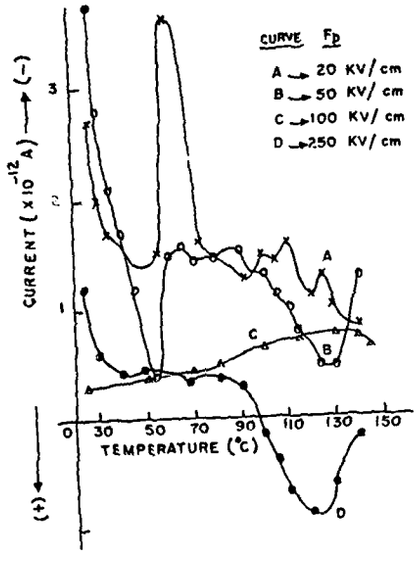

Fig.1. TSC curves for samples poled at 20°C with various field (F_p) values.

Considering a set of trapping levels with detrapping time constant for each level to be of standard Boltzmann form 2, it can easily be concluded that levels with detrapping times smaller than the charging time will fail to retain charge, while the levels with detrapping times greater than the charging time will be holding the charge at the completion of charging. Such analysis accounts for the observed decrease in magnitude at low temperature peak, appearing at about 60°C for room-temperature charged samples, and its shift towards higher temperatures with

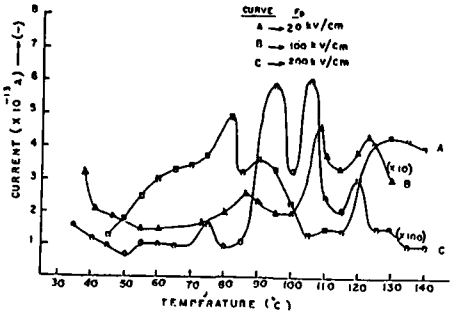

Fig.2. TSC curves for samples poled at 100°C with various fields.

increase in poling temperature. This peak appears at about 75°C for 100°C- charged samples and merges with 100°C-peak for 140°C-charged samples (Figs.1-3). Clearly the high-temperature poling favours the shift of the carriers from shallower to deeper traps.

A further conclusion drawn from the observed behaviour of low-temperature peak is that we have a distribution of trapping levels for this peak. The fact that the TSC for samples charged at 140°C with low fields is the envelop of TSCs for samples charged at lower temperature in conjunction with the peak shift to high temperature can only be explained by a trap level distribution.

In addition to the distribution of

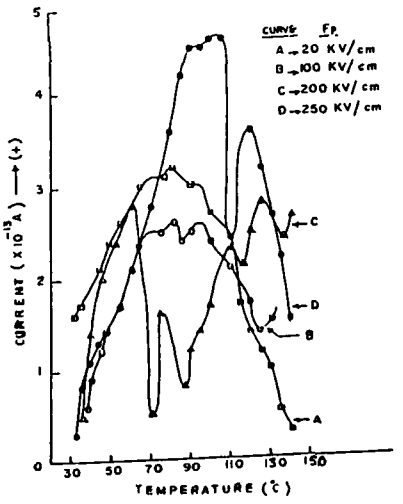

Fig.3. TSC curves for samples poled at 140°C with various fields.

trapping levels for low-temperature peak, the existance of energetically deeper traps is clearly evidenced by the appearance of high temperature peak. Because the carrier mobility increases with temperature and the carrier density injecting from the electrode increases with field, therefore in the case of charging made with higher fields, sufficient number of free carriers, apart from the carriers filling the trapping levels for low temperature peak, will be available to move into the bulk of the sample to fill the deeper traps with a higher release time giving rise to high temperature peak.

The TSCs for samples charged at 140°C with various fields have been found to be anomalous in the sense that current flows in the direction opposite to the charging current (Fig.3). Such behaviour can not be expected from the depolarization by dipoles. Thus the TSCs are likely to be due to space charge carriers injected from the electrodes. The origin of anomalous currents can be understood as explained in the literature [3]. Considering one type of carriers, we may have a distribution of injected homo space charge just after charging where the density n (x,t) drops with increasing 'x' measured from injecting electrode. The field F(0,t) acting on the injecting electrode side of zero field point $\bar{x}$ will be driving the carriers towards the injecting electrode and that on the otherside of $\bar{x}$ towards the other electrode. The appearence of anomalous TSDCs requires the suporession of carriers flow to the injecting electrode, which results in a net carrier flow towards the other electrode and the movement of $\bar{x}$ away from the injecting electrode. As the carrier mobility increases with the temperature and as the density of injected space charge increases with applied field, a high charging field and a high temperature result in a high return rate of carriers to the injecting electrode. As a result, the return rate of carriers may surpass the charge exchange rate

of the electrode. This means a partial blocking of the electrode which suppresses the carrier flow to the injecting electrode and results in the movement of $\bar{x}$ away from the injecting electrode causing an anamolous TSC. Theoretical analysis shows that the anomalous TSC cannot be generated with ohmic contacts, hence the observed anomalous TSCs are concluded to be caused by injected space charge with blocking electrodes.

REFERENCES

1. G.M. Sessler (Ed), Electrets (Springer Verlag, Berlin, 1980).
2. G.M. Sessler and J.E. West, J. Appl. Phys. 43, 922 (1972).
3. T. Mizutani, K. Kanero and M. Ieda, Jpn. J. Appl. Phys. 20, 1443 (1981).

PYROELECTRIC APPLICATIONS OF FERROELECTRIC POLYMERS

Sidney B. Lang

Department of Chemical Engineering
Ben-Gurion University of the Negev
84105 Beer Sheva, Israel

Xiao Ding-Quan

Department of Physics
Sichuan University
Chengdu 610064, People's Republic of China

ABSTRACT

The major application of pyroelectric materials is in infrared detection, although their unique thermal sensitivity is utilized in a number of other ways. Ferroelectric polymers such as polyvinylidene fluoride (PVDF) and vinylidene fluoride-based copolymers have the special advantage of availability as large surface area, thin, flexible, low-cost sheets. This paper reviews some of the applications of these materials.

INTRODUCTION

The piezoelectric effect in ferroelectric polymers has been used in a broad spectrum of applications. Less well known are the uses of their pyroelectric properties. Pyroelectric single crystals and ceramics have a number of characteristics listed in Table 1 which make them suitable for applications in infrared detection and many other areas. Polymers have the additional advantages listed in Table 2. Many applications of pyroelectric polymers are given in Table 3.

EXAMPLES OF APPLICATIONS

An application from each of the sections in Table 3 is described. These applications were possible only because of the unusual characteristics of pyroelectric polymers.

CH2593-2/ 88/ 0000-0251$01.00 Copyright 1988 IEEE

Table 1. Important features of pyroelectric devices

Electrical response to rate of change of temperature
Capacitative behavior
High responsivity and low noise
Response independent of wavelength of radiation
High speed
Cooling not required

Table 2. Additional features of pyroelectric polymers

Large surface areas
Extremely thin films possible
Flexibility for conformity to curved surfaces
Selective area poling and electroding
Low cost

Table 3. Applications of pyro lectric polymers

Infrared detection	
Single-element detector	1- and 2-D arrays
IR reflectrometry	Radiometer
Vidicon	Laser profile or power
CO2 line spectrometer	Intrusion detector
Heat and other electromagnetic radiation detection	
Micro- & millimeter waves	Nerve excitation studies
Optical fibre attenuation	Heat generation in retina
Photopyroelectric spectroscopy & thin film calorimetry	
Thermal diffusivity	Scanning microscopy
Phase transition studies	Standing light waves
Pulsed laser annealing	Laser-induced desorption
Electronic defect centers	Anemometer
Concave lens	Plasmon surface polaritons
Other applications	
Copying	Solar energy conversion
Electrophotography	Ultraheavy nuclei detect.
Thermodielectric energy	Heat to electricity conv.
Cosmic dust detection	Electric field sensor

Electronic readout spectrometer for CO2 lasers [1]

In many applications of CO_2 lasers, it is necessary to know on which spectral line the laser is oscillating. Edwards, Jefferies, and Ridgen constructed a grating spectrometer with a PVDF film detector, as shown in Figure 1. Ray tracing was used to calculate the positions at which 50 of the principal wavelengths in the P and R branches of the CO_2 spectrum would fall on the detector. A mask was prepared and the aluminum electrodes on the PVDF were photo-etched to give an array of electrodes at the precise positions of the spectral lines. The dynamic range of the instrument was 3000:1 so that weak satellite lines could be observed. The minimum energy and power requirements were 1 μJ and 0.5 mW for pulsed and continuous lasers, respectively.

Optical fiber absorption loss measurement [2]

Kashyap and Pantelis developed a calorimetric technique for measuring the absorption loss in optical fibers. Small-bore thick-walled PVDF tubing (1.409 mm OD, 0.941 mm ID) was produced continuously using a screw extruder followed by a corona poling process during drawing. The tubing was filled with water and the optical fiber was centrally aligned within the tube as shown in Figure 2. Emission from a Nd:YAG laser operating at 1.06 μm was admitted into the fiber and the output power measured at the far end. The fiber was heated by absorption and the heat was conducted through the water into the PVDF which generated pyroelectric charge. The minimum measurable loss was about 0.07 dB/km with an injected power of 1 W and a tube length of 500 mm.

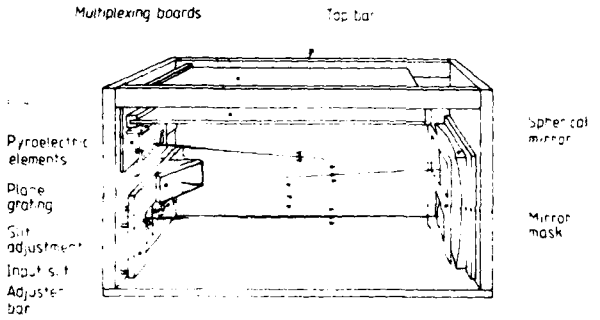

Figure 1. Spectrometer for CO2 laser analysis

Standing light wave in front of a silver mirror [3]

Electromagnetic theory predicts that standing light waves will form if a light beam is reflected from a metallic mirror. Knoll and Coufal coated a 20-μm thick PVDF film with silver electrodes. Various numbers of 5-nm thick transparent Cd-arachidate (CdA) layers were deposited upon the detector by a Langmuir-Blodgett technique. A monolayer of a cyanine dye deposited on the top CdA layer was exposed to a visible light beam produced by a spectrometer. The measured pyroelectric signals were composed of responses due to heat absorbed on the silver mirror, and heat absorbed from the standing waves by the dye which was conducted through the CdA to the detector. The signal varied sinusoidally

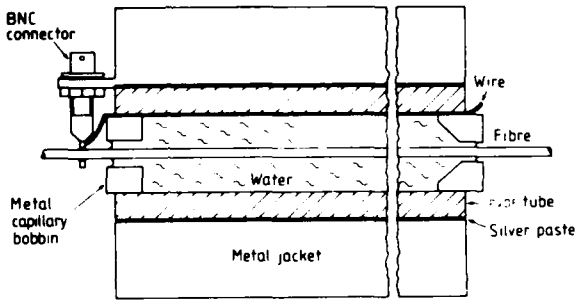

Figure 2. Measurement of optical fiber absorption loss

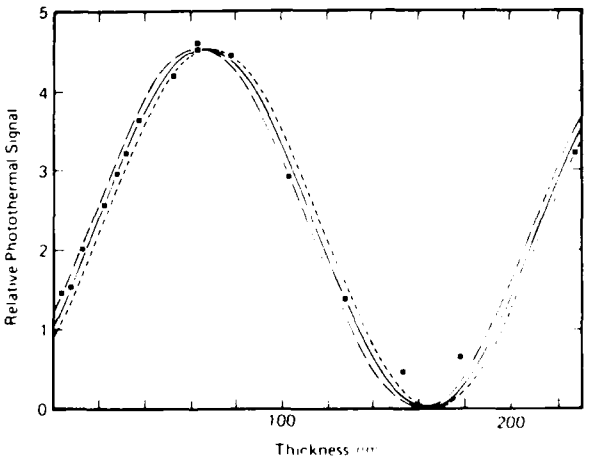

Figure 3. Measurement of standing light wave intensity

with thickness of the CdA as shown in Figure 3 and the calculated phase shift of 124° at the mirror (solid line) was in good agreement with theory.

Cometary and interplanetary dust detector [4]

Perkins, Simpson, and Tuzzolino developed PVDF dust counters and mass analyzers (DUCMA) which were mounted on two USSR Vega spacecraft and sent on a mission through the tail of Halley's Comet in March 1986. The detectors (28-μm in thickness and 75 cm^2 in area) were placed beneath a thermal blanket and adjacent to a small PVDF acoustic noise detector as shown in Figure 4. The major signal caused by an impacting high velocity dust particle was due to thermal depolarization with an additional small pyroelectric component. The minimal mass sensitivity of DUCMA was about 10^{-13} g.

REFERENCES

[1] J. G. Edwards, R. Jeffries and J. D. Ridgen, J. Phys. E, Vol. 14, p. 731-734 (1981).

[2] R. Kashyap and P. Pantelis, J. Phys. D, Vol. 18, p. 1709-1721 (1985).

[3] W. Knoll and H. J. Coufal, Appl. Phys. Lett., Vol. 51, p. 892-894 (1987).

[4] M. A. Perkins, J. A. Simpson and A. J. Tuzzolino, Nucl. Instrum. Meth. Phys. Res., Vol. A239, p. 310-323 (1985).

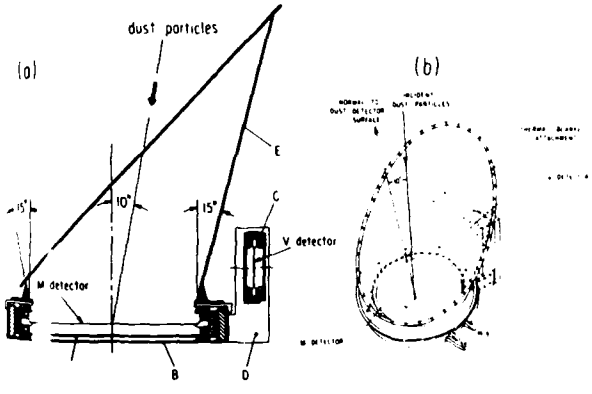

Figure 4. PVDF dust counter and mass analyzer

PIEZOELECTRICITY IN NYLON 5,7

P. E. Dunn and S. H. Carr

Department of Materials Science and Engineering and the Materials Research Center, Northwestern University, 2145 Sheridan Road, Evanston, Illinois, 60208

We have investigated nylon 5,7 as a piezoelectric polymer which can potentially exhibit very high activity. Nylon 5,7 is synthesized using improved procedures, and the product polymer is characterized by X-ray diffraction, calorimetry, and the thermally stimulated current. Films are prepared by quenching from the melt. The piezoelectric response is compared to other odd polyamides.

Of all the polymers investigated to date, none has exhibited the magnitude of the piezoelectric response which has been found in polyvinylidene fluoride (PVF_2). The highest piezoelectric strain constant available is d_{31}= 28 pC/N [1]. This is followed by copolymers of vinylidene fluoride-trifluoroethylene, d_{31}= 12 pC/N [2] and nylon 11, d_{31}= 6 pC/N [3] (values obtained at room temperature). The potential for a higher piezoelectric response from lower members of the series of odd nylons $[HN(CH_2)_xCO]_n$ and odd,odd nylons $[HN(CH_2)_yNHOC(CH_2)_zCO]_n$ (where x is even, y and z are odd) has been theorized over the last decade [4]. This is based on the aggregate effects of the following properties:

1. The large dipole moment in the chemical repeat unit of 3.7 Debye, compared to 1.52 Debye in that for PVF_2
2. The ability to crystallize with a net dipole moment per unit cell.
3. A large potential polarization, based on the theoretical dipole concentration per unit volume.

A comparison of the theoretical dipole concentrations for PVF_2 and the low, odd nylons is shown in table I. These values were calculated by dividing the net dipole moment in the unit cell by the unit cell volume. PVF_2 can have a dipole concentration as high as 29 Debye per cubic nanometer [4]. Unit cells for nylon 11, nylon 9 and nylon 7 are triclinic, containing one polymer repeat [4,5]. Unit cell volumes for nylon 11 and nylon 7 were calculated by Litt et. al. [4]. Unit cell dimensions for

CH2593-2/ 88/ 0000-0256$01.00 Copyright 1988 IEEE

the lower numbered nylons were calculated by assuming that the unit cells were also triclinic and contained one polymer repeat. Nylon 11 has ten methylene ($-CH_2-$) groups between amide linkages and therefore has only half the dipole concentration of PVF_2. However, as the number of methylene groups in the repeat unit of nylon is decreased, there is a correspondingly higher potential polarization which surpasses PVF_2 below nylon 5. As this repeat distance decreases there is an associated increase in the crystal density [6], which would result in an even higher dipole concentration than that calculated for the lower numbered members. This implies that the lower polyamides could yield a potential polarization per unit volume which greatly exceeds that of PVF_2, if they crystallize in an asymmetric form and in conformations in which the dipole moments are additive.

Table I: Theoretical dipole concentration

PVF_2	$29D/nm^3$
nylon 11	14
nylon 9	17
nylon 7	21
nylon 5	28
nylon 3	41
nylon 1	75

The main constraint in determining the piezoelectric response of the low, odd numbered nylons has been their lack of availability. Of the odd numbered nylons shown in table I only nylon 11 and nylon 9 are available commercially. Measurements on the lower members of this series, and the low numbered odd, odd nylons still await their synthesis. Owing to the sensitivity of the piezoelectric activity in polymers to the specimen preparation and poling conditions [7], one finds that it is difficult to attain the optimum activity. The optimum piezoelectric activity of nylon 11 (d_{31} = 6 pC/N to date) has not been reproduced by other researchers; however, in a comparative study of nylon 11 and nylon 9 by Wu, Yano and Soen [5], and of nylon 11 and nylon 7 by Mathur [8] both were found to surpass the piezoelectric activity of nylon 11. This indicates that the theoretical prediction for higher activity in the low, odd nylons may in fact be correct. To test this hypothesis further, we chose to synthesize the lower numbered members of the odd,odd nylons — nylon 5,7, nylon 3,5 and nylon 1,3 and

then to measure their piezoelectric activity. The first nylon in this series has been synthesized.

SYNTHESIS

The synthesis of polyamides from diacids and diamines by high temperature melt polymerization follows the form:

$$nH_2N(CH_2)_yNH_2 + nHOOC(CH_2)_zCOOH \longrightarrow$$

$$H[HN(CH_2)_yNHOC(CH_2)_zCO]_nOH + (2n-1)H_2O \quad (1)$$

This procedure demands high purity of monomers and stoichiometric balance of reactants to obtain high molecular weight polymer. An appropriate time and temperature regime must be chosen, compatible with the kinetics of the polymerization reaction, for effective removal of the the water of condensation. A polymer of high molecular weight is important for piezoelectric activity, as it imparts ductility to the polymer films. Ductility is necessary in obtaining high piezoelectric properties as well as good mechanical strength.

In the synthesis of nylon 5,7, the monomers 1,5-pentane diamine and heptanedioic acid were purified and combined as alcoholic solutions to form a balanced salt. These operations were performed in an inert atmosphere to prevent degradation of the amine. The salt was then subjected to a carefully designed schedule of time, temperature, and atmosphere (vacuum). The resultant polymer, after dissolving in formic acid and precipitating in water, has a fibrous morphology, characteristic of a high molecular weight polymer.

SAMPLE PREPARATION

Films of nylon 5,7 were made by placing the polymer between two sheets of aluminum foil with a 100μm thick brass spacer. It was pressed at 220°C for five minutes and quenched onto chilled plates. Gold electrodes were applied to both sides of the film by vacuum evaporation. Samples were polarized using an "Electret Thermal Analyzer", manufactured by Toyo-Seiki Seisaku-Sho, Ltd. The films were poled under vacuum in an electric field of 175 kV/cm for 15 minutes at 80°C and then cooled in the same field to room temperature.

STRUCTURAL AND PIEZOELECTRIC MEASUREMENTS

Because it is the way the chains pack that is key to getting high piezoelectric properties, the following studies were undertaken. The crystal structure of nylon 5,7 is reported [9] to be monoclinic, belonging to the P_b space group and containing two monomer repeats per unit cell. This generates a chain packing which allows a net dipole moment in the unit cell and the potential for electrical activity. X-ray scattering from the product material obtained in this study is consistent with [9]. Differential scanning calorimetry was used to characterize the effect of thermal history on melting behavior. The thermally stimulated discharge current (TSDC) technique was employed to evaluate the origins of the electrical induced polarization (dipolar, ionic or electronic space charge) [10].

The piezoelectric $g_{3,1}$ constant was measured at 80Hz by applying an oscillatory force from a B and K model 4810 mechanical transducer, attached to the film sample, and measuring the electric field generated across the sample thickness (voltage). The input (force) and output (voltage) were displayed on an oscilloscope. The ratio of the amplitudes of the signals (V/F) was used to calculate the piezoelectric $g_{3,1}$ constant, and converted to the $d_{3,1}$ constant.

Initial measurements on poled nylon 5,7 resulted in a piezoelectric strain coefficient $d_{3,1} = 0.4$ pC/N. In comparison, $d_{3,1}$ values in the literature [5] for nylon 11 and nylon 9 at more than twice the field strength are presented in the following table (film forming conditions, poling time and temperature being the same). This indicates that at an equivalent field strength of 400kV/cm, nylon 5,7 could surpass the piezoelectric activity of nylon 9 and verify the theoretical prediction of increased activity in the lower, odd nylons.

Table II

	Field strength, kV/cm	$d_{3,1}$, pC/N
nylon 11	400	0.6
nylon 9	400	1.1
nylon 5,7	175	0.4

REFERENCES

[1] H. Ohigashi, "Electromechanical Properties of Polarized Polyvinylidene Fluoride Films as Studied by the Piezoelectric Resonance Method", J. Appl. Phys., Vol. 47, pp. 949-955, 1976.

[2] G. M. Sessler in Topics in Applied Physics, Vol. 60 (Electrets), edited by G. M. Sessler, Springer-Verlag, New York, pp. 370, 1987.

[3] S. C. Mathur, J. I. Scheinbeim and B. A. Newman, "Piezoelectric Properties and Ferroelectric Hysteresis Effects in Uniaxially Stretched Nylon 11 Films", J. Appl. Phys., Vol. 56, No. 9, pp. 2419-2425, 1984.

[4] M. H. Litt, C. Hsu and P. Basu, "Pyroelectricity and Piezoelectricity in Nylon 11", J. Appl. Phys., Vol. 48, No. 6, pp. 2208-2212, 1977.

[5] G. Wu, O. Yano and T. Soen, "Dielectric and Piezoelectric Properties of Nylon 9 and Nylon 11", Polymer J., Vol. 18, No. 1, pp. 51-61, 1986.

[6] J. H. Magill, "Formation of Spherulites in Polyamides. V. Odd-Odd Polyamides", J. Polymer Sci.:A-2, Vol. 9, pp. 815-827, 1971.

[7] B. A. Newman, P. Chen, K. D. Pae and J. I. Scheinbeim, "Piezoelectricity in Nylon 11", J. Appl. Phys., Vol. 51, No. 10, pp. 5161-5164, 1980.

[8] S. C. Mathur, "Piezoelectric Properties of Nylon 11 and Nylon 7", Ph. D. Thesis, Rutgers University, New Brunswick, New Jersey, 1986.

[9] J. C. Lin, M. H. Litt and G. Froyer, "X-Ray and Thermal Studies of Nylon 5,7", J. Polymer Sci.: Polymer Chem. Edn., Vol. 19, pp. 165-174, 1981.

[10] K. Kojima, P. Dunn and S. H. Carr, "TSDC Study on the Polarization of Nylon 5,7", in preparation.

ELECTRO ACTIVE PROPERTIES OF CERAMIC-POLYMER COMPOSITES

M.J. Abdullah and D.K. Das-Gupta

School of Electronic Engineering Science, University College of North Wales, Bangor, Gwynedd, U.K.

Abstract

The nature of dielectric behaviour and pyroelectric properties of three ceramic/polymer composites have been studied. One of the composites shows a significantly higher pyroelectric figure of merit than that of PZT. The loss process appears to be due to polymer phase with an added contribution from ceramic phase at low frequencies and high temperatures regime.

INTRODUCTION

Present work reports the results of a study of dielectric and pyroelectric behaviour in three different composites, i.e. composite A: PZT5/VDF-TrFE (50/50), composite B: PZT8/PVDF (50/50) and composite C: PZT8/ polypropylene (50/50). Copolymer VDF/TrFE and polymer PVDF are both solef grades while polypropylene was supplied by Hercules Corporaton (USA).

EXPERIMENTAL

Composites were prepared by mixing an equal volume fraction of ceramic powder (obtained from Unilator, U.K.) and polymer pellets at appropriate temperatures (composites A and B at 442K and composite C at 413K) using hot roller and then pressing into films of approximately 200 μm in a temperature controlled hydraulic press. Aluminium electrodes (area 2 cm x 2 cm, thickness 700 A) were vacuum deposited on both sides of the samples. The preconditioning of the samples at 373K in the evacuated measurement chamber ($<10^{-5}$ torr), the apparatus and the measurements procedure for dielectric and pyroelectric data were the same as those reported in the previous work [1-3].

CH2593-2/ 88/ 0000-0261$01.00 Copyright 1988 IEEE

RESULTS AND DISCUSSIONS

The dielectric behaviour (ϵ' and ϵ'') of the three composites are shown in Fig.1. For the ease of comparison, the values of ϵ' and ϵ'' for composite C have been multiplied by a factor of 10 in Fig. 1. Following the expression given by Yamada et al [4] for the permittivity of such composite system, and using the value of shape factor m=8, ϵ'(PVDF)=12, ϵ' (PZT) = 1300, ϵ'(PP)=2, the calculated values of the permittivities for PZT/PVDF and PZT/PP composites are 96 and 18 respectively which are in good agreement with the experimentally observed values (i.e. composite A: ϵ'=100, composite B:ϵ'=105, and composite C: ϵ'=15.5 at 1kHz at 363K).

The behaviour of ϵ'' in composites A and B (Fig.1) show a broad relaxation peak at around 1 kHz and it may be attributed to α_c-relaxation of the PVDF phase. Composite C does not show any relaxation behaviour of ϵ'' in the present frequency range at 363K. At high temperatures, the magnitude of ϵ'' is observed to increase [3], which may be effectively due to ionic conductivity.

The pyroelectric coefficient p, was obtained from the reversible thermally stimulated discharge current (TSDC). The unusual pyroelectric behaviour of the composite C is shown in Fig. 2 from which it may be observed that the polarity of the pyroelectric current reverses at ~345K and this behaviour is reproducible even after three successive TSDC runs. The value of p in composite C is extremely low which may possibly mean that the applied field was not sufficient to polarize the PZT particles located in the amorphous phase of the polymer because of the very low electrical conductivity of the polymer.

Composites A and B show an increase in p-values with temperature (Fig. 3). The difference in magnitudes in the p-values of the two composites tend to reduce progressively with increasing temperatures. Such a behaviour may originate from the localised energy levels of space charges in the

amorphous and interface regions of the ceramic-polymer composites and further work is necessary to clarify the observed behaviour of p(T).

The dependence of pyroelectric coefficient on poling parameters is shown in Fig. 4. It may be observed that efficient poling can be achieved at high temperature and high poling field as long as it does not reach a limit of breakdown strength of the sample. Extending poling time (t_p) beyond 3 hours would not give very much improvement in the value of p (i.e. the saturation value of p is only 15% higher than that obtained for 3 hours poling time). Using the value of $p=1.5\times10^{-4}$ $C/m^2/K$, the pyroelectric figure of merit (p/ϵ') of composite A is about 1.6×10^{-6} $C/m^2/K$, which is about 4.2 times greater than that of PZT ($\tilde{}3.8\times10^{-7}$ $C/m^2/K$) at 343K.

ACKNOWLEDGEMENTS

This work is financed by a research grant from the European Research Office of the U.S. Army. One of the authors (MJA) is grateful to the Public Service Department of Malaysia for a scholarship and to the Universiti Sains Malaysia for granting a study leave and a maintenance allowance.

REFERENCES

[1] D.K. Das-Gupta and M.J. Abdullah, "Electro-active characterisation of polymer-ceramic composite," British Ceramic Proceedings, Ed. R.W. Davidge, No. 38, p. 231-243, 1986.

[2] M.J. Abdullah and D.K. Das-Gupta, "Dielectric and Pyroelectric Properties of Polymer-Ceramic Composites", Ferroelectrics, Vol. 76, pp. 393-401, 1987.

[3] D.K. Das-Gupta and M.J. Abdullah, "Dielectric and Pyroelectric Properties of Polymer/ Ceramic Composites", J. Mater. Sci. Lett., Vol. 7. pp. 167-170, 1988.

[4] T. Yamada, T. Ueda and T. Kitayama, "Piezoelectricity of a high-content lead zirconate titanate/polymer composite," J. Appl. Phys., Vol. 53(6), pp. 4328-4332, 1982.

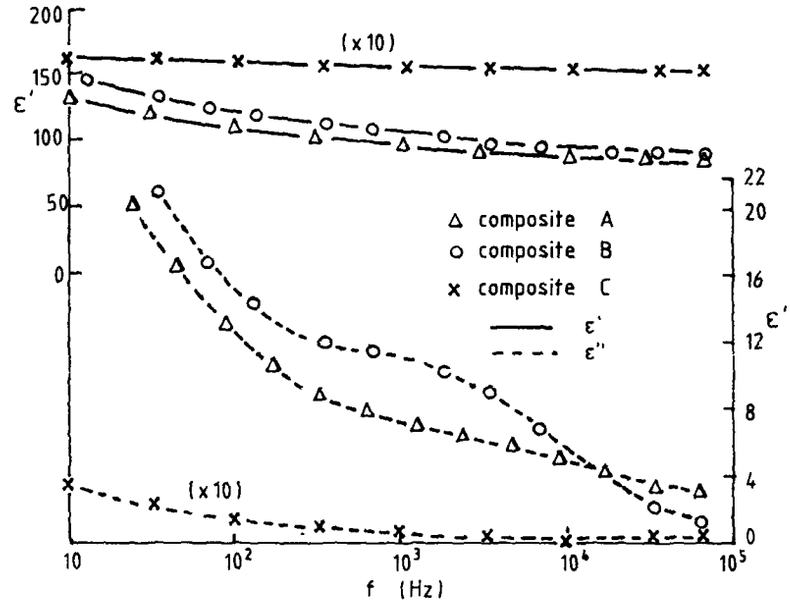

Figure 1. The behaviour of ε' and ε'' against frequency in ceramic/polymer composites at 363 K.

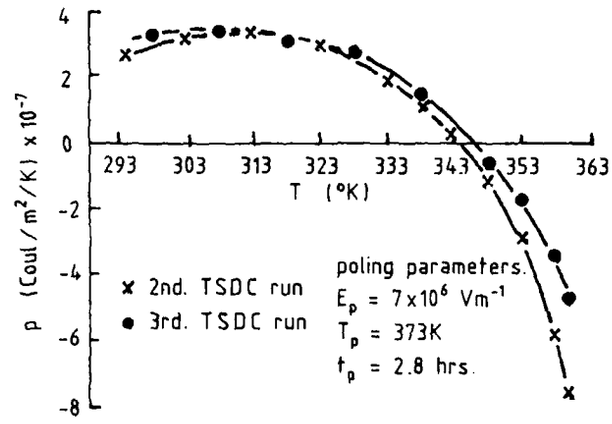

Figure 2. Pyroelectric coefficient against temperature in composite C.

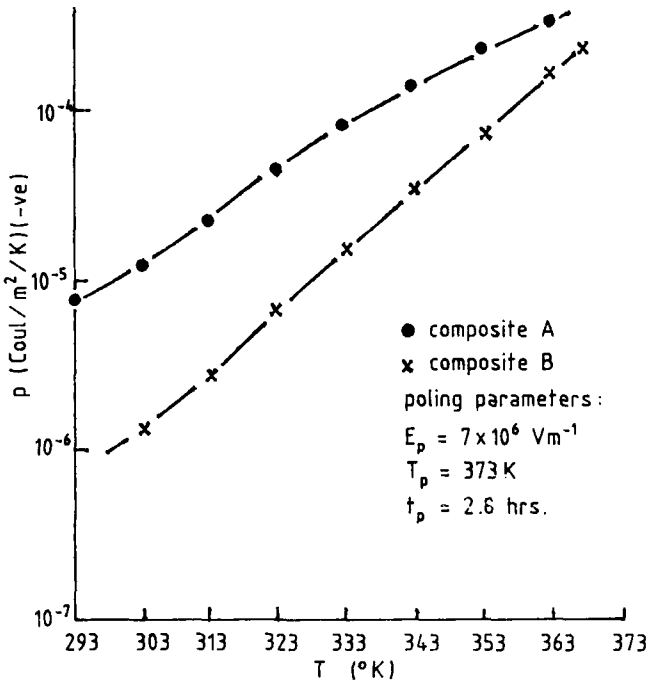

Figure 3. Pyroelectric coefficient against temperature in composites A & B.

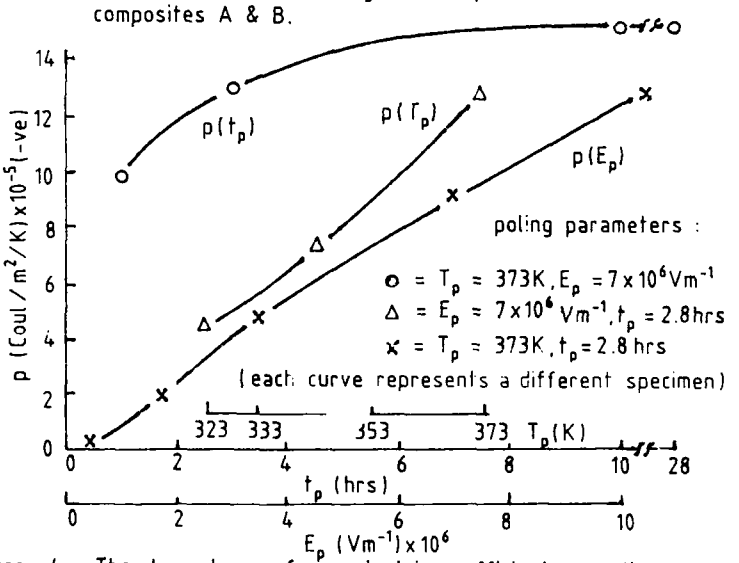

Figure 4. The dependence of pyroelectric coefficient on poling parameters at 343K in composite A.

DIELECTRIC STUDY OF Al-HYDROXY-NONTRONITE

A. Anagnostopoulou-Konsta, N.H.J. Gangas*, P. Pissis,
L. Apekis, D. Petridis**

National Technical University of Athens, Zografou Campus,
15773 Athens, Greece

ABSTRACT

The dielectric behaviour of aluminium-hydroxy-nontronite has been studied by the TSDC method as a function of water content, in the 0-20% h-range. Recorded spectra exhibit three main relaxation regions, corresponding to temperatures 77-130, 130-200 and 200-300 K respectively, and depending on hydration. The use of special experimental techniques allows to attribute the first region to dipolar reorientation and the second one to the release of charge carriers, most probably of protonic nature, trapped into the clay structure, whereas the third region seems to be directly related to the quality of the contact of the sample-electrodes configuration.

INTRODUCTION

Naturally occurring swelling clays (smectites) have a layered structure and are characterized by a large interlayer surface: therefore smectites have been intensively used as hosts for inserting in their interlamellar space a variety of cations and neutral molecules.

Recently a novel class of microporous materials emerged by intercalating smectites with polynuclear cations of metals. Upon firing these precursors to about 500 C the large intercallated molecular moieties transform to metal oxide pillars propping apart the silicate layers [1] (Fig. 1). The resulting pillared layered clays (PILCs) have a surface area in the range of 200 to 500 m^2/g and a high protonic acidity. These features make PILCs suitable materials for catalysis and molecular sieving [2].

*Kifissias Avenue 108, 11526, Athens, Greece
**Nuclear Research Centre DEMOCRITOS, Athens, Greece

CH2593-2/ 88/ 0000-0266$01.00 Copyright 1988 IEEE

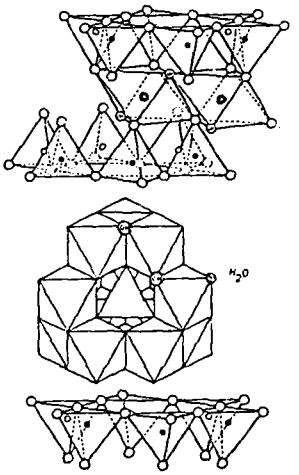

Fig. 1. Model structure of a smectite intercalated with Keggin ion: $[Al_{13}O_4(OH)_{24}(H_2O)_{12}]^{7+}$.

O : Oxygen

OH : Hydroxyl

O : Al, Fe, Mg

∘ and • : Si, occasionally Al

Intensive work has recently aimed at the characterization of the PILCs structure with a variety of techniques, as IR [3], magic-angle-spinning NMR [3], DTA, EPR [4] and Moessbauer spectroscopy [5]. In the present communication we report, for the first time to our best knowledge, results concerning the dielectric behaviour of a PILC precursor hydrated at room temperature up to water contents of about 21% w/w. We employed the method of Thermally Stimulated Depolarization Currents (TSDC) and data were obtained in the temperature range 180 to 290 K.

EXPERIMENTAL

The PILC precursor was prepared by treating a 1% w/w water suspension of Na^+ nontronite clay fraction with Al-hydroxy oligomers, prepared according to [1]. The resulting solid was first dried at room temperature and then hydrated at controlled relative humidities. The principle of the TSDC method, as well as the experimental procedure and apparatus used, are described in [6].

RESULTS AND DISCUSSION

Fig. 2 shows TSDC plots obtained with PILC precursor pellets in direct contact with the brass electrodes of the measuring capacitor, for different water contents, h. Four relaxation peaks are immediately discerned, which will be referred to as I, II, III and IV, in order of increasing temperature.

TSDC plots recorded with the same sample but with three different polarizing voltage values are shown in Fig. 3, while Fig. 4 displays the effect of the electric contact configuration on the recorded peaks.

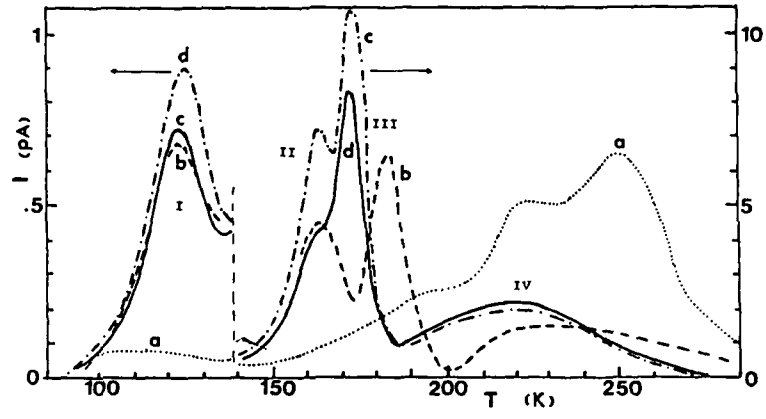

Fig. 2. TSDC plots of pillared clay samples with 4 different water contents: 3%(a), 11%(b), 17%(c) and 20.6%(d).

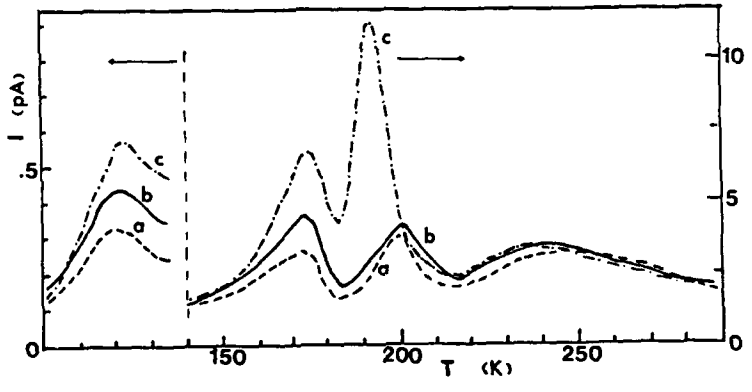

Fig. 3. TSDC plots of a sample recorded with 3 different polarizing field values: 100(a), 200(b) and 300(c) V/mm.

Peaks I and II seem to behave in practically the same way. Their maximum current and depolarization charge increase linearly with the polarizing voltage value (Fig. 3). They continue to subsist with completely blocking electrodes (Ho) whereas both peaks are masked by the third one, when silver paste (Ag) contacts are used (Fig. 4).

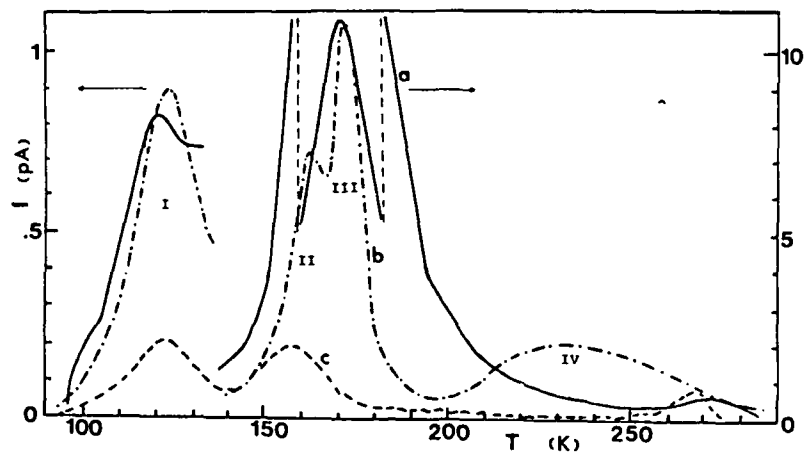

Fig. 4. TSDC plots of samples provided with silver paste (Ag) contacts(a), direct contact(b) and thin insulating foils (Ho) of Hostaphan(c) between sample and electrodes.

With increasing water content, peak III is constantly displaced towards the lower temperatures and its charge is enhanced. It disappears with the use of blocking electrodes (Ho), but becomes huge and masks all other contributions when the samples are provided with silver paste contacts. The influence of the polarizing voltage on this peak is not very clear.

Peak IV, finally, is very broad and not very well defined. It remains almost unaffected by the polarizing field but is almost absent when either very conducting or completely blocking electrodes are used (Fig. 4: a, c).

Starting with this last peak, we note that on the basis of its general behaviour it cannot in principle be attributed to dipolar relaxation. Its remarkable reduction with silver paste contacts (which constitute a very good electrical contact between sample and electrodes) would rather indicate that it is generated by the depolarization of space-charge carriers trapped at the boundaries between sample and electrodes. As this charge is accumulated during the polarizing step of the whole process, it practically disappears when conductivity through the sample is blocked (Fig. 4: c).

Peak III, is also directly related to the conductivity of the sample-electrodes system. It is obviously produced by the release of charge carriers trapped in the bulk of the sample during the polarizing step, as revealed by its disappearance with insulating electrodes (Ho) and its tremendous enhancement with very conducting contacts (Ag). These charge carriers are most probably due to the known interlayer protonic acidity of these systems which increases upon dehydration [1,7]. This is also in accord with TDA and NMR results reported by other authors [2,8]. We plan now to perform TSDC measurements in these samples with proton injecting electrodes and upon hydrating the material with heavy water in order to elucidate this point.

Both peaks I and II are undoubtedly of dipolar origin. The present experimental data do yet allow us to identify the exact nature and source of the reorientating dipoles. However, on the basis of data obtained with other hydrated systems (e.g. [9]), peak I might well be due to relaxation of very loosely bound water molecules, for example water molecules coordinated to the intercalated Al-hydroxy complexes (Fig. 1). Measurements with PILCs prepared from heavy water solutions could throw more light on this matter.

REFERENCES

1. G.W. Brindley and R.E. Sempels, Clays and clay minerals 12 (1977) 229, T.J. Pinnavaya, Science 220 (1983) 365.
2. J.J. Fripiat, Clays and Clay Minerals 34 (1986) 501.
3. D. Plee, F. Borg, L. Gatineau and J.J. Fripiat, J. Amer. Chem. Soc. 107 (1985) 2362.
4. O. Braddell, R.C. Barklie, D.H. Doff, N.H.J. Gangas and A. McKimm, Zeit. Phys. Chem. 151 (1987) 3081.
5. N.H.J. Gangas, J. van Wonterghem, S. Morup and C.J.W. Koch, J. Phys. C 18 (1985) L1011.
6. P. Pissis, J. Phys. D: Appl. Phys. 18 (1985) 1897.
7. M.L. Occelli and R.M. Tindwa, Clays and clay minerals 31, (1983) 22.
8. P. Heokstra and W.T. Doyle, J. Coll. Inter. Sci. 36 (1971) 513.
9. A. Anagnostopoulou-Konsta and P. Pissis, J. Phys. D: Appl. Phys. 20 (1987) 1168.

DIELECTRIC STUDY OF THE INTERACTION OF DNA AND WATER

A. Anagnostopoulou-Konsta, D. Daoukaki-Diamanti, P. Pissis and E. Sideris*

National Technical University of Athens, Zografou Campus, 157 73 Athens, GREECE.

ABSTRACT

The ways in which water molecules bind to DNA are studied with the aid of Thermally Stimulated Depolarization Currents (TSDC) measurements of hydrated solid DNA samples and dilute aqueous solutions, in the temperature range 80-300 K. The first two peaks of the recorded spectrum are interpreted on the basis of free water and loosely bound water dipoles reorientation respectively. It is shown that water sorbed up to at least 25% w/w is irrotationally bound to the DNA molecule. Additional dispersions, eliminated with the use of insulating foils, are attributed to space-charge depolarization connected to d.c. conductively.

INTRODUCTION

Water plays a significant role in modifying the conformational structure and stability of DNA as illustrated by solution and solid state hydration studies. A variety of physicochemical methods have been applied to the study of DNA-water interactions. Among them we can mention X-ray diffraction, IR absorption, Raman spectroscopy, NMR, electrical and dielectric measurements. [1-4].

Results obtained with the above methods are not always in accord with each other, as far as the fraction of bound water is concerned, due mainly to the fact that the hydration (or bound) water is not a precisely defined quantity and different measurement techniques are sensitive to different properties of the water fraction.

In this work we report preliminary results obtained with TSDC measurements performed on hydrated solid samples and

*Nuclear Research Centre Democritos, Athens, GREECE

CH2593-2/ 88/ 0000-0271$01.00 Copyright 1988 IEEE

dilute aqueous solutions of DNA, with the aim to investigate the role of the water of hydration and to determine the fractions of tightly and loosely bound water.

EXPERIMENTAL

Test samples of salmon testes DNA (Na salt, type III, Sigma Chem. Co) were either pressed into disks or made into aqueous solutions of concentrations ranging from 0.1 to 1% w/w. The solid samples were hydrated or dehydrated over saturated salt solutions in sealed jars at controlled relative humidities. The water content, h, defined as a percentage of the dry sample weight, varied between 3 and 90%. The principle of the TSDC method, the apparatus used and the experimental procedure followed are described in |5|.

RESULTS AND DISCUSSION

TSDC plots recorded with a DNA solid sample sandwiched between two insulating foils of Hostaphan (Ho) as a function of water content h, are shown in Fig. 1. Ho contacts were used in order to eliminate a certain number of additional peaks originating from space-charge depolarization connected with d.c. conductivity, as shown in Fig. 3. (It is to be noted that Ho contacts introduce a spurious peak at about 260 K). TSDC spectra obtained with DNA solutions of three different concentrations are illustrated in Fig. 4.

The similarity between spectra recorded with DNA solutions and highly hydrated solid samples is striking. We note that the three main peaks (Fig. 2) labelled I, II, and III respectively in order of increasing temperature, are also present in the plot of a solid sample containing 90% water; peaks I and III at exactly the sampe position, peak II slightly displaced towards the higher temperatures (Fig. 1). For less hydrated samples, i.e. for $40 < h < 75\%$, peaks I and II merge into one broad peak, whose position does not change, but whose height is constantly diminishing with decreasing h. It disappears for h somewhere between 25 and 40%.

Separation of peak I from peak II with the use of the thermal sampling technique has shown that peak I is well defined with a very narrow relaxation times distribution

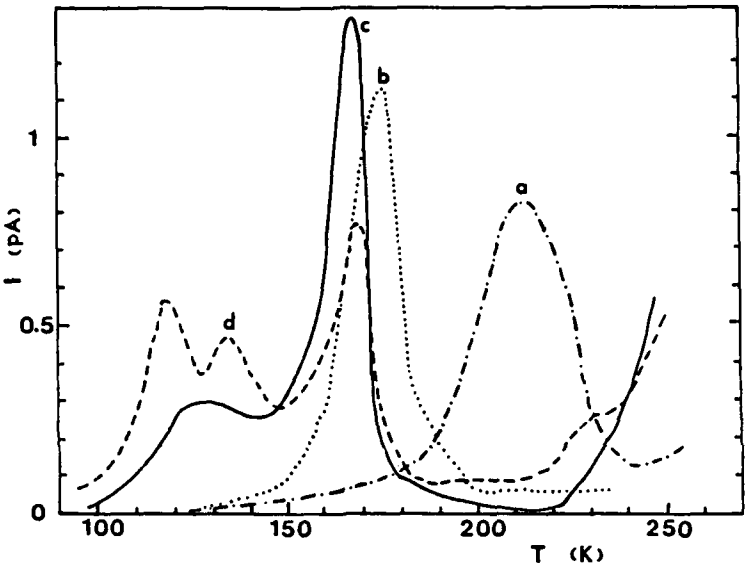

Fig. 1. TSDC plots recorded with a Na DNA sample for 4 different h values: 7%(a), 24%(b), 54%(c) and 90%(d).

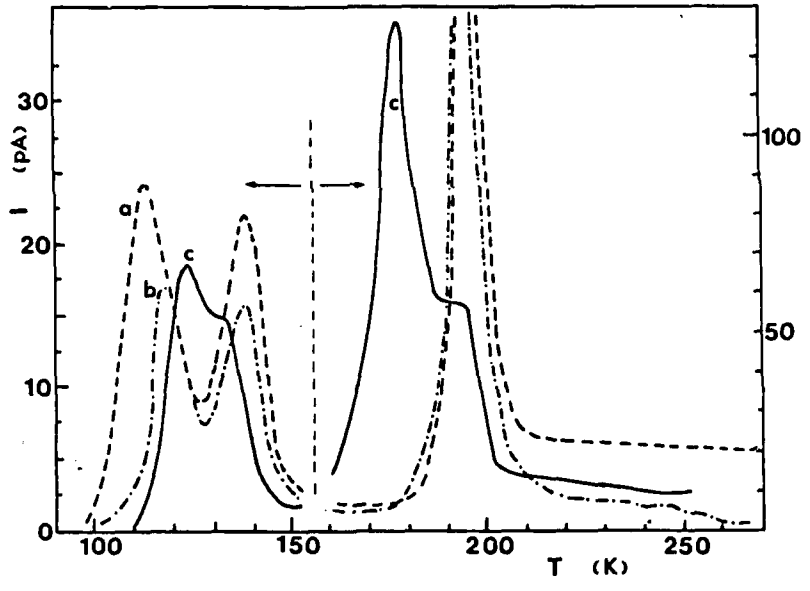

Fig. 2. TSDC plots of three Na DNA solutions with concentrations: 0.1%(a), 0.5%(b) and 1%(c).

and an activation energy of 0.26±0.07 eV, whereas the process responsible for peak II is distributed, with a mean activation energy of the order of 0.36 eV.

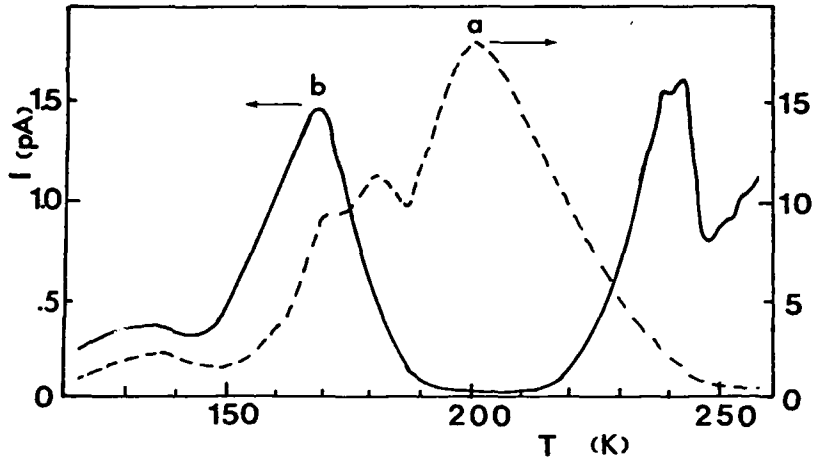

Fig. 3. TSDC plots of a DNA sample with h=45% in direct contact with the brass electrodes (a) and with Ho foils between sample and electrodes (b). Note that the two curves correspond to different scales.

Consideration of the above data, as well as comparison with TSDC plots obtained with bulk ice |6|, hydrated proteins |7| and aqueous solutions of other organic systems |8|, allows to attribute peak I to the reorientation of dipoles of the free water fraction and peak II to the loosely bound water fraction. The presence of bulk water in the solid sample may be due to capillary condensation.

In fact it has been found that the peak occurring in bulk ice is situated at 120 K, corresponds to a very narrow relaxation times distribution and has an activation energy of 0.25±0.04 eV. On the other hand loosely or semi-bound water is characterized by a rather broad spectrum of activation energies, and a somewhat larger mean activation energy.

The dielectric behaviour of DNA has been investigated by Takahashi et al [2] at frequencies between 0.1 MHz and 70 GHz. As reported by these authors the relaxation frequency of water in DNA solution is lower than that of pure water by 1-3 GHz, in accord with our results. Obviously this is a mean relaxation frequency value, comprising both free and semi-bound water, since the A.C. method does not allow to discriminate between very close lying relaxation mechanisms.

The fact that the complex peak (I+II) is missing from spectra recorded for h < 24% indicates that all water molecules sorbed up to at least this h-value are irrotationally bound to the DNA structure. In order to determine the precise value of the tightly and loosely bound water fraction, a series of systematic measurements in the h region between 24 and 90% is needed.

The origin of peak III cannot be unambiguously determined from data obtained up to now. The use of special experimental techniques offered by the TSDC method may help to the interpretation of its mechanism.

REFERENCES

1. J. Texter, Prog. Biophys. Molec. Biol. 33, (1978) 83-97.
2. S. Takashima, C. Gabriel, R.J. Sheppard and E.H. Grant, Bioph. J. 46 (1984) 29-34.
3. T.E. Cross and R. Pethig, Int. J. Quantum Chem.: Quantum Biology Symposium 10 (1983) 143-152.
4. Y. Tominaga, M. Shida, K. Kubota, H. Urabe, Y. Nishimura and M. Tsuboi, J. Chem. Phys. 83 (1985) 5072-5975.
5. P. Pissis, A. Anagnostopoulou-Konsta and A. Apekis, J. Exp. Botany 38 (1987) 1528-1540.
6. L. Apekis, P. Pissis and G. Boudouris, Nuovo Cimento D 2 (1983) 932-946.
7. A. Anagnostopoulou-Konsta and P. Pissis, J. Phys. D: Appl. Phys. 20 (1987) 1168-1174.
8. D. Daoukaki-Diamanti, P. Pissis and G. Boudouris, Chem. Phys. 91 (1984) 315-325.

DIELECTRIC STUDY OF DRY AND HYDRATED MICROCRYSTALLINE CELLULOSE

L. Apekis

National Technical University of Athens, Zografou Campus, 15773 Athens, Greece

ABSTRACT

Thermally Stimulated Depolarization Current (TSDC) measurements on dry and hydrated compressed pellets of microcrystalline cellulose, in the temperature range of 77-300K, show three main dielectric dispersion bands: (i) a complex band in the region of 80-200K attributed to the reorientation of polar groups of cellulose, (ii) a broad peak in the region of 128-145K attributed to the polarization of loosely bound sorbed water molecules, which for high water content dominates in this temperature region, and (iii) a broad dispersion peak appearing in the region of 180-260K which is attributed to the motion of polar groups of cellulose facilitated by sorbed water.

INTRODUCTION

The dielectric properties of dry and hydrated cellulose and cellulose derivatives have been studied by many investigators using dielectric loss methods [1-4] and thermally stimulated depolarization current (TSDC) method [5-7]. However, some questions concerning the hydration mechanism of cellulose and the influence of hydration on the dielectric behaviour of cellulose are still open.

In this work the dielectric behaviour of dry and hydrated (up to 14.8%) compressed pellets of microcrystalline cellulose (MCC) was studied by the TSDC method, in the temperature range of 77-300K.

EXPERIMENTAL

The TSDC method consists of studying the thermally activated release of stored dielectric polarization [7,8]

CH2593-2/ 88/ 0000-0276$01.00 Copyright 1988 IEEE

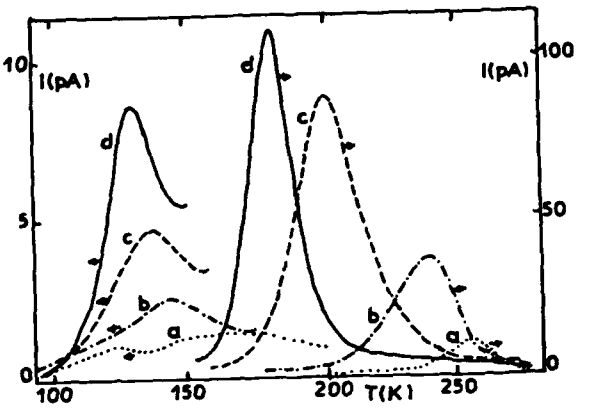

Fig. 1. TSDC plots of MCC samples with different water contents : 0.6%(a), 3.7%(b), 8.5%(c) and 13.2%(d).

Measurements have been made using microcrystalline cellulose (MCC) powder (type 20, SIGMA, approx. particle size : 20 µm), compressed to cylindrical pellets of 13 mm diameter and various values of thickness (1.33 to 1.55 mm) and density (1.41 to 1.47 $g \cdot cm^{-3}$). The samples were provided with contacts of silver paste. The water content h of the samples, defined as the ratio of the weight of the sorbed water to the weight of dry cellulose, was varied between 0 and 14.8%. Typical values for the experimental conditions were 5kV/cm for the polarizing electric field, 300K for the polarization temperature, 3 min for the polarization time, 10 K/min for the cooling rate down to 77K and 3 K/min for the heating rate.

RESULTS AND DISCUSSION

Fig. 1 shows typical TSDC plots measured on MCC samples with different water contents, h = 0.6, 3.7, 8.5 and 13.2%. Each plot shows a low-temperature band and a high-temperature broad peak, whose shape and position in the plot are affected by the water sorbtion.

Measurements on dry samples show a broad dispersion in the region of 80-200K with two maxima, one at about 140K and another at about 170K. By increasing the water content, the first peak (first in order of increasing temperature) seems to be practically unaffected, while the second peak

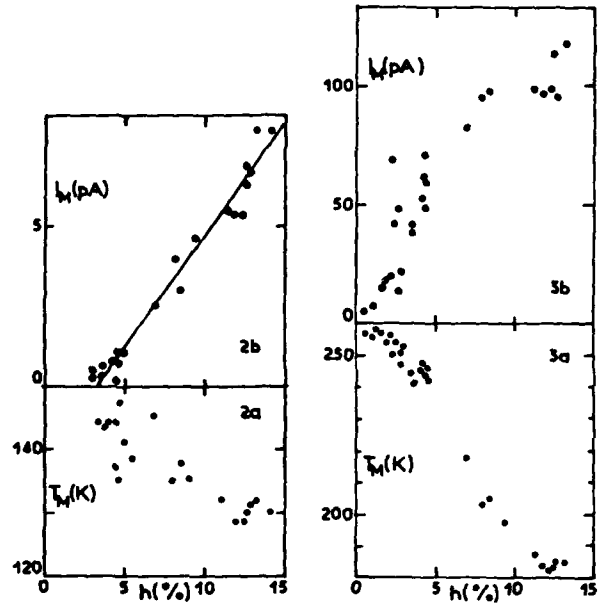

Fig.2. Peak temperature T_M and current maximum I_M of the low-temperature TSDC peak as a function of the water content h.

Fig.3. Peak temperature T_M and current maximum I_M of the high-temperature TSDC peak as a function of the water content h.

shifts to lower temperatures. There is experimental evidence that both peaks are of dipolar origin. The peak at about 140K may be of the same origin as those obtained by TSDC measurements on completely dried [5] and hydrated cellulose [6], which are both attributed to the motion of primary hydroxyl groups of glucose residue in the amorphous regions of cellulose. In the case of microcrystalline cellulose of our measurements hydroxyl groups of the surface of the crystallites and even of the crystalline regions might participate to the polarization. The origin of the second peak of the low-temperature dispersion may be due to dipolar groups of cellulose whose motion is made easier by sorbed water.

For water content higher than about 3.5% the low - tempe-

rature dispersion is dominated by a broad peak whose position in the plot (peak temperature T_M) shifts from about 145K to 128K (fig.2a) and whose magnitude (current maximum I_M after subtracting the broad band measured on dry and low-hydration samples) increases with increasing water content (fig.2b). Thermal sampling and partial heating analysis [8] of this peak showed a relaxation mechanism characterized by a continuous distribution of relaxation times with an activation energy ranging continuously from 0.20 to 0.45 eV.

The comparison of these results with those reported from TSDC measurements on cellulose [6] and AC measurements on MCC [1], permits us to adopt the same interpretation and attribute the distributed relaxation mechanism observed in the low-temperature region, for water content higher than about 3.5%, to orientational polarization of loosely bound sorbed water molecules and consider all water molecules, for water contents up to 3.5%, as tightly (irrotationally) bound to cellulose. The shift of this dispersion to lower relaxation times with increasing water content (fig.2a) may be due to a continuous transition from loosely bound to free water. This shift, which was not observed in cellulose [6], possibly suggests a difference in the hydration mechanisms of the two materials. Our results did not confirm the dependence of the activation energy values on the water content, reported in [1].

As fig. 3 shows, the polarization mechanism causing the high-temperature TSDC peak of MCC, becomes faster (shifting of T_M to lower values, fig. 3a) and is enhanced (increase of I_M, fig. 3b) with increasing water content. The influence of the water is very pronounced for h values between 3 and 9%. Experimental tests offered by the TSDC method [8] show that this peak must be due mainly to dipolar polarization. Similar results have been obtained by TSDC measurements on hydrated cellulose [6,7] and mechanical and dielectric loss measurements on hydrated cellulose and cellulose derivatives [3,9] and were attributed to the motion of $CH_2OH - H_2O$ or glucopyranose rings relieved by water in the amorphous regions. This is an interpretation which may well be adopted for the high-temperature peak of our measurements. With the difference that, as the magnitude of the peak suggests, the crystalline regions of MCC may also contribute to this polari-

zation mechanism.

REFERENCES

1. M. Kent and W. Meyer, J. Phys. D : Appl. Phys. 16 (1983) 915.
2. C. Ballario, A. Bonincontro, C. Cametti and A. di Biasio, J. Coll. Interface Sci. 78 (1980) 242.
3. R.W. Seymour, S. Weinhold and S.K. Haynes, J. Macromol. Sci. - Phys. B 16 (1979) 337.
4. J.E.Algie, in Applied Fibre Science, ed. F. Happey (Academic, N. York, 1979) Vol.2, pp. 169-203.
5. A. Sawatari, in Charge Transport and Electrostatics with their Applications (Elsevier Amsterdam 1979) p.347.
6. P. Pissis, J. Phys. D : Appl. Phys. 18 (1985) 1897.
7. P. Pissis and A. Anagnostopoulou-Konsta, Proc. 5th Int. Symp. Electrets, eds G.M. Sessler and P. Gerhardt-Multhaupt (IEEE, N. York, 1985), p.842.
8. J. Vanderschueren and J. Gasiot, in Thermally Stimulated Relaxation in Solids; ed. P. Braunlich (Springer, Berlin, 1979) pp.135-223.
9. M. Kimura and J. Nakano, J. Polym. Sci. Lett. Ed. 14 (1976) 741.

DIELECTRIC PROPERTIES OF POLYURETHANE BLOCK COPOLYMERS

L. Apekis, P. Pissis and C. Christodoulides
Department of Physics

G. Spathis, E. Kontou and V. Kefalas
Section of Mechanics

National Technical University of Athens, Zografou Campus, GR 15773 Athens, Greece

ABSTRACT

The dielectric behaviour of polyurethane block copolymers with various molecular weights and amounts of soft and hard block segments was studied by the Thermally Stimulated Depolarization Current (TSDC) method, in the temperature range of 77-370K. TSDC measurements show a double low-temperature dispersion attributed to γ and β relaxations and a peak at about 240K probably due to the glass transition of the amorphous soft phase of the copolymer. A peak also appears between 255 and 270K related to MWS-type polarization, occuring mainly in the amorphous soft phase.

INTRODUCTION

The dielectric properties of polyurethanes have mainly been studied by the a.c. dielectric loss method [1-6].

This work deals with a study of the dielectric behaviour of polyurethane block copolymers with various molecular weights and amounts of soft and hard block segments by means of the Thermally Stimulated Depolarization Current (TSDC) method in the temperature range 77-370K.

EXPERIMENTAL

The TSDC method consists of studying the thermally activated release of stored dielectric polarization [7]. The copolymers studied are segmented polyurethanes prepared by reacting the symmetric methylenediphenyl isocyanate (MDI) with a hydroxy-terminated polyester (PE) to form a soft block segment. The polyester used is polyethylene

CH2593-2/ 88/ 0000-0281$01.00 Copyright 1988 IEEE

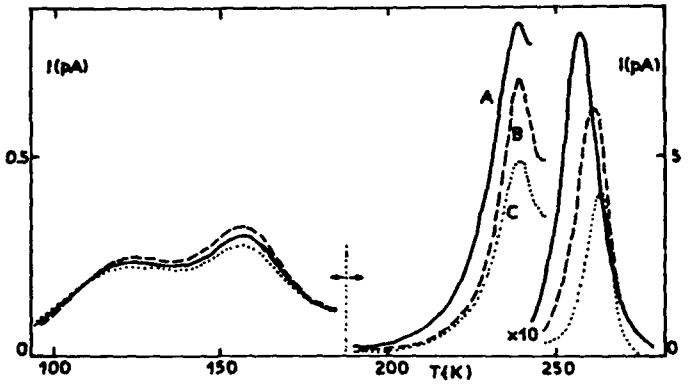

Fig.1. TSDC plots for three different types (A,B,C) of polyurethane block copolymers, normalized to the same polarizing field of 3.5 kV/cm.

adipate with an average molecular weight of 2000. The resultant polymer is then extended with butanediol (BDO) to form a hard block segment. Five types of specimens were prepared with stoichiometric amounts of MDI forming five different linear types of molecules with various molecular weights and various amounts of soft and hard segments [8]. The initial concentrations of reactants for the five types of polyurethane were (MDI : BDO : PE, in mols/lit) : 2:1:1 (A-type), 3:2:1 (B-type), 4:3:1 (C-type), 5:4:1 (D-type) and 6:5:1 (E-type).

The samples measured were cylindrical discs of about 13mm diameter and various thicknesses (0.51 to 2.17mm). Typical values for the experimental conditions were 300K for the polarization temperature, 5min for the polarization time, 10 K/min for the cooling rate down to 77K, 3 K/min for the heating rate and 3.5 - 13 kV/cm for the polarizing electric field.

RESULTS AND DISCUSSION

In fig.1 are shown TSDC plots of three different types of the polyurethanes studied. The plots show a broad dispersion with two maxima, at about 120K and 160K in the low-temperature region and two peaks, one at about 240K (peak I) and another appearing between 255-270K (peak II),

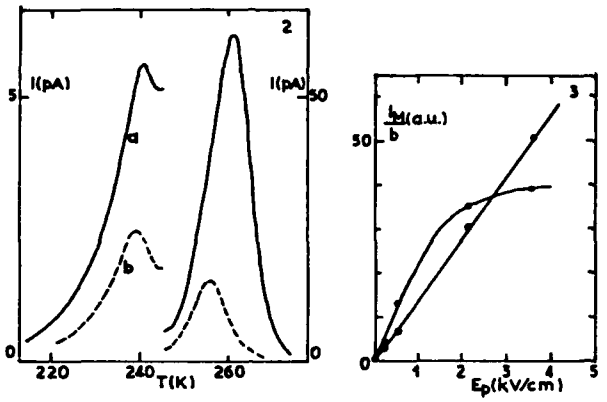

Fig.2. The high-temperature TSDC band with brass electrodes (a) and with teflon sheets between sample and electrodes (b), (A-type).

Fig.3. Current maxima (normalized to the same heating rate b) of peaks I (empty points) and II (full points) versus polarizing field.

in the high-temperature region.

Measurements show that the low-temperature peaks have practically the same shape, position and magnitude for all the types of polyurethane studied (with the exception of the samples of E-type, in the plots of which the two peaks are of lower magnitude). Results to be reported elsewhere show that sorbed water does not affect the peak at about 120K, while it enhances the peak at about 160K. These two peaks may be attributed to γ and β relaxations respectively, observed in polyurethanes and polyamides [6].

In the present work we studied in detail the high-temperature dispersions, peak I and peak II. Figures 2 and 3 show an example of the influence on peaks I and II of the kind of electrodes used (insulating or not) as well as of the polarizing electric field. Similar behaviour has been observed in all the samples of the five types of polyurethane. According to these results peak I must be due to volume dipolar polarization and peak II may be due to

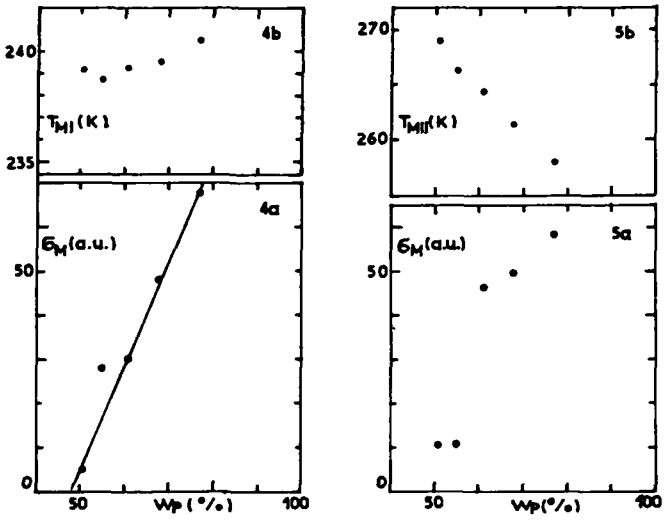

Fig.4. Variation with the initial polyester content W_p, of (a) : normalized current maxima, σ_M and (b); peak temperature T_M of peak I.

Fig.5. Variation with W_p of (a) : normalized current maxima and (b) : peak temperature of peak II.

Maxwell-Wagner-Silars polarization, rather than to space charges related to the dc conductivity [7].

Figures 4 and 5 show for peaks I and II respectively, their position in the TSDC plots (peak temperature T_M) and their magnitudes (current maxima I_M normalized to the same polarizing field, heating rate and cross section for all samples) for the five types of polyurethane studied. The results are plotted as a function of the initial weight content in polyester, W_p.

The dipolar origin of peak I and the fact that its magnitude is a linearly increasing function of the initial polyester content (fig.4), might justify the attribution of this peak to the glass transition of elastometric phase of the copolymer, in accordance with Dev et al. [2]. As fig.4 shows, this transition could be observed for copo-

lymers with initial polyester contents higher than about 50%. Fig.4 also shows, that variation of the initial polyester content does not result in a significant change of the transition temperature.

The increase in magnitude of peak II with increasing initial polyester content shown in fig.5, indicates that the ionic MWS polarization which is probably the cause of peak II, must be occuring mainly in the amorphous phase of the copolymer. The systematic variation in the position of peak II with W_p (fig.5) may be related to a corresponding variation in ionic mobility or to a variation of the mobility of the amorphous soft phase. Similar results have been reported by Dev et al [2].

REFERENCES

1. A.M. North and J.C. Reid, Europ. Polym. J. 8 (1972) 11299.
2. S.B. Dev, A.M. North and J.C. Reid, in "Dielectric Properties of Polymers", ed. F.E. Karasz (Plenum, N.York, 1972).
3. C. Delides and R.A. Pethrick, Europ. Polym. J. 17 (1981) 675.
4. R. Zielinski and M. Rutkowska, J. Appl. Polym. Sci. 31 (1986) 1111.
5. G. Banhegyi, M.K. Rho, J.C.W. Chien and F.E. Karasz, J. Polym. Sci : Part B : Polym. Phys. 25 (1987) 57.
6. P. Hedvig, in "Dielectric Spectroscopy of Polymers", ed. A. Hilger (Techno House, Bristol, 1977).
7. J. Vanderschueren and J. Gasiot, in "Thermally Stimulated Relaxation in Solids", ed. P. Braunlich (Springer, Berlin, 1979) pp. 135-223.
8. L.H. Peebles, Macromolecules, 7 (1974) 872.

CONCERNING THE ρ RELAXATION DURING AMORPHOUS PET CRYSTALLIZATION BY THERMALLY STIMULATED DISCHARGE

J.Belana and P.Colomer

Escuela Tecnica Superior de Ingenieros Industriales (UPC)
Colón 11, 08222 Terrassa (Barcelona),Spain.

ABSTRACT

The thermal depolarization of amorphous PET electrets metallized on one side and corona charged at T_p>70ºC provides,between 20ºC and 105ºC,three relaxations: α ,ρ_1 and ρ_2. The origin of ρ_2 is free charge injected from the electrodes while ρ_1 could be asociated with a uniform bulk mechanism. The ρ_1 peak has been located in electrets metallized on both sides and polarized ,between 73ºC and 79ºC, only in the isothermic phase so that at T_p>79ºC it overlaps with ρ. The stimulated crystallization by thermal steps in PET-a samples, metallized on both sides,lets us to think that ρ_1 changes with the crystallinity and becomes the α_c relaxation of the PET-c.

INTRODUCTION

The discharge of amorphous polyethylene terephthalate (PET-a) electrets metallized by both sides provides two relaxations (α and ρ) between 20ºC and 105ºC. The first is the α relaxation which is polar. The ρ relaxation has been related to space charge although the results attained in corona charged samples [1] lead us to believe that this relaxation is compound.On the other hand, on increasing the crystallinity of the samples by the process of thermal stimulation by steps [2] α does not evolve in a continuous way until α_c of the PET-c.For a certain crystallinity degree, a simultaneous ocurrence of α , α_c and ρ is achieved, which suggests that α_c could originate from one relaxation masked by α or ρ .

The aim of this paper is to make evident that the ρ relaxation is compound, to analyse the origin of the mechanisms of which it is composed and to prove that α_c comes from one of these mechanisms.

CH2593-2/ 88/ 0000-0286$01.00 Copyright 1988 IEEE

EXPERIMENTAL PART

The experiments have been carried out on commercial PET with a molecular weight of 20,000 measured by viscosimetry. The PET-a films were prepared, with a diameter of 2 cm and thickness of about 250μm, by fusion and quenching in molds.The conditioning and the experimental dis position have been explained in detail in another work [3] The corona charging has been done using samples metallized on one side with aluminium, leaving an air gap of 1 mm between the polarization electrode and the non meta llized side. The heating rate has been 2ºC/min in all cases. With the purpose of studying the crystallinity effect we have used the method of thermal stimulation by steps (TSS) consisting in, once the sample is polarized at a fixed temperature T_p, finalizing each discharge at a temperature higher than the preceeding discharge.

RESULTS AND DISCUSSION

While the discharges of electrets metallized on both sides provides, between 20ºC and 105ºC, two relaxation peaks (α and ρ), the discharge of electrets metallized on one side and corona charged allows to observe three relaxations in the same range of temperature (fig.1).

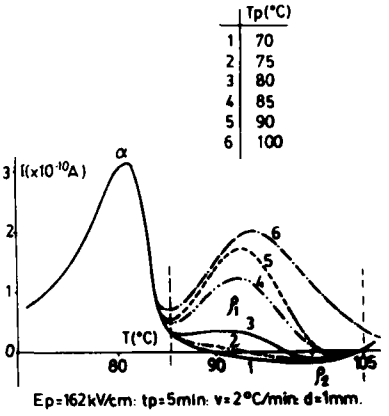

Fig 1. TSD curves of corona charged electrets at different T_p.

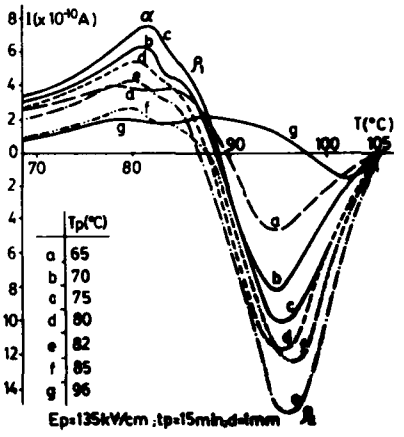

Fig 2. TSD curves at different T_p in a corona charged isothermic electret

The first is the α relaxation and the other two,named ρ_1 and ρ_2, appear in the thermal range of the ρ peak .While ρ_1 is always heteropolar, the ρ_2 peak is homopolar. On increasing the polarization temperature T_p , ρ_1 increases while ρ_2 decreases so that at T_p>90ºC only ρ_1 (which is concurrent with ρ) appears in the thermogram.

In fig 2, the curves obtained in the discharge (TSD) of a corona charged isothermic electret at different T_p can be seen. This electret has been polarized without the applied field E_p during the cooling.The methode is more selective with the mechanisms activated at T_p because any superposition of the former with the mechanisms which might be activated during the cooling phase is prevented

We observe that ρ_1 peak follows the same variations as α and its intensity increases with T_p, reaching a maximum at T_p=75ºC;while the ρ_2 homopolar peak, which also increases with T_p, reaches a maximum at T_p=82ºC and then decreases until disappearing.

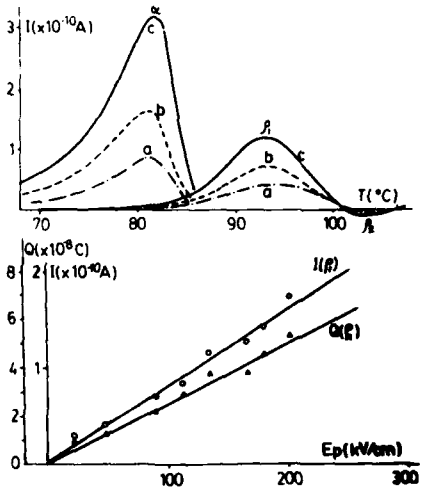

Fig.3. a)Peak Cleaning.
b)Charge and Intensity vs E_p
T_p=85ºC,t_{pi}=15 min.
E_p:(a)45Kv/cm,(b) 90Kv/cm,
(c) 157,5Kv/cm.

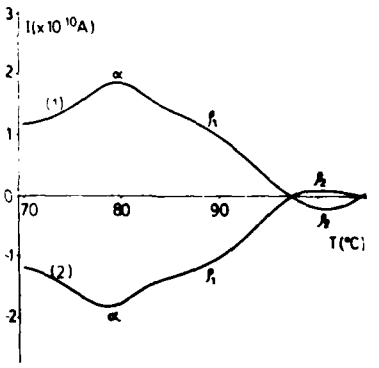

Fig.4. Effect of the polarity of the electrodes. T_p=82ºC,t_{pi}=15 min
(1) E_p=112Kv/cm (-)
(2) E_p=112Kv/cm (+)

While the origin of ρ_2 is due to injected charge from electrodes, that of ρ_1 is more confusing .Because of the range of temperature which it appears, it seems to be related to free charge. However a wider analysis permits us to observe, by the peak cleaning technique, that its charge and intensity plotted as a function of the applied field is linear, increasing its heteropolar character with the applied field. It also shows an elevated simetry when the polarity of electrodes is changed (fig 3,4).

All these facts, lead us to think that ρ_1 is polar and that it should correspond with a mechanism situated over the T_g which isn't seen in the discharge of electrets metallized on both sides and polarized in its conventional form.

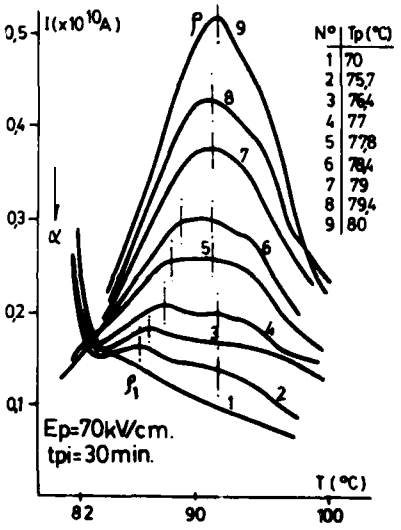

Fig 5. TSD curves of an isothermic electret at different T_p.

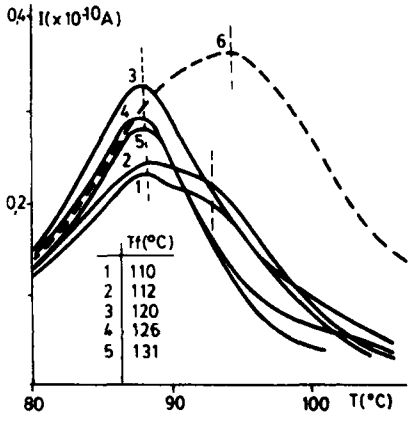

Fig 6. TSD curves obtained by the application of TSS method (1-5). T_f is the final temperature reached in the preceeding discharge. T_p=77ºC, E_p=70Kv/cm, t_{pi}=40min (6): TSD curve of the same electret polarized at T_p=90º in its conventional form. E_p=70Kv/cm, t_{pi}=40 min.

The localization of this relaxation is verified applying the TSD technique to isothermic electrets of PET-a with crystallinity degree χ_c=3%. In fig 5 the TSD thermogram at T_p between 70ºC and 80ºC is shown. ρ_1 and ρ appears at T_p< 80ºCso that at T_p> 80ºC there is an overlapping of both mechanisms.

The effect of the crystallinity over ρ_1 has been verified in an isothermic electret by the TSS method.In fig 6, some of the discharges obtained at applying this method at 77ºC are represented,showing the evolution of ρ_1 from 1 (PET-a) until 5 (PET-c, χ_c=35%) which presents the maximum at a temperature T_M=87ºC.The peak of this electret,which varies with the T_p, presents at T_p=90ºC the maximum at T_M=93ºC when forming the electret in its conventional form (maintaining the applied field during the cooling) which proves, in accordance with [2] that it is α_c of the crystalline sample (fig 6,curve 6).

ACKNOWLEDGMENT

This work is a part of Research Project Nº 0395/85 supported by the Comisión Asesora de Investigación Científica y Técnica (Spain)

REFERENCES

1. J.Belana,M.Pujal and E.Menéndez. To be published in Makromol.Chem. International Symposium on Polymer Materials,San Sebastian (Spain),1987.

2. J.Belana,M.Pujal,P.Colomer and S.Montserrat. To be published in Polymer.

3. J.Belana,P.Colomer,M.Pujal and S.Montserrat. J.Macromol.Sci.-Phys.B23(4-6),467-481 (1984-85).

INVESTIGATION OF CRYSTALLINE ORIENTATION, THERMODYNAMIC PROPERTIES AND CURIE TRANSITION ON FERROELECTRIC VF_2/TrFE COPOLYMERS

Alain Chalumeau

Thomson-Sintra ASM, Valbonne, France

ABSTRACT

VC_2/TrFE copolymers have been investigated by means of X-ray diffraction, Differential Scanning Calorimetry, optical microscopy and piezoelectric characterization.

The orientation of crystalline axes have been determined by pole figure analysis as a function of poling and processing history.

Morphology and crystallization kinetics have been studied with an optical microscope, during isothermal crystallization on 70/30 copolymer. Thermodynamic equilibrium temperature and infinite crystal enthalpy were extrapolated from melting temperatures and heats of fusion, measured on D.S.C. thermodiagrams.

The influence of monomer composition, processing history and poling on Curie transition have been investigated by D.S.C. Analysis and the resulting piezoelectric characteristics have been determined.

ON THE FIELD DISTRIBUTION AND EFFECTIVE PERMITTIVITY OF TWO-LAYERED CAPACITORS

R. Coelho

Laboratoire de Physique des Décharges (ER 114) du CNRS - ESE 91190 Gif-Sur-Yvette France

A. Cansell

ATESYS - 67160 Wissembourg France

Abstract

High voltage, high energy two-layered capacitors have been developed recently. This work deals with the field distribution and effective permittivity of such capacitors. The use of a simple empirical formula for the field-dependence of the conductivity of non-ohmic materials permits a detailed discussion of the field distribution and the electrostatic energy stored in the device.

I. INTRODUCTION. GENERAL RELATIONS FOR A TWO-LAYERED STRUCTURE

If a two-layered structure such as shown in Fig. 1, with ohmic materials 1 and 2 is submitted to a voltage step V, the equations for the fields E_1 and E_2 in the layers 1 and 2 resp. are derived from

1) the continuity of the total current at the interface :

$$(\epsilon_1 d/dt+\sigma_1)E_1 = (\epsilon_2 d/dt+\sigma_2)E_2 \quad (1)$$

2) the boudary condition :

$$\lambda E_1 + (1-\lambda)E_2 = E_a \quad (2)$$

where E_a is the applied field V/L.

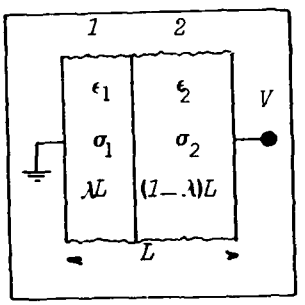

Figure 1

Elimination of E_2 - for example - between eqns. (2) and (2) yields a differential equation for E of the form :

$$dE_1/dt = E_a/T_2 - E_1/\tau \quad (3)$$

where

$$T_2 = [\lambda\epsilon_2 + (1-\lambda)\epsilon_1]/\sigma_2 ,$$

CH2593-2/ 88/ 0000-0292$01.00 Copyright 1988 IEEE

and $\tau = [\lambda\varepsilon_2 + (1-\lambda)\varepsilon_1]/[\lambda\sigma_2 + (1-\lambda)\sigma_1]$

is the dielectric relaxation time of the structure.

The differential equation (3) describes the exponential transition between the capacitive divider configuration with dominating displacement current at short time, and the resistive divider configuration with dominating conduction at longer time. If the field is applied gradually, eqn. (3) must be integrated with the proper $E_a(t)$ to obtain the variations of E_1 and E_2.

In the general case where $\varepsilon_1/\varepsilon_2 \neq \sigma_1/\sigma_2$ (untuned divider), if the constitutive layers undergo their breakdown fields in the capacitive regime, one of them will break during the transient. Nevertheless, it will be assumed here that the field is applied so slowly that both layers remain practically in the resistive state. In other words, the time constant of voltage application is assumed much longer that τ.

Under this assumption, the conduction current is continuous at the interface, and eqn. (1) reduces to :

$$\sigma_1 E_1 = \sigma_2 E_2 = i \tag{4}$$

i.e.

$$\frac{v}{\lambda/\sigma_1} = \frac{V - v}{(1-\lambda)/\sigma_2} = \frac{V}{\lambda/\sigma_1 + (1-\lambda)/\sigma_2} \tag{5}$$

where v, the voltage at the interface between the two layers, can be written in terms of V and $s = \sigma_1/\sigma_2$:

$$v = \left[1 + (1-\lambda)s/\lambda\right]^{-1} V \tag{6}$$

In the particular case of a tune divider ($s=e\equiv\varepsilon_2/\varepsilon_2$), v varies **exactly** as predicted by (6).

Using the above expression of v, the fields E_1 and E_2 can be written :

$$\begin{pmatrix} E_1 \\ E_2 \end{pmatrix} = \begin{pmatrix} 1 \\ s \end{pmatrix} \frac{E_a}{\lambda + (1-\lambda)s} \tag{7-8}$$

2. STORED ENERGY BY UNIT EREA

The total stored energy by unit erea in the structure is

$$W = W_1 + W_2 = \left[\lambda\varepsilon_1 E_1^2 + (1-\lambda)\varepsilon_2 E_2^2\right] L/2 \tag{9}$$

Using relations (7-8) for E_1 and E_2 in (9), W takes the form

$$W = \bar{\varepsilon} V^2/2L \tag{10}$$

where $\bar{\varepsilon}$ is the effective permittivity of the structure, given by

$$\bar{\varepsilon} = \varepsilon_2 \frac{\lambda e + (1-\lambda)s^2}{[\lambda + (1-\lambda)s]^2} \tag{11}$$

This effective permittivity varies from ε_2 for $\lambda = 0$ to ε_1 for $\lambda = 1$, and assumes a maximum

$$\bar{\varepsilon}_m = \varepsilon_2 \frac{(e-s^2)^2}{4s(1-s)(e-s)} \tag{12}$$

for

$$\lambda = \lambda_m = \frac{s}{1-s} \frac{s^2 - 2s + e}{e - s^2} \tag{13}$$

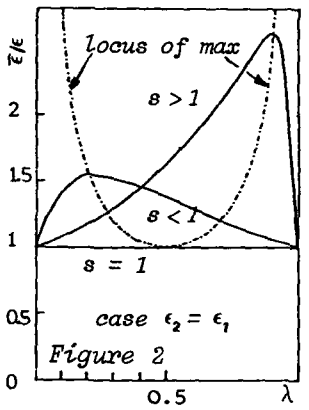

Figure 2

The simple case $\varepsilon_2 = \varepsilon_1(e=1)$ is illustrated on figure 2. The effective reduced permittivity is then maximum for $\lambda_m = s/s+1$, and its maximum $(s+1)^2/4s$ is much larger than unity whenever s is very small or very large compared to unity, i.e. when the layers have very different conductivities.

3. MAXIMUM APPLIED VOLTAGE

The maximum voltage V_m which can be applied to the structure is that for which E_1 or E_2 first reaches its maximum, E_1^* or E_2^* respectively. For instance, if E_1 first reaches the value E_1^*, E_2 then reaches the value sE_1^* which is assumed lower than E_2^*, and the maximum applied voltage is

$$V_m = [\lambda + (1-\lambda)q]E_1^* L \tag{14}$$

This shows that if both materials are ohmic, the layers cannot both work optimally unless $E_2^* = sE_1^*$, which corresponds to a unique value i_m of the current density

$$\sigma_1 E_1^* = \sigma_2 E_2^* = i_m \tag{15}$$

In practice, the materials are never ohmic, and their conductivities increase with increasing field. We shall

see in the following sections that this may cause either a balance or an unbalance of the fields in the constitutive layers, depending on the materials characteristics, which should be chosen such as to produce field balance for optimal behaviour.

4. A SIMPLE MODEL FOR THE FIELD DEPENDENT CONDUCTIVITY

The usual relationships for $\sigma(E)$ such as the Poole-Frenkel formula leading here to untractable calculations, we have deliberately chosen to use the simplest empirical relation accounting for the fact that σ increases from $\sigma(0)$ to infinity as E increases from 0 to the breakdown value E*. This is

$$\sigma(E) = (1 - E/E^*)^{-1}\sigma(0) \tag{16}$$

In our problem, the values $\sigma_1(0)$ and $\sigma_2(0)$ are noted σ_1^o and σ_2^o respectively, and the breakdown fields are E_1^* and E_2^*. Thus, under the same assumptions and with the same notations as used in section I, the conductivities σ_1 and σ_2 in layers 1 and 2 are

$$\sigma_1 = (1 - v/\lambda LE_1^*)^{-1}\sigma_1^o \tag{17}$$

and

$$\sigma_2 = \left[1 - (V-v)/(1-\lambda)LE_2^*\right]^{-1}\sigma_2^o \tag{18}$$

and the continuity of the current at the interface (eqn. (4)) can be written, after some algebraic manipulation, under the reduced form :

$$Ax^2 - Bx + \lambda = 0 \tag{19}$$

where $x = v/V$,

$$A = (E_2^*/E_1^* - s)E_a/E_2^*, \quad \text{with } s = \sigma_1^o/\sigma_2^o$$

and $B = \lambda - (1-\lambda)s + A$

6. DISCUSSION OF EQUATION (19)

First, it can be seen that A vanishes if $E_2^*/E_1^* = s$. In that case, eqn. (19) reduces to a first degree equation having the single root

$$x_o = \lambda/B = \frac{\lambda}{\lambda + (1-\lambda)s},$$

the same as found earlier in eqn. (6).

In the general case $E_2^*/E_1^* \neq s$, eqn. (19) has two roots :

$$x_{1,2} = (B/2A)\left(1 \pm \sqrt{1-4A\lambda/B^2}\right) \tag{20}$$

Here, we may note that A is usually quite small compared to unity, firstly because the factor E_a/E_2^* is small, except when the applied field E_a approaches the breakdown level, and secondly because the factor (E_2^*/E_1^*-s) is also small, since breakdown fields are usually high for low conductivity materials, and vice-versa.

Consequently, the square root in eqn. (20) can be approximated by a first-order expansion, and the only physically significant root (that one which is smaller than unity) is

$$x_1 = \frac{\lambda}{\lambda + (1-\lambda)s + A} \tag{21}$$

This can be written in terms of the value x_o corresponding to the case of ohmic layers :

$$x_1 = \left[1 + \frac{A}{\lambda + (1-\lambda)s}\right]^{-1} x_o \tag{22}$$

or, in view of the small value of A

$$x_1 \simeq \left[1 - \frac{A}{\lambda + (1-\lambda)s}\right] x_o \tag{23}$$

The new field E_1' in layer 1 can also be written in terms of the field E_1 given in eqn. (7) for ohmic materials under the same applied field

$$E_1' \simeq \left[1 - \frac{A}{\lambda + (1-\lambda)s}\right] E_1 \tag{24}$$

This shows that $E_1' < E_1$ if $s < E_2^*/E_1^*$, and vice-versa.

In just the same way, one can calculate the value of the field E_2' in terms of E_2, and obtain :

$$E_2' = \left[1 + \frac{\lambda A}{(1-\lambda)(\lambda + (1-\lambda)s)s}\right] E_2 \tag{25}$$

so that $E_2' > E_2$ if $s < E_2^*/E_1^*$, and vice-versa.

Summing up, the conditions to be fulfilled so that an increase of the applied stress tends to balance the field between the two layers are :

$$E_1 < E_2 \ (s>1) \text{ requires } E_1' > E_1 \text{ or } s > E_2^*/E_1^*$$

$$E_1 > E_2 \ (s<1) \text{ requires } E_1'/E_1 \text{ or } s < E_2^*/E_1$$

These conditions can be condensed in the unique inequality :

$$(s-1)(s - E_2^*/E_1^*) > 0 \qquad (26)$$

which simply means that s must be **outside** the interval $[1, E_2^*/E_1^*]$, $\forall\ E_2^*/E_1^*$.

6. ENERGY STORED IN THE NON-OHMIC STRUCTURE

Following the same reasoning as in Section 2, but now accounting for the new values E_1' of E_1 and E_2' of E_2 given in eqns. (24) and (25), one can write the new energy W' in terms of W, as an expansion of increasing powers of A. It is interesting to note, as the calculation is performed, that the first-order term in A, hence in E_a, vanishes, so that, to the second order, one has

$$W' \simeq W \qquad (27)$$

7. CONCLUSION

A simple empirical relation for the field-dependence of the conductivity has been proposed. Using this relation for a two-layered structure, a condition for optimal behaviour-namely a balance of the stress among the constituents under applied field - has been formulated. This involves only the low-field conductivities and the breakdown fields of the constituents.

Both E_2^*/E_1^* and s are either smaller or larger than unity, but it is further required, for optimal behaviour, that s differs more from unity that E_2^*/E_1^*. Also, the thickness ratio λ should be chosen close to the value for which the effective permittivity of the structure is maximum. For materials of similar permittivities, λ should be of the order of s/(s+1).

Finally, the fact that the total stored energy calculated with our $\sigma(E)$ is unaffected, to the first order in the applied field, can be regarded as supporting our approach.

OPTO-FERROELECTRIC MEMORIES USING VINYLIDENE FLUORODE COPOLYMERS

M.Date, T.Furukawa and T.Yamaguchi*

The Institute of Physical and Chemical Research, Wako, Saitama 351-01, Japan
*Ricoh Co.Ltd., Kouhoku, Yokohama 223, Japan

ABSTRACT

We have demonstrated that ferroelectric polymers may be applied to erasable optical memories. The media developed consist of a 1μ m thick layer of a dye-doped vinylidene fluoride / trifluoroethylene copolymer spin-coated onto an ITO-coated glass plate. Information is written in terms of sequences of positive and negative polarizations, which are generated by irradiating a focused laser beam c. 5μ m in diameter with the aid of a sign-controlled electric field. The data is read out pyroelectrically by scanning the laser beam.

Introduction

Ferroelectrics have stable remnant polarization under zero electric field. The sign of the remnant polarization is controlled by the external field. By assigning the positive and negative remnant polarizations to 0/1 binary data, we can construct a non-volatile memory using ferroelectrics.
Vinylidene fluoride copolymers, well-known as ferroelectric polymer, in particular, do not need an elongation treatment for ferroelectric properties to appear; unlike poly vinylidene-fluoride. Therefore, it is easy to make a thin ferroelectric film via the spin-coat method.
The present paper is mainly concerned with the fundamental characteristics of the ferroelectric polymers in relation to their memory applications.

Principle

To construct a multi-bits memory, it is required to controll the polarity of polarization at a selected location without affecting other locations. This can be

CH2593-2/ 88/ 0000-0298$01.00 Copyright 1988 IEEE

achieved by two methods, a multi-electrode method and single-electrode method. The former requires matrix array of electrodes as used in an IC memory. In the latter, data are recorded locally by heating a spatially addressed point under an electric field. The strength of the applied electric field must be smaller than the coercive field (E_c) at its environmental temperature. Since the coercive field decreases with increasing temperature, only the polarization of the heated point is reversed. [1] We adopted the latter method to our memory.

Figure 1 shows a schematic diagram of the read-write processes of our memories. Erasing process (a) consists of applying an electric field greater than the coercive field to erase the previous polarization pattern. Writing process (b) reverses the polarization of the selected area by irradiating the laser beam under a weak field opposite in sign. These processes, (a) and (b), are used in the writing of the write-after-erase mode. In this mode, simultaneous verification can be performed by monitoring the current associated with polarization reversal.
Writing process (c) sets the direction of polarization at a heated point independently of the previous direction of polarization. The sign of the applied field is controlled according to the data to be written. This writing mode corresponds to the over-write mode in the opto-magnetic memories. Reading process (d) reads the polarization pattern by the sign of the pyroelectric current induced by laser scanning.

Media

The media used in the memories of this experiment were made of a VDF/TrFE (65/35 mol%) copolymer provided by Daikin Kogyo Co.. The memory was made by the following procedure. The DMF solution of a dye-doped copolymer was spin-coated onto an ITO coated glass plate. The thickness of the copolymer layer was about 1μ m. After drying, it was annealed in a vacuum for one hour at 150 ℃ . The counter aluminum electrode was deposited onto the coated layer. The writing laser beam was exposed on the ITO coated side.

Results and Discussion

Figure 2 shows typical D-E hysteresis curves measured at room temperature (a), 80°C (b) and 90°C (c). It was seen that the coercive field is decreased as the temperature is raised.
Figure 3 shows the field dependence of the reversal temperature. As the field is lowed, the temperature reaches the Curie temperature.

Figure 4 shows the changes in polarization caused by the application of reverse electric pulse train at 100Hz at room temperature. We find that the reverse electric field lower than $1/2E_c$ does not affect the polarization. This means that the writing of the new data at a location at $E=1/2E_c$ does not interfere with the stored data at the other locations.

Figure 5 shows examples of memory patterns in the sample. The height of the pattern corresponds to the value of the polarization. These patterns were obtained by the pyroelectric response under a raster scanned laser beam. Its diameter at the focal point was 5μ m. The flat levels correspond to the non-electroded portions.
The conditions of the process were as follows:
(a) A field of !00MV/m was applied to initialize the memory (first erasing).
(b) A single line was written using 10mW laser power, 30MV/m reverse field and 100ms exposure.
(c) 100MV/m was applied to re_erase previous pattern.
(d) 10 line were written using laser powers from 12mW (left side) to 2mW (right side) in a 1mW step. The minimum writing power was found to be 4mW. The S/N ratio was about 30 dB under these conditions.

Because of their simple configuration, polymer ferroelectric memories may be adapted mass productive low-cost erasable memories.

References

[1] M.Date, IEEE Trans. ELECTRICAL INSULATION, EI-21, 539 (1986)

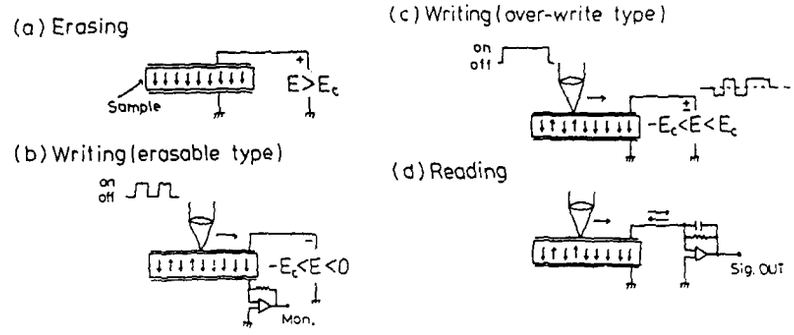

Fig.1 Principles of ferroelectric memory

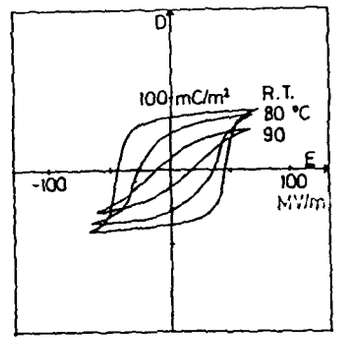

Fig.2

Hysteresis curves of VDF/TrFE copolymer at various temperatures

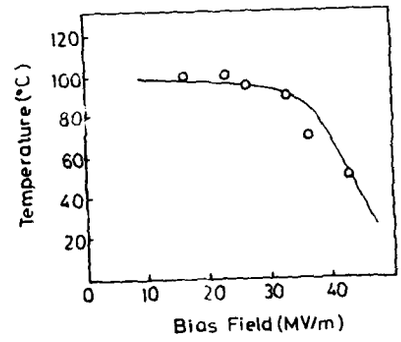

Fig.3

Field strength dependence of temperature of polarization reversal

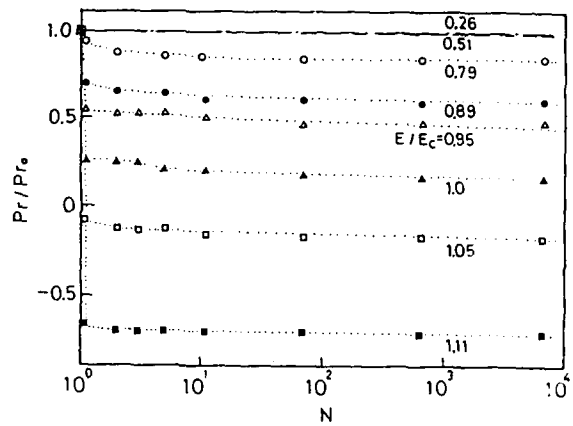

Fig.4 Changes in polarization caused by a pulse train of reverse electric fields

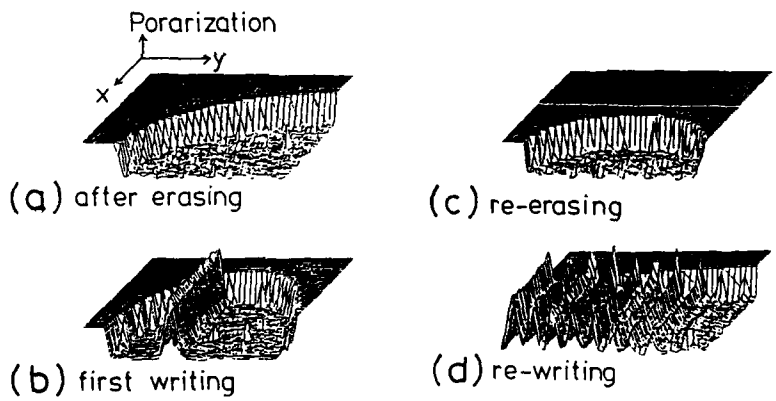

Fig.5 Memory patterns of erased and written states

SHORT-CIRCUIT THERMALLY STIMULATED CURRENTS IN POLYSTYRENE-POLY METHYL METHACRYLATE BLENDS

J.M. Keller, R.S. Baghel, Ranjit Singh and S.C. Datt

Department of Postgraduate Studies and Research in Physics, Rani Durgavati Vishwavidyalaya, Jabalpur -482 001 (MP) India.

ABSTRACT

Investigations of short-circuit thermally stimulated depolarization currents have been made on 20 μm thick, polystyrene (PS)-Polymethyl methacrylate (PMMA) blends containing different weight percentage of PMMA. The observed currents decrease for higher values of forming field and temperature and become anomalous for higher forming fields and temperatures. These characteristics are considered to be due to space charge formation near the electrodes and due to their blocking nature. The TSDC characteristic have been found to be sensitive to blend composition.

INTRODUCTION

Charge transport in insulating organic polymers is still a subject of much controversy [1-3]. This is partly because of their complex structure and partly because of extremely low conductivity and carrier mobility which are rather difficult to be measured accurately. Thermally stimulated depolarization current (TSDC) measurements have been extremely useful for studying electrical transport in these materials.

In the present paper we report the result of short-circuit TSDCs in PS-PMMA blends. Polymer blends are heterogeneous mixtures and the possibility of trapping of charges at the grain boundries of the individual materials is higher in them. The TSDC is considered to give valuable information about the molecular interaction between the individual components and the effect of structure on the electrical

CH2593-2/ 88/ 0000-0303$01.00 Copyright 1988 IEEE

transport in the blends.

EXPERIMENTAL

The materials used in the present investigation were commercial grade PS and PMMA supplied by M/s Chemicals Agency, Bombay, India. Blend films of thickness 20 μm were grown from a solution of the polymers in chemically pure benzene containing 6, 10 and 15 weight percentage of PMMA. The samples were outgassed in air at 80°C for 24 h followed by a room-temperature outgassing at 10^{-4} torr for a further period of 24 h. Both the surfaces of the samples were then vacuum aluminised over a central circular area of 42 mm diameter.

The samples were thermally polarized with polarizing fields of 10, 15, 20 and 25 kV/cm at temperatures 40, 60 and 80°C. After polarizing for 1 h at the desired temperature, the samples were cooled to room-temperature under the application of field. Total time of polarisation was adjusted to be 2½ h in each case. The TSDCs of polarized samples were obtained by reheating the sample at a rate of 3°C/min and the current was monitored using a 610C Keithley electrometer.

RESULTS AND DISCUSSION

Typical TSDCs for samples containing 6% PMMA (by wt.) and polarised at different temperatures with different fields are shown in Figs.1 and 2. It is seen that for specimens polarised at 80°C, the magnitude of TSDC increases with forming field; however, for highest field i.e. 25 kV/cm, it becomes anomalous and flows in the same direction as the polarising current. Further, for specimens polarised with 25 kV/cm, the magnitude of TSDC decreases with rise in forming temperature and becomes anomalous for 80°C.

Anomalous TSDC in plastic insulators have been reported by a number of workers [3, 4]. In HD-PE, anomalous TSDCs have been considered to originate from the injected space charges [3].

In the present case also, the anomalous TSDC may be considered to be due to the injected space charges since the concentration of free charge carriers in polymers is negligibly small. These injected space charges are trapped in various traps existing in the polymer.

In a polarized short circuited specimen, the concentration of trapped carriers is higher near the carrier injecting electrode and it decreases with distance towards the non-injecting electrode [4]. The movement of carriers towards the injecting electrode during depolarization process gives rise to normal TSDC. Any suppression of the carrier flow towards the injecting electrode results in a net carrier flow towards the rear non-injecting electrode giving rise to anomalous current. Such supression is considered to be due to blocking nature of metal-polymer contact.

With increase in forming field, density of injected space charge increases. Further, the

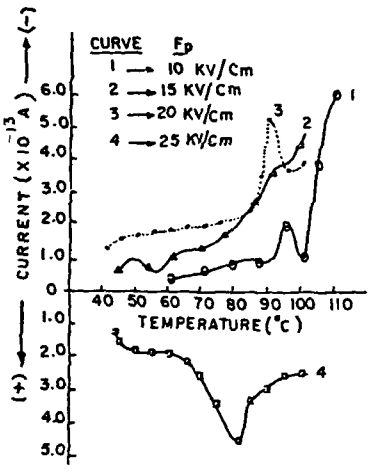

Fig.1. TSC spectra for PS with 6% PMMA poled at 80°C with various fields.

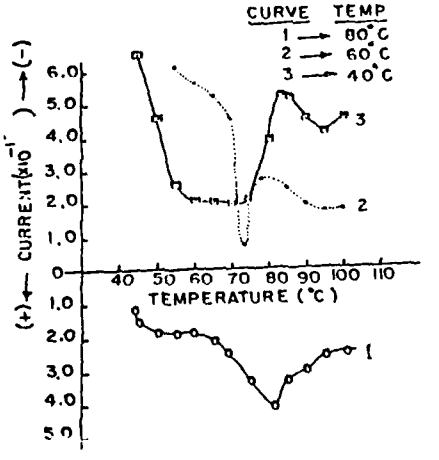

Fig.2. TSC spectra for PS with 6% PMMA poled with 25 kV/cm at various temperatures.

mobility of charge carriers increases with rise in temperature. This increased density of space charge together with increased mobility of carriers may result in high return rate of carriers towards the injecting electrode. Under conditions of high forming field and temperature, this high return rate of carriers may surpass the charge exchange rate at the electrode leading to blocking of electrode and hence anomalous TSDC.

Fig . 3 shows the TSDCs of specimen having different compositions and polarised under different forming conditions. It is seen that for specimens containing higher weight percentage of PMMA, anomalous TSDCs are observed for lower forming temperatures (60°C). However, for higher forming temperatures the current flows in the normal sense. This may be understood in terms of distribution of trap levels in the material. At high forming field, density of injected charge is very high. Since the mobility of charge carriers is low at lower

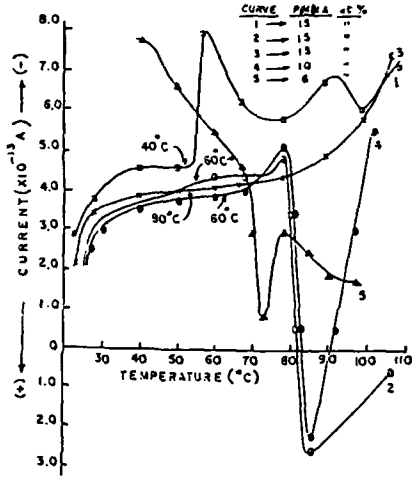

Fig.3. TSC spectra of PS blended with PMMA and poled with 25 kV/cm.

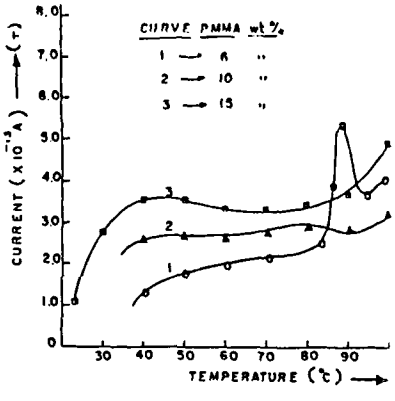

Fig.4. TSC spectra of PS blended with PMMA and poled at 80°C with 20 kV/cm.

temperature only shallower traps are filled, release of charge carriers from which being very small normal TSDC is observed. As temperature increases, mobility of carriers also increases, hence, at moderate temperature deeper traps are also filled. Release of a large number of charge carriers from the traps during depolarizing cycle may then result in high return rate of carriers leading to blocking of electrode. With increasing amount of PMMA in PS, number of traps and hence the density of injected space charge increases giving anomalous TSDCs at lower forming temperatures. At still higher temperatures mobility of carriers becomes appreciably high and hence only deep traps are filled. Number of charge carriers released from these may not be sufficient so as to cause blocking of electrode and hence TSDC flows in the normal sense for specimen polarised at 80°C. This is further reflected in the anomalous behaviour becoming normal as the temperature increases during depolarisation process.

Fig. 4 shows TSDCs of specimen having different compositions and polarised at highest forming temperature (80°C) with moderate field (20kV/cm). Normal TSDCs are observed for such specimens. At higher temperatures, mobility of carriers is very high. Since the field is moderate, despite increasing amount of PMMA in PS, density of charge carriers may not become high enough to cause blocking of electrode. Consequently, normal TSDCs are observed.

REFERENCES

1. H.J. Wintle and G.M. Tibensky; J. Polymer Sci. 11, 25 (1973).
2. K. Tahira and K.C. Kao; D: Appl. Phys. 18, 2247 (1985).
3. T. Mizutani and M. Ieda; D: Appl. Phys. 11, 185 (1978).
4. T. Mizutani, M. Ieda and I.D. Jordan; Jpn. J. Appl. Phys. 18, 65 (1979).

A STUDY OF ABSORPTION CURRENTS IN ACRYLIC ACID-DOPED POLYSTYRENE

Ranjit Singh, R.S. Baghel, J.M. Keller and S.C. Datt

Department of Postgraduate Studies and Research in Physics, Rani Durgavati Vishwavidyalaya, Jabalpur -482 001 (MP), India.

ABSTRACT

The absorption currents in the discharge mode in acrylic acid (AA)-doped solution-grown polystyrene (PS) films, prepolarized at 358 K with different fields, have been analysed in temperature range 313-358 K. Space charge due to trapping of injected charge carriers in energetically distributed traps is considered to account for the observed currents. Two relaxation peaks centred at 328 K and approximately at 348 K have been observed in the isochronal current thermograms.

INTRODUCTION

Transient current measurements have been considered to be helpful to understand the effect of controlled doping on polarization processes in polymers [1,2]. The present paper reports the discharging behaviour of polystyrene (PS) films doped with acrylic acid (AA), using transient current measurement technique.

EXPERIMENTAL

AA-doped PS films were grown from solutions of 10 g of PS in well-stirred mixtures of AA and benzene. The dopant concentration was changed by varying the amount of AA added to the solvent such that the total volume of the solvent and AA was always 100 ml. Samples with low, medium and high dopant concentrations having 1,3 and 5 ml of AA in 99, 97 and 95 ml

CH2593-2/ 88/ 0000-0308$01.00 Copyright 1988 IEEE

of benzene have been used for the present work.

Both side vacuum aluminized 50 μm thick samples were polarized in a programmed oven at 358 K for 1 h with different fields and then were cooled, under the application of field, to appropriate temperature at which the absorption current was measured in the discharge mode by short-circuiting the sample through a 610C Keithley electrometer. The currents were recorded as a function of time in the range $10-10^3$ sec.

RESULTS AND DISCUSSION

Typical plots of discharge current (I_d) at various temperatures for samples with different dopant concentrations are shown in Figs.1-3. These plots have been found to be characterized with two linear regions; one, short-time region (I) and the other, long-time region (II). The current in both the regions may be represented by the Curie-Von Schweidler law [3]

$$I_d(t) = A(T)\ t^{-n} \qquad (1)$$

where t is the time and A(T) is temperature

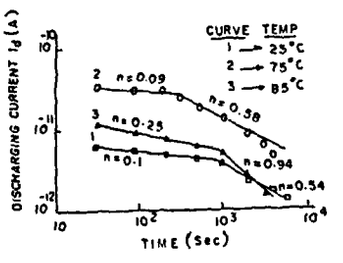

Fig.1. I_d versus time plots at different temperatures for 20 kV/cm poled samples with low doping.

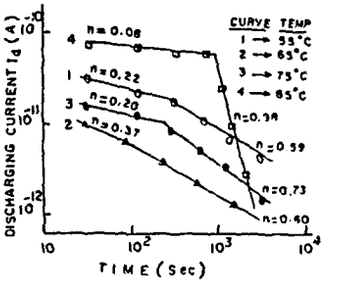

Fig.2. I_d versus time plots at different temperatures for 10 kV/cm poled samples with medium doping.

dependence factor. The values of index n for both regions of discharging current are shown in Figs.1-3. It is noted that in region I, n remains less than 0.5, whereas in region II, n lies between 0.5 and 1. In the long-time region n is found to increase with temperature for samples polarized under identical conditions with each dopant concentration. The temperature dependence of discharging current is shown clearly when the current (measured at constant time) is plotted against temperature. Activation energy values obtained from activation plots of the discharging current at various prescribed times for various samples are found to vary from 0.21 to 0.95 eV. The values are found to increase with increasing time of measurement and decreasing dopant concentration.

Number of mechanisms have been considered to lead to the Curie-Von Schweidler type of time dependence [3]. It is rather difficult to specify the origin of absorption current unambiguously from the time-dependence alone. However, the various facts including the weak polar structure of PS, power law dependence of current on charging voltage, observed values of n, and thermal activation of current over certain temperature range as observed in the present case indicate that the space charge due to accumulation of charge carriers near the electrodes and trapping in the bulk may be supposed to account for the observed current.

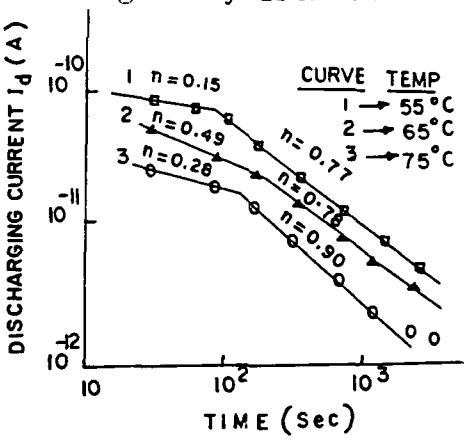

Fig.3. I_d versus time plots at different temperatures for 15 kV/cm poled samples with high doping.

The faster decay of current in long-time region for different samples indicates the existence of energetically distributed localized trap levels in the sample. It seems that at shorter times only shallow traps get emptied contributing to stronger current. However, at longer times deeper traps with long detrapping time release the charge due to which the current decays with faster rate at longer times.

The AA doping is considered to play an important role in modifying the nature of electrical conduction[4] . The dopant used in the present work is an α - β unsaturated carbonyl compound. It posses both a C=C and a C-O double bond and exhibits the properties of both fundamental groups. Moreover, AA may be regarded as an electronegative acceptor because of the electron-attracting carbonyl group, the adjacent double bond increasing the tendency of the proton to escape. Hence AA molecules trapped in the chain structure or present in the interstitial positions can form CTCs.

The dopant molecules present in very less number in PS matrix may provide additional traps, however, formation of CTCs may effectively decrease the trapping effect by "handling on" the carriers. At the formation of CTCs, links between the trapping centres are produced due to the increase in the orbital overlaps. Such a phenomena would result in the reduction of the activation energy and would increase the mobility of the carriers. The observed decrease of activation energy values and increase in current values with increasing doping concentration supports the above role of CTCs.

Typical examples of discharge currents measured at a constant times (isochronals) plotted against temperature are shown in Fig.4. These isochronals are characterized by two well defined peaks located at about 323 and 348 K.

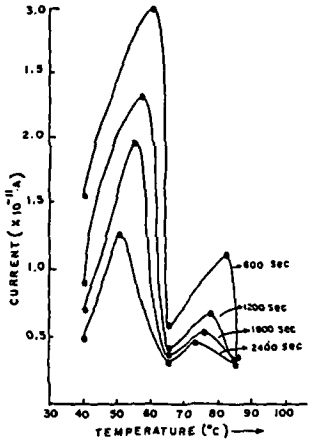

Fig.4. Isochronal discharge current at different temperatures. Pre-applied field: 15 kV/cm; doping: medium.

Both these peaks shift to lower temperature with increasing time, which is a characteristic of relaxation processes.

The activation energy values, calculated from the Arrhenius shift of the peaks, for low-and high temperature peaks for samples with different doping have been found out to be 0.85 ± 0.12 eV and 0.54 ± 0.13 eV, respectively. The activation energy values for both the peaks have been found to decrease with increase in doping concentration. Charges releasing from shallow and deep traps can be considered to contribute to these peaks.

The work for the fuller specification of these peaks is in progress.

REFERENCES

1. P.K.C. Pillai and Rashmi, Europian Polym. J. 17, 611 (1981).
2. T. Mizutani, K. Mitani and M. Ieda, J. Phys. D· Appl. Phys. 17, 1477 (1984).
3. J. Vanderschueren and A. Linkens, J. Appl. Phys. 49, 4195 (1978).
4. H.C. Sinha, I.M. Talwar and A.P.Srivastava, Thin Solid Films 82, 229 (1981).

THERMALLY STIMULATED AND ISOTHERMAL DISCHARGE OF CORONA-CHARGED POLYPROPYLENE

Ranjit Singh, J.M. Keller and S.C. Datt
Department of Postgraduate Studies and Research in Physics, Rani Durgavati Vishwavidyalaya, Jabalpur -482 001 (M.P.), India.

ABSTRACT

The paper reports details of short- and open-circuit thermally stimulated current (TSC), and also of isothermal charge decay and absorption current measurements made on corona-charged 50 μm thick commercial grade isotactic polypropylene (PP).

INTRODUCTION

Regardless of various advances made in the past, the charging and discharging processes in most of the polymers, including polypropylene (PP), can not be considered to be fully understood [1,2] . The paper, therefore, reports a combined study of short-and open-circuit thermally stimulated currents (TSCs) alongwith that of isothermal charge decay and absorption current on PP foils.

EXPERIMENTAL

Measurements were made on one-sided vacuum aluminized 50 μm thick commercial grade isotactic PP films. Samples were corona-charged negatively with corona voltages (V_p) of 7-12kV at temperatures ranging from 30 to 140°C in all experiments.

Surface charge measurements were followed by short- and open-circuit TSC measurements on two separate batches of electrets, charged under identical conditions. Absorption current in the discharge mode was measured at different fixed temperatures as a function of time. The measurements were made with pre-polarized samples. The details of the experimental techniques for different measurements are described elsewhere [3,4] .

CH2593-2/ 88/ 0000-0313$01.00 Copyright 1988 IEEE

RESULTS AND DISCUSSION

The characteristic curves for various experimental findings are shown in Figs. 1-5. At each charging temperature (T_p) a rapid increase in charge with V_p tending to saturate at higher values of V_p is observed (Fig.2). It is further noted that at each V_p, the charge after increasing with T_p starts decreasing with further rise in T_p. Short-circuit TSCs (Fig.3) are characterized with three peaks located approximately at 50, 90 and 120°C. However, open-circuit TSCs (Fig.4) show four peaks centred at 50, 105, 135 and 145°C.

The enhancement of initial charge density with V_p at each T_p indicates that the build up of polarization is due to the charge penetrating through the non-metallized surface into the near surface region of the sample and its subsequent trapping in various available traps. This is further evidenced by the observed variation of charge Q (released under all the

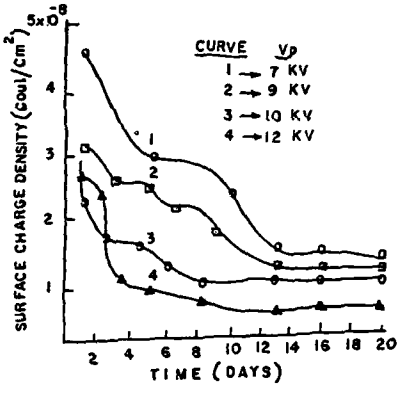

Fig.1. Surface charge decay curves of 100°C-charged samples with various (V_p) values.

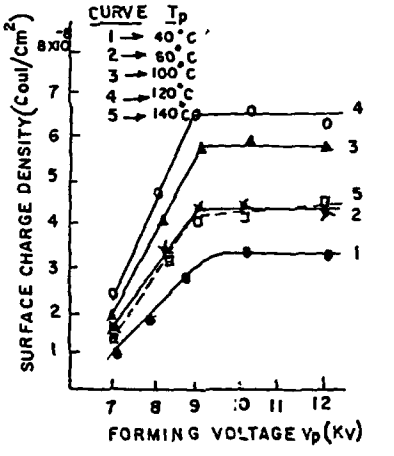

Fig.2. Corona voltage (V_p) dependence of surface charge density at various charging temperatures (T_p).

peaks of short-circuit TSCs) with V_p at various values of T_p (results not shown) which is characteristic of non-uniform volume polarization produced by space-charge build-up near samples. The increase in Q values with T_p and V_p before reaching saturation is characteristic of incomplete filling of trapping sites.

The appearance of a peak centred at 140° C in open-circuit TSCs, while its absence in short-circuit TSCs shows that this peak is due to the charge trapped in trapping sites located at surface or near surface region. However, the traps giving rise to the other three peaks, common to both type of TSCs, are clearly bulk traps.

Anomalous short-circuit TSCs (flowing in the same direction as the charging current) observed with high-temperature charged samples, can be understood in terms of space-charge-limited (SCL) drift of charge carriers towards the collecting

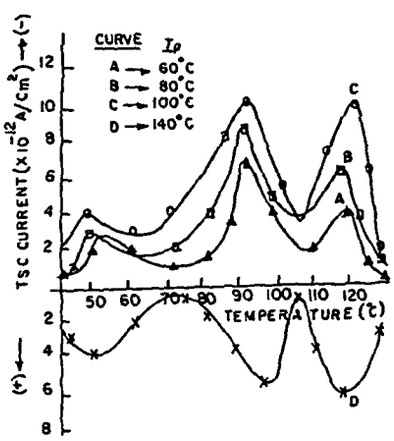

Fig.3. Short-circuit TSC curves for samples charged with 10 kV at various T_p values.

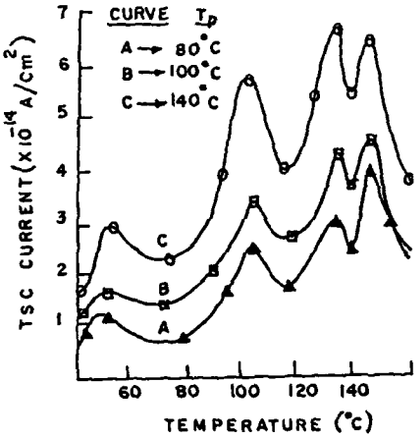

Fig.4. Open-circuit TSC curves for samples charged with 12 kV at various T_p values.

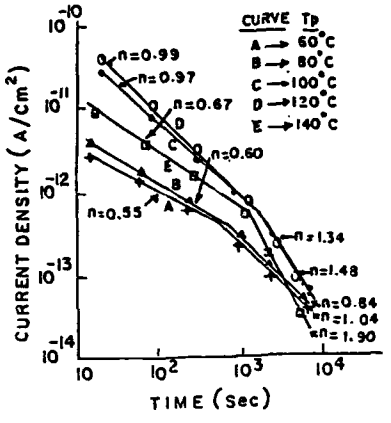

Fig.5. Time dependence of discharge current (I_d) at various temperatures for samples charged at 140°C with 10 kV. Values of n for both branches are indicated in the figure.

electrode [5]. The high return rate of carriers towards the collecting electrode exceeding the charge exchange rate at the electrode causes the current to be anomalous. Such situation is expected to arise in high temperature charged samples due to higher concentration of space charge near collecting electrode in such samples.

Typical plots as shown in Fig. 5, show that the discharge current I_d follows t^{-n} time dependence, where t is the time measured after removal of V_p. Discharge current measured at various prescribed times versus temperature plots, constructed from time-dependence curves of I_d at various fixed temperatures, show that the isochronals so obtained, are characterized by a single peak. The position of the peak shifts towards lower temperature at higher values of discharge time. The activation energy evaluated from the Arrhenius shift of this peak have been found to be 1.25 ± 0.02 eV, which is approximately the same as that for 90°C peak in short-circuit TSC.

REFERENCES

1. G.M. Sessler (Ed.), Electrets (Springer verlag, Berlin, 1980).
2. J. van Turnhout, Thermally Stimulated Discharge of Polymer Electrets (Elsevier, Amsterdam, 1975).

3. R. Singh and S.C. Datt, in Proc. 5th Intern. Symp. Electrets, Heideberg 1985, ed. by G.M. Sessler and R.G. Multhaupt (IEEE Service Center, Piscataway, NJ, USA) pp. 191-195.
4. S.C. Datt and R. Singh, in Proc. 5th Intern. Symp. Electrets, Heidelberg 1985, ed. by G.M. Sessler and R.G. Multhaupt (IEEE Service Center, Piscataway, NJ, USA) pp. 196-201.
5. T. Mizutani, K. Kaneko and M. Ieda, Jpn. J. Appl. Phys. 90, 1443 (1981).

POLARIZATION BEHAVIOUR OF IODINE-DOPED POLYSTYRENE

Ranjit Singh, S.Nayak, J.M.Keller and S.C.Datt

Department of Postgraduate Studies and Research in Physics, Rani Durgavati Vishwavidyalaya, Jabalpur -482 001 (MP), India.

ABSTRACT

Thermally stimulated currents (TSCs) from iodine-doped polystyrene (PS) thermoelectrets have indicated the polarization to be due to the localization of injected charge in geometrically and energetically distributed traps. Anomalous TSCs, observed with strongly doped samples, are considered to be due to release of injected space charge carriers and the partial blocking of metal-polymer contact.

INTRODUCTION

Inspite of many publications on polarization behaviour of polymers doped with impurities, the mechanism of impurity effects on such behaviour is not yet well understood [1].

In this paper thermal polarization of iodine-doped PS has been investigated using thermally stimulated current (TSC) technique.

EXPERIMENTAL

Iodine-doped 50 μm thick PS films, grown from a benzene solution containing 10 g of PS and 0.4, 2.0 and 4.0 g of iodine $(100\ cm^3)^{-1}$ respectively, have been used for the present work.

TSCs for both sided vacuum aluminized samples, polarized under different field and temperature conditions for total polarization time of 4h, were observed by short-circuiting the samples through a Keithly 610C electrometer and heating

CH2593-2/ 88/ 0000-0318$01.00 Copyright 1988 IEEE

them with a heating rate of 3°C/min.

RESULTS AND DISCUSSION

For simplicity we designate iodine doping with 0.4, 2.0 and 4.0 g of iodine $(100\ cm^3)^{-1}$ as low, medium and strong doping.

Characteristic TSCs for samples with different dopant concentration and polarized under different field and temperature conditions are shown in Figs. 1-4. It is observed that room-temperature (22°C) charged samples are characterized with a single broad peak around 70°C. It is further noted that the samples with strong doping give rise to anomalous TSC in the sense that the current flows in the direction opposite to that of the charging current.

Samples polarized at 70 and 100°C generally give rise to three peaks located around 40-60, 75-100 and 110-120°C. For various dopant concentrations except for strongest one, the observed TSCs are normal. In such cases the low-temperature peak decreases, while the two peaks on higher temperature side increase in

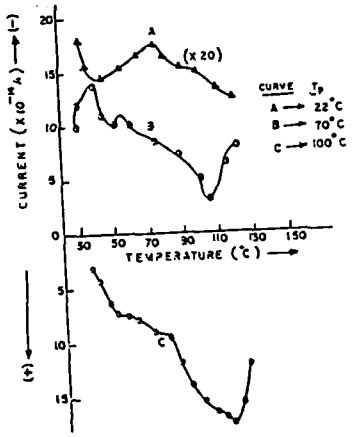

Fig.1. TSC curves for samples with low doping polarized at various temperatures with 10 kV/cm.

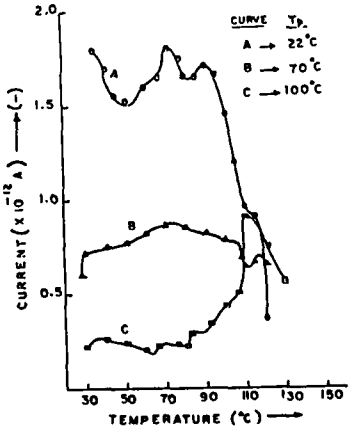

Fig.2. TSC curves for samples with medium doping polarized at various temperatures with 10 kV/cm.

magnitude with increase in charging temperature and field values. TSCs for samples charged at these temperatures with strong doping have been found to be characterized with an anomalous peak located at 90-115°C alongwith two normal peaks, one, on lower and the other, on higher temperature side of the above peak. Generally, the discharge current increases with increasing dopant concentration.

The observed TSC characteristics in the present case indicate that the TSCs are contributed by space charge, and the dopant molecules added in different concentrations modity them to a large extent. Iodine molecule, being strongly electronegative, is supposed to easily accepts electron from polymer molecule creating a hole on it, and thus to form charge-transfer complex (CTC).

The CTCs may reduce the barrier of the amorphous-crystalline interfaces and provide conducting paths for the charge carriers through these boundaries. The increase in peak currents with increased doping under identical charging field and temperature conditions supports the above role of CTCs.

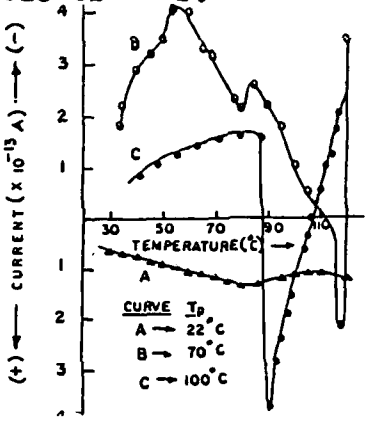

Fig.3. TSC curves for samples with strong doping polarized at different temperatures with 10 kV/cm.

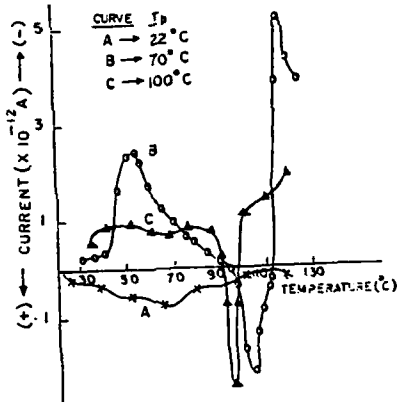

Fig.4. TSC curves for samples with strong doping polarized at different temperatures with 100 kV/cm.

Various results obtained in the present case indicate the existence of surface and bulk traps with distribution in energy. Assuming a discrete set of trapping levels with detrapping time constant for each level to be of standard Boltzmann form [2], it can easily be concluded that for any level to hold the charge during charging its detrapping time should be greater than the charging time. Thus, for charging at lower temperature trapping sites with small detrapping time and hence with low activation energy are occupied, however, with increasing charging temperature only energetically deeper traps with long detrapping time will be occupied. This explains the appearance of only a single peak around 70°C for room-temperature charged samples. This also accounts for the decrease of low-temperature peak and the corresponding increase of the peaks on higher temperature side with increasing charging temperature.

The broadness of the peak observed with room-temperature charged samples and also that of low-temperature peak of samples charged at higher temperatures, indicates a distribution of trapping levels for this peak. Further, the existence of energetically deeper traps is clearly evidenced by the appearance of the two peaks on higher temperature side for samples charged at elevated temperatures. Due to the increase in carrier mobility with temperature sufficient number of carriers move into the bulk of the sample to fill the deeper traps giving rise to high-temperature peaks for high temperature charging.

The anomalous TSCs observed under certain charging field and temperature conditions for strongly doped samples can be understood to be due to the injected homo space charge and partial blocking of the metal-polymer contact as suggested in the literature [3,4].

As the number of shallow traps with small detrapping time is considered to increase

with increasing dopant concentration, the space charged density will be relatively greater in room-temperature charged samples with strong doping than that in samples charged at this temperature with weaker doping. Rather easier release of carriers from these traps causes the high return rate of carriers to the injecting electrode resulting into partial blocking of the electrode which makes the observed current to be anomalous for such samples.

The transfer of charge from shallow to deeper traps for high-temperature charged samples reduces the return rate of carriers releasing from shallow traps, due to which the low-temperature peak for such samples has been found to be normal as opposed to the anomalous peak, located in this temperature range, for room-temperature charged samples with strong doping. However, the anomalous high-temperature charged samples may be attributed to the increase in carrier return rate releasing from deeper traps due to increased concentration of space charge in such traps. The normal peak appearing on higher temperature side of anomalous peak indicates the lesser amount of space in comparatively deeper traps.

REFERENCES

1. G.M. Sessler (Ed), Electrets (Springer Verlag, Berlin, 1980).
2. G.M. Sessler and J.E. West, J. Appl. Phys. 43, 922 (1972).
3. T. Mizutani, K. Kaneko and M. Ieda, Jpn. J. Appl. Phys. 20, 1443 (1981).
4. T. Mizutani, T. Oomura and M. Ieda, Jpn. J. Appl. Phys. 21, 1195 (1982).

ELECTRICAL CONDUCTION IN ACRYLIC ACID DOPED POLYSTYRENE

A.R.K. Murthy, R.S. Baghel, Ranjit Singh and S.C. Datt

Department of Postgraduate Studies and Research in Physics, Rani Durgavati Vishwavidyalaya, Jabalpur -482 001 (MP), India.

ABSTRACT

The electrical conductivity of acrylic acid (AA)-doped polystyrene films (about 100 μm thick) has been studied as a function of temperature in the range 20-85°C. Power-law dependence of current on voltage ($I \propto V^m$) has been observed at various temperatures. The value of the power has been found to decrease with increasing temperature and also with increasing dopant concentration. The conductivity was found to increase with increase in dopant concentration. These effects has been attributed to the formation of charge-transfer complexes (CTCs).

INTRODUCTION

The d.c. electrical conductivity study on polystyrene (PS) is of major interest not only from a technological viewpoint since PS is a good insulator used in electronics having very low dielectric losses, but also, because it permit a new insight into the control of the structure and properties of the material [1]. Considerable attention has been devoted to the problems of the change in electrical conduction in polymers due to intentional doping with low molecular compounds [2]. However, the mechanism of impurity effects on electrical conduction are not yet well understood.

This paper reports some of our findings on steady state electrical conduction in acrylic acid (AA)-doped polystyrene (PS) films.

EXPERIMENTAL

AA-doped PS films were grown from solutions of

CH2593-2/ 88/ 0000-0323$01.00 Copyright 1988 IEEE

10 g of commercially available atactic PS in well-stirred mixtures of AA and chemically pure benzene. Samples of about 100 μm thickness with two dopant concentrations, having 0.5 and 3 ml of AA in 99.5 and 97 ml of benzene, were used for the present work.

Steady state current was measured as a function of voltage at various fixed temperatures by increasing and also by decreasing the applied voltage in equal steps. The measurements were made on both sided vacuum aluminized samples.

RESULTS AND DISCUSSION

Typical current-voltage (I-V) curves, obtained with increasing and also with decreasing the voltage, for low and high dopant concentrations are shown in Figs. 1 and 2. It is seen that, at each temperature, the curves for increasing

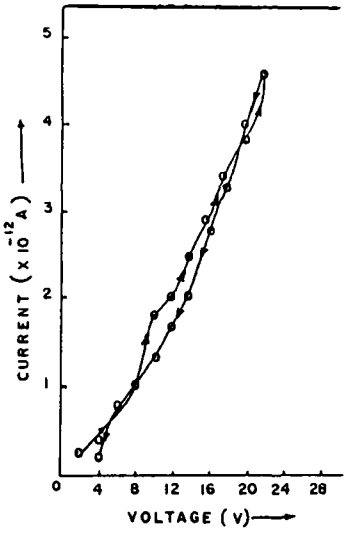

Fig.1. Variation of current with voltage at 20°C for samples doped to a low concentration.

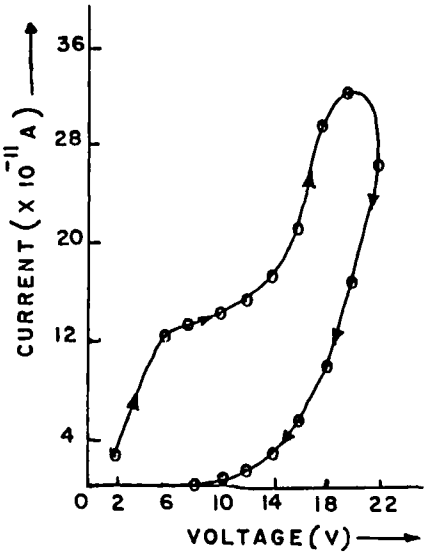

Fig.2. Variation of current with voltage at 65°C for samples doped to a high concentration.

and for decreasing the voltage are quite different and distinct showing the hysteresis effect. The arrows put over each curve indicate the manner in which the voltage was varied. On decreasing the voltage the current was found always to be less than its corresponding value during increasing cycle of voltage. This can be understood in terms of the charge injection from electrodes with subsequent trapping of injected charges in near surface region giving rise to homo space charge, and the sufficiently slow thermal release of charge carriers from the traps. Before the trapped space charge, injected at higher voltage, is thermally released, a space charge barrier is presented to the electrode which suppresses the entrance of charge carriers into the sample. Thus the observed current remains smaller than its

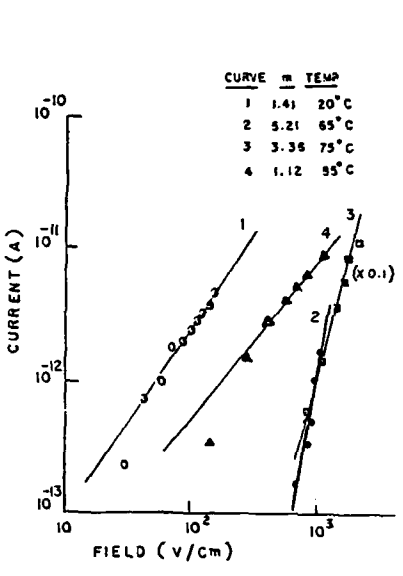

Fig.3. I-V characteristics at different temperatures for samples with low dopant concentration.

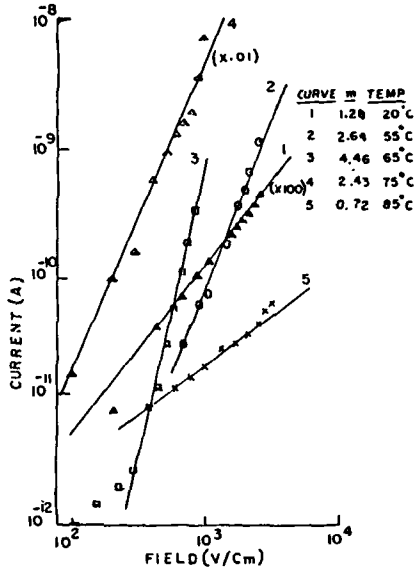

Fig.4. I-V characteristics at different temperatures for samples doped to a high concentration.

corresponding value when the voltage was increasing.

The I-V characteristics at various fixed temperatures for decreasing branch of voltage are shown in Figs.3 and 4. At each temperature the current has been observed to follow $I \propto V^m$ relationship, where m is a power. The value of m for each curve is shown in the figures. The relationship indicates that the conduction is space charge limited in PS samples with low as well as high dopant concentration.

In the temperature range above 65°C, the values of m have been found to decrease continually with increasing temperature. This is in accordance with the space charge limited conduction in the presence of exponential distribution of traps in energy for which the exponent m is equated with $(T_c/T)+1$, where T is the absolute temperature for the observation of current and T_c is the characteristic temperature [3] . However, it is not possible to specify the mechanism of electrical conduction in polymeric complex structures from analysis of voltage depence alone. In materials with high activation energies like PS, the charge carrier transport is believed to take place by hopping over energetic shallow band tail states with frequent trapping in energetic deeper traps which are responsible for the experimentally observed activation energies[4].

On increasing the dopant concentration there is an overall increase in the conductivity of the material. Moreover, the value of the exponent m decreases with increasing AA-doping at each temperature. This, in turn, implies that the thermal activation energy of the current decreases with increase in doping. These effects of AA may be explained as follows.

The dopant AA used in the present work is an α-β unsaturated carbonyl compound. It may be regarded as an electronegative acceptor due to the electron-attracting carbonyl group, present in it. Thus, AA molecules trapped in the chain

structure of PS matrix or present in interstitial positions can form charge-transfer complexes (CTCs). The CTCs, if formed, will provide conducting pathways through the amorphous regions of the polymer and would result in the enhancement of its conductivity. The observation that the current in PS does in fact increase with the increase in AA concentration supports the formation of CTC. Furthermore, the presence of CTCs causes a reduction in the barrier at the amorphous-crystalline interfaces of the polymer. The observation of the decrease in m values at various temperatures with increasing dopant concentration, implying the decrease in the activation energy of charge carriers responsible for conduction with the increase in AA concentration, confirms the formation of CTC when PS is doped with AA.

REFERENCES

1. V. Adamec and J.H. Calderwood, J. Phys. D: Appl. Phys. 11, 781 (1978).
2. P.C. Mahendru, N.L. Pathak, K. Jain and P. Mahendru, Phys. Stat. Sol. A 42, 403 (1977).
3. M.L. Lampert and P. Mark, Current Injection in Solids (Academic Press, New York, 1970).
4. G. Phister and H. Seher, Phys. Rev. B15, 2062 (1977).

PERSONNEL RADIATION DOSIMETRY USING ELECTRET IONISATION CHAMBERS

K. Doughty & I. Fleming,
School of Electronic Engineering Science,
University College of North Wales,
Dean Street,
BANGOR, Gwynedd, LL57 1UT,
United Kingdom.

Abstract

A new personnel dosimetry system has been developed to satisfy the protection needs of non-registered radiation workers in hospitals and nuclear installations. It consists of up to 200 special badges, each containing a charged electret film, and a microprocessor-controlled reader unit which calculates the cumulative radiation dose by measuring the surface potential of the electret non-invasively. A badge can be read frequently without destroying the cumulative information on dose.

Introduction

Recently, the theory of charge reduction in electret ionisation chambers (EIC) by x-rays and gamma-rays has been well developed [1]. Many designs of EIC have been produced and have been proposed as being suitable for personnel radiation dosimetry [2,3,4]. These devices have not yet gained the confidence of the end-users, not only because of the resistance of the market to new ideas but also because they generally lack a sophisticated electronic measuring system to read and record cumulative dose.

In the present work we have considered the advantages and the disadvantages of the EIC in detail and have performed a thorough market survey of the needs of potential users. This has enabled us to identify a particular market niche in which a customised EIC dosimetry system would be ideal and other dosimetry systems (such as film badge and TLD) would be unsuitable. We have developed a complete personnel dosimetry system based on the electret principle and herein

CH2593-2/ 88/ 0000-0328$01.00 Copyright 1988 IEEE

describe the technical features of the system.

Market Analysis

The major drawbacks of film badge and TLD badge systems were found to be:
1) the non-linear low energy response.
2) the loss of information on reading.
3) badges are routinely read only once a month.
4) the record systems are too formal for non-registered workers and for visitors.

EICs by their very nature do not suffer from these problems and, by careful design, we set out to produce a system which would compliment existing badge dosimetry systems. We therefore targetted those sectors which now rely on expensive battery-powered hand-held meters as well as those which have previously resisted the need to employ any form of dosimetry.

Our market survey identified the following:
1) Health Authorities - requiring a small-scale dosimetry system for improved detection of diagnostic x-rays and for monitoring staff, visitors & patients who "come and go" from supervised radiation areas.
2) Nuclear Industries - requiring a system to compliment statutory systems to improve day to day control and to monitor visitors and the work-force of contractors.
3) Research Laboratories - requiring monitoring system for visiting staff and scientists.

System Design

Our specification was for a system of EICs in the form of small badges which could be read by a member of the public using a purpose-built reader unit. The reader unit would contain all the necessary electronics to recognise a badge, and to read and record its dose. The badge would be read unopened and without handling the electret film. It would contain no electronic circuitry.

Reader Unit

Standard methods of measuring surface potential of electrets require access to the film surface and were unsuitable for our specification. Sonic

methods [4] were considered but were rejected due to inaccuracies associated with dimensional variations and the effects of environment.

Our solution was similar to the sonic method in that the EIC was employed to detect a mechanical oscillation. However, whilst other workers have used the magnitude of the a.c. response as an indication of the electret charge, we have used a null method in which a d.c. voltage is applied to the EIC until the a.c. effect disappears. This technique is independent of errors associated with the output level of the oscillator and other environmental factors. A block-diagram of the system is drawn in Figure 1.

The principle of operation is as follows, the mechanical oscillation of the top of the badge being performed by a miniature solenoid which is operated at 180Hz. This produces an a.c. signal across the load resistor which is measured with an electrometer circuit (see Figure 2).

Charge is now forced onto the bottom plate of the badge from the high-voltage amplifier which is driven by the ramp generator (an integrator). The effect of this charge is to lower the effective field in the EIC. This produces a reduced a.c. signal. Ultimately, if equal and opposite charges exist on the surface of the electret and on the bottom plate of the EIC then there will be zero electric field in the air gap in the EIC and there will be no a.c. signal generated in response to the vibration of the top plate. This is the null point and can be used to calculate the surface potential on the electret in a straighforward manner. If further charge is forced onto the bottom plate of the EIC an a.c. signal of opposite face will be detected in the electrometer circuit.

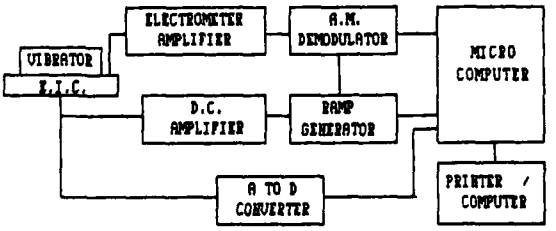

Figure 1. Block diagram of electronic charge measurement system.

EIC Design

It was necessary for the electret to be housed in a chamber which held the electret film in a position between two conducting faces which were insulated from each other. For the above measurement technique it was also essential that one of the badge faces could be vibrated using only a small force. Commercial pressures also indicated the need for a small simple design from materials which matched body tissue as closely as possible whilst being resistant to attack from chemicals and from the environment.

These criteria were satisfied in the design shown in Figure 3 in which the top and bottom of the chamber are each manufactured from conductive plastic. They are separated by a gasket of PVC which both provides the necessary insulation between the faces and acts as a spacer to create a specified air gap within the EIC (this is shown in Fig.4). The PVC sheet has been extended for attaching the badge to the user and for printing the bar-code which is used for identification. The electret material selected was FEP/TFE because of its excellent charge retention.

A computer spread-sheet was developed to incorporate the standard relationships for the reduction of charge in a EIC as a function of dose. For a given range of dose it is possible to calculate a whole family of dimensions which would satisfy these relationships. However, we decided that for ease of wearing, the badge should be small (less than 5mm. thick). We also considered the range of useful electric field to be 10000 to 40000 volts per metre.

Thus, we could, for an electret initially charged to 100 volts, produce a device with a dose range of 128mSv using electrets of 1.6mm. thickness in an air gap of 2.5mm. This range of dose may be too great for some applications and it may not be difficult to adjust the geometry and initial surface potential to deal with the user's requirement.

Similarly, the dose sensitivity is dependent on the resolution with which the surface potential can be measured. In general, levels of sensitivity down to 0.001mSv. may be required and this involves measuring voltage over 6 orders of magnitude to achieve the desired head-room.

Testing the System

We will not discuss the experimental verification of the EIC in this paper as this is now well established. Calibration trials and energy dependence tests are also under way on our system in an independent laboratory and will be published elsewhere. We have investigated repeatability & sensitivity of the new system of charge measurement and have been encouraged.

A series of electrets were supplied with different surface potentials in the range 20 to 200 volts. Our system was able to read the voltage repeatably (3 successive occasions) to 4 significant figures in each case. Furthermore, measurements of surface voltage were in agreement with other conventional methods proving that the measurement procedure does not affect the charge.

The above tests indicate that it is possible to produce a system with sensitivity of better than .01mSv. with a range of 100mSv. using a single type of electret and badge. The range may be extended in both ways by employing two badges or by incorporating two electrets of different thickness and/or surface charges in the EIC.

Conclusions

We have developed a novel electronic system for the measurement of surface potential on an electret film inside a sealed badge which has been designed as an electret ionisation chamber. The system may be employed, in certain circumstances, for personnel radiation dosimetry.

Acknowledgements

One of the authors (IF) was leader of a student Product Enterprise group which also included M. Crosby, J. Gittins, J. Goodman, S. Hinde, K. Karavadra, L. Newbigging & J. Stone. This 2 year project of design, development & market analysis was undertaken as part of their M. Eng. course.

References

[1] G. Pretzch, B. Dorschel & A. Leuschner:

Radiat. Prot. Dosim.; 4, 79 (1983)
[2] H. Bauser & W. Ronge:
Health Physics; 34, 97 (1978)
[3] J.R. Cameron & S. Mascarenas:
Proc. 6th. Conf. on Dosimetry (1980)
[4] M. Ikeya & T. Miki:
Health Physics; 39, 797 (1980)
[5] R.P.C. Product Enterprise Final Report:
Univ. College of Wales, Bangor (1988)

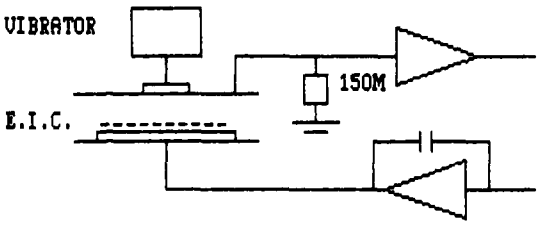

Figure 2. Basic charge measurement circuit.

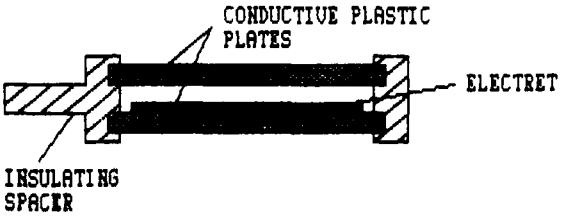

Figure 3. Plastic Electret Ionisation Chamber (section).

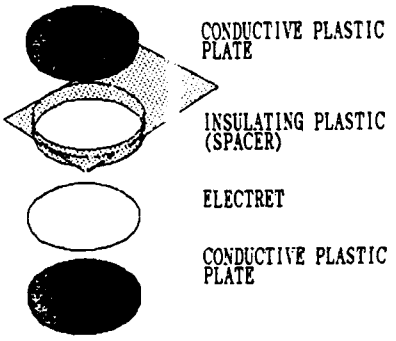

Figure 4. Exploded view of E.I.C.

ELECTRO-OPTICAL BEHAVIOUR OF FERROELECTRIC LIQUID CRYSTAL (FLC) MIXTURES

H.-R. Dübal, C. Escher, and D. Ohlendorf

HOECHST AG, Postfach 800320, D-6230 Frankfurt 80, F.R.G.

Abstract: Surface stabilised ferroelectric liquid crystal displays are sensitive to ac electric fields. Their smectic layer structure and thus their texture is irreversibly changed by exceeding a critical ac field amplitude that depends on the frequency, the temperature, and some material properties. In the altered textures the same FLC material exhibits strikingly different electro-optical properties.

INTRODUCTION

The surface stabilised ferroelectric liquid crystal display (SSFLC) [1,2] is a promising technique for applications which require video frame rate and high spatial resolution, such as TV and computer monitors. It is a highly multiplexable flat and thin matrix display with low driving voltage, power consumption, and weight. In combination with the fabrication technique and the driving electronics the material parameters [3] determine the static and dynamic director configuration and, therefore, the electro-optical behaviour of the display. In our paper, we describe another important parameter which is the type of the FLC texture that is induced by the application of ac electric fields.

AC FIELD DEPENDENT TEXTURES

We have performed the experiments with our FLC mixtures FELIX-001, FELIX-002, and FELIX-004 in polyimide-coated cells with thicknesses between 1.5 µm and 3.3 µm. For FELIX-001, we compile some material parameters in table 1.

CH2593-2/ 88/ 0000-0334$01.00 Copyright 1988 IEEE

Fig. 1a: texture I
(virgin)

Fig. 1b: texture II
(roof)

Fig. 1c: texture III
(stripes)

Fig. 1d: texture IV
(grooves)

Table 1: Material parameters of FELIX-001 (physical data at 20 °C)

Phases: X - 7 SmC* 79 S_A* 83 N* 99 I

P_S = 7.5 nC/cm^2	$\Delta\varepsilon$ = - 0.8
γ_φ (c) = 64 mPas	Δ n = 0.126
$t_{0,90}$ = 205 µs	

critical field (200 µs, 1.5 µm cell, virgin texture) = 6 V/µm

The cells are filled by capillary action and oriented homogeneously by cooling from the isotropic phase down to the SmC* phase. The so obtained smectic layer structure leads to a texture as in Fig. 1a showing the so-called zig-zag disclinations [4] which are compatible with the chevron local layer structure model [5]. Starting from this texture (I) we apply a sine-wave of various field amplitudes and frequencies over a period of one minute and inspect the texture microscopically.

As an example, let us consider the texture changes of FELIX-001 at 60 °C. By exceeding a field of 6 V/µm at 10 Hz and 60 °C, the virgin texture transforms into texture II, as in Figure 1 b [6], exhibiting "roof-shaped" disclinations. At 13 V/µm, stripes occur (texture III, Fig. 1c) parallel to the rubbing direction. Finally, by exceeding 20 V/µm we obtain the texture IV, characterised by the appearance of grooves oriented obliquely to the rubbing direction (Fig. 1d). By performing such experiments for frequencies up to 20 kHz we finally end up with a field-frequency diagram as in Figure 2.

From these and other measurements, we conclude, that the sensitivity of SSFLC-devices increases with increasing temperature (see Fig. 2). Comparative experiments with other mixtures show a strong dependence on the spontaneous polarisation. The high P_S-mixture FELIX-002 is much more sensitive to ac-fields. The practical relevance of our findings comes from the fact, that the electro-optical properties are strongly influenced by the ac-field treatment. For a pulse width of 200 µs, the latching field for FELIX-001 is 6 V/µm (1.5 µm cell thickness) in the virginal texture whereas we obtain 15 V/µm in texture II.

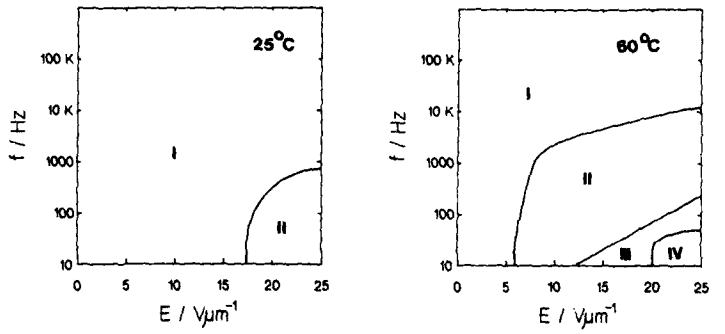

Figure 2: Field-frequency diagram for FELIX-001 (a) at 25 °C (b) at 60 °C. The roman numbers correspond to Figure 1

Schiller et al. [7] and Sato et al. [8] have reported similar structural changes in achiral and chiral SmC* phases, respectively. Thus, the ac-field dependent textures seem to be a rather universal phenomenon in SSFLC displays. The increasing optical response time, the increasing effective optical tilt angle and contrast and the stepwise disappearance of the zig-zag disclination lines during the transition from texture I to IV support our interpretation of a transition from a virgin tilted layer structure (e.g. a chevron structure) to an inhomogeneous geometry with upright layers (local bookshelf geometry), while II and III are intermediate states.

FOURIER ANALYSIS OF DRIVING SCHEMES

To elucidate the significance of our findings for a practical matrix display let us consider Figure 3(a), which shows an example of a pulse sequence used to simulate the voltage that is applied to a SSFLC pixel.

From the three voltage levels (select, halfselect, and non-select) the non-select pulses are the most important ones and lead to the prominent peaks in the spectrum occuring at the relatively high frequencies ν, 3ν, 5ν, ... with ν = 1/400 μs = 2.5 kHz in our example. For video applications ν is even in the order of 10 kHz and from Figure 2 it is clear, that such a high frequency is rather inactive in altering the texture.

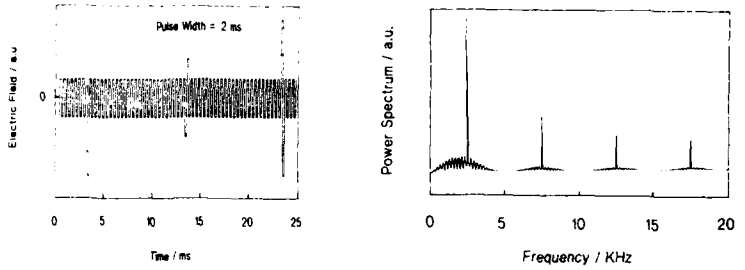

Figure 3(a): Driving waveform (pulse width 200 µs)
(b) Power spectrum, calculated by numerical Fourier transform of 3(a)

However, particularly at higher temperature and for large spontaneous polarisation mixtures, the low frequency part of the driving signal might give rise to texture problems and slow optical response. A square wave of the same frequency and amplitude as a sine wave is more active due to the higher effective voltage applied to the cell.

From our field frequency diagram we conclude that FELIX-001 is very resistant against ac-fields even at higher operation temperature and therefore texture changes are unlikely to occur with this mixture under practical driving conditions.

REFERENCES

1. R.B. Meyer, L. Liébert, L. Strzlecki, and P. Keller; J. Phys. (Paris) Lett. 36, L-69 (1975)
2. N.A. Clark and S.T. Lagerwall; Appl. Phys. Lett. 36, 899 (1980)
3. C. Escher; Kontakte 2, 3 (1986)
4. Y. Ouchi, H. Takano, H. Takezoe, and A. Fukuda; Jap. J. Appl. Phys. 27, 1 (1988)
5. T.P. Rieker, N.A. Clark, G.S. Smith, D.S. Parmar, E.B. Sirota, and C.S. Safinya; Phys. Rev. Lett. 59, 2658 (1987)
6. The photographs are actually taken at 70 °C for FELIX-004 under a polarising microscope (crossed polarisers) FELIX-001 and FELIX-002 show textures of the same kind.
7. P. Schiller, G. Pelze, and D. Demus; Liquid Crystals 2, 21 (1987)
8. Y. Sato, T. Tanaka, M. Nagata, H. Takeshita, and S. Morozumi; Proceedings of the 6th International Research Conference, Tokyo 1986, page 348.

DIELECTRIC α RELAXATION STUDY OF POLYETHYLENE BY THERMALLY STIMULATED DEPOLARIZATION CURRENTS AND THERMAL SAMPLING.

J.M.Meseguer Dueñas*;R.Diaz Calleja;J.L.Gómez Ribelles

Laboratorio de Termodinámica y Fisicoquímica.
(*)Departamento de Física Aplicada.
Universidad Politécnica de Valencia.
bop.:22012. 46071 Valencia. Spain.

ABSTRACT:

The dielectric α relaxation zone of branched low density and linear high density Polyethylene has been studied by thermally stimulated depolarization currents. Tow relaxations, α and α', have been found, with maxima in the temperature range between 270K and 300K. Thermal sampling measurements showed that the α' relaxation is distributed in both polyethylenes, and appears at higher temperatures and with lower activation energy in the branched polyethylene than in the linear one. The activation energy of the α relaxation is not distributed, appearing at the same temperature in both polyethylenes. The behaviour of the α' relaxation agrees with the hypothesis of a molecular origin in the crystalline-amorphous interface of polyethylenes, the α relaxation being due to molecular motions whithin the crystalline phase.

INTRODUCTION:

The aim of this work is to characterize the α dielectric relaxation of Polyethylene(PE) by means of thermally stimulated depolarization currents(TSDC) an thermal sampling(TS) techniques. Two commercial Dow PEs were used: a low density branched PE710 and a high density linear PE10062. The samples were prepared by melting at a temperature 30K above the melting temperature(T_m), determined as the maximun of the DSC scan of each PE. The samples were annealed at T_m for an hour and then quenched to room temperature. The TSDC and TS techniques have been explained in previous works[1-3]. The characteristic parameters of the TSDC

CH2593-2/ 88/ 0000-0339$01.00 Copyright 1988 IEEE

experiments were: Polarization temperature 300K; Polarization time 10 minutes (considered enough to attain the saturation of the sample); cooling rate 4K/min; Shortcircuit temperature 113K; heating rate 2K/min; Polarization field 5KV/mm in PE10062 sample and 1KV/mm in PE710 sample. The TS experiments were carried out with polarization windows of 5K. The polarization field was 1KV/mm in both polymers. The samples were metallized with coloidal silver. In the PE710 samples maximun temperature of these experiments was 305K so avoiding changes in the crystalline morphology of the samples during the experiment.

The polarizability of PE samples is very variable since it is mainly due to polar groups and the presence of impurities; so the intensity of TSDC spectrum of different samples is not strictly comparable.

TSDC AND TS RESULTS:

The TSDC spectrum of both PEs is represented in figure 1 in the temperature range corresponding to the dielectric α relaxation zone. The spectrum shows the existence of three peaks called hereafter α', α and ρ in order of increasing temperatures. The temperature of the maximun and the equivalent alternative frequency, which may be calculated from the TSDC measurements, indicate that the two first relaxations correspond to the α' and α relaxations determined by alternative dielectric measurements, reported in the literature.

The ρ peak, due to the space charges present in the sample, is not very repetitive but always appears at a temperatures higher than the other two relaxations.

In the PE10062 sample, the temperature of the α' maximun appears at 297K and overlaps at the high temperature side with the ρ peak. In the PE710 sample both, the α' and α maxima, have a similar intensity appearing at 282 and 296K respectively.

Thermal sampling experiments were carried out with polarization windows covering the range of temperatures between 250 and 325K. The results in both PEs are similar. Figure 2 shows the depolarization curves measured in PE710. The arrows in each curve indicate the polarization temperature. It is interesting to note that in several depolarization curves there appear two maxima; in these cases the two peaks were analitically separed in order to calculate the characterystics

parameters of each peak. Figure 3 shows the temperature of the maximun of the polarization peaks against its polarization temperature. In both polymers there appears a non-distributed relaxation with maximun temperature independent of the polarization temperature. In both cases the temperature of this relaxation is coincident with that of the α relaxation of TSDC measurements. At temperatures below this relaxation the points corresponding to the different polarization windows fall on a straight line covering the range of temperatures of the TSDC α' relaxation.

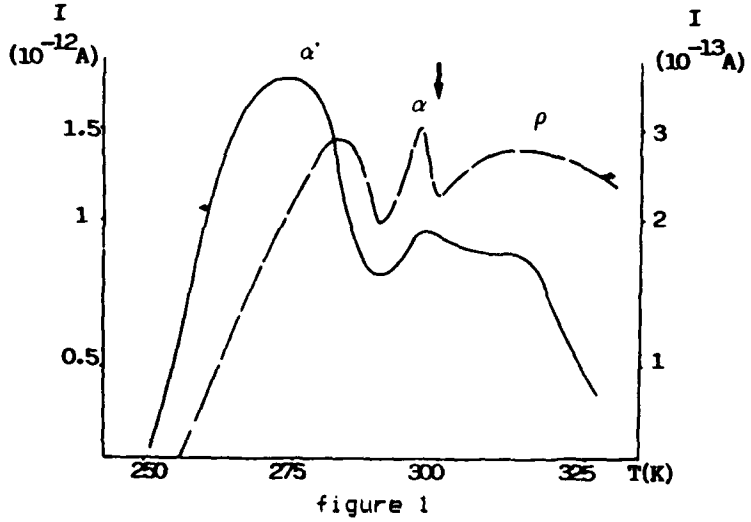

figure 1
TSDC results in PE10062(——) and PE710(— —)

The depolarization peaks corresponding to the α relaxation have similar activation energy (figure 4) with maximun value of 42Kcal/mol and a narrow range of variation due to the overlapping with the α' and ∫ relaxation zones.The peaks corresponding to the α relaxation have a higher activation energy in PE10062 (about 25Kcal/mol) than in the PE710 (about 12Kcal/mol) and the maximun activation energy appears, in a plot against polarization temperature, about 30K higher for the last polymer than for the linear PE.

DISCUSSION:

The α relaxation zone is generally ascribed to

molecular motions, in the crystalline phase of PE[4-6].

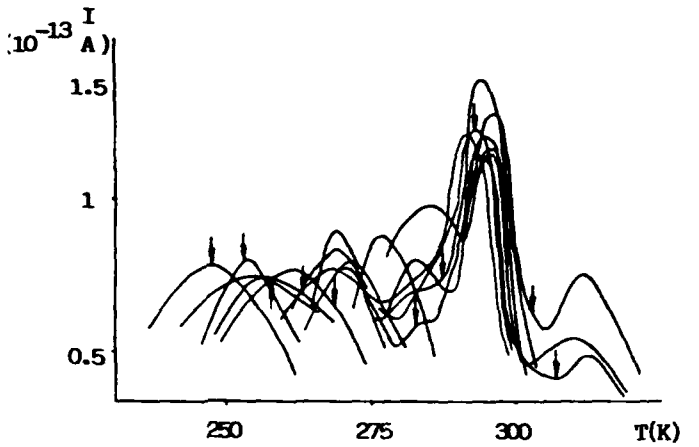

figure 2
TS measurements in PE710

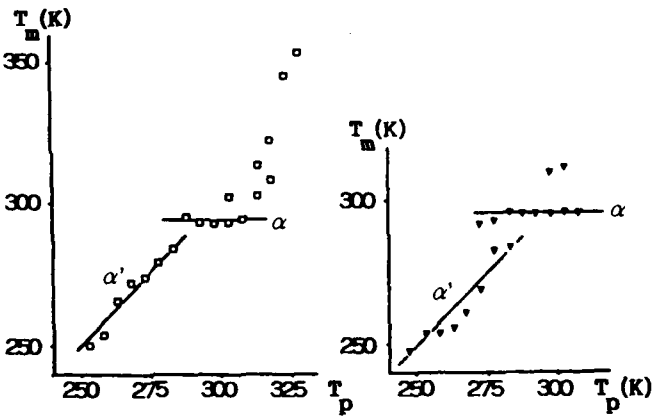

figure 3
Temperature of the maximun against polarization temperature of TS measurements in PE10062(□) and PE710(▼)

The α peak is produced by motions whithin the crystalline phase[7,8] and the α' is related to motions in the amorphous-crystalline interphase on the surface of the crystals or perhaps to motions in imperfect crystals[9]. The crystalline morphology of linear and

branched PE is very different as concerne the distribution of crystalline sizes[9].

In the results reported in this work the parameters characterizing the α relaxation are equal in both PE: the maximun appears in TSDC at 296÷297K and with activation energy in TS about 42Kcal/mol. Thus supporting the idea of an origin inside the most perfect crystals sice they sould be similar in both polymers The α' relaxation appears at 275K in PE10062 and 282K in Pe710 in TSDC and the latter has smaller activation energy. If the molecular origin for this relaxation given in the bibliografy is accepted, the important differences found in the dielectric relaxation spectrum in the α' zone must be attributed to the differences in the crystalline morphology between the two polymers.

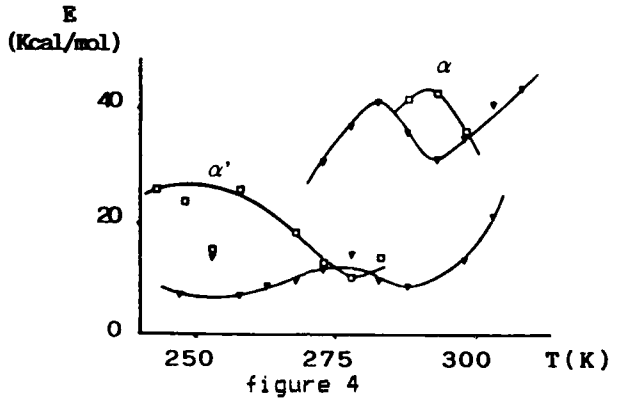

figure 4

Activation energy v.s. polarization temperature of the TS measurements in PE10062(□) and PE710(▼)

REFERENCES:

1-Van turnhout J.: Thesis. Leiden(1972)
2-Bucci C., Fieschi R.: Phys.Rev.Letters. 12,16(1964)
3-Diaz R.,Meseguer J.M.:XX Bien.RSEFQ.Castellón(1984)
4-Ascraft R.H.,Boyd R.H.:J.Polym.Phys.Ed.:14,2133(1976)
5-Kakizaki M., Hideshima T.: Rep.Prog.Polym.Phys. 14,447(1971)
6-Ishida Y., Yamafuyi K.: Koll.Z.Z.Polym. 202,26(1965)
7-Ribes A.: Thesis. Valencia(1986)
8-Kakizaki M., Kakudate.: J.Polym.Sci. Polym.Phys.Ed. 23,809(1985)
9-Ribes A., Diaz R.: J.Appl.Polym.Sci. 34,2819(1987)

EFFECT OF ELECTRODE COATING ON LEAKAGE CURRENT AND SURFACE FLASHOVER STRENGTH IN POLYMERS

Fathi M.H. Youssef and Taher D. Eish

Electrical Engineering Dept., Faculty of Engineering, Mansoura University, Mansoura; Egypt.

ABSTRACT.

The influence of electrode coating on the leakage current of three polymer insulating materials, namely, polystrene (PS), polyvinyl chloride (PVC) and polymethylmethacrylate (PMMA) is investigated. The insulating materials have been subjected to alternating voltage (50 Hz) under inhomogeneous field conditions (rod-plate electrode system) . Thereby, experimental investigations on the effect of specimen thickness on leakage current and flashover voltage have been carried out under bare electrode conditions as well as under coated electrode conditions. The results illustrating the effect of electrode coating on leakage current and surface flashover voltage are presented and discussed in this paper.

INTRODUCTION.

Insulating polymers are of good electrical properties (high electrical strength, high resistivity, and low dielectric losses) in addition to good mechanical properties, and they are recently widely used as electrical insulators [1]. Moreover, some insulating polymers show excellent charge storage capabilities and have received wide applications such as electrets [2]. In order to improve polymeric insulators or to develop the practical applications mentioned above, it is necessary to understand fundamental properties of polymers such as electrical conduction and flashover. This paper presents results of investigations of flashover and leakage current in three polymer insulating materials. The effect of electrode coating by electrical insulating materials, just like varnish, are also reported.

CH2593-2/ 88/ 0000-0344$01.00 Copyright 1988 IEEE

EXPERIMENTAL SET UP.

The experimental set up used is composed from a rod-plate electrode system mounted inside a PVC vessel. The rod electrode is formed from solid steel of 2 mm diameter and the earthed plate electrode is 50 mm in diameter. The specimens are square shaped with 100 mm sides. Three types of polymeric materials are investigated here to study the flashover voltage and leakage current characteristics under different operating conditions. The materials under investigation are PS, PVC and PMMA.

The high AC voltage is obtained from a 220 V/80 kV, 8 kVA test transformer. The output voltage is measured by means of an electrostatic voltmeter in conjunction with resistive potential divider arranged in such away to give a direct reading (r.m.s.). The accuracy of voltage measurement is $\pm$ 2%. The AC voltage is applied to the rod electrode and the leakage current is measured at the plate electrode means of an electrometer. After applying the voltage, the readings of the leakage currents are taken after dyring away of any transient currents. Each flashover voltage value or leakage current value reported in this work represent the average value of ten readings.

The coating of the electrodes by electrical insulating varnish has been undertaken by means of a hand brush. The brushing of the liquid varnish on the electrodes has been repeated to give an approximately 0.1 mm smooth, uniform tickness of the varnish layer.

RESULTS AND DISCUSSION.

The variation of AC flashover voltage values with insulating material thickness, for different polymer materials, is illustrated in Fig.1. for both cases bare and warnish coated electrodes. In general, the flashover voltage increases with increasing the specimen thickness. This is expected, since with increasing the specimen thickness a decrease of the electric field strength for the same voltage level results and meanwhile an increase of the discharge path occurs. It is seen also from the figure, that the flashover voltage values under coated electrodes are higher than those under bare electrodes. This fact can be explained through the resulting elongation to the flashover path caused by the

insulating coating material. On the otherhand, the coating suppresses the generation of free charges on the electrodes [3], which results in a higher flashover strength for the same arrangement.

Fig.2 shows the relationship between leakage current (for different polymer insulating materials of an 8 mm thickness) and the applied AC voltage under bare electrode conditions. It is generally noticed, that the leakage current increases as the applied voltage increases. These results are in line with [4] and can be laid back to the fact, that the leakage current is mainly a capacitive one, which can also be noticed from the linearity of the curves in the figure.

To study the effect of polymer material thickness on the leakage current of polymer materials, investigations have been carried out under constant 20 kV AC voltage stress for different material thickness for both cases of bare electrodes and warnish coated electrodes. The results of these investigations are illustrated in Fig.3. It is generally noticed, that the leakage current decreases as the specimen thickness increases. This is expected, since the capacitance of the arrangement decreases with increasing the specimen thickness. Accordingly, the leakage current, which is mainly a capacitive one decreases as the specimen thickness increases.

It is also noticed from Fig.3 that the leakage current values under coated electrodes are higher than the corresponding values under bare electrode conditions. This may be attributed by the increase of the capacitance value of the arrangement due to the coating. The insulating coating film, which possesses a higher permittivity than that of air, enlarges the capacitance of the arrangement and consequently causes an increase in the leakage current.

CONCLUSION.

The main flashover voltage and leakage current characteristics of three different polymeric materials, namely PS, PMMA and PVC, are introduced in this paper. It has been found, that the flashover voltage increases in general as the insulating material thickness increases. On the contrary, the leakage current decreases in general with the increase of the material thickness. A remarkable effect of electrode coating on the flashover voltage as well as on the leakage current is

demonstrated in this paper. The coating of electrodes is found to increase the flashover voltage withstanding capability of the arrangement remarkably, although the leakage current thereby noticeably increases.

REFERENCES.

[1] M. Ieda. IEEE Trans. Elec. Ins. Vol. EI-15, pp. 206-244, 1980.

[2] G. M. Sessler: "Electrets", Springer-Verlag, Berlin, 1980.

[3] F. Endo, T. Yamagiwa, T. Ishikawa, and M. Hosokawa, IEEE, Vol. PWRD-1, No. 1, January, pp. 58-65, 1986.

[4] T.D. Eish, M.H. Abdel-Rahman, F.M.H. Youssef and H. A. El-Behairy: To appear in (IEE), 5th Intern. Conference on Dielectric Materials Measurements and Applications, June 27-30, 1988.

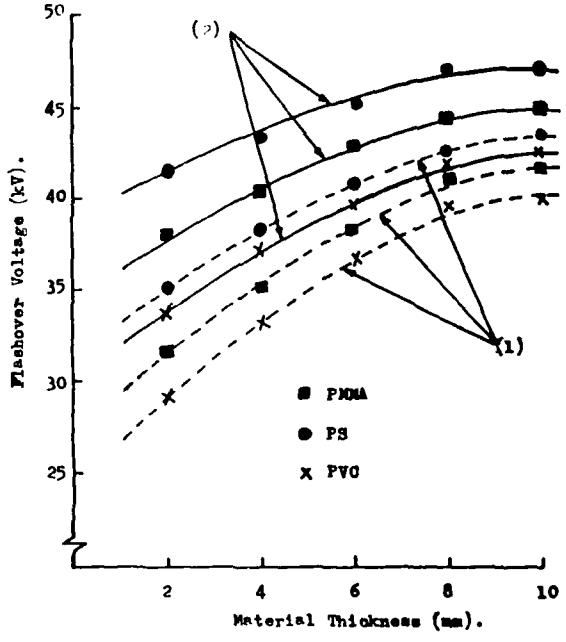

Fig. 1: Variation of AC flashover voltage with material thickness for various polymers.
(1) Bare electrodes.
(2) With varnish coated electrodes.

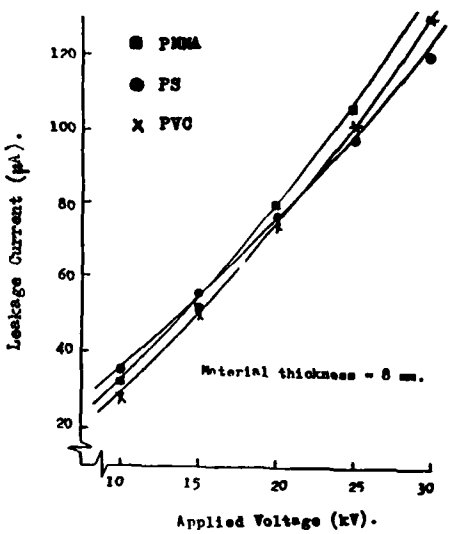

Fig. 2: Variation of leakage current with applied voltage for various polymers (under clean electrode conditions).

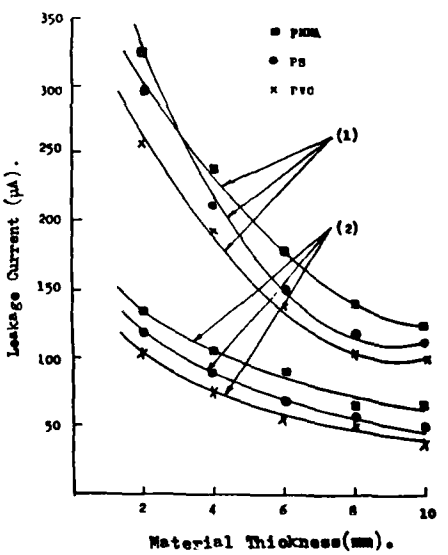

Fig. 3: Variation of leakage current with material thickness under applied AC voltage of 20 kv.
(1) with varnish coated electrodes.
(2) dare electrodes.

SURFACE FLASHOVER AND SURFACE DETERIORATION OF POLYMER INSULATIONS IN VACUUM

Taher D. Eish and Fathi M.H. Youssef

Electrical Engineering Dept., Faculty of Engineering, Mansoura University, Mansoura, Egypt.

ABSTRACT.

This paper introduces the results of investigations carried out to record the various factors affecting the surface flashover strength across perspex (PMMA) and teflon (TFP) insulators in vacuum. The factors studied include the dependance of flashover AC and DC voltage stresses on sample length and field conditions. The influence of the number of sequential flashovers on the magintude of flashover voltage and on the surface deterioration of the polymer samples in vacuum is also introduced.

INTRODUCTION.

The effect of deterioration and conditioning of the insulator surface and electrodes is particularly critical. Deterioration and conditioning can aries due to relatively low energy partial discharges on the insulator surface or to high energy discharges between the electrodes. These events can affect gas pressure near the the insulator surface, the insulator surface resistivity, secondary emission coefficient, and topograph, the electrode electrom emission characteristics or the triple junction geometry and emission characteristics [1,2]. The presence of deterioration events implies that the physical parameters of the insulator system change as a function of time. The changing conditions should be considered when evaluating the system performance. In this paper observations concerning the dependence of flashover characteristics on insulator length, on sequential flashover number, on uniform and non-uniform field conditions and on deterioration of the polymer samples are introduced.

EXPERIMENTAL TECHNIQUES.

Two types of electrode configurations are used to simulate uniform and non-uniform fields. The uniform field is attained

CH2593-2/ 88/ 0000-0349$01.00 Copyright 1988 IEEE

by using two parallel copper plate electrodes of 50 mm diameter and radius of curvature at the edges of the electrodes of 2 mm. The non-uniform field is obtained by using a rod-plate arrangement with a steel rod electrode of 2 mm diameter and copper plate electrode of 30 mm diameter.

The insulator samples are solid cylinders of 50 mm diameter and different thickness, namely, 10, 20, 30 and 40 mm. The polymeric materials under investigation are PMMA and TFP. The sample is then placed in a PVC vessel, which is then evacuated by a cryogenic absorption pump to an ulitinate pressure of 0.1 Pa. The AC voltage required for investigations is obtained by means of a 220 V/ 80 kV, 8 kVA testing transformer. The DC voltage is obtained by means of the same transformer connected in series with rectifier and smoothing capacitors. Both AC and DC voltages are measured by means of electrostatic voltmeter in conjunction with a resistive divider. The accuracy of voltage measurment is $\pm$ 2%. Each flashover voltage reported is the average of ten readings.

The rate of decrease of the successive flashover voltages was used as an indication of the rate of deterioration of the insulator surface. Later, the surfaces of the samples were examined by using an electron microscope.

RESULTS AND DISCUSSION.

The flashover AC and DC voltages have been found to increase with the length of the specimen under non-uniform field conditions as shown in Fig. 1. However, the rate of increase is found to be different for each type of applied voltage and also for each material. The flashover voltage, as a function of insulator length, can be represented approximately by the product of the square root of the insulator length and a constant, the value of which depends on the type of insulator and the type of test voltage used. Under all tests, the flashover voltage for PMMA is higher than that of TFP. The flashover voltage characteristics obtained (Fig. 1) show that the negative polarity and positive polarity of DC flashover values exceed the AC values and that the DC values for PMMA always exceed the corresponding values for TFP. It is also seen from Fig. 1 that the flashover voltage for negative polarity is always greater than those for positive polarity.

It has been also observed that ultimate surface insulation

strength depends upon the type and magnitude of the conditioning voltage used. Conditioning using AC voltage is more effective. It is likely that conditioning leads to more rapid removal of impurities, concentrated on the insulator surface. Prebreakdown discharges and flashovers may also modify the secondary electron emission from the dielectric surface [3]. This has a strong influence on the flashover voltage. The effect of uniform and non-uniform field conditions on flashover voltage as a function of sample length has also been determined. Fig. 2 shows the flashover voltage along the TFP insulator as a function of the sample length. The Figure shows that for all investigated sample lengths, the flashover voltage under non-uniform field is higher than that of uniform field. These results are in line with [4] and can be laid back to the fact, that the factor is probably associated with peculiarities of the breakdown preparatory stage in the vacuum gap. On the other hand, it should be noted that the flashover length under non-uniform field condition is greater than that under uniform conditions.

The flashover voltage of a given sample is found to increase initially by sequential conditional flashovers (Fig.3). After 10 to 30 flashovers, the flashover voltage remains essentially constant. However, after 35 flashovers, the flashover voltage is found to decrease due to surface deterioration. Examination of samples implied that the decrease of flashover voltage is a result of conducting tracks formed on the dielectric surface. The test samples, after flashovers, are found to have tree-type paths (tracks) on the surfaces. The tracks have been examined by means of an electron microscope to evaluate the shape and rate of growth. It has been observed that the surface damage is in the form of branching, tree like paths eroded into the insulator. The tree begin at the cathode and transfer insulator material to the anode. similar channel behavior has been also observed for AC excitation. Predominate channel ultimately developed from the cathode has an appearance similar to those observed for DC excitation.

CONCLUSIONS.

The factors affecting the surface flashover strength across perspex and Teflon insulating materials, in vacuum, are presented and discussed in this paper. Under an ultimate pressure of 0.1 Pa., it has been found that the flashover voltage for perspex is always higher than that of teflon material. Thereby, the DC flashover voltage values are

higher than those of AC values, whereby the negative polarity flashover voltage is higher than that of the positive polarity. The flashover voltage increases in general with increased sample length. Thereby, the flashover voltage values under non-uniform fields are found to be higher than those under uniform field conditions. The flashover voltage decreases first after about 35 flashovers. Such a sequential conditional number of flashover is necessary to cause tree like eroded paths on the insulating surface and thus leading to a remarkable decrease of flashover voltage value.

REFERENCES.

[1] C.H. DeTourreil and K.D. Srivastava: IEEE Trans. Elec. Ins., Vol. EI-8, pp. 17-21, 1973.

[2] R. Lee, T.S. Sudarshan, J.E. Thompson and G.R. Nagabhushana: ibid., Vol. EI-18, pp. 280-286, 1983.

[3] S. Grzybowski, E. Kuffel, and J.P.C. McMath: ibid, Vol. EI-7, pp. 180-185, 1972.

[4] I.I. Kaljatsky, G.M. Kassirov, and F.G. Sekisov: ibid, Vol. EI-20, pp. 701-703, 1985.

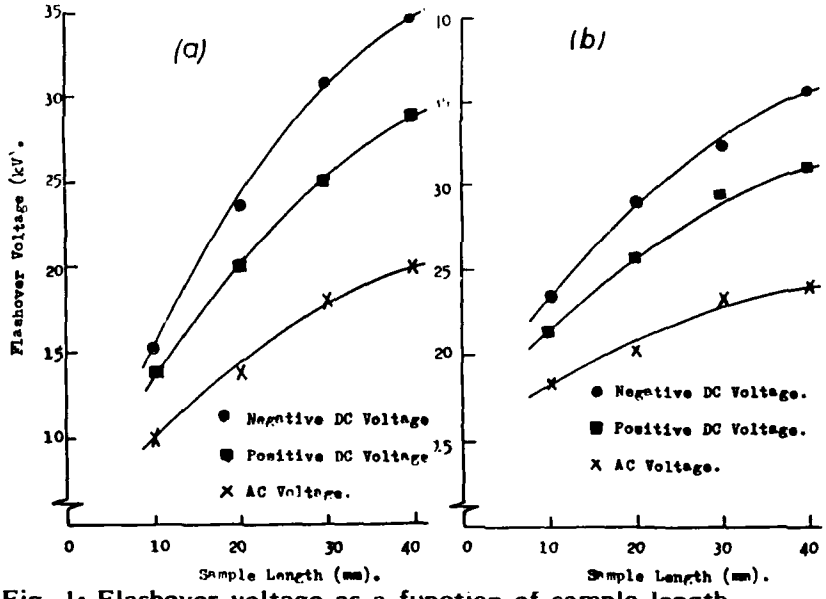

Fig. 1: Flashover voltage as a function of sample length under non-uniform field.
(a) For TFP Sample.
(b) For PMMA Sample.

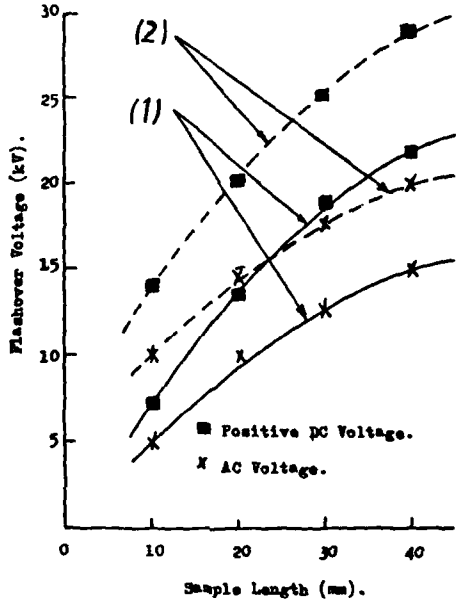

Fig. 2: Flashover voltage as a function of TFP Sample length
(1) Uniform field
(2) Non-unform field.

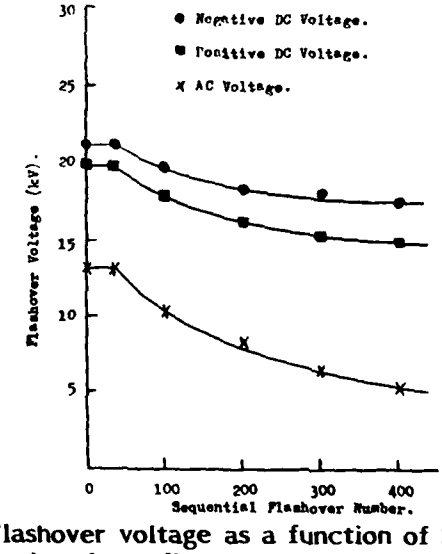

Fig. 3: Flashover voltage as a function of Sequential flashover number for teflon under non-uniform field and Samples 30 mm thick

FACTORS AFFECTING CREEPAGE AND CLEARANCE DISTANCES OF POLYMER INSULATORS IN COASTAL AND MARINE ELECTRICAL EQUIPMENT

S. S. El-Dessouky
Elect. Eng. Dept.
Faculty of Eng.
Suez Canal Univ.
Port Said; Egypt

Fathi M. H. Youssef
Elect. Eng. Dept.
Faculty of Eng.
Mansoura Univ.
Mansoura; Egypt

ABSTRACT.

The smaller creepage distances in unfavorable service conditions may lead, in marine electrical equipment, to tracking and cause short-circuits between parts having different potentials. Too big distances result in uneconomical dimensions of equipment. In this paper, the influence of ionic liquid contaminants upon tracking behaviour of four typical polymeric insulants is measured and recorded in terms of electrode seperation and voltage. The insulants treated in this work are Bakelite, Polyvinyl chloride (PVC), polymethyl methacrylate (PMMA) and Polystrene (PS). Investigations to relate time-to-track and distance between electrodes are introduced.

INTRODUCTION.

Creepage distances have for a long time been a problem in marine electrical equipment [1]. They are critically influenced by external conditions as well as by properties of the insulation itself. This makes the choice of optimum creepage distance to be difficult.

Acreepage distance is specified to limit leakage currents passing through surface contaminants and thus prevent tracking. Tracking is initiated by minute sparks or arcs resulting from the interruption of leakage current across the surface of the insulation. The degree of resistance to tracking of a material depends upon its chemical nature and the manner in which it breaks down when subjected to very high temperatures of the small surface arcs [2].

The present work introduces a study to the creepage of some

CH2593-2/ 88/ 0000-0354$01.00 Copyright 1988 IEEE

of the widely used polymeric materials at up to 440 volts AC (ships power operating voltage). Thereby, investigations to relate time-to-track and distance between electrodes as well as time-to-track and flashover voltage are introduced.

TEST PROCEDURE.

Tests have been carried out by means of an arrangement as illustrated in Fig. 1. This arrangement makes it possible to seperate stainless steel electrodes having the same shape as those used in the IEC standard for the measurement of tracking resistance [3].

Test voltages up to 600 V, 50 Hz have been applied between electrodes by means of using a step up transformer, whose input can be varied through a variac. The short-circuit current has been limited to a value of 1.25 A.

The test insulating samples were square shaped of 5 cm aside. The PVC and PMMA specimens were of 3mm thickness PS and bakelite specimens were of only 1mm thickness. Therefore, by testing these materials 3 samples were always taken together to ensure a thickness of 3mm.

Wetting the surface between the electrodes have been undertaken by means of drops of the test solution at intervals of 35 s . The drops have been let to fall centrally from a 30 mm height. A hypodermic needle has been found to be suitable for a droping device.

Two test solutions have been used in this work;

* Solution A : 0.1 ± 0.002% by mass ammonium chloride (NH_4Ch) in distilled water. This is the main test solution as specified by the IEC standards.
** Solution B: 0.1 ± 0.002% by sodium chloride (Nacl) in distilled water. This solution is used in this work for comparative Purposes.

RESULTS AND DISCUSSION.

Fig. 2. illustrates the time-to-track behaviour, for all 4 polymer materials under discussion, versus the applied AC voltage. The spacing between the electrodes is thereby hold constant at 4mm and the contaminant solution used is solution

A. As clearly seen from the figure, the bakelite insulating material is that of the worst tracking behaviour followed by the polystrene insulating material as the second worst one. On the other hand, the PVC insulating material has been found to have the best tracking behaviour followed by the PMMA insulating material. This results can be generally explained through the main characteristics of these materials [4].

Both bakelite and polystrene materials have the disadvantage of being of law Martens temperature. They have poor arc resistance and tendency to track, leaving carbonized traces on the surface. The knee point existing in both curves of Ba. and PS gives a point of change from the tracking characteristics of the material itself into tracking characteristics of a totaly carbonized surface, which does not represent the real material any more.
The better tracking behaviour of both PVC and PMMA materials can be laid back to the fact, that both materials evolve gaseous products of decomposition which foster extinction of the arc, if acted upon by an electric arc. This explains also the less damage caused by tracking in these materials than that caused in Ba. and PS materials.

For the special case of 440 AC voltage and under test solution A, Fig.3. illustrates the mean values of the creepage distances at which the material withstands 50 drops without tracking. For this particular voltage, the PS material has been giving better tracking conditions than PMMA material, which in turn has been giving better results than PVC material. Ba. material is by all means the worst of all.
Fig. 4. demonstrate a comparison of the average time-to-track of all discussed materials under 440 AC voltage and by a constant electrode seperation of 4 mm for three different test conditions: (1)Under test solution A, (2) Under test solution B and (3) Under test solution A with specimens soaked in diesel engine oil for 7 days. This latest condition is to simulate natural working conditions on ship board. The results show that the different specimen materials have the same tracking tendency in all test conditions. However, diesel engine oil caused an effective delayment of specimen failure, presumably by preventing wetting of the surface.

CONCLUSION.

The creepage and tracking behaviour of bakelite, PS, PMMA and PVC insulating materials are presented and discussed in this paper. Both bakelite and PS materials have the disadvantage of being of low Martens temperature. Therefore, they have more tendency to track leaving carbonized traces on the surface. PVC and PMMA insulating materials have better tracking behaviours. They evolve gaseous products of decomposition which foster extinction of the arc. Soaking the insulating specimens in diesel engine oil delayed failure effectively, presumably by preventing wetting of the surface.

REFERENCES.

[1] Kaszewski, B; IEEE Trans. Electr. Insul., Vol. EI-14, No. 3, pp. 167-170, June 1979.
[2] Day, A., G. and Stonard, D. J., IEEE Trans. Electr. Insul., Vol. EI-12 No. 3, June 1977.
[3] IEC standard publication 112 third edition (1979).
[4] Koritsky, Yu.; Electrical Engineering Materials, MIR Publishers Moscow, 1970

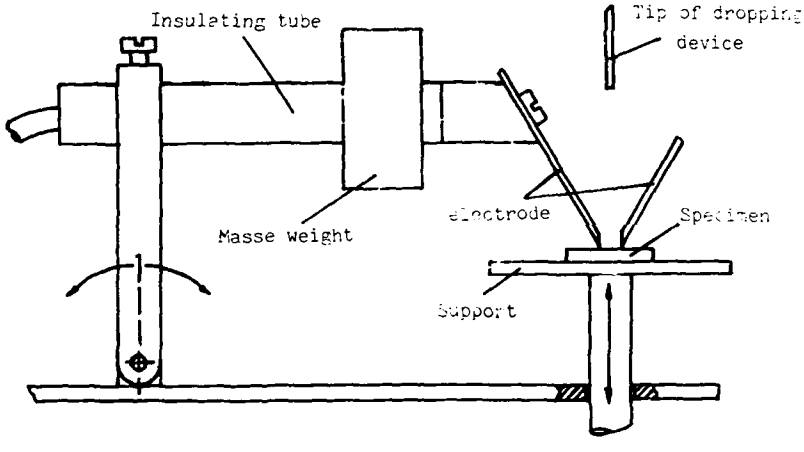

Fig.1 Test arrangement

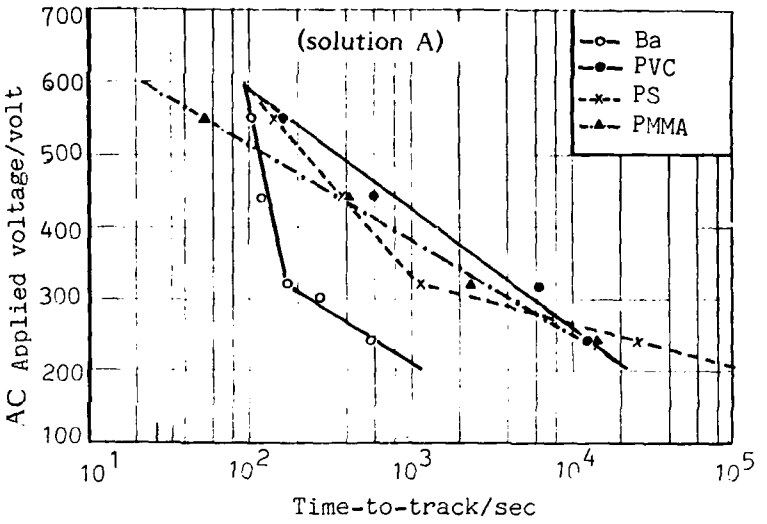

Fig.2. Relation between time- to - track and applied voltage.

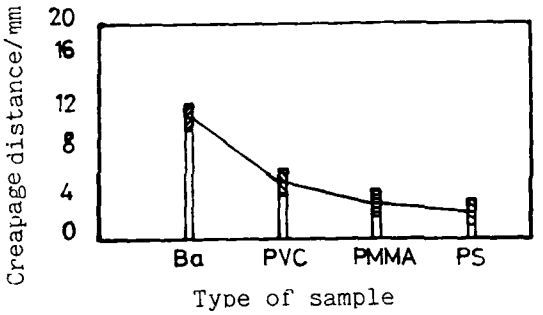

Fig.3. Mean creepage distance values(440 AC voltage, solution A).

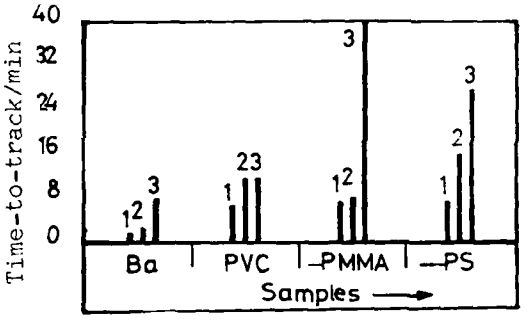

Fig.4. Time- to - track for different conditions as in text.

Dynamics of Polarization Growth and Polarization Reversal in PVDF Films

M. Womes, E. Bihler and W. Eisenmenger
Physikalisches Institut, Universität Stuttgart, Pfaffenwaldring 57,
D-7000 Stuttgart 80

1.Introduction

The risetime of the polarization response to electrical field steps in form I PVDF (high β-crystallite content) was investigated by several authors /1,2/. In these fast rise time switching experiments yet the amount of persistent polarization after field removal has not been determined. In this contribution we present measurements of the maximum displacement at the end of a rectangular high voltage pulse together with the remanent polarization after the pulse under short circuit condition as a function of the polarizing pulse end length. The pulse length varied from 10 μs to 100 s, the field strength ranged from 0.8 MV/cm to 2 MV/cm. The original samples were reversely polarized or unpolarized 12 μm thick films from Kureha Chem. Ltd containing 37% β-material /3/.

2. Experimental

Fig.1 shows the high voltage pulse generator. High voltage is applied to the sample by closing switch S1 and opening S2, shorting the sample is provided by reverse operation. The switches S1 and S2 consist of field-effect power transistors and are triggered by external pulse generators.

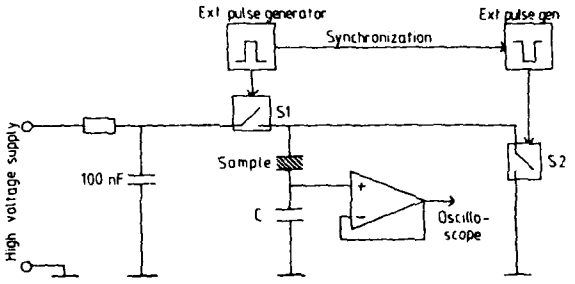

Fig.1: Block diagram of the high voltage pulse generator used for polarizing the samples.

The dielectric displacement D at the end of the field pulse is calculated from the charge on capacitor C. The remanent polarization P caused by the pulse is measured after several minutes under short circuit conditions with the PPS-method (piezoelectrically generated pressure step) /4,5/. The result of this measurement is called the remanent polarization P in the further context.

CH2593-2/ 88/ 0000-0359$01.00 Copyright 1988 IEEE

3. Results

a) unpolarized films:

The dielectric displacement D and the remanent polarization P were measured for the electric field of 2 MV/cm as function of the pulse duration (fig.2).

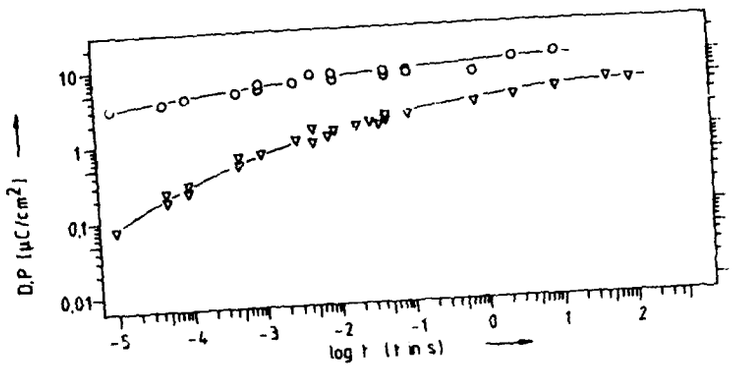

Fig.2: Development of the displacement D (o) and the remanent polarization P (∇), unpolarized samples, E = 2MV/cm.

The development of the remanent polarization is significantly delayed against the fast build up of the dielectric displacement under the applied electric field. This shows a comparison of the times after which half of the long time (10 s) values have been reached:

	after 10 s	the half of this value is reached after
displacement D	10 $\mu C/cm^2$	200 μs
remanent polarization P	4 $\mu C/cm^2$	100 ms

Between 200 μs and 10s the displacement doubles its value, while during the same time intervall the remanent polarization increases by a factor of 10.

A comparison of fig.2 with the results obtained under 1.2 MV/cm (fig.3) and 0.8 MV/cm (fig.4) shows, that the time delay of the beginning development of the remanent polarization depends critically on the field strength:

field strength	development of the remanent polarization
0.8 MV/cm	1s
1.2 MV/cm	10 ms
2.0 MV/cm	< 10 μs

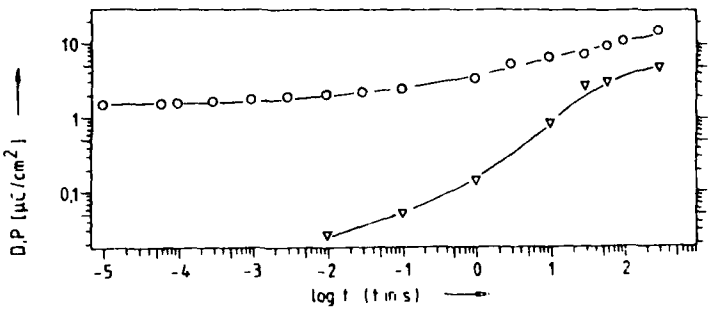

Fig.3: Development of the displacement D (o) and the remanent polarization P (∇), unpolarized samples, E = 1.2 MV/cm.

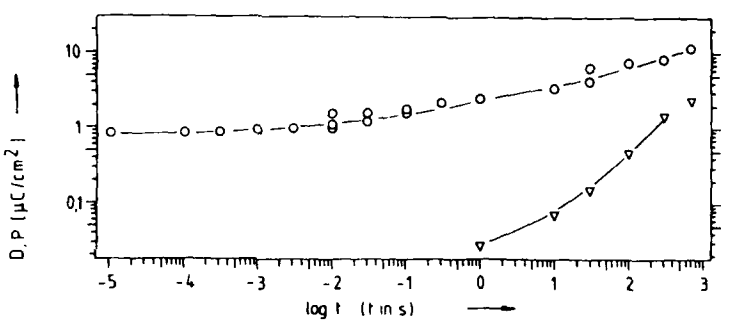

Fig.4: Development of the displacement D (o) and the remanent polarization P (∇), unpolarized samples, E = 0.8 MV/cm.

b) Polarized films:

The poling procedure was the same as Furukawa's and Johnson's /1/. The samples were polarized under 2 MV/cm for 100 s and then kept under short circuit conditions for another 100 s. After this procedure the samples had a remanent polarization of 4.8 $\mu C/cm^2$ ± 10%. Then a reversly directed field pulse of 2 MV/cm was applied and the displacement D and the remanent polarization P were measured as before. Fig.5 shows the result.

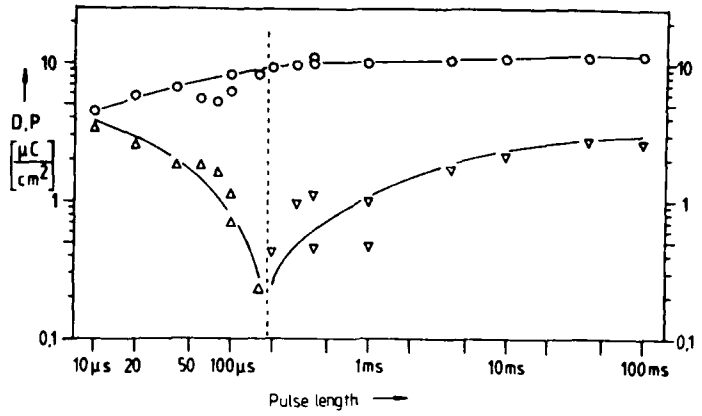

Fig.5: Reversal of the remanent polarization in prepolarized samples, reversed field 2MV/cm, o: displacement D, Δ: remanent polarization, original direction, ∇: remanent polarization, reversed direction.

After 200 μs the initially fast build up of the displacement is finished and is replaced by a slow ascent. This point marks the "switching time t_S" as defined by Furukawa /1/. We see that, with respect to the remanent polarization, this definition is not applicable, since at this time the remanent polarization first reduced to zero begins to change its sign. After 100 ms the polarization has reached only 60% of its initial value the opposite direction, a complete reversal takes more than 100 ms. After having changed its sign, the remanent polarization grows faster and reaches a higher value after 100 ms as compared to the unpolarized samples (cf.fig.2).

In comparison to Furukawa's and Johnson's results /1/ obtained with 7 μm thick films with possibly higher content of β-material, our samples show a somewhat different displacement increase. Under the same electrical field conditions in Furukawa's experiment the fast build up of the displacement is finished after 10 μs with no further increase following. In our experiment the corresponding times amount to 200 - 400 μs. At lower fields of 0.8 MV/cm...1.2 MV/cm, but after the same poling procedure, the times in our experiments necessary to change the sign of the remanent polarization became very long. So we were able to perform a time resolved poling experiment in the PPS-apparatus by connecting the sample with a high voltage source through an additional metallized PET-film /6/. The PPS-signals were recorded with a video system. Under a field of 1 MV/cm it takes 4.6 s for the apparent polarization to change its sign, but when we remove the field after 4.6 s, the polarization returns to its original direction and has still one third of its original value. Under fields of 0.8 MV/cm and 1MV/cm no complete reversal of the remanent polarization could be obtained after 40 and 15 minutes respectively. The development of the PPS-signal shows that under a field of 0.8 MV/cm no complete reversal of the remanent polarization is possible at all.

4. Discussion

The switching back of a large amount of the polarization after removal of the electric field and the significantly delay of the development of the remanent polarization compared to the displacement cannot be explained by a 6-site potential combined with cooperative behaviour alone, as suggested by Broadhurst and Davis /7/. The most simple explanation of our results gives a model of charge injection and trapping /4,8/. The number of deep traps is directly proportional to the polarization. The charges are trapped by dipole ends at the surfaces of the crystallites in PVDF.

In unpolarized films the dipoles become oriented under an external field, but switch back after removal of the field if not stabilized by trapped charges. This leads to a delay of the development of the remanent polarization (fig.2). The dynamics of the dipole orientation under field as well as the injection current depend on the field strength. This leads to a strong field dependence of the dynamics of the remanent polarization (fig.3,4).

In polarized films the dipoles align with the direction of the reversed electric field, but switch back after removal of the field, because trapped charges still stabilize the original direction. On the other hand the field induced chain rotation destroys the former trapping sites, the charges are able to move away and find new traps where they stabilize the reversed orientation. This leads to a slow and delayed reversal of the remanent polarization as compared to the faster displacement D (fig.5). The probability of field induced chain rotation and the mobility of the charges in the sample both depend on the field strength. Hence the times necessary to reverse the remanent polarization depend strongly on the field strength. This model also explains the faster development of the reversed remanent polarization in prepolarized films as compared to unpolarized films, since injected charges are already present in prepolarized films.

5. Conclusion

The cooperative model combined with a 6-site potential alone cannot explain the observed switching back of the remanent polarization, its delayed development, and the long times necessary for polarization reversal. The results are qualitatively consistent with a model of charge injection and charge trapping at polarized crystallites.

6. References

/1/ T.Furukawa, G.E.Johnson, Appl.Phys.Lett., 38, 1027 (1981)
/2/ Y.Takase, A.Odajima, Jap.J.Appl.Phys., 21, 707 (1982)
/3/ calculated from the IR absorption, measured by K.Thonke, A.Dörnen and T.Wildermann, Universität Stuttgart, 1987
/4/ W.Eisenmenger, M.Haardt, Sol.State Comm., 41, 917 (1982)
/5/ M.Haardt, W.Eisenmenger, IEEE 1982 Annual Report CEIDP, p.46
/6/ K.Holdik, thesis, Universität Stuttgart, 1985
/7/ G.Broadhurst, G.T.Davis, Ferroelectrics, 32 , 177 (1981)
/8/ W.Eisenmenger, M.Haardt K. Holdik, IEEE 1982 Annual Report CEIDP, p.52

Negative Charging and Secondary Emission of Teflon FEP under Electron Irradiation

A. Berraissoul, B. Gross*

Institute for Electroacoustics, Technical University of Darmstadt, Merckstrasse 25, D-6100 Darmstadt, Federal Republic of Germany.

Abstract: One-side metalized Teflon FEP films of 25 µm thickness were irradiated on the nonmetalized side with electron beams of energy above that of the second cross-over point E_{II}. E_{II} is the energy at which the number of emitted secondary electrons equals the number of incident primaries. For a beam energy $E_b = 12$ keV, the sample surface reaches a potential of $V_s = 10.5$ kV corresponding to a value $E_{II} = 1.5$ keV. Due to this charging, the effective energy of the incident electrons decreases. Measurements of the induction current into the rear electrode allow one to determine the secondary-emission yield as a function of energy. Results are compared with data published by other authors, and represented by an approximate relation.

1. INTRODUCTION

For the purpose of investigating surface charging and secondary electron emission for irradiation with electrons of energy E_b above the second cross-over point, i.e. for $E_b > E_{II}$, the sample is irradiated without a bias voltage at a constant beam energy E_b, as shown in **Fig.1.** During charging the rear current I is measured. The surface potential V_s becomes negative, and the effectve electron energy $E = E_b + eV_s$ decreases. This process continues until the second cross-over point has been reached at $eV_s = E_{II} - E_b$; simultaneously $I_r = I_b$ and $I = 0$, where I_r is the sum of secondary emission and backscatter. If would the charging process continue, i.e. if V_s became even more negative, E would drop below E_{II}, and thus $I_r > I_b$. This means that any

---

*Present address: Institut of Physics and Chemistry of Sao Carlos, University of Sao Paulo,CEP 13.560 Sao Carlos, SP, Brazil

CH2593-2/ 88/ 0000-0364$01.00 Copyright 1988 IEEE

attempt of the potential to fall below E_{II}, would lead to a current reversal, and the potential would increase again. Thus the surface potential runs into the second cross-over point.

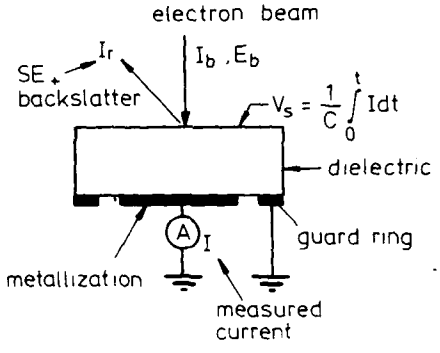

Fig. 1 Schematic diagram of the experimental configuration

2. RESULTS AND DISCUSSIONS

For Teflon FEP we found in previous measurments [1] [2] a value of $E_{II} = 1.5$ keV. This means that with an electron energy of 12 keV, a Teflon sample should get charged to -10.5 keV. Results are plotted in **Fig.2**, which shows the current I as a function of time t. As

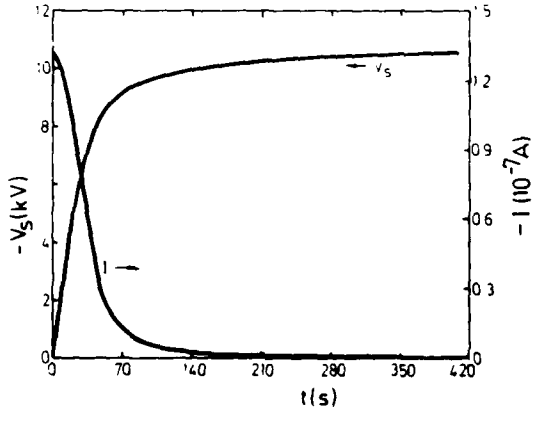

Fig. 2 negative charging of FEP. Measured current I and surface potential $V_s(t)$ as function of time t.

expected, the current decreases fast and eventually approaches zero. The initial increase of the slope of the current curve is due to electron backscattering. The surface potential, also shown in **Fig.2** was determined, as in[1] by means of the relation:

$$V_s(t) = 1/C \int_0^t I(t)dt. \qquad (1)$$

where C is the capacitiance of the irradiated region of the sample. $V_s(t)$ decreases to -10.47 keV, with a value of $E_{II} = 1.53$ keV following from $E_{II} - E = eV_s$, in agreement with the result obtained in previous paper.

In logarithmic scale **Fig.3** shows the secondary emission yield $\delta = -I_r/I_b$ as a function of E. A straight line results for values between $E = E_{II}$ and $E = 5$ keV. It is given by the approximate relation $\delta = A/E^n$ with $A = 1.2$ and $n = 0.4$

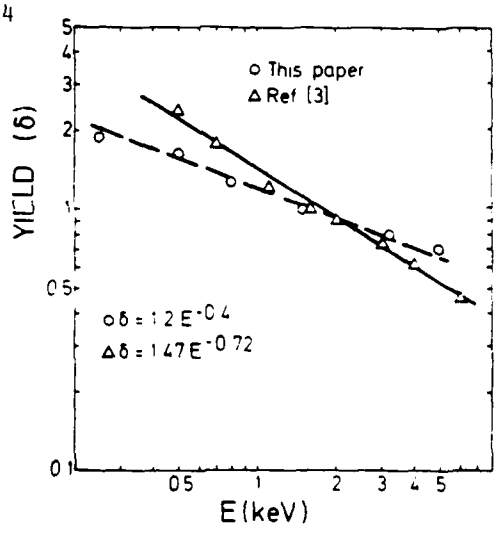

Fig.3 Secondary emission yield in logarithmic scale. Comparison of the results of Hazelton et al. [3]and those of the present paper.

Hazelton et al. [3] have also determined the secondary emission yield for Teflon. In the energy interval $0.5 < E < 4$ keV they found a relation $\delta = 1.47\, E^{-0.72}$. Extrapolating this relation up to their beam energy of

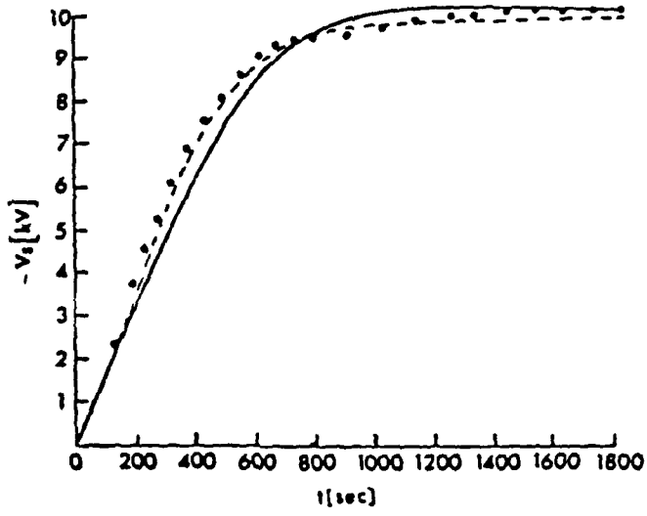

Fig.4 Results of Hazelton et al. [3]. Comparison between theory and measurments. Dots:Measured values. Solid line:Theory. Dashed line:Calculated by Eq.(1).

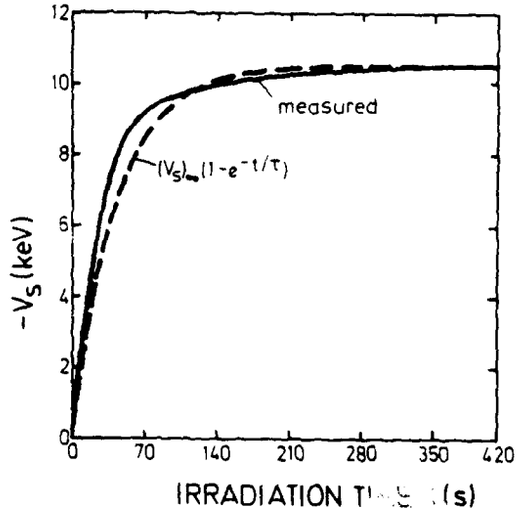

Fig.5 Approximation of the charging curve of **Fig.2** by means of an exponential function, Eq.(2).

12 keV they calculated the charging curve $V_s(t)$. Their results as shown in **Fig.4** give satisfactory agreement between calculated and measured values.

The function $V_s(t)$ is, however, very insensitive to change of the function $\delta(E)$. To show this we have used an alternative approach and shown that the curve $V_s(t)$ can be approximated by means of an exponential function:

$$V_s(t) = (V_s)_\infty [1 - \exp(-t/\tau)], \qquad (2)$$

which is the solution of the differential equation $dV/dt + V/\tau = V_\infty/\tau$. **Fig.5** shows a comparison of the calculated and measured curves with $(V_s)_\infty = -10.47$ keV and $\tau = 42$ s. Agreement is as good as shown by Hazelton et al. [3], although Eq.(2) is based on a relation between I_r and E, which is quite different from that used in [3].

3. CONCLUSION

During irradiation of Teflon with electrons of energies above the second cross-over point, the surface potential as a function of time can be calculated in terms of a simple exponential equation.

Acknowledgments. The authors are indebted to Prof.Dr.G.M.Sessler for stimulating discussions, to Mr.H.Eisenhauer for sample preparations, and to the Deutsche Forschungsgemeinschaft as well as the Stiftung Volkswagenwerk for generous financial support.

REFERENCES

[1] B. Gross, H. von Seggern, A. Berraissoul: IEEE Transactions on Electrical Insulation. **EI-22**, 23-28 (1987)

[2] H. von Seggern: IEEE Transactions on Nuclear Science, **NS-32**, 1503-1511(1985)

[3] R. C. Hazelton, E. J. Yadlowsky and R. J. Churchill: IEEE Transactions on Nuclear Science, **NS-28**, 4541-4546 (1981).

TSDC ANALYSIS OF THE POLY(TRANS 1-OCTENYLENE)

J.Fraile, A.Torres, J.Jiménez, J.A. de Saja

Departamento de Física de la Materia Condensada.
Facultad de Ciencias. 47011 - Valladolid (Spain).

ABSTRACT

The TSDC spectrum of the Poly(trans 1-octenylene), $[CH=CH-(CH_2)_6]_n$ is analyzed by means of the thermal sampling technique over the 150-320K temperature range. Three relaxation zones are so defined in the spectrum. In addition, a shoulder localized in a narrow temperature interval (220-250K) of the TSDC spectrum is observed.It was found to be correlated with a change in the slope of the microhardness (Vickers) vs T plot.

INTRODUCTION

The analysis of the TSDC (Thermally Stimulated Discharge Current) spectrum of the poly(trans 1-octenylene), usually known as polyoctenamer or P8, is done by the thermal sample technique. This spectrum exhibits two broad bands in the 150K-320K temperature range, the maxima are around 180K and 283K respectively.

The analysis of this spectrum leads to the characterization of three relaxations, which in the increasing temperature order, are associated with: dipolar motion in the amorphous phase; relaxations at the amorphous-crystalline interface and discharge in the crystalline phase.However, the sensitivity of the experimental procedure allows us the observation of a fourth relaxation, which was correlated to a thermoelastic transition observed in the microhardness vs T plot. The analysis of the single TSDC peaks obtained by thermal sampling is done by fitting the experimental peaks to a current density expression, deduced from the general order kinetics equation of the dipolar relaxation. This leads to a relaxation time with three fitting parameters, i.e. activation energy, preexponential factor and a third parameter, Q, which when the relaxation deals with dipolar motion was called interaction parameter. This equation has been largely described and successfully used

CH2593-2/ 88/ 0000-0369$01.00 Copyright 1988 IEEE

in other materials, leading to a realiable description of the different temperature relaxation zones of such materials [1,2].

EXPERIMENTAL

The Poly(trans 1-octenylene), which the formula is $[-CH=CH-(CH_2)_6-]_n$ is a polymer characterized by high mechanical and thermal stabilities due to its rather few branches [3]. It contains 70-80% trans double bonds. The melt point is 324K as deduced by DSC. The specimens for measurements were obtained submitting molten polymer at 373K during 5 minutes at 4MPa, cooling down to 293K and annealed for 24 hours at 315K. The samples so obtained were 65μm thick. They were cut for TSDC measurements in specimens of 5x5mm^2. The TSDC measurements were carried out with a classical experimental equipment, which has been largely described in previous papers [1,2]. The electrical measurements are made with a digital electrometer (Keithley 616). The samples were under 10^{-5}torr vacuum, coated copper electrodes were used. The resolution of the TSDC spectrum in single peaks was made by the thermal sampling technique [2,4].

RESULTS AND DISCUSSION

The TSDC spectrum of P8 is represented in fig. 1. This spectrum presents two well defined bands, around 180K and 283K respectively. These bands are labeled β and α in agreement with the usual nomenclature. The thermal sampling is carried out every 5K, which allows the obtention of 32 single peaks, fig.1. The characteristic relaxation parameters are obtained by fitting every single peak to the following expression for the current density:

$$I = s^{-1}\left[P_0^{1-Q} + (Q-1)\int_0^T s^{-1} f'(T')\,dT'\right]^{-Q/(Q-1)} \qquad (1)$$

where P_o is the initial polarization at t=0; $s=\tau_o \exp(E/kT)$ τ_o is the preexponential factor with time dimensions; E is the activation energy; k is the Boltzmann constant; Q is a fitting parameter, coincident with the kinetic order, it is called the interaction parameter as an

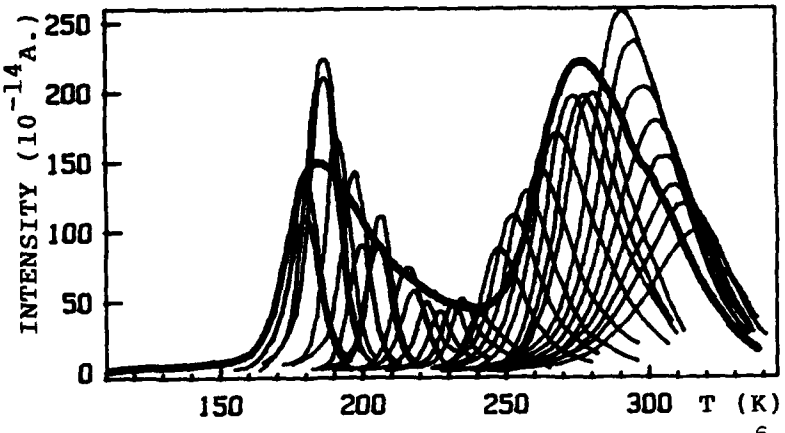

FIG.1:(▬) Global TSDC spectrum obtained by poling with E_p=3.8x10^6V/m during tp=5 min. at Tp=314K. (——) Thermal sampled curves obtained by varying Tp from 158 to 313K. The depolarization temperature is 5K below Tp, and the depolarization time is 5 min.

extension of the meaning it has when the relaxation is purely dipolar; finalyy f'(T') is the inverse of the heating rate. Equation 1 is deduced from the expression $J=-dP/dt=P/\tau$, where τ is a complex relaxation time obeying the equation:

$$\tau(T) = \tau_0 \, (P_0/P)^{Q-1} \exp(E/kT) \qquad (2)$$

where P is the remaining polarization at T. The meaning of this relaxation time has been the matter of other previous articles [5,2]. An adequate choice of the three parameters E,τ_o and Q, allows a quite satisfactory fitting of the equation 1 to the experimental single peaks, fig.2. The different temperature relaxation zones are determined on the basis of the evolution with temperature of these three parameters. Fig.3 represents E, τ_o and Q as a function of maximum temperature of the indiviudal TSDC peaks resolved by thermal sampling. The temperature dependence of τ_o and E is quite similar, the difference between both lies in the fact while E increases, τ_o decreases and vice versa. This is due to the exponential relation between both. The parameter Q exhibits a different temperature dependence, which is in agreement with the interpretation of this parameter.
In fig.3 the temperatures limiting the four deduced relaxation zones are indicated. The first zone (lowest

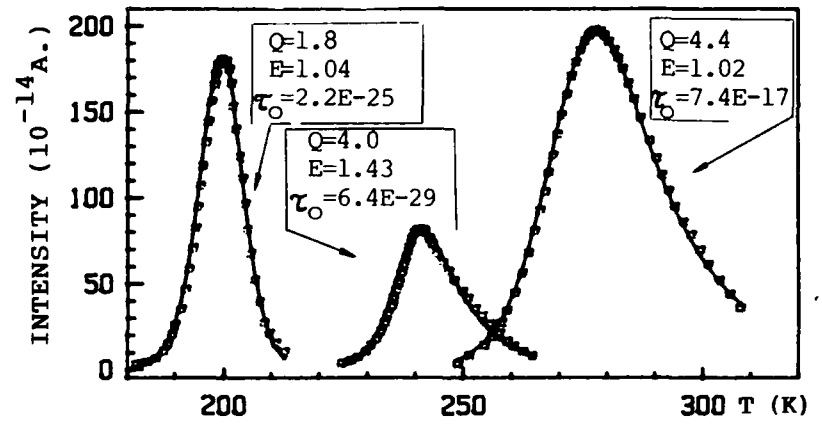

FIG.2:Examples of fitting (——) using eq. (1) to the experimental points (□ □ □). Left:Tp=188K. Middle:Tp=233K. Right:Tp=268K. The intensities of both left and middle curves are multiplied by 2.

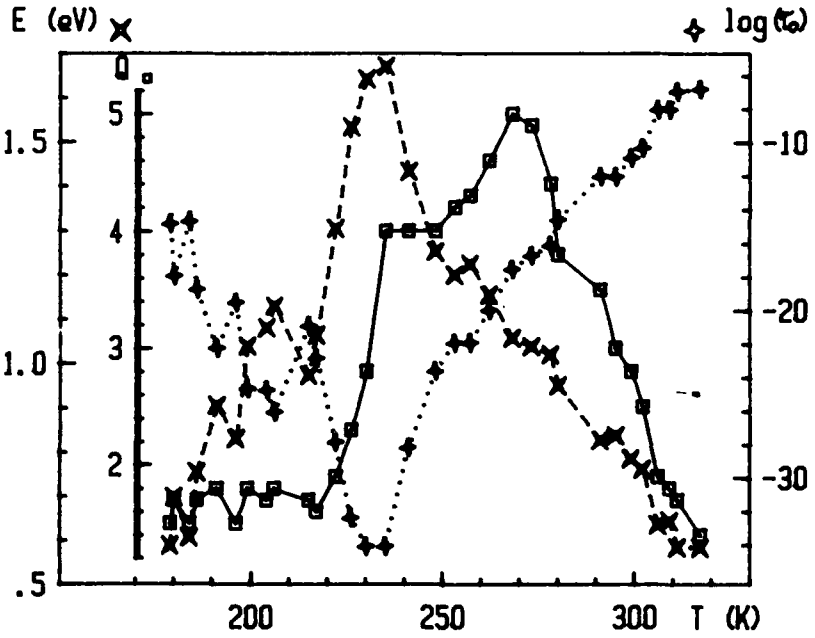

FIG.3:Relaxation parameters vs Tm plots, Tm being the temperature at the maximun for each thermal sampled curve.
E: (X- -X). log(τ_o): (+...+). Q: (□——□).

temperature range) is limited by the glass transition temperature Tg=208K; Q lie around 1.7 over all this temperature margin; this relaxation is ascribed to a dipolar reorientation mechanism taking place at the amorphous phase. The second zone is observed between 220K and 250K. The single peaks corresponding to such an interval are not well fitted to eq. 1; this is due to the low electric current signal observed in this temperature range, however it should mainly related to the existence of an additional polarization, which has been found to be related to a thermoelastic transition observed by microhardness measurements [6] in the same temperature range. This relaxation would be associated with the motion of the polymeric chains bounded at the amorphous-crystalline interface. The third relaxation is observed between 250 and 290K, it is characterized by high values of Q. This relaxation is probably related to the detrapping of the space charge induced at the amorphous-crystalline interface traps. It should be noted that the liquid-liquid transition temperature lies in this temperature range. Finally, a change in the slope of E, τ_o and Q vs T plots at 290K allows us to identify the fourth relaxation zone; this is particulary conspicuous for Q. It is rather probably that this relaxation would be related to detrapping of carriers at the crystalline region, this process should be due to a decrease in the crystalline/amorphous ratio, when the temperature increases in such a range. It should be noted that this transition has been reported to be reversible, a cooling of the specimen restores the initial crystalline content.

REFERENCES

[1] A. Torres, J. Jiménez, V. Carbayo, J.A. de Saja. Phys. Stat. Sol. (a) Vol. 78, pp 671-677, 1983.

[2] A. Torres, J. Jiménez, B. Vega, J.A. de Saja. J.Mat. Sci. Vol. 22, pp 1623-1629, 1987.

[3] A. Draexler. Kautsch. Gummi,Kunstst. Vol. 34, pp 185-190, 1981

[4] J. Vanderschueren, J.Gasiot. Field-induced thermally stimulated currents, in: P.Braeunlich Ed., Thermally stimulated relaxation in solids. Springer, New York 1979, pp 135,223

[5] A. Torres, J.Jiménez, J.C. Merino, J.A. de Saja. J. Phys. Chem. Solids. Vol. 46, pp 665-674, 1985.

[6] B. Martin, J.M.Pastor. Private communication.

PVDF SENSOR ARRAY FOR HUMAN BODY DETECTION

Reinhard Freitag, Hans Meixner
Siemens AG, Corporate Research and Development
Munich, West Germany

ABSTRACT

The pyroelectric polymer PVDF is particularly suitable for sensor arrays because of its low lateral heat flow. Sensor arrays can be used to determine the direction and, knowing the distance between detector and heat source, the velocity of a heat source. An IR detector based on PVDF is presented in which a sensor array is combined with a suitable optical unit and an amplifier circuit to form a single complete device. There is a great number of applications such as human body detection, automatic actuation of devices in installations, security and control engineering.

INTRODUCTION

The polymer PVDF is known for its good pyroelectric properties, which are in every respect comparable to those of pyroelectric monocrystals and ceramics. The capacity for large-area fabrication, simple machining and low material price opens up a wide field of applications for PVDF in passive IR detectors. Beyond this, its special thermal properties permit technical solutions which are not possible with conventional materials.

IMPORTANT MATERIAL PARAMETERS FOR PRODUCING A SENSOR ARRAY

For numerous applications such as the automatic actuation of devices in installation engineering and the security sector (property safeguarding, access control) it is desirable to detect the presence of human beings with a passive IR detector, to determine their direction of motion and, where the distance is known, their angular velocity as well. For simply detecting human beings, a single sensor is sufficient, but at least two sensors or even better a sensor array are required to determine their direction of motion and velocity.

To use sensor arrays in IR detectors, parameters such as the pyroelectric signal voltage, response speed and lateral thermal resolution are of particular interest for selecting a suitable sensor material. Because its temperature is higher than ambient, the human body emits about 60 W of infrared radiation onto its surroundings. Since the radiation intensity decreases approximately in inverse proportion to the square of the distance between the radiating body and the

CH2593-2/ 88/ 0000-0374$01.00 Copyright 1988 IEEE

detector, the material must supply a signal voltage which can still be effectively evaluated at greater distances (e.g. 10 m). A measure of the signal voltage is provided by the pyroelectric voltage coefficient (P_y) of the respective material. An important parameter for detecting movements is the response speed of the sensor element. This depends less on the kind of pyroelectric material used than on its thickness. The third parameter of interest is the lateral thermal resolution, which is determined principally by the lateral thermal heat conductivity of the sensor material. The smaller the heat conductivity of the sensor material, the smaller the crosstalk from one element to the adjacent element. Figure 1 shows a comparison of different sensor materials with respect to signal voltage, response velocity and lateral resolution.

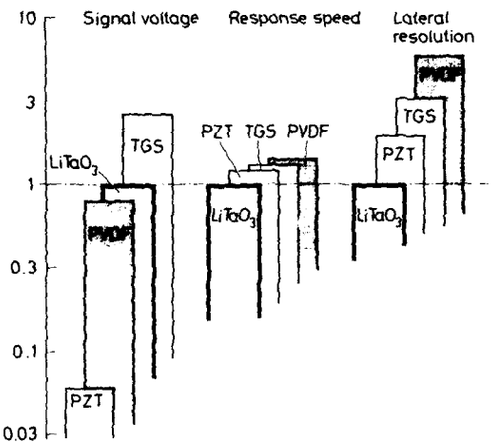

Figure 1: Principal sensor properties (signal voltage, response speed, lateral resolution) of various pyroelectric materials normalized to the values of $LiTaO_3$ of identical thickness

The values marked in the diagram were calculated from values given in the literature for the most common sensor materials [1,2,3] and standardized with respect to lithium tantalate, the pyroelectric material most commonly used up to now.

It can be seen from the diagram that although PVDF exhibits about 80 % of the signal of $LiTaO_3$, it allows the highest spatial resolution to be attained due to its thermal conductivity. Figure 2 shows the influence of the thermal conductivity on crosstalk. The 25µm thickness of the $LiTaO_3$ corresponds to the minimun thickness available on the market. None of the known pyroelectric materials is as well suited for arrays as PVDF.

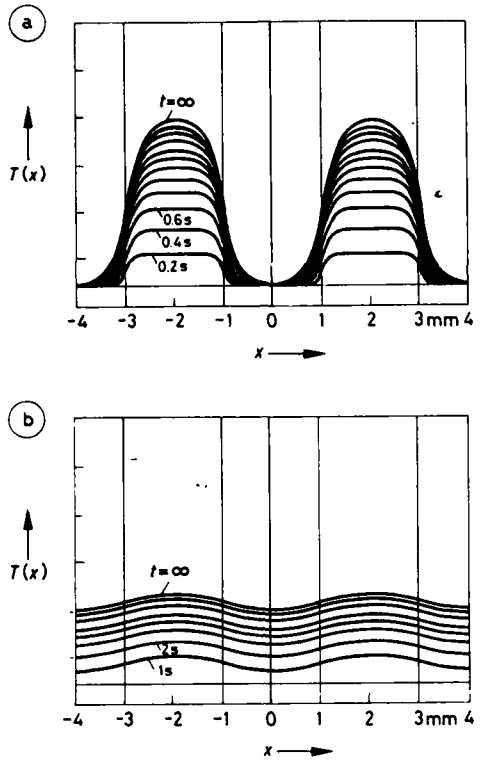

Figure 2: Calculated one-dimensional temperature profiles in arbitrary units in the self supporting pyroelectric material during a heating process. The sensors are arrayed with a spatial period of 2 mm. Every second sensor is irradiated. The absorbed thermal power is transferred to the environment (air) with a heat transfer coefficient of $11 W/(m^2 \cdot K)$.
(a) Polymer (PVDF of thickness 10 µm)
(b) single cristal material ($LiTaO_3$ of thickness 25 µm)

THE USE OF A PVDF ARRAY IN A PASSIVE IR DETECTOR

In order to obtain a thermal image on a PVDF array, an optical system is reqired. Either a lens (e.g. fresnel lens) or a spherical mirror are suitable for this purpose. The PVDF can be arranged in a hollow mirror so that the optical axis lies either normal to or in the PVDF plane. The latter case will be considered more closely.

There are many applications requiring a large horizontal angular detection region (up to 120^0) with high angular resolution and in which a limitation to a narrower vertical zone is of advantage. The schematic representation in Fig. 3 shows the optical system and an array configuration for a sensor of this type. A plane pyroelectric PVDF film is placed in the middle of a spherical mirror. The semicircular array of sensor elements is arranged on the film in such a way that the elements are placed at the foci of the IR rays entering at different angles of incidence (Fig. 3a). In this configuration, the sensor material is irradiated from both sides, which results in a shorter response time than for unilateral irradiation (as when using a Fresnel lens) [4].

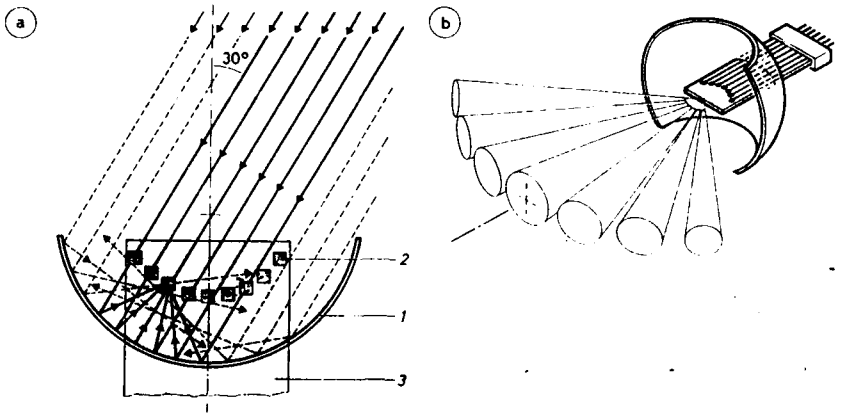

Figure 3: Broad angle IR detector with linear PVDF sensor array.
(a) Beam path of spherical reflector for radiation incident at oblique angles. (1) Spherical reflector, (2) Sensing element, (3) PVDF film
(b) Sensor array and directional characteristics

SIMPLE WIDE-ANGLE DETECTOR WITH A 4-ELEMENT ARRAY

A simple design of a wide-angle detector with only four elements is shown in Fig. 4. The thickness of the PVDF film used is 10 µm. The electrode structure of the elements and their feed lines can be fabricated by etching a previously metallized PVDF film. A technical superior solution, suited especially for serial production, is achieved by structuring the electrodes by means of lasers. In this case, the metallization is vaporized from both front and rear sides of the PVDF film by the pulse of a spread laser beam. The future electrodes are covered by masks [5].

An ideal approach would be to use a transparent electrode material so that the absorption bands of the PVDF can be exploited in the wavelength range from 7 - 12 µm. However, transparent electrodes can be produced only at a temperature at which the PVDF would depolarize. The usual electrode materials (such as Al, Cr, Ni, Ag and Au) reflect the IR radiation focussed from the mirror onto the film. The film is therefore covered with a special resist whose absorption bands lie in the wavelength range between 6 and 16 µm. this corresponds to the IR radiation emitted by human beings. Visible light and near IR radiation are not absorbed and therefore cannot give rise to any disturbances. The film is additionally protected from moisture, which could reduce the high impedance output signal.

To process the signal from the individual sensor elements, amplifiers with a high input impedance are required, e.g. amplifier circuits in C-MOS technology. The amplifiers and the array must be shielded from electromagnetic interference by a conductive housing and a conductive grid placed in front of the mirror. A polyethylene film transparent to IR radiation ensures that air currents arround the PVDF film which rests loosely in a frame cannot cause disturbances due to the piezoelectric effect of PVDF.

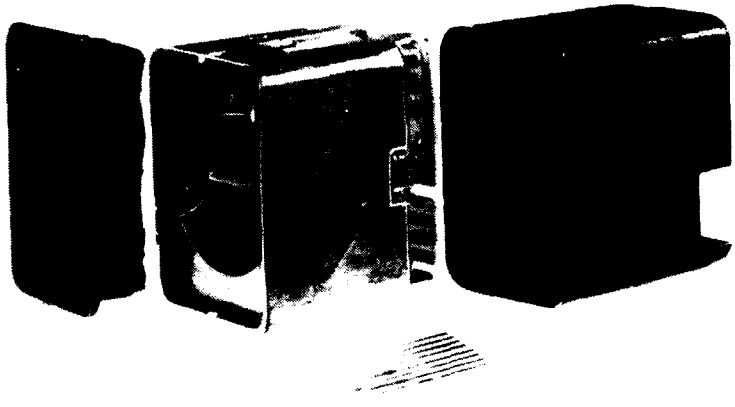

Figure 4: Complete IR detector with a 4-element array (prototype in open state)

CONCLUSION

Future research activities in the field of sensors based on polymers are aimed at the development of large-area n x m matrix sensors in conjunction with Fresnel lenses to determine the area of an object emitting IR radiation.

REFERENCES

[1] W. Heywang (Ed), Sensorik, pp. 135-164, Springer Verlag,Berlin (1984)
[2] H. Meixner, G. Mader, P. Kleinschmidt, Siemens Forsch.- u. Entwickl.-Ber. 15, Nr.3, pp. 105-114 (1986)
[3] Das Polyvinylidenfluorid von Solvay BR 1292 d-B-1.5-0685 (1985)
[4] H. Meixner, G. Mader, R. Freitag, Pat.Nr. 86P1281DE (1986)
[5] H. Meixner, R. Freitag, E. Krimmel, Pat.Nr. 85P1610DE (1985)

ULTRASONIC TRANSDUCERS USING PIEZOELECTRIC PVDF FILMS

Nils Kroemer, Wolfgang Manthey

Technical University Karl-Marx-Stadt,
Reichenhainer Str.70, 9022 Karl-Marx-Stadt,
German Democratic Republic

Wolfgang Kuenstler, Rudi Danz and Detlev Geiss

Institute of Polymer Chemistry "Erich Correns"
Academy of Sciences of the GDR, Kantstr. 55
1530 Teltow, German Democratic Republic

ABSTRACT

Piezoelectric ultrasonic transducers are used in sensing systems of industrial robots.Transducers using PVDF films have some advantages compared to conventional ceramic transducers. The broad frequency range allows a high resolution of the measured distance and a small minimum detection range. High reliability is achieved by microcomputer signal processing. Adaptation of acoustic parameters as sound beam pattern and operation frequency to special measuring problems is effected by variation of geometrical transducer characteristics. Multielement transducers were also created for electronically controlled variation of sound beam pattern.

INTRODUCTION

Contactless distance measurement using ultrasound in air allows effective and low cost solutions for many tasks in robot technology. The efficiency of ultrasonic measurement systems mainly depends on the electroacoustic transducers. Widely used piezo ceramic transducers are compact and low cost

CH2593-2/ 88/ 0000-0379$01.00 Copyright 1988 IEEE

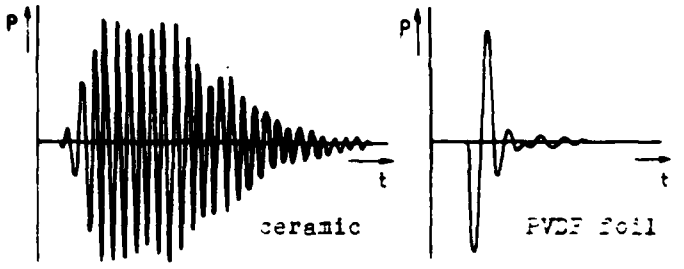

Fig. 1 Response on a voltage step of a piezo polymer foil and a piezo ceramic

components, but they show an unsatisfactory transient pulse response if the electric driving signal is a rectangular pulse or step signal. Moreover the form of the received signal depends to a high degree on reflection conditions and the sound radiation direction relative to the transducer. Therefore signal processing becomes complicated.
Ultrasonic transducers using piezoelectric polymer films of PVDF or related materials show very good dynamic properties because of the low mass and high mechanical losses of such foils. The transmitted acoustic signal is a good image of the electric driving signal.
High distance resolution can be achieved by simple signal processing. Moreover the minimum detection range of the transducer becomes very small especially if single pulses or short bursts are used. Fig. 1 shows the typical response on a voltage step of a piezo polymer foil transducer and a piezo ceramic transducer as described in [1].

EXPERIMENTAL

The principle construction of a multielement foil transducer for use in an object detection system of a robot is illustrated in Fig. 2. The single elements are cylindrically shaped foam supported stripes of a uniaxially orien-

ted PVDF foil. Every single element may be used as transmitter and receiver independently of the other elements. Because of the lateral clamping the length extension of the foil is converted into a radial motion (transmitter) and reverse (receiver) [2].

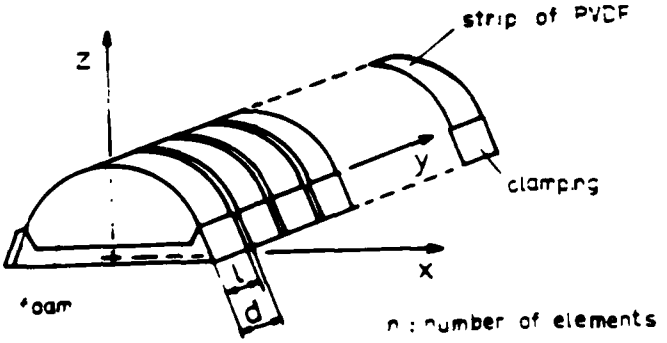

Fig. 2 Multielement foil transducer

The acoustic radiation pattern of the transducer in the yz-area can be changed over a wide range by phase shifted driving of the single element. The sound beam pattern may be calculated by the term

$$R(\gamma) = R_{FE} \cdot R_{FM}$$

with $$R_{FE} = \frac{\sin((kl \cdot \sin\gamma)/2)}{(kl \cdot \sin\gamma)/2}$$

and $$R_{FM} = \frac{\sin(n(kd \cdot \sin\gamma - \varphi)/2)}{n \cdot \sin((kd \sin\gamma - \varphi)/2)} \quad .$$

$k = 2\pi/\lambda$

γ : angle between z-axis and any point in the far field within the yz-area

φ : phase shift between adjoining single elements

λ : sound wave length in air.

R_{FE} describes the sound beam pattern of a single element while R_{FM} represents the group

characteristic. The maximum electric phase shift is $\pm\pi$ if the driving signal is a pulse burst. The electronic scanning has some advantages compared to systems using mechanically moved transducers as described in [3]. However the maximum scanning range decreases with increasing frequencies as follows from [1].
Fig. 3 shows some examples of measured and calculated sound beam patterns of the multielement transducer with φ as parameter. The resonance frequency f_R of the transducer is mainly determined by the geometric size of the cylindrically shaped membrane and may be varied over a wide range because of the high flexibility of the foil [4]. Because of the sound attenuation in air, frequencies below 200 kHz are usual if the maximum detection range is more than 2 meters. For rectangular pulses the useful frequency range of the transducer is about $0.7f_R$ ... $1.4f_R$.
The ultrasonic measurement system is controlled by a microprocessor. In the transmitter mode the electric phase shift between the single element of the transducer can be varried in steps of $\pi/8$ from $-\pi$ to $+\pi$.

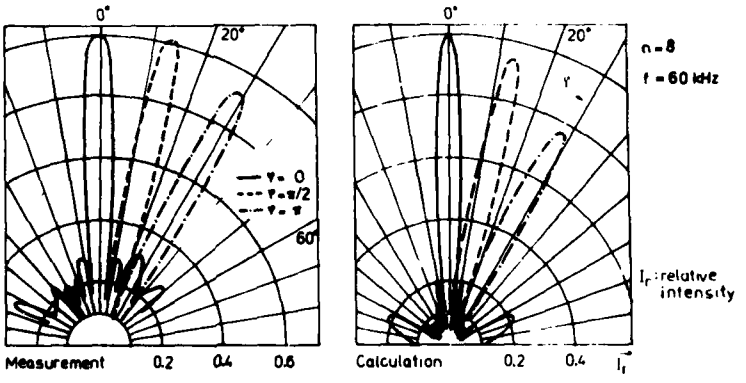

Fig. 3 Sound beam pattern of a multielement transducer

Any number of elements can be used as receiver.The distance measurement is carried out by measuring the transit time of the sound waves from the transducer to the surface of the reflecting object and back. The obtained distance resolution is 0.1 mm registering the zero transitions of the received signal which are independent of the signal amplitude. One complete measurement cycle takes about 20 ms.

High reliability and noise immunity are achieved by combining different measures:
- signal identification
- logic result test
- mean value calculation
- variation of frequency.

To suppress environmental influences such as changes in air temperature or relative humidity the measurement system is periodically calibrated by the help of a reflector which is placed in a fixed distance to the transducer.

REFERENCES

[1]P. Kleinschmidt and V. Magori, "Ultrasonic Robotic-Sensors for Exact Short Range Distance Measurement and Object Identification", Proc. IEEE Ultrasonics Symposium Oct. 16-18,1985,pp.457-462.

[2]M. Tamura et al., "Electroacoustic Transducers with High Polymer Films", J. Audio Eng. Soc. Vol. 23, pp. 21-26, 1975.

[3]K. Sasaki et al.,"Development of Ultrasonic Robot Sensor, Design and Synthesis", H. Yoshikawa (Ed.), Elsevier Science Publishers B. H. (North Holland), 1985.

[4]R. Lerch, "Untersuchungen an Piezopolymer-Mikrophonen", Diss. TH Darmstadt, 1980.

PIEZOELECTRICITY AND POLARIZATION IN ACRYLONITRILE/METHYLACRYLATE COPOLYMER

Wolfgang Kuenstler, Hans von Berlepsch, Armin Wedel, Rudi Danz and Detlev Geiss

Institute of Polymer Chemistry "Erich Correns" Academy of Sciences of the GDR, Kantstr. 55, 1530 Teltow, German Democratic Republic

ABSTRACT

The piezoelectric strain coefficient d_{31} of stretched and unstretched acrylonitrile/methylacrylate copolymer films has been investigated in dependence on poling conditions. The maximum value of $d_{31} \approx 3$ pC/N is obtained for stretched films. The time stability of piezoelectricity is relatively low. A hysteresis loop of electric displacement vs. electric field has been observed for the first time indicating of a ferroelectriclike behaviour.

INTRODUCTION

The polymer with the strongest piezoelectric activity arising from dipole orientation is poly(vinylidene fluoride) (PVDF) [1]. Whereas the $-CF_2-$ group has a dipole moment of 2.1 D, the nitril side group of poly(acrylonitrile) (PAN) has a dipole moment of about 3.5 D. If these dipoles can be oriented by an applied field, a piezoelectric activity can be expected. Indeed, it could be observed [2-4].
The aim of the present study was to gain more insight into the nature of piezoelectricity in PAN. Owing to the better processability instead of AN homopolymer a copolymer of AN (≈93%) and methylacrylate (6-7%) (P(AN-MA)) was used.

EXPERIMENTAL

Films of the copolymer were cast from a dime-

CH2593-2/ 88/ 0000-0384$01.00 Copyright 1988 IEEE

thylformamide solution, dried in an evacuated oven, uniaxially stretched (draw ratio about 4), electroded with aluminium and poled [3]. The sample thickness varied from 10 to 15 μm. The measurement of d_{31} was carried out at room temperature two days after poling. The hysteresis loops were measured by the conventional Sawyer-Tower method using a triangular electric field of 0.2 Hz (standard regime) at various temperatures up to 90°C.

RESULTS

Fig. 1 represents the poling field strength E_p dependence of d_{31} for stretched and unstretched films. The poling time t_p was chosen as 10 s. In the case of stretched films two different poling temperatures of T_p=90°C and 140°C, respectively were used. The same saturation value of $d_{31} \approx 3$ pC/N is reached in both cases. Secondly the poling time was varied between 10 s and 25 min. For stretched samples poled at 90°C under E_p=8x10^{7}V/m a value of $d_{31} \approx 3$ pC/N was also found independent of t_p.
The piezoelectric activity strongly depends on the poling temperature as shown in Fig. 2. Very little activity is found unless T_p is greater than a critical value of about 50°C. At E_p=8x10^7 V/m d_{31} increases sharply when the

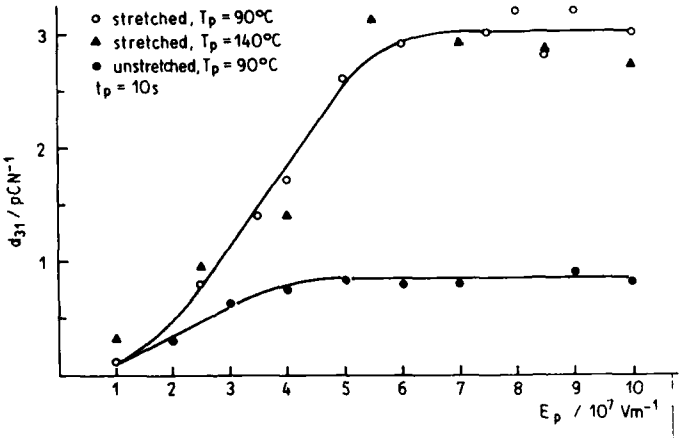

Fig. 1 Poling field strength dependence of d_{31}.

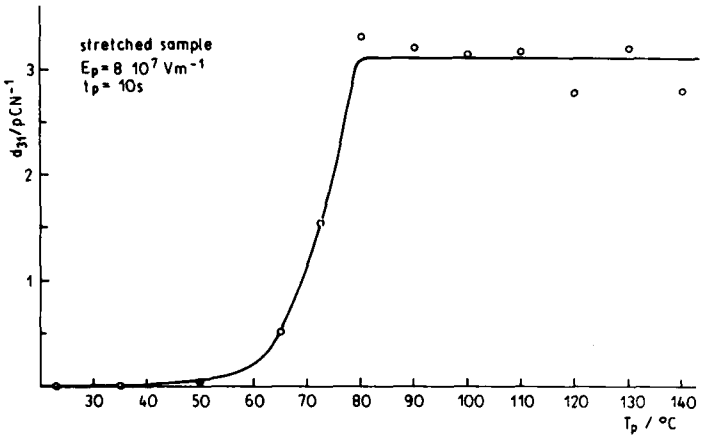

Fig. 2 Poling temperature dependence of d_{31}.

poling temperature exceeds 65°C and reaches its saturation value around 80°C. This behaviour is related with the glass transition. By dynamic mechanical measurements T_g was found to be $\approx$ 95°C. The temperature region above 50°C coincides closely with the loss of elastic modulus.

To obtain information on the stability of the piezoelectric properties the storage time dependence of d_{31} at room temperature was investigated. The piezoelectric decay follows logarithmic kinetics [4]. The isothermal investigations were supplemented by thermally stimulated measurements. For this reason an initially poled sample was annealed stepwise at rising temperatures T_a for 30 min and quickly cooled down to room temperature. After each annealing step the residual d_{31} coefficient was estimated. This procedure was carried out on three samples which were previously stored different times (2d, 7d, 200d) at room temperature. Fig.3 gives the plots of d_{31} vs. T_a. We note a nearly linear decay of d_{31} after an initial constant plateau. For aged samples the loss of piezoelectricity sets in at higher temperatures compared with the fresh sample. However, the initial value of d_{31} is smaller originating in the foregoing isothermal aging. The most con-

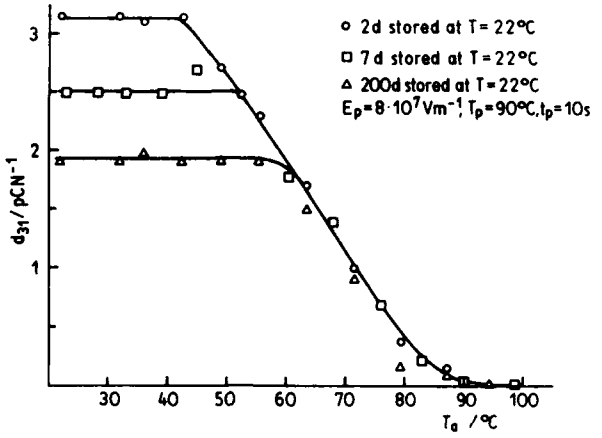

Fig. 3 Annealing temperature dependence of d_{31} for differently stored samples.

spicuous fact is the sample history independent linear loss of piezoelectricity at higher temperatures.
In Fig. 4 a characteristic hysteresis loop for a field amplitude of 1.05×10^8 V/m is plotted. The loops after two cycles were found to be almost stationary and their shape is nearly independent of the frequency (ranging from 0.03 to 0.2 Hz). For higher fields and temperatures the loops are distorted by the effect due to dc conduction.

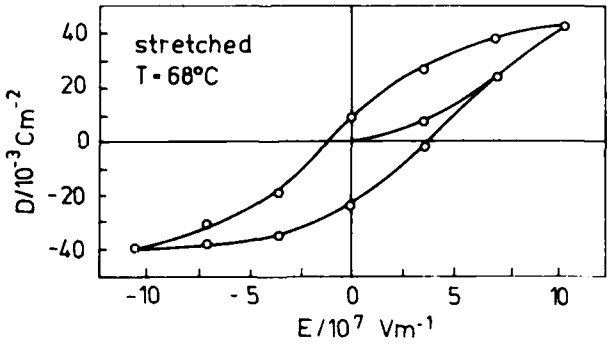

Fig. 4 Hysteresis curve for P(AN-MA).

CONCLUSIONS

As demonstrated, both homo [2] and copolymers of AN possess appreciable piezoelectric activity in spite of their assumed helical conformation [5]. This is in contrast to literature [6] where it is suggested that PAN should not show any piezoelectricity as the result of the cancellation of dipoles. The present investigations indicate that the polarization arises at least partially from a preferential orientation of dipoles. The hysteresis phenomenon observed suggests the copolymer to be quasi ferroelectric. Only quasi ferroelectric, because the piezoelectric state is obviously metastable as its low time stability shows. In order to clarify the origin of piezoelectricity in more detail investigations in relation to the structure are necessary.

REFERENCES

[1]T.Furukawa,"Piezoelectricity and Pyroelectricity in Ferroelectric Polymers",Proc. 5th Intern.Symp.Electrets,Heidelberg 1985 (IEEE,New York,1985),pp.883-888.

[2]H.Ueda and S.H.Carr,"Piezoelectricity in Polyacrylonitrile",Polymer J.,Vol.16,pp.661-667,1984.

[3]H.v.Berlepsch,W.Kuenstler and R.Danz,"Piezoelectricty in Acrylonitrile/Methylacrylate Copolymer",Ferroelectrics, in press.

[4]H.v.Berlepsch and W.Kuenstler,"Piezoelectricity in Acrylonitrile/Methylacrylate Copolymer",submitted to Polymer Bull..

[5]G.Henrici-Olivé and S.Olivé,"Molecular Interactions and Macroscopic Properties of Polyacrylonitrile and Model Substances", Adv. Polym. Sci., Vol.32,pp.123-152,1979.

[6]H.K.Hall jr., R.J.H.Chan, J.Oku, O.R.Hughes, J.Scheinbeim and B.Newman,"Piezoelectric activity in films of poly(1-bicyclobutanecarbonitrile)",Polymer Bull.,Vol. 17,pp.135-136,1987.

INFLUENCE AND IMPLICATIONS OF SURFACE CONTAMINATIONS ON THE CHARGE DECAY IN ELECTRETS

Wolfgang Stark, Rudi Danz, Wolfgang Künstler and Detlev Geiß

Institute of Polymer Chemistry "Erich Correns", Academy of Science of the GDR, 1530 Teltow-Seehof, Kantstr. 55, German Democratic Republic

ABSTRACT

Investigating charge decay of FEP electrets at elevated temperatures considerable differences from sample to sample were found. Stronger charge decay at open stored samples suggest that surface contaminations must have a significant influence on decay rate. For cleaning destilled acetone was used. Cleaned samples had good reproducibility and a lower charge decay rate. Thermally stimulated charge decay measurements (TSCD) showed that cleaning shifts the charge decay into ranges of higher temperature.

INTRODUCTION

Thermally stimulated charge decay investigations belong to the most powerful tools for investigating charge storage properties of electrets /1/. We used isothermal charge decay measurements at 150°C and thermally stimulated charge decay (TSCD).

EXPERIMENTAL

The electret material used was TEFLON-FEP (DuPont) foils 12.7 /um thick. The electret charge was generated by current limited discharge in small air-gap /2/. Electret

CH2593-2/ 88/ 0000-0389$01.00 Copyright 1988 IEEE

charge was measured by the compensation method /3/.

RESULTS AND DISCUSSION

Isothermal charge decay at 150°C

In measuring isothermal charge decay at 150°C distinct differences from sample to sample were found - Fig.1. The fact that these differences increased when foils were stored unprotected before charging - see Fig.2 - gave a first hint that surface contaminations must have a considerable influence on charge decay at elevated temperatures.
Therefore we looked for a possibility to clean the foils before charging.
A method using freshly destilled acetone to wash dust particles from glass tubes for light scattering investigations /4/ turned out to be also well suited for foil cleaning. A detailed description of the cleaning device used is given in /5/.
With the cleaned foils a good reproducibility was reached - Fig.3.
Cleaned foils, after a first measurement, were stored for 24 h either dust protected or open. Then again isothermal charge decay was measured. The results are represented in Fig.4. With samples stored dust protected in the second measurement charge decay continued at low rate but open stored samples showed a sharp potential decrease.
This means that washing with acetone must lead to the removal of surface contaminations, causing increased charge stability. Reappearence of these contaminations leads to the same bad stability typical of non-cleaned foils.
The effect of surface contaminations on charge decay is unknown. We could show that there is no effect of increased surface conductivity /6/.
Therefore we assume that dust particles enter

the FEP foil softened at 150°C and increase the conductivity in the upper part of the foil volume. This leads to a fast charge decay in the first minutes which slows down when the charge carriers have reached the non-influenced volume.

Thermally stimulated charge decay (TSCD)

The results of TSCD measurements may also be influenced by surface contaminations. Therefore we measured TSCD (heating rate 1 K/min) of original and cleaned foils with different starting potential.
Typical results are summarized in Fig. 5. Cleaned foils (solid curves) show a shift of the temperature where charge decay starts by about 40 K. Only with cleaned foils the expected correlation between the starting potential and temperature of charge decay comes into effect.
For potential change equation (1) holds /1/:

$$\frac{dV}{dt} = - \frac{/u(T)}{\varepsilon_o \varepsilon} \int_0^l \varrho(x,t) E(x,t) dx \qquad (1)$$

$/u(T)$ - charge carrier mobility,
$\varrho(x,t)$ - charge density

using the Poisson equation follows

$$\frac{dV}{dt} = - \frac{1}{2} /u(T) E^2(1,t) \qquad (2)$$

For times smaller than the transit time one gets

$$\frac{dV}{dt} = - \frac{1}{2d^2} /u(T(t)) U_{E1o}^2 \qquad (3)$$

U_{E1o} - starting electret potential

That means since dU_{El}/dt at beginning of charge decay is the same for all curves we have

$$/u(T_d) \cdot U_{Elo}^2 = \text{const} \qquad (4)$$

T_d - temperature of charge decay

Using

$$/u(T) = /u_0 \cdot \exp(-A/kt) \qquad (5)$$

an activation energy A can be calculated.
A semilogarithmic plot of $\ln U_{Elo}$ as a function of $1/T_d$ for the cleaned foils gave a straight line allowing an activation energy for the very first charge decay of 0.65 eV to be calculated.

REFERENCES

/1/ J. van Turnhout, Thermally Stimulated Discharge of Electrets
Elsevier Scientific Publishing Corporation, 1975.

/2/ W. Stark, R. Danz and W. Künstler
Experimentelle Technik der Physik
Vol 29, p 223, 1981.

/3/ C. W. Reedyk and M. M. Perlman
J. Electrochem. Soc.
Vol 115, p 49, 1968.

/4/ H. Dautzenberg, private communication
R. H. Shipman and E. Farber
J. Polymer Sci. Part B, Pol. Letters
Vol 1, p 65, 1963.

/5/ W. Stark and R. Danz
Acta Polymerica Vol 33, p 9, 1982.

/6/ W. Stark and R. Danz
Plaste und Kautschuck
Vol 35, p 109, 1988.

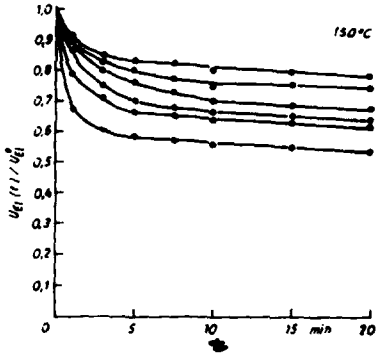

Fig. 1 Isothermal charge decay, original foil

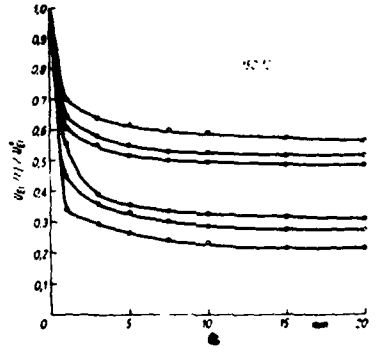

Fig. 2 Isothermal charge decay, foil 24 h open stored before charging

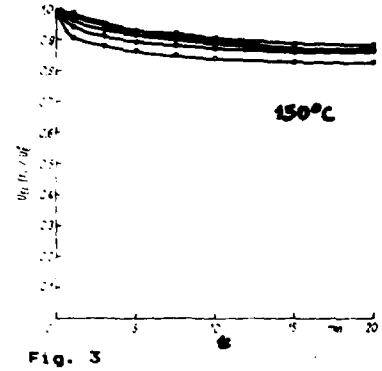

Fig. 3

Isothermal charge decay, foil cleaned before charging

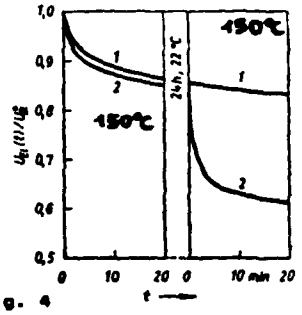

Fig. 4

Isothermal charge decay, foils cleaned before charging, after first measurement 24 h stored open (2) or dust protected (1)

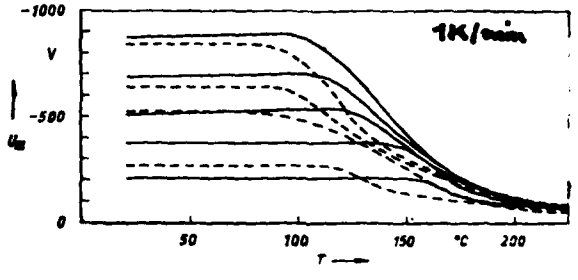

Fig. 5 TSCD curves for original and cleaned foils.

STOCHASTIC HOPPING TRANSPORT IN DISORDERED POLYMERS

Ingolf Mueller, Ludwig Brehmer, Detlev Geiss

Institute of Polymer Chemistry "Erich Correns"
Academy of Sciences of G.D.R.,Kantstr. 55,
1530 Teltow, German Democratic Republic

Eckhard Platen, Alfred Liemant and Wolfgang Wagner

Institute of Mathematics "Carl Weierstrass"
Academy of Sciences of G.D.R., Hausvogteiplatz
1086 Berlin, German Democratic Republic

ABSTRACT

A stochastic approach to electronic charge transport in disordered materials on the basis of a hopping mechanism is presented. The field strength dependence of the space charge evolution is calculated for a defined concentration and distribution of localized levels.

INTRODUCTION

The disordered organic, polymeric and inorganic materials play an increasing part in the field of electronic properties and devices.
But until now the charge carrier transport processes and the electrical direct current properties of strongly disordered or amorphous materials have not been completely elucidated. Furthermore, the knowledge of the space charge dynamics as a result of the transport process is necessary for the optimization of such important technological procedures as electrophotography, electrets, insulation and breakdown.
In this paper we briefly discuss a new quantitative description of a hopping process in amorphous solids, the numerical solution procedure and first results taking into consi-

CH2593-2/ 88/ 0000-0394$01.00 Copyright 1988 IEEE

deration the temperature and field strength of the process. In an previous paper [1] we dealt with a stochastic description of the non-equilibrium charge carrier transport process in polymer insulators, discussing the experimental results and the mathematical assumptions.

TRANSPORT MODEL

Now the mathematical treatment is generalized [2] and the temperature and electric field strength are taken into consideration. The localized levels, distributed randomly in space and energy can be occupied only by one electron. The transition intensity w of an electron from an occupied level u into an unoccupied one v is given by

$$w(u,v)=a^{-b}g\ \exp\{-2a^{-1}\,|u-v| + \frac{e}{2kT}(v-u)\,F\}$$

$$\times\ \exp\{-(v_e-u_e)+\frac{1}{kT}\}\quad , \qquad (1)$$

with $d+ = d$ when $d \geq 0$, else zero;
g : constant; a : localization radius;
k : Boltzmann constant; T : temperature;
F : electric field strength;
e : elementary charge.

The macroscopic dynamics of the charge carrier transport can be expressed by the normalized degree of occupation in x-direction h(x), which is an biunique solution of the non-linear partial differential equation (PDE)

$$\frac{\partial}{\partial t}h_\epsilon(x) = \frac{1}{2}\,b\left(\frac{\partial}{\partial x}\left(D(h_\epsilon(x))\right)\frac{\partial}{\partial x}h_\epsilon(x) - \frac{e\cdot Fx}{kT}\,W(h_\epsilon(x))\,\frac{\partial}{\partial x}h_\epsilon(x)\right) \qquad (2)$$

RESULTS

The numerical solution of this PDE was obtained by an efficient difference alogrithm with a dynamic time-step control.This numerical procedure allows the PDE to be solved in a wide variation of initial and boundary conditions. The generalized diffusion coefficient D(h) and the generalized mobility W(h) were calculated in a sophisticated manner by numerical integration using Kronrod's formula.
With the calculated function h(x) we can estimate the space charge evolution and other ovservables (current, surface potential).
In order to study the competition between the diffusion term and the generalized mobility, one h(x) was calculated for different electric field strengths F and temperatures T.
According to our experimental results for poly(ethylene) the boundary conditions are $h_t(0) = 1$ for $t \geq 0$ (injecting electrode)
and
$h_t(L) = 0$ for $t \geq 0$ (absorbing electrode),
and the initial conditions is
$h_{t=0}(x) = 0$ for all $x > 0$.
In the following the disordered solid is simulated by $N = 10^{28} m^{-3}$ localized levels, distributed homogeneously in space and Gaussian in an energy range from 0 eV to -1 eV with an expectation value of -0,5 eV and a variation of 0,25 eV, a localization radius $a = 10^{-9} m$ and b=1. The results are presented for T=300 K and field strength F=0 (only diffusion) and $F=1,29\ 10^{7} Vm^{-1}$ in figure 1 and 2, respectively.
We can see in a quantiative manner the strong influence of the field strength on the charge carrier evolution process under these conditions. This problem and the consequences for the space charge carrier evolution process under this conditions. This problem and the consequences to the space evolution will be discussed in the poster in more detail.

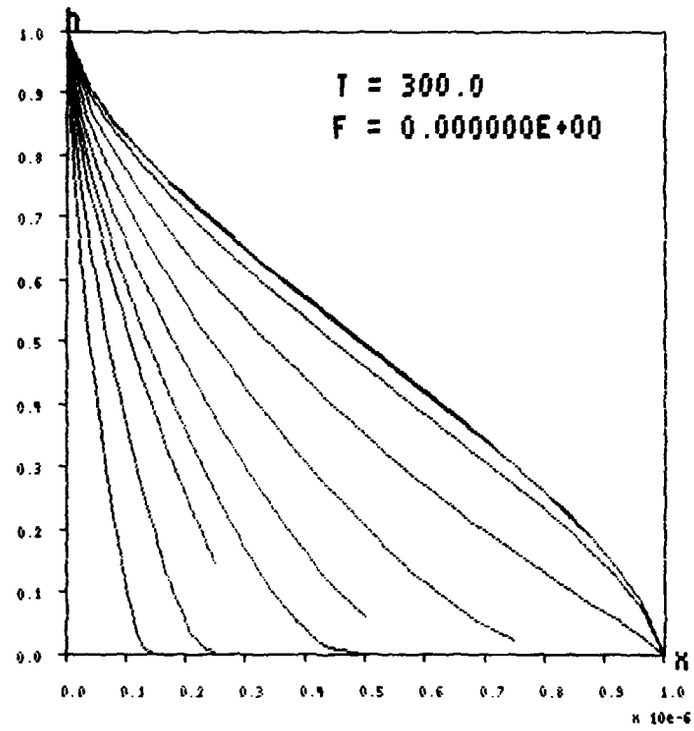
n
T = 300.0
F = 0.000000E+00
1.0
0.9
0.8
0.7
0.6
0.5
0.4
0.3
0.2
0.1
0.0
0.0 0.1 0.2 0.3 0.4 0.5 0.6 0.7 0.8 0.9 1.0
x
x 10e-6

Fig. 1

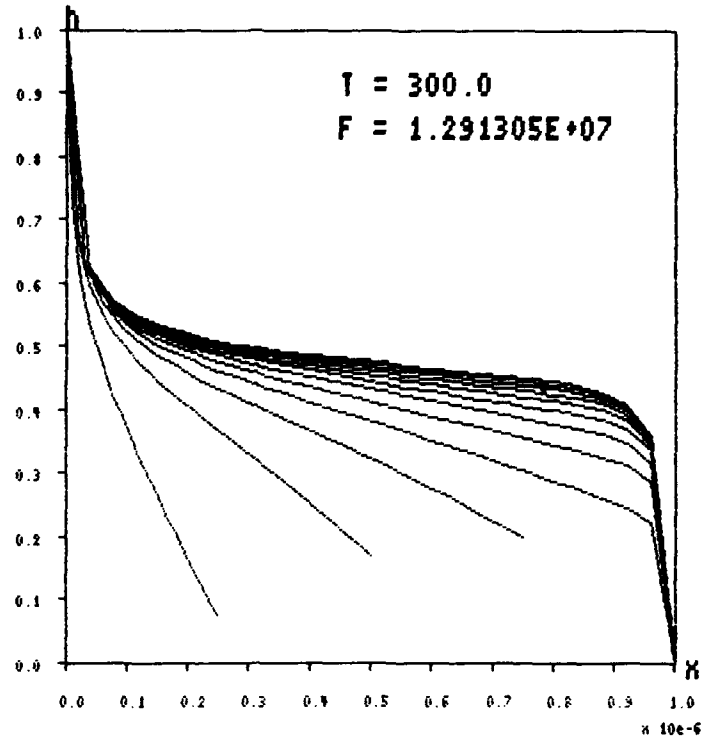

Fig. 2

REFERENCES

[1]L.Brehmer,E.Platen, D.Fanter and A.Liemant "A stochastic description of the non-equi- charge-carrier transport process in polymer insulators",IEEE Trans. Elec. Ins. Vol. EI22, pp. 245-248, 1987

[2]E.Platen, L.Brehmer, A.Liemant, I.Mueller and W.Wagner, "Mathematische Modellierung des Ladungstransportes in polymeren Isola- toren", Preprint P-Math-33/87 of the Insti- tute of Mathematics of the Academy of Sciences of the G.D.R.,Berlin 1987

DETECTION OF LASER RADIATION USING PVDF-FILMS

Burkhard Elling, Wolfgang Kuenstler, Rudi Danz and Detlev Geiss

Institute of Polymer Chemistry "Erich Correns" Academy of Science of the GDR, Kantstr. 55, 1530 Teltow, German Democratic Republic

Werner Bohmeyer

Central Institute of Electron Physics Academy of Science of the GDR, Hausvogteiplatz 5-7, 1086 Berlin, German Democratic Republic

ABSTRACT

For the active sensor element of a pyroelectric device exist two ways of absorbtion of radiation, either within the polymer foil or by the front electrode. Optimization of pyroelectric detector performance in view of measuring short laser pulses requires an adapted device construction. Detector elements were prepared with pure and doped PVDF-films. In the case of optimized volume and wave guided absorption, rise times in the sub-nanosecond range were achieved.

INTRODUCTION

Pyroelectric detectors offer some particular advantages,e.g. high sensitivity, low response time and simple design. For special experiments fast detectors are required to be compatible with oscilloscope direct-access mode of operation [1].
As an active element PVDF becomes more important in comparison with conventional pyroelectric materials, because PVDF is available in films of desired area and thickness, exhibits resistance to humidity and chemicals and has favourable mechanical properties.

CH2593-2/ 88/ 0000-0399$01.00 Copyright 1988 IEEE

The application of PVDF in measuring devices for power and energy of lasers requires special design depending primarily on the electrical and optical parameters and the mode of operation. In particular, if very short laser pulses are to be measured it is necessary to optimize the detector design [2]. An aspect is to reduce the electrical active volume, based on the surface electrode arrangement, to the thermal active volume, based on the absorption depth of incoming radiation. In this view the origin of pyroelectricity is important for explanation the fast response [3]. Therefore the dyeing of PVDF becomes important for a high absorption in the volume immediately and reducing the absorption depth.

EXPERIMENTAL

Pyroelectric detectors were built with different types of active elements: pure and doped PVDF. The pure PVDF is a commercial film from Solvay, Belgium. The doped PVDF film is prepared by solving the polymer and additive in dimethyl sulfoxide and cast onto glass. An effective additive is hexamethyl parosaniline (crystal violet). The additive acts as an absorber for incident radiation in a special spectral range and influences the structure of films casted from solution. The films were four times stretched and electroded by thermal vacuum deposition with gold or aluminium on both surfaces. Semitransparent front electrodes were created by gold deposition of 10 nm thickness. Subsequently the films were poled in strong electric fields from 2 MV/cm up to 3.5 MV/cm. The films were arranged in the detector by a simple clamping on a heat sink to prevent thermal destruction during irradiation. The pyroelectric signals due to irradiation with low power lasers (He-Ne laser) were measured with a phase sensitive voltmeter at a modulation frequency of 80 Hz.

In order to detect the time resolution of high power laser pulses the detector is directly connected to a high speed oscilloscope. The lasers used for the investigations have the following operation characteristics:

type	wave length	pulse duration	power
excimer	308 nm	7.5 ns	8 MW
N_2	337 nm	3 to 10 ns	1 MW
He-Ne	632.8 nm	cw	40 mW
CO_2-TEA	10.6 µm	1 to 5 µs	1 MW

RESULTS

To protect optimal absorption conditions several kinds of element constructions were designed and tested.
The pulse power of a CO_2-TEA laser was measured by the absorption of the radiation across a semitransparent gold electrode. The time resolved power pulse of a CO_2-TEA laser is shown in Fig. 1.
The electric time constant of 5 ns was obtained with a load resistance of 50 ohm and an effective sensor capacitance of 100 pf.

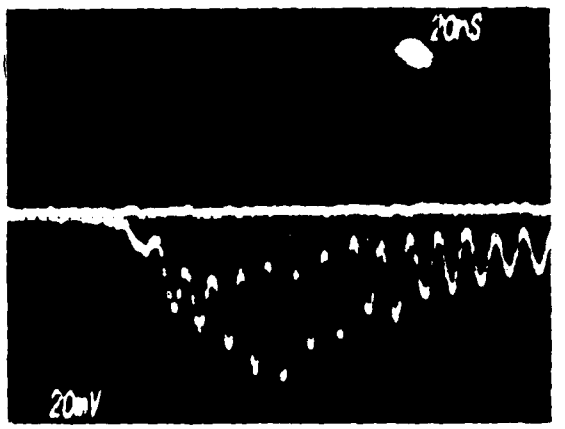

Fig. 1 Time dependence of the CO_2-TEA laser power pulse (mode locking)
time resolution: 20 ns/div

One problem in measuring high laser powers is the thermal destruction of the thin semi-transparent gold electrodes after several irradiations.
To avoid this disadvantage a wave guided arrangement was tested. The investigation of responsivity as a function of the irradiation angle shows a strong influence on the multiple reflections inside the element volume and therefore on the absorption conditions for a crystal violet doped sensor element. The pyroelectric responsivity of doped PVDF is larger than 30 times in comparison to unmodified sensor elements.
In short time experiments the radiation of a N_2-laser was led into the volume of the active PVDF sensing element in this way. With a detector capacitance of 40 pf and a load resistance of 25 ohm an electric time constant of 1 ns was obtained. In this way it is possible to detect the time resolved power pulse of a N_2-laser. The rise time of the pulse is about 800 ps and will be exactly restored by the pyroelectric detector.

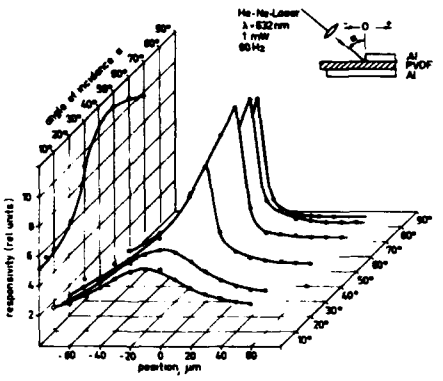

Fig. 2 Pyroelectric responsivity of doped detector elements as a function of the angle of incidence

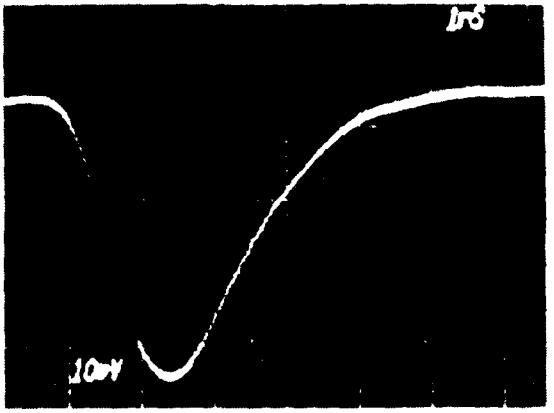

Fig. 3 Time resolved power pulse shape of a N_2-laser
time resolution: 1 ns/div

The wave guided arrangement protects a good electrical and thermal contact between the pyroelectric active element and the mounting. Therefore repetition rates in the order of several thousand cycles per second are possible. The fast response experimental results indicate a significant fraction of primary pyroelectricity in PVDF. With a farther more decrease of the electrical time constant more shorter pulses are detectable.

REFERENCES

[1] S.C. Stotlar, E.J. McLellan, A.J. Gibbs, J. Webb, "10.6 µm damage threshold measurements on sub-one-hundred-ps pyroelectric detectors", Ferroelectrics, Vol. 28, pp.325-327, 1980.

[2] W. Bohmeyer, W. Kabel, H. Volkmann, R. Danz, B. Elling, W. Stark,"Pyroelectric detectors on the basis of PVF_2", Exp. Techn.Phys., Vol. 30, pp. 65-74,1982.

[3] R.G. Kepler, R.A. Anderson, "On the origin of pyroelectricity in polyvinylidene fluoride", J.Appl.Phys.,Vol.49, pp. 4918-4921, 1978.

CONSTANT CURRENT CORONA TRIODE WITH BIAS GRID VOLTAGE CONTROL

José A. Giacometti and J. Sinézio Campos+

Instituto de Física e Química de São Carlos
Universidade de São Paulo - CP 369
13560 - São Carlos - Brasil
+Departamento de Ciências
Universidade Estadual Paulista J. Mesquita Filho
15378 - Ilha Solteira - Brasil

ABSTRACT

A new version of a corona triode alowing charging dielectric foils with a constant current was developed. The charging current is kept constant by controlling the bias grid voltage. We describe how the sample potential is measured and present results of the uniformity of charge deposition and some measurements performed with Teflon FEP and PVDF films.

INTRODUCTION

The corona triode with constant current had proved to be a powerful technique to study the charge transport in dielectric foils. The method allows to follow the entire charging and discharging cycle for a sample charged with a constant current[1,2]. Previously, to achieve a constant charging current a feedback circuit was used to control the corona tip voltage. The surface potential measurement is based upon the method of the dynamic capacitor[3].

The new version of a corona triode uses a constant current source as the charging current and measures the corresponding grid voltage[4]. The surface potential may be inferred using a calibration curve, as will be explained shortly. Furthermore, the apparatus allows to improve the surface charge uniformity during charging mainly due to a polarized cylinder above the grid. Some measurements with Teflon FEP and PVDF samples are also shown.

CH2593-2/ 88/ 0000-0404$01.00 Copyright 1988 IEEE

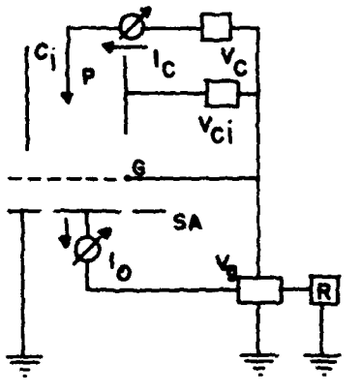

FIGURE 1. Diagram of the measurement setup

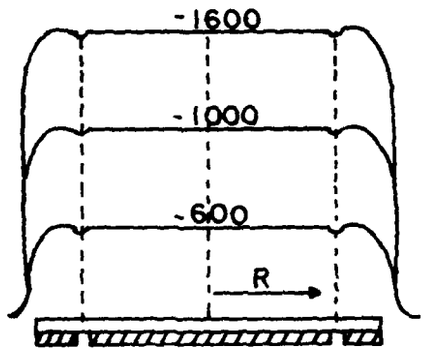

FIGURE 2. Charge uniformity (FEP)

EXPERIMENTAL SETUP

A positive or negative corona discharge is generated applying a voltage to a tip placed inside a biased metallic cylinder, as figure (1) shows. A metallic grid is inserted between the tip and the sample holder to constitute the corona triode. The constant current corona and the cylinder voltage supplies are floating over the grid voltage supply V_g. The voltage bias applied to the cylinder allows to improve the radial current distribution produced by the corona discharge[3]. The charging current I_o is monitored by an electrometer and a recorder is connected to the V_g supply output.

CURRENT CONTROL AND THE POTENTIAL DETERMINATION

To kept constant the current I_o the output signal of the electrometer is fed in to the grid voltage supply to control the bias grid voltage in order to compensate the decrease of the charging current when the sample voltage increases. Then, V_g must increases in the same proportion of the sample voltage in order to keep the charging current I_o constant[5].

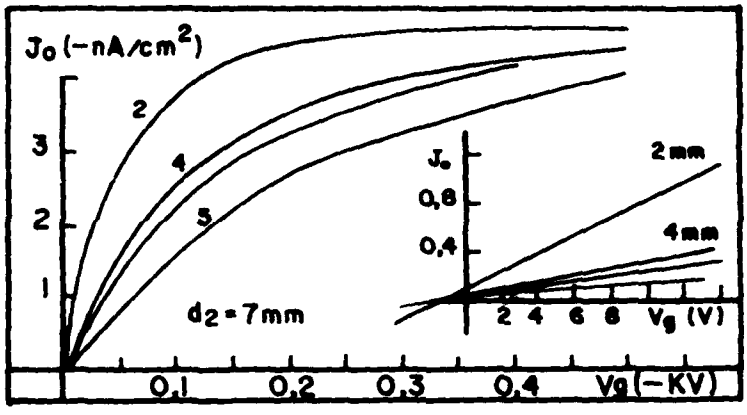

FIGURE 3. Electric characteristics of the new corona triode. Calibration curves for determination of potential for differents operating conditions. The inset shows the current for small values of V_g showing the effect of corona wind. Corona current I_c = -5uA.

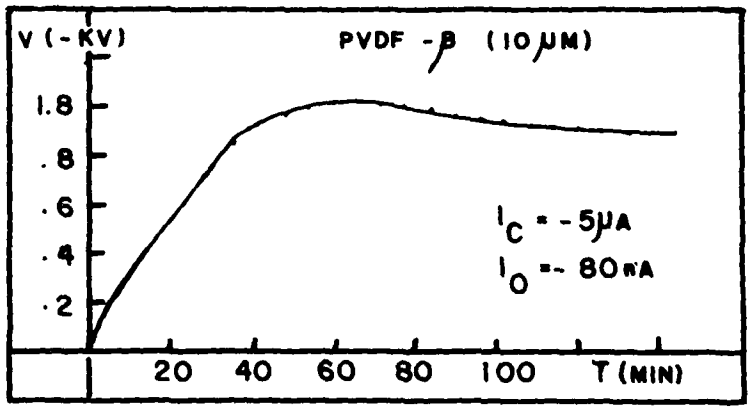

FIGURE 4. Potential build-up for a β-PVDF sample 10 μm of thickness. Negative charge.

Since the electric gap field is due to the applied grid voltage V_g the surface sample charge and to the space charge formed by the ions in the gap[4], the grid voltage is equal to

$$V_g(t) = V(t) + V_s \qquad (1)$$

where $V(t)$ and V_s are the sample potential and the potential drop due the space charge (which remains constant in a given experiment). $V(t)$ may be determined using the equation (1) and the value of V_s obtained measuring V_g without the sample but with the same current I_o (that is, $V_g=V_s$). V_s depends only on I_o and the geometry and a set of curves for different grid to sample distances are showed in the figure (2). The inset shows the dependence of the current for small values of V_g.

SURFACE CHARGING UNIFORMITY

An important requirement for a meaningful measurement of the surface potential is the charging uniformity over the sample. In the past a special double grid was used to provide almost uniform charge profiles[1-3]. With the bias grid voltage control a grid with a single mesh produces a very uniform charge profile[4]. Figure (3) shows the evolution of the surface potential as function of the sample radial position. The uniformity obtained with this technique is better than those obtained with the corona voltage control and increases when operating the system with small grid to sample distances. The space charge appearing in the gap and the biased metallic cylinder are responsible for the good charge profile[4].

RESULTS FOR TEFLON FEP AND PVDF

Measurements performed with Teflon samples showed that $V(t)$ increases linearly with the time when charged at moderate surface charge density[2]. Table I shows the rate $R = dV(t)/dt$ of the potential build up for different current and sample thickness. The sample capacitance determined by $C = I_o/R$ agrees within 5% with the value C_b measured using a capacitance bridge.

TABLE I

L	I_o	dV/dt	V_f	C_b	C_b/C
um	-nA	-V/sec	-V	nF	
25	1.3	3.67	1.89	.344	Ø.97
25	3.5	1Ø.5	2.16	.344	1.Ø3
5Ø	3.3	16.67	4.Ø	.2Ø4	1.Ø3
5Ø	6.5	31.83	4.Ø	.2Ø4	.989
75	1.7	13.45	3.32	.132	1.Ø5
75	4.8	38.25	3.56	.132	1.Ø5

V_f- final sample voltage
L-sample thickness C_b-sample cap.(bridge)

Figure (4) show the potential build up for samples of β-PVDF. At the beginning of the charging the sample voltage increases fast, then a knee appears and finally a steady state is reached. At moment we believe that the knee is due the polarization switching which happens at critical electric field. The steady state is supposed to be due electric sample conductivity[6].

ACKNOWLEDGMENTS: Authors are thanked to CNPq and TELEBRAS for the financial help and to G.F. Leal Ferreira.

REFERENCES

1. J.A Giacometti. PhD. Thesis. "Corona with constant current: A new method...." Universidade de São Paulo - São Carlos - Brasil. 1982
2. B. Gross, J.A. Giacometti and G.F. Leal Ferreira. "Corona Method for investigation fo charge storage and transport in dielectrics". An. Rep. IEEE-CEIDP, pp39-44(1979)
3. R.A. Moreno and B. Gross. "Measurement of potential build up and decay, surface charge..". J. Appl. Phys., vol47, pp3397-3402(1976)
4. J.A.Giacometti. "Radial current-density distr., sample charge unif. in a corona triode". J.Phys.D:Appl.Phys., vol2Ø, pp675-682(1987)
5. R. Haug. French Patent 8414209 (1984)
6. B. Gross, J.A. Giacometti, G.F. Leal Ferreira O.N.Oliveira. "Constant current corona charg. of PVDF". J.Appl.Phys.,vol56,pp 1487-1491(1984)

PEAK SHIFT DUE TO THE ELECTRIC FIELD ON PETP CORONA CHARGED FOILS

José A. Malmonge+, G.F. Leal Ferreira, José A. Giacometti and R.A. Moreno++

Instituto de Física e Química de São Carlos
Universidade de São Paulo - CP 369
13560 - São Carlos - Brasil
+Departamento de Ciências - 15378-Ilha Solteira
++Departamento de Física - 13500 - Rio Claro
Universidade Estadual Paulista J. Mesquita Filho

ABSTRACT

Annealed PETP samples corona charged give only one open circuit current peak on heating from room temperature, the thermograms being independent of the polarity and metal electrodes. However, the peak shifts to lower temperature for increasing initial potential. These results seem to indicate that an electric field activated conductivity is at work. Frozen free volume charges may explain higher currents observed on the low temperature part of the thermogram.

INTRODUCTION

Measurement of TSD in corona charged annealed PETP (polyethylene terephthalate) samples were carried out in a variety of ways, attempting to clarify the nature of the conduction process. A shift of the TSD peak to lower temperature with increasing field was observed.

EXPERIMENTAL DETAILS

All measurements of thermally stimulated current in open circuit were performed with 25 μm Mylar-A samples supplied by DuPont Nemours. They are discs carrying a vacuum deposited Al electrode in one side. A few measurements with another kind of metal electrode or in two side metallized samples were also performed. Samples were charged either positive or negatively using a corona triode. The open circuit TSD measurements were carried out using a oven controlled by a microcomputer which also allows

CH2593-2/ 88/ 0000-0409$01.00 Copyright 1988 IEEE

to digitize the experimental results. The heating rate was between Ø.5 to 4.5°C/min. Prior to each measurement the samples were annealed and quenched in order to freeze a free volume, thus eliminating the first current peak, with a maximum around 76°C, appearing in as received (that, is aged) samples and believed at the transition temperature[1].

EXPERIMENTAL RESULTS

The crosses in figure (1) and (2) show the TSD current for one side metallized samples charged at different initial potentials. The results show that the temperature T_p where the maximum occurs decreases as function of the initial sample voltage, see the inset of figure (1). It was found that the current peak shape is essentially independent of the charging polarity, nature and number (one or two) of electrodes used, for voltages not exceeding 5ØØ volts. By means of the heat pulse technique it was found that the position of the charge centroid was always located at the sample surface independently of temperature, initial potential, polarity and other parameters. All these results seems to indicate that the potential decay is due to intrinsic mobile carriers, that is, to a conductivity process, as already proposed[2].

THE TRANSPORT MODEL

In a first attempt, an electric field and temperature dependent conductivity of the sinh type[3] was unsucessfully used to fit the results: neither the larger initial rise nor the peak shape and position were correctly obtained. A better fitting was obtained (lines in fig. (1) and (2)) assuming:

1) that, according to Adamec and Calderwood[4] the density of intrinsic carriers is electric field dependent due to a kind of Poole-Frenkel dissociation. The dissociation is also activated, with energy U_1.
2) that, the mobility of the free carriers is dependent on the free volume [5], which is higher than the equilibrium value below the

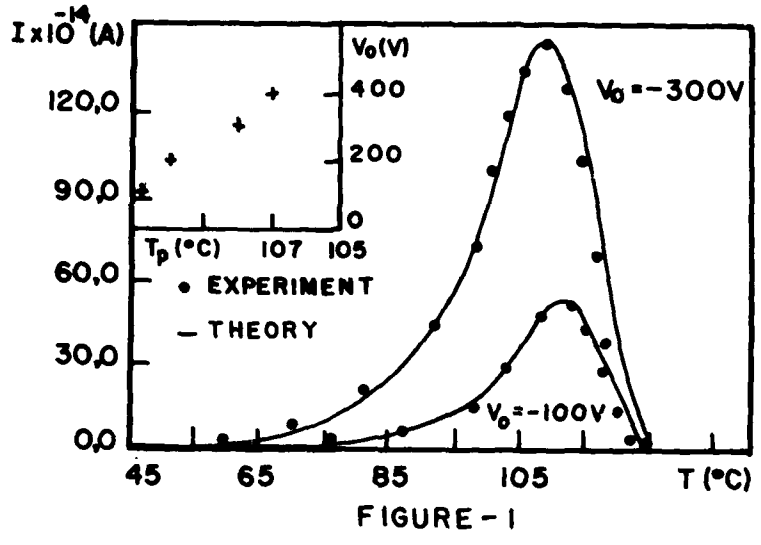

FIGURE - 1

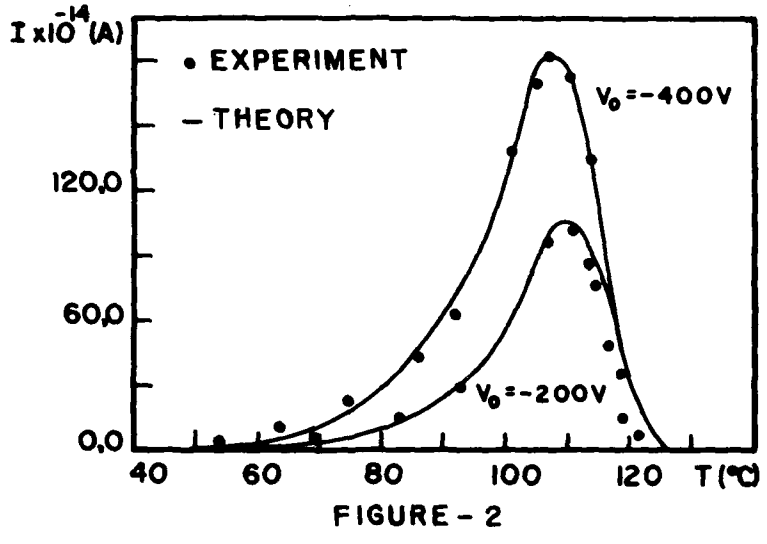

FIGURE - 2

FIGURE (1) and (2). Open TSD measurements for 25 μm PETP samples charged at different initial potential V_o. The inset of figure shows the dependence of peak temperature T_p as function of V_o.

glass-plastic transition temperature T_m (at 78°C, approximately in Mylar). Using the free volume dependent expression for the jumping frequency v_o [6],

$$v = v_o[\exp(-xU_2/kT)]\exp[-(1-x)U_2/kT^*]$$

where x measures the part of the jumping activation energy U_2 due to the free volume, which is dependent of T^*, the fictive temperature. In general[7] $T^* = T + \frac{v - v_\infty}{\alpha\, v_\infty}$

where v and v_∞ are the actual and the equilibrium volume and α the mean dilation coefficient. During cooling T^* is very close to T for $T>T_m$ and equal to T_m for $T<T_m$[5]. This is not exactly so in the subsequent heating but the figures are still good approximations, which greatly simplify the calculations. With this, the conductivity g becomes

$$g = \{N_o e^2 a^2[\exp(-U_1/2kT)][1+A\sinh A-\cosh A]/A^2T\}.$$

$$.v_o[\exp(-xU_2/kT)]\exp[-(1-x)U_2/kT^*] \quad \text{mho/cm}$$

with $A = 49.2\sqrt{V}/T$, for Mylar 25 μm samples. N_o is the density of dissociating centers, a the jumping distance, e the electronic charge and V the sample potential in volts.

The fittings provided the following set of parameters: U_1=Ø.4 eV, U_2=1.8 eV, x=Ø.6, but a new set U_1', U_2' and x′ such that $U_1'+U_2' = 2$ eV and $U_1'(1-x')$=Ø.72 will also work. A bad feature of the model is the high value of v_o thus obtained (for $N_o=10^{22}cm^{-3}$, $v_o \sim 10^{22}Hz$) for reasonably a jumping distance of a few Angstrons. In figure 3 the constant temperature current calculated with the above g value is compared is with the measured ones. For values of the potential less than 500 volts, the agreement is fairly good.

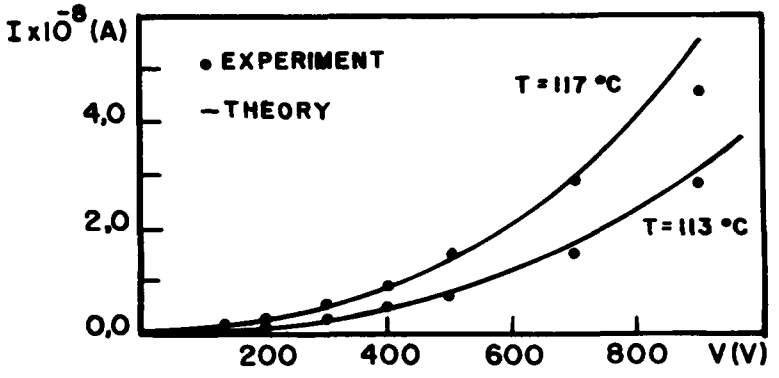

FIGURE (3). Short circuit currents for PETP samples at different temperatures. The fitting parameters are the same used to fit TSD measurements.

ACKNOWLEDGMENTS: The authors are thanked to FAPESP and TELEBRAS for the financial support.

REFERENCES

1- D. Broemme. "Isot. and Therm. stim. discharge PETP foils". Ann.Rep.IEEE-CEIDP. pp129-135(1981)
2- L.E.Amborski. "Structural dependence of the electrical condutivity of PETP". J.Polym.Sci., vol62, pp331-345(1962)
3- V. Adamec and J.H. Calderwood. "Electrical conduction is dieletrics at high fields". J. Phys. D: Appl. Phys. vol 8, pp 551-560(1975)
4- A.J.Kovacs and J.M.Hutchinson. "Isobaric Thermal behaviour during cooling and heating". J.Poly.Sci:Phys. Ed. vol 17, pp2031-2058(1979)
5- O.s.Narayanaswamy."A model of struc. rel. in glasses".J.Am.Ceram.Soc.,vol 54, pp491-498(1971)
6- A.J.Kovacs, J.M.Hutchinson and J.J.Aklonis. "Isobaric vol. and enthalpy recovery of glasses". Structure Cryst. Mat., P.H.Gaskell, Ed. Taylor-Francis. London, pp 153-163(1977)

SOME STUDIES ON GLASS FIBRE REINFORCED POLYMER COMPOSITES

Malti Goel

Department of Science & Technology
Technology Bhawan
New Delhi-110 016

ABSTRACT

Composites are novel materials, having two or more components. In composite formation specific properties of one of the component are considerably improved by addition of the other component. Most developed modern composite materials are fibre reinforced composites, known for their improved mechanical properties such as strength and stiffness. Investigations on electrical and polarization properties are relatively less. The present article concerns the effect of fibrous fillers on dielectric properties and the role played by interface in polymer composites. Physical properties of composites can be described in terms of series or parallel coupling or those based on structure and composite geometry. Some results obtained on short glass fibre reinforced polypropylene composites will be discussed.

INTRODUCTION

Glass fibre reinforced polymer composites are essentially two phase materials with polymer acting as continuous phase, called matrix and glass fibre as dispersed phase, called filler. Fillers could be continuous or discontinuous. Mechanical properties like stiffness and toughness are considerably improved by addition of glass fibres. This has led to the advancement of Technology, for many light weight structural applications. When enhancement in electrical properties was looked, conducting filler, such as carbon black (1) or metallic fibres have been used. Detail investigations of electrical properties have not been carried on composites having glass as fibres. Glass though nonpolar, has conduc-

CH2593-2/ 88/ 0000-0414$01.00 Copyright 1988 IEEE

tivity 100 times that of Polypropylene and therefore, can play important role in electrical polarisation and dielectric measurements.

EXPERIMENTAL

Experimental set up used for measuring thermally stimulated current has been described in a previous publication (2). The thermal cycle for conductivity measurement consists of heating to a temperature upto 150 °C at a constant rate, in the presence of external electrical field. Current is measured across the sample with the help of Keithley Electrometer 610 C.

RESULTS AND DISCUSSIONS

Many theories have been proposed to derive expressions for physical properties of a composite, on the basis of sum properties of constituents. These derivations are based on the assumption that composite is istropic on macroscale. The resultant physical property in case of unidirectional fibrous or cylindrical fillers are emperically derived by applying the Rule of mixtures.

For a series distribution of the filler in matrix it can be stated as

$$K_{comp} = \frac{K_1 K_2}{vK_2 + (1-v)K_1} \quad \ldots(1)$$

K stands for the physical property of two components with subscripts 1 and 2, and v is volume fraction of the filler. K could be electrical conductivity, dielectric constant, dielectric loss or Young's modulus along the alignment direction, as the case may be.

For the case of parallel coupling between two components, physical property would be

$$K_{com} = (1-v)K_1 + vK_2 \quad \ldots(2)$$

Consideration of polarity of matrix and fillers are also important for determining dielectric behaviour. In case of non-polar fillers such as glass,

in non-polar matrix, a two layer capacitor model has been suggested (3) for finding the value of composite dielectric constant interms of permittivities, conductivities and volume fractions of its components,

$$\epsilon^* = \frac{v\epsilon_2\sigma_1^2 + (1-v)\epsilon_1\sigma_2^2}{\left[v\sigma_1 + (1-v)\sigma_2\right]^2} \qquad \ldots\ldots(3)$$

Here v is volume fraction of the filler. ϵ and σ are the dielectric constant and conductivity of two components with subscript 1 and 2. Calculated value of dielectric constant however is found to lower than the observed value of 2.38 at 100 Hz.

According to Hale (4) resultant composite property could either be SUM or PRODUCT property of its constitutent phases. Conductivity mismatch at the interface plays an important role. Interfacial polarisation losses arise since the ratio of dielectric constant and d.c. conductivity is different for polypropylene and glass. The emperical relations based on sum properties do not take into account this aspect as well as fibre dimensions. Van Suchetelen (5) proposed that all possible interactions between two phases should be considered while describing any physical property of the composite. This behaviour is explained on the basis of product properties and the composite may have entirely new set of properties as differentiated from its components.

Electrical conductivity measurements are shown in Fig.1 as a function of temperature. Matrix behaviour dominates upto a temperature of 44 °C. Above this temperature, composite conductivity is raised by an order of magnitude than that of polypropylene. Glass itself showed conductivity due to carriers injected from electrodes as well localised processes invoking activated transitions from occupied site to nearby site, which is several orders higher than polypropylene, where stochastic transport model for amorphous materials seems to be applicable. Within the polymer surface conductivity of glass fibres is much higher than its volume conductivity. Glass fibres act as nucleating agents during the formation and a narrower distribution

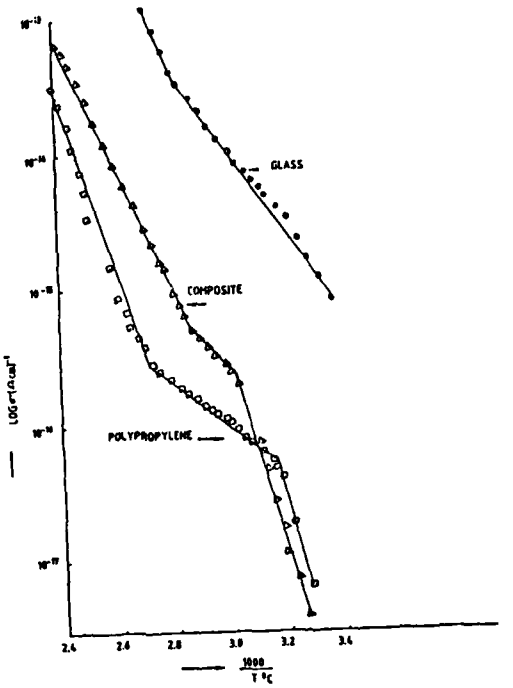

Fig.1. Plot of log conductivity vs inverse of temperature

of crystalline size is observed in their vicinity. At a temperature corresponding to dielectric relaxa tion (2) bound charge at amorphous-crystallite boundaries or polymer glass boundaries is released giving rise to recombination processes and a decrease in the slope of $\log \sigma$ *vs* $\frac{1}{T}$ *curve.*

TSC measurements on Electrets prepared from these samples have shown interesting evidence of product behaviour. In the case of composite, peak current is increased by a factor more than two. Higher polarisation results from accumulation of charge at the polymer-glass interface, even though, taken individuallytheir polarisabilities are not so different. At the same time lower mobility in composite arises from hindrance due to large surface area of fibre matrix interface. It is relevant to mention here that Data on stiffness measurements is also compared

(6). Eq (1) and (2) above do not give the resultant behaviour. The observations are explained taking aspect ratio of fibres and role played by interface into account.

CONCLUSION

Measurement of dielectric constant electrical Conductivity andpolarization has shown that product behaviour is predominant in short glass fibre reinforced polypropylene.

ACKNOWLEDGEMENT

Author expresses her gratefulness to Prof.PKC Pillai and Prof.VB Gupta at Indian Institute of Technology for providing the facilities and many fruitful discussions. She is grateful to Department of Science & Technology for other assistance.

REFERENCES

1. S.K.Bhattacharya and A.C.D.Chaklader,Polym.Plast. Tech. Eng.,19(1),21(1982)
2. Malti Goel,VB Gupta and P.K.C.Pillai, Polymer Bulletin;7,69 (1967).
3. L.K.H. Van Beek,Progress in Dielectrics;7,69(1967)
4. D.K.Hale,J.Mat.Sci.,11,2105(1976)
5. J.Van Suchtelen,Philips Res.Repts.,27,28(1972)
6. Malti Goel andV.B.Gupta (to be published)

ELECTRIC POLARIZATION OF POLYMERS IN METAL-DIELECTRIC-METAL SYSTEMS

Goldade V., Pinchuk L., and Voronezhtsev Yu.

Institute of Mechanics of Metal-Polymer Systems,
Byelorussian SSR Academy of Sciences,
246652 Gomel, USSR

ABSTRACT

The phenomenon of electric polarization was observed in polymeric interlayers, and existence of an electret state in polymers, when spontaneous thermally stimulated currents (TSC) passed across a metal 1 - polymer - metal 2 (M1 - P - M2) system. This type of polarized state was termed " metal - polymer electret " (MPE). The amount of the volume charge determined by the thermally stimulated depolarization (TSD) method was shown to reach the value of 10^{-5} C/cm sq. ; the charge being distributed in the near-electrode layers of 20 - 80 microns thick. The electrode metals were found to diffuse in the polymeric matrix; a correlation was established between the distribution of the metal and the volume charge throughout the MPE depth. The structure and properties of MPE were investigated. The mechanism of electric polarization of polymers was discussed for M1-P-M2 systems as resulting from the formation and degradation of organometallic species in the polymeric matrix.

INTRODUCTION

In recent years, the process of current generation in M1-P-M2 systems has been given much attention. A number of authors used a great variety of polymers in studying spontaneous TSC, which depend on the open-circuit voltage generated between electrodes. The present authors assume an electrochemical origin of this voltage [1]; work [2] describes an electrochemical model where the electrode reactions at the metal-polymer interface are treated as a basis for the open-circuit voltage. A metal 1 -polymer-metal 2 system can be treated as a galvanic cell with a high internal resistance; then the

CH2593-2/ 88/ 0000-0419$01.00 Copyright IEEE

open-circuit voltage can be described by the differences in the oxidation potentials of the metals, or in other words, by the difference in free energies of the oxides formation [3]. The galvanic effect can significantly influence the electrical properties of polymers in weak fields. It appears that TSC passing through M1-P-M2 systems lead to electric polarization of the polymer interlayer, and the electret state occurs [4].

RESULTS

Unlike thermal electrets that acquire stable charge in strong electric fields (dozens kV/cm), MPE are formed without voltage from external sources. A necessary and adequate condition for MPE formation is that the polymeric material must be thermally treated between short-circuited electrodes of dissimilar metals. The volume charge density in MPE (σ_{TSD}) can reach values of 10^{-5} C/cm^2, and exceed by several orders of magnitude the effective surface charge density (σ_{eff}) measured by the contact-free induction method (Table 1).

TABLE 1

Fabrication Conditions and MPE Charges when Cu - Al Electrodes Were Used

Polymer	T, K	τ, ks	Charge density, C/cm^2	
			σ_{TSD}	σ_{eff}
PE	440	10.8	6×10^{-8}	8×10^{-10}
PMMA	400	2.4	1.7×10^{-5}	2.4×10^{-9}
PVB	407	3.9	1.9×10^{-5}	1.5×10^{-8}

It is characteristic that MPE formed by polarization of films in contact with dissimilar metals possess homocharge, i. e., the charge sign in the electret surface coincides with the polarity of the corresponding electrode from the electrochemical series of metals.

The results of investigations in the charge distribution across the MPE volume indicate that the polarization charge is mostly concentrated in the surface layers of the specimens (Figure 1, curve 1). After polarization between Cu - Al electrodes, the charge localized near the copper electrode is higher than that near the aluminum electrode [5].

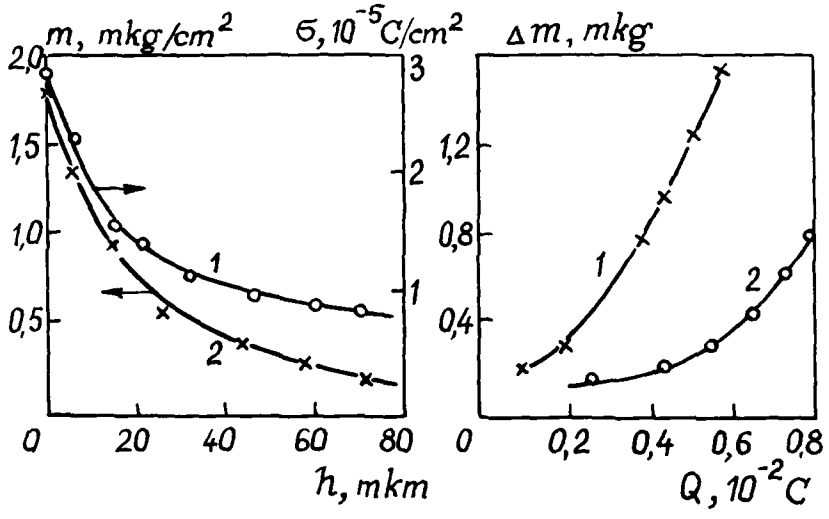

Figure 1. TSD charge density (1) and copper content (2) in polarized PVB (Cu - Al electrodes) vs. thickness of layers cut from the surface. Initial film thickness was 300 microns

Figure 2. Mass differences for copper (1) and aluminum (2) in polarized (Cu - Al) and reference PVB vs. polarization charge

The MPE charge magnitude is affected by the following factors : plasticization and doping of the polymer, deformation of samples, and gamma-irradiation.

Polarization of a polymer in contact with dissimilar metals is accompanied by transfer of metals from the electrodes into the polymeric matrix [6]. For instance, after PVB was polarized between Cu - Al electrodes, the copper content in the polymer approached 2 mkg/cm^3 (Figure 1, curve 2), aluminum 0.25 mkg/cm^3. For the reference samples thermally treated in contact with open circuit electrodes, the values were lower by 2 - 5 times. The quantity of the metal diffused in the polymeric layer increased with the polarization charge (Figure 2).

The diffusion of metal in polymer and the volume charge generated lead to structural rearrangements in the near-electrode polymeric layer [7]. For instance, with penton the roentgen degree of crystallinity in the polarized samples increased by 4% on the part of the Cu electrode, and 6% on the part of the Al electrode, as compared to the thermally treated unpolarized samples.

Modification of MPE surface layers changes their physical-and-mechanical properties [8]. The breaking tensile stress increases by 1.2 - 1.8 times for polarized film samples of PVB, PVC, PA and penton as compared to unpolarized samples. The strengths of polymer-metal adhesion bonds increased by 1.5 - 2 times. The vapour sorption of organic solvents dropped by 10 - 50 times (for diethyleneglycol, benzene, etc.).

DISCUSSION

On the basis of the experimental data analysis, a mechanism of MPE polarization is proposed that combines the electrochemical and volume charge polarizations [9]. As the result of electrochemical reactions of the diffused metallic ions and carboxyl groups of the polymer in the near-electrode layers, metal-containing species are formed, particularly salts of carboxylic acids, which subsequently

decompose to give metallic particles. Decomposition of the metal-containing species accumulated in the near-electrode zone results in an unbalanced dis - tribution of the charges and electric polarization of the polymers.The electret charge is generated by the capture of charge carriers by the structural traps resulted from both the structure irregularities in the polymer itself, and the polymer - metal particle interfaces (Maxwell - Wagner polarization).

REFERENCES

[1] V. A. Belyi, V. A. Goldade, A. S. Neverov, and L. S. Pinchuk,"Study of Physico-Chemical Interactions in Metal-Polymer Systems", J. Polym. Sci.: Pol. Chem. Ed., Vol. 17, pp. 3193 - 3203, 1979.

[2] A. K. Vijh,"Electrochemical Effects as the Source of Electromotive Force in M1-P-M2 Systems", J. Appl. Phys., Vol. 49, pp. 3621 - 3624, 1978.

[3] J.-P. Crine and A. K. Vijh,"The Electrochemical Origins of Open-Circuit Voltages Observed During Heating of Metal-Polymer-Metal Systems", Materials Chemistry ans Physics, Vol. 11, pp. 85-98,1984

[4] V. A. Bely, V. A. Goldade, A. S. Neverov, and L.S. Pinchuk, "Electret State of Polymers in Joints of Dissimilar Metals", USSR Academic Reports(Rus) Vol. 245, pp. 132 - 134, 1979.

[5] Yu. I. Voronezhtsev, V. A. Goldade, L. S. Pinchuk, and G. V. Rechits,"Effect of Charge Volume Distribution on Friction Characteristics of Polymeric Electrets", Soviet Friction and Wear J.(Rus.ed.), Vol. 5, pp. 138 - 142, 1984.

[6] Yu. I. Voronezhtsev, V. A. Goldade, and L. S. Pinchuk, "On the Mechanism of Polymer Polarization in M1-P-M2 Systems", BSSR Academic Reports, Vol. 28, pp. 534 - 536, 1984.

[7] V. A. Bely, I. M. Vertiachikh, Yu. I. Voronezhtsev, V. A. Goldade, and L. S. Pinchuk, "Strength of Polymeric Composites Formed in Contact with Metals", USSR Academic Reports, Vol. 275, pp. 639 - 641, 1984.

[8] I. M. Vertiachikh, Yu. I. Voronezhtsev, V. A. Goldade, and L. S. Pinchuk, "Properties of Polymeric Electrets Formed in Contact with Dissimilar Metals," Plastics (Rus), No. 3, pp. 30 - 32, 1986.

[9] V.Goldade et al.,Vysokomol.soed.,Vol.30,p.328,1988.

CHARGE STORAGE AND RELAXATION $SrTiO_3$ AND $KTaO_3$ CRYSTALS

Yu. Gorokhovatsky and Yu. Sezonov

Moscow Institute of Electronic Engineering, Moscow, USSR.

ABSTRACT

Charge relaxation in $SrTiO_3$ and $KTaO_3$ single crystals was studied by thermally stimulated depolarization (TSD) technique.

TSD currents measurements of photo- and thermoelectret state in crystals showed the close relation of high temperature peaks to volume charge storage at hole capture centers. The energies of these centers are determined by fractional TSD techniques.

We obtained three quasi-discrete levels with energies 0,22; 0,25; 0,43 eV in $KTaO_3$. In case of $SrTiO_3$ only one quasi-discrete level with energy 0,56 eV was determined, but also a number of levels with continuous energy distribution in the range of 0,15 - 0,22 eV.

TSD CURRENTS IN THERMALLY AGED AND β-IRRADIATED POLYETHYLENETEREPHTALATE FILM

S.M. Gubanski[+], A. Gubanski[+], B. Macalik[x]

[+]Technical University of Wroclaw, ul. Wybrzeże Wyspianskiego 27, 50-370 Wroclaw, Poland

[x]Institute of Low Temperatures and Structure Research, Polish Academy of Sciences, P.O. Box 937, Wroclaw, Poland

ABSTRACT

Influences of thermal ageing and β-irradiation on TSD current spectra of the PET film were studied. A dynamics of the complex ageing as well as changes in activation energies temperature distributions were found.

INTRODUCTION

Attempts to study a multistress ageing characteristics of different insulating materials are recently often undertaken. Out of many factors that may interact with the materials most interesting are temperature, electric field, different types of irradiation and mechanical stresses. This work presents the study of the joint influence of β-irradiation and thermal ageing on thermostimulated depolarization current spectra of the polyethyleneterephtalate film. Authors have recently proposed [1] to apply the TSD measurements for the temperature indice TI prediction of PET polymeric films. Therefore, it was also interesting to study how the two-stress ageing influences the PET film TSD current spectra.

EXPERIMENTAL PROCEDURE

A commercial ESTROFOL PET film, 36μm thick, was investigated. It was characterized by a high degree of crystallinity ~70%. The TSD currents measurements were conducted in vacuum (10^{-4} Tr) in the temperature range 80K to 500K.

CH2593-2/ 88/ 0000-0425$01.00 Copyright 1988 IEEE

Samples were β-irradiated with three different doses of 5, 10 and 15 Mrads and then thermally aged in air chambers at temperatures 105, 160 and 200 °C for 5, 10 and 100 hours.

RESULTS AND THEIR DISCUSSION

A typical TSD spectrum for the fresh PET film is shown in Fig.1. The literature data [2,3] and the earlier authors studies [1,4] indicate that the low temperature relaxation β (120-210K) results most probably of a movement of side polymer polar groups in its glassy state. A conformational rearrangement of the main polymer chains, when it reaches the glass transition temperature, is reflected by the appearence of the α peak in the temperature about 360K. Finally, above the temperature of 380K the ϱ peak appeares and it is attributed to a space charge formation at locallized states.

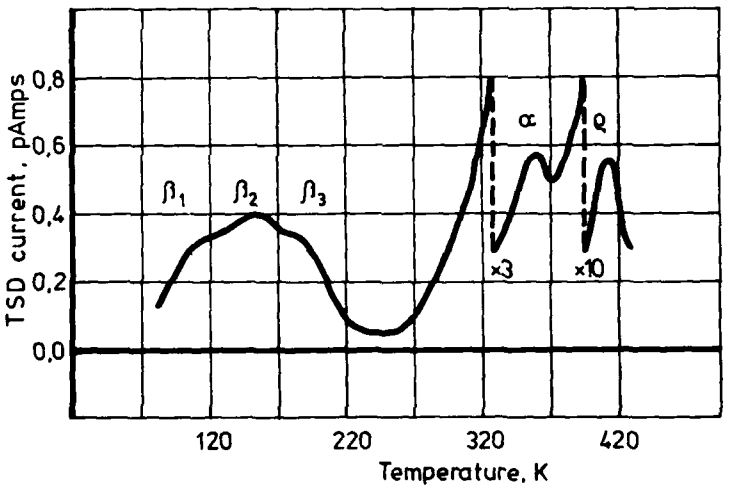

Fig. 1. TSD current spectrum of the fresh PET film charged at 390K - 100V - 1800s.

The β-irradiation of the film causes a change of both, i.e. α and ϱ peaks intensities. The ϱ peak increases, whereas its maximum temperature remains unchanged. At the same time the α peak decreases, and this may be related to

an additional crosslinking of the polymer chains in its amorphous phase. The ϱ peak increase is caused by creation of additional charge traps.

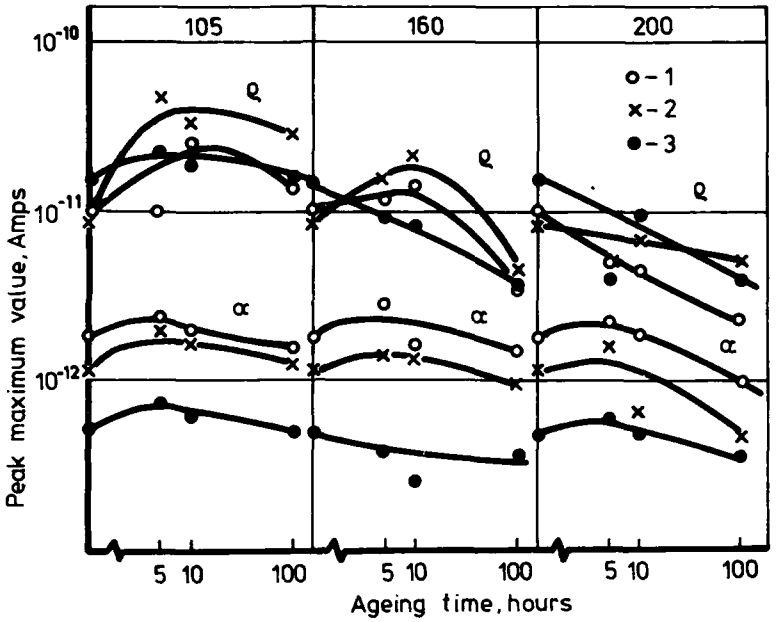

Fig. 2. Ageing time influence on the α and ϱ current peaks maxima for different ageing temperatures and irradiation doses.

Qualitative changes of the α and ϱ peaks caused by thermal ageing of previously irradiated samples are shown in Fig.2. The α peak intensity, for all ageing temperatures, increases initially and then, after reaching a maximum value, decreases. Similar behaviour may be noticed for the ϱ peak measured on samples aged at temperatures 105 and 160°C. On the other hand, the ageing at the temperature of 200°C causes a monotonous decrease of the ϱ peak intensity.

When applying the partial heating technics,

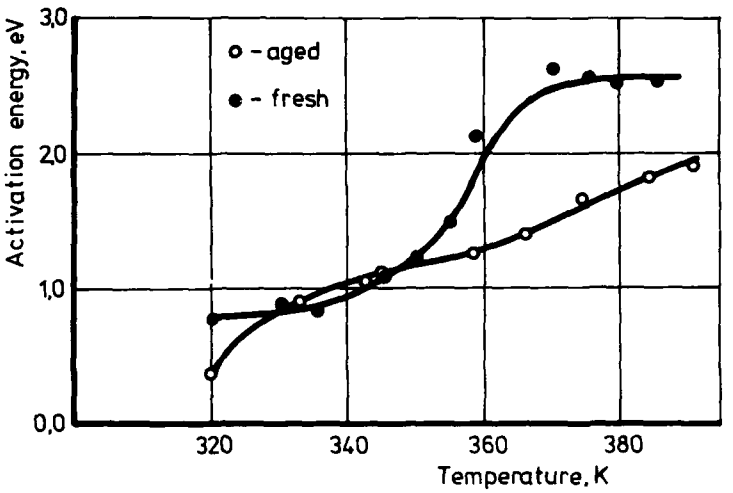

Fig. 3. Activation energies distributions for fresh and thermally aged (160°C, 1700h) PET samples.

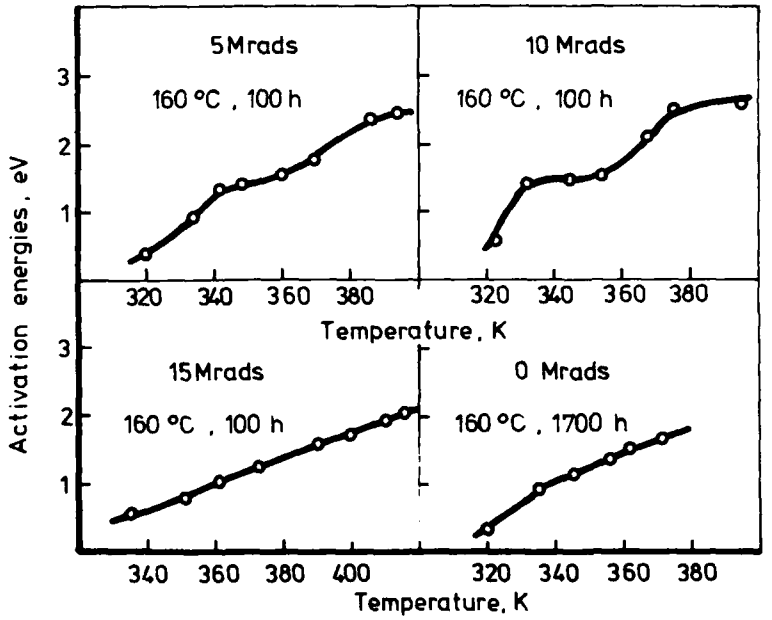

Fig. 4. Activation energies distributions for β-irradiated and thermally aged PET samples.

a distribution of activation energies of relaxation processes, being responsible for the α and ρ peaks, was found. In the α relaxation case the distribution is due to different lengths of the main polymer chains, when for the ρ peak it is due to different depths of space charge traps. The prolonged thermal ageing causes a decrease of activation energies in both cases as it is shown in Fig.3.

A comparison of the activation energies distributions, for a fresh samples and β-irradiated with the dose of 15 Mrads and subsequently thermally aged samples, shows that the character of the thermal dependence of activation energies also changes. There exists a lack of defined energy levels, though the range of the activation energies remain similar. It is presented in Fig.4. A different behaviour, however, was observed for the samples that were irradiated with 5 and 10 Mrads doses. In that case creation of a new energetic level in the range of 1.2 - 1.9 eV was observed.

REFERENCES

1. S.M. Gubanski, A. Gubanski - "An Attempt to Evaluate the Polyethyleneterephtalate Foil Temperature Indice on the TSD Measurements Basis", Materials Science, Vol. XIII, No 1-2, 1987, pp. 79-82.
2. J. Vanderschueren - Ph.D. Thesis, Liege, Belgium, 1974.
3. I. van Turnhout - "Thermally Stimulated Discharge of Polymer Electrets", Elsevier Publ. Co. Amsterdam, 1975.
4. A. Gubanski, S.M. Gubanski - "Thermostimulated Depolarization Currents in Thermally Aged Polyethyleneterephtalate PET Films", Proceedings of the ICPADM-88 Conference, Tsinghua University, Beijing, China, 12-16 Sept. 1988, to be published.

APPLICATION OF A SECOND ORDER RESPONSE THEORY TO THE NONLINEAR PIEZOELECTRICITY OF PVDF

P. HARNISCHFEGER, B.J. Jungnickel

Deutsches Kunststoff-Institut, Schloßgartenstr. 6R, D-6100 Darmstadt, West Germany

ABSTRACT

The piezoelectric response of Poly(vinylidene fluoride) is known to be a nonlinear function of the stress. In the present paper, a second order response theory is applied to this phenomenon. The derived equations allow the determination of nonlinear coefficients already from the linear part of the response if a static stress has been applied before. Our experimental results leads to the conclusion that two molecular processes contribute to the macroscopic piezoelectricity which differ in the sign of their polarization.

1 INTRODUCTION

PVDF is known for its large piezoelectric response in comparison with other piezoelectric materials [1]. By application of a strong electrical field to an oriented PVDF film, a macroscopical electrical polarization is generated which changes if a mechanical force is applied, later. Usually, the piezoelectric properties of such PVDF films (drawing direction 1, poling direction 3) are described by a linear relation between mechanical stress T and polarization P:

$$P_i = d_{ij} T_j, \quad \text{if } E_k = 0 \qquad (1)$$

where d_{ij} is the piezoelectric constant and E_k an electrical field. It turns out that d_{32} depends on the applied stress in such a manner that it even changes its sign with increasing stress. Furthermore, by appli-

CH2593-2/ 88/ 0000-0430$01.00 Copyright 1988 IEEE

cation of a sinusoidal stress, a phase shift of up to -180° appears between excitation and response [2], and frequency doubling is observed [3]. The present paper is concerned with the theoretical description of these nonlinear phenomenona by a second order response theory, which is applied to experimental results of PVDF.

2 THEORY

In order to include nonlinear effects, Eq. (1) is extended (in the following the tensor character of the quantities is neglected):

$$P = P_0 + d_S T_S + \beta_S T_S^2 . \qquad (2)$$

P_0 describes the permanent polarization, β is the nonlinear coefficient and the subscript S indicates that we are concerned with static quantities. If the applied stress is time dependent, Eq. (2) has to be replaced by [4]

$$P(t) = P_0 + d_\infty T_d(t) + \beta_\infty T_d^2(t) + \int_{-\infty}^{t} g_1(t-t')\, T_d(t')\, dt' + \int_{-\infty}^{t}\int_{-\infty}^{t} g_2(t-t', t-t'')\, T_d(t')\, T_d(t'')\, dt'dt'' \qquad (3)$$

d_∞ and β_∞ describe the immediate response and the $g_i(t)$ are response functions. Assuming a single Debye-type relaxation, isothermal conditions, and consideration of the Markovian approximation, Sauermann et al. [5] derived an analytical expression between the response function of second order and the linear response. Using their result, we get:

$$P(t) = P_0 + d_\infty T_d(t) + \beta_\infty T^2{}_d(t) + a\int_{-\infty}^{t} e^{-\Gamma(t-t')}\, T_d(t')\, dt' + b\int_{-\infty}^{t} e^{-\Gamma(t-t')}\, T_d^2(t')\, dt' + c\int_{-\infty}^{t} e^{-\Gamma(t-t')}\, T_d(t') \int_{t'}^{t} T_d(t'')\, dt''\, dt' \qquad (4)$$

where

$$a = X\,\Gamma, \quad 2b = (X\Gamma)' + X\Gamma', \quad c = X\,\Gamma\,\Gamma'. \quad (5)$$

$X = d_0 - d_\infty$ and Γ is the inverse relaxation time. Both quantities can be functions of a static stress T_S and the derivation with respect to T_S is indicated by the primed quantities.

Assuming that the total stress consists of a static stress T_S and a superimposed harmonic stress of amplitude T_0, Eq. (4) results in:

$$P(t) = P_0 + P_B + d_d T_0 \cos(\omega t - \Phi_L) + \\ + \beta_d T_0^2 \cos(2\omega t - \Phi_q) \quad (6)$$

with

$$2P_B = T_0^2 \,(\beta_\infty + b\Gamma + c/(\Gamma^2+\omega^2)) \quad (7)$$

$$\text{tg}\,\Phi_L = d''/d', \quad \text{tg}\,\Phi_q = \beta''/\beta' \quad (8)$$

$$d_d = |d^*|, \; d^* = d' - id'' = d_\infty + X\Gamma/(\Gamma+i\omega) \quad (9)$$

$$\beta_d = |\beta^*|, \; \beta^* = \beta' - i\beta'' = \beta_\infty + b/(\Gamma+2i\omega) + \\ c/(\beta+i\omega)(\beta+2i\omega) \quad (10)$$

The time-dependent polarization can be described in formal analogy to the static one:

$$P^*(t) = P_0 + d^* T^* + e^* T^{*2} \quad (11)$$

Eq. (6) reveals the well known properties of nonlinear relaxations which are in accordance with the findings for PVDF: a stationary background response P_B which is linked with the second order response, an in-frequency-response and a second harmonic response. In addition, the theory gives analytic results for the phase shifts (Eq. (8)-(10)).

3 EXPERIMENTAL RESULTS AND DISCUSSION

PVDF films were drawn up to a ratio of four and poled by corona discharging in order to get ferroelectric samples. By application of a step-like stress superimposed on a static stress of different strength, the relaxation

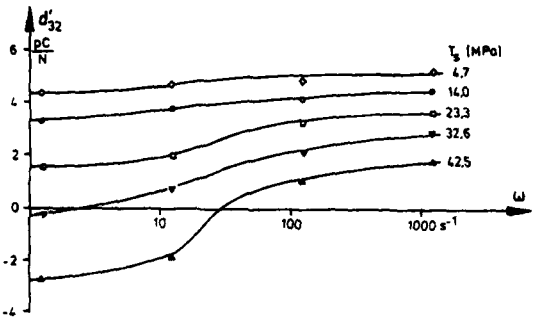

Fig.1: Real part of $d_{32}^*(\omega)$ (i.e. d_{32}')

time could be estimated; in the limit of negligible static stress it amounts to about 35 ms and it depends weakly on T_s.

The nonlinear behaviour can already be determined from the in-frequency response after simulatanoursly application of a harmonic and static stress (cf. Eq. (6)-(10)). Fig. 1 shows the dispersion curve $d_{32}'(\omega)$ which displays a characteristic shape for single mode relaxations. But in contrast to the usual results of dielectric and mechanical measurements, the relaxation strength and the position of the inflection point depend on the strength of the superimposed static stress. This is clearly marked in the static limit $d_{32}^*(T_s)\big|_{\omega\to 0}$ (Fig. 2), from which the linear and nonlinear static coefficients (as defined

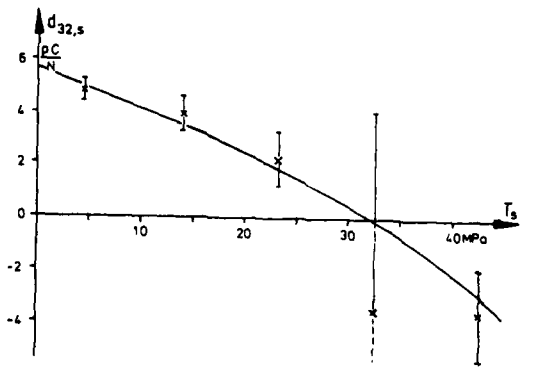

Fig.2: The static limit of $d_{32}^*(T_s)$

by Eq. (2)) are estimated. The values of $d_{32,S} = 5.7$ pC/N and $\beta_{322,S} = -7.7\ 10^{-20}$ pC²/N² indicate that the stress induced polarization changes its sign at a static stress of about 75 MPa. It should be emphasized that the dynamic piezoelectric constant $d_d = |d^*|$ exhibits a minimum which is shifted to higher stress-values with increasing frequency but which is always a positive quantitiy. Simultanously, a phase shift of up to -180° appears which exhibits -90° at the mentioned minimum.

The observed dependences of the piezoelectric coefficients on the frequency and in particular, the change in sign of d_{32}' at a certain static stress, suggests the conclusion that two types of molecular motions contribute to the observed piezoelectricity which differ in the sign of the polarization that they induce; the contribution of each process depends on the static stress and frequency. The determination of the molecular origin of these processes are the aim of further investigations.

The application of the second order theory to the nonlinear piezoelectricity of PVDF is described in more detail in [6].

REFERENCES

[1] M.G. Broadhurst, G.T. Davis, J.E. McKinney, R.E. Collins, J. Appl. Phys. 49 4992 (1987)

[2] B.R. Hahn, J. Appl. Phys. 57, 1294 (1985)

[3] E. Fukada, M. Date, H.E. Neumann, J.H. Wendorff, J. Appl. Phys. 60 (1988)

[4] P.N. Butcher: Nonlinear Optical Phenomena Ohio State University Engineering Publications. Columbus (1965)

[5] G. Sauermann, W. Just, K.P. Karmann, Physica 140A, 597 (1987)

[6] P. Harnischfeger, B.J. Jungnickel, Ferroelectrics, (1988), submitted

A METHOD FOR SPACE CHARGE DISTRIBUTION DETERMINING IN THICK DIELECTRIC SAMPLES.

Ryszard Kacprzyk

Wrocław Technical University, Institute of Funadmentals of Electrical Engineering.
Pl. Grunwaldzki 13, 50-377 Wrocław, Poland.

ABSTRACT

A method for determining the space charge distribution on thick samples of dielectrics is presented. The method is based on measurements of the effective surface charge density on the one side of the plane parallel sample, when the other side is simultanously dissolved in conducting or dielectric solvent. A possible application of the method was chacked on wax electrets.

INTRODUCTION

Investigations of space charge distribution in thick dielectric samples are very often difficult or simply impossible. This is caused by the fact, that there are no universal methods, and those in use are applicable only to materials with specific physical properties. In this paper, a method similar to the virtual electrode method [1] is presented. The method was developed for samples with thicknesses of the order of a few millimeters.

THEORY

Let's consider the model illustrated in Fig.1 A sample of the investigated dielectric with a relative dielectric permittivity ε_1 and thickness d has a space charge $q_V(x)$ distributed along the x axis. The corresponding effective surface charge density q_S induces on the measuring electrode with a surface s (placed at a distance 1 from the analysed sample surface) a q_S' charge density. The other side of the sample is covered by a "moving"

CH2593-2/ 88/ 0000-0435$01.00 Copyright 1988 IEEE

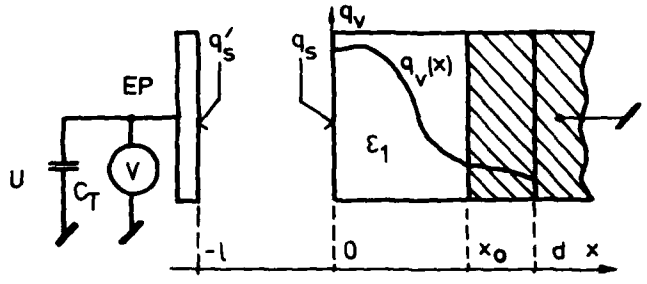

Fig.1. A model of measuring circuit for analysis with a conducting solvent.

conducting electrode (created by solvent) which can translocate through the entire sample thickness. If the moving electrode is placed at a distance x_o, the effective surface charge density $q_s(x_o)$ is as follows:

$$q_s(x_o) = \frac{1}{x_o} \int_0^{x_o} (x_o - x) q_v(x) dx$$

Differentiation of the expression under the integral and combining the result with the expression for q'_s (measured charge density) finally gives (by the assumption that $l \gg x_o$) the following one:

$$q_v(x_o) \simeq \frac{C_T \cdot \varepsilon_1 \cdot l}{s} \cdot \frac{d^2[U(x_o)]}{dx_o^2}$$

If the experiment is carried out in a circuit similar to that shown in Fig.1, the voltage $U(x_o)$ across the total capacitance C_T is measured as a function of time and the sample thickness x_o.

Similar analysis carried out for the case with dielectric solvent gives the following expression:

$$q_v(x_o) \simeq \frac{C_T}{s}\left(1+\varepsilon_2\cdot\frac{1}{b}\right)\frac{dU(x_o)}{dx_o}$$

where ε_2 is a relative dielectric permittivity of the solvent and bits layer thickness.

EXPERIMENTAL SETUP AND RESULTS

A sketch of the experimental setup used is shown in Fig.2. The electret (1) is pressed by the metal ring (2) to the rubber ring gasket (3) and to the bottom of the measuring container (4). The measuring electrode (5) covered by screens (6,7) and held by an insulator (8), is placed on the axis of the cylindrical measuring container. The voltage on the measuring electrode was measured by an electrometer (9) RFT type 6350, and registered by an x-t recorder (10). The container with a mounted sample was filled with the analysing solvent (11) and closed with a cover with a mounted electrical mixer.

A possible application of the method described above was checked on wax electrets made of a melt of 50% bees wax and 50% balsamic calophony. Electrets were formed using injecting and blocking electrodes. The melted mixture was polarized at a temperature of 353K in the field 1 MV/m. The final thickness of the electrets was about 3 mm.

An exemple of the result obtained for electrets formed with injecting electrodes and analysed in a conducting solvent (tetrahydrofurane) is shown in the Fig.3 in the form $U(x_o)$ curve, and in the final form $q_v(x_o)$. The results obtained for electrets formed with injecting and blocking electrodes (non presented) seem to be similar to those of Walker-Jefimenko[2].

SUMMARY

A dissolving method for space charge distribution determining was presented. A variant with conducting solvent was checked on the

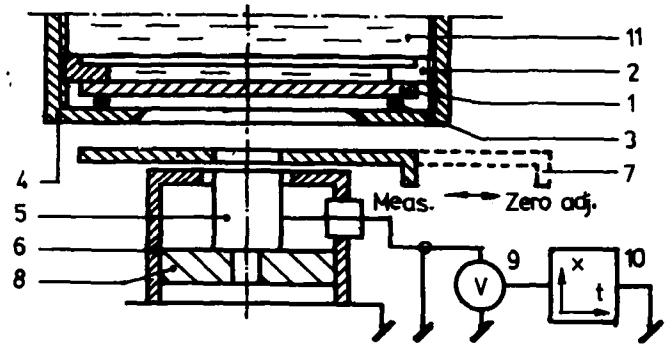

Fig.2. A sketch of measuring circuit.

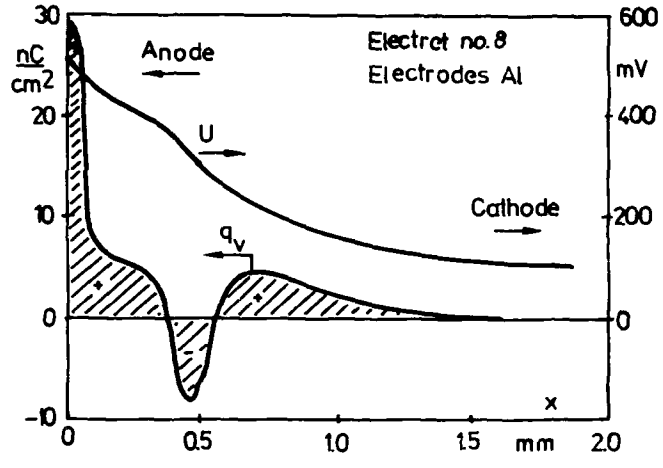

Fig.3. Voltage and space charge distribution for the electret formed with injecting electrodes.

example of wax electrets and a good comparison to the literature data [2] was obtained. The resolution of the method depends on the dissolving velocity and in the case of wax electrets (dissolved in tetrahydrofurane) can be valued as high as 10 μm.

REFERENCES

[1] G.M.Sessler, J.E. West, H. von Seggern, Electron beam method for detecting charge distributions in PET films. J. Appl. Phys. 6, 4320-4327, (1972).

[2] D.D. Walker, O. Jefimenko. Volume charge distribution in carnauba wax electrets J. Appl. Phys. 8, 3959-3964, (1973).

EFFECT OF ANTISTATIC AGENT ON ELECTRICAL CONDUCTION OF POLYPROPYLENE FOIL

Ryszard Kacprzyk and Edmund Motyl

Technical University of Wroclaw, Poland.

ABSTRACT

The effect of the Polstat 12-14 antistatic agent on electrical conductivity, thermally stimulated currents and decay of surface charges in polypropylene foil was investigated. It was found, that antistatic dopant evidently increases electrical conductivity in the temperature range 293-380 K. Conductivity as the reciprocal temperature function shows two activation processes. The values of activation energy computed from the conductivity characteristics and from the TSD spectra are compared. It was stated that the antistatic agent produces deep traps for the injected charge carriers and cause an increase of their relaxation times.

A SURFACE T.S.C STUDY OF THE INTERACTION BETWEEN A GAS AND AN EPOXY RESIN

Farid KAOUAH, Mohamed BENDAOUD, and Noureddine BOUCHTOUT

Laboratoire des Dielectriques, Institut de Physique,
U.S.T.H.B B.P. N°32 El-Alia Algiers (ALGERIA).

ABSTRACT: The thermally stimulated surface current has been measured by special electrodes metalized on the same side of a sample of a DGEBA/IPD resin system. The surface TSC diagrams have been compared to the TSC volume measurements. Then the interaction between the polymer and the atmosphere, in which it has been placed, has been studied: viz. humid atmosphere, nitrogen, and carbon dioxide.

1. INTRODUCTION

The thermally stimulated current method has been widely used for the study of molecular mechanisms which occur in the polymer bulk, in the course of the different relaxations and transitions [1]. On the other hand, surface TSC measurements permitted Despax et al [2,3] and Peres [4] to observe the influence of different gases on the surface dielectric properties of silica. The aim of this paper is to continue this work with a study of the interaction between a polymer and the atmosphere in which it has been placed.

2. EXPERIMENTAL

The samples were prepared with a diglycidyl ether of bisphenol A resin cured with isophorm diamine (DGEBA/IPD) in the proportions of 100 gm of DGEBA with 24 gm of IPD. The mixture was degassed for one hour, and then it was poured between two aluminium plates. The system was kept at 140° for 8 hours. The comb-shaped aluminium electrodes were deposited on the same side of the sample, according to the technique described by Despax [3]. The inter-electrodes distance was 18 μm with a total length of 60cm. During the measurements the sample was placed in a stainless steel cell. The temperature was measured with a platinum resistance connected to a digital thermometer, and the current by a Keithley 642 electrometer. The Conditions of polarization have been indicated in the figures, during the depolarization the sample was warmed at 6°C/mn.

CH2593-2/ 88/ 0000-0441$01.00 Copyright 1988 IEEE

3. RESULTS OBTAINED WITH DEGASSED SAMPLES

3.1 The figure (1) represents the evolution of the surface TSC as a function of the temperature, when the sample was kept in a dry atmosphere. The sample had been degassed for 24 hours at 40°C at 10^{-6} mb. The curve I shows, at low temperature, a peak whose maximum was situated at -96°C preceded by a shoulder; another peak was also observed at 85°C. Volume TSC measurements gave similar results however the peak at high temperature was displaced to 118°C.

3.2 The peak and the shoulder which appear at low temperature are due to a β relaxation due to the crankshaft motion of the chains sequences, and to the rotation of the lateral groups. A resolution of this relaxation into elementary peaks (fig.4) by the fractional polarizations method applied to the surface TSC gives activation energies from 0.14 to 0.57 eV. Su et al. [5] have studied, from volume TSC measurements, the β relaxation in a TGDDM/DDS resin system. Although these authors have operated with a system different from that of ours we have obtained results in agreement with theirs. This relaxation did not appear to have been affected by the change of the resin structure or the curing agent nature; this fact has been observed by Williams [6]. On the other hand the curing conditions influence this relaxation.

3.3 As opposed to the β relaxation, the glass transition temperature depends on the resin, curing agent, and also on the curing conditions as shown in the literature: T_g = 247°C in TGDDM/DDS [7], 137°C in DGEBA/DDM [8], 75°C in DGEBA/EDA [9], from 28°C to 62°C in DGEBA/DSA [10]. The peak which has been obtained in our volume TSC diagram at 118°C is due to an α relaxation which appears in the neighbourhood of T_g. This peak is situated at lower temperature in the surface TSC diagrams: The branching and the crosslinking density is more feeble in the vicinity of the sample surface than in the bulk. Consequently, the movements of the surface chains become more easy, and begin at lower temperature.

4. INFLUENCE OF MOISTURE

A number of studies [7,8,11] have shown that the epoxy resins are very sensitive to moisture which have influence on the relaxations. Evidently this influence will be very much marked on the movements of the mobile units found

near the sample surface. In order to study this action, we have used three series of samples: Those of the series II and I have been kept in an atmosphere of 80% relative humidity for 1 hour and 48 hours respectively. The cell after having been evacuated, was filled with dry nitrogen at 100 mb to assure good thermal conduction, and the measurements were immediatly taken. As for the samples of serie III, after having been taken out of the dessicator, they were degassed under conditions given in paragraph 3.1 The results obtained have been illustrated by the fig. 3.

4.1 It was observed that the α relaxation which took place at 85°C was amplified and displaced toward lower temperature down to 60°C as the water content in the surface sample increased. Water here appeared to act as a plasticizer facilitating the movements of the chains. Banks et al. [8] had observed, by proton NMR, the same phenomenon with a DGEBA/DDM system; the Tg passes from 137°C to 105°C. They postulated that the chain movements are increased as a "result of the disruption of hydroxyl groups hydrogen bonds by the absorbed water molecules". Keenan et al. [7] had not observed this effect in the TGDDM/DDS resin system. They think that "the fact that T_g (247°C) was well above 100°C contributed in eliminating moisture from the sample by the time Tg was reached". However they have shown evidence for existence of a relaxation at about 100°C, which they called ω transition which depends strongly on humidity. Strark et al. [11] have studied the effect of the H_2O molecules introduced during the course of the curing reaction of a TGDDM/DDS system. They had observed a small decrease of Tg, and only in the case of the samples cured in a humid atmosphere, the appearance of a peak at 80°C which was attributed to the ω relaxation identified by Keenan. Thus it follows from what was dicussed above that moisture has an important influence on the relaxations taking place at about 100°C. The water molecules adsorbed by the sample diminishes the croslinking density by breaking the hydrogen bonds which results in a lowering of the temperature of these transitions and an increase of their intensities.

4.2 Influence of the moisture on the β relaxation: Just as it happened in the case of the α relaxation the water molecules act as a plasticizer, but this action is much less marked.

4.3 The two relaxations which appear at medium temperatu-

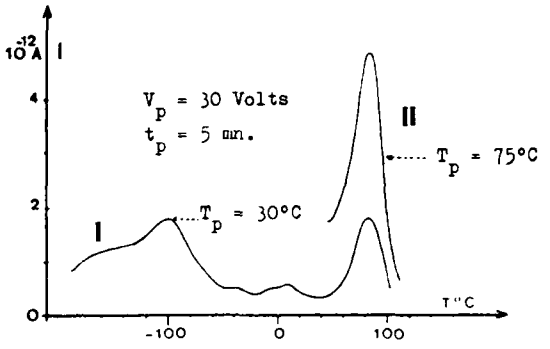

Fig. 1 : Degassed sample.

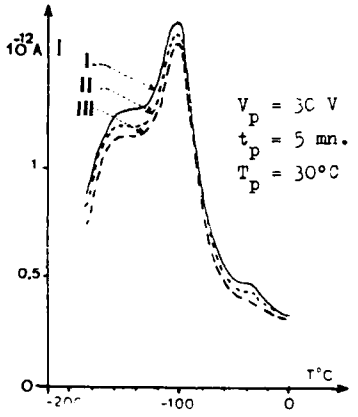

Fig. 2 : Influence of N_2.

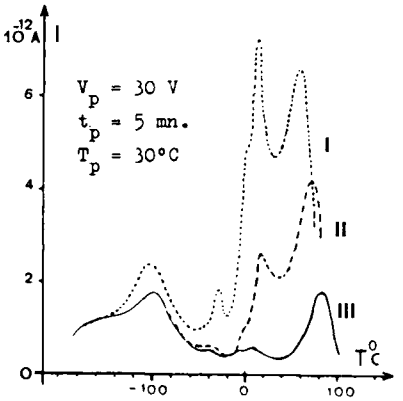

Fig. 3 : Influence of moisture

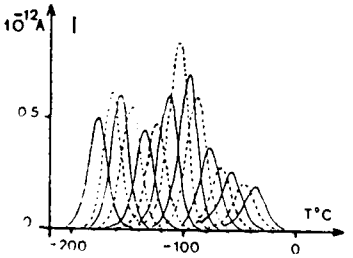

Fig. 4 : Elementary peaks.

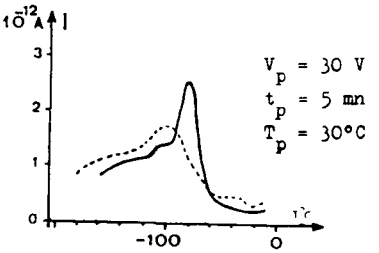

Fig. 5 : Influence of CO_2.

re between -30°C and 30°C in the surface TSC diagrams (fig.3) do not appear in the volume TSC diagrams. They are hence due to the movement of the free water molecules or feebly bonded to the lateral groups . Ellis et al., cited by Banks [8], have shown, by infra-red spectroscopy, that adsorbed water is hydrogen bonded to hydroxyl groups in epoxy resin at room temperature.

5. INFLUENCE OF N_2 AND CO_2.

The influence of these two gases have been studied at low temperatures where one can eliminate all traces of water of sorption from the sample surface. The curves given in the figure (2), have been obtained with samples kept for 5 minutes (I), 24 hours (II), and96 hours (III) in an atmosphere of dry nitrogen. The influence of this gas results in a feeble diminution of the amplitude of the β relaxation. The adsorbed nitrogen molecules occupy a part of the free volume and hinder the movements of lateral groups and the chain segments responsible for this relaxation

The same effect was observed with a sample kept in a CO_2 atmosphere for 24 hours (fig.5), however in this case, a new peak was observed at - 80°C. Despax et al. [2] have observed a surface TSC peak at - 100°C, in the case of a silica sample kept in a CO_2 atmosphere. These authors do not exclude the possibility of a chimisorption phenomenon enhanced by the presence of trapped charges. The peak which appears at - 80°C in the figure (5), is due to the carbon dioxide molecules bonded to the hydroxyl lateral groups.

ACKNOWLEDGEMENTS: We thank Drs Bui Ai, Despax, and Ms Arles of the" laboratoire de Genie Electrique" of the Toulouse University, and Dr Krishnan of the Algiers University, for their help.

REFERENCES:

[1] J. VANDERSCHUEREN : Thesis Liège (1975)
[2] B. DESPAX, BUI Ai, M. ABDULLAH, C.HURAUX: Appl. Phys. Lett. 39, 220 (1981)
[3] B. DESPAX, C.HURAUX, R.LACOSTE, M.ABDULLAH: J. of Mat. Sc. 18, 2544, (1983)
[4] P. PERES : Thesis Toulouse (1984)
[5] W.F. SU, S.H.CARR, J.BRITTAN: J. of Appl. Polym. Sc. 25, 1355, (1980)
[6] J.G.WILLIAMS: J. of Appl. Polym. Sc. 23, 3433 (1979)
[7] J.D.KEENAN, J.C.SEFERIS, J.T.QUINLIVAN: J. of Appl. Polym. Sc. 24,2375(1979)
[8] L. BANAS, B.ELLIS : Polym. Bul. 1, 377 (1979)
[9] C.C. RICCARDI, H.ADDABC, R.WILLIAMS: J. Appl. Polym. Sc. 29, 2481 (1984)
[10] N. SHITO: J. of Polym. Sc. 23, 569, (1968)
[11] E.STARK, A.M.IBRAHIM, T.E.MUNIS: J. of Appl. Polym. Sc. 30,1717,(1985)

THE FORMATION OF DEEP TRAPS IN THE NEAR SURFACE LAYERS OF FLUOROPOLYMER CORONA ELECTRETS

V.G. Boitsov, A.A. Rychkov and V.V. Schvetz

Herzen Pedagogical Institute of Leningrad, Leningrad, USSR.

ABSTRACT

The stability of positive homocharge in nonpolar fluoropolymer Corona electrets is due to the polymer surface states. The electrets stability can be controlled by changing of the trapping levels spectrum in the thin near surface dielectrics layers. The formation methods of deep trapping in fluoropolymer dielectrics before polarization and in the process of the electret state formation are considered. It is shown that the formation of deep traps for the positive homocharge in the fluoropolymer dielectrics essentially depends on the duration of adsorbtion process. The fraction of deep traps in surface states spectrum increases with time of treatment. This process is considerably intensified during the treatment of films initially charged by positive homocharge or during triboactivation of surface in the process of treatment.

On the basis of the model conceptions the energy spectrum of near surface trap layers of polymer is determined and the correlation of spectrum with the surface structure is established.

TIME AND FREQUENCY DOMAIN PERFORMANCE OF ULTRASONIC TRANSDUCERS

R. Lal and D.K. Das-Gupta

School of Electronic Engineering Science,
University College of North Wales,
Dean Street, Bangor, Gwynedd. LL57 1UT

Abstract
This paper provides a discussion on methods used in the analysis of piezoelectric transducers for high frequency applications. The influence of mechanical and electrical loading on transducers constructed from PZT and PVDF are evaluated in the time domain. Frequency domain information is acquired by the use of a Fast Fourier Transform (FFT) algorithm.

The effects of excitation/reception circuitry on a transducer operated in its thickness mode are also studied. The results obtained in this manner, are then compared with theoretical simulation plots, calculated using Z-transform techniques.

INTRODUCTION

Ultrasonic transducers are gathering increasing popularity in such fields as medical imaging, non-destructive testing and in acoustic microscopy applications. The demand for efficient generators and receivers of acoustic energy is greater than ever before. It therefore, becomes important to comprehend fully the underlying mechanisms controlling the characteristics of such devices. The most comprehensive treatment to the one-dimensional lossless thickness mode transducer in the time domain has been given by Hayward and Jackson [1], [2]. In this paper, two very simple cases are presented to illustrate the use of this technique.

EXPERIMENTAL

In order to measure the impulse response of the transducers, the excitation circuitry consisted of a fast switching MOSFET, type IRF840, capable of switching up to 500V in approximately 10nS. A

CH2593-2/ 88/ 0000-0447$01.00 Copyright 1988 IEEE

circuit was constructed similar to that of Ramos-Fernandez et al [3], with provision for altering excitation pulse characteristics.

Only very simple construction strategy is employed here. A poled and electroded PZT5 disc, 860μm thick, 20mm in diameter was held secured at one end of a cylindrical PTFE mould, 60mm long, with an inner diameter of 20mm. The centre conductor of a coaxial cable, type RG174A/U, was connected to the the back face of the piezo disc by means of silver loaded cement. The braid of the cable was pulled out of the mould via a cut in the PTFE cylinder, see fig. 1 (a) and (b). Upon drying of the cement, epoxy encapsulating compound was poured into the mould. Having allowed time for the expoxy to set, the final contact to the outer electrode was made by forming a conductive track between the electrode and the braid. The design facilitated good mechanical support whilst maintaining a smooth front face, as well as, eliminating the need for any additional glue layers.

Transducers made using 138μm PVDF, followed a similar design procedure, except, the PVDF film was initially held stretched by two concentric rings and the diameter of the active area was reduced to 10mm. This is shown in Fig.1 (c).

For the results presented below, identical devices were used to transmit and receive. The transducers were axially aligned in a tank containing deionised water. The receiver was connected, as shown in Fig.2, to a digital storage oscilloscope featuring a sampling speed of up to 100 MHz, with, 1024 points per waveform. The received echo was thus digitised, stored and subsequently transferred to a micro. Any digitisation noise was removed from the echo under observation, the data then further processed with the aid of a FFT algorithm to estimate its power spectra. The simulation plots were performed on a mainframe computer.

TYPICAL WAVEFORMS

Two identical transducers constructed from PZT5 were connected as described above. Fig 3(a) and 3(b) show respectively, the simulated and the measured time responses for this setup. As can be seen from these plots, an excellent agreement is achieved between them. The corresponding frequency domain spectra are compared in Fig. 3(c). This graph shows the resonance frequency to be identical, though, the measured response shows a slightly larger bandwidth. Thus, the transducer may be fully characterised in this way and influence of any parameter changes may be studied with great precision.

Fig 4(a) shows the measured and the predicted time domain responses of two identically manufactured, 138μm PVDF transducers used in the transmit/receive mode. Again, an excellent agreement is seen, though, the measured signal is considerably lower in amplitude. This is possibly due to losses in the water medium, the reception circuitry and the material itself. The frequency domain data are plotted in Fig. 4(b), showing good agreement. The bandwidth and the resonance frequency are seen to be appreciably lower than expected. This may be due to the uncertainty in the physical parameters of the device. The thickness direction velocity was taken to be 2260m/s [4], whereas, the quoted value by the manufacturer was nearer 2500m/s. Similarly, the quoted thickness of PVDF was 138μm with a 5% tolerance. These factors combined with the fact that the internal losses of PVDF were ignored in the simulations, may serve to explain the discrepancies.

REFERENCES

[1] G. Hayward, M.N. Jackson, "Discrete-Time modelling of the thickness mode piezoelectric transducer", IEEE Trans. Son. Ultrason., vol. SU-31, pp. 137-150, 1984.

[2] G. Hayward, M.N. Jackson, "A lattice model of the thickness-mode piezoelectric transducer", IEEE Trans. Ultrason. Ferroelec. F- Con., vol. UFFC-33, pp. 41-50, 1986.

[3] A. Ramos-Fernandez, P.T. Sanz-Sanchez, F.R. Montero de Espinosa, "Broad-band driving of echographic arrays using 10ns-500V efficient pulse generators", Ultrasonics, pp. 221-228, 1987.

[4] H. Ohigashi, "Electromechanical properties of polarised PVDF films as studied by the piezoelectric resonance method", J. Appl. Phys., vol. 47, pp. 949-955, 1976.

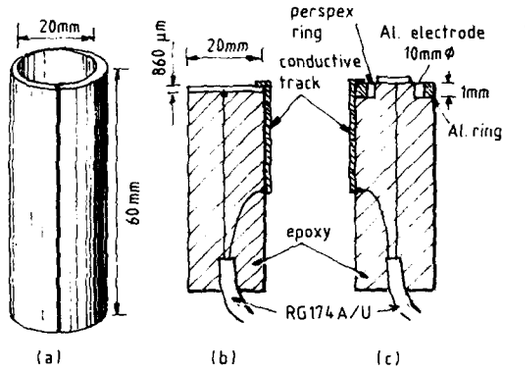

Fig. 1. Transducer construction.

(a) PTFE mould
(b) PZT Transducer
(c) PVDF Transducer

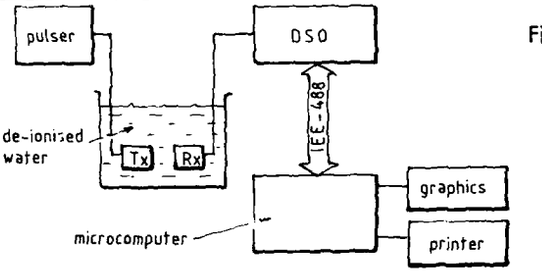

Fig. 2. Experimental arrangement.

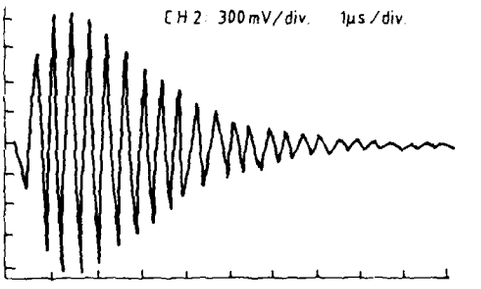

Fig. 3(a). Simulated PZT response.

density	=	7700Kgm^{-3}
ε_r	=	1700
velocity	=	4200ms^{-1}
thickness	=	860 µm
diameter	=	20mm
h_{33}	=	2.1x10^{9}Vm^{-1}
Z_{epoxy}	=	2.5 MRayl
Z_{water}	=	1.5 MRayl

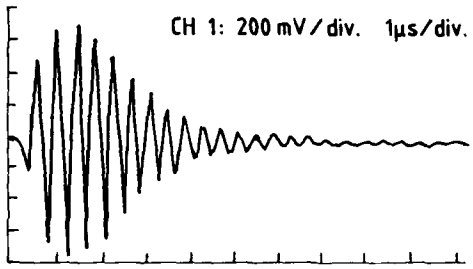

Fig. 3(b). Measured PZT response

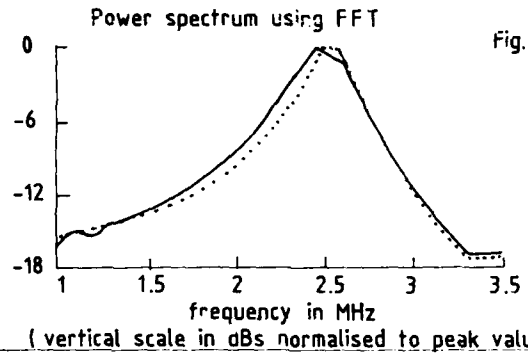

Fig. 3(c). Frequency spectra of (a) and (b).

..... simulated
—— measured

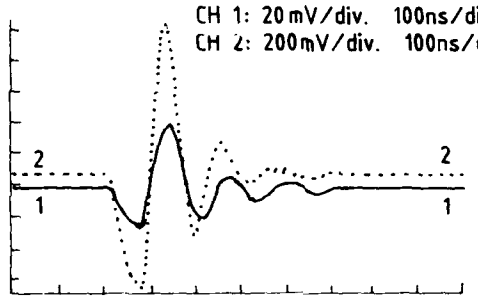

Fig. 4(a). Simulated PVDF response.

density	=	1780 Kgm^{-3}
ε_r	=	11
velocity	=	2260 ms^{-1}
thickness	=	138 μm
diameter	=	10 mm
h_{33}	=	$1.65 \times 10^9 Vm^{-1}$
Z_{epoxy}	=	2.5 MRayl
Z_{water}	=	1.5 MRayl

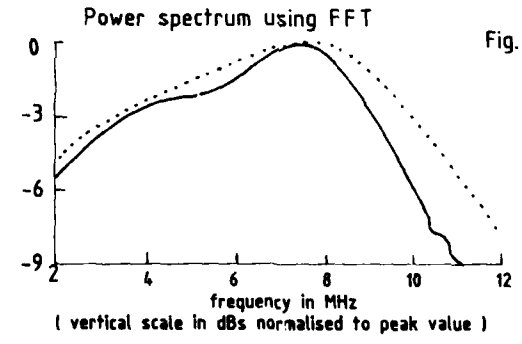

Fig. 4(b). Frequency spectra of 4(a).

..... simulated
—— measured

POLARIZATION PHENOMENA AS A CHARACTERISTIC OF THE "STRUCTURE" OF THE POLYMERIC AMORPHOUS PHASE

A. BERNES,

SOLOMAT France S.A., 91160 Toulouse Cédex

D. CHATAIN, C. LACABANNE,

Laboratoire de Physique des Solides Associé au CNRS,
Université Paul Sabatier
31062 Toulouse Cédex (France)

ABSTRACT

Polarization phenomena of polycarbonate have been investigated by Thermally Stimulated Current spectroscopy. The relaxation modes are characteristic of its thermodynamic history. Moreover, the existence of compensation laws reveal the presence of local order in the amorphous phase of polycarbonate. The existence of domains of some 20 to 40 A has been postulated according to the granular model of Yeh.

INTRODUCTION

Polycarbonate has a peculiar place among thermoplastics because of its excellent mechanical properties. Its crystalline phase has been widely studied [1] ; contrarily, less work has been devoted to its amorphous phase. The aim of this paper is to investigate the polarization phenomena associated to this amorphous phase. Lexan bisphenol A polycarbonate has been studied by Thermally Stimulated Current (TSC) spectroscopy.

RELAXATION SPECTRA

Figure 1 shows the TSC spectra of reference (*solid line*) and annealed (*dashed line*) polycarbonate. On this figure, the "dipolar" conductivity σ has been reported versus temperature T ; the arrows indicate the polarization temperatures. For reference polycarbonate, a TSC peak is observed around 155°C

CH2593-2/ 88/ 0000-0452$01.00 Copyright IEEE

i.e. in the vicinity of the glass transition temperature. So, this peak has been associated to the

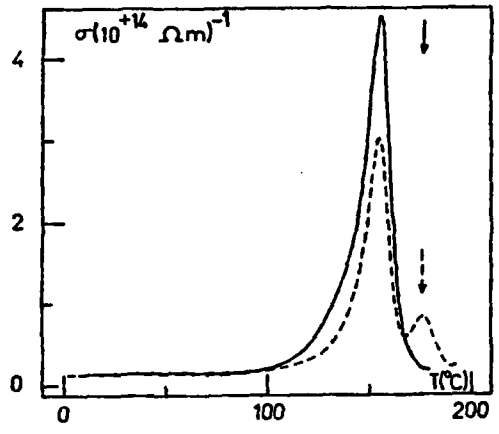

Figure 1
TSC spectra of polycarbonate
—— reference ;
--- annealed.

dielectric manifestation of the glass transition Tg. After annealing 20 minutes at 230°C, a new TSC peak is found at 175°C and the sub Tg mode decreases.

RELAXATION MAPS

The resolution of complex TSC spectra into elementary TSC spectra has been undertaken by using fractional polarizations. Then, the obtained dielectric relaxation times τ have been plotted on relaxation maps (Figure 2).

Arrhenian Relaxation Times

The TSC peaks situated at $120°C < Tm < 173.5°C$ in reference polycarbonate and at $133.5°C < Tm < 176.5°C$ in annealed polycarbonate are characterized by relaxation times following an Arrhenius equation. Note that the correlation coefficients are higher than 0.95. The corresponding pre-exponential factors τ_{oa} and activation enthalpies ΔH have been listed on Table 1a and b respectively. The letter C indicates

that the corresponding relaxation time follows a compensation law. For reference polycarbonate the compensation temperature and time are respectively 182°C and 0.7 sec ; for annealed polycarbonate 165°C and 6.2 sec.

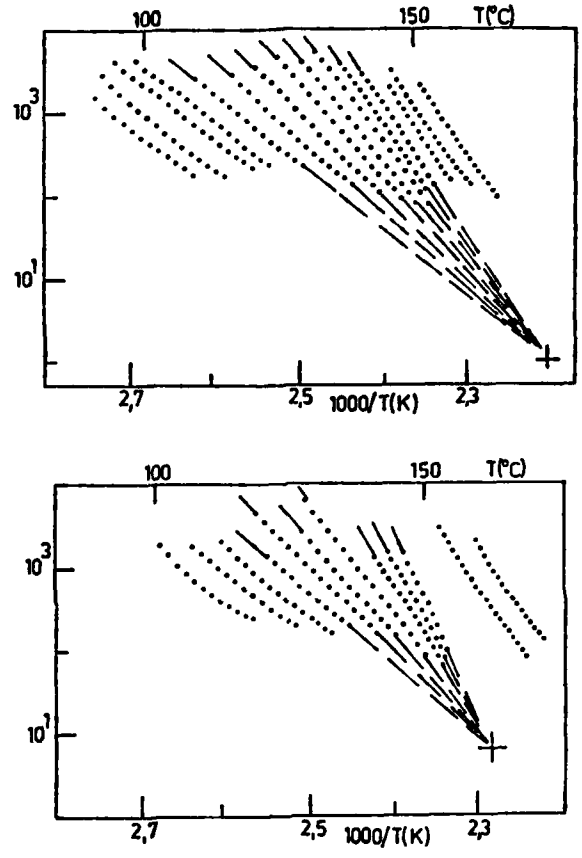

Figure 2.- Arrhenius diagrams of relaxation time.

Vogelian Relaxation Times

The TSC peaks situated at 116°C in reference polycarbonate and at 128 and 182°C in annealed polycarbonate have correlation coefficients of 0.95 with "apparent" parameters indicated on Table 1

(*subscript "ap"*). A best fit of experimental points is obtained with a Vogel equation :

$$\tau(T) = \tau_{ov} \exp \{ \alpha_f (T - T_\infty) \}^{-1}$$

where τ_{ov} is the pre-exponential factor, α_f is the thermal expansion coefficient of the free volume and T_∞ is the critical temperature at which any molecular movement is frozen. The corresponding parameters have been plotted in Table 2.

Table 1.- Activation parameters of relaxation times
(a) reference polycarbonate
(b) annealed polycarbonate

(a)

Tm (°C)	ΔH (eV)	τ_{oa} (sec)	
116	1.64 ap	$3.60\ 10^{-20}$	ap
120	1.63	$9.65\ 10^{-20}$	
128.5	1.60	$5.65\ 10^{-19}$	
131	1.62	$4.90\ 10^{-19}$	
139.5	1.72	$5.85\ 10^{-20}$	c
144.5	1.94	$2.00\ 10^{-22}$	c
149.5	2.02	$3.80\ 10^{-23}$	c
152.5	2.33	$1.30\ 10^{-26}$	c
155	2.55	$3.80\ 10^{-29}$	c
156.5	2.64	$5.55\ 10^{-30}$	c
157	2.96	$1.25\ 10^{-33}$	c
158	3.29	$2.40\ 10^{-37}$	c
166	3.02	$9.45\ 10^{-34}$	
170	2.94	$1.25\ 10^{-32}$	
173.5	2.94	$2.85\ 10^{-32}$	

(b)

Tm (°C)	ΔH (eV)	τ_{oa} (sec)	
128	1.61 ap	$2.95\ 10^{-19}$	ap
133.5	1.65	$2.50\ 10^{-19}$	
141	1.75	$2.70\ 10^{-20}$	
145.5	1.87	$1.25\ 10^{-21}$	c
151	1.91	$9.00\ 10^{-22}$	c
152.5	2.28	$3.80\ 19^{-26}$	c
155	2.60	$1.00\ 10^{-29}$	c
156.5	3.17	$3.05\ 10^{-36}$	c
157.5	3.63	$1.55\ 10^{-41}$	c
158.5	4.59	$9.35\ 10^{-53}$	c
176.5	3.00	$9.15\ 10^{-33}$	
182	2.88 ap	$7.95\ 10^{-31}$	ap

Table 2.- Parameters of Vogelian relaxation times.

Polycarbonate	Tm (°C)	T_∞ (°C)	α_f (10^{-3} deg^{-1})	τ_{ov} (sec)
Reference	116	44	2.4	0.23
Annealed [	128	77	8.25	10
	182	100	1.2	$1.9\ 10^{-3}$

DISCUSSION

We will discuss now the polarization phenomena observed around and below the glass transition temperature.

Glass Transition / Relaxation

The TSC peak observed around the glass transition temperature is constituted of elementary processes with relaxation times following a compensation law. It is interesting to rate that Tc - Tg ~ 20°C. Such an empirical relationship has been yet observed in either oriented or doped amorphous polymers and in semi crystalline polymers. So, this behavior has been attributed to the existence of local order.

Sub-Glass Relaxation

This mode situated between 90 and 140°C is essentially constituted of Vogelian processes. From values of Table 2, we can calculate the fractional free volume at Tm : the values are ranging from 0.168 in reference polycarbonate to 0.421 in annealed polycarbonate. It is interesting to note that these values are higher than the one (0.083) recorded in polystyrene at the liquid-liquid transition i.e. same 50° above the glass transition.

CONCLUSION

Polarization phenomena of polycarbonate have been found to be strongly related to its "physical structure". Indeed, relaxation modes are characteristic of physical aging and local order in the amorphous phase. The existence of domains of 20 to 40 Å has been postulated according to the granular model of Yeh [2].

REFERENCES

[1] Ch. Bailly, M.Daumerie, R. Legras and J.P. Mercier,*J. Polym. Sci.*, Vol.**23**, 751-770 (1985).

[2] G.S.Y. Yeh, *J. Macromol. Sci. Phys.* **B6(3)**, 465-478 (1972).

CHARACTERIZATION OF THE MICROSCTRUCTURE OF LATEXES BY THERMALLY STIMULATED CURRENTS

P. CEBEILLAC, C. LACABANNE,

Laboratoire de Physique des Solides, Associé au CNRS, Université Paul Sabatier, 31062 Toulouse Cédex, France

and P. DUPUIS,

Centre de Recherches d'Aubervilliers, Rhône-Poulenc Recherches, 93308 Aubervilliers Cédex, France.

ABSTRACT

The microstructure of latexes has been investigated by Differential Scanning Calorimetry/DSC and ThermoStimulated Currents/TSC. The SC copolymer obtained by semi-continuous feeding, is characterized by a narrow glass transition and a single TSC peak. Moreover, the analysis of the fine structure of the TSC peak shows that it is associated with a single compensation law. This behavior is typical for a statistical copolymer. Contrarily, the SAS and ASS copolymers prepared by step feeding, have a broad glass transition and two TSC peaks. This behavior is characteristic of block copolymers. This result is confirmed by the existence of two compensation laws indicating a biphasic structure. The SAS copolymer has been found to have a higher segregation than ASS probably because of higher reactivity of styrene and of its hydrophobicity.

INTRODUCTION

The aim of this wo[illegible]s the characterization of the microstructures of amorphous copolymers of styrene and n butyl acrylate. Indeed, it is well known that by varying feeding conditions, the rheological properties of the obtained copolymers can be very different. So, it would be of interest to relate the evolution of rheological properties to their microstructure.

CH2593-2/ 88/ 0000-0457$01 00 Copyright 1988 IEEE

MATERIALS

The studied copolymers have been prepared by emulsion copolymerization of 45% styrene (S) and 55% n butyl acrylate.

Three series of samples have been prepared :

- SC copolymer : it has been obtained by semi-continuous (SC) feeding with A and S

- ASS and SAS copolymers : both copolymers have been prepared by step (S) feeding with A and S,
  . copolymerization of A and then S (ASS)
  . copolymerization of S and then A (SAS).

METHODS

Differential Scanning Calorimetry (DSC) has been used as reference technique ; Thermally Stimulated Currents (TSC) for investigating the fine structure of relaxation spectra.

DSC and TSC complex spectra of copolymers

DSC/Thermograms of the three copolymers have been represented on Figure 1. The transition zone is narrower for SC copolymer than for ASS and SAS. The broadening of the transition zone may be attributed to step feeding during the copolymerization.

TSC/Complex spectra of SC, ASS and SAS copolymers have been reported on Figure 2. The thermocurrent has been normalized to the external electrical field and the dynamic conductivity (σ) has been indicated on the Figure. The temperature variation of σ shows the existence of a single peak in the SC copolymer and of two well resolved peaks in both ASS and SAS copolymers. In ASS and SAS, the low temperature peak has been associated to the glass transition of acrylic sequences ; the high temperature peak has been related to the glass transition of styrenic sequences. The single peak observed in SC copolymer may also be attributed to the glass transition.

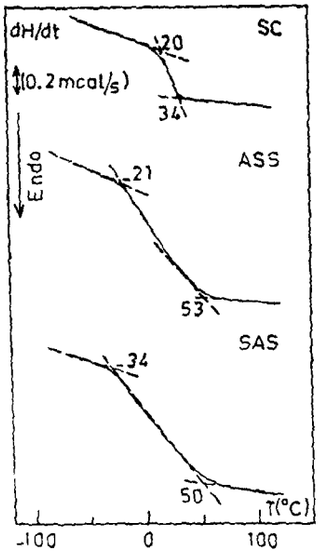

FIGURE 1.- DSC Thermograms for SC, ASS and SAS copolymers.

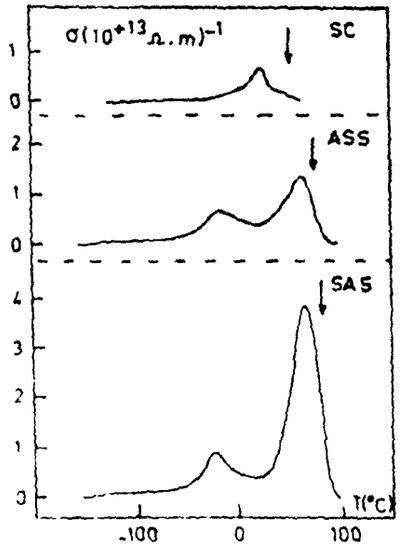

FIGURE 2.- TSC thermograms for SC, ASS and SAS copolymers.

Fine structure of TSC spectra of copolymers

The technique of fractional polarizations has been used for resolving the complex TSC spectra of copolymers. The corresponding elementary TSC spectra have been well described by Arrhenian relaxation times and the variation of the preexponential factor (τ_o) has been plotted versus the activation enthalpy (ΔH) [Figure 3]. For the SC copolymer, a single compensation line, characteristic of a monophasic structure is observed ; for the ASS and SAS copolymers, two compensation lines have been found. They indicate the existence of a biphasic structure.

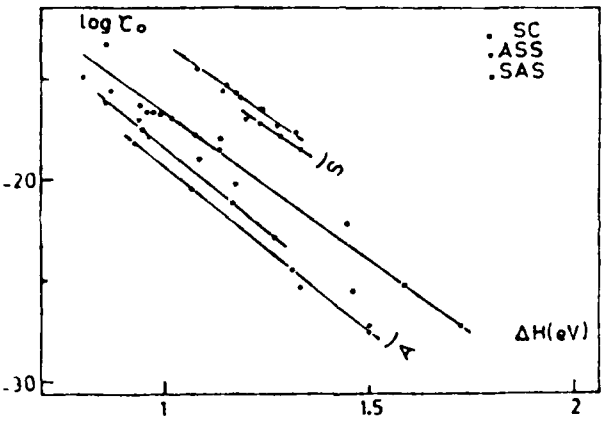

FIGURE 3.- Compensation diagrams for SC, ASS and SAS copolymers.

DISCUSSION

SC Copolymer prepared by semicontinuous feeding.

For this copolymer, the DSC and TSC spectra are typical of an homopolymer. The glass transition temperature and the TSC maximum temperature ($T_{g/m}$) obey a Fox equation :

$$1/T_{g/m} = Xa/T_{g/m,a} + Xs/T_{g/m,s}$$

where Xa is the weight fraction of A ; Xs is the weight fraction of S, $T_{g/m,a}$ is the glass

transition/TSC maximum temperature of A ; and $T_{g/m,s}$ is the glass transition/TSC maximum temperature of S. This behavior is characteristic of a statistical copolymer. This result is confirmed by the single compensation line deduced from the analysis of the fine structure.

ASS and SAS copolymers prepared by step feeding.

In both copolymers, DSC spectra show a significant broadening of the transition zone. In fact, TSC complex spectra show the existence of two well resolved relaxation modes. They have been attributed to the dielectric manifestation of the glass transition of acrylic and styrenic sequences, respectively. This behavior is characteristic of block copolymers. The analysis of the fine structure confirms the existence of a biphasic structure : indeed two compensation lines are observed.

It is interesting to note that the compensation diagram shows significant differences between ASS and SAS. Indeed, phase segregation is not achieved : it is higher in SAS than in ASS. For explaining this result, it is necessary to take into account the morphology of the copolymers. Previous work [1] has shown the existence of core-shell structures : acrylic core and styrenic shell for ASS ; styrenic core and acrylic shell for SAS. The higher reactivity of styrene [2] together with its hydrophobicity might explain the higher phase segregation of SAS.

REFERENCES

[1] T.I. Min, A. Klein, M.S. El Aasser ; J. Polym. Sci. Chem. Ed. **21**, 2045-61 (1983).
[2] J. Snuparek and F. Krska, J. Applied Polym. Sci. **20**, 1753-64 (1976).

ROLE OF INTERFACES ON A NATURAL COMPOSITE BIOELECTRET : BONE

A. LAMURE, M.J. FAURAN-CLAVEL, C. LACABANNE,

Université Toulouse III
31062 Toulouse Cédex (France)

M.F. HARMAND,

Université de Bordeaux II
33076 Bordeaux Cédex (France)

M. VIGNOLES and G. BONEL,

Institut National Polytechnique,
31077 Toulouse Cédex (France)

ABSTRACT

The aim of this work is the characterization of interfaces in calcified tissues. Thermally Stimulated Currents and Gel Permeation Chromatography have been used for investigating extracts and residues from calf femoral diaphysis, at various stages of demineralization. In residues, the evolution of molecular mobility shows that the organic-mineral linkage is insered by several proteins : Collagen is not directly linked to apatite.

INTRODUCTION

On a physico-chemical point of view, calcified tissues may be considered as natural composites. Their final properties are not only dependent upon the properties of each constituent but also of the molecular interfaces between the various constituents. Those interfaces have been characterized by Gel Permeation Chromatography/GPC and Thermally Stimulated Current-/TSC. 120 days old calves femoral diaphysis have been examined at various stages of demineralization. 0.5 M EDTA extracts and residues have been considered first; then, a highly dissociative buffer (4M guanidinium chloride) has allowed us to separate collagen from the

CH2593-2/ 88/ 0000-0462$01.00 Copyright IEEE

other organic constituents strongly bound to collagen.

MATERIALS AND METHODS

All the samples have been extracted from a 120 days-old calf femoral diaphysis, then carefully washed for being free of marrow and finally deprived from periosteum. This bone has been ground at liquid nitrogen temperature and demineralized in a 0.5 M EDTA solution at pH 7.4 with proteases inhibitors (10 ml solution per powder bone gram). This lost residue has been treated 48 hours by 4 M guanidine HCl, pH 7.4, in order to separate collagen from the remaining organic constituents of bone. The Table I summarizes the procedure of extraction of the various fractions.

TABLE I.- Demineralization sequences of bone.

	SAMPLES	0	1	2	3	4
EXTRACTION TIME (days)	0.5 M EDTA	0	11	10	21	21
	4 M GuHCl	0	0	0	0	2

The last extracts have been analyzed by exclusion chromatography. The identification of the remaining proteins has been done by UV spectroscopy at 280 nm. The proteins titration has been actived according to the Lowry method [1].

The residues have been dried and compressed into pellets. For Thermally Stimulated Current experiments, a voltage of 200 V has been applied at 25°C. Then, the temperature of the sample has been decreased till LNT where the electric field has been cut off. During the controlled increase of temperature, the polarization vanishes. Then, dielectric energy losses are observed.

RESULTS AND DISCUSSION

Bone powder will be studied as reference. It will be designated as "residue 0". After four days of EDTA demineralization, 9% of proteins are isolated and we are left with residue R2. Then, after 21 days of EDTA

demineralization, another 10% of proteins are isolated (residue R3). Using highly dissociative buffer as 4 M guanidine HCl, 3% of tighly bound proteins are extracted (residue R4).

Thermally Stimulated Currents spectra of the five residues have been investigated. Three groups of spectra can be distinguished : one for residues 0 and 1, another for residues 2 and 3, a last one for residue 4. The various TSC spectra have been analyzed by the technique of fractional polarization [2]. So, the complex TSC spectra have been resolved experimentally into elementary TSC spectra. Each elementary TSC spectra has been associated with a dielectric relaxation time (τ) following an Arrhenius equation:

$$\tau = \tau_o \exp \Delta H / kT$$

where τ_o is the preexponential factor, ΔH is the activation enthalpy, and k is the Boltzmann constant.

For characterizing the various residues, the logarithmic variation of τ_o has been plotted versus ΔH. Linear variations indicates the existence of a compensation phenomena. Figure 1 shows the "compensation diagram" of residue 0. The same diagram is also found in residue 1 i.e. after extraction of the first group of proteins comprising osteocalcin. The analogy between residue 0 and 1 shows that this first group of proteins does not interact with the mineral phase. Indeed, by analogy with previous work on stoechiometric [3] and non stoechiometric [4] synthetic apatites, this mobility has been associated with reorientations of hydroxyl ions into the apatitic channels.

Figure 2 represents data obtained with residue 2. The diagram recorded for residue 3 is quite analogous. This second group of extracted proteins with in particular phosphoproteins is slightly bound to the mineral phase since the response of this last one is no longer longer observed on a compensation diagram. A very significant difference is observed for residue 4 as

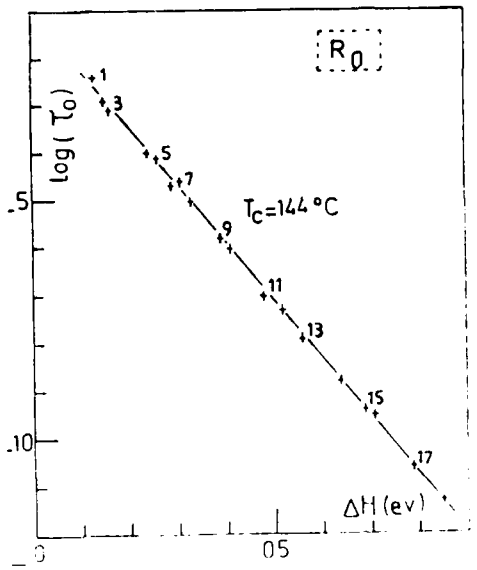

FIGURE 1.- Compensation diagram of bone powder i.e. residue 0.

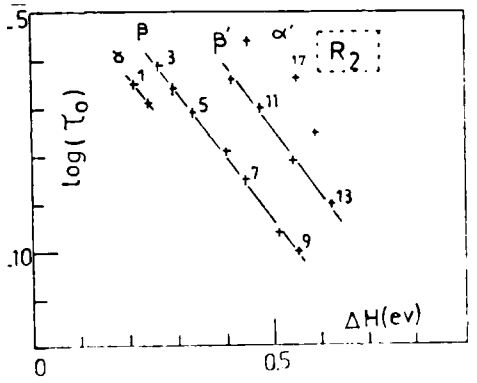

FIGURE 2.- Compensation diagram of residue 2.

shown on Figure 3. It is important to note here that this last diagram is comparable with the one observed for type I collagen [2]. From previous work, the γ and β lines associated with the γ and β relaxation modes, corresponds to intramolecular mobility while the α' one reflects the intermolecular mobility.

The analysis of Figures 2 and 3 shows that the β and γ modes associated with residues 2, 3 and 4, have the

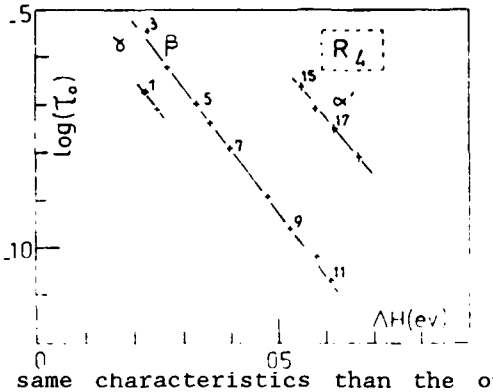

FIGURE 3.- Compensation diagram of residue 4.

same characteristics than the ones found in type I collagen. So, the intramolecular mobility of collagen is not modified by the presence of proteins. Contrarily, the last group highly bound proteins removed by 4 M guanidine HCl modify the intermolecular mobility since the characteristics of the α mode are different in residue 2, 3 and 4. Those proteins may be located in the hollow of the quarter-stagger structure, near the telopeptidic regions.

CONCLUSION

Data from biochemical and biophysical studies show that non collageneous proteins play a key role in interfaces of calcified tissues. The first group of extracted non collageneous proteins with osteocalcin are only loosely bound. Contrarily, phosphoproteins desappear together with the classical pattern of the mineral phase. The interaction with the apatitic structure may be insured by the polar orthophosphate groups. The last stage of demineralization shows the interaction of collagen with the remaining proteins. So multiples proteins are involved in the organic mineral linkage in calcified tissue.

REFERENCES

[1] O.H. Lowry et al. ; J. Biol. Chem. 1,93, 265 (1951).
[2] A. Lamure et al.; IEEE Transactions on Electrical Insulation, EI 21, 443 (1986).
[3] N. Hitmi et al. ; Calcified Tiss. Intl. 38, 252 (1986).
[4] A. Lamure et al. ; Gordon Research Conference on Calcium Phosphate ; Plymouth 22-26/06/1987.

PHASE TRANSITION INVESTIGATION IN VINYLIDENE FLUORIDE/TRIFLUOROETHYLENE COPOLYMERS BY THERMALLY STIMULATED CONDUCTIVITY MEASUREMENTS.

M. Latour, R. M. Faria*, and R. L. Moreira.

Groupe de Dynamique des Phases Condensées - LA 223, U.S.T.L., Place Eugène Bataillon
34060 Montpellier Cedex, France.

ABSTRACT

An additional ferroelectric phase transition, beside the well known ferro-to-paraelectric one, was detected in Vinylidene fluoride/Trifluoroethylene copolymers by Thermally Stimulated techniques with the help of a superimposed piezoelectric noise. Differential Scanning Calorimetry measurements were in agreement with these results. With the initial rise method applied to the glow curves, it was possible to calculate the activation energies of the relaxation connected with the both transitions. We found 0.73 eV and .33 eV respectively for the F-P and for the additional phase transitions.

INTRODUCTION

The high piezoelectric activity of the polarized ß-PVDF films [1] was responsible for an extensive study of this material during two decades. Despite its ferroelectric properties, it does not present the ferro-to-para structural transition, since it remains ferroelectric up to the melting point.

Vinylidene fluoride/Trifluoroethylene copolymers (VDF/TrFE) have piezoelectric and pyroelectric properties similar to those presented by the ß-PVDF [2,3]. Moreover, they and have the advantage to present, in appropriated molar ratios, the Curie temperature [4].

CH2593-2/ 88/ 0000-0467$01.00 Copyright 1988 IEEE

In the present paper Thermally Stimulated Processes are used to study the phase transitions on 90/10 and 70/30 mol % VDF/TrFE copolymers. It is known hitherto that the 90/10 crystallizes in the conformation TGTG', similar to that presented by the α-PVDF, while the 70/30 copolymer takes a trans-planar conformation, similar to ß-PVDF. We found out two peaks on Thermally Stimulated Depolarization (TSD) measurements for both materials in the range 40 to 130 °C. With a help of a superimposed "piezoelectric noise" on the TSD curves, we identified the peak of higher temperature as due to the well known ferro-to-paraelectric (F-P) transition, and the other as a ferro-to-ferroelectric (F-F) transition, in the sense that the ferroelectric properties remain unchanged before and after the corresponding peak. DSC measurements confirmed these transitions. We also obtained the activation energies of the long relaxation processes whose accompanied both peaks.

EXPERIMENTAL PROCEDURES

The copolymer films were prepared from resins provided by Atochem (France), whose were pressed at 200 °C and quenched to the room temperature. Samples were circular with a diameter of 4 cm and thickness of 50 µm. Rectangular aluminum electrodes (1.0 by 2.5 cm) were high vacuum deposited on both sides. TSD measurements were carried out with a linear rate of 1.9 °C/min, and the samples were polarized at 65 °C under a field of 500 kV/cm. A slight mechanical vibration (around 1 Hz) was imposed to the sample, which created a "piezoelectric noise" on the TSD recorded measurements. DSC measurements were performed in non polarized samples with a DSC 4 Perkin-Elmer apparatus with a scan rate of 20 °C/min.

RESULTS

Typical TSD curves obtained are presented in the figure 1. Two peaks were observed in the

70/30 sample (curve a), at 102 and 108 °C, called A and B peaks respectively. In the 90/10 copolymer also two peaks appeared, at 63 and 120 °C. The amplitudes of the peaks of 70/30 sample are higher than that presented by 90/10 one, however their widths are narrower. On both curves a noise was present. Its amplitude increased with the temperature up to the begining of the B peak, then decreased and dissapeared completely after its maximum was reached. This noise was not detected on non piezoelectric materials. So we concluded that it has a piezoelectric origin due to the mechanical vibration. The DSC measurements show two endothermic peaks for the 70/30 sample at temperatures close to that presented in the TSD thermogram (Fig. 2). A peak around 60 °C and a initial rise starting at 100 °C were recorded for the 10/90 sample.

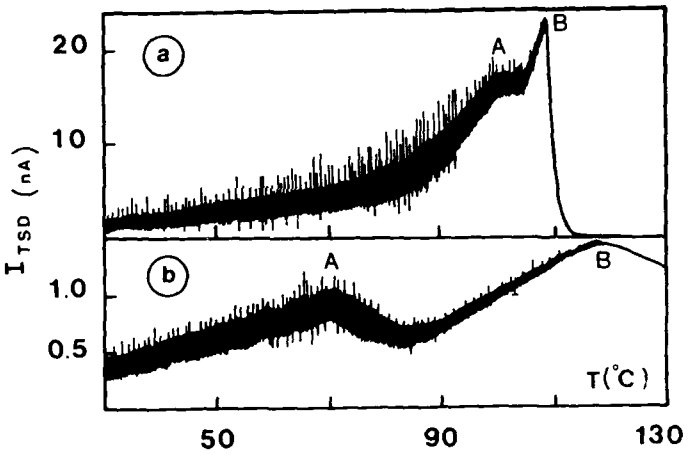

Fig. 1 - TSD curves with a superimposed piezoelectric noise. (a) 70/30 and (b) 10/90 mol % VDF/TrFE copolymers.

In figure 3 we present charge densities variation (corresponding to the remanent polarization) with temperature, derived from the TSD curves of 70/30 and 60/40 (this one non presented here) copolymers.

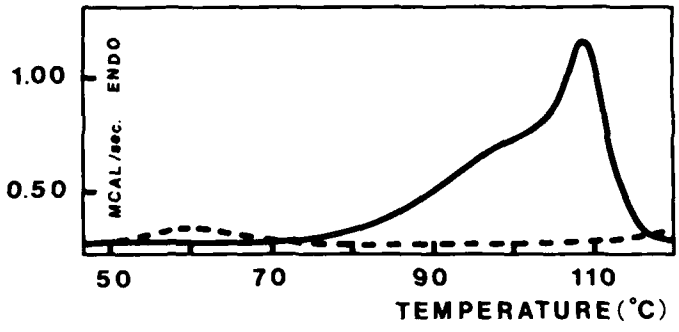

Fig. 2 - DSC measurements. (a) 70/30 and (b) 90/10 mol % VDF/TrFE copolymers.

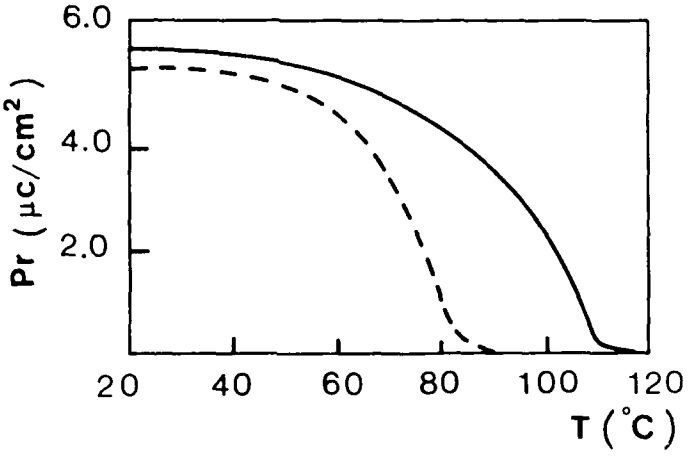

Fig. 3 - Remanent polarization curves. (—) 70/30 and (---) 60/40 mol % VDF/TrFE copolymers.

DISCUSSION

The DSC measurements make clear that two transitions take place in 70/30 mol % VDF/TrFE copolymer, around 100 and 110 °C. For the 90/10 copolymer just one transition was detected cle-

arly (at 60 °C). Due to the similarities of the TSD and DSC measurements, we might assume that they have the same physical origin. The peaks of higher temperature in the measurements of the 70/30 copolymer were identified with the ferro-to-paraelectric structural transition. In the TSD curve its decay is very abrupt in agreement with a first-order transition. The piezoelectric noise on the TSD curve is in accordance with the conclusion of a F-P transition. The transition at lower temperature was assumed to be a ferro-to-ferroelectric transition, since the material continues to present a piezoelectric activity. The activation energies connected with the relaxations of the A and B peaks were calculated by the initial rise method. The obtained values were respectively .33 and .73 eV. The curve presented in the figure 3 shows the characteristic remanent polarization decay of this copolymer. By the other hand, the 90/10 copolymer also presents the piezoelectric noise despite its conformation similar to that presented by α-PVDF [5].

*Permanent adress- Instituto de Física e Química de São Carlos, USP - Brasil.

Acknowlegments - R. M. Faria and R. L. Moreira gratefully acknowledege the Brazilian agency CNPq for fellowship supports during this work.

REFERENCES

[1] H. Kawai, Jpn. J. Apll. Phys. 8, 975 (1969)
[2] Y. Tajitsu, A. Chiba, T. Furukawa, M. Date, and E. Fukada, Appl. Phys. Lett. 36, 286 (1980).
[3] T. Furukawa, J. X. Wen, K. Suzuki, Y. Takashina, and M. Date, J. Appl. Phys. 56, 829 (1984).
[4] T. Yamada and T. Kitayama, J. Appl. Phys. 52, 6859 (1981).
[5] M. Latour and R.L. Moreira, J. Polym. Sci.: Part B: Polym. Phys. 25, 1717 (1987).

THERMALLY STIMULATED CURRENT STUDY ON POLYIMIDE FILM

Lei Qingquan and Wang Fulei

Department of Electrical Materials Engineering
Harbin Institute of Electrical Technology
Harbin, China

ABSTRACT

We have experimentally observed that there are two peaks in TSC-specrta of Du Pont polyimide film, the low temperature peak in range of 50-70°C is ascribed to dipole depolarization of unimidized polyamic acid in film, whereas, the high temperature peak in range of 160-180 °C is clearly manifested with our experimental results to be due to depolarization of space charge of ions generated through ionization of unimidized polyamic acid, ionic impureties and water, then bound into Fröhlich's two potential well.

INTRODUCTION

Because polyimide(PI) up to 300°C high temperature still possesses the excellent dielectric properties, it has been widely used in electrical equipments and integrated circuits, the investigations have been reported on dielectric behaviours at DC and AC voltages [1-3]. In order to further clarify its dielectric relaxation mechanism, only Tanaka [4], at first using TSC technique, has experimentally researched and suggested that the low temperature peak(β) at 50°C is due to dipole orientation polarization probably associated wirh residual reactive groups in PI, and the high temperature(α) is caused by release of trapped electron.

Based on some results obtained from TSC and DC conduction measurements, we shall further discuss and reveal the nature of (α) peak in PI.

EXPERIMENTAL

All specimens of Du Pont PI of 50 μm thickness were first cleaned with alcohol, then two-side-

CH2593-2/ 88/ 0000-0472$01.00 Copyright 1988 IEEE

metallized in vacuum with aluminium, the diameter of Al-electrodes is of 20 mm. The specimens provided with Al-electrodes were treated at 70°C(PI-1) and at 370°C(PI-2) for 24 h in air, respectively. Except PI-1 and PI-2, other specimens were previously processed with N,N-dimethylformamide(DMF) at room temperature for 72 h to solve unimidized polyamic acid in film, then vacuum-evaporated with Al, refered to as PI-3.

The poling parameters are as follows: E_p=2-70 kV/mm, T_p=25, 170°C, t_p=15 min, 1 or 3h, b=dT/dt=60°K/h, the currents were measured with a model FJ-365 electrometer.

RESULTS AND DISCUSSION

Fig. 1 shows short-circuit(bias field E_b=0)TSC spectra of PI-1 and PI-2 poled with E_p=50 kV/mm at T_p=170°C, Fig. 2 presents TSC for PI-2 at various poling fields, in which there are a shoulder near 70°C(β) and a pronounced near 170 °C(α). For determining the mechanism of creating both the peaks, their peak currents as a function of poling field are plotted in Fig. 3 and Fig. 4, respectively. From linear dependence of β peak on E_p, it is fully manifested that the β peak is related to existence of unimidied polyamic acid in PI. Besides, both peaks(α and β) of PI-2 in Fig. 1 are lower than that of PI-1 demonstrating the unimidized polyamic acid during treating at 200-370°C further produced imidization reaction; even in the case of extremely low poling field, α peak can be observed, which probably proves ion feature of α peak.

From Fig. 4 we can find that α peak currents with increase of E_p will tend to reach saturation value, as a result, we shall employ Fröhlich's two potential well model [5] to analyse the mechanism responsible for α peak. By comparing the experimental values with theoretical ones, it can be seen that the saturation behaviour of α peak predicted by Fröhlich's model is possibly better responsible for depolarization of ions from such a bound state than of electrons from Coulombic trap.

Through peak cleaning technique, an isolated α peak can be acquired, using initial rise method the migration activation energy is evaluated to be 1.21 eV. In order to further identify ionic characteristic of α peak, we have measured temperature dependence of steady state DC conduction current in PI-2, from slope of Arrhenius plot, the activation energy of conduction is easily calculated to be 1.31 eV, it is almost equal to activation energy of proton conduction obtained by Sacher [3](1.39 eV). Because of short-circuit measurement of TSC, the activation energies responsible for α peak and DC conduction are nearly equal, which interprets why the mechanism of α peak is attributed to depolarization of ionic space charges.

Although both E_p and t_p indicated in Fig. 5 are much higher than that in Fig. 2, the β peak in the former is much lower than that in the latler, the α peak in the former vanichs, the reason is that at lower poling temperature, dipole groups can not fully be orientated, and that ion space charge polarization can not be created due to difficulty of ionization of unimidized polyamic acid.

Fig. 6 shows TSC-spectra of PI-2 and PI-3 at E_p =70 kV/mm. The α peak of PI-3 almost disappears manifesting ion concentration in PI treated previously with the above solvent lowers distinctly. Since N,N-dimethylformamide can solve the unimidized polyamic acid in PI. However, β peak in PI-3 is higher than that in PI-2, this indicates that DMF can also swell PI and make it to contain more polar groups, then to possess higher β peak.

CONCLUSION

It comes to the conclusion that the β peak of PI is possibly ascribed to dipole depolarization of unimidized polyamic acid; the α peak is due to depolarization of space charge of ions mainly generated by ionization of unimidized polyamic acid, and then bound into Fröhlich's two potential-well, which can be explained by the following facts: (1) the saturation

behaviour of α peak predicted by Fröhlich's two potential well model; (2) even at poling field much lower than that of threshold field of electron emission, α peak still exists; (3) activation energy of α peak is nearly equal to that of DC conduction; (4) α peak for PI treated by solvent(DMF) basically disappears.

REFERENCES

[1] W. Wrasidio, J. Polym. Sci., Polym. Phys. Ed., Vol. 11, 2143, 1973.
[2] E. Sacher, IEEE Trans. Elec. Ins. Vol. EI-13, 94, 1978.
[3] E. Sacher, IEEE Trans. Elec. Ins. Vol. EI-14, 85, 1979.
[4] T. Tanaka, J. Appl. Phys., Vol. 49, 784, 1978.
[5] H. Fröhlich, Theory of Dielectrics, Clarendon, Oxford 1958, Chapter 2.

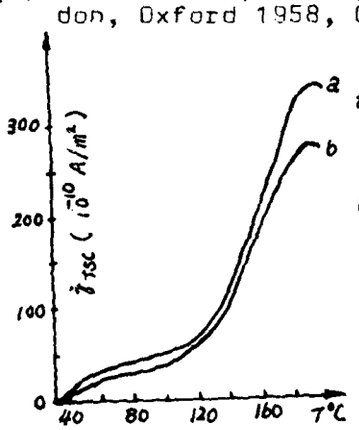

Fig.1 Short-circuit TSC spectra of PI-1 (a) and PI-2(b) at E_p=50 kV/mm and t_p^p=170°C.

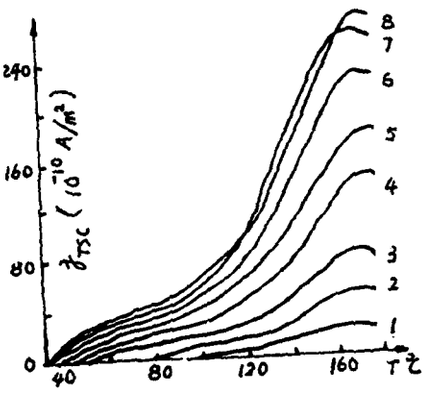

Fig.2 TSC spectra of PI-2 at different poling field (kV/mm): 1-2, 2-6, 3-10, 4-20, 5-30, 6-40, 7-50, 8-60.

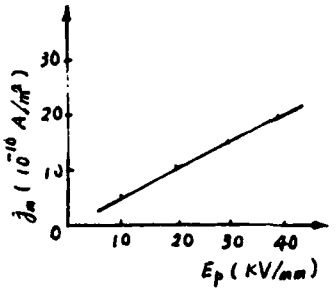

Fig.3 ß peak current as a function of poling field.

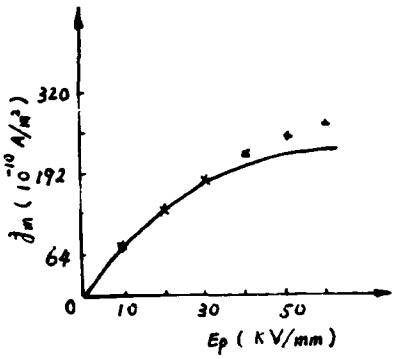

Fig.4 peak current as a function of poling field. x: experimental values; solid curve: theoretical values.

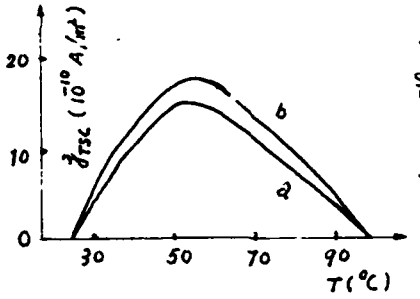

Fig.5 TSC spectra for PI-2 at E_p=70 kV/mm and T_p=25°C. (a) t_p =1 h, (b) t_p=3 h.

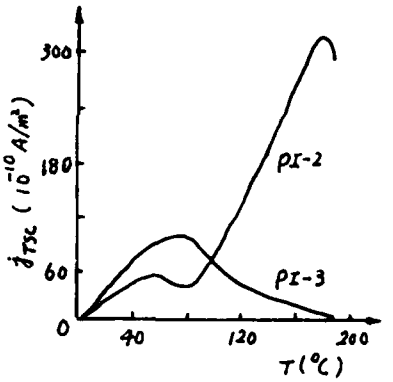

Fig.6 TSC spectra of PI-3 and PI-2 at poling field of 70 kV/mm.

METHD OF MEASUREMENT OF SPACE CHARGE DISTRIBUTION IN DOUBLE-LAYER COMPOSITE DIELECTRICS

Zhang, Yewen; Tu, Demin and Liu, Yaonan

Dept. of Electri. Engin., Xi'an Jiaotong University, Xi'an, Shaanxi Province, P. R. China

ABSTRACT

In this paper, a new method for measuring space charge in double-layer composite dielectrics was given. Using the method of Pressure Step Wave, considering the transmission and reflection of the pressure wave on the interface, and the superposition of the signals obtained, the potentials distribution in the double-layer composite dielectrics may be obtained by measuring the open-circuit voltage through simple calculation. The experimental equipment mainly consists of the shock tube and the stroage oscilloscope. For the sample of composite dielectrics consisting of 0.5mm polymethymethacrylate (PMMA) and 0.16mm fluorinated ethylene propylene(FEP), the experimental results show that this method is successful.

I. INTRODUCTION

For the measurement of space charge distribution in solid dielectrics, the pressure wave method is used widely[1-5] and has been used to conduct the research of the charge injection from an electrode in insulating material under high field[6]. For the insulating structure in practical cases, the double-layer composite dielectrics is used very often. And the space charge is easily to be created and accumulated in it. So, it is necessary to measure and to study the space charge distribution in double-layer composite dielectrics. Being measured with the pressure wave method, it is necessary to consider the reflection and the transmission of pressure wave (stress wave) at the interface, and the superposition by the action of pressure wave (stress wave).

II. THEORETICAL ANALYSIS

1. Reflection and transmission of pressure wave[1]

When an elastic wave with its propagating direction normal to the interface propagates from medium 1 to medium 2, by assuming these two kinds of medium to be kept to contact on the interface, and applying to the law of conservation of momentum at wave front, we can get

$$\begin{cases} p_f = F p_I, \quad p_T = T p_I \\ F=(1-n)/(1+n), \quad T=2/(1+n), \quad n=(\rho_0 C)_1/(\rho_0 C)_2 \end{cases}, \tag{1}$$

CH2593-2/ 88/ 0000-0477$01.00 Copyright 1988 IEEE

where, F and T are reflection coefficient and transmission coefficient respectively, n is the radio of acoustic impedance, $\rho_0 C$ is acoustic impedance, ρ_0 is initial density, C is sound velocity, p is stress and the subscripts I, T, and F show incidence, transmission, and reflection respectively.

For the plane wave in a thin plate or film, it can be seen as one-dimensional elastic longitudinal wave, its wave velocity is

$$C=\left[\frac{(1-\nu)E}{\rho_0(1+\nu)(1-2\nu)}\right]^{1/2} \quad , \tag{2}$$

where, E is Young's modulus, and ν is Possion's ratio. And,

$$E_L=\frac{(1-\nu)E}{(1+\nu)(1-2\nu)} \quad , \tag{3}$$

where, E_L is side limited elastic modulus. From these two equations, we can get

$$E_L=\rho_0 C^2 \quad . \tag{4}$$

Eq. 4 can be used to measure side elastic modulus E_L. In addition, the compressibility χ in the case of one-dimension can be defined as follows,

$$\chi=\frac{1}{z}\cdot\frac{dz}{dp} \quad , \tag{5}$$

and the relationship between E_L and χ is

$$\chi=-\frac{1}{E_L} \quad . \tag{6}$$

2. Method of step pressure wave

Let a step pressure wave propagate along z-axis, shown in Fig. 1. The origin of coordinates is at electrode I and moves with the motion of Electrode I. Taking the electrode I as potential reference point, the potential V(t) of the electrode II is studied. The quantities with superscript ' show the physical quantities in the compression area and that without superscript ' in non-compression area. Then,

$$\begin{cases} V(t)=-[1-\frac{\varepsilon}{\varepsilon'}(1+\chi p)]\Phi(z) \\ z=Ct \end{cases} \tag{7}$$

where, $\Phi(z)$ is the initial potential distribution in the dielectrics. If pressure wave is a tensile wave (expansion wave), p will be negative. Let a step pressure wave

propagate along the neverse direction of z-axis, the other conditions are remained as same as above, shown in Fig. 2. Then,

$$\begin{cases} V(t)=[1-\frac{\varepsilon}{\varepsilon'}(1+\chi p)]\Phi(z) \\ z=d_0+Ct \end{cases} \quad (8)$$

Eq. 8 is alike in expression to Eq. 7 except one sign. For the tensile wave (expansion wave), p will be likewise negative.

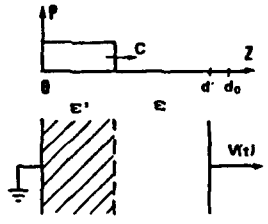

Fig. 1 pressure wave along z-axis

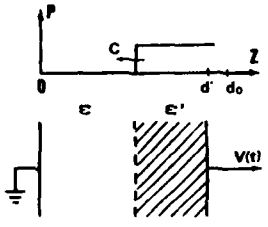

Fig. 2 pressure wave along rev. z-axis

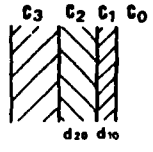

Fig. 3 medium structure of double-layer composite dielectrics

3. Measurement of space charge in double-layer composite dielectric

The medium structure for the pressure wave propagation can be seen as shown in Fig. 3. The measuring electrode is very thin and can be neglected. Medium 0 is air, medium 3 is a backplate made of brass, while medium 1 and 2 are composite dielectrics to be measured. d0 and C are their original thicknesses and sound velocity respectively. p1 and p2 are stress intension of incidence wave in medium 1 and medium 2 respectively. Tmn and Fmn are the transmission factor and the reflection factor from medium m to medium n.

Given: $d_{20}>d_{10}$ and $|d_{10}/C_1|<|d_{20}/C_2|<|2d_{10}/C_1|$. So, the relationship between open voltage V(t) and space potential distribution $\Phi(z)$ is different in different time interval.

(1) Before the reflection at the interface,

$$\begin{cases} V_1(t)=[1-\frac{\varepsilon_1}{\varepsilon_1'}(1+\chi_1 p_1)]\Phi(z) \\ z=d_{10}+d_{20}+C_1 t \\ 0<t<-d_{10}/C_1 \end{cases} \quad (9)$$

Considering the amplification factor of the measuring system and the relationship between dielectric constant

and stress p, using

$$1-\frac{\varepsilon}{\varepsilon'}(1+\chi p)=-\chi p\left(\frac{\varepsilon}{3}+\frac{4}{3}-\frac{2}{3\varepsilon}\right) \quad , \tag{10}$$

the measuring signal $V_1^*(t)$ is

$$V_1^*(t)=KV_1(t)=-K\chi_1 p_1\left(\frac{\varepsilon_1}{3}+\frac{4}{3}-\frac{2}{3\varepsilon_1}\right)\Phi_1(z) \quad . \tag{11}$$

(2) Arriving at the interface, the step pressure wave will creats transmission and the reflection. For the transmission wave $p_2=T_{12}p_1$, and for the reflection wave, $p_1'=F_{12}p_1$. Considering the simultaneous action of p_2 and p_1', sususbstiuting the initial condition and Eq.11 into the susuperposed differential equation, we can get the relationship between the open-circuit voltage $V^*(t)$ measured and $V_2^*(t)$, in which the proportionality coefficient between $V_2^*(t)$ and $\Phi_2(z_2)$ has the same value as that in Eq.11.

$$\begin{cases} V_2^*(t)-V_1^*(-d_{10}/C_1)=\dfrac{\chi_1\left(\frac{\varepsilon_1}{3}+\frac{4}{3}-\frac{2}{3\varepsilon_1}\right)}{T_{12}\chi_2\left(\frac{\varepsilon_2}{3}+\frac{4}{3}-\frac{2}{3\varepsilon_2}\right)}\{V^*(t)-V_1(-d_{10}/C_1) \\ \qquad +F_{12}[V_1^*(-d_{10}/C_1-t)-V_1^*(-d_{10}/C_1)]\} \\ -d_{10}/C_1<t<-2d_{10}/C_1 \end{cases} \tag{12}$$

(3) The pressure wave from the interface reflection will be creats the second reflection at the interface between medium 1 and medium 0. As stated similarly as above, the relationship between $V_2^*(t)$ and the open-circuit voltage $V^*(t)$ can be shown as follows,

$$\begin{cases} V_2^*(t)-V_1^*(-d_{10}/C_1)=\dfrac{\chi_1\left(\frac{\varepsilon_1}{3}+\frac{4}{3}-\frac{2}{3\varepsilon_1}\right)}{T_{12}\chi_2\left(\frac{\varepsilon_2}{3}+\frac{4}{3}-\frac{2}{3\varepsilon_2}\right)}\{V^*(t)-V_1^*(-d_{10}/C_1) \\ \qquad -F_{12}F_{10}V_1^*(t+2d_{10}/C_1)-F_{12}V_1^*(-d_{10}/C_1)\} \\ -d_{10}/C_1<t<-2d_{20}/C_2-d_{10}/C_1 \end{cases} \tag{13}$$

So, $V_2^*(t)$ that is directly proportional to the potential distribution $\Phi(z)$ in the dielectrics sample can be obtained by measuring the open-circuit voltage $V^*(t)$, which the proportional coefficient is $-K\chi_1 p_1(\varepsilon_1+4-2/\varepsilon_1)/3$.

III. EXPERIMENTAL EQUIPMENT AND TEST RESULTS

The step pressure wave is created by a shock tube. The sample to be studied is mounted on the end of the shock tube. The diameter of sample is 75mm. The electrode on the sample is made of Al vaporized in vacuum, and the relative intensity of shock wave is about 0.1~0.2MPa.

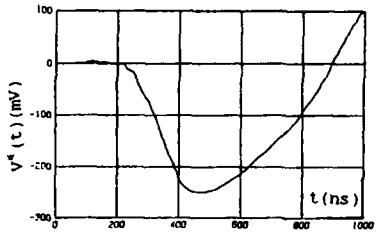

Fig. 4 open-circuit voltage $V^*(t)$

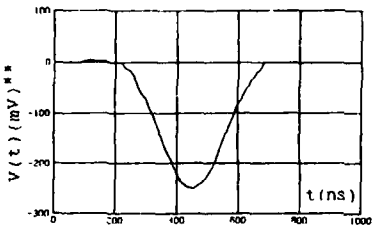

Fig. 5 potential distribution in sample, **directly proportional to $\Phi(z)$, on the time axis

The double-layer composite dielectric sample, consisting of 0.13mm FEP and 0.5mm PMMA, is to be acted under 1000V DC at least 40 hours, then the open-circuit voltage $V^*(t)$ under the action of step pressure wave can be measured as shown in Fig. 4. In accordance with the sound velocity and the density of its own, the compressibility and the transmission coefficient as well as the reflection coefficient can be obtained. Putting the data in Fig. 4 into a microcomputer and using above mentioned method, the results is shown in Fig. 5, which shows the potential distribution of the sample as indicated on the time axis. The peak point on the potential distribution is right over the position of the interface in sample. Because of no charge injection processing from an electrode under electric field, there existed no space charge except that at the interface.

IV. CONCLUSION

The said method for measuring space charge in double-layer composite dielectric is successful. Its accuracy depends greatly on the measuring accuracy of sound velocity. This method can be also used to study the space charge distribution in laminated composite dielectrics.

V. REFERENCE

1. C. Alquie, et al, Phys. Rev. Lett., vol. 47, p. 1483-7, 1981.
2. R. Gerhard-Multhaupt, et al, J. Appl. Phys., vol. 55, p. 2769-75, 1984.
3. A. G. Rozno, et al, IEEE Trans. on Electr. Insula., vol. EI-21, p. 417-25, 1986.
4. R. Gerhard-Multhaupt, IEEE Trans. on Electr. Insula., vol. EI-22, p. 431-54, 1987.
5. M. Haardt, et al, Ann. Rep. Conf. Electr. Diele. Phenom., p. 46-51, 1982.
6. F. Chapeau, et al, IEEE Trans. on Electr. Insula., vol. EI-21, p. 405-10, 1986.
7. John S. Rinehart, "Stress Transients in Solids", New Mexico, 1975.

BEHAVIOR OF NEGATIVELY CORONA CHARGING TEFLON-FEP AT ELEVATED TEMPERATURE

Lu Ting-ji, Yang Guo-mao and Sun Xi-min

Pohl-Institute of Solid State Physics, Tongji University, Shanghai, China

ABSTRACT

In this paper we study the behavior of negatively corona charging Teflon-FEP at elevated temperatures. Equivalent surface voltages, charge centroids, total charges per unit area and TSC of samples are determined under different charging temperatures and charging times. from their relationships we found several interesting results. For example, under elevated temperature there are limitation of charge centroid in depth and maximum of total charge per unit area. Further we can chose one best charging temperature and charging time. Then stability of negatively corona charging Teflon-FEP will be improved.

INTRODUCTION

One of important characters of electret, the charge stability, is concerned with material as well as charging method[1]. In recent years the Teflon-FEP has been widely used as a good electret material. It has been shown that the pre-quenching before corona charging and the annealing at elevated temperature after charging can improve the charge stability of Teflon-FEP because these thermal treatments contribute to increasing the charges trapped by deep bulk traps and erasing the charges trapped by shallow traps[2].

In this paper we study the behavior of negatively corona

CH2593-2/ 88/ 0000-0482$01.00 Copyright 1988 IEEE

charging Teflon-FEP at elevated temperature. As long as the charging temperature and the charging time are properly chosen, the Teflon-FEP electret foil of high stability is obtained.

EXPERIMENTAL PARAMETERS

All experiments were carried out with circular samples of Teflon-FEP, 7.2cm in diameter and 25.4μm thick. One side of samples was aluminized (back electrode).

All samples were charged by corona-grid charger[3] in an oven. Corona charging voltage V_c=-8.0kv. Grid voltage V_g, charging time t_c and charging temperature T_c are controllable.

The thermally stimulated current (TSC) measurements[1] were performed with equipment, having a probe diameter of 50mm and a distance from probe to sample of 4mm, using a heating rate of 4 °C/min in the range of 20 to 250 °C.

For measurements of the charge centroid $\bar{x}$ and the total charge per unit area in the sample we used the thermal-pulse technique[4].

EXPERIMENTAL RESULTS

The open circuit TSC measurements of samples which charged at elevated temperature were shown in Fig 1. The 30 °C charged sample shows three current peaks; one at about 155 °C and others at 180 °C and 220 °C. For increasing of charging temperature the two low temperature peaks decrease gradually to vanish and the high temperature peak shifts toward higher temperature. There is only one high temperature peak for 180 °C charged sample. Activation energies calculated

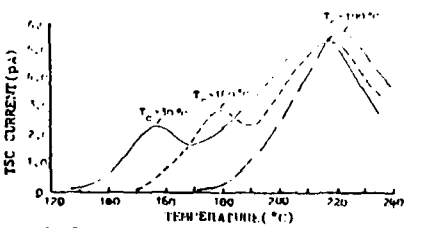

FIG.1. TSC measurement of samples at elevated temperatures; V_c=-8.0kv, V_g=-500v, t_c=10min.

by initial rise metnod are about 1.2and2.0 eV respectively.

The benaviors of initial surface voltage V_{so}, charge centroid $\bar{x}$ and total charge per unit area σ_T in the sample vary with charging temperature T_c are shown in Fig.2.

The initial surface voltage of the sample which is charging at elevated temperature (for example 180°C or above 180°C) is quickly increasing to a saturate volue in a few seconds, as shown in Fig. 3(a).

Charge centroid becomes deeper as the charging time increases and remain a stationary position, as shown in Fig. 3(b). Total charge per unit area becomes bigger as the charging time increases and gradually trends toward a maximum, as shown in Fig. 3(c).

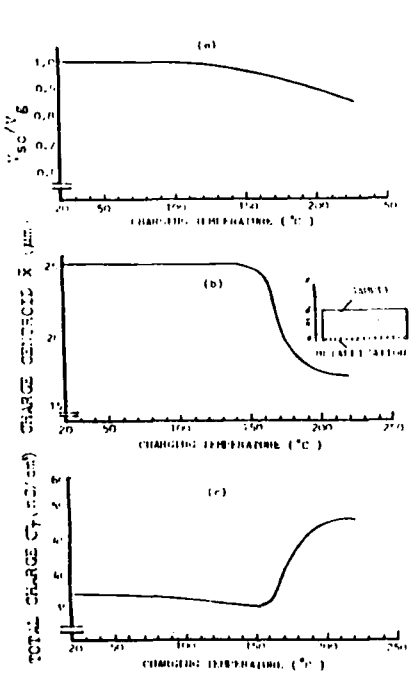

Fig.2. V_{so}/V_g, $\bar{x}$ and σ_T as a function of T_c (V_c = -8.0kv, V_g = -500V, t_c = 10 min)

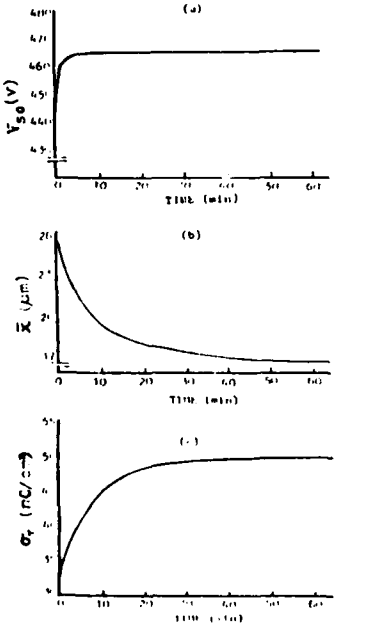

Fig.3. V_{so}, $\bar{x}$ and σ_T as a function of charging time. (V_c=-8.0kv, V_g=-500v, T_c=180°C)

DISCUSSION

Heinz von Seggen concluded[5] that the low temperature TSC peaks (155 and 170°C) are caused by carriers which are activated from energetically shallow traps at surface or near surface, while the high temperature peak (200°C) is caused by carriers which are activated from deep traps in bulk. Our TSC measurements at elevated temperature coincide basically with above conclusion. It will be seen from this that for up to 180°C charged sample carriers are trapped by deep bulk traps. The surface voltage is related to charge distribution in the sample by the following equation[6]

$$V_{so} = -\frac{d}{\varepsilon_0 \varepsilon}\left[\sigma + \frac{1}{d}\int_0^d x\rho(x,t)\,dx\right] \qquad (1)$$

where d is the thickness of a sample, ε_0 the permittivity of free space, ε the dielectric constant, σ the surface charge density and $\rho(x,t)$ the space and time dependent bulk charge density. The location x is measured from the rear metallization.

For corona charging it is known the all charged particals fall onto the surface and stay there in traps[3]. For the reason that the energies of these carriers are very small (about 1eV). At a temperature T°K the probability that an electron will escape from energy trap of depth E is [7]

$$p = \nu \exp(-\frac{E}{KT}) \qquad (2)$$

were ν is the attempt to escape frequency.

It is notable in Fig.3 that $\bar{x}$ starts moving at about 150°C and σ_T starts increasing at about 160°C. These facts indicate: rising with charging temperature (from about 150 to 170°C) the probability that an electron will escape from trap of activation energy of 1.2eV becomes enough big . Therefor, the carriers stored in shallow surface traps are released and drift in their self-field into near sur-

face or bulk. As the temperature rises up to 170°C, the near surface charges are also activated. It leads up to decreasing surface voltage. One part of these carriers will be trapped in deep bulk traps and another part reach the metal electrode to be neutralized. Since the sample is continued to charge, the amount of carriers trapped in deep bulk traps increases gradually to a certain value.

According to Fig.3, when the sample is charged at elevate temperature, there is a difference between grid and surface voltage. This indicates there is a certain current flowing through the sample. So, rising with charging time more and more carriers are trapped by the deep bulk traps . Through a certain time almost all deep bulk traps are fulled by carriers, $\bar{x}$ stays at a constant location $x \simeq 17$ μm, σ_r tends to a maximum too. Trap density of the sample has been inferred from the maximum of total charge. Full trap density in volume is about $1.3X10^{14}cm^{-3}$.

If the sample is charged at proper elevated temperature for enough charging time, more carriers can be trapped in deep bulk traps. Once the sample is conserved at room temperature, it is very difficult that the carriers detrap from deep bulk traps. These charges can be stored for a long period of time at room temperature. In summary , the corona charging method at elevated temperature is a valid method in order to improving charge stability.

ACKNOWLEDGEMENT

This work is supported by VW-Stiftung of F.R.Germany. The authors are indebted to Prof. G.M.Sessler for his friendly helping.

[1] G.M.Sessler(Ed.) Electrets, Springer, Berlin, New York (1980)
[2] Lu Ting-Ji, Electrostatistical Technology, No 1-2 of 1986, 70-76 (1986)
[3] R.A.Moreno and B.Gross, J.Appl.Phys. 47, 3587 (1976)
[4] R.E.Collins, Rev.Sci.Instrum. 48, 83 (1977)
[5] H.von Seggern, J.Appl.Phys. 50, 2817 (1979)
[6] G.M.Sessler in Electrical Properties of Polymer, Ed. D.A.Seanor, Academic Press, New York, London (1982)
[7] K.H. Nicholas and J.Woods, Brit.J.Appl.Phys. 15, 784 (1964)

THERMALLY STIMULATED CURRENTS OF CORONA TREATED TEFLON-FEP ELECTRETS

C.J. Dias, J.N. Marat-Mendes and J.A. Giacometti*

Faculdade de Ciências e Tecnologia#
Universidade Nova de Lisboa
Torre, 2825 Monte da Caparica, Portugal

*IFQSC- Universidade de S. Paulo
C.P. 369, 13560 São Carlos - SP , Brazil

Abstract: Thermally stimulated currents of corona charged Teflon-Fep electrets show a single peak around 210°C for short polarization times. However when the polarization time or the corona current are increased, changes either in the maximum or, in the position of the peak occur. At the same time a new broad current band in the range between 100-180°C appears, while a liquid is formed over the electret surface. Measurements of the charge centroid show no detectable change in its location. The results are tentatively explained in terms of surface traps becoming shallower.

I - INTRODUCTION:

Thermally Stimulated Discharge currents (TSD) studies are a powerful tool and have been widely used for investigating the charge stability of polymer electrets [1-3]. In one of its versions, the so-called open circuit TSC, the charged surface of the sample is left free,i.e, it does not touch the upper electrode. This method is very much suitable for studies of the electret surface.

On the other hand corona discharge provides a good mean of treating polymer surfaces, changing its physical and chemical properties [3-7]. By treatment we mean the modification that occurs on the properties of the polymer surface, mainly due to the action of excited neutral species,produced under the corona discharge. It has been proposed that the corona treatment of polymer surfaces leads to bond breaking and creation of polar groups [4]. It has also been proposed for some polymers that the effect of the neutral molecules is associated with the injection of charge into the bulk of the polymer. Teflon-Fep is one of the most used polymers in the electret production, corona discharge is the common polarization industrial process. The study of its surface treatment is of practical interest [8].

---

and Centro de Física Molecular das Universidades de Lisboa (INIC).

CH2593-2/ 88/ 0000-0487$01.00 Copyright 1988 IEEE

II - EXPERIMENTAL DETAILS

The front surface of circular Teflon-Fep samples, (diameter 2.2cm, thickness d ≈ 12.7μm, assembled between two metallic rings) is non-metallized and left electrically floating. The rear surface is metallized with a vacuum deposited aluminium electrode (diameter 1.5cm and ≈ 500Å thickness).

The samples were polarized on the corona triode as it is shown in fig.1 a). In order to charge the sample negatively with a given voltage, a positive bias voltage was applied to the sample holder and a constant current to the negative corona tip [9]. Currents between -1 and - 100μA were used. The sample surface voltage was measured by the Kelvin's method [10]. Initial surface voltages were around - 430 Volts. When a sample is corona charged, in this mode of operation, both ions and excited molecules impinge the sample. This sample is called a "treated " sample, by the excited molecules. To avoid a sample to be treated during charging, air is blown laterally to the electret surface to prevent the excited molecules to reach the sample. This is called an "untreated"sample. A sample can also be treated either before or after charging it, in both cases a negative bias voltage is applied to the sample holder. In this way the field opposes the movement of negative ions towards the sample surface.

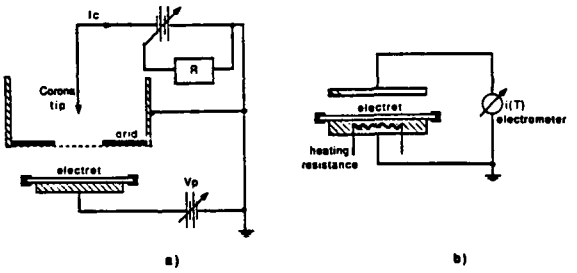

Fig. 1- Schematic setup of the corona triode (a), and the open circuit TSD equipment (b). R- Corona current regulator.

The TSD measurements were performed with the set up schematically illustrated in fig.1 b). The sample was heated up at a constant rate β = 3,5° C/minute, by a back side heater shielded to the ground. The decay of its surface potential was measured as a function of temperature, by measuring the variation of induced charge on a metallic plate placed 0,1 cm above the sample. The measurements of the centroid of the charge distribution were carried out using the heat pulse technique [11].

III - EXPERIMENTAL RESULTS AND DISCUSSION

TSD currents of Teflon-Fep untreated and treated samples are shown in fig.2. The untreated sample (charged with air blowing laterally and therefore with treatment time tc=0min) shows a current peak with a maximum at 207°C, while the treated sample (tc = 3 min) shows a narrow peak pointing at 212°C and a broad band on its low temperature tail.

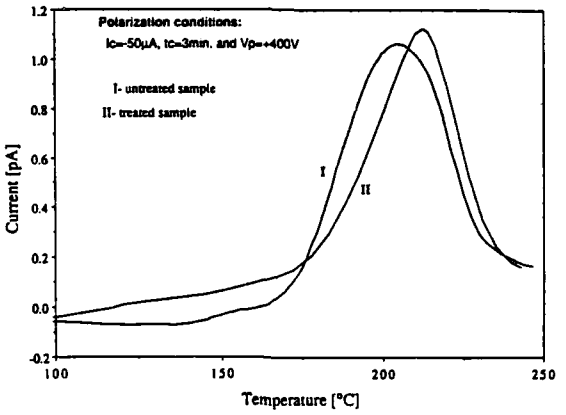

Fig. 2 - Open-circuit TSD measurements for corona charged samples showing the effect of corona treatment.

The effect of corona treatment is expected to depend on the corona current Ic and on the treatment time tc. In order to study these effects we performed two sets of experiments, the results of the last one are shown in fig.3.

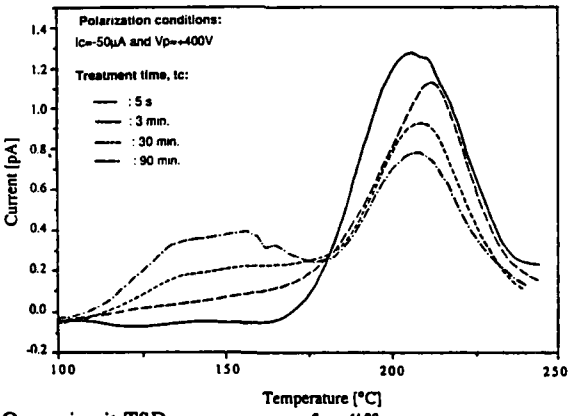

Fig. 3 - Open circuit TSD measurements for different corona treatment times tc.

Both results however have shown that the maximum of the high temperature peak firstly shifts from 207° C to 212° C and then moves back, decreasing in height as the treatment time increases. At the same time a broad band develops on the low temperature tail, the effect being clearly evident for long exposures time. Simultaneously small liquid droplets appear on the sample surface. For even longer exposures, a liquid covers most of the polymer surface.

Measurements of the charge centroid after treatment, show that it is always located at the sample surface, therefore the excited molecules do not induce charge injection in Teflon Fep an explanation that has been proposed for other polymers [11]. The TSD currents spectra show however, a decrease in the charge stability of the electret induced by the treatment, since the development of the TSD band in the low temperature range means an earlier potential surface decay. The presence of the liquid must be related to this decay.

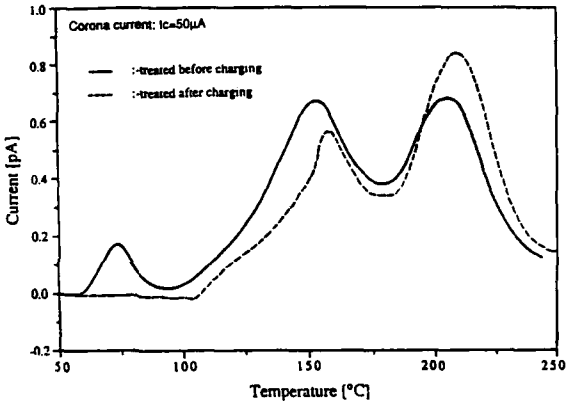

Fig. 4 - The effect of the liquid on the thermal charge stability. ___ : sample charged for 30min before charging; --- : sample treated and charged simultaneously for 30 min.

In order to investigate the role of the liquid in the process, we carried on experiments, treating the samples previously, without allowing the ions to reach the sample (Ic = -50μ A, tc = 30 min and $V_p = 0$); before charging it (Ic = -50μA, tc = 1 min., V_p = + 400V). In fig.4 we compare this result with one of a sample treated after charging it. Apart from the small low temperature peak at 75° C, no major qualitative differences seem to occur. This result confirms that it is the liquid, and not the excited molecules the responsible for the changes in the thermogram of a treated sample.

We also carried on experiments to investigate whether the treatment produces other degradation or permanent damage of the sample. The liquid was removed from the treated sample by dissolution, simply by emerging it in ethyl alcohol. Then the same sample was corona charged

without treatment. A thermogram was then carried on, and the result is shown in fig.5. The figure also presents a thermogram of a treated sample (treated before charging) where it can be seen that the electrical properties of the surface were not qualitatively modified by the previous corona exposure treatment. The differences from fig.2, namely the fact the 207°C has not been totally recovered, may rather be explained by a remnant contamination or by some alteration attributable to the alcohol molecules.

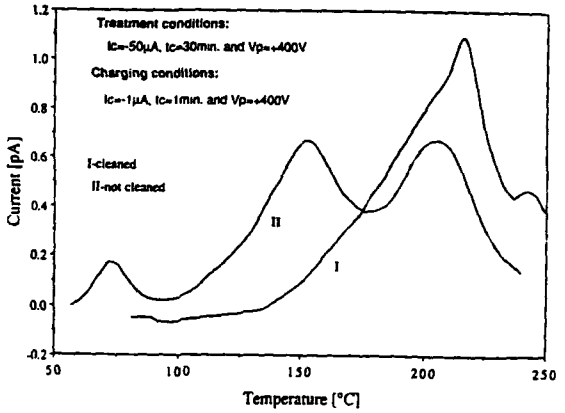

Fig. 5 - The removal of the liquid. I- sample treated then cleaned before charging; II- sample treated then charged.

IV - CONCLUSIONS

It was shown that Teflon Fep negatively corona charged electrets present a single TSD current peak around 207°C. This peak is related to charges located in traps at the sample surface. The trapping of these charges is the result of the interaction of the corona negative ions with the polymer surface. However, if before, during or after corona charging, other types of corona produced species, besides negative ions, i.e. excited molecules of the corona wind, collide against the polymer surface, a new broad current band appears in the low temperature side of the TSD spectrum. At the same time some changes occur also on the shape of the 207° C peak. We interpret these changes on the basis that there are more than one kind of traps, i.e. surface and near surface traps [12], giving current peaks very close to each other.

As the centroid measurements show that it remains at the sample surface during the corona treatment we can conclude that the excited molecules do not induce charge injection into the bulk. However they may provide the energy to activate the chemical reactions leading to the liquid formation. The charge centroid moves to the sample bulk only after heating the sample.

We interpret the thermogram changes of the treated sample on the basis of surface traps becoming shallower in the presence of the liquid. This would explain the formation of the low temperature broad band associated to the decrease of the electret charge stability. It also agrees with the results of the increase of the surface charge injection when the sample is heated. Therefore in order to get Teflon Fep electrets the formation of the liquid has to be avoided.

V - ACKNOWLEDGMENTS

The authors are grateful to G.L. Ferreira for stimulating discussions and to the Conselho Nacional de Desenvolvimento Científico (CNPq-Brazil), Junta Nacional de Investigação Científica e Tecnológica (JNICT-Portugal), Ministério da Indústria (MI-Portugal) and Instituto Nacional de Investigação Científica (INIC-Portugal) for the financial support.

VI-REFERENCES

[1] - J. van Turnhout: in "Electrets", ed. by G.M. Sessler, Springer Verlag, Berlin 1980.

[2] - H.Von Seggern: J. Appl. Phys. 50, 2817 (1979).

[3] - J.A. Giacometti, J.A. Malmonge and J.N. Guimarães Neto: IEEE Trans. Elect.Insul. EI-21, 283 (1985).

[4] - A. Goldman and Amoroux: in "Electrical Breakdown and Discharge in Gases" Part B; ed. E.E. Kunhardt and L.H.Luessen, Plenum Press, 1983 (pp. 293-346).

[5] - N. Takahashi, J. Rault, A. Goldman and M. Goldman. Proceedings of the 2nd International Conference on Conduction in Solid Dielectrics, Erlangen, W.Germany, July 1986.

[6] - E.A. Baum, T.J. Lewis and R. Toomer, J. Phys. D: Appl. Phys. 11, 963 (1978).

[7] - K.J. Kao, S.S. Bamji and M.M. Perlman, J. Appl. Phys. 50, 8181 (1979).

[8] - C.J. Dias, J.A. Giacometti and J.N. Marat-Mendes: Ferroelectrics 76, 469 (1979).

[9] - R.A. Moreno and B. Gross: J. Appl. Phys. 47, 3397 (1976)

[10] - J.A. Giacometti: J. Phys. D: Appl. Phys. 20, 675 (1987).

[11] - R.E. Collins: Rev. Sci.Instrum.48, 83 (1977).

[12] - H.V. Seggern: J. Appl. Phys. 50, 2817 (1979).

ISOTHERMAL CHARGE DECAY OF TEFLON-FEP ELECTRETS UNDER A CORONA DISCHARGE

C.J. Dias, J.N. Marat-Mendes and J.A. Giacometti*

Faculdade de Ciências e Tecnologia #
Universidade Nova de Lisboa
Torre, 2825 Monte da Caparica, Portugal

*IFQSC- Universidade de S. Paulo
C.P. 369, 13560 São Carlos - S.P., Brazil

Abstract: Corona polarized Teflon-Fep electrets, set on earthed or with a negative bias voltage at the sample holder of a corona triode, show a decrease on the surface potential. Heat pulse measurements taken while treating the sample, gives information that the charge centroid remains always on the sample surface, giving evidence that there is no charge injection into the bulk, as has been suggested for others polymers. No losses of charge by surface conductivity was observed also. The results are tentatively explained by charge compensation with positive ions arriving at the sample surface.

I- INTRODUCTION

Corona discharge in air in a configuration called corona triode is a mean of depositing charge over an insulating surface [1], leading for instance to the formation of electrets. In this configuration there is a corona point, a sample holder and a grid controlling the surface potential of the electret.

Others corona effects beyond the charging, were studied in polymers. They were related to by-products of corona, such as neutral excited species, produced by ion-molecule collisions, during the motion of ions in the corona gap field. The excited molecules were assumed to release charge from surface shallow traps, in negatively charged poliethylene, followed by a charge injection into the bulk under the charge's own field [2,3]. This process leads to a surface potential decay, as the charge centroid penetrates into the polymer.

Recently, it was observed that in Teflon-Fep these molecules lead to a liquid formation over the sample surface, changing the stability of surface traps [4,5] . However, no charge injection was observed. The change in surface traps was apparent in an open-circuit TSC experiment, in the form of a broad current band appearing in the 100-180°C range.

A mechanism of lateral charge spreading leading to a surface

and Centro de Física Molecular das Universidades de Lisboa (INIC).

CH2593-2/ 88/ 0000-0493$01.00 Copyright 1988 IEEE

potential decay, was also reported in Mylar [6].

Here we report, the surface potential decay in negatively charged Teflon-Fep when exposed to a negative corona discharge source, in a corona triode configuration. The above mechanisms does not explain all the experimental results. Our interpretation calls for an electronic component of the corona current that under suitable conditions would lead to positive ions formation. The ions would compensate the negative charge on the electret, thus reducing its surface potential.

II - EXPERIMENTAL

A - Samples

Samples were circular foils of Teflon-Fep [7] , 12.7μm thick. They were metallized on one surface, with a vacuum-deposited aluminium electrode approximately 500Å thick and a diameter of 1.5cm. The other surface remained non-metallized in order to receive ions from the negative corona discharge. The sample was slightly stretched between two concentric metallic rings 2.2 cm in diameter to remain flat during the experimental procedures.

B - Corona triode

The corona triode setup used in all experiments is schematically shown in fig.1. Its constituents are: a metallic point (a sewing needle), a metallic grid, a brass sample-holder and a metallic shutter between the sample holder and the grid. The grid had a 750μm spaced mesh, with brass wires 160μm in diameter. The distances between point-to-grid (corona gap) and grid-to-sample (air gap) were 0.6cm and 0.5cm respectively.

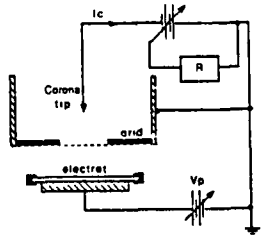

Fig. 1 - Electret in a corona configuration. R- corona current regulator

This triode is operated in the following way: an adjustable negative point-to-grid voltage V_c is applied in order to get a constant corona current (I_c). This negative current is independent of what is happening in the air gap between the grid and the sample, and is in the range 1-100μA. This negative current will be the sum of the grid current (I_g), and the sample-holder current (I_p). The sample-holder current I_p, normally a small fraction of the grid current is the electret polarization

current It strongly depends on the field in the air gap and is weakly dependent on the electrical transparency of the grid and on the corona wind [8]. As a first approximation, we can say that the polarization current stops when the surface of the electret is at the grid potential. So when we apply a positive voltage at the sample holder a current (i.e negative ions/electrons) will flow in the air gap, depositing negative charge on the surface of the polymer.

The surface potential thus decreases and eventually reaches zero in a few seconds therefore we end up with a foil whose non-metallized surface has -400V relative to the back electrode.

For longer exposure times to corona discharge, other discharge products such as neutral excited molecules will go on striking the surface of the Teflon. These excited molecules produced in the corona gap by ion-neutral molecule collisions are corona current dependent. The total number of excited molecules is thus both proportional to the exposure time and to the corona current. They are carried to the sample by the corona wind and in some experiments they were diverted by blowing air tangentially to the sample.

In the following we will refer to a corona experiment by its corona current I_c, the voltage applied to the sample holder V_p, and the exposure time t_c.

C - Surface Potential and Centroid Measurements

The mean surface potential of the sample was measured by mechanically vibrating the sample and using the Kelvin's method [9]. A scanning capacitive probe was also used to draw the surface potential profile of the sample [10]. The probe resolution is of the order of $0.1 cm^2$.

The charge centroid was measured using the Collins' heat pulse method in open circuit, in order not to spoil the electret.

III - RESULTS AND DISCUSSION

In fig.2 the surface potential profiles of a sample after polarization ($I_c = -1\mu A$ $t_c = 1min$ $V_p = +400V$), is shown, compared with that of the same sample, which afterwards was exposed for 30min to the corona discharge with -1000V applied to the sample holder ($I_c = -50\mu A$ $t_c = 30min.$ $V_p = -1000V$). With this reversed bias voltage the potential difference between the polymer surface and the grid is -1400V at the beginning of the exposure time, thus preventing the depositing of any negative charges on the sample surface. We can see that the surface potential has decreased (becoming positive) in the center. There is also no sign of lateral spreading of charge.

The surface potential decay can then be attributed either to: (a) an injection of charge into the bulk; (b) negative charges released from surface traps by the action of the excited molecules, leaving the surface

and moving upwards towards the grid or finally, (c) to positive ions coming from the grid, compensating the negative charge of the electret. In the first case the process would be independent of the air gap field, since the excited molecules are carried by the corona wind and charge injection does not depend either on it.

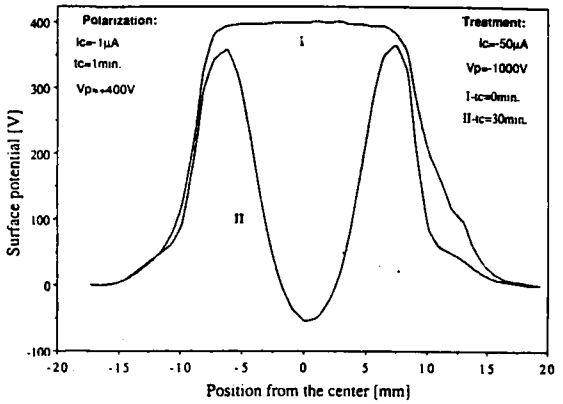

Fig. 2 - Surface potential profiles of a sample after polarization and after 30min of exposure time.

Another set of the experiments consisted in plotting the surface potential of the sample center versus time for various reversed bias voltages, fig.3. It is shown that the decay is proportional to the air gap field, which kept always the same sign in the course of the experiments.

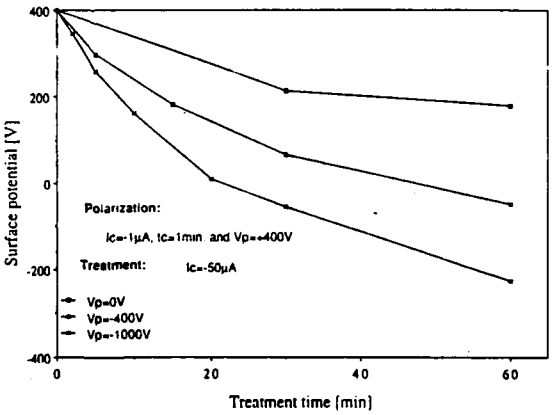

Fig. 3 - Surface potential decay in the center of the sample for various reversed bias voltages.

The charge centroid was also measured and no penetration into the bulk was observed.

A polarized sample was then exposed to the corona discharge while air was blown tangentially to the sample surface, thus removing all the excited molecules away, fig.4. No significant change in the surface potential decay is observed when compared with one obtained in similar conditions but without blowing air.

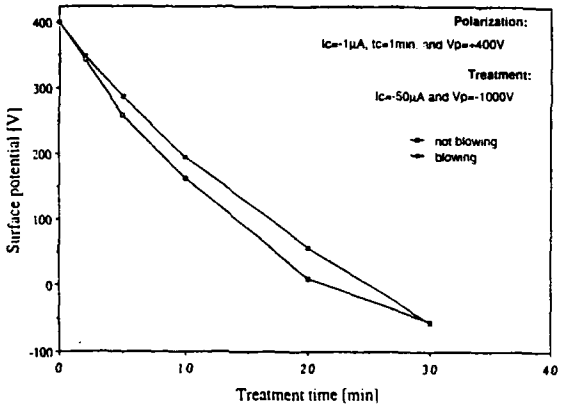

Fig. 4 - Surface potential decay showing the effect of blowing air tangentially to the sample.

A possible explanation calls for an electronic component of the corona current for short point-to-grid distances. These electrons are hot electrons, and their energies at high fields may be as high as a few eV [12]. Those electrons passing through the grid and returning to it, due to the reversed field between the grid and the electret surface may create pairs when losing their energies. The positive ions created would be driven to the sample surface by the electric field. Those positive ions by compensation of charge would then lead to the observed surface potential decay. The faster decay in the center, can be explained in terms of an higher density of electrons in this region.

IV - ACKNOWLEDGMENTS

The authors are grateful to G.L. Ferreira for stimulating discussions, to P.G. Sustelo for his help in this work and to the Conselho Nacional de Desenvolvimento Científico (CNPq-Brazil), Junta Nacional de Investigação Científica e Tecnológica (JNICT-Portugal), Ministério da Indústria (MI-Portugal) and Instituto Nacional de Investigação Científica (INIC-Portugal) for the financial support.

V - REFERENCES

[1] R.A. Moreno and B. Gross: J. Appl. Phys. 47 (8), 3397 (1976).

[2] E.A. Baum, T.J. Lewis and R. Toomer: J. Phys. D: Appl. Phys. 10, 487 (1977).
[3] K.J. Kao, S.S. Bamji and M.M. Perlman J. Appl. Phys. 50 (12), 8181 (1979).
[4] C.J. Dias, J.A. Giacometti and J.N. Marat-Mendes: Ferroelectrics 76, 469 (1987).
[5] C.J. Dias, J.A. Giacometti and J.N. Marat-Mendes: J. Phys. D: Appl. Phys. (to be published).
[6] E.A. Baum, T.J. Lewis and R. Toomer: J.Phys. D: Appl. Phys. 11, 963 (1978).
[7] Teflon-Fep is a trade mark of Dupont & Nemours and the samples were supplied by Societé de Plastiques Nobles (SPN), France.
[8] O.N. Oliveira, Jr and G. Leal Ferreira: Rev. Sci. Instrum. 56 (10), 1957 (1985).
[9] J.A. Giacometti: J. Phys. D: Appl. Phys. 20, 675 (1987).
[10] R. Gerhard-Multhaupt and W. Petry: J. Phys. E: Sci. Instrum. 16, 418 (1983).
[11] R.E. Collins: J. Appl. Phys. 51 (6), 2973 (1980).
[12] A. von Engel: in "Ionized Gases", Oxford University Press, 1965 (pp. 122).

DOSIMETRY AT INTERFACES : MEASUREMENTS BY POLYPROPYLENE ELECTRETS AT AND NEAR PLANE INTERFACES BETWEEN DIFFERENT MATERIALS (C, Al, Cu, Sn, Pb) IRRADIATED WITH COBALT 60 GAMMA RAYS

Paule-Noëlle MARTIN
Laboratoire des Radiations Ionisantes - Faculté des Sciences-
123, avenue Albert Thomas - 87060 LIMOGES CEDEX - FRANCE

ABSTRACT

The electret surface charge density σ deposited by corona effect is function of the gamma photon exposition. The relative variations of $\sigma = q/q_0$ are function of the ionization created in the air cavity which contains the electret, (if the initial and final charges of the electret are q_0 and q).

A multilaminary system made with two materials , (metal Z and carbon C) allowed us to measure the relative ionization to the carbon at all points. The same evolution was obtained with a traditional ionization chamber used under the same experimental conditions.

INTRODUCTION

A preliminary study enable us to show the interesting behaviour of the polypropylene electret as a dosimeter [Be 80]. [Ma 85],which is charged by corona method and placed in a cavity inside the medium studied. It is the variation of the charge of the electret $\phi = (q_0-q)/q_0$ which is an image of the ionization created in the cavity or of the received dose [Ma 85] [Ma 87].

CH2593-2/ 88/ 0000-0499$01.00 Copyright IEEE

EXPERIMENTAL SET UP

With the help of apparatus developed in our laboratory, we are going to follow the evolution of the surface charge on polarised samples subject to the radiation. The polypropylene electrets are produced by corona discharge in the air surrounding them . For the electret charge measurements, a coaxial insulated metal chamber, connected to a Keithley electrometer model 616 is used in the total influence conditions [Ma 85].

IRRADIATION TECHNIQUE

Ionization measurement at the interface and in the medium

In order to analyse the environment conditions during irradiations of electrets, the chamber was built in order to permit different application conditions (fig. 1). Figure 2 shows four of these configurations.

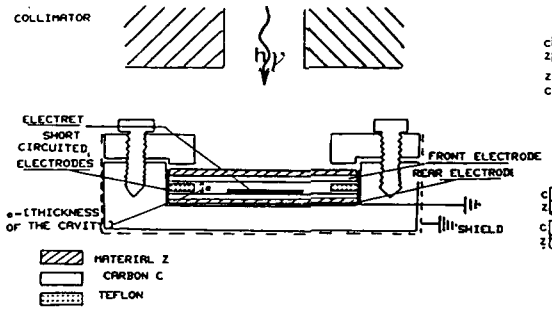

FIG -1- ELECTRET CHAMBER

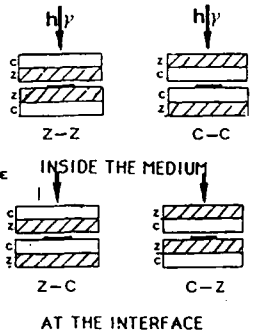

FIG -2-IRRADIATION CONDITION

Typical curves are shown in figure 3 for the copper and 4 for the lead.

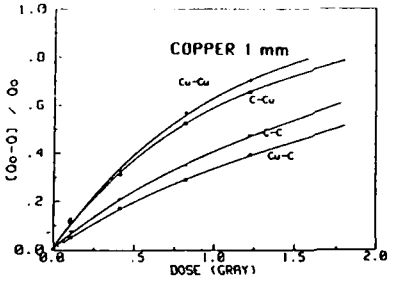

FIG -3-VARIATION OF THE ELECTRET RECEIVED CHARGE Φ (COPPER)

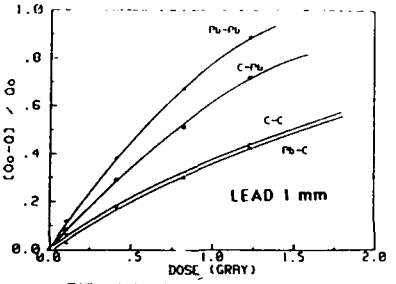

FIG -4-VARIATION OF THE ELECTRET RECEIVED CHARGE Φ (LEAD)

Ionization measurement near the interface

A multilaminary system (fig. 5 (a)) enabled us to measure the ionization near the plane interface. The electret which has a thickness of 25 µm is placed in a cavity 0,2 mm high. The advantage of the small thickness of Bolloré polypropylene exhibits a minimum of photonic and electronic perturbations.

The correction of the air cavity introduction is shown on figure 5 (b) .

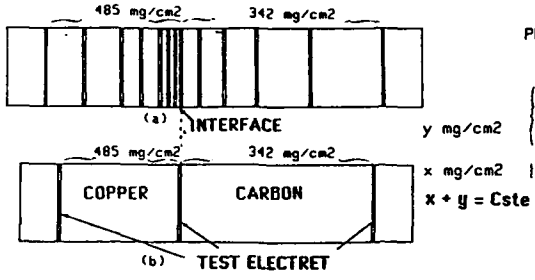

FIG -5-MULTILAMINARY ELECTRET SYSTEM

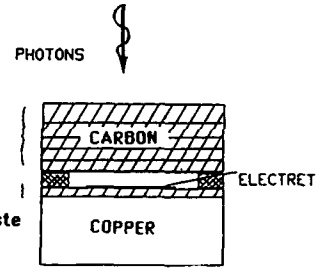

FIG -6-LAYOUT OF THE ELECTRET CHAMBER MAKING IT POSSIBLE TO MEASURE IONIZATION IN THE TRANSITION ZONE

The air cavity introduction ,above the electret prevents the discharge when there is not a good contact, by alcontrary,if it is introduced in the irradiated medium it produces a perturbation. KAPPAS has explained this phenomena [Ka 86].

To get round this fact we did a measurement using three test electrets, one at the interface, the other two inside the media and we have reported the values found with the multielectret system of case (a) to those of case (b).

To check our results we have measured ionization in the region of non electronic equilibrium with the set up, indicated on figure 6 ,which makes it possible to deplace the cavity inside the media.

EXPERIMENTAL RESULTS AND DISCUSSION

Exemples of ionization curves obtained,with the electrets multilaminary system ,for the interfaces Cu-C, Pb-C are showed figures 7-8.

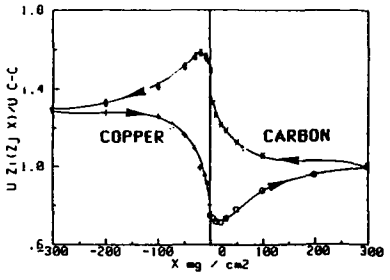

FIG -7-IONIZATION MEASURED VALUES
(COPPER-CARBON INTERFACE)

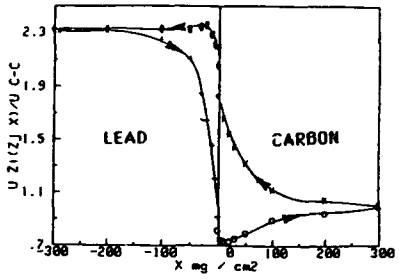

FIG -8-IONIZATION MEASURED VALUES
(LEAD-CARBON INTERFACE)

From observations of ionization in an air cavity, with a traditional ionization chamber polarized with a constant field; DUTREIX and BERNARD [Du 66], MARTIN [Ma 68], WALL and BURKE [Wa 70] have reported the ionization distribution in the vicinity of an interface between two media irradiated by a ^{60}Co gamma ray source (interface Al-C, Cu-C, Sn-C, Pb-C, for the first and Al-Mg, Cu-Al and Mo-Al for the last one).

With the multielectret system chamber we found the same evolutions.

1- Direction carbon C - material Z (C < Z) (here Z= Al,Cu, Sn, Pb)

- the ionization in a high Z material behind one of lower Z (here the carbon C),is enhanced,rather than reduced,and reaches a maximum after the interface at a small distance from the boundary.

- the ionization,on both sides of the interface,is enhaced when the gamma ray beam penetrates the law Z material first.

2 - Direction material Z - carbon C (Z > C)

-the ionization in a low material Z (here carbon) behind one of greater Z is reduced relative to the equilibrium ionization,and a minimum at a small distance from the boundary occurs between 20 to 50 mg/cm^2 from the interface.

These particularities are confined to the transition regions of electronic non equilibrium which exist on either side of the interface,and whose thickness is of the order of the range of the maximum energy secondary electron producted.

It occurs because both the spectrum of secondary electrons arising in the media,and their rate of energy loss,are different for the two media from their differing absorption and scattering properties.

Monte-Carlo technique shows the same particular finite discontinuities near the interface [We 79], [De 72].

CONCLUSION

The results show that significant variations in dose distributions occur at high photon energy where the mass energy absorption coefficients differ relatively little from one material to another.

The enhancement or reduction in ionization becomes very sensitive to the direction of the incident photon beam.

The energy deposited in a material is enhanced when it is next to one of lower atomic number provided the gamma beam penetrates the lower atomic number material first.

A reversal in beam direction reduces the ionization to a level below which it could be for either material alone.

BIBLIOGRAPHY

[Be 80] - BERNARD M., MARTIN P.N. - Radiophysique - XIXème Congrès de la Société des Physiciens d'Hôpitaux - Reims 1980, p. 164-171.

[De 72] - DELLIN Th. A., MAC GALLUM G.J., SCLRR 720086 Sandia Laboratories

[Du 66] - DUTREIX J., BERNARD M., Brit. Journ. of Radiol., 39, p. 205-210, (1966).

[Ka 86] - KAPPAS C., thèse Docteur ès Sciences, Fac. Sciences Toulouse (France).

[Ma 68] - MARTIN P.N., DES Sciences Physiques, Fac. Sciences Limoges (1968).

[Ma 85] - MARTIN P.N., BERNARD M., Proc. 5th Int. Symposium Electrets, Heildelberg 1985, p. 696-707.

[Ma 87] - MARTIN P.N., thèse Docteur ès Sciences. n° 38-87, Limoges (France).

CALCULATIONS OF THE IONIZATION DISTRIBUTION AT, AND NEAR, THE INTERFACES BETWEEN TWO MEDIA USING P.N. JUNCTION AND ELECTRETS DETECTORS

Paule-Noëlle MARTIN
Laboratoire des Radiations Ionisantes-Faculté des Sciences-
123,avenue Albert Thomas-87060 LIMOGES CEDEX - FRANCE

A knowledge of the energy distribution,of the secondary electrons travelling past a point in the medium under irradiation of γ rays is necessary for a complete understanding of the physical and biological processes which occur during irradiation.

A quantitative theory of the effect of electron multiple scattering upon the ionization at and near a plane interface, between different media is made using the DUTREIX-BERNARD theory [Be 64]. To perform their theory :

-We have used P.N. junction and electret measurements. P.N. junction allows us to measure the relative variations of F (Forward) and B (backward) emissions in the transition region, they are functions of the interface distance and the adjacent environment.

-We have measured, with electrets, the relative ionization at several points during a same irradiation, which enables us to calculate the forward, backward and the backscatter coefficient b in any point. Consequently we can calculate the ionization in any point and prove that it depends on both environment and distance.

INTRODUCTION

Ionization profiles in two adjacent materials of different atomic number were measured with an multielectret chamber. The results show that significant variations in these ionization distributions occur at high photon energies and the perturbation is not a sample function of atomic number alone.

The enhancement or reduction in ionization is very sensitive to the direction of the incident photon beam.

CH2593-2/ 88/ 0000-0504$01.00 Copyright 1988 IEEE

At each location within the transition regions there exist electrons which have crossed the interface and whose energies are a function of the scattering properties of both media.

PRELIMINARY THEORY [Be 64]

Let us consider a point in a material Z_i thick enough to give electronic equilibrium. F_{Zi} (forward) is the ionization component from the electron generated in front of it which traverses it for the first time and B_{Zi} (backward) is the corresponding from electrons generated behind it.

-The total ionization U_{ZiZi} in the material Z_i is ; $$U_{ZiZi} = \frac{F_{Zi} + B_{Zi}}{I - B_{Zi}}$$

where b_Z is the backscatter coefficient of the medium Z.

-In the case of an interface Z_i - C the ionization depends of the direction of the incident photon beam, we get a system of four relations which represents ionizations at the interfaces between two media Z_i and Z_j ($Z_i \neq Z_j$) or identical ($Z_i \equiv Z_j$) (ionization inside the medium):

$$\frac{U_{Z-Z}}{U_{C-C}} = \frac{F_Z + B_Z}{I - b_Z} \qquad \frac{U_{C-C}}{U_{C-C}} = \frac{F_C + B_C}{I - b_C} \qquad (I)$$

$$\frac{U_{Zi-Zj}}{U_{C-C}} = \frac{F_{Zi}(I + b_{Zj}) + B_{Zj}(I + b_{Zi})}{I - b_{Zi} \cdot b_{Zj}} \qquad \frac{U_{Zj-Zi}}{U_{C-C}} = \frac{F_{Zj}(I + B_{Zi}) + B_{Zi}(I + b_{Zj})}{I - B_{Zi}\, b_{Zj}}$$

Development elaboration of this theory was undertaken from experiments with electret chambers and P.N. junction.

Theoretical and experimental study of the coefficients F, B and b inside the media and at the interface

The experimental study of various ionization inside medium, at the interfaces and in

the transition region,has been done using an electret chamber which is described in n° 1. For each medium,and for each interface,we have study the adjacent materials Al-C, Cu-C, Sn-C, Pb-C and U-C and measured the different ionizations, we added the study of Cu-Al and Sn-Cu. So we have solved the system of 18 equations and 18 parameters from (I).

The solutions are represented on table I and in table II. We compare the experimental values measured and the theorical values.

Z	U_{Z-Z}/U_{C-C}	U_{Z-C}/U_{C-C}	U_{C-Z}/U_{C-C}	F_Z	B_Z	b_Z
C	1	1	1	0,76	0,023	0,219
Al	1,07	0,90	1,19	0,640	0,096	0,291
Cu	1,293	0,78	1,46	0,562	0,253	0,370
Sn	1,58	0,70	1,74	0,502	0,375	0,445
Pb	2,32	0,86	1,954	0,587	0,438	0,558
U	2,72	0,93	2,05	0,641	0,501	0,557

TABLE - I- RELATIVES VALUES TO THE CARBON OF F_{Zi}, B_{Zi}, b_{Zi}

Z	Z'	C	Al	Cu	Sn	Pb	U
C	m	1	1,19	1,465	1,74	1,96	2,05
	c	1,002	1,19	1,468	1,72	1,96	2,04
Al	m	0,88	1,07	1,38	1,65	1,92	
	c	0,87	1,07	1,389	1,68	1,96	2,06
Cu	m	0,78	0,94	1,29	1,62	1,87	
	c	0,78	0,968	1,293	1,59	1,86	1,96
Sn	m	0,70	0,87	1,20	1,58	1,90	
	c	0,71	0,908	1,26	1,58	1,88	1,96
Pb	m	0,86	1,10	1,52	1,87	1,90	
	c	0,856	1,10	1,51	1,90	1,88	2,00
U	m	0,93					
	c	0,93	1,19	1,60	2,007	2,43	2,580

TABLE - II- RELATIVES IONIZATIONS TO THE CARBON AT THE INTERFACES Z-Z' AND IN THE MEDIA (C,Al,Cu,Sn,Pb and U)

The different variations of ionization obtained in function of the atomic number are showed on figure1.

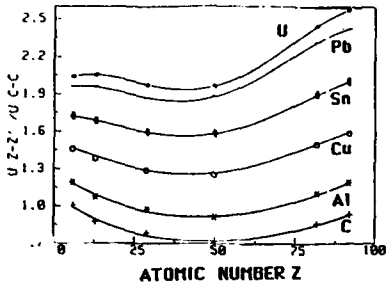

FIG -1-COMPARED VALUES OF IONIZATIONS AT ANY INTERFACES - DIRECTION Z-Z'

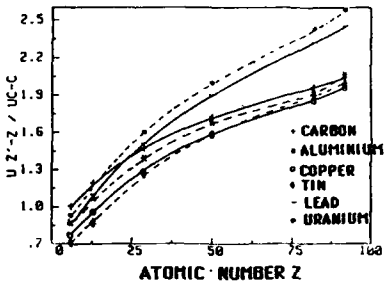

FIG -2-COMPARED VALUES OF IONIZATIONS AT ANY INTERFACES - DIRECTION Z'-Z

Experimental and theoretical study of the coefficient $F_{Zi}(Z_j, x)$, $B_{Zi}(Z_j, x)$, $b_{Zi}(Z_j, x)$ near the interface.

1 - The elementary components of electronic flux which are initially directed towards the half space caracterised by the coefficients b. We call them by b_{Zi} in the zone of electronic equilibrium and by $b_{Zi}(Z_j, x)$ near the interface. The term $b_{Zi}(Z_j, x)$ means that it is the coefficient in Z_i depending of the second medium Z_j and on the distance x from the interface. The total ionization in the medium Z_i is represented by two relations related with the direction of the photon beam through the interface.

$$\text{I} \quad U_{Zi}(Z_j,x) = \frac{F_{Zi}\{1 + b_{Zi}(Z_j,x)\} + B_{Zi}(Z_j,x)\{1 + b_{Zi}\}}{1 - b_{Zi} \cdot b_{Zi}(Z_j,x)} \qquad \text{II} \quad U'_{Zi}(Z_j,x) = \frac{F_{Zi}(Z_j,x)[1 + b_{Zi}] + B_{Zi}[1 + b_{Zi}(Z_j,x)]}{1 - b_{Zi} \cdot b_{Zi}(Z_j,x)}$$

We have measured each parameter F and B using a P.N. junction which have a small depletion layer (figure 3,4).

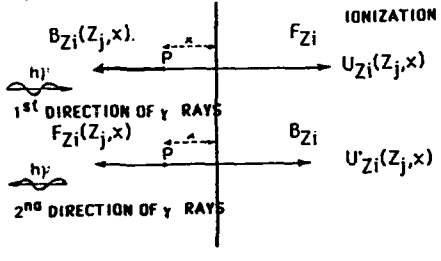

FIG -3-TOTAL IONIZATION RELATED WITH THE DIRECTION OF PHOTON BEAM

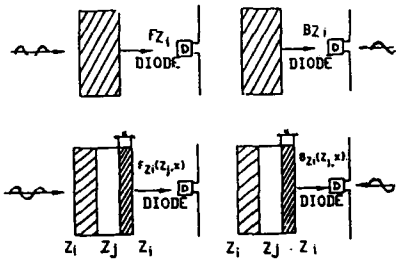

FIG -4-MEASURE OF THE FORWARD F AND THE BACKWARD B WITH P.N.JUNCTION

EXPERIMENTAL RESULTS

From the P.N. junction experiments, we deduced the variations of ΔF and ΔB in function of the massique thickness x from the interface, and we can calculate $F_{Zi(Zj, x)}$ and $B_{Zi(Zj, x)}$ in any point [Ma 87].

The measurement of $U_{Zi\,(Zj, x)}$ et $U'_{Zi(Zj, x)}$ obtained with the electret chambers permits us to calculate the different values of $b_{(Zj, x)}$ [Ma 87]

the general expression II and III then become.

$$U_{Zi}(Z_j,x) = \frac{F_{Zi}\left[1 + b_{Zi} + (b_{Zj}-b_{Zi})\,e^{-kx}\right] + \left[B_{Zi} + (B_{Zj}-B_{Zi})e^{k(Zj,x)}\right](1 + b_{Zi})}{1 - b_{Zi}\left[b_{Zi} + (b_{Zj} - b_{Zi})\,e^{kx}\right]}$$

$$U'_{Zi}(Z_j,x) = \frac{\left[F_{Zi} + (F_{Zj}-F_{Zi})e^{-k(Z_j,x)}\right](1+b_{Zi}) + B_{Zi}\left[1+b_{Zi} + (b_{Zj}-b_{Zi})e^{-kx}\right]}{1-b_{Zi}\left[b_{Zi}+(b_{Zj}-b_{Zi})e^{-kx}\right]}$$

ou

$$\text{Log } K(Z) = 0{,}0085 + 0{,}0147\,Z$$

$$k = 0{,}0289\ cm^2 \cdot mg^{-1}$$

We represent in figure 5 the calculated values in the case of the pair Cu-C and in fioure 6 for the case Pb-C.

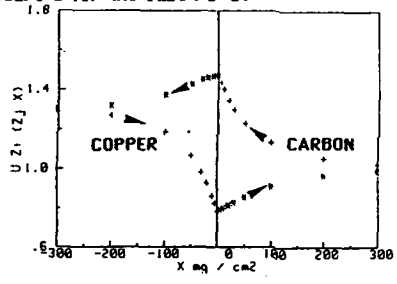

FIG -5-IONIZATION CALCULATED VALUES (COPPER-CARBON INTERFACE)

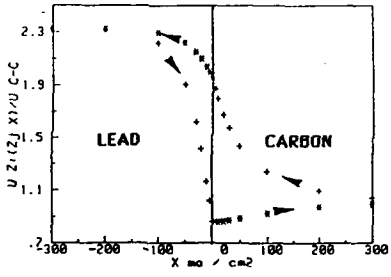

FIG -6-IONIZATION CALCULATED VALUES (LEAD-CARBON INTERFACE)

CONCLUSION

Using multilaminary electrets system we have been able to measure the ionization near the interface, we have used a P.N. junction to measure the variation of the Forward and the Backward. The depletion layer of this junction which replace the cavity of an ionization chamber. We have modelized the mechanism of the ionization near the interfaces.

BIBLIOGRAPHY

[Be 64] - BERNARD M., thèse Docteur ès Sciences, série A n° 51 90, Paris 1964.

[Ma 87] - MARTIN P.N., thèse Docteur ès Sciences, Limoges 1987.

ACKNOWLEDGEMENTS :The author gratefully acknowledge thesupport in the electret research by BOLLORE TECHNOLOGIE - 29195 QUIMPER CEDEX FRANCE.

KINETICS OF RADIATION-INDUCED DIELECTRIC EFFECT IN POLYMERS

V.I. Arkhipov, V.R. Nikitenko and A.I. Rudenko

Moscow Engineering Physics Institute, Moscow, USSR.

ABSTRACT

There exist numerous applications of insulators, for which their dielectric properties are of special importance. In particular, polarization of dielectrics plays a dominating role in the process of electret formation. We should note, that irradiation is one of the most effective methods of electret production. Thus, one needs to know how irradiation changes the dielectric constant of insulators.

In the present paper we suggest a model of non-equilibrium radiation-induced dielectric effect in disordered insulators. The model is based on the concept of geminate recombination of carriers under the condition of dispersive (non-equilibrium) transport regime. This effect results in the appearance of additional time- dependent polarization of irradiated insulator. The model predicts that radiation-induced polarization of insulators may increase after pulse electric field is switched off. Further polarization decays, and depolarization current decreases as a power function of time: $j \alpha t^{-\alpha-1}$, where α is the dispersive parameter. $\alpha = kT/E_o$ (T is the temperature, E_o is a characteristic depth of localized state energy distribution, which controls the carrier transport).

ELECTRET STATE OF BUTADIENE-STYRENE COPOLYMERS

R.Capelletti and J.Pospisil*

Physics Department - University of Parma and G.N.S.M. - C.I.S.M.
Viale delle Scienze - 43100 - Parma - ITALY

*Department of Polymer Physics - Mathematics and Physics Faculty
Charles University - 18000 Praha - CZECHOSLOVAKIA

ABSTRACT

Thermally stimulated depolarization currents (TSDC) in the range 120-350 K are exploited to study either triblock and statistical styrene-butadiene copolymers. TSDC peaks occur at the butadiene phase glass transition, due to the reorientation of butadiene dipolar groups. The peak is accounted for by a distribution of relaxation times. In block copolymers TSDC signal is monitored at the butadiene phase transition temperature even if the sample is not previously polarized: ordering effects induced by the sample preparation are discussed.

1 - INTRODUCTION

The butadiene (B)- styrene (S) copolymer systems exhibit different structures due either to the statistical or to block distribution of butadiene and styrene, to the different molecular masses of the blocks, to the butadiene-styrene ratio, and to the different microstructure of butadiene (cis-, trans-, and vinyl contents).

The relaxation processes (mechanical and electrical) are deeply affected by the structural changes which such systems undergo when they are submitted to a thermal cycle up to temperatures close to the melting point. In the present paper we are mainly concerned with the dielectric relaxation mechanisms, monitored by means of TSDC technique, either in amorphous statistical B-S copolymers and in block copolymers (triblock copolymers, where S-B-S units are present in the structure).

The mechanical relaxation mechanisms of B-S copolymers have been already investigated by means of viscoelastic measurements [1]. The block copolymers exhibit two relaxation regions: the former at low temperature $T_{g,B}$ due to the glass transition of butadiene (or better of the butadiene phase) and the latter at higher temperature $T_{g,S}$ due to the glass transition of styrene, namely to the melting of styrene domains (crystallites), which build the network of such thermoplastic rubbers. In statistical B-S copolymers only one relaxation occurs at a temperature intermediate between $T_{g,B}$ and $T_{g,S}$ and increases by increasing the styrene contents. Since electric dipole moments are present on the styrene molecule and on the cis and vinyl form of 1,2 addition of butadi-

CH2503-2/88/0000-0510$01.00 Copyright 1988 IEEE

ene, one expects that reorientation of such dipoles can take place under electric field.

2 - EXPERIMENTAL DETAILS

The block copolymer samples used were triblock copolymers (S-B-S). Table I shows the relative content (in weight) of butadiene and styrene and the block dimensions of styrene (S) and of butadiene (B) as given by the average molecular weight $\overline{M}_n$. The microstructure of butadiene is, for samples 1 and 2 respectively, as follows: 30 and 32 % of 1,4 addition (cis); 19 and 19.9 % of 1,4 addition (trans) and 51 and 48.1 % of 1,2 addition (vinyl). The high content of vinyl 1,2 addition of butadiene in samples 1 and 2 is responsible for the shift of $T_{g,B}$ towards higher temperatures.

TABLE I

sample	styrene content [%]	butadiene content [%]	$\overline{M}_n$ of the S block	$\overline{M}_n$ of the B block
1	30	70	9000	48000
2	16	84	6300	76000

The statistical copolymer, with 40 wt % of bound styrene, is a commercial product (Krylene 1516), supplied by Polysar Corp..

The samples were pellets 1 mm thick prepared by applying a pressure of 200 N/cm^2 at 400 K to the copolymer.

The TSDC measurements have been performed according to the usual procedure [2]. As a rule the polarization temperature T_p was 300 K and the polarization time t_p was 3 min., even if different figures were used to put in evidence the existence of relaxation time distribution (see §3b and fig.3b). The polarization field ranged between 10^2 and 10^4 V/cm. The heating rate during the TSDC recording was 7K/min. "Blank" measurements were performed according to the usual procedure, but no electric field was applied to the sample.

3 - EXPERIMENTAL RESULTS

a - "Blank" measurements. Typical TSDC "blank" spectra are shown in fig.1a for block copolymer samples 1 and 2 (see Table I): only one main peak is present, whose maximum occurs at 217 and 224 K respectively. The temperatures at which the TSDC peaks occur are close to the $T_{g,B}$ (butadiene phase) of the two samples (218 and 224 K) as monitored by viscoelastic and calorimetric measurements.

The amplitude of the peak is function of the thermal history of the sample: if the sample is annealed for short time (3 min) at temperatures T_a's ranging between room temperature and temperatures close to the melting point, the TSDC signal in the subsequent "blank" increases, see fig. 1b. However if the sample is annealed for two hours at temperatures close to the melting point, the subsequent "blank" doesn't exhibit any longer TSDC signal. It should be stressed that the TSDC signals were found only in the "blank" measurements performed on block copolymers, but not on the statistical ones.

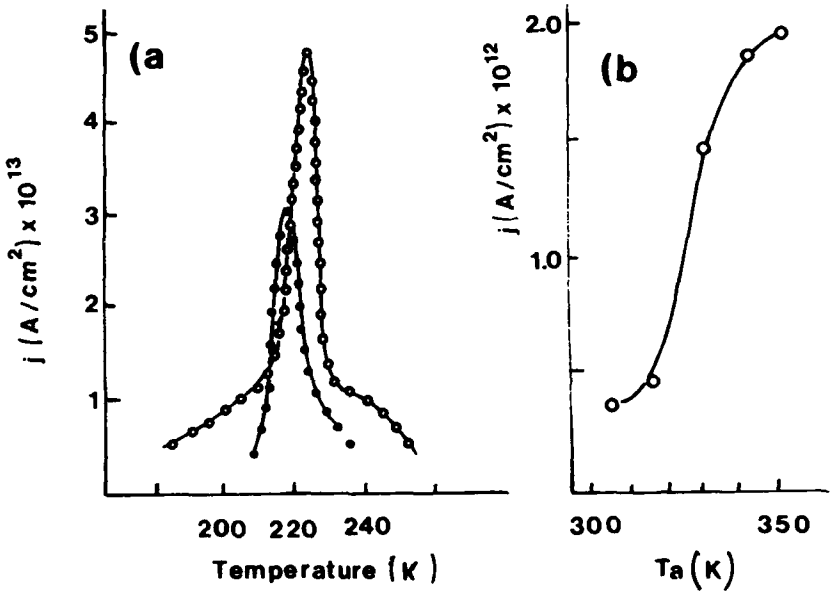

Fig.1a - TSDC "blank" measurements of block copolymers vs. temperature: full circles - sample 1; open circles - sample 2.

Fig.1b - Amplitude of TSDC peak in a "blank" vs.annealing temperature T_a for a block copolymer.

b - Normal TSDC spectra. The normal TSDC spectra, namely obtained by applying an external electric field, are displayed in fig.2 for block copolymers (samples 1 and 2) and for statistical copolymer (sample 3) . Again only one main peak is present, which occurs at temperatures close to $T_{g,B}$ of the block copolymers and to the glass-rubber transition temperature of the statistical copolymer, as monitired by viscoelastic measurements. The main features of such spectra can be summarized as follows: 1) the peak amplitude is linear function of the external applied field E_p at least up to 1.6×10^4 V/cm, see fig.3a, while the peak position

does not depend on E_p; 2) the shape of the peak and its position (see fig.3b) depend on the polarization temperature T_p, if this is lower than the temperature T^* at which the peak occurs, for instance, as shown in fig.2; 3) if T_p is chosen lower enough than T^*, the peak position and amplitude depend on the polarization time t_p as well. The last two results are meaningful of relaxation time distribution [2; 3], see §4.

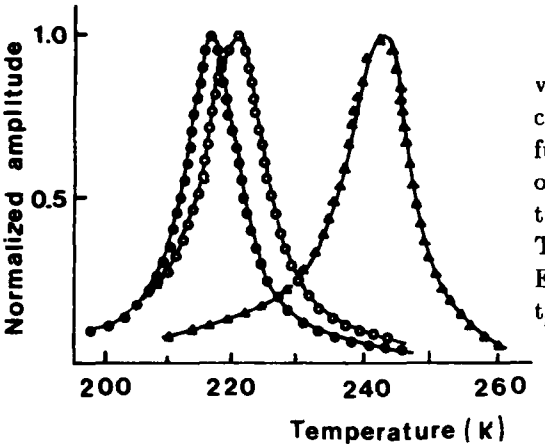

Fig.2 - TSDC plots vs. temperature for B-S copolymers:
full circles - sample 1;
open circles - sample 2;
triangles - sample 3
T_p = 300 K ;
$E_p \simeq 5 \times 10^3$ V/cm ;
t_p = 180 sec.

4 - DISCUSSION

The presence of TSDC signal in "blank" measurements performed on block copolymers is at first sight surprising and can be interpreted in the following way. The stress field used to prepare samples as pellets (see §2) could have induced the S-B-S block ordering with the consequent partial alignment of the butadiene chains (bearing a dipole moment of .403 D in the cis form of the 1.2 addition). The subsequent heating (to monitor TSDC spectrum) through the butadiene phase transition temperature involves an increasing mobility of dipolar groups of butadiene, with the consequent detection of weak displacement currents. The sample heating for time long enough (2 hours)at temperatures close to the melting point (see §3a) destroys the order previously induced by the stress field, and no TSDC signal is any longer detected in the subsequent "blank" measurement. The absence of TSDC signal in "blanks" of statistical copolymers can be attributed to the amorphous state of such samples which cannot be changed into a partially ordered one by the stress field used for the sample preparation.

The normal TSDC spectra can be explained in a similar way: the partial alignment of butadiene dipolar groups is induced by the electric field. At the phase transition, dipoles gain mobility, get random orientations (no electric field being applied) and give rise to the TSDC signal.

The linear dependence of the peak amplitude on the electric field (see fig.3a) supports that dipolar reorientation is responsible for the TSDC peak.

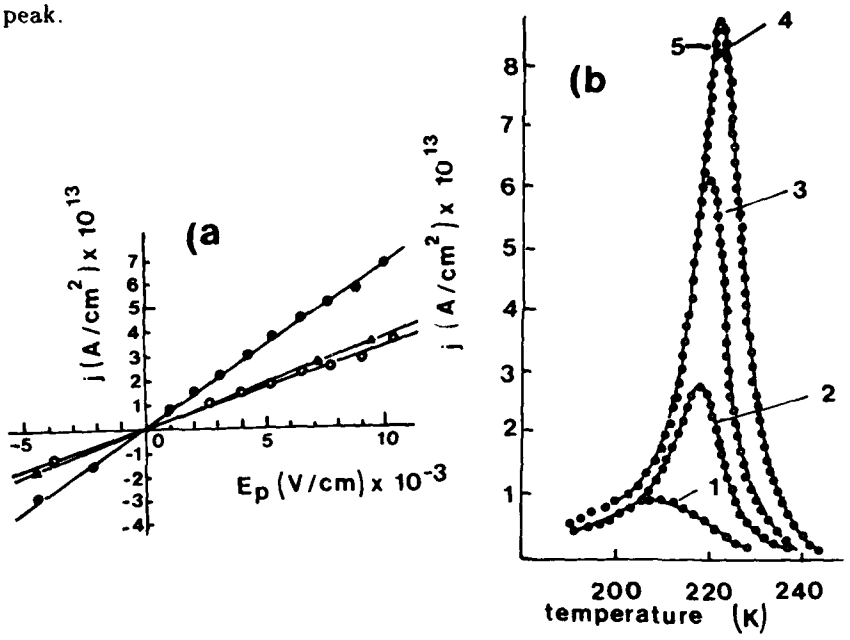

Fig.3a - *TSDC peak amplitude vs. applied field* E_p : full circles - sample 1; open circles - sample 2 ; triangles - sample 3. T_p =300 K ; t_p = 180 sec.

Fig.3b - TSDC peak dependence on the polarization temperature T_p for block copolymer (sample 2) as follows: curve 1, T_p=190K; curve 2, T_p=203K; curve 3, T_p=207K; curve 4, T_p=223K and curve 5, T_p=237K. E_p=5.5 x 10^3 V/cm ; t_p=180 sec.

The dependence of the peak position on T_p and t_p (see §3b and fig.3b) is meaningful for a distribution of relaxation times, which is expected indeed to occur in a polymeric structure, where dipoles are embedded in many different surroundings: therefore their reorientation take: place with different reorientation energies and pre-exponential factors.

5 - REFERENCES

[1] J.Pospisil and A.Havranek - in "Morphology of Polymers" , B. Sedlacek ed.; Waller de Gruyter, Berlin,N.Y., (1986) p.399

[2] R.Capelletti - in "Defects in Solids", A.V.Chadwick and M.Terenzi eds.; Plenum Publ. Corp., N.Y., (1986) p.407

[3] J.Van Turnhout - in "Electrets" , G.M Sessler ed.; Springer, Berlin, (1980) p.81

CHARGING CHARACTERISTICS OF A NON-WOVEN SHEET AIR FILTER

Tetsuji Oda and Jun Ochiai

Department of Electrical Engineering, University of Tokyo
3-1 Hongo-7chome, Bunkyo-ku, Tokyo 113, Japan

Corona-charging characteristics of a non-woven poly-propylene sheet of 140 μm thickness are studied related to the charging conditions. When the grid voltage, Vg (which control the surface potential of the film) is - 3 kV, the surface potential profile of the charged sheet is non-uniform. On the other hand, the profile is very uniform when Vg is only -1 kV. The average surface potential of the charged sheet is roughly -500 V in both cases if charging time is enough, such as more than 30 minutes. The experimental results of charge decay with time, resistivity in normal or ion-rich conditions and TSDC curves are also reported.

INTRODUCTION

The electret filter is very effective to remove submicron dust particles from air with little pressure loss and is already used as the human mask and so on. Many works on that filtration performance have been reported. However, charging performance has not yet analyzed sufficiently. In this report, electrical characteristics of a corona-charged electret filter are described related with its charging current, charge life time, resistivity, etc.

SAMPLE AND EXPERIMENTAL

A test sample is a non-woven poly-propylene sheet (PP thickness: 140μm, diameter of fiber:1.6μm,see Fig.1). The sheet is electrified by corona ions produced by needles. The charging is controlled by the screen

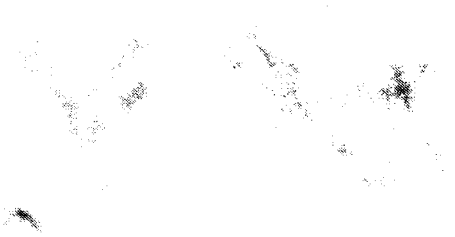

Fig.1 Photogragh of a filter sheet

CH2593-2/ 88/ 0000-0515$01.00 Copyright 1988 IEEE

grid (grid voltage:Vg) located 20mm above the sheet. The typical charging time is 30 min. at room temperature. After the corona-charging, a surface potential profile is measured by a surface potential probe (Monroe 244) and a X-Y stage which are controlled and processed by a personal computer system (FM77AV and others). Thermally stimulated discharge currents (TSDCs) of the sheet are observed by the automatic TSDC system[1]. The conductive current through the sample in corona ion rich atmosphere is measured compared with the normal resistivity. The normal resistivity is measured by using a commercial high resistance meter and a adapter including two electrodes (YHP4329A + YHP16008A applied voltage is from 25V to 1000V). Filtration efficiency are checked by a condensation nucleus counter (CNC:KANOMAX 3020).

SURFACE POTENTIAL PROFILE

Average surface potentials of the charged sheets are between -350V and -600V where typical grid voltages Vg are -1k, -2k or -3kV. In general, the surface potential of the dielectric film such as teflon sheet charged by this system is mostly as same as the grid voltage, Vg, when the Vg is small enough. This difference, that is, the surface potential of the filter sheet is limited to be -600V, is assumed to be due to the local discharge inside the film because this sheet is very porous or,

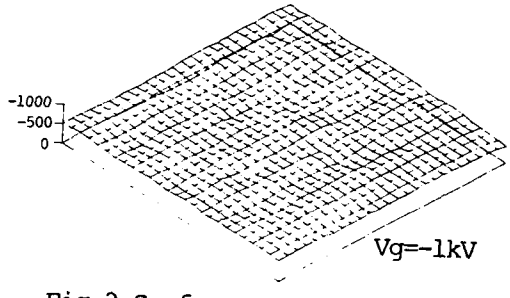

Fig.2 Surface potential profile of the sheet

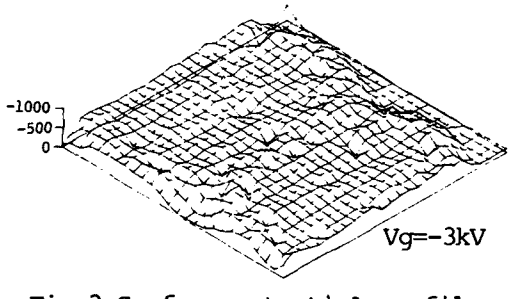

Fig.3 Surface potential profile of the sheet

Table1 Surface potential decay

SAMPLE	Vg[kV]	tp[min]	ORIGINAL (A)	1 HOUR LATER	1 DAY	1 WEEK (B)	B/A[%]
A	3	5	-579	-552	-541	-529	91.4
B	3	30	-473	-468	-448	-442	93.4
C	1	5	-359	-284	-251	-226	63.0
D	1	30	-524	-495	-472	-420	80.2

in other word, the PP space factor is very poor. Examples of surface potential profiles of those charged nonwoven PP sheet are shown in Figs.2 and 3. The potential profile of the sheet charged at the Vg of - 3kV in Fig.3 is very rough compared with the relatively smooth potential profile in Fig.2 suggesting the local discharge is stronger in large Vg than that in small Vg. Table 1 shows the averaged surface potential changes with stored time for various samples in open condition which means that the sample is laid on the metal plate and the surface is not covered with anything. When the both sample surfaces are covered with metal foils, this condition is called "in short condition". The surface potential profile of the electrified sheet stored in desiccator in open condition for one week after the charging shows that the averaged potential decreased to be 80% of the original one. On the contrary, the averaged potential of the sheet stored in open condition in room atmosphere is only 59% of the original. The moisture in atmosphere has clearly great influence on the charge decay in the filter. As the filter was made of many fibers, the net surface area is very large. Then conservation of charges in the sample depends much on the moisture in the air. When the sample is stored in short condition, the surface potential remains better.

THERMALLY STIMULATED DISCHARGE CURRENT (TSDC)

Thermally stimulated discharge currents(TSDC) of the negatively electrified sheet are hetero-current in every case. Two peaks of TSDC are observed at about 80°C and 140°C where those temperatures are mostly independent on the charging conditions, such as Vg or charging temperature shown in Fig.4. However, the charging temperature Tc affects the peak value, that is, the peak at low temperature of about 80°C is very small when Tc is high

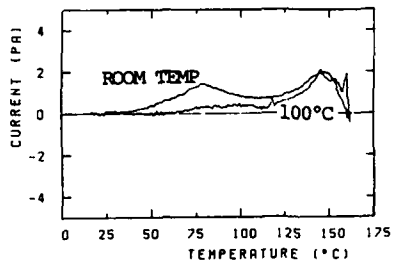

Fig.4 TSDCs of electrified filter

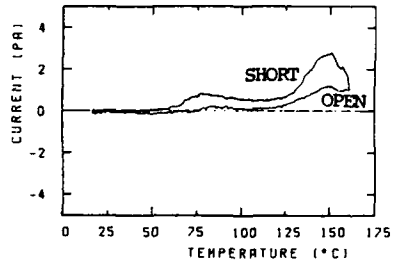

Fig.5 TSDCs of electrified filter

enough.

When a charged sample is stored in a metal box in open condition, the decay of the lower peak value of TSDC at about 80 °C is very large and that peak decreased to be zero in a week or so. The another peak at 140 °C also dec reases. The appearance of hetero-current may be explained as followings : injected charges inside the sheet form dipole-like pairs on counter side of each fiber. When thermal stimulation becomes large and trapped charges can move, those recombine together. Those phenomena are observed as hetero-current. On the other hand, the decay of the peak value at 80 °C in short condition is not so large as that in open condition,and the peak at 140 °C increases with time. The peak at 80 °C correspond to the discharge from shallow traps and the peak at 140 °C is assumed to be due to transition point of PP. In the case of the sample charged at 100 °C or the sample stored in short condition, charges trapped once at the shallow level are discharged from the trap and retrapped at the deeper traps.

CURRENT THROUGH THE CHARGING SAMPLE

The corona charging current through the sample is observed and saved anothe personal computer. Figures 6 and 7 show the current versus time at Vg = - 100V and at Vg = - 150V. When Vg is - 100 V, the current becomes smaller with time. How-

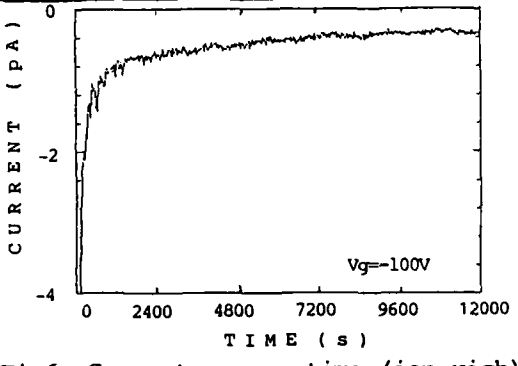

Fig6. Current versus time (ion rich)

ever, when Vg exceeds-150 V, the current signal is unstable and shows many spike-like noise, indicating the existence of the local discharge inside the sample.

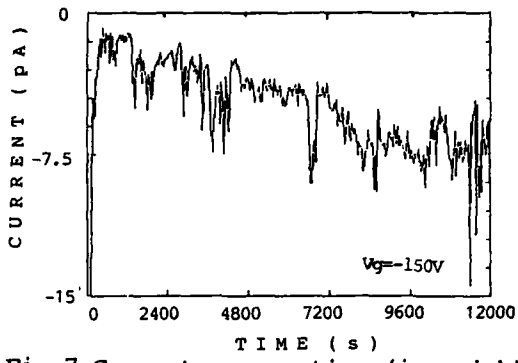

Fig.7 Current versus time (ion rich)

Fig.8 is the normal current characteristics where the D.C. high voltage Va is applied between two metal electrodes. When Va is less than 500V, the current decreases with time similar to that in Fig.6. However, the apparent discharge in the sheet occurs and resistivity cannot be measured when Va is 1000 V range. It is convinced that corona ions surely contribute the generation of local discharge in the sheet. However, the discharge light is not yet observed.

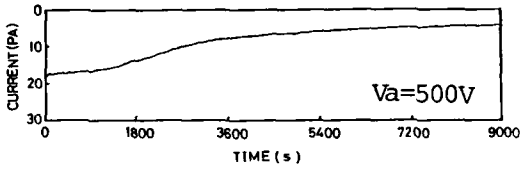

Fig.8 Current versus time (normal)

FILTRATION EFFICIENCY

The filtration efficiency of the electrified sheet for room air was 99.8% where the number of dust particles in air or cleaned air was counted by a CNC and the effective filter diameter was 55mm. The filtration efficiency of the original was also very high, 99.4%. The electrification effect is not yet obvious.

ACKNOWLEDGMENTS

The authors express their thanks to Dr. K.Ando at Toray for supplying special samples of non-woven PP.

REFERENCES

1] T.Oda: Proc.Inst.Electrost. Jpn. vol.8 pp223-231 (1984) (in Japanese).

POLARIZATION PHENOMENA OF BIOLOGICAL DIELECTRIC UNDER THE INFLUENCE OF ELECTRIC AND MAGNETIC FIELD

J.C.Paul

Department of Electrical Engineering
Tripura Engineering College
Tripura India-799055

Abstract

Polarization phenomena in dielectrics including charge storage and transport have been the subject of considerable study and research for the long time. In recent years increasing attention is being given to studies of dielectric properties of biological materials. In the present paper polorization phenomena of biological dielectric under the influence of electric and magnetic field have been presented which has not been reported so far in the available literature.

Theory

It is alreadyknown that when an electric field E is applied to a dielectric, the distortion polarization(P_1) will be established very quickly, but the remaining dipolar part of the polarization(P_2) takes time to reach its equilibrium value. However, the rate of change of P_2 may be expressed as [1]

$$\frac{dP}{dt} = \frac{P-P_1-P_2}{\gamma} \qquad \ldots(1)$$

where P is the equilibrium value of the total polarization and γ is called the relaxation time. If the applied field is alternating with circular frequency W then such a field may be expressed as $E = E_o \exp(jwt)$ and in that case dP_2/dt may be related as

CH2593-2/ 88/ 0000-0520$01.00 Copyright 1988 IEEE

$$\frac{dP_2}{dt} = \frac{\epsilon}{4\pi\tau}(\epsilon_0 - n^2) E_0 \exp(jwt) - \frac{P_2}{\tau} \quad \ldots (2)$$

where the static permittivity and refractive index are defined in terms of P and P_1 by

$$4\pi P = \epsilon(\epsilon_0 - 1) E \quad \ldots (3)$$

$$4\pi P_1 = \epsilon(n^2 - 1) E \quad \ldots (4)$$

and finally P_2 may be expressed as

$$P_2 = \epsilon(\epsilon_0 - n^2) E / 4\pi(1 + jw\tau) \quad \ldots (5)$$

The ratio of P_2/E becomes a complex quantity and it is possible to write the following equation

$$P_1 + P_2 = P' - jP'' = \frac{\epsilon}{4\pi}(n^2 - 1) E + \frac{\epsilon(\epsilon_0 - n^2)}{4\pi(1 + jw\tau)} E \quad (6)$$

The permittivity must also become complex and it may be expressed as

$$\epsilon^* = \epsilon' - j\epsilon'' = n^2 + (\epsilon_0 - n^2)/(1 + jw\tau) \quad \ldots (7)$$

where both ϵ' and ϵ'' are real and ϵ' and ϵ'' may be expressed as follows

$$\epsilon' = n^2 + (\epsilon_0 - n^2)/(1 + w^2\tau^2) \quad \ldots (8)$$

$$\epsilon'' = (\epsilon_0 - n^2) w\tau/(1 + w^2\tau^2) \quad \ldots (9)$$

Effect of magnetic field

In addition to electric field if now a cross magnetic field is applied in that case the effective field becomes as $E = vxB$ where B is the magnetic field and v is the velocity. Under this condition the value of P will be changed and the relaxation time will no longer be a constant. It has been reported that under the influence of magnetic field there may be various changes on the biological dielectric. It is known that

for the detection of cancer NMR is used in which the patient is placed inside a large magnetic coli. The coil causes the magnetic dipoles of hydrogen protons in the subject's body to align. The machine then applies a radio pulse with an alternating magnetic field at right angle to the first. The second field twist the dipoles of the hydrogen nuclei out of their alignment. When the radio pulse ceases, the nuclei return to their former state and emit their own characteristic radio signals. These signals are picked up and processed and then converted into two-dimensional images displayed in either black and white or colour. Although NMR is the best method for the detection of cancer , but acceptance of the same will depend on socioeconomic factors as well as on technical advances. Even in the USA the cost of NMR are not covered by most major third-party health -care payers, although some insurance companies are paying for scans of selected patients.

It may be suggested that by measuring the relaxation time under the influence of electric and magnetic field the cancerous and non-cancerous tissue may be differentiated. Knowing the values of relaxation time the permittivity may be determined from the equations as stated above for both cancerous and non-cancerous tissues.

Mammography is currently the most sensitive method for the detection of breast cancer. The female breast is one of the most radiosensetive organs and irradiation causes breast cancer. It may be stated that each mammography might double the risk of cancer in the high risk group. In view of this it is felt that the measurement of relaxation time is the best solution for the detection of cancer in which there is no risk factor.

Polarization as a Function of Time

The behaviour of the polarization as a function of time or frequency may be expressed in terms of a decay function [1] and it is possible to

express the orientation polarization $P_2(t)$ as

$$P_2(t) = \alpha_0 E/(1+j\omega\tau) \quad \cdots \quad (10)$$

where α_0 is the dipolar contribution to the polarizability. But in addition to electric field if a cross-magnetic field is also applied in that case $P_2(t)$ may be represented as

$$P_2(t) = \alpha_0(E+v\times B)/(1+j\omega\tau) \quad (11)$$

It may be stated that orientation polarization in biological dielectric may occur in two ways i.e by rotation of the group within the molecule , and by rotation of the molecule as a whole. Itis to be expected that the latter process will depend on the viscosity of the medium , while the former, since it causes little disturbance of the surroundings,will be fairly insensitive to the nature of this medium.The relative lengths of the relaxation times associated with the two processes will vary from dielectric to dielectric, the relaxation time for the intramolecular process being dependent on the magnitude of the potential barriers the rotating dipole must overcome.

Discussion and Conclusion

It is known that human tissues contain more than 70% water, exceptions are adipose tissue (50%), bone(30%) and teeth(5%). In its capacity as a solvant, water plays a fundamental role in cellular reactions. A very large number of substances are soluble in water, other substances such as fats can be carried in fine emulsion rendered water-soluble in other ways, for example by combining with proteins, It may be said that as soon as cancer is developed there should be significant increase in the motional freedom of water in the malignant tissue.As a result of this there will be various changes in the electrical properties in the cancerous tissues in comparison with normal tissues.It

may be stated that under the influence of cross magnetic field ions/electrons , instead of moving in straight lines between collisions, are defàected and as a result of which there may be increase in collision frequency and reduction in mean free path. As a result of which there may be various changes ia the biological dielectric under the influence of electric and magnetic field. There may be change in the dipole moment of the molecules, there may be distortation of valance angles, or there may be orientation of the spins of the molecules.There should be change in the polarization of the molecules,as it is evident from equations discussed earlier. It may be stated that by measuring the relaxation time under the influence of both electric and magnetic field the cancerous and non-cancerous tissue may be differentiated.Knowing the values of relaxation times it is possible to determine the values of permittivitţes for both cancerous and non-cancerous tissues from the equations as stated earlier.

References

1.Nora E.Hill,Worth,E.Vanghan,Price,A.H Davies,M :Dielectric properties & molecular behaviour,Van Nostramd ReinholdCo,London, (1969)
2.Paul,J.C. :Int.Sym.H.V.Engg.Zurich,360(1975)
3.Paul,J.C. :Ind.J.Phys,53B,85,(1979)
4.Paul,J.C. :Ind.J.Phys,53B,96,(1979)
5.Paul,J.C. :J.I.E(I),EE,64,84,(1983)
6.John,H. :IEEE Spectrum,January,89,(1985)
7.Paul,J.C.:5th Int.Sym.Electrets,947,(1985)
8.Paul,J.C.:J.Ind. Med.Asso. Communicated
9.Suchet,J.P.:Electrical conduction in solid materials,Pergaman Press (1975)

A.C. POLING OF SOLUTION CAST FILMS OF POLYVINYLEDENE FLUORIDE/LEAD ZIRCONATE COMPOSITES

Dolly Sinha and P.K.C. Pillai

Indian Institute of Technology, New Delhi, India.

ABSTRACT

Composite samples were prepared in the form of thin films (50-80μm) by solution cast techniques for different weight fractions of PZT in PVDF matrix. Samples were a.c. poled at a temperature of ~180°C. The a.c. poling at elevated temperature considerably enhances the dielectric constant and is found to be a more efficient way of poling composite films than conventional d.c. poling. SEM and XRD studies were done to correlate the increment in dielectric constant with structural modification.

ELECTRET FORMATION AND CHARGE STORAGE IN SINGLE CRYSTAL ZIRCONIA

O. P. Puri, Om Sinha, Kofi Bota and Terry Harrington

Clark-Atlanta University, Atlanta, Georgia 30314

Fully stabilized zirconia ZrO_2-Y_2O_3, 9.8 molar Y O exhibits behavior characteristic of electrets in most respects. Samples are characterized with attention given to "quasipermanent charge retention".

A theory has been developed for the formation and decay of thermoelectrects to qualitatively explain different materials under different conditions and semi-quantitatively explain their decay and thermally stimulated discharge process.

X-Ray diffraction studies are being undertaken to explain the theory developed.

INTRODUCTION

Tests are in progress studying polarization in fully stabilized Zirconia (ZrO_2-Y_2O_3), henceforth referred to as Zirconia. Other and current results have shown that Zirconia exhibits behavior that is characteristic of electrets. This study evaluates Zirconia mostly at room temperature. We have considered the effects of material orientation, sample thickness and low temperature on charge storage in Zirconia.

SAMPLE PREPARATION AND POLARIZATION

Samples 1.1 centimeter used for these tests were sliced from a single crystal Zirconia and polarized in an electric field was applied across the parallel surfaces of the sample and charge density was measured.

CH2593-2/ 88/ 0000-0526$01.00 Copyright 1988 IEEE

BEHAVIOR OF SURFACE CHARGE AND POLARIZING CURRENT

Zirconia samples polarized for the first time were observed to have higher polarizing currents compared to the currents for the same samples during subsequent tests. The initial polarizing current at the beginning of each test was about the same as that flowing at the end of the prior test. Differences in Laue diffraction photographs of polarized and unpolarized samples were not observed.

EFFECT OF SAMPLE THICKNESS ON CHARGE STORAGE

Zirconia samples of various thicknesses were polarized at three kilovolts (3 kV) for three hours at room temperature. The surface charge density on the samples was determined after each polarization. The graph of the maximum surface charge density versus sample thickness (Figure 1) shows that the

Fig 1 EFFECT OF SAMPLE THICKNESS ON CHARGE DENSITY

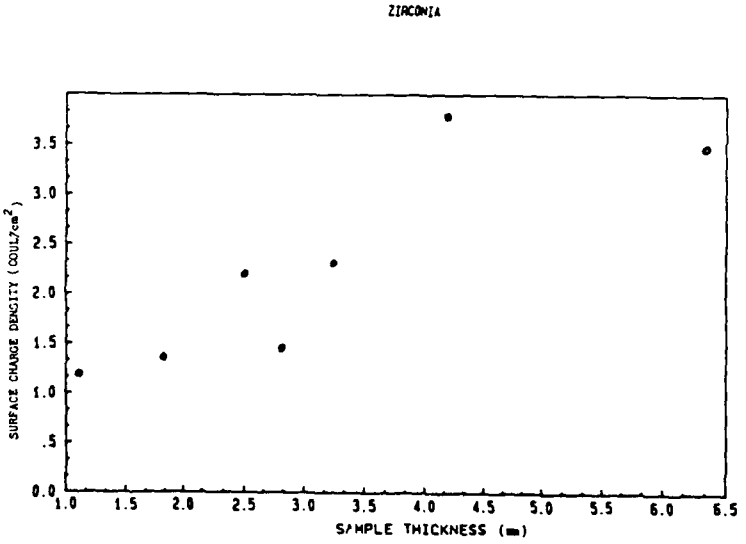

surface charge density on the zirconia samples is proportional to the sample thicknesses used.

Fig 2

SURFACE CHARGE DENSITY VS TIME
ZIRCONIA AT ROOM TEMPERATURE

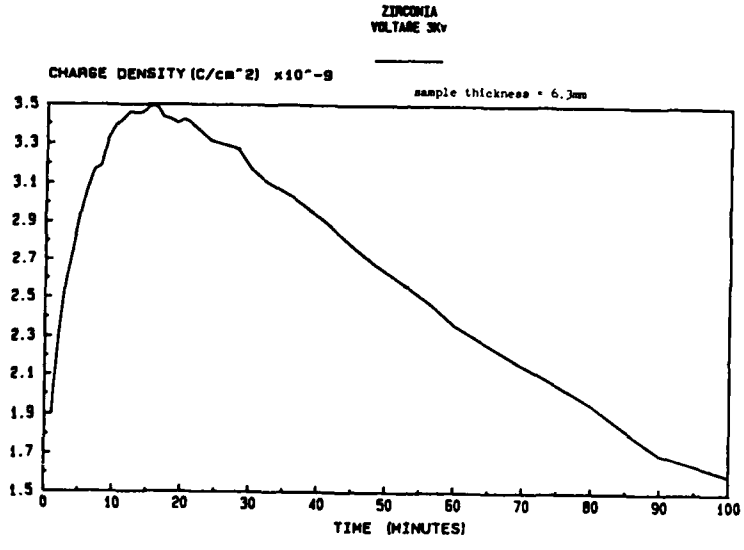

Fig 3

SURFACE CHARGE DENSITY VS TIME
ZIRCONIA AT ROOM TEMPERATURE

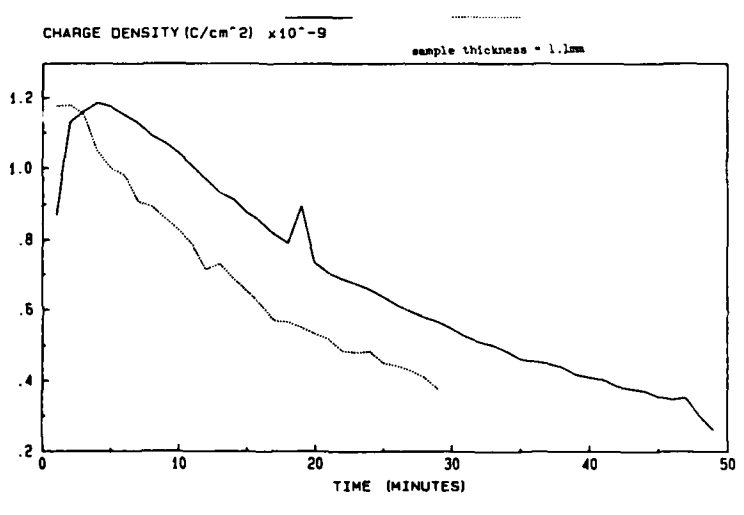

EFFECT OF LOW TEMPERATURE (-10 C)

Freezing polarized samples to -10 C was observed to increase the life of the surface charge density. Polarized samples were transferred into a freezer after the surface charge density was measured for the first ten minutes of life. The results show that the surface charge density increased within the first ten minutes of life to a maximum before the decay process started. Each time that the sample was removed from the freezer and surface charge density measured, it increased from a low value to a maximum before the decay process started. The reason for this behavior has not been determined, however, the result suggest that surface charge decay in zirconium is influenced by ionic diffusion and that low temperature decreased the diffusion rate.

EFFECT OF HEAT ASSISTED POLARIZATION ON CHARGE DENSITY

The maximum charge density obtained on a polarized sample of zirconia has been in the order of 10 Coulomb/cm2. Attempts were made to obtain higher charge density. Zirconia samples (6 mm in thickness) were pre-heated to 60 C in an oven for one hour and polarized at 3 kV for 3 hours. The oven was turned off after two hours of polarization and the sample cooled to room temperature before the polarization process was stopped. The result of this test did not show an appreciable difference in the surface charge density compared to the maximum charge density from room temperature polarization.

EFFECT OF MATERIAL ORIENTATION

Zirconia samples of equal thicknesses were prepared from the (100), (111), (101) crystallographic directions. These samples were polarized at room temperature to 3 kV for 3 hours. Comparison of the surface charge density observed on the samples showed no significant difference.

SUMMARY AND CONCLUSION

(a) The memory effect of the polarizing current during subsequent polarizations of a zirconia sample at room temperature. (b) The proportionality between the surface charge density and the zirconia sample thickness. The thicker the sample, the more the surface charge measured. (c) The influence of low temperature -10 C in extending the life of the surface charge density. (d) Obtaining the maximum surface charge on zirconia is independent of the crystallographic orientation of zirconia, it is also independent of the polarizing temperature (room or high temperature). Other properties not contained in this paper have been reported elsewhere. Complete charac-terization of the electret properties require the knowledge of it's microstructural behavior during and after a polarization process. This is our next interest. A mathematical model has been developed to quantify charge relaxation in thermoelectrets (2, 3).

ACKNOWLEDGEMENT

This work was supported by the U. S. Department of Energy, Office of Energy Research, Grant # DE-FG05-84ER45128.

REFERENCES

1. Harrington, T.L., Charge Storage and Transport in Fully Stabilized Zirconia. Masters Thesis 1987.
2. Puri, O. P., Investigations of Charge Transport in the Thermoelectret State of Some Gases and Ceramics. Fifth International Symposium on Electrets, Heidelberg, West Germany, 1985.
3. Puri, O. P. et al, Charge and Polarization Relaxation in Thermoelectricts. 1986 Sixth IEEE International Symposium, Bethlehem, Pa.

THERMALLY STIMULATED CURRENTS IN SODIUM BOROSILICATE GLASS

E. Rysiakiewicz-Pasek, V. Graveris, I. Krumins*

Institute of Physics,
Technical University of Wrocław, Wybrzeże Wyspiańskiego 27, 50-370 Wrocław (Poland)
*Institute of Solid State Physics,
Latvian State University, Kengaraga 8,
226063 Riga (USSR)

The thermally stimulated method (TSP, TSD) was used to investigate sodium ions motion in borosilicate glass. Two TSD peaks were observed. The results of experiments point out the dipole polarization nature of the low temperature peak. This peak can be related with a short range sodium ions motion.

INTRODUCTION

Results of thermally stimulated currents measurements : thermally stimulated polarization TSP and thermally stimulated depolarization TSD have provided useful information on trapping, storage and thermally activated release of electrical charge in many dielectrics [1,2]. This technique can be used for investigation of ionic motion in sodium silicate glasses [3,4] and in other glasses [5,6]. This paper describes the results of TSP/TSD measurements for sodium borosilicate glass.

EXPERIMENT

The measurements were carried out in the following way.
Firstly the sample was cooled to the temperature T_o (=100 K). Than the sample was heated at a constant rate b=0.1 K/s with the external field applied (E_p=2.10^5 V/m). The measured current was denoted as TSP-1. With an electric

CH2593-2/ 88/ 0000-0531$01 00 Copyright 1988 IEEE

field still applied, the sample was again cooled to T_o and heated for the second time (TSP-2). No current peak due to dipole orientation was observed because the dipoles became oriented during the first heating. The TSP-2 current can be used for calculating the dc conductivity of the sample. At higher temperature TSP-1 and TSP-2 became essentially identical. Subsequently the sample was rapidly cooled to T_o with E_p applied. Than the field was removed. The sample was heated and TSD-3 current was measured. The measurements of the thermally stimulated currents (TSP, TSD) were performed with the system consisting with: TSD cell, vacuum system and electrometer. Either graphite or gold paste electrodes were applied for these measurements. The samples were of dimension: 10x10x1 mm. the surfaces were ground and polished from the both sides.
The subject of investigations was the glass with composition (in % by weight): 40% SiO_2, 40% B_2O_3, 20% Na_2O.

RESULTS

In Fig.1 the typical TSP/TSD curves (with gold electrodes) are shown. Identical curves using the graphite electrodes have been observed. In the temperature range between 140 K and 400 K there are no TSP peaks, but the TSD high temperature peak appears. No peak is observed in either TSP-1 or TSP-2 currents because of the large dc conductivity.
Polarizing the sample at lower temperatures the low temperature peak appears (Fig.2). The temperature of the peak (T_m) and height of the low temperature peak increase with increasing polarization temperature. The height of this peak increases linearly with E_p. The size of the low temperature peak is independent on the material of electrodes.
To separate the transient polarization from the dc conductivity, the teflon electrodes are helpful. For the measurements a thin layer of teflon (50 μm) was placed between the glass sample and the chromic electrodes. Teflon eliminates

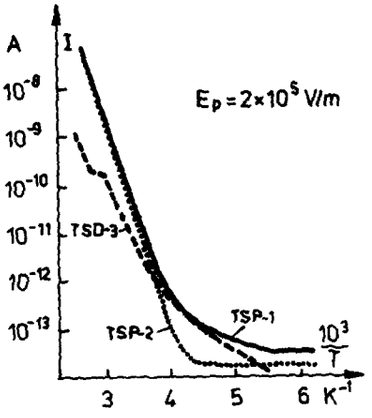

Fig.1. TSP/TSD curves

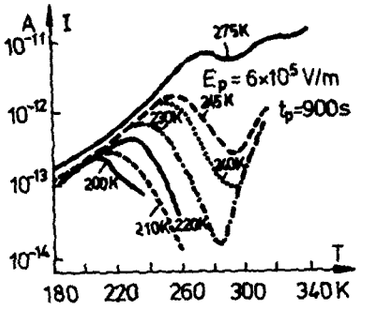

Fig.2. Dependence of TSD curves on T_p

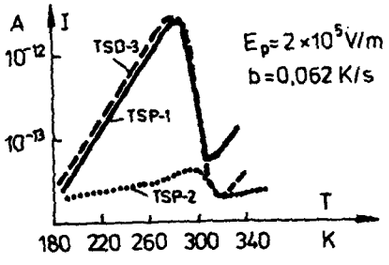

Fig.3. TSP/TSD curves measured with the teflon electrodes

the dc conductivity and the low temperature TSD peak is observed (Fig.3.). Activation energy for the dc conductivity was calculated from TSP-2 curve. The obtained values: 0.85 eV (gold electrodes) and 0.88 eV (graphite electrodes) agree very well with previous our measurements [7].

The shift of the low temperature peak maximum to the higher temperature can be releated with a distribution of the activation energies. The activation energy for TSD peaks were determined by the partial-discharge technique [2]. The calculated values of the activation energies for the subsequent cycles are: 0.42, 0.48, 0.54, 0.58, 0.59, 0.61 eV (low temperature peak) and 0.66, 0.71, 0.72, 0.74 eV (high temperature peak).

DISCUSSION

Interpretation of the TSD peaks is based on the fact that the activation energy for the high temperature peak is higher than that for the low temperature TSD peak, but the activation energy for both TSD peaks is lower than for the dc conductivity.

At lower temperature a very localized motion is possible only, whereas at higher temperature translation throught the glass network can also occur. The linear dependence of the low temperature peak height on E_p, independent on the electrodes material, and existence of this peak on TSP-1 and TSD-3 (teflon electrodes) are consistent with the dipole than space charge polarization.

The structural studies [8,9] of the sodium borosilicate glasses indicate that for the investigated glass Na^+ ions should be associated with $[BO4]^-$ tetrahedra and existence of the nonbridging oxygens is possible, but not in silicon-oxygen sites.

The value of the ionic conductivity appearing together with the low temperature TSD peak ($=10^{-16}\ \Omega/m$) corresponds well with the ionic conductivity value for the low temperature peak for sodium silicate glasses [3,4].

Quite the same activation energy and height of this low temperature peak for the sodium borosilicate glass and those for the sodium silicate glass indicate with this peak is similar for both glasses.

For the sodium silicate glass, the low temperature had be related with the orientational polarization connected with the sodium ion (Na^+) jump from one to another nearly equivalent sites around the same nonbridging oxygen ion $[NBO]^-$. But it is also possible that, in the investigated glass, with the external electric field applied, orientation of Na^+ ions around $[BO4]^-$ tetrahedra occurs [10]. This motion of Na^+ ions can be also responsible for the low temperature TSD peak.

In the investigated glass no phase separation

was detectable with electron miscroscop at magnifications up to 5900. The experiments [11] had shown that in these sodium borosilicate glasses sodium ions are not homogeneously distributed.
Up to now the origin of the high temperature TSD peak is not quite clear. It can be supposed that existence of this peak is related with heterogeneity of the glass structure.

REFERENCES

[1] G.M.Sesler, Electrets, Springer-Verlag, Berlin,Heidelberg, New York, 1980.
[2] C.Bucci, R.Fieschi, G.Guidi, Phys.Rev., 148,1966,816.
[3] A.K.Agarwall, D.E.Day, J.Amer.Ceram.Soc., 65,1981,227.
[4] C.M.Hong, D.E.Day, J.Amer.Ceram.Soc.,64, 1981,61.
[5] I.Thurzo, Acta Phys.Slov.,29,1979,46.
[6] A.Doi, S.Maruno, Mat.Sci.,52,1981,3433.
[7] W.Magierski, E.Rysiakiewicz-Pasek, Proc. 3-th Conf.Electrostatics, Kraków, Poland 1981,214.
[8] M.P.Brungs, E.R.McCartney, Phys.Chem.Glass. 16,1975,48.
[9] Y.H.Yun, P.B.Bray, J.Non.Cryst.Sol.,27, 1978,363.
[10] B.Dutta, D.E.Day, J.Non.Cryst.Sol.,48, 1982,345.
[11] A.A.Appen, Chimija stekla, Chimija,

MECHANISM OF CHARGE FORMATION IN THE IRRADIATED POLYETHYLENE

V.V. Gromov, A.G. Rozno and O.V. Procopiev

Institute of Physical Chemistry, Academy of Science of the USSR, Moscow, USSR.

ABSTRACT

Using the acoustic wave method the electric charge distribution in high- and low pression polyethylene was studied. It was established the correlation between the charge accumulation and portion of crosslinking of the irradiated polyethylene. Mechanism of the electric charge accumulation in connection with the molecular structure of polyethylene and different polymers are discussed.

INCREASE OF REFRACTIVE INDICES IN LIQUID DIELECTRICS BY SPACE CHARGE ACCUMULATION

Tadashi Sato

Faculty of Engineering, Iwate University, Japan.

ABSTRACT

Distributions of refractive indices were measured with Mach-Zehnder and Schlieren technique in liquid dielectrics where space charge conduction took place with parallel plane electrode configuration under direct voltage application.

Al-SiO-Au emitter for hexane, discharging plasma in gaseous space and aqueous solutions of electrolytes for mineral and silicone oil were employed as charge emitters.

Space charge distributions were determined graphically from curves of potential distributions measured with electrostatic probe.

Comparisons of the distributions of refractive index to those of space charge show that refractive indices increase with space charge by the rate of $1.7\times10^{-5}/10^{-3}C/m^3$ for mineral oil at room temperature.

INVESTIGATION OF CORONA-CHARGING OF POLYPROPYLENE AT ELEVATED TEMPERATURES

DING Hai and XIA Zhongfu

Pohl Institute, Tongji University, Shanghai, P.R.China
and
Institute for Electroacoustics, Technical University of Darmstadt, Darmstadt, F.R.Germany

ABSTRACT

Stabilization of negative charge in polypropylene (PP) corona-charged at elevated temperatures is investigated. Measurements of corona current and TSC (thermally stimulated current) yield the charging efficiency and the structure of the trapping levels, respectively. With increase of charging temperatures, the TSC peaks shift to higher temperatures, while the charging efficiency drops, which can be made up partially by prolonging the charging time. A continuous distribution of trap levels has to be assumed and a new phenomenological theory is suggested. To explain the shift of TSC peaks, trapping and detrapping should be taken into account.

INTRODUCTION

Electrets have found widespread use in industry ⟨1,2⟩. In some applications, such as in the production of air filters, demand of electret materials is in large quantity, so an inexpensive material is requried. Polypropylene (PP) is an ideal material for this, although its charge retention properties are not as good as those of polytetrafluoroethylene (PTFE) and its copolymer (FEP) ⟨3,4⟩.

In the past, many studies on PP using TSC techniques were published ⟨5-9⟩. Bamji et al (1979) observed peaks at 65° C and 105° C for samples corona-charged at RT (room temperature) and 120°C respectively ⟨5⟩. Baba and Ikezaki (1984) found four peaks for positively and negatively corona-charged samples under different heat treatment ⟨6⟩. Myśliński and Kryszewski (1980) reported two peaks located at 90°C and 120°C for samples charged

CH2593-2/ 88/ 0000-0538$01.00 Copyright 1988 IEEE

with an electric field of 8kv/cm at 105°C for 2 min. ⟨7⟩. Singh and Datt (1984) obtained a single peak at 114° C for PP polarized at 145° C with 100 kv/cm field ⟨8⟩. Keller and Datt (1985) detected a characteristic peak at 393K for samples Townsend-charged with different poling fields and polarities (9). Although these authors obtained different results because of differences in materials and methods used, they agreed that negative carriers are more stably trapped in PP.

EXPERIMENT

The polypropylene material used is 15 μm NND 15 Trespaphan made by Kalle, Wiesbaden, F. R. G. The samples are one-side metalized with 1000Å aluminum with a guard ring of 5.5 cm in diameter. As shown in Fig. 1, the charging apparatus includes (1) a tungsten needle baised to -10 kv, (2) a wire grid baised to -500 v and (3) a brass base grounded over a Keithley galvanometer. The set is shieled in a mesh cage and placed in a thermostat.

After charging, samples are taken out of the thermostat as soon as possible and cooled down to RT. The surface potential is measured with a Monroe 175 electrostatic

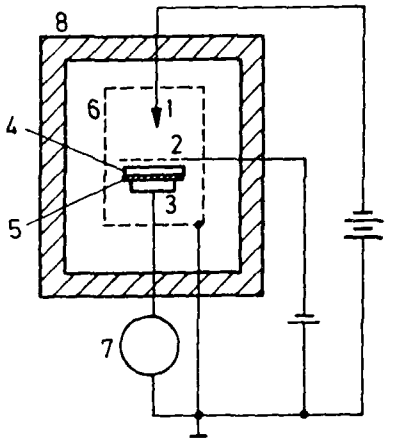

Fig.1. Schematic drowing of corona charging apparatus. 1 tungsten needle, 2 wire grid, 3 brass base,4 sample, 5 metalization, 6 mesh cage, 7 Keithley, 8 thermostat

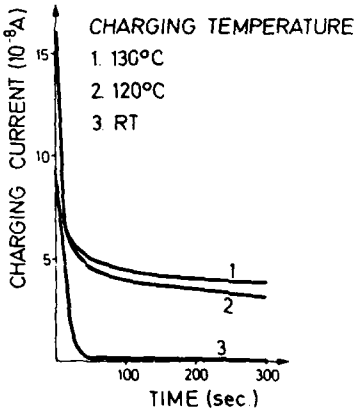

Fig.2. Corona current at different temperatures.

voltmeter and the TSC is performed with a Keithley 600-B using a heating rate of 1.67°C/min.

RESULTS AND DISCUSSION

Fig. 2 dipicts typical corona current curves at different temperatures. At the begining, the current is the maximum and then decreases. At RT, it reaches a very small steady state value in about 40 s. By contrast, at high temperatures the current decreases not so fast and still drops after 300 s. The steady state current value of curve 3 is as small as $4*10^{-11}$ A and is due to leakage; it does not contribute to charge injection. For curves 1 and 2, the current is larger than $3*10^{-8}$ A after 300 s. It proably results from an increase of conductivity as well as from trapping and detrapping processes. Conductivity should be time-independent during charging and the leakage does not contribute to surface potential buildup, while the trapping current, which decreases with time, increases the surface potential. Correspondingly, the surface potential of the sample charged at RT assumes a saturation value, namely the grid voltage, in 40 s. This value is not reached for samples charged at elevated temperatures. By prolonging the charging time, the surface potential will increase, but it remains below the grid voltage. The decrease of charging efficiecy with temperature seems to be due to the fact that constant charging current is used. When the conductivity is raised, a large portion of the current passes through the sample as conductive current. Thus, less current is available for trap filling while detrapping increases.

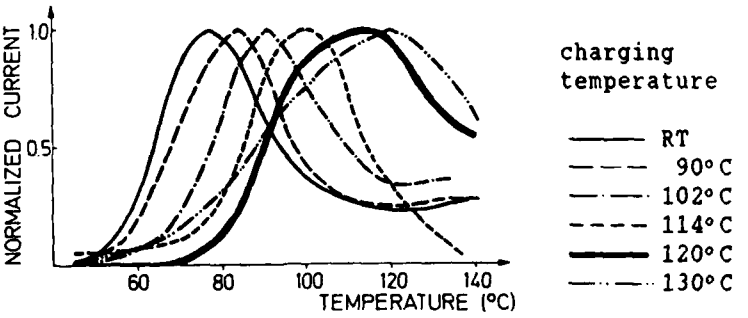

Fig.3. TSC spectra of PP corona-charged at different temperatures.

Fig.3 dipicts TSC spectra of PP. It is obvious that the detrapping peak shifts to higher temperature with increase of charging temperature. For the RT-charged sample,the peak is located at 77° C, while peaks are at 84°C, 91°C, 101°C, 115°C and 120°C for samples charged at 90°C, 102°C, 114°C, 120°C and 130°C respectively. The peaks are broader than those observed by other authors, which indicates that they are due to emptying of traps with a distribution of activation energies.

During corona charging, both trapping and detrapping are taken into account. Van Turnhout ⟨10⟩ discribed the trapping kinetics with

$$\partial m/\partial t = C_m n\langle M-m\rangle - \nu(T)\,m, \qquad (1)$$

where m and n are the concentration of traped and free electrons, M is the total number of available traps with a cross section C_m and $\nu(T)$ is the escape rate. According to Boltzmann statistics,

$$\nu(T) = \nu_0 \exp(-U/kT). \qquad (2)$$

As most carriers are released at 77° C for a sample charged at RT, one can assume that different C_m-values apply to traps of different activation energy. The dependence of C_m on activation energy U is assumed to be

$$C_m(U) = C_0 \exp(A/U), \qquad (3)$$

where C_0 is a coefficient and A is a characteristic energy. That means traps with low activation energy have larger cross section than those with high energy. So the injected carriers are first captured by low-energy traps. When the temperature is elevated, the second term in equation (1) increases rapidly and, for low-energy traps, approaches the first term, while it is still much smaller than the first term for high-energy traps. So carriers will fill the high-energy traps. In this way, we explain the shift of TSC peaks with the increase of the charging temperature.

As is well known, the glass-rubber transition temperature is 238-299K ⟨11⟩. In our TSC, there is a contribution from polarization since PP is a polar material and we charged it at elevated temperatures. However,

the above theory with proper modification applies also to polarization. In the present paper, there is no attempt to identify how much of TSC currents is contributed by real charge and how much by polarization.

CONCLUSION

TSC from PP corona-charged at elevated temperatures shows that the peak shifts to higher temperatures with increase of charging temperatures. Traps with low activation energy have larger cross section than higher energy traps. Since the charging current is constant while the conductivity increases at elevated temperatures, the charging efficiency drops for the higher temperature experiments.

ACKNOWLEDGEMENTS

The authors are greatful to Prof. G. M. Sessler and Dr. R. Gerhard-Multhaupt for stimulating discussion and valuable comments on the manuscript. Thanks are also given to Mr. H.Eisenhauer for sample preparation. The financial support of this work by the Stiftung Volkswagenwerk is gratefully acknowledged.

REFERENCES

(1) G.M.Sessler: Electrets (Springer-Verlag, Berlin, Heidelberg, New York, London, Paris, Tokyo, 1987) pp.347-81, 415-20
(2) R.Gerhard-Multhaupt: IEEE Trans. Electr. Insul. EL-22, 1987, pp.531-54
(3) P.H.de Haan, J.van Turnhout, K.E.D.Wapenaar: Proc. 5th Int. Symp. on Electrets, Heidelderg (IEEE Serv. Center, Piscataway, NJ 1985) pp.756-65
(4) D.B.Blackford, R.C.Brown: (In Ref. 3, pp.766-71)
(5) S.S.Bamji, K.J.Kao, M.M.Perlman: J.Electrostat. 6 (1979) 373
(6) A.Baba, K.Ikezaki: J. Appl. Phys. 57 (1985) 359
(7) P.Myśliński, M.Kryszewski: Poly. Bull. 2 (1980) 761
(8) R.Singh, S.C.Datt: (In Ref. 3, pp.202-7)
(9) J.M.Keller, S.C.Datt: Phys. stat. sol. (a) 91 (1985) 205
(10) J.van Turnhout: (In Ref. 1, p.136)
(11) D.W.van Krerelen: Properties of Polymers (Elsvier Sci. Publ. Comp., Amsterdan, 1976) p.428

INFLUENCE OF QUENCHING ON THE CHARGE STABILITY OF POLYMER ELECTRETS

Xia Zhongfu

*Pohl Institute, Tongji University, Shanghai, P.R.China
and Institute for Electroacoustics, Technical University of Darmstadt, F.R.Germany

ABSTRACT

The influence of heat treatment (heating followed by quenching prior to charging) on charge storage in polymer foils has been studied by TSD and surface-potential decay measurements of FEP, PETP, and PP foils charged by corona discharge or electron beam. It is shown that the heating rate before quenching and the quenching temperature affect the charge-decay time and the TSD-peak temperature. Crystallinity and crystal granular size have been measured before and after quenching by means of X-ray diffraction. The different charge stabilities can be explained qualitatively by morphology changes.

INTRODUCTION

Annealing and quenching can change the charge-storage capabilities of polymer materials, since any thermal treatment usually induces changes in the physical properties of the dielectric [1]. In this paper, we discuss the influence of several heat-treatment parameters on the charge stability in electret samples.

EXPERIMENTAL PROCEDURE

Samples consisting mostly of Teflon FEP (Dupont, 25 μm) with evaporated aluminium electrodes (100nm) on one side were used. Care must be taken to select samples which have approximately the same initial morphology; therefore, all samp es were taken from the central part of the respective polymer roll. Heating is performed in an oven (Heraeus, F.R.G.) with a controlled linear temperature rise of 3 to 46K/min. After heating to a predetermined temperature, the samples are kept at this temperature for 1 min. It is necessary to use sufficiently thin samples (25 μm) and a quenching medium 'water) with a high heat-transfer coefficient so that the high temperature morphology is "frozen in" after quenching. (For

CH2593-2/ 88/ 0000-0543$01.00 Copyright 1988 IEEE

Teflon FEP, the quenching temperature T_q is 19°C). In order to minimize the temperature change during transfer of the very thin samples from the oven to the quenching bath, the quenching is carried out in the oven and must be as rapid as possible. After this heat treatment, the samples are charged by means of a corona discharge or an electron beam [1]. Then open-circuit TSD measurements with a heating rate of 3.3K/min. are performed.

RESULTS AND DISCUSSION

1.Qualitative interpretation of the improvement of charge stability by quenching

The TSD curves of Fig.1 illustrate that for quenched samples the space charge peak at about 146°C is decreased and the peak at about 210°C is shifted towards a higher temperature than that found with nonquenched samples. The experimental results suggest that most of the space charge is trapped at deeper levels; the stability of charge storage is improved markedly. When the sample is heated to T ($T_g<T<T_m$) before quenching, the material melts gradually. The arrangement of molecular chains tends to randomize. During this period, crystal blocks break into smaller grains (or lamellae) which are dispersed in an amorphous liquid. This morphology exhibits a larger crystalline-amorphous interface region than that existing before quenching. While being quenched, the viscosity of the melt is increased rapidly. Because of relaxation, the random molecular chains do not have enough time to crystallize. The smaller grains in the melt are frozen in. Therefore, the number of crystal granules is increased. More and more complex defects are formed [1]. Thus, trapping due to the Maxwell-Wagner effect is reinforced and charge storage is improved. X-ray diffraction (Fig.2) shows that, upon quenching, the crystallinity of the sample hardly changes, but that the average diameter of the crystallites is only about 3/4 of that of a nonquenched sample. Consequently, isothermal (RT) surface-potential decay curves of PP (TORAY FAN BO,24μm) over a period of six months exhibit a drop of only 6% for quenched samples compared to 25% for nonquenched samples.

2.Heating rate before quenching

The heating rate β_1 before quenching will affect the charge-storage capability. If β_1 is fairly large, the sample will reach the melting point in a short time

(such as 2-5 min.). Due to the slowness of the relaxation, the quenching starts before all the molecular chains randomize and before the grains of the primary structure fully dissociate. Therefore, the modification of the material is incomplete. This is evident from a comparison of the dashed line in Fig.1 with the curves in Fig.3.

3.Depth dependence of hardening

For successful quenching, the cooling rate of the sample on immersion must be fast enough to ensure that no observable property variation happens during cooling [2]. For polymer foils, the thermal conductivity k affects the hardenability markedly. The thermal transfer equation [3] is given by

$$C_p \partial^2 T/\partial t^2 = k \cdot \Delta T + q^*, \qquad (1)$$

where q^* is the heat loss per unit area. For thin foils, thermal transfer occurs only along the thickness direction of the sample; furthermore we suppose that the heat profile does not change with time. Then eq.(1) yields

$$Q = Aq^* = -kA\partial^2 T/\partial x^2 . \qquad (2)$$

Obviously, thermal transfer by the sample itself is proportional to k. Because the thermal conductivity of Teflon FEP is quite low (k=0.25J/msK, which is only 1% of that of most metals), it is difficult to reduce its temperature in the bath within a short time. This could prevent the quenched sample from freezing in the high temperature state. In addition, cooling of the sample is faster at the surface than in the bulk. Thus, internal stress, which comprises thermal stress and tissue stress, is produced by the non-uniform cooling and leads to stretching of the molecular chains [4,5]. While this benefits crystal growth and segment joining, it is harmful for the charge stability. After quenching, the samples are charged by means of electron beams with different beam energies, but with the same total injected charge. From Fig.4, we find that t[illegible]bility is different for charge layers located at [illegible]ent depths: The stability of corona-charged samples is the best; the larger the distance of the charge from the surface, the worse is the charge stability. This result supports the above interpretation.

4.Choice of the optimal quenching temperature
There is a significant influence of temperature on the polymer crystal. If the quenching temperature would be near T_m, the crystal nuclei would be fewer and less stable [6]. We expect that a larger number of smaller grains is obtained by means of quenching. From our experiments and from published results [6], it follows that the quenching temperature should be near T_g. After having done many experiments at various quenching temperatures and by comparing the results of TSD spectra, the best quenching temperature is found. The chosen quenching temperatures for PP and PETP are -7°C (T_g=-35/+26°C) and 95°C (T_g=69/77°C), respectively, which are closer to T_g, but farther from T_m.

CONCLUSION

If we suitably prolong the quenching time, decrease the heating rate prior to quenching, and choose the proper quenching temperature for the respective material, the stability of electrets charged by corona or low-energy electron beams can be improved significantly.

ACKNOWLEDGMENTS

The author is grateful to Prof.Dr.G.M.Sessler and Dr.R.Gerhard-Multhaupt for stimulating discussions and valuable comments on the manuscript and to Mr.H.Eisenhauer for sample preparation. Thanks are also due to the Stiftung Volkswagenwerk for financial support.

REFERENCES AND FOOTNOTE

1. G.M.Sessler, Electrets, 2nd ed. (Springer 1987).
2. D.P.Birnie,III,W.D.Kingery,J.Mater.Sci.20,2193(1985).
3. Carslaw,H.S.andJ.C.Jaeger, Conduction of Heat in Solids, 2nd ed. (Oxford Univ.Press 1959).
4. A.Aref-Azar et al., Polymer(GB) 24, 1245-51 (1983).
5. S.Lee,H.Miyaji and P.H.Geil, J.Macromol.Sci-Phys. B22, 489-496 (1983).
6. Science and Technology University of China, The Structure and Properties of Polymers (Science Publishing Company Beijing 1981), p122.
*Permanent address

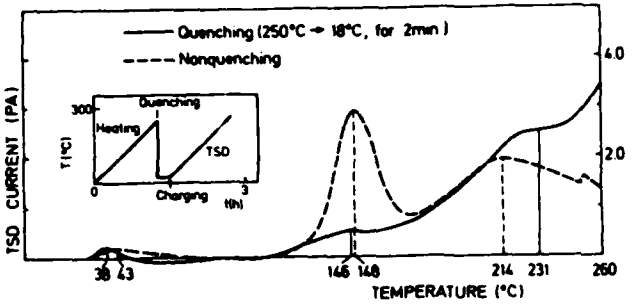

Fig.1. Current TSD of FEP foils before quenching as compared with that after quenching

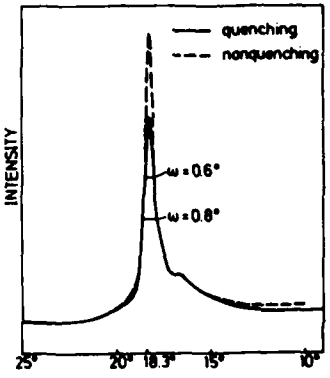

Fig.2. X-ray diffraction curves of Teflon FEP before and after quenching

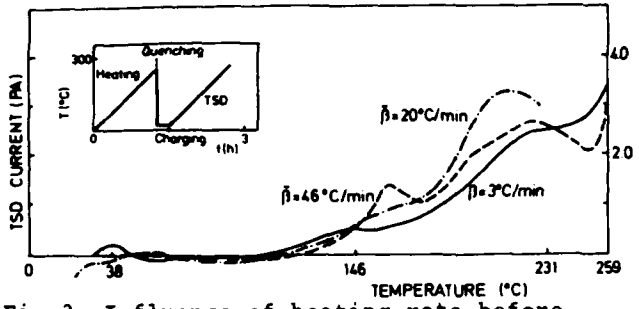

Fig.3. Influence of heating rate before quenching on current TSD of FEP

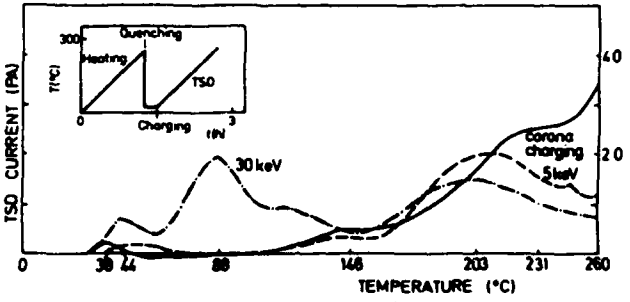

Fig.4.Current TSD of FEP foils after quenching by corona charging as compared with that of different electro-beam energy

ALUMINIUM POROUS OXIDE FOR ELECTRETS

V.I. Shershulsky and D.V. Yakovlev

Minsk Radioengineering Institute, Minsk, USSR.

ABSTRACT

The progress in functional electronics needs the development of new electret materials exhibiting high electret characteristics and compatibility with electronic technology. A couple anodic oxide - polymer is perspective electret material. The proper choice of electrolyte composition and anodization regime yields porous oxide films with different geometry of regular pores. It is shown that pore growth is a result of etching and oxidation concurrence. Pore parameters and their change owing to regime switching are computer simulated and incorporated space charge influence to leakage current is estimated.

ELECTRET AIR FILTER USED FOR GETTING RID OF BACTERIA

Shi Linsheng Chen Baoji Wang Yude

Pohl-Institute of Solid State Phsics, Tongji University, Shanghai, China

ABSTRACT

In this paper we report some experimental results of bacteria filtering through an electret air filter which has the laminated structure made from a plurality of electret pp film spaced by aluminium foil from each other. We measure the bacteria filtering efficiency of the electret air filter in natural environment. We also explain its mechanism and discusse the possibility of its applications on pharmaceutical factory and bacteria-free room.

INTRODUCTION

Recently, the receach and applications of faberic electret air filter have got in many success(1). But it has a disadvantage of high flow resistance. The present work was begun to stady an electret air filter which has the laminated structure made from a plurality of electret pp film spaced by corrugated aluminium foil from each other. In fact, it is a kind of Electrostatic precipitator without source. The flow resistance of this filter is very small($2\sim3mmH_2O$). Its filtering efficiency for powder or dust of the order of μm magnitude is greater than 90%(2). It belongs to secondary or superior air filter.

Bacteria is a particle of an order of magnitude from submicrometer to micrometer, its surface always charges negatively. It floats in air as dust particle. We use this electret air filter for getting rid of floating

CH2593-2/ 88/ 0000-0549$01.00 Copyright 1988 IEEE

bacteria in air and get a satisiactory result. This electret filter has a low flow resistance and without power supply, therefore it has a vast prospects of application.

PREPARATION OF ELECTRET AIR FILTER

Owing to the electical stability of pp film in high humidity(RH=95%)[4], we take it as a charging material of electret air filter. The pp film of 15μm thick was cut into a long strip of 30mm width, and a strip aluminium of 0.12mm thick and 30mm width was rolled in rippled surface. The pp film will be charged through a grid controlling corona charging in moving state, when this electret filter was winding process. The diagram of preparation is shown in figure 1.(3)

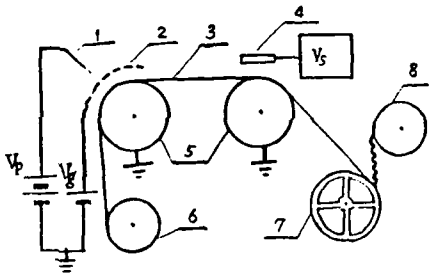

Figure 1. sketch of charging and winding of of electret air filter

1-discharging needle, 2-grid, 3-pp film, 4- probe of surface potentiometer, 5-grounding metal wheel, 6-wheel for pp film supply, 7-electret air filter, 8-wheel for aluminium riple strip supply

The pp film is charged positively. As bacteria usually is charged negatively and the positive charging of pp film has advantage of stability(5). The charging conditions are Vc=+10kv, Vg=+1.5kv in air. The surface potential of pp film just after charged may be monitored by KAWAGUSHI S-210.

The electret filter unit is made in single element of 60mm diameter.A suitably practical electret air filter may be obtained through several element connecting in parallel or in series.

MEASUREMENT OF BACTERIA FILTERING EFFICIENCY

For measuring the bacteria filtering efficiency of electret air filter, we parallelly arrange seven electret air filter unit of diameter 6cm as a enlarged filter and put it in a air channel of diameter 20cm. The arrangement of measuring bacteria filtering eifficiency is combined with air channel,electret air filter, air-blower, bacteria culture vessel and etc, as shown schematically in figure 2.

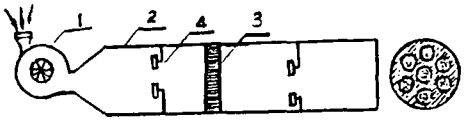

Figure 2. The arrangement of measuring bacteria filteration efficiency
1-air-blower, 2-air channel, 3-electret air filter, 4-bacteria culture vessel

We put bacteria culture vessals, from which can measure the number of bacteria, on both sides of elctret air filter. The air-blower can produce the air blast of 1m/sec. if there are any bacterias adsorpte on the culture medium in vessel. after culturing for 48 hours we can read the number of bacterias adsorpted on it. Compairing with the number of bacterias of both sides. We can get the bacteria filtering efficiency η:

$$\eta = \frac{n_1 - n_2}{n_1} \quad 100\%$$

where n_1 is the number of bacterias befor filteration, n_2 the number of bacterias after filteration .The result of this measurement is show in the following table

(measuring in ordinany room, at room temperature.measuring time is 25 min)

times	n1	n2	n(%)
1	98	9	91
2	74	3	96
3	41	2	95

DISCUSSION

There is a very high electric field E between pp film and corrugated aluminium strip of electret air filter. According the Deutsch's formular

$$\eta = 1 - \exp (- vf)$$

where η is the filtering efficiency, v is moving speed of dust partical, we explain the relation between the efficiency of air filter and other parameters qualitatively. If the air filter is rectangular (l in length, b in width and h in high), we have

$$f = \frac{l}{hu}$$

where u is the air flowing speed.
Therefore

$$\eta = 1 - \exp (- v \frac{l}{hu})$$

If the length of electret air filter increases, the η will increase too. however, we find there isn't notable increasing of efficiency but the tliwing resistance is linerally increasing if the length of electret air filter l>30mm. If the partical carried charge (eg.

bacteria), it's more easy to be captured when it goes through the electret air filter because there is a very high electric field in it, so the filteration efficiency is much better for these kind partical.

In summary, the electret air filter is very efficient for getting rid of bacteria because bacterias usually are carring charge. As this kind filter is a second-level filter, the efficiency will be improved if we add a thin fible air filter acting as a primary filter to erase dust and part of bacteria, then, we can develope many applications on bacteria-free room, pharmaceutical factory and food processing.

ACKNOWLEDGEMENT

This work is supported by Stiftung Volkswagenwerk. We wish also to thank Prof. Sun Xi-min

REFERENCES

1. Baumgart.H. et al, Proc. 5th Intern. Symp. Electrets, pp 772-777, Heidelberg 1985
2. Blackford D.B. et al. Proc. 5th Intern. Symp Electrets, pp 766-770, Heidelberg 1985
3. Shi Linsheng and Wang Yude, Proc. 4th. Chinese Academic Conf. on Dielectric Phys. P146, Shanghai 1987
4. Zhu shaonan(Ed.) The Application and Mordifying of Polypropylene Plastics, Chinese Light Industry Press, 1982
5. Mizutani T. et al. Japanese J.Appl. Phys. 24, 1164, 1985

TSC DUE TO POLARIZATION BY TRANSFERENCE OF SPACE CHARGE

Kimio SHINDO

Department of Physics, Faculty of Education,
Shiga University
2-5-1, Hiratsu, Otsu-shi, Shiga-ken, 520 Japan

ABSTRACT

We attempted two kinds of experiment to investigate space charge near surface of polymer electret. The one is removal of thin layer from surfaces of an electret. The electret shows far smaller TSDC after removal than before. The other one is an experiment of piled electret. A pile of three sheets of polymer film is polarized and separated into three parts. We measured TSDC of each sheet. TSDC of outer two sheets are much more than that of the middle one, showing that space charge gather near the surfaces.

1. INTRODUCTION

The mobility of space charge in a polymer increases remarkably at temperature over glass

CH2593-2/ 88/ 0000-0554$01.00 Copyright 1988 IEEE

transition point T_g. Transfered space charge makes a kind of polarization whose behavior is different from that of polarization caused by other origin such as dipole orientation.

I have observed thermally stimulated depolarization current (TSDC) at high temperature over T_g of polyethylene terephthalate (PET). A thermogram of a TSDC shows a steep peak near highest temperature whose magnitude is far greater than that of peaks below T_g, and this large peak may come from the polarization by transference of space charge.

If space charge stay near surfaces, they will be taken away by removal of thin layer from the surfaces. I tried a simple test and got expected results.

I tried another experiment of piled electret. Three sheets of polymer film are piled and sandwiched between two electrodes, and are polarized in a field. If space charge transfer near surfeces,i.e. near electrodes, then they will gather in outer sheets. This assumption is verified.

2. REMOVAL OF THIN LAYER

A disk of PET film with a diameter of 2cm and a thickness of 183micron is polarized in a field of $7.98*10^6$V/m at 150°C. We measured TSDC after removing a thin layer of about 12

micron from the bottom surface, and compared it with a ordinary TSDC. We noticed that removal of a thin layer makes remarkable reduction in TSDC. Removal from the top surface showed similar effect. Fig.1. shows an ordinary TSDC and the one after removal of thin layers from both surfaces. We can see the reduction of peak obviously.

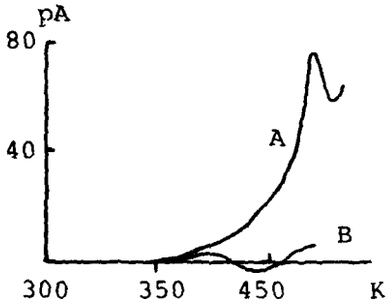

Fig.1. TSDC of PET
A: ordinary TSDC
B: TSDC after removal of thin layer

3. PILED ELECTRET

Structure of a pile is shown in Fig.2. Three sheets of polymer film are put together, with or without metal foils between them.

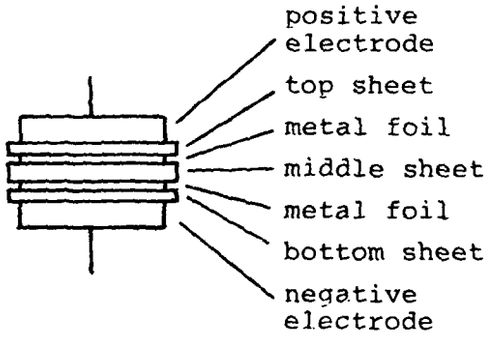

Fig.2. Structure of a pile

i) WITHOUT METAL FOIL

An example is shown here. Three PET sheets of thickness 25, 100, 25 micron are put together without metal foil. They are polarized in an electric potential 796V at 180°C. After cooling and separating into three parts, we measured TSDC of each sheet. They are shown in Fig.3. The current of top and bottom sheet are much larger than that of middle sheet at temperature over 420K. This fact suggests that charges involved in top and bottom sheet are much more than that in middle sheet.

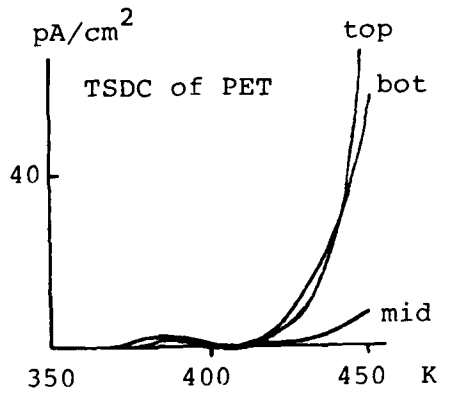

Fig.3. TSDC of each sheet polarized in a pile

ii) WITH METAL FOIL

An example with Sn foil. Three PET sheet of the same size above mentioned are put together

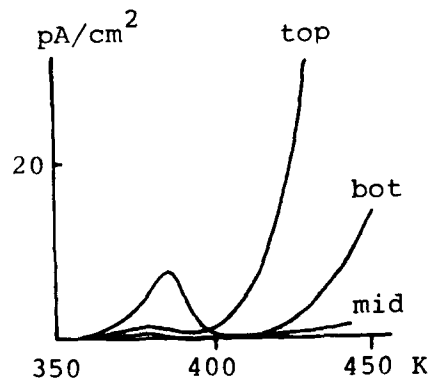

Fig.4. TSDC of each sheet polarized with Sn foils

with Sn foils between them. After polarization with the same condition they are cooled to room temperature. Their TSDC are shown in Fig.4. We notice that TSDC of top and bottom sheet rise at 400K much steeper than that of middle one. We see similar feature as in the case wothout metal foil.

We made same experiments with polypropylene (PP) and got similar results.

4. THERMALLY STIMULATED POLARIZATION CURRENT

We measured thermally stimulated polarization current (TSPC) too. We compared TSPC of pile without metal foil with TSPC's of piles with foils of various kind of metal; Sn, Al, Cu, Ag, Pt, Ni. A result by PET is shown in Fig.5. Obviously, TSPC without metal foil is larger than that with metal foils. We got similar results by PP. We speculate that the main part of carrier in polymer may not be electrons and /or holes, because they can go through metal easily. Majority of space charge may be ions.

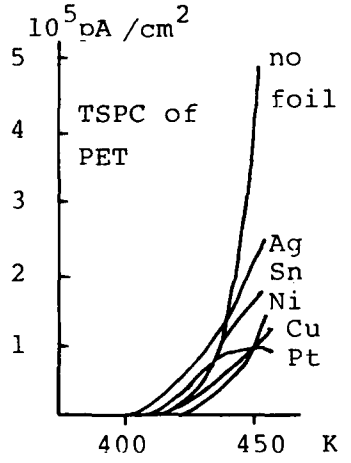

Fig.5. TSPC of pile with various foil.

THERMALLY STIMULATED CURRENTS IN POLYMERS AND DIELECTRICS

A. Mandowski and J. Swiatek

Institute of Physics, Pedagogical University, Poland.

ABSTRACT

One of the main problems in the theory of thermally stimulated currents (TSC) is to take into account retrapping effects which take place during thermal release of trapped carriers. The problem is still far from being satisfactorily solved, except a few special cases, because of mathematical complexity of the equations describing those phenomena. In this work we derived an equation in generalized Randall- Wilkins form in the case when there is only one type of charge carrier, and the whole observed current originates from space-charge carriers trapped in the sample. This involved equation was obtained for an arbitrary form of the relation $I=I(n_c)$ and for an arbitrary number of discrete trap levels. We also present a method of applying this equation to the curve fitting procedure, and discuss inverted problem - a way of calculating TSC curve when all parameters are known. Numerical calculations have been done to compare the results with Randall-Wilkins solution.

LATERAL NONHOMOGENEOUS DECAYS OF SURFACE CHARGE ON TEFLON-FEP FILMS

Sun Xi-min, Yang Ding-guo

Pohl Institute of Solid-State Physics, Tongji University, Shanghai, China

ABSTRACT

In an negatively grid-control corona charging of Teflon--FEP, we discover nonhomogoneous charge decays along lateral surface, i.e. isothermal charge decay of the central region is faster than that of the border part. Similarly, the more rapid decay of central regin also be observed on negative charging Teflon-FEP at elevated temperature. In negatively liquid-contact charging of Teflon-FEP, this phenomenon of nonhomogeneous decays also exist. We consider these phenomena mainly originate from electrons drift of various parts under different normal component of electret self-field along the lateral surface. The surface Charge density at any part during decay process may be estimated by an empirical formula.

INTRODUCTION

Teflon-FEP is a copolymer of tetrafluoroethylene and hexafluoropropylene. It has an excellent charge retention, therefore this copolymer may be often used as many electret devices. Its main behaviours are dependent upon type of charge and charging conditions[1].

The present work was begun to study decays of negatively charging Teflon-FEP of grid-control corona and liquid--contact methods.

CH2593-2/ 88/ 0000-0560$01.00 Copyright 1988 IEEE

EXPERIMENTAL PROCEDURES

Samples of Teflon-FEP-50A(Du-pont) and 12.7μm thick are metallized with aluminum on one surface and stretched firmly onto a circular ring metal clamp, the evaporated aluminium surface will be contacted with metal grounding electrode, and the free surface may be charged negatively coronacharging at room temperature or any elevated temperature (figure 1). After charging, the surface

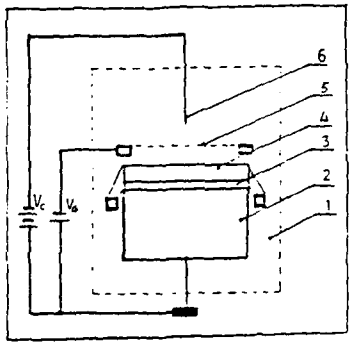

Fig 1. Sketch of corona charging: 1 - over., 2 - metal support, 3 - evaporated aluminium, 4 - Teflon FEP film, 5 - grid, 6 - needle

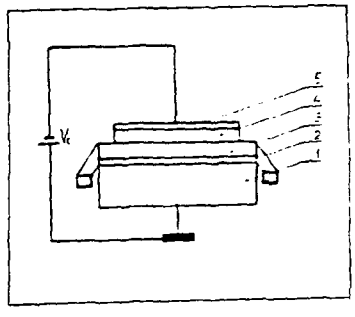

Fig 2. Sketch of liquid-contact charging:
1 -metal support, 2 -evaporated aluminium, 3. Teflon FEP film, 4 -soft wet mead, 5 -metal electrode

potential distributions will be measured by Model 244 Isoprobe with a space resolution 100um.

An experimental diagram of negatively liquid-contact method is shown as in figure 2. The sample which preparation of Teflon-FEP is like mention above will be brought on a grounding metal support. An negativel discharging flat-softwet head should be closely into contact with the upward free surface of Teflon-FEP for charging. The surface potential distributions may be measured by Model 244 isoprobe similarly.

EXPERIMENTAL RESULTS

Decaies of negatively corona charging of Teflon-FEP at

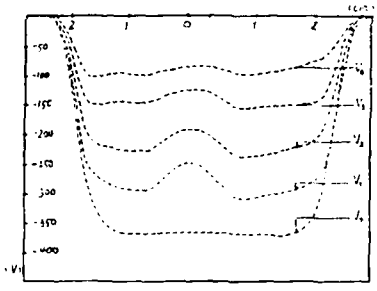

Fig 4. Isothermal decay of corona charging at elevated temperature: V_0 -initial potential, V_1, V_2, V_3, V_4 -corresponding to 30,150, [illegible] heating 1 hour progressively

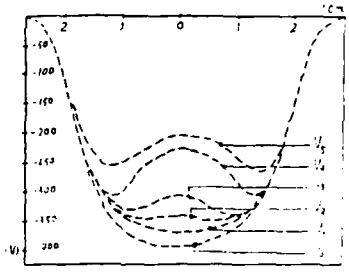

Fig 5. Isothermal decay of corona charging at room temperature: V_0-initial potential, V_1, V_2, V_3, V_4, V_5 -corresponding to surface potential after 12,17,28,60,97 days past respectively

room temperature are shown as in figure 3. We see potential decay of the central region is faster than that of border part.

Figure 4 shows central-line profiles of isothermal decay of surface potential for negatively corona charging at different elevated temperature.

For negatively liquid-contact charging of Teflon-FEP, the lateral nonhomogeneous decay which the potential of central region is rapider than that of border part are also be observed (figure 5)

DISCUSSION

Owing to the stability of charge retention of Teflon-FEP in normal conditions, the decay of negative potential of central region being faster than that of border part only be observed in a long period for several months or years.

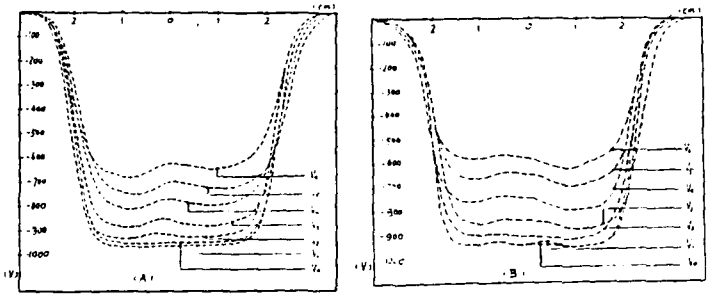

Fig 5. Isothermal decay of liquid-contact charging at elevated temperature: V_0 -initial potential, (A) $V_1, V_2, \cdots, V_6$ -potential corresponding to 60, 80, 100, 120, 140, 160°C heated 1 hour progressively. (B) potential and heating temperature of decay profiles in a similar way to (A)

According to the "principle of time-temperature equivalent effect of polymer", the phenomenon of lateral nonhomogeneous decay of surface charge (electron) would be observed in a shorter period at elevated isothermal temperature (figure 4).

In negatively liquid-contact method, a certain magnitude and uniform charge distribution may be recieved. In general, the charge retention of this method will be stabler than that of corona charging at same charging conditions. The more rapid decay of potential in the central region may also be observed at different isothermal temperature (figure 5).
For nonpolar-molecular material polymers from PE to PTFE, lateral nonhomogeneous decay perhaps may be a kind of general characteristics, when these materials were charged negatively. This characteristic should influence the feature of negative electret device used for long period.

Baum explained the reason for the central region more rapid decay of negatively corona-charged polyethylene was that only central region recieved corona light incident[2]. But this reason could not be used to explain the

similar phenomenon of lateral nonhomogeneous decay of negatively liquid-contact charged Teflon-FEP. It is possible that different rates of negatively potential decaies are due to electron drifts under different normal component of electret self-field along surface.

We suggest an empirical formula for estimating charge density at any part during isothermal decay process

$$\sigma = \sigma_0 \exp\left[-K t/(r+b)^2\right]$$

where σ_0 is initial charge density just after charging, t decay time, r distance from the centre along polymer surface, K decay constant, and b parameter. The later constant K and parameter b are dependent on the material, charging and decay conditions

AKNOWLEGLENTS

This work is supported by stiftung Volkswagenwerk. We are much indebted to professor G.M.Sessler for his help.

REFERENCES

[1] G.M.Sessler, Electrets (springer-Verlarg Berlin Heidelberg New York London Paris Tokyo,1987)

[2] E.A.Baum, T.J.Lewis and R.Toomer, J. Inys. D.Appl. Phys., Vol.10,1977.

ELECTRIFICATION AND ELECTRET EFFECT IN POLYMER FRICTION

Sviridyonok A. I., Klimovich A. F., and Guzenkov S. I.

Institute of Mechanics of Metal-Polymer Systems,
Byelorussian SSR Academy of Sciences,
246652 Gomel, USSR

ABSTRACT

A conception is advanced and supported experimentally on the common nature of the processes of electrification and electret state generation in polymers and their composites at mechanical effects, such as rubbing, which is manifested by means of electret-triboelectrification superposition, transformation of electret state, and subsequent changes in electrophysical, physicomechanical and tribological properties of polymers and composites. The mechanism of polymer electrification and electretization at rubbing conditions is discussed.

INTRODUCTION

Numerous theoretical and experimental studies evidence to a responsibility of electrical phenomena at rubbing conditions for the initiation and outcome of such events as emission, adhesion, and deformation, metal hydrogenation, tribopolymerization and transfer, mechanodestruction, wear, etc. [1-3]. Triboelectrification is the main aspect in the set of electrophysical phenomena in polymer friction [2, 4]. Electrification at rubbing conditions is a common feature occurring at all types of friction with any combination of contacting bodies. However, the role of electrification processes in polymer friction has not been identified unambiguously. The present authors carried out complex studies on polymer friction, and saw that electret state in polymers is a direct consequence of electrification [2, 5].

RESULTS AND DISCUSSION

Analyses of contact interaction of a polymer particle collective with a metallic surface in terms of the principle of closed circulation, revealed a high

CH2593-2/ 88/ 0000-0565$01.00 Copyright 1988 IEEE

level of electrification in dispersed polymers : at the speed of 20 m/s potentials can reach the value of 250 kV. The results of the investigations evidence to deep structural changes in polymers at mechanical effects, and allow an assumption that high local temperatures (1 000 K) can exist at microcontacts [5].

The data obtained on friction electrification of polycaproamide (PCA) show a close relationship between the rate of electrification and friction parameters [2]. Figure 1 representing diagrams of simultaneous recording of the electrification current and friction force, shows a correlation between $I - \tau$ and $F - \tau$ dependences. With increased periods of interaction, the friction force increases. The $I - \tau$ dependence passes through the maximum with a subsequent current inversion. The electrification analogies observed in numerous experiments with polar, nonpolar, and dispersed polymers, together with analytical treatments, showed that current inversion can be regarded as a common feature of electrification processes in polymer friction, thus evidencing to a complexity of electrification phenomenon, and supporting its adequate relation to the physical-and-chemical events in polymers [2].

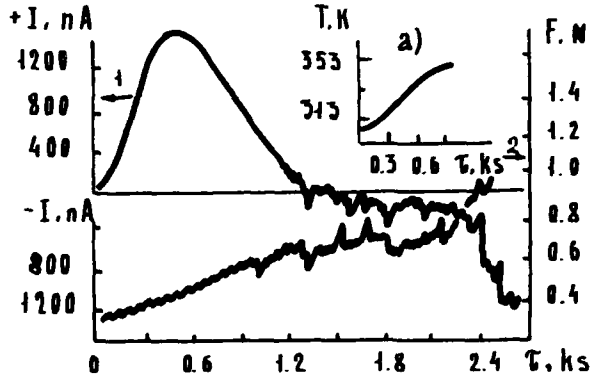

Figure 1 Kinetics of electrification current I (1) and friction force (2) recorded simultaneously for PCA – steel pairs : a, temperature variations in the metallic element during rubbing

TABLE 1

Dependence of Surface Charge Density ($-\mu C/m^2$) on Exposure Time for Mechanically Activated Dispersed Fluoroplastic [5].

Exposure conditions	Time of exposure, hours				
	5	20	40	120	200
In air	80	26	20	9	3
In desiccator	140	65	52	48	47

Electrophysical investigations showed [2 - 6] that mechanical effects on polymers lead to deep structural transformations, electrification, and initiation of electret states as well (Table 1). Analyses of interrelations between structural transformations of particles, their morphological changes, rate of electrification, and the electret state revealed a most important role of temperature in the above set of events. The electrophysical properties of the contacting materials (electron work function, presence and characteristics of surface states, permittivity and conductivity), as well as the parameters of contact interaction, electrical diagram of contact, and the environments influence significantly the electrification processes in polymer friction. One of the important aspects of the electrification effect on polymer friction and wear is that friction forces increase owing to the electrostatic interaction of the surfaces in contact [2, 3].

Investigations into the electrification identified electret states in polymers rubbed in air or in liquids, both dielectrics and electrolytes [7]. Two features in electrification have been found to influence the polymer friction and wear : i) supermolecular structure transformations and ii) electret triboelectrification superposition [2, 8]. It was discovered that electret fillers in polymers affect the triboelectret properties of composites. The field generated during triboelectrification can be weakened or strengthened depending on the direction of the field intensity vector of the electret fillers, i. e., the principle of

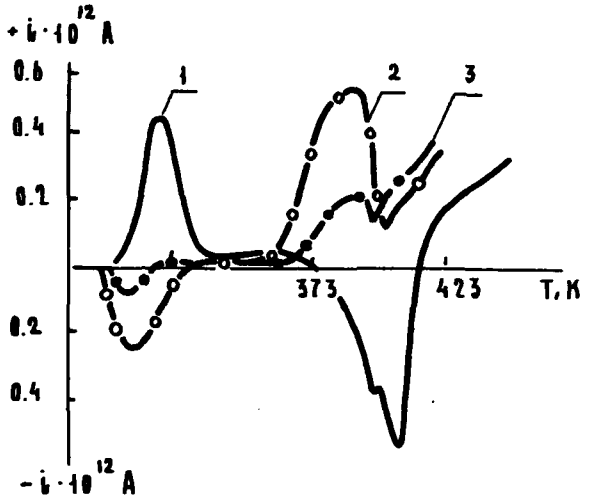

Figure 2 TSC curves for polyethylene coatings containing 75 % wt dispersed fluoroplastic: 1, initial coating; 2, 3, rubbed coating ; 2, untreated filler; 1, 3, mechanically activated filler

electret triboelectrification superposition can be provided, Figure 2. The electret state generated in a polymer can change physicomechanical properties, decrease friction forces (in run-in period by 10 - 30 %), and wear rate by 1.5 - 3 times [9]

The available literature, and our experimental findings allow a suggestion of a mechanism of polymer electrification and electretization at mechanical effects, based on the applicability of the fundamental laws of the electrostatic theory of adhesion. Application of the electron theory of unordered systems and surface states provides deeper understanding of the suggested mechanism of electrification, particularly existence of surface states and their filling with injected charge carriers on contact separation; electric charge appears on polymer surfaces. Under

the effect of surface charge field, the charge gets redistributed within the near-surface region; spat ial charge area (SCA) and a double electric layer are formed, which charge density and structure depend on surface state characteristics. During electrification, and surface charge and SCA formation, poly - meric materials get polarized in the field of the latter two, and as a result, electret state is formed, which parameters depend on the free injected charge carriers, and polarization.

REFERENCES

[1] V. A. Bely, A. I. Sviridyonok, M. I. Petrokovets, and V. G. Savkin, Friction and Wear of Polymer Based Materials, Nauka i tekhnika, Minsk, 1976.

[2] A. F. Klimovich and V. S. Mironov, "Electric Events in Polymer Friction", Soviet Friction and Wear J., vol. 6, No. 5, pp. 796 - 806; No. 6, pp. 1026 - 1033, 1985.

[3] B. V. Deriaguin, N. A. Krotova, and V. P. Smilga, Adhesion of Solids, Nauka, Moscow, 1973.

[4] J. Lowell and A. C. Rose-Innes, "Contact Electrification", Advances in Physics, vol. 29, No. 6, pp. 947 - 1023, 1980.

[5] A. F. Klimovich, "Study of Contact Electrification in Polymers", DAN BSSR (USSR), vol. 24, No. 3, pp. 238 - 241, 1980.

[6] Electrets, Edited by G. M. Sessler, Springer - Verlag, Berlin-Heidelberg-New York, 1980.

[7] A. F. Klimovich, V. S. Mironov, and S. I. Guzenkov, "On the Electret Effect During Rubbing of Polymers in Liquids", DAN BSSR (USSR), vol. 30, No. 6, pp. 517 - 520, 1986.

[8] S. I. Guzenkov, Yu. V. Gromyko, and A. F. Klimovich, "On the Electret Triboelectrification Superposition During Rubbing of a Composite Containing an Electret Fil'er", Soviet Friction and Wear J., vol. 8, No. 1, pp. 136 - 140, 1987.

[9] V. S. Mironov, Yu. I. Voronezhtsev, A. F. Klimovich, and V. A. Goldade, "Effect of Electrification and Electric Polarization on Polymer Friction and Wear", in Proc. Tashkent International Friction, Wear and Lubricants Conf., 1985, vol. 5, pp.50-51

ELECTRODE EFFECT ON THERMALLY STIMULATED DISCHARGE CURRENT IN POLYSTYRENE FILMS

A.R. Tiwari

Department of Physics, S.R.T.N.E.S. College, Barman, India.

and

K.K. Saraf and A.P. Srivastava

Department of Physics, Dr. H.S. Gour Vishwavidyalaya, India.

ABSTRACT

The thermally stimulated discharge (TSD) current excited at $90^{o}c$ by 27 KV Cm^{-1} in 20μm thick polystyrene (PS) films in contact with Al, Pb, Cu, Ni, Cd, and Zn have been measured keeping the other electrode as Al. TSC parameters are observed to change with the choice of electrode material. Maximum charge is stored by PS films in contact with Cu. The observed polarization is explained in terms of detrapping of charge injected from the electrode and in terms of space charge effect.

NUMERICAL SIMULATION OF NON-ISOTHERMAL DISPERSIVE CARRIER TRANSPORT

Władysław Tomaszewicz

Laboratory of Organic Dielectrics and Semiconductors, Technical University of Gdańsk, Majakowskiego 11/12, 80-952 Gdańsk, Poland.

ABSTRACT

A Monte-Carlo study of thermally simulated currents (TSC) due to trap-controlled dispersive carrier transport in an insulator is presented. The calculations are performed for exponential and quasi-Gaussian trap distributions. The numerical results are in a good agreement with the previously derived approximate formulae, describing TSCs, and prove its usefulness in analysing the experimental data.

INTRODUCTION

In eighties, a new theory of TSC has been developed, which takes into account dispersive character of carrier transport in disordered solids [1 - 4]. In the present communication, the TSCscaused by multiple-trapping dispersive carrier transport are calculated by a Monte - Carlo method. The obtained TSC curves are compared with those calculated from the approximate formulae, derived before, which enables us to determine its accuracy.

MONTE-CARLO METHOD

The numerical procedure is similar to that used in the isothermal case, e.g. [5]. It consists in calculating repeatedly the free carrier time-of-life Δt_f, the trap depth ε_o and the trapped carrier time-of-life Δt_{tr}, according to the equations

$$\Delta t_f = -\tau_f \ln x', \qquad (1)$$

CH2593-2/ 88/ 0000-0571$01.00 Copyright 1988 IEEE

$$\int_{\varepsilon_t^o}^{\varepsilon_o} \frac{N_t'(\varepsilon)}{N_{tot}} d\varepsilon = x'' , \qquad (2)$$

$$\nu_o \int_{t_{tr}}^{t_{tr}+\Delta t_{tr}} \exp\left[-\frac{\varepsilon_o}{kT(t)}\right] dt = -\ln x''' . \qquad (3)$$

Here, τ_f is the mean free carrier time-of-life, $N_t'(\varepsilon)$ is the trap density per unit of energy ε, N_{tot} is the total trap density, ε_t^o is the depth of the shallowest traps, ν_o is the frequency factor, k is the Boltzmann constant, $T(t)$ is the sample temperature at the time t, t_{tr} is the moment of carrier capture, x', x'', x''' are the random numbers between zero and unity. The free carrier displacement and the resulting current, flowing in the external circuit, are given by $\Delta x = d \cdot \Delta t_f / \tau_o$ and $j = e/\tau_o$, where d is the sample thickness, τ_o is the free-carrier time-of-flight and e is the elementary charge. The linear heating scheme is assumed, $T(t) = T_o + \beta t$, where T_o is the initial temperature and β is the heating rate.

The calculations are carried out for exponential and quasi- Gaussian trap distributions,

$$N_t'(\varepsilon) = \frac{N_{tot}}{kT_c} \exp\left[-\frac{(\varepsilon - \varepsilon_t^o)}{kT_c}\right], \qquad (4)$$

$$N_t'(\varepsilon) = \frac{2N_{tot}(\varepsilon - \varepsilon_t^o)}{(kT_c)^2} \exp\left[-\left(\frac{\varepsilon - \varepsilon_t^o}{kT_c}\right)^2\right], \qquad (5)$$

where the characteristic temperature T_c determines the rate of trap density variation with energy. The insertion of these equations into Eq. (2) yields explicit formulae for the ε_0 energy. Eq. (3), determining the Δt_{tr} time, is solved numerically.

The above calculations are continued up to the moment of carrier transit through the sample. By repeating this procedure for a large number L of the carriers and averaging the induced current one obtains the TSC curve.

Results and Discussion

The TSC peaks, calculated numerically for the trap distributions (4) and (5) with two different values of the T_c parameter, are shown in Figs. 1 and 2, respectively (denoted by points). For comparison, the TSC curves calculated from the approximate formulae, derived in [5], are also presented (denoted by solid and dashed lines; the dashed lines represent limit formulae, valid for low / high-temperature region). The TSC intensity $I(t)$ is normalized to $I_0 = e_0/\tau_0$, where e_0 is the charge generated in the sample. The values of the parameters used in calculations are given in Table 1.

Table 1: Data sets used in calculations.

Fig.	$\tau_f \cdot \beta / T_0$	T_c/T_0	ε_t^0/kT_0	L
1 (a)	2.28×10^{-13}	5	30.0	10000
1 (b)	2.51×10^{-15}	5	30.0	500
2 (a)	5.35×10^{-12}	10	19.5	5000
2 (b)	9.90×10^{-15}	12	22.4	2500

Figs. 1-2 : $\tau_0 \cdot \beta/T_0 = 10^{-10}$; $\nu_0 \cdot T_0/\beta = 10^{15}$; $T_0 = 100K$.

In general, the agreement between numerical and analytical results seems to be quite satisfactory, though in Figs. 1(b) and 2(b) slight

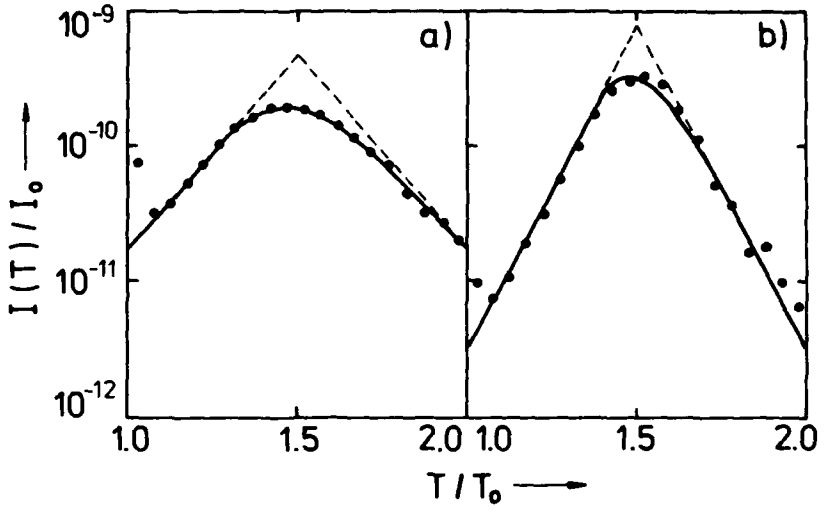

Fig.1: TSC curves for exponential trap distribution.

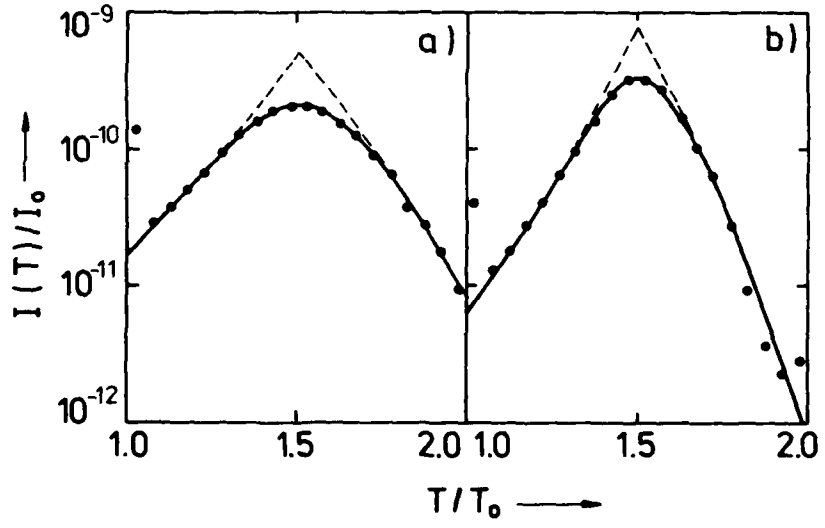

Fig.2: TSC curves for quasi-Gaussian trap distribution.

systematic deviations in the vicinity of the TSC maxima are seen. The discrepancies in the high-temperature part of the TSC curves are probably due to statistical fluctuations. It could be noted that the TSC peaks, calculated for quasi-Gaussian trap distribution, reveal much higher asymmetry than those obtained for exponential one.

In conclusion, the results obtained prove the usefulness of the formulae, derived in [5] in determining the shape of the trap distribution as well as some trap parameters from the TSC measurements.

REFERENCES

[1] M.Samoć and A.Samoć "Thermally stimulated currents with participation of two trapping levels. Extension of the model", Phys.Stat.Sol.A.Vol.57, pp.667-674, 1980.

[2] J.Plans, M.Zielinski and M.Kryszewski, "Theory of the thermally-stimulated-current transport peak. Application to a dispersive transport case", Phys. Rev. B.Vol.25, pp.5557 - 5569, 1981.

[3] A.Tomaszewicz and J.Zachym, "Dispersive carrier transport in solids with continuous trap distribution", J.Non - Cryst. Solids Vol.65, pp. 193-213, 1984.

[4] B.Schrader and M.Kryszewski, "Multiple trapping approach to the TSC drift experiment ", Phys.Stat. Sol.A.Vol.91, pp.243-253, 1985.

[5] J.T.Marshall, "A trap limited model for dispersive transport in semiconductors", Philos.Mag.Vol.36, pp. 959 - 975,1977.

EXPERIMENTAL DETERMINATION OF THE DISPERSION SPECTRUM OF ZEOLITES

Manuel Hernández Vélez
Rolando Roque-Malherbe

Instituto Superior Pedagógico "E.J.V.",
Facultad de Física, Ciudad Libertad,
Marianao, Ciudad de La Habana, Cuba.

ABSTRACT

This paper describes a device to measure complex permittivity and some results obtained using the device in the study of dielectrical properties of zeolite samples. The device is very reliable and precise. It allows for a frequency sweep from 0.03 to 100 Khz and from 0.001 to 10 Mhz. Moreover, it can calculate very small capacities and has also been used to measure the dispersion spectrum under conditions of adsorption of gases and vapours. As a result of the study, some important deductions concerning the structure and heterogeneity of zeolites have been made.

THEORY AND EXPERIMENT

The equipment designed for the experiment consists of a circuit to determine complex permittivity and a vacuum line.

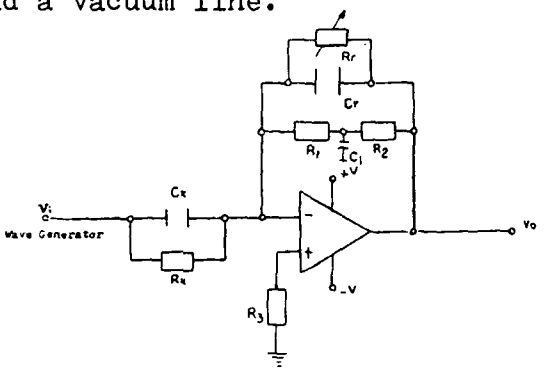

Figure 1

CH2593-2/ 88/ 0000-0576$01.00 Copyright 1988 IEEE

The transferential function of the circuit (see Fig. 1) is such that the amplitude of the output signal is independent of the frequency and is purely a function of the capacity and resistance of the material placed in a cylindrical capacitive cell, which constitutes the capacity (Cx) to be determined.

The circuit functions with a polarised high frequency response operational amplifier with resistances R1, R2, and R3. The role of C1 is to eliminate the negative feedback which R1 and R2 can introduce up to 30 Hz. Given the high value of Rx and Rr, the following working equation is derived:

$$Cx = Cr(Vo/Vi) \qquad (1)$$

To calibrate the circuit, the resonance method was used with a Phillips Standard Condenser of a capacity range between 100 and 1100 pF and a sensitivity of 0.2 pF. The reference capacity determined by this method yielded the value of:

$$Cr = 108.6 \text{ pF} \pm 10\%$$

The cylindrical cell where the sample is placed has a vacuum capacity of 1.5 pF. The real part of permittivity is determined on the basis of the empirical equation:

$$\varepsilon(w) = AVo-B \qquad (2)$$

where A is a constant which depends on the design and geometry of the system;
B is a constant which depends on the capacity of the assembly of the system.

The vacuum line is made of Pyrex and different calibrated volumes of different gases or vapours can de directly connected to it. This design allows for the study of the dielectrical spectrum under adsorption conditions.

Due to the adsorptive properties of zeolites, it was first necessary to de-gas the samples

by placing them in a vacuum at 300 degrees Celsius for 18 hours.

Once the results were obtained, a phenomenological model was designed to explain the dielectrical behaviour of the samples in the range of 2 to 15 Khz., and 100 to 200 degrees Celsius. The model is derived from the existence of a sole mechanism of polarisation -- in the case of homoionic samples -- consisting of thermically activated cationic jumps, thus obtaining for the dielectrical susceptibility the following expression:

$$X(w) = X(0)/(1\ iw/QD) \qquad (3)$$

where X(0) is the susceptibility for zero frequency of the field;
Q is a constant which depends on the sample's characteristics;
D is the auto-diffusion cationic coefficient.

RESULTS AND CONCLUSIONS

Figure 2 shows an example of the spectrum obtained for a mordenite with different percentages of adsorbed water.

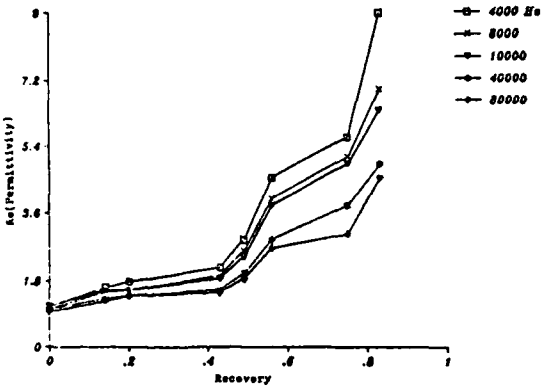

Figure 2

The greater values of ε for low frequencies indicate the presence of interfacial polarisation. The different slopes in the curves are

due to different bonding states of the water in the structure of the material. In the zone of low recovery of water, all the curves tend to have the same value which coincides with the response of the de-gassed material.

Figures 3 and 4 show the results obtained with clinoptilolite in the form of Na and Ca.

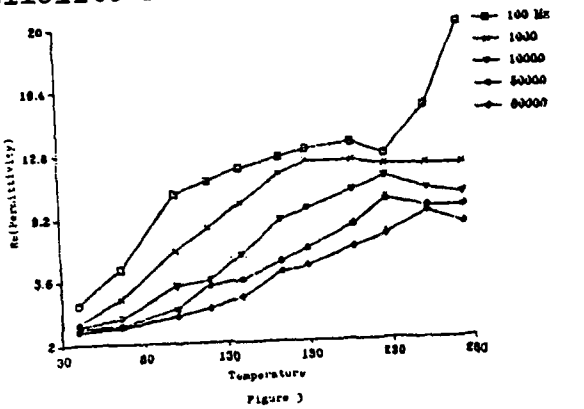

Figure 3

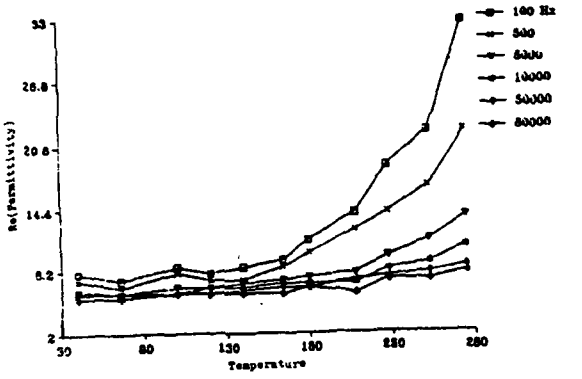

Figure 4

From the form of these curves, it is possible to identify the type of cation which predominates in the structure.

Figure 5 is an example of how the model fits the experimental data obtained with an erionite For frequencies higher than approximately 15 Khz., other mechanisms of polarisation appear which overlap with cationic migration.

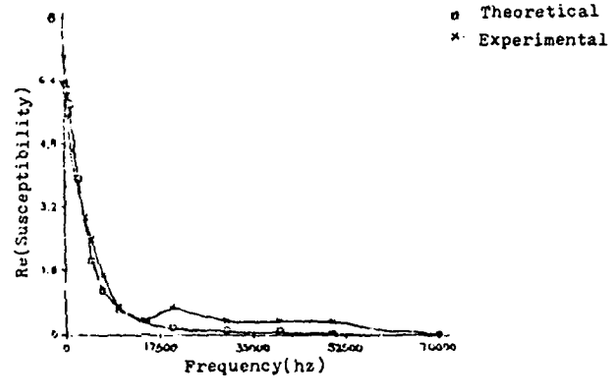

Figure 5

Finally, Tables I and II show the activation energy and the diffusion coefficients respectively, calculated on the basis of the model and the experimental data obtained.

Table I

C1Me	C2Me	C4Me	Phy	MeX	Et
21.2	26.9	31.6	24.6	24.4	28.6

Table II

Temp (°K)	Coef.	C1Me	C2Me	C4Me	Phy (x10-15)	MeX	Et (x10-13)
413	D_0	2800	15000	-	8100	-	140000
	D	7.9	9.8	-	9.9	-	2
437	D_0	4600	18000	52000	9760	-	140000
	D	13.4	11.6	8.6	10	-	5.2
453	D_0	4500	18000	63000	14000	1700	470000
	D	16	14	14	19	2.6	23
461	D_0	3000	-	-	-	1600	360000
	D	15	-	-	-	3.5	28
501	D_0	-	-	-	-	1400	520000
	D	-	-	-	-	3.9	62

These results corroborate the reliability of the equipment and the method of measurement used.

BIBLIOGRAPHY

Hernández Vélez, Manuel, PhD Thesis, CENIC, Cuba, 1987.

Roque-Malherbe, R. et.al, J. Thermal Analysis 31, 41, 1986.

Roque-Malherbe, R., PhD Thesis, Mosocow, 1978.

DIELECTRIC EFFECTS OF THE TUNNEL MECHANISM OF RELAXATION

V. Veksler and Y. Orlova

Department of Physics, Polytechnical Institute of Karaganda, Karaganda, USSR.

ABSTRACT

Dielectric characteristics of crystals are calculated with quasiclassical approximation for weak fields. The calculation is carried out on the basis of the developed theory of dielectric relaxation with complete consideration of relaxator quantum behaviour. The results of complex dielectric susceptibility calculated for rectangular and parabolic barriers satisfactorily agree with experimental data.

MICROMACHINING OF ELECTRET MATERIALS, ADVANTAGES AND POSSIBILITIES

J.A. Voorthuyzen and P. Bergveld

Twente University, P.O. Box 217, 7500 AE Enschede
The Netherlands

ABSTRACT

In this paper we describe a process for the micromachining of organic electret materials like Teflon-FEP. We have used photolithography and plasma etching, by which electrets can be etched selectively.

The advantages of, in such a way micromachined electrets are numerous. Miniature sensors like microphones and pressure sensors, containig local areas with Teflon, have been realized in our laboratories. The process can also be used for electret research. An example is the overall reduction of electret film thickness, by which we have determined the average penetration depth of accelerated electrons in Teflon-FEP.

INTRODUCTION

The application of carbon-fluor polymers for electrets is well known. Teflon-FEP has a resistivity of 10^{21} Ωcm and a reported charge-decay time of more than 10 years [1]. The use of Teflon-PTFE for electret and piezoelectric applications is also well known.

The electret properties of such polymers appear to depend on the film thickness. Useful values, and commercially available are 12.5 and 25 μm [1]. In many applications the thickness of the foil and the size of the structures to be realized are not very critical.

However, in the Biosensor Research Group of Twente University we are considering the application of Teflon foils in the development of microtransducers with submillimeter dimensions [2]-[6]. In that case the lateral dimensions of the foil as well as its thickness are very important and should be controlled in a well-defined way.

A very useful tool in the realization of microsensors is photolithography. This technique enables us to pattern thin films in many different profiles. The process consists of several steps, as schematically drawn in figure 1 and described below.

CH2593-2/ 88/ 0000-0582$01.00 Copyright 1988 IEEE

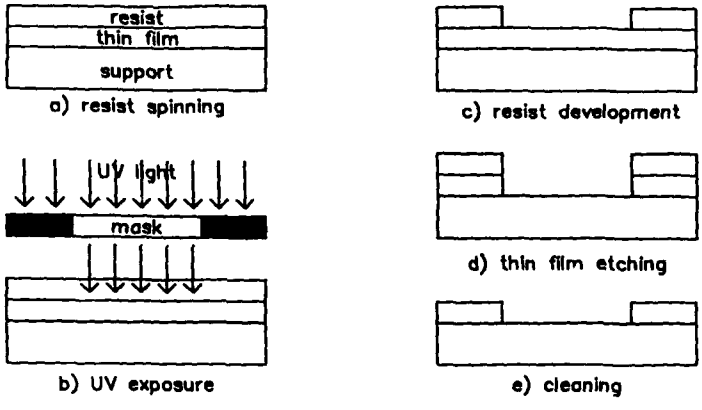

Figure 1: consecutive steps in photolithography.

PHOTOLITHOGRAPHY

The film, deposited on a support (usually a silicon wafer) is spin-coated with a 2-3 μm thick layer of photoresist. The resist is pre-polymerized during 20 minutes at 90 °C. The wafer is positioned under a mask and then exposed to UV-light, causing exposed parts of the resist to depolymerize (for so-called positive resist) and non-exposed parts to remain unchanged. Then the wafer is developed and the UV-radiated resist is solved. The wafer is post-baked to complete polymerization and then placed in an etching liquid or gas, specific for the material of the thin film. Finally the resist layer itself is removed and the locally etched wafer is cleaned.

ETCHING OF CARBON-FLUOR POLYMERS

The use of wet chemical etchants for photolithography is rather cheap and easy. For many materials selective etchants are known.

However, for carbon-fluor polymers such etchants are not known. In literature the use of a sodium dispersion suspended in naphtalene has been reported for the etching of Teflon, but it appears only to remove fluorine atoms from the surface, facilitating its bonding to other materials, and not to etch with a reasonable speed [7].

A quite different possibility is to use a plasma.

Generally a plasma is created by applying a high voltage between two electrodes in a vacuum chamber in which a certain gas is injected. For several materials, like silicon and silicon dioxide, it has been found that plasma's from CCl_4 and CH_3F respectively can be used for the selectively plasma etching of these materials. It has also been found that an O_2 plasma can be used for the plasma etching of Teflon [8].

In a plasma different etching mechanisms may be active, depending on the processing parameters like power-density, gas flow and substrate temperature. The etching characteristics, like selectivity (the preferential etching of one material) and anisotropy (the etching speed lateral to the substrate differs from that in perpendicular direction) for those mechanisms are quite different:

1) Physical etching:

In the plasma, ions are created and accelerated in the applied electric field. They strike the surface of the thin film which will be damaged and is thus etched. Due to the acceleration of ions in one direction it is anisotropic, causing rather perpendicular etched profiles if a patterned masking layer is used. However, this mechanism is not very selective, causing that layers of different materials are etched with comparable speed.

2) Chemical etching:

In the plasma also radicals of the gas are formed which may chemically react and have a preferential etching behaviour for one specific material. The transport of radicals in the plasma is not determined by the applied electric field, and thus will result in isotropic etching causing considerable underetching.

3) Physically enhanced chemical etching:

A combination of both processes may of course also occur. The chemical etching with radicals may be enhanced by ion bombardment. It will result in more underetching than physical etching, but is also more selective. The exact properties depend on the relative influence of both mechanisms on the etching characteristics.

EXPERIMENTAL

We have investigated the etching characteristics of Teflon FEP in an oxygen plasma in a barrel reactor and a plasma-etcher.

In a barrel reactor the applied electric field is parallel to the thin film surface and in a plasma etcher perpendicular to it. This means that in a barrel reactor the etching will be of chemical origin, while in a plasma etcher

all mechanisms mentioned above may occur.

The etching of Teflon in the barrel reactor appeared to be negligibe, although in the same reactor layers of resist have been etched favourably with considerable speed (about 0.1-0.2 μm/min.). In the plasma-etcher Teflon has been etched with a speed of about 0.15-0.30 μm/min.), which implies an overall etching time of about 80-40 min for 12.5 μm foils. The underetching appeared to be less than the intial thickness of the Teflon layer. The etching speed can be controlled by the power-density. In general it may be attractive to use the highest etching speed as possible. However, we have found that in that case a residual layer of unknown composition is formed, that can not be removed. Using an etching speed of 0.15 μm/min. this effect was not observed.

To pattern a Teflon layer a mask is required. In this case photoresist could not be used, because it is also etched in an O_2 plasma with at least the same speed as Teflon.We have found that a 0.2 μm thick layer of aluminium, deposited by evaporation and patterned by photolithography can be used succesfully. It will be clear that after the Teflon etching process, the aluminium mask has to be removed.

Considering the rather high selectivity of the etch-process between Teflon and aluminium, the observed under-etching and the low etching speed in a barrel reactor, we conclude that the etching mechanism of Teflon in an oxygen plasma is physically enhanced chemical etching.

OTHER APPLICATIONS

We have described a process that enables to shape Teflon layers for use in microsensors e.g. for blood pressure and acoustic pressure, as described elsewhere [2]-[6].

The same process can also be used for determining the average penetration depth of electron beams in flat Teflon samples. We have realized Teflon samples on a conductive support with different thicknesses by changing the etch-time. The thickness has been measured by determining the weight loss after etching. In all samples the same amount of electric charge has been injected by a SEM. This implies that the surface potential linearly depends on the electret thickness. Plotting the surface potential (as measured by a Monroe Probe) of the various electrets versus the electret thickness, the intersection with the x-axis yields the average penetration depth, as shown in figure 2. The acceleration voltage was 15 kV. We observe an average penetration depth of 2.5 μm, which corresponds rather well to the value reported elsewhere [1].

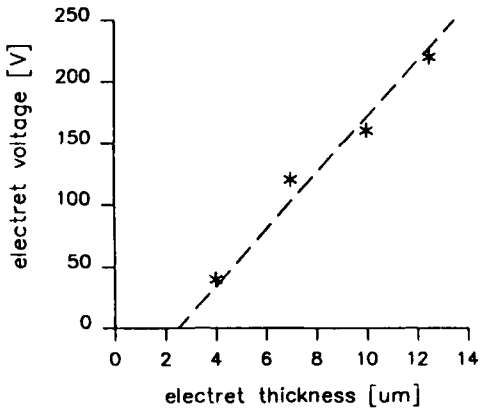

Figure 2: measured electret surface potential as a fucntion of electret thickness.

REFERENCES

[1] G.M. Sessler, "Topics in applied physics, vol. 33; Electrets", Springer-Verlag, Berlin, 1980.
[2] J.A. Voorthuyzen and P. Bergveld, "Theoretical considerations in the design of integrated semiconductor sensors applying electrets", IEEE Trans. Electron Dev., vol. ED-32, no. 7, pp. 1185-1190, July 1985.
[3] A.J. Sprenkels, J.A. Voorthuyzen and P. Bergveld, "A theoretical analysis of the electret air-gap field effect structure for sensor application", Sensors and Actuators, vol. 9, pp. 59-72, 1986.
[4] J.A. Voorthuyzen, "The PRESSFET, an integrated electret-MOSFET structure for application as a catheter-tip blood pressure sensor", Thesis, Twente University, 1986.
[5] A.J. Sprenkels, "A silicon subminiature electret microphone ", Thesis, Twente University, 1988.
[6] A.J. Sprenkels and P. Bergveld, "The use of silicon technology for an electret microphone construction", This proceedings.
[7] S.J. Updike, M.C. Shults and M. Busby, "Continuous glucose monitor based on an immobilized enzyme electrode detector", J. Lab. Clin. Med., vol. 93, no. 4, pp. 518-527, 1979.
[8] L.A. Perderson, "Structural composition of polymers relative to their plasma etch characteristics", J. Electrochem. Soc., vol. 129, no. 1, pp. 205-208, Jan. 1982.

AN ELECTRET-BASED PRESSURE SENSITIVE MOS TRANSISTOR

J.A. Voorthuyzen and P. Bergveld

Twente University, P.O. Box 217, 7500 AE Enschede
The Netherlands

ABSTRACT

The operation of the Metal Oxide Semiconductor Field Effect Transistor (MOSFET) is based on the fact that the lateral conductivity of silicon at the silicon dioxide-silicon interface strongly depends on the transverse electric field in the oxide. Adding a small air-filled spacer between metal gate and oxide, and applying a voltage across the insulator on top of the silicon, the lateral conductivity can become pressure sensitive.

The generation of the electric field in the insulator can however also be provided by means of an electret. In this paper the integrated Electret-MOSFET based pressure sensor is presented with respect to its theory, realization and performance.

THEORY

The MOS transistor has appeared to be a useful electronic component for the realization of small solid-state chemical and biochemical sensors. The purpose of this work was to investigate the application of the MOSFET as a pressure sensitive device [1], [2].

The MOSFET, as drawn in figure 1, consists of two heavily phosphorus doped silicon regions (called the source and drain) in a lightly boron doped silicon substrate (called the bulk). The electric conductivity in the source and drain is determined by electrons and in the bulk by holes. As long as no electrons are present in the bulk no current can flow between source and drain. Applying however a positive voltage to the gate with respect to the bulk a negative surface charge and thus a conductive path at the silicon-silicon dioxide interface is created.

Satisfying several conditions it appears that the current I from drain to source can be written as:

CH2593-2/ 88/ 0000-0587$01.00 Copyright 1988 IEEE

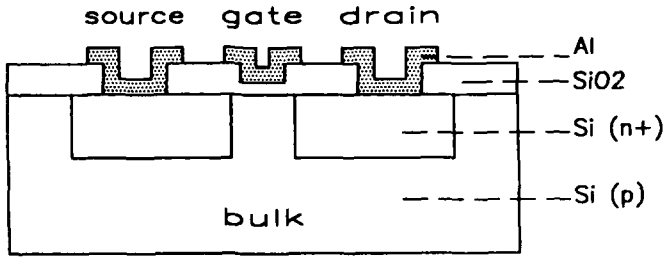

Figure 1: Cross section of the MOS transistor.

$$I = K\,C_i\,((V_{gs}-V_t)V_{ds}-0.5V_{ds}^2) \qquad \text{if } V_{ds} <= V_{gs} \qquad (1)$$

$$I = K\,C_i\,(V_{gs}-V_t)^2/2 \qquad \text{if } V_{ds} >= V_{gs} \qquad (2)$$

with K a constant, C_i the capacitance per unit area of the insulator between gate and silicon, V_{gs} the voltage between gate and source and V_{ds} the voltage between source and drain. V_t is the threshold voltage, which is the required minimum value of V_{gs} to realize a conductive path between source and drain.

The threshold voltage depends on the value of the capacitance C_i as follows:

$$V_t = V_o - Q_i/C_i \qquad (3)$$

with V_o a voltage which in our case is approximately equal to - 0.3 V and Q_i the fixed charge present at the silicon-silicon dioxide interface.

The insulator capacitance C_i is inversely proportional to the insulator thickness. In figure 2 some theoretical curves are presented of the current as a function of the oxide thickness, with the gate-source voltage as a parameter.

Adding a small air-filled spacer between gate and insulator and exposing the top side of this structure to the pressure to be measured we obtain a pressure dependent

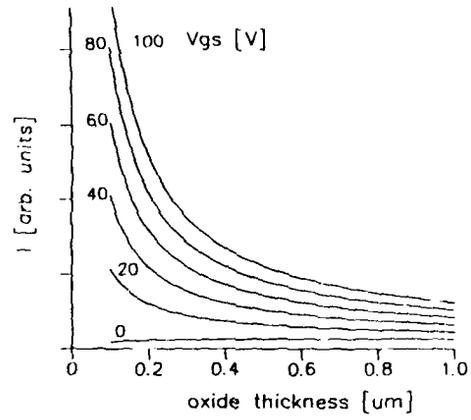

Figure 2: Theoretical behaviour of the MOSFET with variable insulator thickness.

insulator thickness (air is also an insulator), and thus a pressure sensitive MOSFET.

Considering figure 2 we observe that the sensitivity, defined as the current change to insulator thickness variations, increases almost linear with increasing V_{gs}.

The use of large, externally applied voltages is however not always practicle, and therefore we have decided to incorporate an electret with a considerable charge density.

Due to the fact that the long term stability of Teflon FEP is well known, we have used this material, and developed a technique to attach foils to a silicon wafer. In the theory we can account for an electret in different ways, as described elsewhere [2], [3]. A possibility is to consider the electret voltage, defined as the electret charge divided by the electret capacitance, to be in series with the gate voltage. Due to the fact that Teflon electrets can be charged up to 300 V, it will be clear that we obtain a pressure sensor with high sensitivity.

SENSOR FABRICATION

The sensors are fabricated by integrated circuit and thin film technologies. The sensor realization is rather complex and requires at least nine photolithography steps. The most important are described briefly.

Using the standard NMOS process of the Sensors and Actuators Laboratory of Twente University, in each 2 inch

silicon wafer 300 MOSFET's are realized.

Holes through the wafer (designed as glue passage for diaphragm attachment and air duct to the air gap) nearby each MOSFET are realized by means of anisotropic silicon etching.

Teflon FEP is deposited on the whole wafer by a heat-sealing technique and afterwards patterned by a plasma-etch process [4]. This patterning is required for contacting the source, bulk and drain area's.

The Teflon is charged in vacuum by a SEM and controlled by measuring in the vacuum chamber the charge induced at the back of the silicon wafer. Knowing the radiated area we also know the charge density of the electret. We have used a value of -30 nC/cm·cm.

Finally an 8 μm aluminum diaphragm is mounted on top of the structure and glue-bonded to it via holes around the sensor. A cross section is drawn in figure 3.

EXPERIMENTAL

Using reasonable values for all parameters the pressure sensitivity of sensors with outer dimensions of 1mm * 2mm *0.3 mm has been calculated. We found a pressure sensitivity of 0.6 μA/kPa and a zero pressure current of 3 mA for a V_{ds} of 1 V.

We have measured our sensors by using a fast pressure actuator that generates pressures between -15 and +60 kPa relative to atmospheric pressure at frequencies between 0 and 100 Hz. This pressure is exposed to the top side of the sensing diaphragm while the other side is exposed to the barometric pressure via the air duct, as drawn in figure 3.

We have measured an average pressure sensitivity of about 0.2 μA/kPa in the pressure range between -15 and +60 kPa. This is three times lower than the calculated value and might be due to a smaller deflection of the diaphragm.

The linearity of these sensors is good, but they display a rather large temperature sensitivity of about 10 μA/°C, which implies that a temperature change of 1 °C corresponds to a pressure of 50 kPa. It will be clear that this temperature sensitivity has to be reduced by adding compensating electronic circuitry to the sensor.

CONCLUSIONS

Comparing the sensitivity of the electret-MOSFET pressure sensor and the piezoresistive pressure sensor it appears that the sensitivity of the first is at least ten times higher. Its

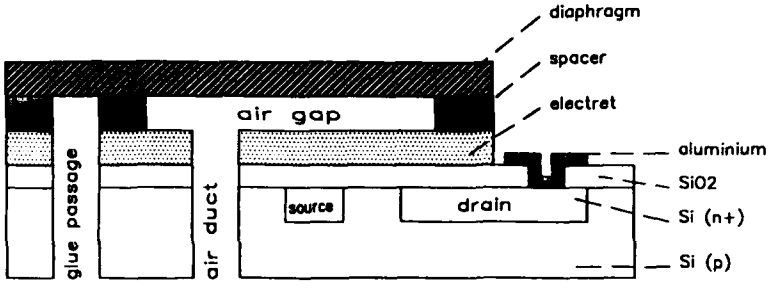

Fig. 3: Cross section of the electret MOSFET pressure sensor.

temperature sensitivity is however much larger.

The introduction of Teflon in MOSFET's is rather complex. For instance: after Teflon deposition no high temperature processing is allowed to avoid its decomposition. We discovered however that silicon dioxide can also be used as electret. This is very interesting, because it reduces the complexity of the sensor fabrication. Due to the fact that silicon dioxide electrets can be much thinner than Teflon electrets the use of silicon dioxide may yield sensors with increased sensitivity [5].

REFERENCES

[1] P. Bergveld, " The impact of MOSFET-based sensors", Sensors and Actuators, vol. 8, pp. 109-127, 1985.

[2] J.A. Voorthuyzen, "The PRESSFET, an integrated electret-MOSFET structure for application as a catheter-tip blood pressure sensor", Thesis, Twente University, 1986.

[3] A.J. Sprenkels, J.A. Voorthuyzen and P. Bergveld, " A theoretical analysis of the electret air-gap field-effect structure for sensor application", Sensors and Actuators, vol. 9, pp 59-72, 1986.

[4] J.A. Voorthuyzen and P. Bergveld, " Micromachining of electret materials, advances and possibilities", this proceeding

[5] A.J. Sprenkels, "A silicon subminiature electret microphone ", Thesis, Twente University, 1988.

MICA ELECTRETS

I.I. Inculet, R.M. Quigley and A. Garg

Applied Electrostatics Research Centre, Faculty of Engineering Science, The University of Western Ontario, Canada.

ABSTRACT

Currently electrets are manufactured using synthetic materials such as TFE, FEP, PE, PF_2V, PCV etc. The authors have attempted to investigate the possibilities of manufacturing electrets from phillosilicates which are a naturally occurring group of minerals. Such minerals are known to have large net negative charges within their crystalline structure, which under certain circumstances may express themselves as surface charges. Preliminary experiments with mica materials have shown considerable promise. The paper will cover the method used to manufacture the mica electrets, the surface charge densities which were obtained, and the expected life of such electrets.

THE USE OF SILICON TECHNOLOGY FOR AN ELECTRET MICROPHONE CONSTRUCTION

A.J. Sprenkels* and P. Bergveld+

+Twente University, P.O.Box 217,
7500 AE, Enschede, The Netherlands
*Twente Technology Transfer, P.O.Box 545,
7500 AM, Enschede, The Netherlands

ABSTRACT

We present a subminiature electret microphone which has been realized in silicon using wafer processing techniques. The microphone consists of two conducting plates which form a capacitor. The lower plate (backplate) is rigid and fabricated in silicon. The upper plate (diaphragm) consists of a 6 μm thick metallized Mylar foil. In the air cavity between both plates a 1 μm thick silicon dioxide electret is present.

The fabrication process, such as the construction of the silicon backplate, the realization of the electret and the diaphragm attachment are described.

The microphones measure 3 * 3 * 0.3 mm and show a sensitivity of 1.4 mV/μbar and a frequency response within ± 1 dB up to 15 kHz.

INTRODUCTION

Up to now electret microphones are manufactured using conventional construction techniques. Much of the processing is performed manually, which is very labour intensive. Moreover, with these techniques the limits of miniaturization have almost been reached. The application of photolithographic processes and micro-machining for the construction of three dimensional sensor structures is well established nowadays. However, the use of these techniques for the realization of a subminiature microphone is relatively new [1]. For example the microphone in figure 1 includes a 20 μm deep air-gap space, a number of holes (A) to provide the necessary connection between the air gap and the backchamber, and a diaphragm support (S). On top of the air cavity a diaphragm with upper electrode has been fixed to the backplate by means of glue via the holes G through the backplate.

CH2593-2/ 88/ 0000-0593$01.00 Copyright 1988 IEEE

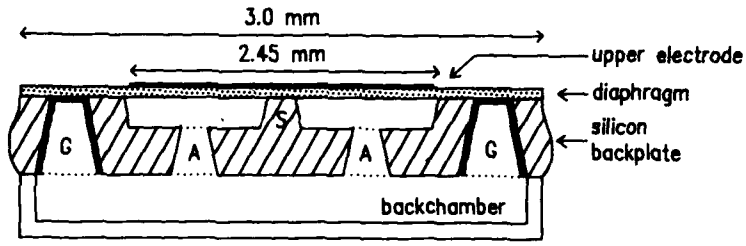

Figure 1 A schematic cross section of a silicon electret microphone.

THEORY

An electret microphone is a capacitor which is charged due to the presence of an electret between both capacitor plates. We have used silicon dioxide as the electret material.

The microphone of figure 1 may be modelled by an air gap capacitance C_a in series with an electret capacitance C_f , while the electret charge per unit area is represented as σ_f as shown in figure 2. The connected amplifier H has an input capacitance C_i and an input resistance R_i. It is of the utmost importance that the amplifier has a low input capacitance C_i and a high input resistance R_i.

Due to the electret charge an electric field exists in the air gap. Sound waves acting on the diaphragm change the air-gap space s_a and thus the air-gap capacitance C_a. Since the total electret charge is constant, a variation in the air-gap capacitance ΔC_a is accompanied by a redistribution of the charge between the upper electrode and the backplate. This charge transfer results in a voltage variation ΔV across the input resistance R_i of the connected amplifier as schematically shown in figure 2. In order to describe the microphone behaviour, the total sensitivity S, expressed in V/μbar can be described as

$$S = S_e \, S_m \, H \, H_c \, , \qquad (1)$$

where S_e is the electrical sensitivity, H is the gain of the amplifier and H_c is the capacitive attenuation by the input capacitance C_i of the amplifier. S_m is determined by the mechanical properties of the diaphragm and the air damping due to the shallow air gap and the backchamber.

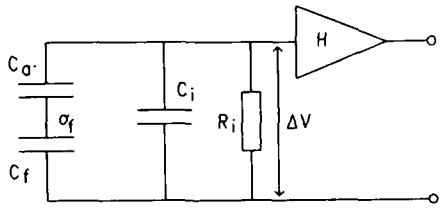

Figure 2 Schematic diagram of the electret microphone, connected to an amplifier.

For variations in the air-gap space s_a, which are fast compared to the time constant τ, (which is determined by R_i, C_a, C_f and C_i) the electrical sensitivity may be approximated by [2]:

$$S_e = \frac{\sigma_f \; s_f}{\epsilon_0(s_f + \epsilon_f s_a)} , \tag{2}$$

where s_f is the thickness and ϵ_f the relative dielectric constant of the electret material. The capacitive attenuation H_c is given by:

$$H_c = \frac{C_m}{C_m + C_i} \tag{3}$$

where

$$C_m = \frac{C_a \; C_f}{C_a + C_f} \tag{4}$$

The mechanical sensitivity S_m is determined by two restoring forces acting on the diaphragm. The first due to the mechanical properties of the diaphragm, the second due to the compression of the entire effective air volume behind the diaphragm. Assuming a zero initial tension in the diaphragm, the mechanical sensitivity of a square diaphragm with side 'a' may be approximated by:

$$S_m = \frac{-1}{\left[\frac{h^3 E(1+1.6(w/h)^2}{0.138\ a^4}\right] + \left[\frac{P_0}{s_0}\right]} , \tag{5}$$

where h is the thickness and E the Young modulus of the diaphragm material, w is the center deflection of the

diaphragm, P_0 is the atmospheric pressure and s_0 is the effective thickness of the backchamber [2,3]. The total approximated sensitivity S is then:

$$S = \frac{\sigma_f \; s_f}{\epsilon_0 (s_f + \epsilon_f s_a)} \; \frac{-1}{\left[\frac{h^3 E (1 + 1.6(w/h)^2}{0.138\, a^4}\right] + \left[\frac{P_0}{s_0}\right]} \; H \; \frac{C_m}{C_m + C_i} \qquad (6)$$

The microphone described in this paper comprises four diaphragm supports, which are necessary to prevent the diaphragm from collapsing towards the backplate which may occur due to the electrostatic attraction. The microphone can thus be considered as to be composed of a number of small unit cells, or small microphones, operating in parallel. The dimensions of the unit cell control the sensitivity and frequency response.

Using this model a sensitivity of about 1.5 mV/μbar can be calculated for a microphone with the following parameters: s_a = 20 μm, s_f = 1.1 μm, V_f = 325 V, E = 5*E9 N/m^2, h = 6 μm, a = 0.6 mm, s_0 = 2 mm.

MICROPHONE FABRICATION

For the realization of the silicon backplates we start with a p-type 5-10 Ωcm (100)-orientated silicon wafer. A 1 μm thick oxide layer is used as a mask for the KOH solution which has been used as the anisotropic etchant. First the air cavities, with a depth of 20 μm, have to be etched. This is performed by etching the patterned wafer in a KOH solution. After subsequent oxidation, both sides of the wafer are patterned and etched simultaneously. On the reversed side of the wafer two types of holes are etched through the wafer. One type (A) end in the air-gap space and form the necessary connection between the air gap and the backchamber behind the backplate. The other type of holes (G) are etched around the air cavity area, in order to be able to glue the diaphragm to the backplate (figure 1). After etching, the SiO_2 the wafer is oxidized again resulting in a 1.1 μm thick SiO_2 layer on the entire wafer. This layer serves as the electret and is chemically treated as described in [2] and [4]. Subsequently it is charged to 315 V using a corona charging method. At this stage of the process the diaphragm has to be attached. This is realized by fixation of a 6 μm thick Mylar foil on top of the complete wafer. The actual attachment results from glue through the holes (G) around the devices. Finally the wafer can be diced resulting in separate microphones.

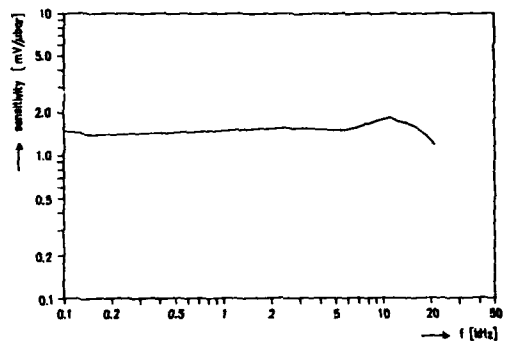

Figure 3 *The measured frequency response of the prototype silicon microphone.*

EXPERIMENTAL

The measured frequency response of the prototype microphones is presented in figure 3. The sensitivity is about 1.4 mV/μbar, which is in good agreement with the calculated value. The curve in figure 4 is a typical example of one of ten microphones which have been tested. None of the ten microphones showed a discrepancy of more than 10 % relative to the given example.

CONCLUSIONS

We have demonstrated that the use of photolithographic processes and anisotropic etching techniques can be succesfully employed in the realization of a subminiature electret microphone. With these techniques a large degree of reproducibility has been achieved.

It has been shown that SiO_2 can be used as an excellent electret material in an electret microphone.

REFERENCES

[1] D. Hohm, "Subminiatur-Silizium-Kondensatormikrofon", Conf. proc. of the DAGA '85, Stuttgart, pp.185-188.

[2] A.J. Sprenkels, A silicon subminiature electret microphone", Thesis, Twente University, 1988.

[3] G.M Sessler, ed., "Topics in applied physics", vol.33, "Electrets", Springer-Verlag, Berlin, 1980.

[4] A.J. Sprenkels, W. Olthuis and P. Bergveld, "The application of silicon dioxide as an electret material", This proceedings.

THE POLING OF MULTIPLE-LAYER POLYVINYLIDENE FLUORIDE FILMS AND THEIR PIEZOELECTRICITIES

Wang Shengjun; Zhao Yanxia; Yan Fuming.

Shandong Institute of Nonmetallic Materials
Jinan, Shandong, P. R. China

ABSTRACT

Poling of multiple-layer polyvinylidene fluoride films has been made. The piezoelectric properties of the poled films are measured. It is found that the polarization is not uniform in thick direction, and that poling of multiple-layer films at elevated temperature and lower field often leads to results that at least one layer of the poled films has strong piezoelectricity. The poling mechanism is also discussed in this article

INTRODUCTION

Since Kawai first reported the drawn and poled Polyvinylidene fluoride (PVDF) has strong piezoelectric activity in 1969,[1]PVDF has been widely studied, and a great grogress in the field of applications of piezoelectric PVDF has been made. In spite of those, the poling process and the mechanism of piezoelectric properties of PVDF have not been very clear so far.[2,3] The nonuniform polarization of poled PVDF was reported by several authors.[4-5] The distributions of polarization reported by the authors are not identical, and the explainations to this phenomenon are rather different.
In this paper, the resuls of studies on the piezoelectricity and polarization in multiple-layer poled PVDF films are presented, the poling mechanism is investigated in connection with thermally-stimulated-discharge (TSD) method and curves of piezoelectric coefficient versus temperature.

EXPERIMENTAL

CH2593-2/ 88/ 0000-0598$01.00 Copyright 1988 IEEE

Polyvinylidene fluoride is offered by Shanghai Institute of organic fluoride materials. The original films were cast from a dimethylacetamide solution of PVDF. The films were uniaxially stretched at 120°C to about four times their original length. X-ray and infrared spectra indicat that the crystalline phase consist of β form in strecthed films. Three stretched films with thicknesses of 30μm were stacked together and subsequently poled in a three-layer structure as shown in Figure 1.

These samples were poled with a dc field of 300kV/cm at 100°C for 60 minutes and then cooled to room temperature, after that, the dc field was removed.

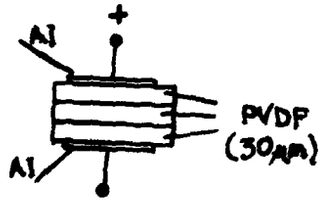

Fig. 1 Poling in a three-layer structure

Aluminium was evaporeted onto the sufaces of the poled films as electrodes.

The piezoelectric coefficients were determinded by Rheovibron DDV-III-EA (TOYO BALDWIN CO.LTD). The thermally stimulated discharge spectra were measured by thermally stimulated current measuring apparatus (TOYO SEIKI SEISAKU-SHO.LTD).

RESULTS AND DISCUSSION

The piezoelectric properties of three-layer poled PVDF films are shown in Table 1

Table 1. The piezoelectric properties of three-layer poled films

group No.	film position	d_{31} (PC/N)
1	P	12
	M	20
	N	9
2	P	16
	M	14
	N	2
3	P	12
	M	20
	N	2

* P contacting positive electrode
  M in the middle
  N contacting negative electrode

From the results we learn that: 1) the polarization is not uniform in the direction of thickness, 2) the location which has the maximum polarization may be between the centre and the suface contacting the positive electrode, 3) the effect of this poling technique on one of the poled films (the one in the middle or contacting positive electrode) is much larger than those of single-layer poling in the same poling condition, and is the same effect as those of single-layer poling in a higher poling field. Same films were poled in the same poling condition in a single-layer poling structure in our laboratory. The piezoelectric coefficient d_{31} of these films are about 9 PC/N. Figure 2 shows the thermally stimulated discharge spectra of group 1. Film which has stronger piezoelectricity has larger discharge current. The films have nearly identical polarizations P_1 and P_2. The obvious differences among the spectra are the polarizations at high temperature.

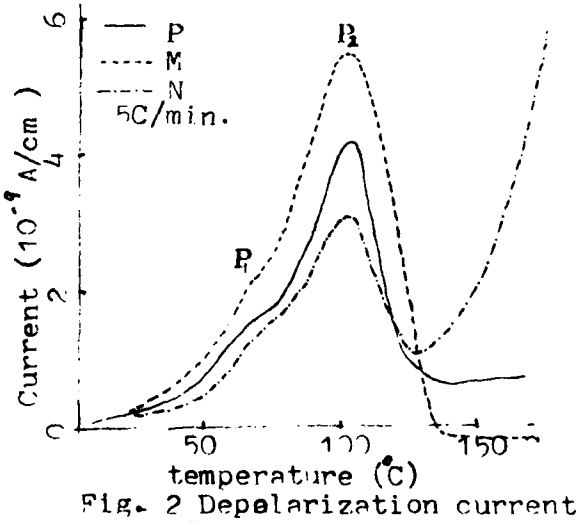

Fig. 2 Depolarization current of group 1

The film N has a large polarization at the temperature near the melting point, the other two films have very small polarizations.
Figure 3 shows the temperature dependence of piezoelectric coefficient e_{31} of group 1.

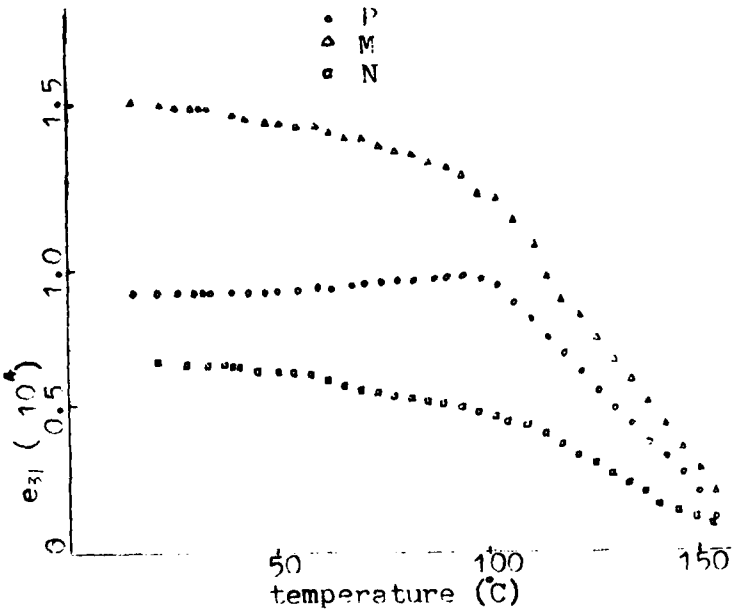

Fig. 3 Temperature dependence of e_{31} of group 1

We found that the decrease of the piezoelectricity parallel the decrease of the polarization.

Sessler proposed that the nonuniform distribution may be due to field distortion caused by charge injection at elevated temperature or by charge migration. In our experiments, it give an evidence to field distortion explaination that one piece of multiple-layer poled samples which were poled at a lower field and elevated temperature has stronger piezoelectricity and polarization than those of single-layer poled samples have. The large depolarization current of the film contacting negative electrode at temperatures near melting point may be due to the negative

charge injected from negative electrode and traped in intersuface of crystalline phase and amorphous phase. this negative charge distort the field greatly, causing decrease of local field near negative electrode and increase of local field of other place. There are also positive charges near positive electrode which are injected from positive electrode, but the amount of those positive charge is much smaller than those of the negative charge near negative electrode.

References

1 H.Kawai, Japan J. Appl.Phys.,8,975(1969)
2 M.G. Broadhurst, G.T. Davis,J.E. Mckinney and R.E. Collins, J. Appl. Phys.,49,4992 (1978)
3 Y. Wada and R. Hayakawa, Ferroelectrics, 32, 115 (1981)
4 H. Sussner, J. polm. Sci. Polm. Phys.Ed., 16,529 (1978)
5 G.M.Sessler, R.Gerhard-Multhaupt, H.Von Seggern, J.E.West, 1984 Annual Report, CEIDP, pp.393
6 M.A.Marcus, Ferroelectrics 32, 149 (1981)

ELECTRET RADIATION DOSIMETER WITH GRID-CONTROL

Zhen-zhong WANG, Ci-zhong XU and Xi-min SUN

Pohl Institute on Solid State Physics, Tongji University, Shanghai, PR CHINA

Abstract

A new method to enlarge the range and improve the sensitivity of electret radiation dosimeter (ERD) is discussed in this paper. It is that the grid mesh nearby the sample surface has been introduced between the front electrode and electret sample. The PTFE sample is negatively corona charged between 160-170°C. The surface voltage of the foil is -1000V. The radiation dose of several tens R can be measured with ERDG. With ERDG we can also radiation charge, obtain expected surface potential.

1. Introduction

It is frequently to use large doses of irradiation for cure tumour patient in radiotherapy in hospitals[1]. Enlarge the range of dosimeter is very important for measurement of exposure. The range of ERD is changed with its geometrical parameters. But it is difficult that the large quantity of exposure can be measured by changing the geometry of ERD. The type of electret radiation dosimeter with grid-control (ERDG) is the electret ionization chamber with grid mesh.

2. Experimental

25.4μm thick PTFE samples were obtained from West Germany. Samples were evaporated aluminium on one surface. The PTFE foil was fixed on a grounded aluminium ring, inner diameter 2.5 cm outer diameter 3.5cm. PTFE was negatively corona-charged at elevated temperature as Fig. 1.

CH2593-2/ 88/ 0000-0603$01.00 Copyright 1988 IEEE

In our experiment, the charging condition is
$V_C = -9.0kV$
$V_G = -1000V$
$T_c = 160-170°C$
$t_c = 5$minutes
The surface voltage of sample can be measured with Model 244 Isoprobe electrometer.

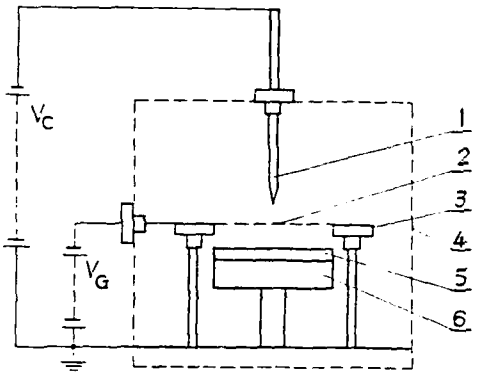

Fig. 1. The cross section of corona-charged device at elevated temerature.
1__wolfram needle, 2__grid mesh, 3__insulator, 4__heating apparatus, 5__electret sample, 6__sample stand

The grid mesh was introduced between the front electrode and electret sample, and was applied negative voltage for enlanging the range of ERD or positive voltage for improve the sensitivity of ERD.

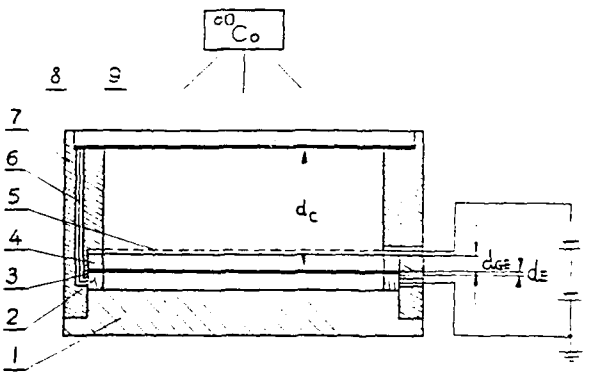

Fig. 2. The cross section of the electret ionization chamber with grid-control.
1__back cover, 2__back electrode, 3__electret sample, 4__insulating ring, 5__grid mesh, 6__conducting wire, 7__shell(PVC), 8__front cover, 9__front electrode.

Samples were irradiated by gamma rays of ^{60}Co as Fig. 2.

3. Results and discussion

Some results are presented in Table 1. It is obviously that there are a lot of difference between ERD and ERDG. During irradiation the surface voltage decay is hindered by use of grid mesh of ERDG so that the measuring range of ERD is enlanged.

Table 1. The surface voltage of ERD and ERDG before and after irradiation. $\eta = \eta/V$. X=40R.

Grid voltage of ERDG V_G (V)	Initial surface voltage V(V)	Surface voltage after irradiation V'(V)	Sensitivity of ERDG η (V/mGy)	Parameter η (1/Gy)
0	-500	0	1.44	
-100	-540	-460	0.23	0.43
-100	-640	-500	0.40	0.63
-200	-470	-390	0.23	0.49
-200	-1120	-910	0.60	0.59
-500	-950	-800	0.20	0.21

As Fig. 2, the negative grid mesh of ERDG is applied to decrease density of positive ions in ionization chamber so that the compound probability of sample-surface negative ions and positive ions in chamber is lowered.

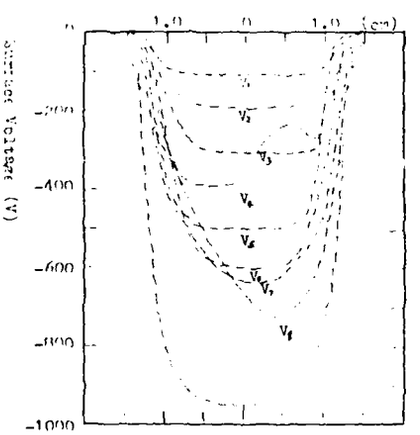

Fig. 3. The surface voltage of sample after irradiation charging at different grid mesh voltage of ERDG V_{G-8} -100, -200, ..., -800V. X = 100R.

As Fig. 3., the ERDG will become irradiation charging when

exposure dose X and exposure rate $\dot{X}$ achieve certain intensity. By use of this method, the even surface potential nearby grid mesh voltage can be gotten.

4. Acknowledgements

This work was supported by Prof. G.M.Sessler and Stiftung Volkswagenwerk. The authors are grateful to Prof. Mu-xian Wu for his first idea of using ERD to measure the large doses of radiation and Dr. R. Gerhard-Multhaupt for his helpful suggestions.

References

[1] Mascarenhas, Sergio. "ELECTRET RADIATION DOSIMETRY: A REVIEW", Proc. 5th Intern. Symp. Electret, Heidelberg 1985.

BULK AND INTERFACIAL DIELECTRIC RESPONSE OF DYSPROSIUM AND YTTERBIUM OXIDE THIN FILM CAPACITORS

T. Wiktorczyk

Institute of Physics, Technical University of Wrocław, Wybrzeże Wyspiańskiego 27, 50-370 Wrocław (Poland)

Characteristics of capacitance, dielectric permittivity and losses as a function of: temperature, frequency, d.c. voltage, insulator thickness and electrodes material for Dy_2O_3 and Yb_2O_3 thin films deposited in MIM sandwiches are presented . Results show that both: volumes of the dielectrics films as well as M/I interfaces (Schottky barriers) are responsible for dielectric response of these capacitors.

INTRODUCTION

Nowadays microelectronic technology is based on a few "clasical" materials like silicon oxide or aluminium oxide used as insulator films for microcircuits. However there has been a sharp increase in investigations of new dielectric materials for thin-film device applications. In this paper experimental data for the dielectric properties of dysprosium and ytterbium oxide thin films are presented. Samples preparation and procedure of measurements have been described elsewhere [1,2].

CAPACITANCE AND DIELECTRIC PERMITTIVITY VERSUS TEMPERATURE

In Fig.1 and 2 C(T) and $\epsilon_r'(T)$ curves of $Al/Dy_2O_3/Al$ and $Al/Yb_2O_3/Al$ capacitors are shown. For the low temperature region (for T below about 350 K) and for higher frequencies (f~1 kHz) experimental curves exhibit a slight rise with temperature in C and ϵ_r' , giving values of temperature coefficient of capacitance of $TCC=2.3 - 3 \cdot 10^{-4}\ K^{-1}$ and $TCC=3.7 \cdot 10^{-4}\ K^{-1}$ for dysprosium and ytterbium oxide capacitors respectively. For high temperatures capacitance and dielectric permittivity increase sharply whereupon they exhibit apparent saturation or tendency to saturation connected with M/I boundaries.

CH2593-2/ 88/ 0000-0607$01.00 Copyright 1988 IEEE

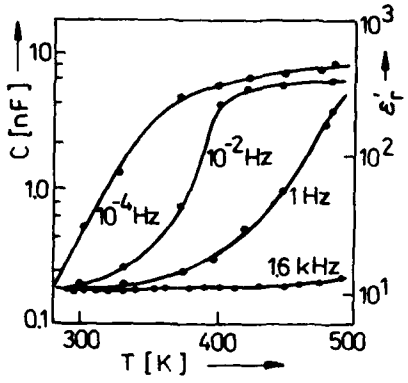

Fig.1. Curves: C(T) and ϵ'_r(T) for Al/Dy_2O_3/Al at different frequencies.

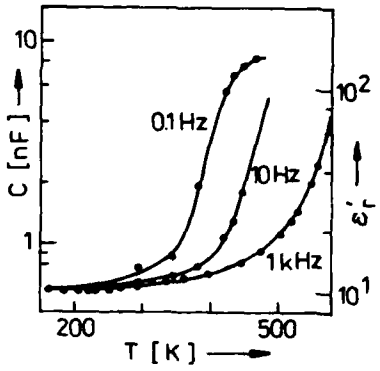

Fig.2. Curves: C(T) and ϵ'_r(T) for Al/Yb_2O_3/Al at different frequencies.

CAPACITANCE VERSUS INSULATOR THICKNESS

Fig.3 shows dependence of the capacitance of dysprosium oxide capacitors versus insulator thickness. For temperature T=300 K and frequency f=1.6 kHz the capacitance depends on thickness giving a "truth" dielectric permittivity of Dy_2O_3 (ϵ'_r=10-18 and depends on sample preparation). For very low frequencies and high temperatures capacitance does not depend on thickness giving capacitance of M/I interfaces. In Fig.4 curves of the capaci-

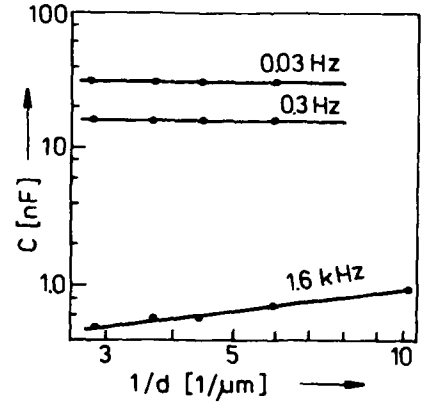

Fig.3. Capacitance vs. thickness of Dy_2O_3 film at T=543 K (upper lines) and T=300 K bottom line), log C-log d^{-1} scale.

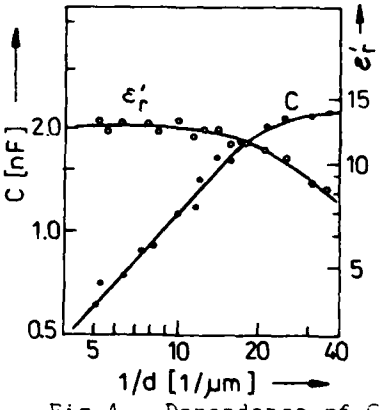

Fig.4. Dependence of C and ϵ'_r on thickness of Yb_2O_3 film (T=300 K , f=1 kHz).

tance and dielectric permittivity measured at f=1 kHz and T=300 K versus dielectric thickness for ytterbium oxide capacitors are presented. For insulator thicknesses greater then 80 nm the value of ϵ'_r is constant (ϵ'_r=12.5 ±1.5). For thiner dielectric films ϵ'_r is becoming smaller with decreasing of the insulator thickness.

FREQUENCY DEPENDENCES OF C AND ϵ'_r

Disperssion characteristics of C and ϵ'_r for Dy_2O_3 sandwiches are shown in Fig.5. For high frequencies and low temperatures C(f) and ϵ'_r(f) curves are almost flat giving bulk dielectric response of Dy_2O_3 itself . For low frequencies and high temperatures these curves increase strongly reaching some saturation region or region of a smaller dispersion, connected with capacitance of M-I regions. ϵ'_r reaches values of order hundreds (see Fig.5) or even thousands [1] in the region under discussion and

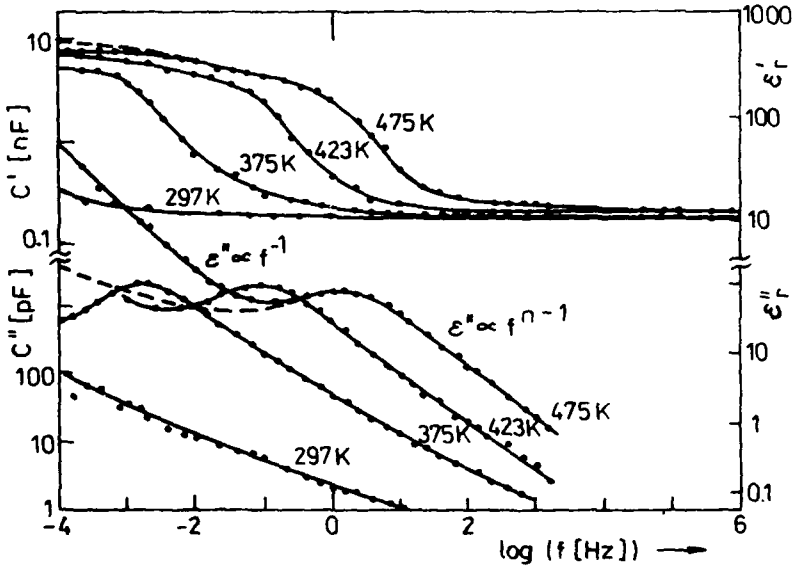

Fig.5. Capacitance and dielectric permittivity versus frequency for Al/Dy_2O_3/Al capacitors : at U=+2 V (solid line) and at U=-2 V (broken line).

Fig.6. Imaginary part of capacitance: C''=G/2πf and imaginary part of dielectric permittivity vs. frequency for Dy_2O_3 capacitors (d(Dy_2O_3)=526 nm, n=0.22-0.60).

has to be taken as an "apparent dielectric permittivity" of these samples. The shape of C(f) curves in this region (their disperssion) depends on polarity of voltage (Fig.5) and is connected with properties of the bottom and the upper M/I interface (see also [2] and [3] for a further explanation).

DIELECTRIC LOSSES IN FREQUENCY DOMAIN

In Fig.6 dissipation curves of dysprosium oxide capacitors are presented. Dissipation peaks are thermally activated (E_b=1.0-1.1 eV) and they come from interaction between the volume of Dy_2O_3 film and Al/Dy_2O_3 interfaces [4,5]. The total dielectric losses of type: $\epsilon''_r \sim f^{-1}$ has been observed for very low frequencies and positive polarisation of the upper electrode coming from d.c. conductivity (σ_{dc}). A contribution of σ_{dc} to ϵ''_r for the negative polarisation was neglible (see Fig.6).
Our a.c. examinations indicate that frequency response of dysprosium oxide capacitors follow "the universal law of dielectric response " (see Fig.6 and [4]).

CAPACITANCE AS A FUNCTION OF A VOLTAGE

In Fig.7 the low-frequency, high-temperature capacitance and high-frequency, low-temperature C-V curves of $Al/Dy_2O_3/Al$ are presented . One can see that the first curve (solid curve) depends strongly on voltage and its form is caused by the capacitances of Schottky barriers

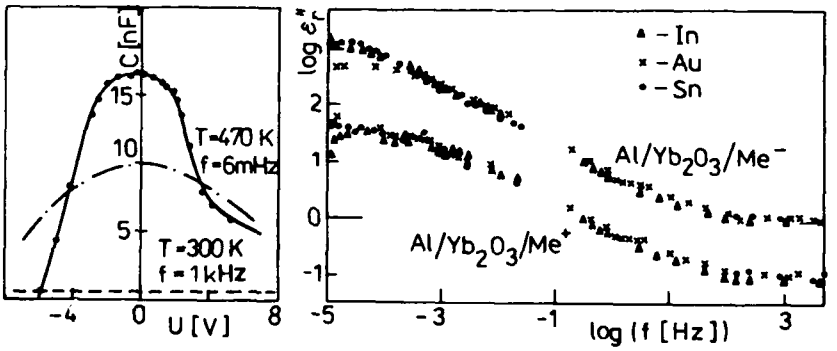

Fig.7. Capacitance vs. voltage for Dy_2O_3 capacitors ($d(Dy_2O_3)$= 273 nm, U_{ac}=50 mV).

Fig.8. $\epsilon''_r(f)$ characteristics for $Al/Yb_2O_3/Me$ samples ($d(Yb_2O_3$=80nm T=300 K). ϵ''_r scale has been shifted by one decade for Me^-.

at M/I boundaries. The second curve (broken line) is almost flat. High voltage aging of samples at high temperatures is also shown in this figure (dashed-dotted curve).

INFLUENCE OF ELECTRODES ON DIELECTRIC RESPONSE

In Fig.8 $\epsilon''_r(f)$ curves for $Al/Yb_2O_3/Me$ capacitors (Me= In, Au, Sn) are presented. These results clearly show that for f>1 mHz dielectric response is the same for each sample, whereas a shape of $\epsilon''_r(f)$ characteristics for lower frequencies depends on electrodes and their polarity and is connected with M/I interfaces.

CONCLUSSIONS

On the basis of the experimental tests the following conclussions can be drawn:

(1) Dielectric properties of dysprosium and ytterbium oxide films studied in MIM structures are similar to each other.

(2) A.c. examinations of $Al/R_2O_3/Al$ sandwiches (where R= Dy, Yb) as well as current response studies after step voltage excitation show that the dielectric response comes from the volume of the insulating thin film and from M/I interfaces.

(3) Schottky barriers are formed at Al/R_2O_3 boundaries and they are responsible for dielectric properties of $Al/R_2O_3/Al$ structures at high temperatures and low frequencies.

(4) High-frequency , low-temperature properties of these capacitors are connected with bulk response of R_2O_3 thin films.

The author thanks to Prof. C. Wesołowska for her constant interest and encouragement . This work was carried out under the Polish Research Project CPBP 01.06-9.01.

REFERENCES

1. T. Wiktorczyk and C. Wesołowska, Vacuum, 37(1987)107.
2. T. Wiktorczyk, K. Nitsch and Z. Bober, Thin Solid Films, 157(1988)13.
3. T. Wiktorczyk, Z. Bober and K. Nitsch, in preparation for publication.
4. T. Wiktorczyk, Solid State Commun., (1988), in press.
5. A.K. Jonscher, C. Pickup and S.H. Zaidi, Semicond. Sci. Technol., 1(1986)71.

STUDY ON THE SPACE CHARGE PEAK OF TSC IN PET FILM

Wu Jiazhen and He Qiwei

Department of Chemical Engineering
Tsinghua University, Beijing, China

ABSTRACT

In this paper, the TSC spectra of the semicrystalline PET film has been investigated. The TSC spectra shows two peaks, α peak temperature is $\approx$105°C, that of negative ρ peak is $\approx$140°C.
The origin of homocharge contributed by itself has been discussed. Four figures of electron spectra have **been** shown. It demonstrated that acetate as catalysis remained at the surface of PET film. The catalysis or the ion disapealed by heating-treatment. Hence, the negative ρ peak of TSC in PET is associated with the surface ion impurity.

INTRODUCTION

Many reports have been published on the TSC by which the polymer molecular relaxations are studied. In recent years authers often ultilize TSC technique to investigate the trapping, migration and transfermation of the charges in electrets by space charge peak [1,2]. There are two different types of charge i.e. heterocharge and homocharge. In general, it is considered that heterocharge is due to dipole polarizetion or space charge produced by conduction in the electrets, while homocharge is due to breakdown between electrode and dielectric, which introduces injection of space charge or due to injecting charge from the electrode. It is nesessar to make discussion on the origin of the homecharge.

The TSC of PET have been reported by many authors [3,4]. It is found that, above the room temperature, there exist four TSC peaks designated P_1, P_2, P_3 and P_4 in ascending order of temperature [5]. Generally, only P_1 and P_2 are discussed. P_1 is called as α peak and attributed to the motion of segments. P_2 is called as ρ peak. It is space

CH2593-2/ 88/ 0000-0612$01.00 Copyright 1988 IEEE

charges peak. But study on the ρ peak is a little. Generally, homocharge is easily generated under higher field and lower temperature. When the homocharge is depolarized, a negetive ρ peak appears in TSC spectra. In this paper, TSC of PET possessing negetive ρ peak has been presented. By TSC spectra of different condition and eletron spectrum, we discuss the origin of the negative ρ peak in PET.

EXPERTMENT

The specimens of test are semicrystalline PET film which is supplied by 2nd film factory of Ministry of Petroleum. The diameter of specimen is 25mm. The external electrode with diameter of 20mm is made. TSC is measured by KH-1 type Thermal Discharge Meter, which is made by Institut of chemistry, Academia Sinica. Electrospectroscopy is obtaind with PHI-5100 esca. In the paper, T_p, t_p and E_p is the poling temperature, time and field, respectively.

RESULT AND DISCUSSION

Fig. 1 shows TSC spectra of semicrystalline PET polarized at higher field and lower temperafure. It resembles a air-gap TSC spectra has been given by sessler [1]. α peak can be observed at about 105°C and at the original position of ρ peak ($\approx$140°C) a negative peak appears. In general, it is considered that positive ρ peaks can be seen as the result of interfacial polarization [1], whereas the negative ρ peak is the result of homocharge discharge, e.g. air gap spark induced the deposition of homocharge or homocharge is generated by charge-injected. [1,6]. As illustrated in Fig. 2, however, after polarization of second times the value of α peak is almost unchanged, while the value of negative ρ peak decreases. This suggest that the negative ρ peak is associated with specimen's charges. As some charges are neutralized during first time depolarizetion and the number of charges gets smaller. Current peak is weaked during second times depolarization. Fig. 3 is TSC spectra of PET at different annealing temperature. It is found that the α peak of the TSC remains unchange. However, along with the annealed temperature increased, the negative ρ peak decrease, then turn to positive. Fig. 4 illustrates the comparision of TSC between annealed and unannealed

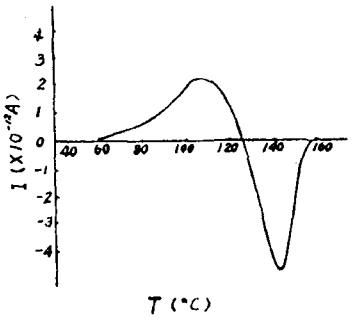

Fig. 1. TSC Spectrum of PET Polarized under Higher Field and Lower Temperature

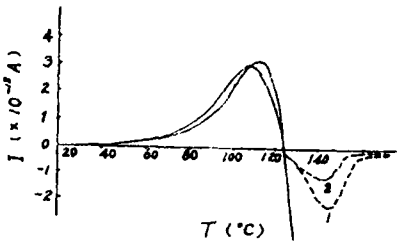

Fig. 2. TSC Spectrum of repeated Polarizetion in PET The dot line represent 10^{-11} A region.
1-first time, 2-second times

PET specimen which is manufactured by Du Pont. Annealization can induce crystallinity to get larger or make dissipation of the impurities on the surface by heating. The experiment shows the later is true. Fig. 5 is Electron Spectra of PET. It shows that C-spectra peak between 280—290ev of annealed sample (a) is higher than that of unannealed sample(b), this means that uncarbonate impurities is relatively diminished after annealing. Fig. 6 shows an expanded C-spectra of PET film, the peak

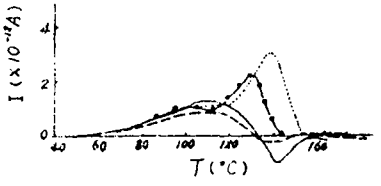

Fig. 3. TSC Spectrum o PET at Various Annealed Temperature
——unannealed --- 80°C
——90°C ... 130°C
T_p=95°C t_p=30min E_p=100 KV/cm

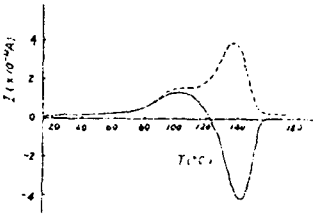

Fig. 4. TSC Spectrum of PET Film of Du pont
——unannealed --- annealed at 110°C for 2h
T_p=150°C t_p=30min E_p=150KV/cm

between 288—290ev assigns to acetate. PET ester-exchange method usually use acetate of Zn, Co, Mn as the catalyst. In Fig. 6(b) no peak appears in the region, whereas (a) shows the existance of the peak. This means that catalyst remained or its ions upon surface dissipate after heat-treatment. As illustrated in Fig. 3 with spot-line, a positive ρ peak appears in TSC spectra of the sample which had been heat-treated.

It is conclued that impurity may tend to concentrate on the surface of specimen and be in ion-state. Under high field, charges upon surface are easilly attenuated by gap discharge between sample and electrode. Its attenuatting process is combination of heterocharges on electrode. Because the temperature is lower, it is disadvantageous to the movements of charges. So relatively more homocharges reside on the surface. We can consider the process as the deposition of homocharges, but the homocharge is not externally injected. Because there is no air gap, under vacuum-deposited electrodes, the surface charge do not exist, and then negative ρ peak do not appear in TSC.

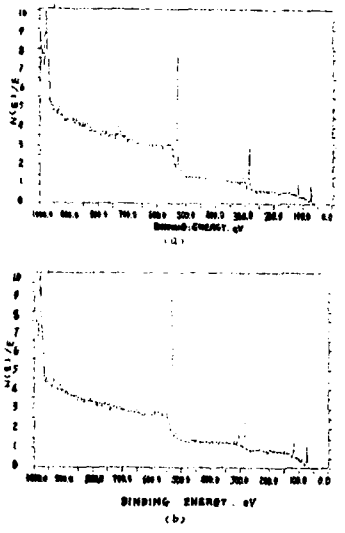

Fig. 5. Electrospectroscopy of PET Film
(a) annealed at 130°C for 2h (b) unanneald

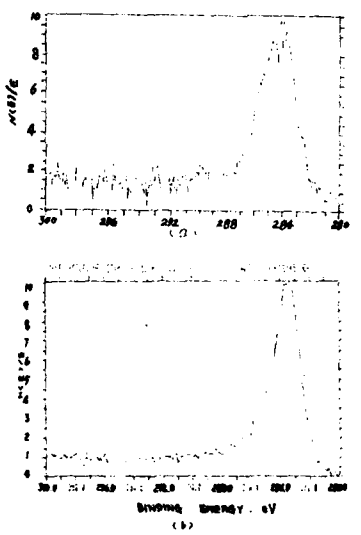

Fig. 6. C-Spectrum of Electrospectroscopy in PET
(a) unanneald (b) annealed at 130°C for 2h

In summary, under lower-temperature and higher-field condition, TSC of semicrystalline PET film represents negative ρ peak. It is attributed to that impurity ions are accumulated on the surface of PET film.

ACKNOWLEDGMENT

The authors thank Mrs. Yong Jingyin for the measument of Electrospectroscopy.

REFERENCES

[1] G. M. Sessler (Ed.), Electrets, Springer, Berlin, 1980.

[2] H. Von Seggern, "CHARGING and POLARIZATION PHENOMENA IN POLYMERS" in Proceedings of the Conference on Electrets, 1985, pp59--71.

[3] T. Hino, "A Method for Measurement of Distribution of Dipolar Relaxation Times by Themally Stimulated Current" Japan J. Appl. Phys., 12, pp611--612 (1973)

[4] Zhou Yiqin, et.al., "Thermal Discharge of PET film" *Communications of* Insulated Material, No. 5-6, pp132--135 (1980)

[5] Keichi Miyairi, Ichiroku Yahagisawa, "Thermally Stimulated Current in Polyehylene Terephthalate in the High Temperature Region" Japan J. Appl. Phys. 17, pp593--594 (1978)

[6] N. Murayama, K. Nakamura, et.al., "The Strong Piezoelectricity in Polyvinylidene Fluroide" Untrasonics, 15, (1976)

A NEW COMPOSITE ELECTRET FILM WHICH IS BASED ON POLYMER PVDF*

YANG Daben

Department of Micro-Electronics Technology
& Electronic Materials
Chengdu Institute of Radio Engineering
610054 Chengdu, Sichuan, P.R.China

ABSTRACT

One type of new flexible composite electret film which is based on polymer PVDF and compounded with ferroelectric ceramics PCM system has been discussed in this paper about its preperation, properties and structure analysis.

INTRODUCTION

Electronic polymer dielectrics and their composite materials are one of the most noticeable direction in the world advancement of piezoelectricity and science of electret materials.

At present, the small piezoelectric constant d_{ij} of pure polymer electret PVDF leads to a certain limitation in their emission type applications. Therefore research has been carried out to add ferroelectric powder with high polarization strength and piezoelectric effect into electret polymer, in order to form a new type of flexible polymer composite electret material. It is obvious that this electret polymer/ferroelectric ceramic composite system with both flexibility and strong piezoelectricity can make compound studies in a selective way in the wide field of electret polymers, e.g. PVDF, PVF, PTFE, Teflon FEP, PP etc, and ferroelectric ceramics, e.g. $BaTiO_3$, PZT, PCM etc.

EXPERIMENTAL

1. Sample Preperation

The refined PCM fine powders are added into carefully made up PVDF resin in a certain proportion, and achieve a polymer composite film(30-100um) of PVDF

* This project supported by National Natural Science Foundation of China

CH2593-2/ 88/ 0000-0617$01.00 Copyright 1988 IEEE

/PCM type with the flow extension compound method. All kinds of proportion and technology of flow extension compound film formation have been tested. Followed by DC high voltage hot polarization electret treatment,and the gets electret piezoelectric oscillators.

2.Property Test

The dielectric parameters(ε, t_δ),piezoelectric parameters(d_{33}, g_{33}) and resonant transducer parameters (f_r, f_a, k_t, Z_a,etc) of PVDF/PCM composite electret film have been measured.The relationships of property parameters of the composite film with temperature(room temperature to 100°C),frequency(50Hz to 300Hz), technological factors and stability have also been tested.The comparison has been given.

3.Structure Analysis

The structure factor of piezoelectric property of PVDF/PCM composite electret film is initially analyzed by metallographic microscope,scanning electron microscope(SEM) and X-ray diffractometer,comparison with the hypothetical model and explanation have been given.

RESULTS AND DISCUSSIONS

1.Piezoelectric Characteristic Parameters

the dielectric and piezoelectric characteristic parameters of the tested PVDF/PCM composite electret film are determined by the properties of polymer base material and the property and content of ferroelectric powder.Besides,they are continuously enhanced when technological factors are improved.The level reached up to date is shoun in Table 1.

Table 1

Material	ε	t_δ	d_{33} 10^{-2}PC/N	g_{33} 10^{-3}Vm/N	K_t%
PVDF	9-15	1.5-2	10-15	70-170	10-15
PCM	1300-1600	0.6-1	400-500	30-40	60-70
PVDF/PCM	40-50	0.3-0.4	20-25	40-65	35-40

The experimental data prove that the larger the dielectric and piezoelectric constants of the polymer base material(p) and ferroelectric powder(c),correspondently the better the dielectric and piezoelec-

tric characterictic parameters of the composite system(&).Such a relationship accords with usual compound calculation formula:

$$\lg \varepsilon_{\&} = N_p \lg \varepsilon_p + N_c \lg \varepsilon_c \qquad (1)$$

$$d = -\,E T^{-1} \qquad (2)$$

The experimental data approximately conform to the calculated result.

2.Dielectric and Piezoelectric T,f Properties

In the temperature relationships(Fig.1),the composite film is usually in high elastic state phase which is above the material PVDF,the composite shows increase of ε and $t_g d$ when T increases in positive range,while decrease of ε in negative (low) temperature range. The correspondent d constants have the same rule of change.Therefore g constant hardly changes in the whole temperature range.
The relationship of PVDF /PCM between ε and frequency has decreasing tendency.

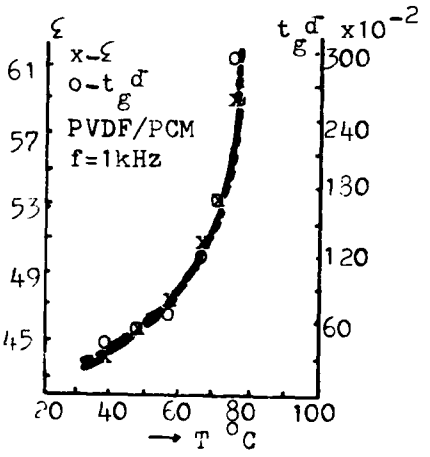

Fig.1

3.Technological Factor Relationship

The piezoelectric property of such flexible polymer composite electret film is strongly relevant to technological factors:
(1)The influence of the proportion of ferroelectric ceramics in the composite film formation,i.e. the content of PCM powder as filler (wt %),on d_{33} of composite film (Fig.2).
Obviously,increase of content of ferroelectric powder(W_ε) will contribute to d_{33} of the composite film nonlinearly in a way of quad-

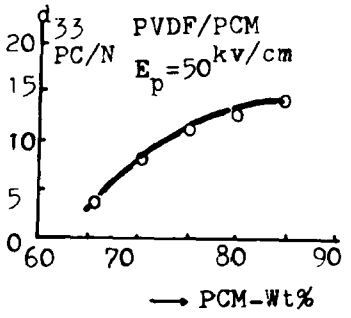

Fig.2

ratic:

$$d_{33\&}=A+BW_c+CW_c^2 \qquad (3)$$

in which,A,B,C-respective coeffients of content influence.Their values can be known with curve fitting method.

(2)Thechnological parameters in electret polarization treatment to composite film,such as E_p,T_p,t_p and pattern will have direct effect on properties of composite .

The effect E_p-wt%-d_{33} is the strongest(Fig.3).This is similar to the quadratic nonlinear relationship.

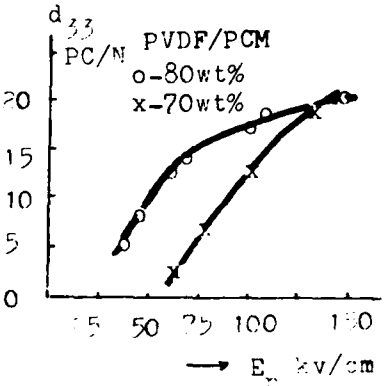

Fig.3

4.Ageing Property

Decay of piezoelectric effect of composite electret is examined in a period of time.The ageing rate is about $+100\times10^{-4}$/10 years.

5.Structure Analysis

The measurements of d_{33} before and after electret polarization treatment to the composite film make it clear that technology of polarization has vital effect on electret property of the composite film.

PVDF/PCM composite electret film after polarization still belongs to C_{6v} symmetry.

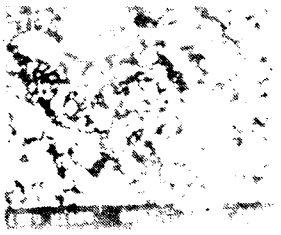

Fig.4

The scanning electron microscope analysis to PVDF/PCM composite film is shown in Fig.4.It reveals quite apparantly here that PCM powder distributes in PVDF polymer system in a form of high scattering phase(about 5-30um).PVDF joins the composite system mainly in d crystal form.

Therefore our research supposes a kind of 0-dimension(a two-phase system composite with 0-3 connectivity) compound model:Ferroelectric ceramics polycrystal(>10μm) approximately evenly inlays in PVDF non-

crystalline or amorphous(crystalline thickness normally < 10μm) linear-chained molecules.Its electric domain spontaneous polarization mechanism hence enhances the piezoelectric effect of the composite electret film system.

Y.Wada thinks that there are two possible piezoelectric mechanisms of compound:(1)Ferroelectrics lead to piezoelectric effect.(2)Polarization charges in ferroelectrics lead to nonhomogeneity of the compound and then the coupling effect.The PVDF/PCM composite electret film here is flexible composite electret piezoelectric system based on PVDF which is in high elastic state at room temperature.So mechanism(2) should be dominant,and it accords with the equation:

$$e=0(3\xi_a/2\xi_0+\xi_c)P_{sc}(\xi_c/2\xi_a+\xi_c.K_a/\xi_a-1/l.\partial l/\partial s) \quad (4)$$

We can see from the X-ray diffraction photograph(Fig.5) that PCM component has very large proportion in PVDF/PCM composite system,therefore influence of mechanism(1) also exists.

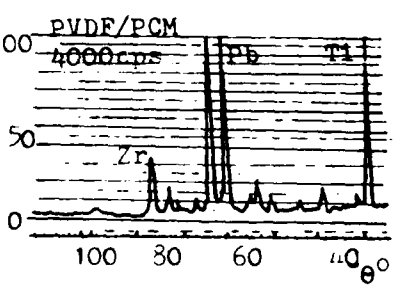

Fig.5

CONCLUSION

1.The polymer and ceramics PVDF/PCM composite is one of the better way of flexible composite electret system.

2.the 0-dimension compound electret piezoelectric mechanism of PVDF/PCM,i.e. Ferroelectric polarization charges under the action of PCM strong piezoelectric effect lead to compound nonhomogeneous coupling ,has the dominant function.

3.Research and development in electronic polymer composite electret film materials have extensive theoretical and practical value in the field of electret transducer effect.

REFERENCES

(1)J.Mort and G.Pfister,Electronic Properties of Polymers,New York,John Wiley,pp.109-160,1982.

(2)G.M.Sessler,Electrets,Topics in Applied physics, Vol 33,Springer Verlag Berlin,1980.

TEMPERATURE DEPENDENCE OF -OH BAND IN VINYL CHLORIDE:VINYL ACETATE:VINYL ALCOHOL TERPOLYMER

V.S. Panwar, Ramadhar Singh, N.P. Gupta* & P.C. Mehendru

National Physical Laboratory, New Delhi-110012, INDIA

ABSTRACT

IR absorption studies of vinyl chloride:vinyl acetate: vinyl alcohol (VC:VAc:VA) terpolymer in the range 4000-400 cm^{-1} at temperatures 298, 323, 348, 373 and 398K show a broad -OH band at $\sim$3460 cm^{-1} with a kink at its shoulder on the higher frequency side at $\sim$3580 cm^{-1}. The IR spectra of the films treated at 323 and 348K show a decrease in the magnitude of the band at $\sim$3460 cm^{-1} with a slight increase in the magnitude of the band at $\sim$3580 cm^{-1} while the IR spectra of films treated at 373 and 398K show, besides a shift in the sharp band towards the higher frequency side, an increase in its magnitude, whereas the broad band (at $\sim$3460 cm^{-1}) continues to decrease in its magnitude with the rise of temperature. The analysis of these bands and their temperature dependence are reported in this paper.

INTRODUCTION

A large number of papers have been published on hydrogen bonding in polymers and corelation between frequency shift as well as change in the band intensity of the -OH group with the strength of hydrogen bonding [1-5]. The present paper reports about the formation of hydrogen bondings and the temperature dependence of -OH band in vinyl chloride:vinyl acetate:vinyl alcohol (VC:VAc:VA) terpolymer.

EXPERIMENTAL

The VC:VAc:VA terpolymer (having weight percentage of VC, VAc and VA as 91, 3 and 6% respectively was obtained from M/s Polysciences, USA. Films of thickness $\sim$20 μm were grown by solution evaporation technique. For the qualitative analysis of the thermal effect on the terpolymer

CH2593-2/ 88/ 0000-0622$01.00 Copyright 1988 IEEE

structure, few films were kept at 323. 348, 373 and 398K for about 16 hours and then allowed to cool fast to room temperature. The normal IR spectra of the terpolymer films with and without quenching thermal treatment were recorded on a double beam spectrometer (Perkin ElmerModel 399) in the frequency range 4000-400 cm^{-1} .

RESULTS AND DISCUSSION

The IR absorption spectrum of terpolymer film at room temperature (298K) in the frequency range 4000-400 cm^{-1} is shown in Fig.1. A broad absorption band at $\sim$3460 cm^{-1} together with a sharp kink of comparatively lesser magnitude onthe high frequency shoulder at $\sim$3580 cm^{-1} is observed. The position of the -OH band of the film treated at 323, 348, 373 and 398K are shown in Fig.2. The IR spectra of the treated films at 323 and 348K show a decrease in the magnitude of the broad band at $\sim$3460 cm^{-1}. On the other hand an increase in the magnitude of the sharp band at $\sim$3580 cm^{-1} is produced by the thermal treatment and in particular, a shift in this sharp band towards the high frequency side alongwith the increase in the magnitude is observed in the films treated at 373 and 398K. Elliott et al [6] have assigned the strong hydrogen bonded -OH stretching band in polyvinyl alcohol at $\sim$3400 cm^{-1}. Two types of hydrogen bonding are possible (i) intramolecular in which the hydrogen atoms are bonded tothe oxygen atoms of the neighbouring monomer units/molecules of the same chain. (ii) intermolecular in which the hydrogen atoms are bonded to the oxygen atoms of neighbouring molecules of the neighbouring chains. The broad band at $\sim$3460 cm^{-1} maybe the result of intermolecular hydrgen bonded -OH stretching vibrations and at

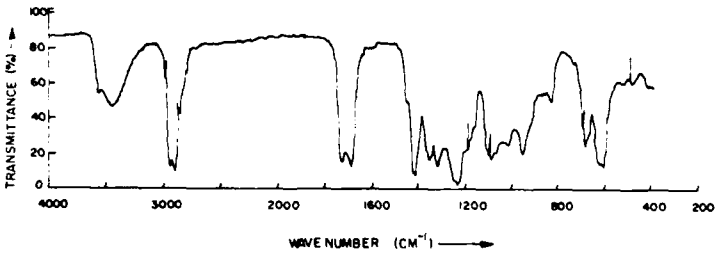

Fig.1. IR spectra of Terpolymer at 298K.

~3580 cm^{-1} it may be either due to the intramolecular hydrogen bonded -OH groups or free -OH groups already present or generated to the breaking of intermolecular hydrogen bonding [1]. Further, this broad band at ~3460 cm^{-1} is not the result of absorbed water as shown by the examination of the thoroughly dried films in which the breadth and intensity of this band would have changed on humidification of the films [7].

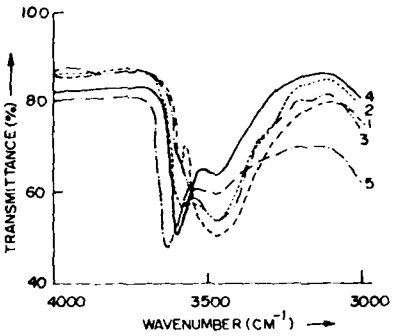

Fig.2. IR spectra of Terpolymer at 1-298,2-323,3-348,4-373 and 5-398K.

The lowering of C=O absorption in carbonyl compounds due to hydrogen bonding by 40-60 cm^{-1} has been reported earlier [8]. In the present investigation the complete elimination of hydrogen bonding on heating is ruled out, therefore, the shift to this extent was not observed. The association of hydrogen bonding with carbonyl groups has been confirmed with the shift of C=O absorption band by ~15 cm^{-1} towards higher frequency side on heating the films from 298 to 398K. In the present studies, the increase in the magnitude of the high frequency sharp band and simultaneous decrease in the magnitude of broad band with the rise of temperature are observed. Particularly, above T_g, there is observed a shift in the high frequency sharp band towards the high frequency side with the rise of temperature. There arises two possibilities:

(a) The broad band at ~3460 cm^{-1} maybe associated with the intermolecular hydrogen bonding. On raising the temperature the intermolecular bonded -OH bonds are broken and set free and their numbers increase with the temperature, thereby showing an increase in ~3580 cm^{-1} band and subsequentlydecrease in the magnitude of the ~3460 cm^{-1} broad band.

On further increase of temperature (beyond T_g) of the films it is changed into the rubber like state in which segments are not much constrained as before (below T_g), showing a little shift in the ~3580 cm^{-1} band, towards

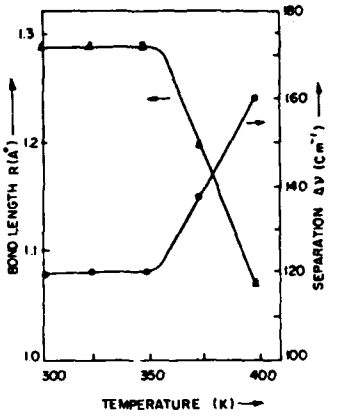

Fig.3. Plot of $\Delta\nu$ and R vs Temperature.

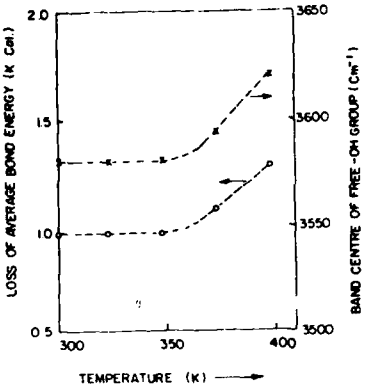

Fig.4. Plot of loss of average bond energy and Band centre of free -OH group vs. Temperature.

high frequency side.

(b) The second possiblity is that the material shows amorphous character [9]. The broad band at $\sim$3460 cm^{-1} may be due to the intermolecular bonded -OH groups in the amorphous region, while the sharp band on the high frequency side, which is observed at a frequency lower than that corresponding to the free -OH groups in liquid/vapour state, may be due to free -OH groups, which are constrained at the lattice sites of the crystalline structure. The separation between the two bonds ($\Delta\nu$) and band length (R) at different temperatures have been calculated [10] and are shown in Fig.3.

These observations are similar to those reported [10] earlier. It has been shown [11] that the stronger the hydrogen bond the greater is $\Delta\nu$. Thus one would expect that the value of $\Delta\nu$ would vary inversely with the length of the hydrogen bond.

Fig.4 shows the loss of energy of the hydrogen bond and the change in the position of band centre of free -OH groups as a function of temperature. It is evident from this figure that above T_g of this terpolymer ($\sim$344K) the loss of energy of hydrogen bond and the change in position of band centre of free -OH groups are clearly noticed.

From the above discussions, it may be concluded that (i) heating to $T > T_g$ breaks intermolecular hydrogen bonds and (ii) slow cooling to $T < T_g$ may make the intermolecular hydrogen bonds once again (iii) quenching tc $T < T_g$ the partial formation of hydrogen bonds may not take place to the extent expected in the process (ii) above.

Thus the magnitude of the absorption bands at $\sim$3460 cm^{-1} and at $\sim$3580 cm^{-1} enable a quantitative estimate of the concentration of "free" and "bound" groups at different stages of heatings.

REFERENCES

[1] R.M. Badger and S.H. Bauer, J. Chem. Phys., 5, 839 (1973).

[2] E.R. Lippincott and E. Schroeder, J. Chem. Phys., 23, 1099 (1955).

[3] A.V. Stuart and G.B.B.M. Sutherland, J. Chem. Phys. 24, 599 (1956).

[4] R. Schroeder and E.R. Lippincott, J. Phys. Chem., 61, 921 (1957).

[5] J.N. Finch and E.R. Lippincott, ibid 61, 894 (1957).

[6] A. Elliott, E.J. Ambrose and R.B. Temple, J. Chem. Phys., 16, 877 (1948).

[7] H.C. Hoss, J. Polym. Sci., 26, 39 (1957).

[8] Y.R. Sharma "Elementary Organic absorption spectroscopy" S. Chand publ., India 1980

[9] V.S. Panwar, R. Singh, G.L. Malhotra, S.K. Sharma, P.C. Mehendru, and N.P. Gupta, J. Mat. Sci. Letters. (In Press).

[10] L.P. Kuhn, J. Am. Chem. Soc. 74, 2492 (1952).

[11] R.M. Badger, J. Chem. Phys., 8, 288 (1940).

*Present Address: Physics Department
J.V. Jain College,
Saharanpur, India

AC CONDUCTIVITY AND DIELECTRIC CONSTANT STUDIES OF VINYL CHLORIDE:VINYL ACETATE COPOLYMERS

P.C. Mehendru, Ramadhar Singh, V.S. Panwar & N.P. Gupta*

National Physical Laboratory, New Delhi - 110012, INDIA

ABSTRACT

AC conductivity $\sigma(\omega)_m$ and dielectric constant ϵ' of vinyl chloride:vinyl acetate (VC:VAc) copolymers having 3,10 and 17% VAc content (by weight) have been measured in the temperature range 77-410K and in the frequency range 50Hz-100kHz. At low temperatures upto 250K, the AC conductivity can be expressed as $\sigma(\omega) = A\omega^s$ where the slope 's' is close to unity and decreases with the increase in temperature. The dielectric constant in this temperature region shows a very weak frequency and temperature dependence. At temperatures (above 300K) the AC conductivity shows a strong temperature dependence. However, the dielectric constant in this temperature region shows a strong frequency dispersion. The mechanisms of conduction in the low and high temperature regions have been discussed in the light of existing theoretical model.

INTRODUCTION

The dielectric relaxations of several polymers have been reported in literature [1]; however, no detailed studies of dielectric constant and ac conductivity of vinyl chloride:vinyl acetate (VC:VAc) copolymers have been reported so far. In the present paper we report the measurement of ac conductivity and dielectric constant of VC:VAc copolymers having 3,10 and 17% VAc content (designated as P1,P2 and P3 respectively) in the frequencyrange 50Hz-100kHz and in the temperature range 77-410K.

EXPERIMENTAL

The copolymers P1,P2 and P3 were obtained from M/s Polysciences, USA. Films $\sim$100 μm thick were grown by solution evaporation technique. Silver electrodes were vacuum deposited on both sides of the sample making an Ag-P-Ag structure. The dielectric measurements were made by using GR1615A Capacitance Bridge.

CH2593-2/ 88/ 0000-0627$01.00 Copyright 1988 IEEE

RESULTS

The temperature dependence of measured ac conductivity $\sigma(\omega)_m$ and the dielectric constant ϵ' of P1 (as representative result) are shown in Figs. 1 and 2, respectively. Fig. 3 shows the variation of $\sigma(\omega)_m$ as a function of frequency in the range 100Hz-100kHz at five different temperatures. Similar results (not shown) have been obtained for copolymers P2 and P3. Fig. 4. shows the behaviour of ϵ' as a function of frequency in the range 50Hz-100kHz at 340K for P1,P2 and P3.

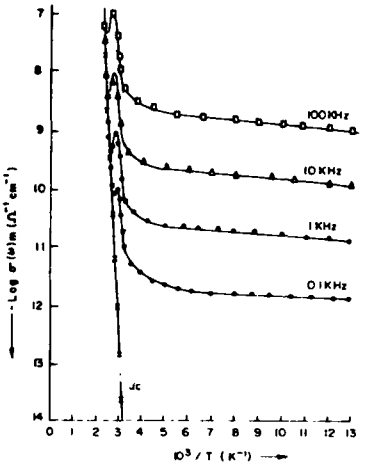

Fig.1. Plot of $\sigma(\omega)_m$ vs. $\frac{1}{T}$

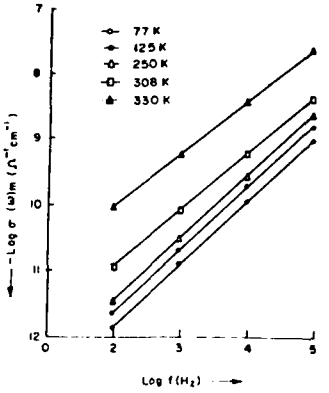

Fig.3. Plot of $\sigma(\omega)_m$ vs. f

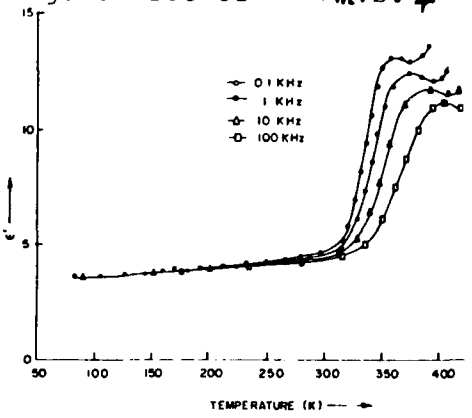

Fig.2. Plot of ϵ' vs. Temp.

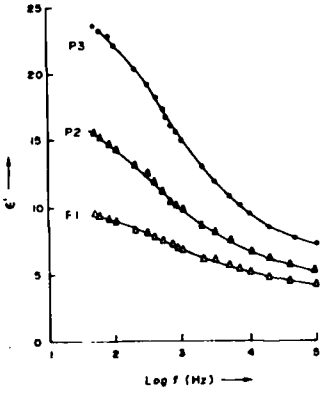

Fig.4. Plot of ϵ' vs f

DISCUSSION

The ac conductivity $\sigma(\omega)$ at low temperature is frequency dependent and can be expressed [2] as

$$\sigma(\omega) = A\omega^s \quad \cdots (1)$$

where 's' ($0.7 < S < 1$) is independent of frequency. At temperatures upto 250K where $\sigma(\omega)_m \gg \sigma_{dc}$, the variation of $\sigma(\omega)_m$ with frequency (Fig.3) can be expressed in terms of Eqn. (1). The value of 's' in this temperature range for P1, P2 and P3 is $\sim$0.94-0.95, however beyond 250K, 's' decreases with the increase in temperature. The activation energy of the carriers calculated at 77K for these copolymers are $\sim$0.01 eV which indicates the evidence of electronic hopping conduction [3] in these materials at low tempertures.

The number of pair centres responsible for ac conductivity can be estimated from Pollak and Geballe [4] which can be expressed for frequency range 100Hz to 100kHz in the following form:

$$\sigma(\omega) = \frac{\pi}{12} \frac{e^2}{kT} N_A N_D \sqrt{S/2} \sqrt{(1-S/2)} (\omega\tau)^S \tau^{-1} (1/\alpha^{-1})^5 \quad \cdots (2)$$

Taking the average value [5] of τ for the frequencty range 100Hz-100kHz of α^{-1} as 4 Å and the values of 's' (at 77K) and $\sigma(\omega)_m$ at 77K and 100kHz the estimated value of $N=(N_A N_D)^{\frac{1}{2}}$ from Eqn. (2) comes $\sim 1\times10^{20}$ cm^{-3}, which is in good agreement with the values reported earlier for amorphous semiconductors [2].

An estimate of the density of states near the Fermi level $N(E_f)$ can be made from the $\sigma(\omega)_m$ at low temperatures where hopping near the Fermi level is expected to dominate. The equation suggested by Pollak [6,7] is similar to that proposed by Austin and Mott [8] but differs in the valuesof the constants. According to Austin & Mott [8]

$$\sigma(\omega) = \frac{1}{3}\pi e^2 KT [N(E_f)]^2 \alpha^{-5} \omega [\ln(\nu_p/\omega)]^4 \quad \cdots (3)$$

The values of $N(E_f)$ calculated from Eqn. (3) assuming $\nu_{ph} \sim 10^{12}$ Hz and α^{-1} as 4Å and using the value of $\sigma(\omega)_m$ at 77K and 100kHz, comes $\sim 10^{21}$ cm^{-3} eV^{-1}. This suggests that hopping near Fermi level is between the nearest neighbour sites. Inspite of the fact that Eqn,.(3) gives a reasonable estimate of $N(E_f)$ it fails to explain the temperature dependence of $\sigma(\omega)$. Equation (3)

predicts a linear temperature dependence of $\sigma(\omega)$, however, the measured values show very weak temperature dependence of $\sigma(\omega)$ in the low temperature region while Eqn. (2) predicts a very weak temperature dependence of $\sigma(\omega)$ which is in good agreement with the observed behaviour. Pollak has argued that the temperature dependence is due to multiple hops but Mansingh et al [9] have shown that multiple hops cannot give a strong temperature dependence of $\sigma(\omega)$ as observed in V_2O_5—P_2O_5 glasses. The measurement of $\sigma(\omega)_m$ as a function of temperature (Fig. 1) shows that the temperature at which σ_{dc} becomes equal to $\sigma(\omega)_m$ for a given frequency, increases with increase in frequency.

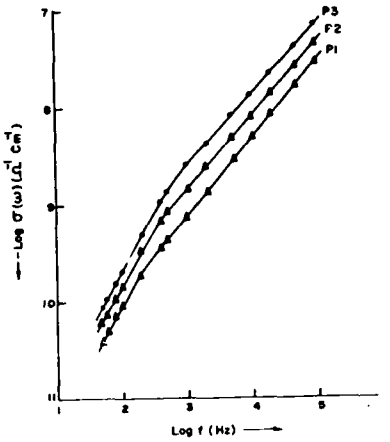

Fig.5. Plot of $\sigma(\omega)_m$ vs. f

At some temperatures, $\sigma(\omega)_m$ for a given frequency and σ_{dc} will appear equal because the dc conductivity may be very much larger than $\sigma(\omega)$ and so $\sigma(\omega)_m$ would appear equal to σ_{dc} within the accuracy of measurement [9]. A similar argument will hold good for the variation of conductivity as a function of frequency at fixed temperatures.

In the low temperature region, carrier hopping occurs with in a system in which a characteristic relaxation frequency f_0 is difficult to define, however, at higher temperatures, where $\sigma(\omega)_m$ approaches σ_{dc} the ac component of conductivity $\sigma(\omega) = \sigma(\omega)_m - \sigma_{dc}$ may show clear evidence for f_0. In particular, ϵ'' will show a Debye type peak at $f=f_0$. A difficulty in this approach is that both $\sigma(\omega)_m$ and σ_{dc} are comparable and the error in $\sigma(\omega)$ is large [9]. It is, therefore, necessary to examine both ϵ' and ϵ'' to justify an analysis in terms of Debye type dispersion. It is seen that the region where there is a strong temperature dependence of ϵ' at a given frequency (Fig.2) is the same in which $\sigma(\omega)_m$ approaches σ_{dc} (Fig.1). Thus the variation of ϵ' with

temperature confirms the existence of Debye type loss peaks indicated in Fig.1. The measured values of ϵ' at 0.1,1, 10 and 100 kHz clearly show a saturation region at the higher temperature end and this may be taken as an estimate of ϵ_0. A plot of $\log \sigma(\omega)$ vs log f at 340K for P1,P2 and P3 (Fig.5) shows a change in slope at a fixed frequency,which corresponds tothe relaxation frequency f_0.

It is evident from Fig.4 that the dielectric constant increases with the increase in VAc content and it is minimum in the copolymer P1 and maximum in the copolymer P3. This temperature of 340K falls in the glass transition region where the materials perhaps turn into a rubbery state and in which the side groups dipoles, whether rigidly or flexibly attached to the main chain of the polymer contribute to the polarization. Further, when VAc content increases the polar character of the materials increases due to the addition of strong polar groups. So the atomic polarizability increases and the effective field in the material medium reduces, which renders an increase in the dielectric constant.

REFERENCES

[1] N.G. McCrum, B.E. Read and G. Williams, "Anelastic and Dielectric Effects in Polymeric Solids", John Wiley and Sons, London (1967).
[2] N.F. Mott and E.A. Davis, "Electronic Processes in Non-Crystalline Materials" Oxford University Press London (1971).
[3] A.K. Jonscher, Thin Solid Films 1, 213 (1967).
[4] M. Pollak and T.H. Geballe, Phys. Rev. 122, 1742 (1961).
[5] A. Mansingh, J.K. Vaid and R.P. Tandon, J. Phys. C: Solid St. Phys. 8, 1023 (1975).
[6] M. Pollak, Phys. Rev. 133, A564 (1964).
[7] M. Pollak, Phil. Mag., 23, 519 (1971).
[8] I.G. Austin and N.F. Mott, Adv. Phys., 18, 41 (1969)
[9] A. Mansingh, R.P. Tandon and J.K. Vaid, J. Phys. Chem. Solids, 36, 1267 (1975).

*Present Address: Physics Department, J.V. Jain College Saharanpur - 247 001, India

The Expreimental Study on The Electret Properties of Carp Scale

Zheng Tong, Wu Zhnghan and Xu Fuelong
Dept. of Phys. and chem. Nanjng Inst. of Tech.

I-Introduction

A lot of biomaterials have general properities of poymers. It display orderly aligment of dipole and it can store charge and ploarization. With a relaxation time. So the techniques used to study the electret effect in biomaterial are essentially the same as for general electret research when we investigate the stucture and physical property of bioelectret.

Scale is the important part that fish make contact with outside world.Studying the electret properties of scale can supply new imformations to analyze physiological phenomenon of fish.So, carp scale was investigated by thermoanalytieal, optical absorption spectra and small angle diffraction of x-ray in this articie.

II-Experimental

Scale Samples were obtained from a live carp directly, In this experimental, scale is taken from flank part of carp. It can be used after it was cleaned and dired.

In order to reduce the gas between the sample and electordes, and avoid the influence of piezoelectric effect.We fit a set of electrodes which surface currature coincide with scale.

TSC charts were obtain from the Electret Analyze which is made of Japan (TOYO SEIKI). the heating rate is 5c MIN^{-1}, scale convex surface downward when the scale heated first time there are two main peaks in the TSC chart.the first peak at 325k. the second at 355k. current dimension about $1*10^{-9}$A if the sample is cooled after the first cycle of TSC and heated

CH2593-2/ 88/ 0000-0632$01.00 Copyright 1988 IEEE

for the second cycle immediatly, both peaks will disappear. if the sample is exposed to atmosphere a few days. the peak will reappear in this cycle, but the current dimension is smaller than last cycle.The scale is dired a few day (about seven days). There is asingle peak at 350k in TSC chart, Current dimension is much small than before; of the sample is polarized at 388k in field of 1KV and polarization time is 5 min. There is a peak at 293k in TSC chart, atter 383k approch to conductance. If convex surface of seale upward, the curren peak change the direction.

There are several methods for calculating the activation evergy of dipoles with a single relaxtion frequency.

Since the temperature is raised linearey with time, the current gensity is a function of temperature

$$j = j_0 \exp\left[-\frac{E_a}{kT} - \frac{1}{\tau_0 \beta}\int_{T_0}^{T} \exp\left(-\frac{E_a}{kT}\right) dT\right] \qquad (1)$$

By differentiat ng (1) with respect to 1/T, we obtain for the initial current rise

$$\frac{d}{d(1/T)} \ln(j/T) = -E_a/k \qquad (2)$$

Thus we can find the activation energy Ea.

The other method for calculating Ea is the use of halfwidth of current peak.So, activation energy can be calculated from

$$\Delta T/T_m \doteq 2.47\, T_m/E_a \qquad (3)$$

By the two methods,we can find the activation energy of that tow peak from thermoanalytical data.

Ea of first peak is 0.64ev, Ea of second peak is 0.87ev.

The aim of infra-red spectrum analysis is to determine the compositions of scale molecule, we obtain the molecular formula by the spectrum $Ca_5[F/(PO_4;CO_3OH)_3]$

We analyze structure of scale by small angle diffraction of x-ray, diffraction curve illustrate that the molecular formula of scale is $Ca_{10}(P,C,O_4)_6(OH,F)_2$,it belong to hexahedron

crystal, a=9.403A, c=6.827A, every cell content a molecula. layer distance of crystal is about 14.4A.

Results and Conclusions

As the result of thermoanalytial, during the sample warm-up the first times, dipoles change direction,charges get rid of trap and palymer lose free water and bound water,so, carp scale present strong TSC,Repeat experiment immed [illegible], there is no TSC phenomenon, it indicate that current originat form electrocctue.

If the scale is turned upside down, the current peaks change direction. it show that there are a few dipoles orderly alignment along the direction that is perpendicular to growth direction of scale.

Scale present strong polarization storage and the polarization storage is recoverable. After dried, scale is heated and polarized, it present current peak in TSC charts. This effect is probable due to the water in polymer and dipoles of collagen orientation alignment.

As the result of smalle angle diffraction of x-ray,interior structure align in periodic [illegible]er, it comform with the mention in references that collagne molecule alignment in helix

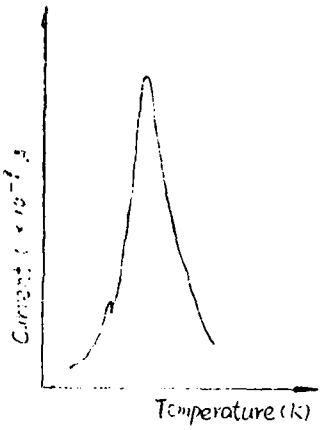

FIG.1 TSC curve of scale in first cycle

FIG. 2 — TSC curve of scale after dlred

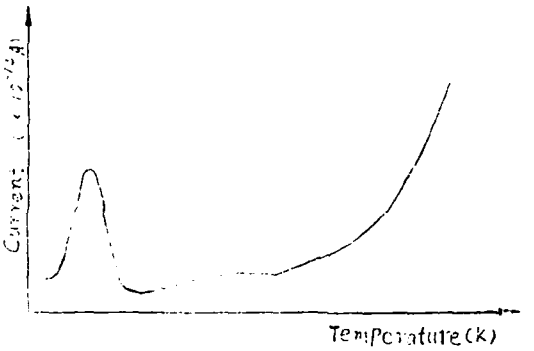

FIG.3- TSC curve of scale after Polarized

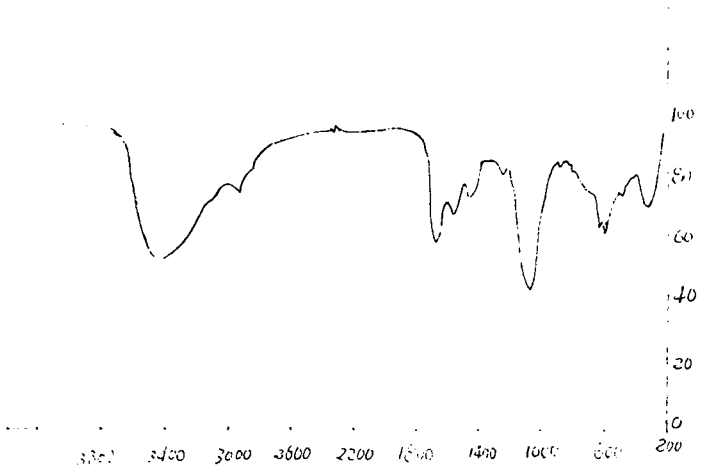

FIG. 4.—Infra-red absorption spectrum

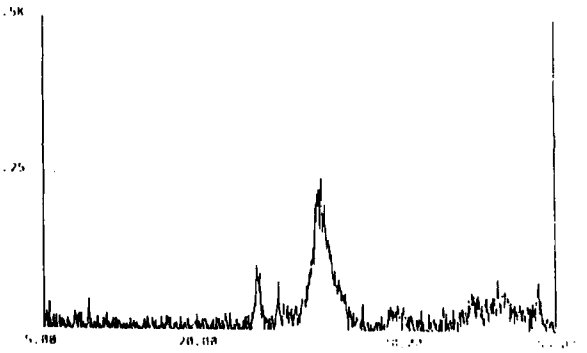

FIG. 5 Small angle diffraction of X-ray
[illegible] of scale

THE ANALYSIS OF THERMALLY STIMULATED CURRENT TO PIG BONE

Zhu Yafei, Wu Zonghan* and Xu Fudong*.

Education Centre, Nanjing Radio Factory.
*Dep. of Phys. and Chem.
Nanjing Inst. of Tech.
Nanjing, P.R. of China

ABSTRACT.

It was found that there was a peak of 10^{-8} A at 75℃ in the TSC spectrum of crude bone. This peak had disappeared in the second cycle of TSC experiment performed immediately after the first cycle or a thermal polarization, but it had reappeared after the sample was exposed to the atmosphere for a few days. When the sample was turned over, the direction of peak was not changed. After the sample was dryed completely, the peak at 75℃ disappeared, but another peak which was much smaller than the peak at 75℃ appeared at around 95℃ and its direction couldn't be reversed by turning the sample over too. In this paper, the method of X ray diffraction and the infrared absorption are used as complementary analysis. It can be concluded from the experiments that the larger peak is originated from the free water and the smaller one is due to the crystallization water, keratin and peptide, etc.

INTRODUCTION:

It has been discovered that there is an obvious charge storage effect in the organs of human being and animals, such as bone, blood vessel, etc.[1] The study of bioelectret is of great significance for seeking the recovery of animal's tissue, and for exploring man-made organ and life phenomenon. In this paper, the electret properties of pig bone was analysed and researched by the method of TSC, and the form of electret state was given by a preliminary explanation.

INSTRUMENT:

It is known how the electrets produce TSC. Its principle is

CH2593-2/ 88/ 0000-0637$01.00 Copyright 1988 IEEE

simply shown in Fig.1. The instrument we use is the Thermally Stimulated Current Measurement Apparatus made in the TOYO SEIKI SEISAKUSHO, ITD. The type of microelectrometre is 410A PICOAMNETER.

SAMPLES:

The samples concerned in this paper are the crude pig-scapula.

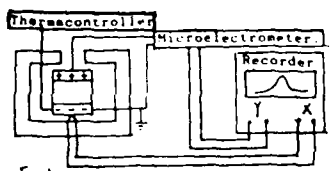

Fig.1.The schematic diagram of TSC.

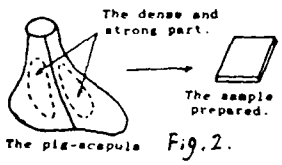

Fig.2.

After clearing the scapula, we can get the dense and strong part of it and grind it to a 0.5 millimetre thick thin slice. A little piece about one square centimetre was cut from the thin slice and marked in No. as shown as Fig.2. Since the polarization inside the sample is the same direction as the growth of biological tissue, so it is parallel to the upper and below surface of the sample we get.

THEORY:

The Analysis of Thermally Stimulated Current:

The principal equation of electret TSC is known as following:

$$j = j_0 \exp\left(-\frac{Ea}{KT}\right) \frac{1}{\tau\beta}\int_0^T \exp\left(-\frac{Ea}{KT}\right)dT$$

In it, $j_0 = P_0 \tau_0$ is the constant of current density; Ea is activation energy; K is the constant of Boltzman; T is the temperature; τ_0 is the relaxation time; β is the rate of heating.

This formula is well fit to the dipoles and charges which possesses a signle activation energy. We can get the peak temperature Tm and activation energy Ea from the experiment curve. Now we use the method of initial rise to obtain the Ea. The data and their calculation is shown in table 1.

Table : 1.

The Sample No.	The sample thickness (cm)	The cycle No.	The interval between two cycles(s)	The peak direction	The order of peak current (A)	The peak temperature (℃)	Activation energy Ea (ev)	Figure No	Remarks
1	0.482	1	/	negative	10^{-8}	77	1.21	2	not dryed
		2	0	No	0	/	/	4	
		3	170	negative	10^{-8}	72	0.65	5	
		4	120	negative	10^{-10}	79	0.86	6	
2	0.510	1	/	negative	10^{-9}	77		7	not dryed
		2	0	No	0	/		8	
		polarisation							Tp=120℃ Vp=500V tp=10min
		3	0	No	0	/		9	not dryed
3	0.500	1	288	negative	10^{-13}	100	/	10	not dryed
		polarisation						11	Tp=130℃ Vp=1kV tp=10min
		2	0	positive	10^{-10}	35	0.19	12	dryed
4	0.501	1	282	negative	10^{-11}	98	1.21	13	dryed
		polarisation						14	Tp=110℃ Vp=1kV tp=10min
		2	0	positive	10^{-10}	65	0.01	15	dryed

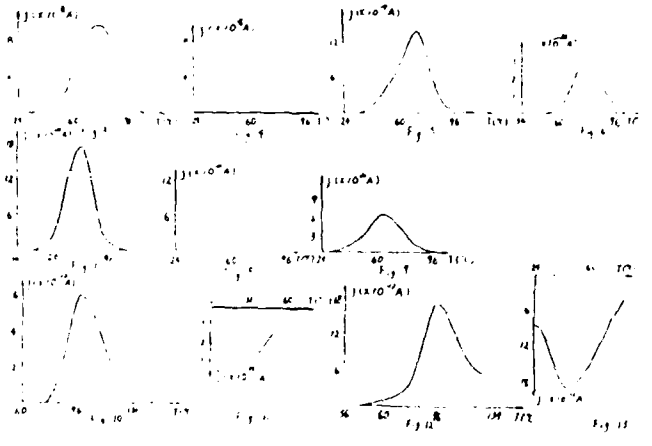

The Analysis of X-Ray Diffraction and The Infrared Absorption Spectrum:

1). X ray diffraction can be seen in Fig.14. We found that several peaks aligned regularly and there exist a big peak. it means that some substance inside bone arranged regularly.
2). The infrared absorption spectrum can be seen in Fig.15. The chemical composition of bone found out from it are carbonat apatite and other basical group, such as CO_3 NH_2 etc.

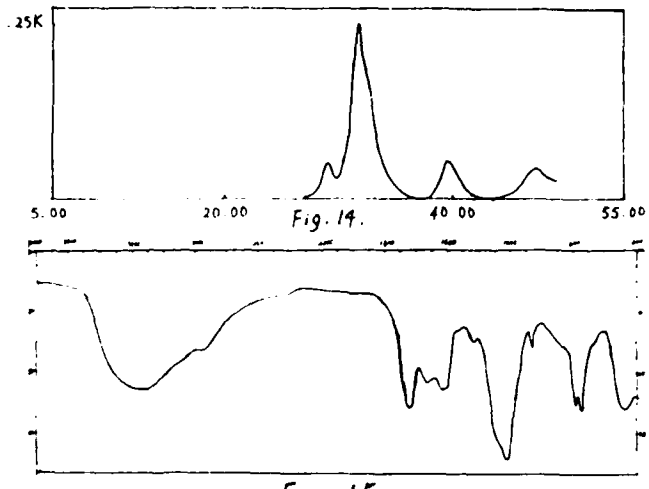

Fig. 14.

Fig. 15.

A PRELIMINARY ANALYSIS:

From the above results, we are able to follow preliminarily that the TSC of crude scapula result mainly from the release of the polarized molecules, such as of water, keratin and peptide, etc. inside sample. This point of view came from following aspects:

1). The bone without any processing contains a lot of water on its surface and inside it, so there exist a obvious peak in TSC. In this experiment, the sample was heated up over 120℃, a lot of water was released, so from the second cycle after the temperature dropped or a thermal polarization was performed there exist no current peak in the measurable range we chose. But after the sample was exposed to the atmosphere without being dryed for a few days, it could suck up moisture from the atmosphere, but the moisture might be unstable to connect with sample and less than that of those not used samples. So the peak had appeared when the second TSC cycle was done, and the temperature and the shape of peak are basically similar to those in the first cycle, but the activation energy Ea is smaller than that one of the first cycle, it is obvious as seen in Table 1.

2). The TSC was still produced by the sample which was dryed, the reason is that TSC was formed by the crystallization water and keratin aligning in order. From the infrared absorption

spectrum, we noted that the sample contained CO and NH. From the X-ray diffraction we predicted that CO, NH arranges in order periodically. It was just consisted with the literature[2] reporting that OCNH possesses the screw structure.

3). The literature[1] had reported that dipoles in the sample had changed its direction obviously when the temperature was heated up over 200℃, but the temperature wasn't heated up over 200℃ in our experiments, and the direction of polarization inside the sample was the same as the one of bone growth, so it was parallel to the upper and below surface of the sample. From the Table 1., we can see that the dryed samples have quite small Ea after polarization. So water play marked role while TSC occurred, the motion of water molecules once released from the stucture of sample wasn't connected with how the sample was set, but the electrode shape and surroundings. It was consistent with the experimental result that the samples dryed and without processing produce the current of same direction whatever direction we put the samples on. So we assume that the release of free water and crystalization water might be the reason of TSC and of the phenomenon which occurred.

CONCLUSION:

1). The contribution to the TSC in bioelectrets is changing according to following order: free water, crystalization water, keratin, peptide. Water in biomaterial has great infuluence to electret property, so it must be given a lot of attentions.

2). On research bioelectrets, the growth direction of biomaterial should be considered carefully when the sample is chosen. Since the direction of polarization inside the sample is the same as the growth direction of tissue. The result would be different if the sample is chosen along the growth direction of the biomaterial or perpendicular to the growth direction. So the infulurence of controlling the biomaterial growth in bioelectrets is connected with the direction.

REFERENCE:

[1]: G.M.Sessler, "Electrets", Springer Verlay Berlin and New York, 1980.

[2]: E.FUKADA, "Organism and Electret", Stett Design. No.163, Page 29.

EFFECTS OF PLASMA TREATMENT OF SURFACES ON CHARGE STORAGE IN POLYPROPYLENE

Hui-juan Zhao, De-min Tu, Liang-yu Gao and Yao-nan Liu

Department of Electrical Engineering, Xi'an Jiaotong University, Xi'an, China

and

Kwan C. Kao

Materials and Devices Research Laboratory, Department of Electrical Engineering, University of Manitoba, Winnipeg, Manitoba, Canada R3T 2N2

ABSTRACT

With the surfaces of polypropylene samples treated in an 800 kHz plasma of air at low temperatures, the level of charge storage in polypropylene is increased, and it depends strongly upon the plasma treatment and charge injection conditions. Under the optimal conditions the polypropylene with plasma treatement may store about 50% in average more charges and the thermally stimulated charge decay becomes much slower than those without treatment. Infrared absorption and photoconductivity spectra indicate that the plasma treatment enhances the formation of C = O and C = C bonds and the degree of crystallinity, which result in an increase of polar groups and deep traps.

INTRODUCTION

It is well known that surface traps play an important role in electrets particularly when surface charging techniques are used for charge injection. In most polymers there exists a large number of surface traps which may be due to chemical impurities, surface oxidation, broken chains, adsorbed molecules, or differences in short-range order of surface and bulk [1]. For polymeric electrets, charges are generally injected into the material through surface states and they are then trapped in the region very close to the surface [2-4]. It is obvious that the charge storage would depend strongly on the behaviour of the surface states and the localized states in the bulk near the surface. Plasma techniques have been widely used for material processing [5]. We therefore carried out an experimental study about the effects of plasma treatment of the surfaces on charge storage in polypropylene. In this paper we

CH2593-2/ 88/ 0000-0642$01.00 Copyright 1988 IEEE

report some new results about these effects under various experimental conditions.

EXPERIMENTAL

The polypropylene was in film form with a thickness of 25 um. Prior to charge injection, the samples were immersed in alcohol for about three hours and then dried under infrared light in order to eliminate any residual space charges at the surface. After this pre-treatment process the samples were treated in a plasma at low temperatures. The plasma was formed in air at a pressure of 10^{-1} torr and a high frequency (800 kHz) operating voltage of 2 kV between two parallel aluminum electrodes of 1.5 cm in separation and 10 cm in electrode diameter. For most experiments the plasma operating voltage V_p was 2 kV and the plasma treatment time t_p was 2 minutes, unless otherwise stated.

Using the conventional corona charging technique, electrons were injected to the polypropylene sample by applying a negative dc voltage V_c to the needle electrode. Multi-needles were used as the negative needle electrode and a stainless steel plate beneath the sample as the grounded positive electrode. The separation between the needle and the plate electrodes was 2 cm and the separa-

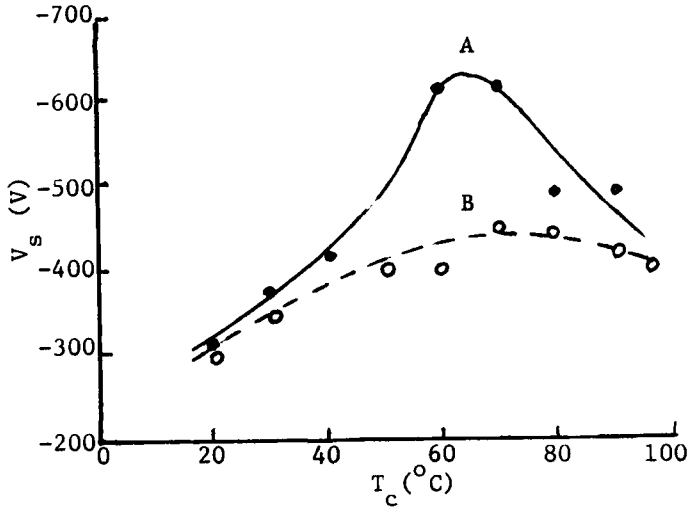

Fig. 1. The surface potential as a function of sample temperature during corona charging injection. (A) With plasma treatment, (B) Without plasma treatment.

tion between two neighbouring needles was 1 cm, the needle radius being 20 um. During charge injection, the sample could be heated to any temperature and maintained at a constant temperature pre-set for particular experiments. After electron injection, the surface potential V_s was measured at room temperature using a potentiometer. We have also made measurements of secondary ion mass spectroscopy, infrared absorption and photoconductivity spectra, and thermally stimulated charge decay in order to study the mechanisms responsible for the effects of plasma treatment.

RESULTS AND DISCUSSION

With the plasma operating voltage V_p = 2 kV and the plasma treatment time t_p = 2 min, the surface potential V_s was measured as a function of sample temperature during charge injection at a fixed corona charging voltage of 4.9 kV and a fix corona charging time of 60 min. The results are shown in Fig. 1. It can be seen that V_s for samples with plasma treatment is generally higher than those without plasma treatment, and that the highest value of V_s occurs at a temperature of 70°C.

With V_p = 2 kV, t_p = 2 min and a fixed corona charging voltage V_c = 4.9 kV and a fixed charge injection temperature T_c = 70°C, the surface potential V_s was measured as a function of corona charging time t_c. The results are shown in Fig. 2. V_s increases with increasing t_c and tends to reach a saturation value at t_c = 50 min.

With V_p = 2 kV, t_p = 2 min, t_c = 60 min, and T_c = 70°C; the results of V_s as a function of V_c are shown in Fig. 3. V_s increases with increasing V_c. However, V_s tends to reach a saturation value at V_c = 4.2 kV.

We have also studied the effects of plasma treatment contions. Figure 4 shows V_s as a function of t_p with a fixed V_p = 2 kV, and V_s as a function of V_p with a fixed t_p = 5 min for V_c = 4.2 kV, t_c = 60 min and T_c = 70°C. From Fig. 4 we can see that V_s is maximum at t_p = 5 min. For higher values of t_p, V_s tends to decrease possibly due to the damage caused by prolonged electron bombardment. The value of V_s also tends to reach a saturation value at V_p = 3.5 kV.

Under optimal conditions: V_p = 3.5 kV, t_p = 5 min, V_c = 4.2 kV, t_c = 60 min and T_c = 70°C, the value of V_s for samples with plasma treatment is about 50% higher than those without plasma treatment.

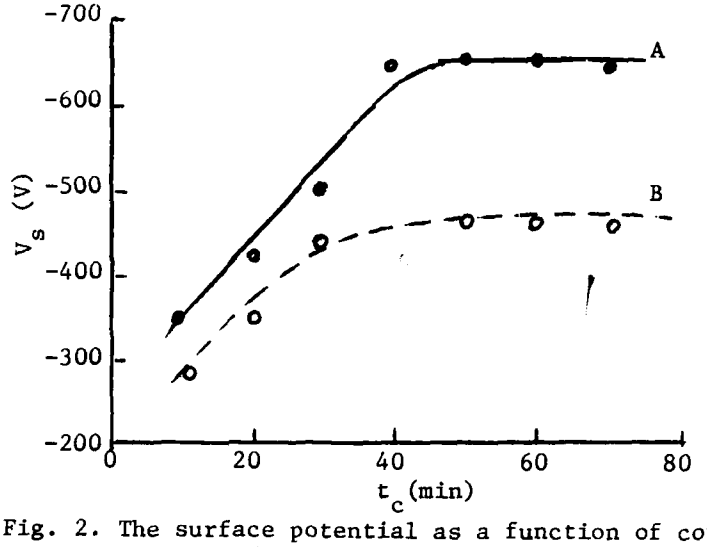

Fig. 2. The surface potential as a function of corona charging time. (A) With plasma treatment, (B) Without plasma treatment.

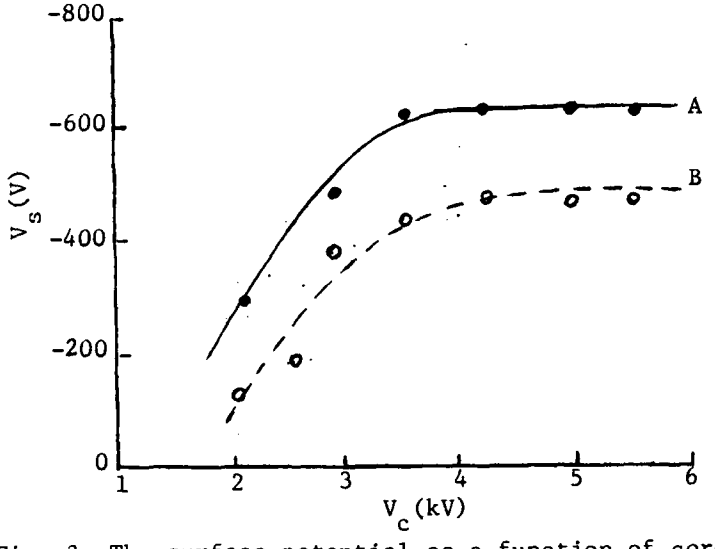

Fig. 3. The surface potential as a function of corona charging voltage. (A) With plasma treatment, (B) Without plasma treatment.

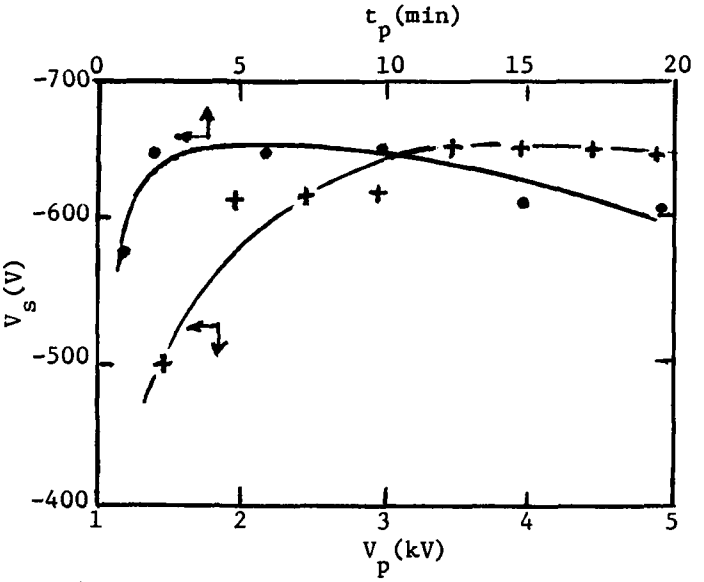

Fig. 4. The surface potential as a function of plasma operating voltage and plasma treatment time.

Other measurements indicate that the plasma treatment introdices more deep traps, higher contents of C = O and C = C bonds and a higher degree of crystallinity, thus improving the capability of charge storage and suppressing the rate of thermally stimulated charge decay.

Financial support of the Natural Sciences and Engineering Research Council of Canada is very much appreciated.

REFERENCES

[1] H. Fuhrmann, J. Electrostat. 4, 109-114, 1978.

[2] T. Mizutani, T. Oomura, and M. Ieda, Japan J. Appl. Phys. 21, 1195-1198, 1982.

[3] G.M. Sessler (Editor), Electrets, Springer-Verlag, New York, 1980.

[4] M. Ieda, IEEE Trans Elec. Insul. EI-22, 261-267, 1987.

[5] S. Sapieha, D. Sadhir, and H.E. Saunders, IEEE Elec. Insul. Mag. 2, 8-14, 1986.

POLYMERIC MATERIALS WITH ENHANCED SECOND ORDER NONLINEARITIES

H.E.Katz, M.L.Schilling, R.B.Comizzoli

AT&T Bell Laboratories, Murray Hill, NJ 07974

K.D.Singer, J.E.Sohn, M.G.Kuzyk, W.R. Holland

AT&T Engineering Research Center, Princeton, NJ 08540

Electric field poling of thin polymer films containing dipolar chromophores provides materials possessing significant bulk second order nonlinear optical susceptibilities. Incorporation of cyanovinyl acceptor groups into the chromophores results in larger susceptibilities than when the more usual nitro group is used. Methods to further augment the electro-optical activity and improve the orientational stability of the materials are under investigation, particularly the covalent attachment of the chromophores to the polymer backbone.

INTRODUCTION

Poled polymers containing conjugated donor- and acceptor-substituted moieties are among the leading candidates for organic electro-optical materials [1]. We have already demonstrated that poly(methyl methacrylate) (PMMA) doped with an azo dye may be applied as a film on a substrate by spin coating, and poled to give a material with a considerable bulk second order susceptibility [2]. Our initial report focussed on materials containing the amino nitro dye 1 (Disperse Red 1). Following our experimental verification of the increased molecular hyperpolarizabilities of di- and tricyanovinyl-substituted anilines and amino azo dyes relative to the nitro compounds [3], we described a series of materials in which cyanovinyl compounds such as 2 were employed as the active species [4]. As expected from the thermodynamic model of the poled polymer system, the bulk susceptibilities of the newer materials were increased

CH2593-2/ 88/ 0000-0647$01.00 Copyright 1988 IEEE

relative to the material containing Disperse Red 1. (This trend is apparent from data listed in Table 1, discussed below.)

The activity of the materials was limited by dilution of the chromophores in the matrix, since the maximum concentration of highly polar dye that could be dissolved in the moderately polar PMMA host before phase separation occurred was only 10-20 weight percent. Partial relaxation of the oriented dyes to a more randomized state was observed after poling, with a concomitant loss of bulk nonlinearity. This paper outlines some ongoing research aimed at overcoming these difficulties.

RESULTS AND DISCUSSION

A conceptually simple modification of our dye-PMMA system that addresses the concentration and relaxation issues is to covalently attach dyes to the PMMA backbone as esters of the methacrylate subunits, as illustrated by structure 3. Covalent attachment effectively "predissolves" the dye in the matrix, and also restricts the molecular motions that lead to orientational randomization. Because of the inhibitory nature of the electron withdrawing substituents on free radical-initiated polymerization, a method was devised for converting pre-polymerized aniline methacrylates to azo dye polymers. By diluting the aniline residues with methyl methacrylate monomeric units, copolymers containing dyes present over a wide range of concentrations could be prepared. The isolation of cyanovinyl aryldiazonium salts of determined purity was essential to the success of the novel azo coupling reactions that led to polymeric dyes. The weight average molecular weights of the isolated polymers was typically 10-20,000 g/mol, while the Tg was 5-30 degrees above that of pure PMMA, and 15-50 degrees above that of PMMA containing Disperse Red 1.

Measurements of second harmonic coefficients d on a corona poled dicyanovinyl azo dye covalently bound to PMMA, 3, are given in Table 1. Also included for comparison are data obtained on corona poled samples of 2 and 1 dissolved in PMMA, and an electrode-poled film of 1 dissolved in the polymer. Films were spin coated onto indium-tin oxide glass

substrates before poling. The use of a corona discharge for poling has been found to be more effective than planar electrode poling, as indicated by the two entries for dye 1. As discussed above, chromophore 2 imparts generally higher bulk susceptibilities on materials than does 1.

The "original" second harmonic intensity (measured immediately after poling) and therefore the net orientation for the covalently bound dye 3 is less than that which would have been predicted from a thermodynamic model of the system for the given number density of chromophores [4]. On the other hand, the stability of the second harmonic signal, and by inference the stability of the orientation, is much improved in the covalently bound system, so that the "final" values of d (measured days to weeks after poling) for 3 differ little from the original values and substantially exceed those of 2 dissolved in PMMA. Taken together, these results suggest that molecular motions associated with both the poling and relaxation processes are more hindered in the dye copolymer than in dye-polymer mixtures. The ratio d_{33}/d_{31} is approximately 3 in all of the samples, in agreement with theoretical expectations for uniaxial films.

Directly measured values of the electro-optic coefficient r for polymer 3 are 18 pm/V and 6 pm/v for the 33 and 13 components respectively, as compared to 30 pm/V and 9 pm/V for the 33 and 13 components of lithium niobate. The calculated figures of merit n^3r/ϵ are of the same order of magnitude for the two materials. Near agreement of our measured values of r and values derived from second harmonic data indicate that the origin of the electro-optic effect in the polymeric materials is predominantly electronic.

In summary, a dye copolymer has been synthesized and processed to yield a novel single-component material with useful, stable bulk hyperpolarizabilities.

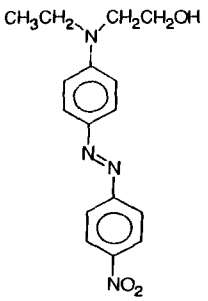

1

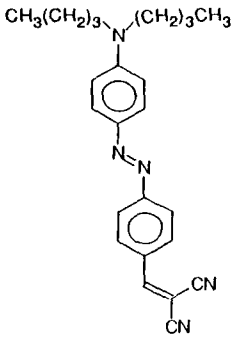

2

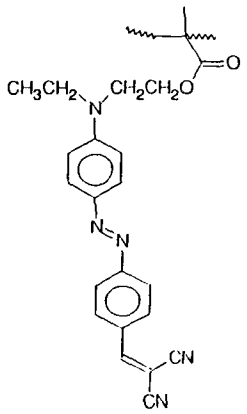

3

TABLE 1

Material	Number Density, (10^{20}/cm^3)	Refractive Index (799 nm)	d(original) (10^{-9} esu) (1.58 um)	d(final) (10^{-9} esu) (1.58 um)
3, PMMA copolymer	8	1.58	d_{33} 51 d_{31} 17	46 15
2, dissolved in PMMA	2.3	1.53	d_{33} 74 d_{31} 25	19 6
1, dissolved in PMMA	2.3	1.52	d_{33} 20 d_{31} 7	—
1, dissolved in PMMA, electrode poled	2.7	1.52	d_{33} 6 d_{31} 2	—

References

[1] Heeger, A.J.; Orenstein, J; Ulrich, D.R., Eds. Mater. Res. Soc. Symp. Proc. 1988, 109.

[2] Singer, K.D.; Sohn, J.E.; Lalama, S.J. Appl. Phys. Lett. 1986, 49, 248.

[3] Katz, H.E.; Singer, K.D.; Sohn, J.E.; Dirk, C.W.; King, L.A.; Gordon, H.M. J. Am. Chem. Soc. 1987, 109, 6561.

[4] Katz, H.E.; Dirk, C.W.; Schilling, M.L.; Singer, K.D.; Sohn, J.E. Mater. Res. Soc. Symp. Proc. 1988, 109, 127.

THE LUMINESCENCE STIMULATED BY TEMPERATURE CHANGE OF CRYSTALLINE FILMS OF N-ISOPROPYLCARBAZOLE*

Z.Dreger and J.Kalinowski

Department of Molecular Physics, Technical University of Gdańsk, 80-952 Gdańsk, Poland

R.Nowak** and J.Sworakowski

Institute of Organic and Physical Chemistry, Technical University of Wrocław, 50-370 Wrocław Poland

ABSTRACT.

The spontaneous emission of light stimulated by temperature change of the vacuum-evaporated crystalline layers of N-isopropylcarbazole (NIPC) has been studied between 100 and 300K.A theoretical model is presented and the temperature evolution of the luminescence is derived including the effects of electrical discharge in the ambient gas due to high electric fields produced by spontaneous polarisation at fresh microcrystal faces emerging during crystallites cracking on cooling or heating of the layer.
Overcome of strength threshold and stress/temperature-induced phase transitions of microcrystallites are assumed to be physical mechanisms responsible for the cracking.

INTRODUCTION.

The spontaneous luminescence observed upon changing temperature of pyroelectric crystals, described recently in literature and referred to as

*The work supported in part by the Polish Academy of Sciences under Program CPBP 01.12.

**Present address: Department of Chemistry, Colorado State University, Fort Collins, Colorado, 80523 U.S.A.

CH2593-2/ 88/ 0000-0652$01.00 Copyright 1988 IEEE

pyroelectric luminescence (PEL)[1-8], is in most cases observed as a sequence of discrete pulses of light. PEL has also been observed on polycrystalline thin films of NIPC [5], its temperature dependence, however, was found to be completely different from that of single crystals and consisted of broad bands appearing below 200K. In this paper, we present results of systematic studies of PEL in vacuum-deposited crystalline thin films of NIPC. We also offer an interpretation of observed phenomena.

RESULTS.

The emission of light from NIPC films can be observed on both cooling and heating the samples, without any previous treatment (cf. Fig. 1). Hereafter,we shall refer to the emission of light observed in the experiments described in this paper as luminescence stimulated by temperature changes (LSTC). The intensity of the luminescence depended on the presence of the ambient gas. The pressure of the gas influenced LSTC intensity only to a minor degree down to ca. 0.01Pa; however, below 0.01Pa the light emission disappeared completely. The most striking

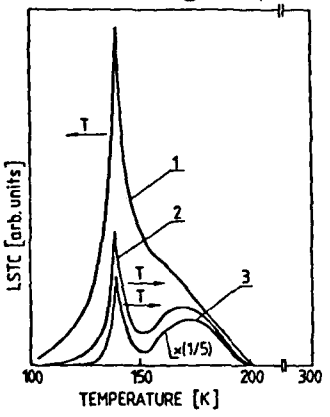

Fig.1.LSTC curves of a NIPC film: 1-cooling; 2,3-heating with two different rates (2-0.2 K/s, 3-0.04 K/s).

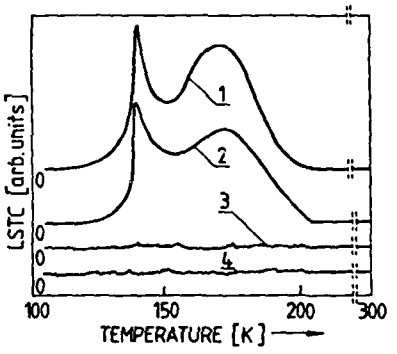

Fig.2.Influence of substrate on LSTC of a NIPC film; substrate : 1-glass, 2-copper, 3-polymer; 4-powder sample.

feature of LSTC of the NIPC films is its dependence on the nature of substrate (Fig. 2).

DISCUSSION AND INTERPRETATION OF RESULTS.

A weak dependence on the pressure of the ambient gas and vanishing of LSTC in vacuum as well as the presence of the emission from the ambient gas in the total LSTC, suggest an important role of electrical discharges in the excitation of LSTC. In principle, the breakdown fields could be generated by the effect postulated for the NIPC single crystals, i.e. as a result of temperature variation of the spontaneous polarisation [8]. However, since LSTC was observed only if the films were deposited onto a substrate having the thermal expansion coefficient significantly different from that of NIPC, it is obvious that mechanical stresses arising during thermal cycling of the samples play an important role. The magnitude of stresses (ξ) appearing in a crystallite attached to a substrate during a temperature change depends primarily on thermal expansion coefficients of the film and substrate, stiffness coefficient (c) of the material, orientation (ϑ) of the crystallites with respect to the substrate, and energy of adhesion of NIPC to the substrate. The stresses lead to cracking the crystallites and detaching them off the substrate. The cracking may appear also as a result of internal stresses in the vicinity of 140 K due to the phase transition, locally modified by external stresses.
The LSTC signal [$\Phi(t)$], i.e. the temporal evolution of the light emission can be expressed as a change of the effective surface of the crystallites due to variation of the temperature,

$$\Phi(T)=\eta N\left\{ s_1 c \int_0^{\vartheta_\rho(T)} [\xi(T,\vartheta)-\xi_\rho] \frac{d\xi(T,\vartheta)}{dT} f(\vartheta)\,d\vartheta + s_2 f(\xi_t) \right\}. \quad (1)$$

The parameter $\vartheta_\rho(T)$, appearing in Eq.(1), is an angle determined at each temperature from the Eq. $\xi[T,\vartheta_\rho(T)]=\xi_\rho$ [ξ_ρ -maximal strain corresponding to the temperature of the LSTC onset (200

K)]; ξ_t is the external strain required to shift the phase transition temperature from $T_t(0)$, to T, and the remaining symbols stand for temperature independent constants, including the luminescence efficiency η and distribution functions $f(\vartheta)$ and $f(\xi_t)$.
The curves determined in such a way are shown and compared with experimental data in Fig. 3.

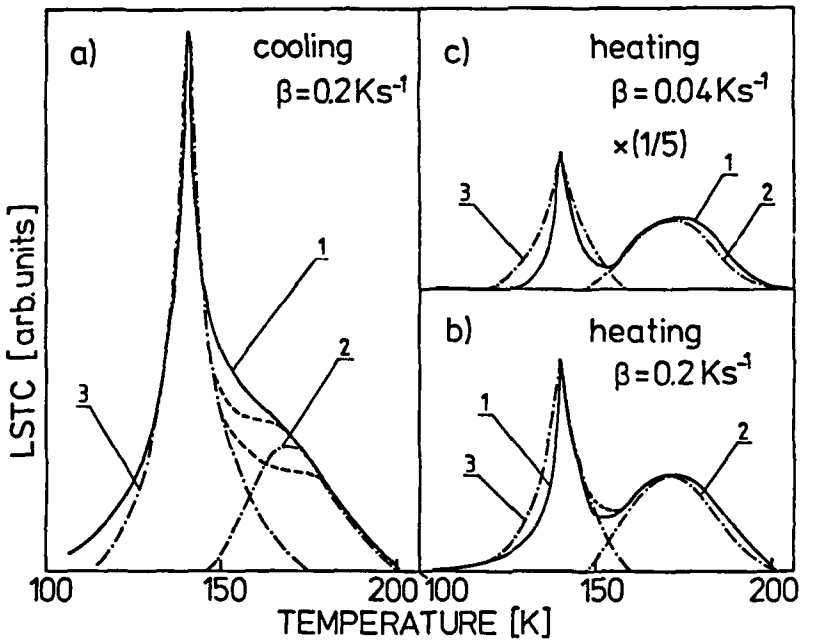

Fig.3. A comparison of experimental (1) and theoretical (2,3) LSTC curves obtained under different conditions. The dashed lines represent the sum of two parts of eq.(1) drawn separately as curves 2 and 3.

In all cases, the calculated curves consisted of two peaks, at 140K and around 170K, corresponding to the second and first term in the brackets of Eq.(1).

CONCLUSION.

LSTC of pyroelectric materials deposited onto rigid substrates is determined by a temperature

evolution of stresses in microcrystallites (contrary to the situation met in freely mounted large single crystals). The source of these stresses lays both in differences of the thermal expansion coefficients of the material and the substrate (external stresses), and in changes of the crystal structure due to the phase transition (internal stresses).
The model of LSTC, taking into account these effects, allowed us to explain all features of the observed phenomena, and to reach at least a qualitative agreement between theory and experiment.

REFERENCES.

[1] I.S.Patel, D.M.Hanson, Nature 293, 451 (1981)
[2] I.S.Patel, D.M.Hanson, Ferroelectrics 38, 923 (1981)
[3] D.M.Hanson, I.S.Patel, M.C.Nelson, Mater. Sci. (Poland) 10, 459 (1984)
[4] R.Nowak, R.Poprawski, Ferroelectrics Lett. 1, 175 (1984)
[5] Z.Dreger, J.Kalinowski, R.Nowak, J.Sworakowski, Mater.Sci. (Poland) 10, 67 (1984)
[6] Z.Dreger, J.Kalinowski, R.Nowak, J.Sworakowski, Chem.Phys.Lett. 116, 192 (1985)
[7] Z.Dreger, Thesis, Technical University of Gdańsk, 1986
[8] J.Kalinowski, Z.Dreger, Phys.Rev. B36 7840 (1987)

TOUCH TRIGGER PROBE WITH PVDF SENSOR

by E. Haeusler and V. Rech
Department of Electrical Engineering
Saarland University
6600 Saarbrücken, Fed. Rep. of Germany

Abstract

A touch trigger probe with PVDF sensor for use in a 3-D-coordinate measurement machine (CMM) was developed. The sensor consists of a circular PVDF film sheet (diameter 2 cm, thickness 20 µm) divided into three electrically insulated segments. The mechanically prestressed PVDF film sensor generates an electric signal if the probe touches an obstacle not depending on the touching direction (axial or transverse). The precision of the probe is in the order of µm).
Construction principle is described and limits of space resolution are discussed.

Introduction

Coordinate measuring machines are used for the exact determination of the dimensions of mechanical structures. The touching point is related to a x-y-z coordinate vector. Using constant translation velocity, the time between two touching points can be transformed into space distance values. With such probes the dimensions of mechanical structures can be determined with a precision in the order of µm. In most cases only mechnical working systems can be used. The necessary contact force of these systems is in the order of 20 gram. In some cases this

CH2593-2/ 88/ 0000-0657$01.00 Copyright 1988 IEEE

force is too high: Sensitive structures can be damaged, for the measurement of deep boreholes long probe heads are required. Therefore, the bending stress produced by the contact force leads to a bending of the probe head and the measurement precision will be reduced. In these cases a reduction of the required contact force can be achieved by application of very sensitive piezoelectric sensors. Application of piezoceramic sensors is known, but these need much more space than piezofilm sensors. Therefore we have developed sensors based on bidirectional PVDF piezofilm [1].

Construction Principle and Properties of the Touch Trigger Probe

Figure 1 shows schematically the construction of the touch trigger probe. The touching stylus is fixed at the force initiation plate. Tangential force at the stylus produces bending stresses of the piezoelement. By dividing the piezoelement into three segments, three separate trigger signals will be generated by bending forces. Some areas of the piezofilm sensor are compressed by the bending force while other areas will be strained. By dividing of the piezoelectric element into three areas (see Figure 2) and differential amplification of the generated electric signals an electric signal not depending on the direction (x or y) of the contact force can be obtained. In this case the contact force is, depending on the stylus length, in the order of 1 gram. The respective signal amplitude is in the order 1 mV and will be processed in a differential amplifier stage with a gain of 60 dB.

A typical trigger signal is shown by Figure 3. This signal was obtained when a contact velocity of 500 mm/min was used. From this a jitter in the order of < 0,3 µm can be expected. Figure 4 shows the complete touch trigger probe with stylus.
The low contact force (ca. 1 gram) high precision (< 0,35 µm) and base resolution (better than 1µm) permits fast, direction independent measurement. False triggering, caused by cross talk of spurious signals can be eliminated by a mechanical switch, which is activated after the electric trigger signal. The coordinate values of the trigger point will be valid only after the mechanical switch is activated.

Sensitivity in z-direction (axial) can be obtained with other electrical signal processing: The differential amplifier will be replaced by a summing amplifier and the output signal of the two amplifiers will fed to an "or" network.

Bibliography

[1] Betz R., Ferroelectrics 75, 1987, pp. 397-404

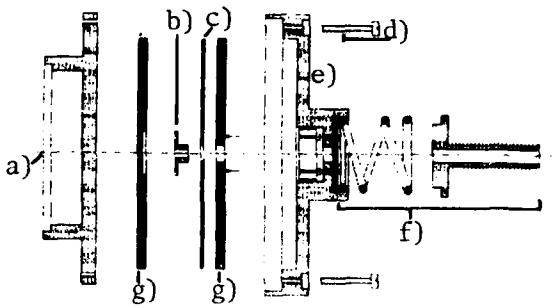

Fig. 1: Construction of the touch trigger probe:
a) force initiation, b) contact ring, c) piezo-element, d) initial stress adjustment, e) force receiving element, f) counteracting force adjustment, g) plexiglas plates.

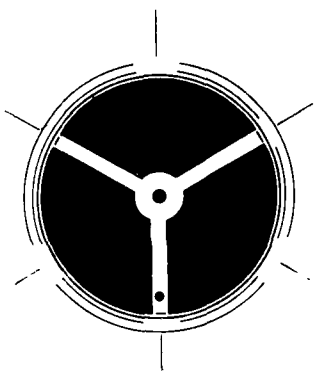

Fig. 2: Piezoelement

Fig. 3: Trigger signal

Fig.: 4: Complete touch trigger probe

COMPUTERIZED ELECTRET DOSIMETER

P.E. Cruvinel and S. Mascarenhas

EMBRAPA/UAPDIA, S. Carlos, SP, Brazil, 13.560

ABSTRACT

An electret dosimeter with a cylindrical active volume has been introduced by Mascarenhas and collaborators[1,2] for possible use in personnel monitoring[3] and in radiotherapy[4]. In this paper we describe a computerized electret dosimeter system for radiation dosimetry that has been developed and built by us. This system allows the measurement of equivalent surface charge up to ±199.9nC on the dosimeter and corresponding dose in the range of 0-0,1Gy as well as the identification of up to 1024 users or more. The computerized electret dosimeter may be operated in two modes automatic and semiautomatic. In the automatic mode data are processed with an 8 bits microcomputer based on a Z80 microprocessor.

(1) Mascarenhas, S. & Zimmerman, R.L. A new electret dosimeter. In: ASSOCIACAO BRASILEIRA DE FISICOS EM MEDICINA. Conferencia do decimo aniversario 1969-1979. Sao Paulo, 1979, p.488-91.
(2) Mascarenhas, S. Bioelectrets in biomaterials and biopolymers. In: SESSLER, G.M., ed. Electrets. 2.ed. Berlin, Springer- Verlag, 1987, p.321-46 (Topics in Applied Physics, 33).
(3) Guerrini, O. Investigations about dosimetry with electrets. Sao Carlos, USP-IFQSC, 1982, 126p, Ma. Sci. Thesis.
(4) Rodrigues, L.N. A new electret dosimeter for radiotherapy. Sao Carlos, USP-IFQSC, 1985. 110p. Ma. Sci. Thesis.

VIBETEK 20* PIEZOELECTRIC CABLE: A CONTINUOUS PROCESS

D R Fox

FOCAS LIMITED, Unit 4, Cheney Manor Ind. Est.
Swindon, Wiltshire SN2 2PJ

ABSTRACT

Piez electric PVdF has been available in thin film from a number of manufacturers for some time. The thick film variant, however, offers advantages in sensitivity and mechanical stability, but has proved less amenable to continuous production. This paper describes an alternative in the form of a coaxial cable, which offers high voltage sensitivity, mechanical robustness and flexibility, as well as continuous production of long lengths. Various key properties are described together with some examples of applications.

INTRODUCTION

Of the piezoelectric polymers, the most exploited material thus far has been poly (vinylidene fluoride), and there are now a number of manufacturers of thin film piezoelectric PVdF. The development of thick film PVdF as an alternative to the more common but less sensitive thin film variant has continued for applications where greater voltage sensitivity is required or where a mechanically more stable product is desired. However, manufacture of thick sheet is not simple and a continuous process is not yet available.

* Trademark of FOCAS Limited.

CH2593-2/ 88/ 0000-0663$01.00 Copyright 1988 IEEE

This paper describes an alternative form of electroactive PVdF. Vibetek 20* is a piezoelectric PVdF coaxial cable which is thick-walled yet extremely flexible. It can be manufactured in long lengths by a continuous process and is highly active, having a hydrostatic voltage coefficient of 130 $mV.mN^{-1}$. Other piezoelectric and physical properties will be presented including its performance under a variety of environmental conditions. Finally, the remarkable versatility of the cable will be exemplified by brief descriptions of some applications, notably in the fields of impact sensing and underwater acoustics.

2. MANUFACTURE

The manufacture of Vibetek 20* piezoelectric cable is carried out in two stages, both of which are continuous processes. The first stage is the coextrusion of PVdF with a suitable low melting point alloy conductor, to form a coaxial wire. The second stage axially stretches this wire at elevated temperatures, up to its natural draw ratio of about 4:1. Either simultaneously with or subsequent to the stretching step, the wire is radially polarised by means of a high electric field. The final stage consists of applying an outer electrode to the cable. This can be done in a variety of ways. It can be coated with a specially formulated silver loaded paint after suitable surface preparation; alternatively braiding and/or jacketing may be carried out using conventional techniques. Standard jackets are a thin crosslinked polyurethane coating over the outer electrode and a crosslinked, modified extruded polyolefin material as outer layer protection.

PROPERTIES

Table 1 shows the properties of Vibetek 20*. All quantities in the table with exception of the g- coefficients and the acoustic impedance have been measured and are not simply derived.

Tensile strength		220 MPa
Elongation to break		35%
Youngs Modulus		2.2 GPa
Volume density		2300 kg m^{-3}
Mass density		4 g/m
Relative permittivity @ 1kHz		12
Dielectric loss @ 1kHz		0.015
Capacitance		600 pF m^{-1}
External electrode resistance		50 ohms m^{-1}
Volume resistivity		3 x 10^{14} ohmscm
Pyroelectric cu ft		35 c m^{-2} k^{-1}
Piezoelectric	g31	280 mV m N^{-1}
Coefficient	g3h	130 mV m_1 N^{-1}
	d31	30 pc N^{-1}
	d3h	14 pc N^{-1}

TABLE 1

It is apparent from the table that the new piezoelectric cable is very flexible, has a low density and its low acoustic impedance allows a better match to water which is of especial benefit to sonar array design. Although the PVdF material has a much lower permittivity than piezo ceramic high device capacitance can be achieved because the coaxial geometry of the Vibetek product results in a cable capacitance of 600 pF per metre.

Vibetek 20* may be used over a wide operating temperature range. Measurements have shown that in the range -20°C to +50°C the g_{3h} coeffient remains essentially constant; in addition, the sensitivity of Vibetek 20* is independent of applied pressure up to at least 15 MPa.

APPLICATIONS

An outstanding feature of Vibetek 20* is its mechanical flexibility, together with the fact that it is available in long lengths, and has a high piezoelectric coefficient. These features offer sensor designers considerable freedom in the development of novel devices, and because of its versatility, the variety of designs is almost limitless. For this reason, it is not proposed to deal at length with device design, but simply to describe a limited number of applications that have been investigated.

One area of application is clearly in the development of acoustic sensors for marine applications. A length of Vibetek 20*, operating in hydrostatic mode has an acoustic sensitivity of about -206dBV/uPa. By winding the cable in a helix, on a thin flexible former, and potting out the whole structure in a suitable elastomer, it is possible to manufacture extended acoustic sensors greater than 1m in length, with sensitivities as high as -184 dBV/uPa. The increase in sensitivity over the base material is a result of exploitation of the longitudinal of -31 mode of the Vibetek 20* cable, together with stress magnification effects resulting from the employment of a thin shell former.

Another major application for Vibetek 20* is for intruder alarms. Again, the mechanical flexibility and robustness of the cable offers considerable versatility in this application. For instance, it can be affixed to various kinds of fences or buried in topsoil, sand or gravel, and unlike many other pressure/vibration intruder alarm systems, there can be a continuous transition between fence and buried protection. Tests have also been performed which show that Vibetek 20* can be used to detect any tampering with a

wall-mounted safe, by bonding the cable to the wall in the vicinity of the safe. The small size of the cable means that it can be made quite unobtrusive and it can completely surround a safe.

A further application is in traffic monitoring or weighing-in-motion systems to replace weigh-bridges. Several lengths of Vibetek 20*, embedded in a suitable potting compound, may be stretched across one or more lanes of highway and connected to suitable electronics and recording apparatus. The flexibility and small size of the materials allows for a considerable reduction in installation costs, whilst its robustness means that replacement costs and down-time are significantly reduced.

SUMMARY

This paper has described a novel piezoelectric cable which can be manufactured on a continuous basis, permitting long continuous lengths to be produced. we have described its important mechanical and electrical properties, together with its performance under a variety of conditions. Its principal features are the considerable mechanical flexibility, high piezoelectric coefficients, and the extremely long lengths available, which allows a remarkable degree of design flexibility never before offered to sensor designers.

Several applications have been outlined, emphasing some of the unique properties of the cable. It cannot be stressed too strongly, however, that these are only a tiny selection of possible application; the development of radically new sensors is now feasible with this unique piezoelectric cable.

THERMALLY STIMULATED CURRENT STUDIES OF CORONA CHARGED TEFZEL

Eugen Neagu,
Department of Physics,
Politechnic Institute of Jassy,
Str. 23 August nr. 11, Jassy-6600, Romania

D.K. Das-Gupta,
School of Electronic Engineering Science,
University College of North Wales,
Bangor, Gwynedd, LL57 1UT, UK

ABSTRACT

Thermally stimulated current spectra from negatively and positively corona charged samples were measured. For negatively corona charged samples the temperature for the maximum current shifts with the charging voltage and the activation energy of the traps increases as the charging voltage increases. The activation energy for positively corona charged Tefzel is greater than that obtained for negatively charged samples. This higher activation energy is associated with ionic traps in amorphous materials. The positions of the two peaks for positively and negatively corona charged samples are very close. The total stored charge strongly increase as the charging voltage increases.

EXPERIMENTAL

Tefzel is a copolymer of polytetrafluoroethylene (PTFE) containing tetrafluorethylene and ethylenetetrafluoroethylene. Thermally stimulated discharge current TSDC measurement is a powerful method to gain insight into the mechanism of charge migration and dipolar motion. The samples were 2.5 x 10^{-5} m thick films of Tefzel type AE obtained from Dupont de Nemour. All experiments were carried out circular samples, 5 cm in diameter. One side of the sample was provided with a vacuum evaporated aluminium electrode.

CH2593-2/ 88/ 0000-0668$01.00 Copyright 1988 IEEE

All samples were corona charged in laboratory air with different corona voltage in the range of -3 to -10kV. The charging time was varied between 5 to 20 minutes at room temperature. The potential of the film surface almost reached the wanted potential within 1 minute and was measured with an electrostatic voltmeter. After charging, an aluminium electrode, 5 cm diameter, was vacuum evaporated onto its charged surface. The sample was short-circuited for at least 0.5 min at room temperature. The TSDC was measured at a constant heating rate of 1.5 K/min in the range 0 to 220°c. The TSDC current was measured with vibrating reed electrometer and recorded appropriately.

RESULTS AND DISCUSSIONS

Figure 1 is a typical TSDC spectrum for negatively corona charged Tefzel as a function of the charging voltage. The samples were maintained in short-circuit condition before TSDC measurements in order to remove the surface charges. As is seen from the figure 1 the TSDC spectra are complex and there are several overlapping peaks. The corresponding electric fields on the sample were 2, 3 and 4 MV/cm for the sample 1, 2, and 3 respectively. The peaks are of negative polarity, the current flow being in the opposite direction as the charging current. The major peak shifts towards lower temperature as the charging voltage increases. At the same time the charge released during TSDC measurements increases which provides a measure of the trapped charge. The dependence of the trapped charge on the charging voltage is not linear. The curve in Fig. 1 has two peaks: one at 75 and has another at 130°c. Sessler [1] gives three peaks for negatively charged FEP, 145, 192 and 220°c. These data are similar to those of electron-beam charged Teflon [2] with main-peak temperature located at 190°c in both cases. For the second curve a single peak was obtained which shifts towards lower temperature, the temperature corresponding to the maximum being 81°c. The fact that the low temperature peak is more pronounced when the charging voltage increases, provides evidence that the deepest traps are filled initially. This is

followed by the filling of shallow traps. To verify this a fresh sample was charged at -5kV, but the charging time was reduced to 10 min and the sample was maintained in short-circuit, after the charging process, for only 0.5 min. The data show that the discharging process starts at a much lower temperature and results in a larger number of peaks than that of the previous sample. Three peaks (see graph 4, figure 1) obtained at 54, 108 and 180°c correspond to different trapping levels. That total charge stored in the sample was determined by the integral over the discharge current. The results obtained are presented in table 1. To obtain the trap depth E_a the initial rise method of Garlick and Gibson [3] was used. Figure 2 shows typical initial rise plots for negatively corona charged samples (No. 1-3) and positively corona charged sample No. 5 (Tefzel).

The concentration of charge carriers n_{to}, captured by traps for the case of mono-molecular recombination conditions and weak retrapping intensity, is given by [4]:

$$n_{to} = \frac{2.7\ J_m\ k\ T_m^{\ 2}}{e\ L\ B\ E_a} \qquad \ldots (1)$$

where J_m is the maximum value of current density, k Boltzmann's constant, T_m the temperature at which the maximum current occur, e the electronic charge, be the heating rate and E_a the activation energy. Table 1 shows the calculated values of n, obtained in this work.

TSDC spectrum for positively corona charged sample shows two peaks and both are negative. The activation energy obtained for the positively charged sample is greater than that for the negatively charged samples. It is likely that the charge are ions, because the activation energies associated with ionic traps in amorphous materials [5,6] are usually higher than that associated with electronic traps.

REFERENCES

1. G.M. Sessler and J.E. West, J. Appl. Phys. 47, 3480 (1976).
2. G.M. Sessler and J.E. West, J. Electrostat. 2, 111 (1976).
3. G.F.J. Garlick and A.F. Gibson, Proc. Phys. Soc. (London), 60, 574 (1948).
4. G.A. Bordovskii, Phys. Stat. Sol. (a) 29, K183 (1975).
5. H. Von Seggern, J. Appl. Phys. 52, 4081 (1981).
6. A.K. Jonscher, Thin Solid Films 1, 213 (1967).

Table 1

Sample	Charging V (kV)	Charging time (min)	T_m (c)	Charge (10^{-8}C)	E_a (eV)	n_{to} ($10^{18}m^{-3}$)
1	-5	20	75 130	3.55	0.55 -	1.0
2	-7.5	20	81	5.16	0.56	1.61
3	-10	20	72	28.46	0.73	2.06
4	-7.5	10	54 108 180	1.47	-	-
5	+7.5	20	73 145	3.82	1.12	0.36

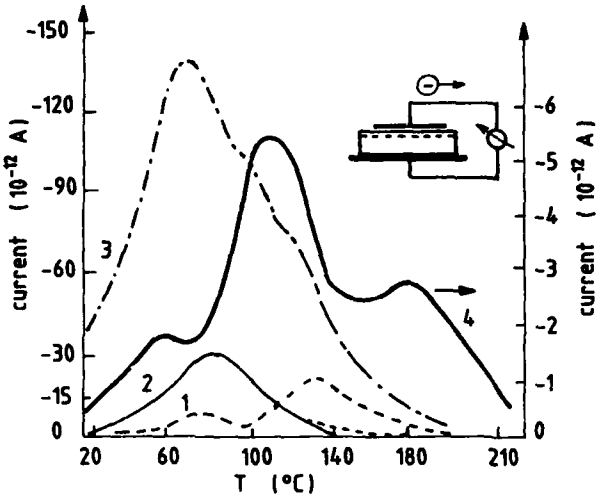

Figure 1. TSDC of corona charged Tefzel poled at different fields.

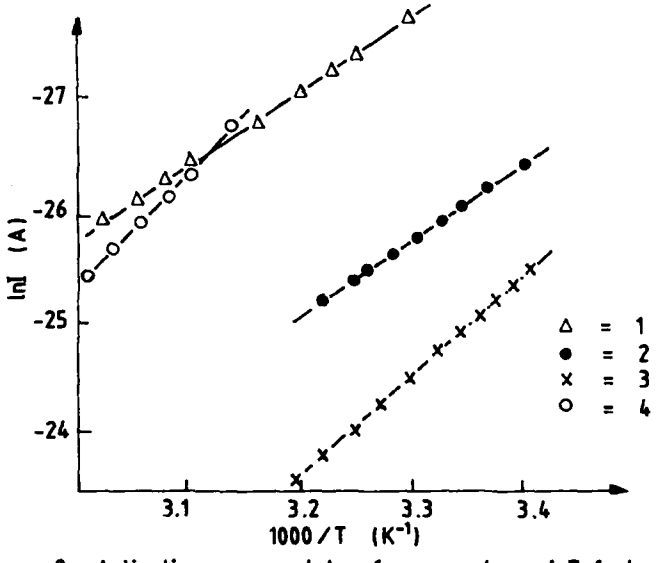

Figure 2. Activation energy plots of corona charged Tefzel.

AUTHOR INDEX

Abdullah M.J. 261
Almairac R. 160
Alquié C. 1, 7
Anagnostopoulou-Konsta A. 266, 271
Apekis L. 266, 276, 281
Arkhipov V.I. 509

Baghel R.S. 246, 303, 308, 323
Bauer S. 28
Belana J. 286
Bendaoud M. 441
Berggren S.R. 170
Bergveld P. 165, 582, 587, 593
Berlepsch H.V. 384
Bernes A. 65, 452
Berraissoul A. 18, 75, 364
Betz R.A. 214
Bihler E. 13, 359
Bohmeyer W. 399
Boitsov V.G. 446
Bonel G. 462
Bota K. 526
Bouchtout N. 441
Brehmer L. 394

Calleja R.D. 339
Cals M.P. 1
Campos J.S 404
Cansell A. 292
Capelletti R. 510
Carr S.H. 256
Cebeillac P. 457
Chalumeau A. 291
Chatain D. 452
Chen B.J. 549
Christodoulides C. 281
Coelho R. 292
Colomer P. 286
Comizzoli R.B. 647
Cruvinel P.E. 662

Dallacasa V. 108
Dandurand J. 241
Danz R. 199, 379, 384, 389, 399

Daoukaki-Diamanti D. 271
Das-Gupta D.K. 261, 447, 668
Date M. 204, 298
Datt S.C. 246, 303, 308, 313, 318, 323
De Bruyne P. 229
De Rooij N. 213
De Rossi D. 234
De Saja J.A. 369
Dias C.J. 487, 493
Ding H. 538
Ditchi T. 7
Domenici C. 234
Döpper H. 98
Doughty K. 328
Dransfeld K. 80
Dreger Z. 652
Dübal H.R. 334
Dueñas J.M.M. 339
Dunn P.E. 256
Dupuis P. 457

Eisenmenger W. 13, 359
Eish T.D. 344, 349
El-Dessouky S.S. 354
Elling B. 199, 399
Escher C. 334

Faria R.M. 70, 467
Fauran-Clavel M.J. 462
Favrie R. 7
Fleming I. 328
Fleming R.J. 118
Fox D.R. 663
Fraile J. 369
Francesconi R. 234
Freitag R. 374
Fukada E. 204
Furukawa T. 182, 298

Gangas N.H.J. 266
Gao L.Y. 642
Garg A. 592
Geiss D. 194, 199, 379, 384, 389, 394, 399
Gerhard-Multhaupt R. 18
Giacometti J.A. 87, 404, 409, 487, 493
Goel M. 414

Goldade V.A. 419
Gorokhovatsky Y. 424
Granz B. 223
Graveris V. 531
Gromov V.V. 536
Gross B. 87, 364
Gubanski A. 425
Gubanski S.M. 425
Günther P. 137
Gupta N.P. 622, 627
Guzenkov S.I. 565

Haeusler E. 657
Harmand M.F. 462
Harnischfeger P. 430
Harrington T. 526
He Q. 612
Holdik K. 13
Holland W.R. 647
Hübschi K. 213

Ibar J.P. 65
Inculet I.I. 592

Jiménez J. 369
Jocteur R. 7
John G. 170
Jorge A. 70
Jungnickel B.J. 430

Kacprzyk R. 435, 440
Kalinowski J. 652
Kao K.C. 642
Kaouah F. 441
Katz H.E. 647
Kefalas V. 281
Keller J.M. 303, 308, 313, 318
Klee D. 92
Klimovich A.F. 565
Koizumi N. 175
Kontou E. 281
Krause G. 92
Kroemer N. 379
Krumins I. 531
Künstler W. 199, 379, 384, 389, 399
Kuzyk M.G. 647

Lacabanne C. 241, 452, 457, 462
Lal R. 447
Lamure A. 462
Lang S.B. 251
Latour M. 160, 467
Leal Ferreira G.F. 87, 104, 409
Lei Q. 472
Lewiner J. 7
Liemant A. 394
Liu Y. 477
Liu Y.N. 642
Lu T.J. 482

Macalik B. 425
Malmonge J.A. 409
Mandowski A. 559
Manthey W. 379
Marat-Mendes J.N. 487, 493
Marchal E. 57
Marque J.P. 1
Martin P.N. 499, 504
Mascarenhas S. 662
Matsubara G. 142
Mehendru P.C. 622, 627
Meixner H. 374
Meurer D. 92
Micheron F. 154
Moisan J.Y. 241
Moreira R.L. 160, 467
Moreno R.A. 409
Motyl E. 440
Müller I. 394
Murata Y. 175
Murphy P. 213
Murthy A.R.K. 323

Nannini A. 234
Narula G.K. 147
Nath R. 47
Nayak S. 318
Neagu E. 668
Nešpurek S. 113
Niezette J. 131
Nikitenko V.R. 509
Nowak R. 652

Ochiai J. 515
Oda T. 142, 515
Ohlendorf D. 334
Olthuis W. 165
Orlova Y. 581

Panwar V.S. 622, 627
Paracchini C. 108
Paul J.C. 520
Perlman M.M. 47
Petridis D. 266
Pillai P.K.C. 147, 525
Pinchuk L.S. 419
Pinnow M. 199
Pissis P. 266, 271, 281
Platen E. 394
Ploss B. 28
Pospisil J. 510
Procopiev O.V. 536
Puri O.P. 526

Quigley R.M. 592

Racine G.A. 213
Reboul J.P. 23
Rech V. 657
Ribelles J.L.G. 339
Roque-Malherbe R. 576
Rozno A.G. 536
Rudenko A.I. 509
Rychkov A.A. 446
Rysiakiewicz-Pasek E. 531

Saffell J.R. 65
Saraf K.K. 570
Sasabe H. 155
Sato T. 537
Schilling D. 80
Schilling M.L. 647
Schmolke R. 199
Schuler S. 80
Schvetz V.V. 446
Sekar R. 147
Servens C. 241
Sessler G.M. 37, 75

Sezonov Y 424
Shershulsky V.I. 548
Shi L.S. 549
Shindo K. 554
Sideris E. 271
Singer K.D. 647
Singh R. 246, 303, 308, 313, 318, 323, 622, 627
Sinha D. 525
Sinha O. 526
Sohn J.E. 647
Spathis G. 281
Sprenkels A.J. 165, 593
Srivastava A.P. 570
Stark W. 389
Sun X.M. 482, 560, 603
Sviridyonok A.I. 565
Swiatek J. 559
Sworakowski J. 113, 652

Takamatsu T. 155
Thomas T. 65
Tiwari A.R. 570
Tomaszewicz W. 571
Torres A. 369
Toureille A. 23
Tripathi A. 147
Tripathi A.K. 147
Tu D. 477
Tu D.M. 642

Utsumi T. 142

Vanderschueren J. 131
Veksler V. 581
Vélez M.H. 576
Vignoles M. 462
Voorthuyzen J.A. 582, 587
Voronezhtsev Y.I. 419

Wagner W. 394
Wang F. 472
Wang S. 598
Wang Y.D. 549
Wang Z.Z. 603
Watson P.K. 52
Wedel A. 199, 384

Wendorff J.H. 204
West J.E. 75, 209
Wiktorczyk T. 607
Wintle H.J. 75
Womes M. 359
Wu J. 612
Wu Z. 632, 637

Xia Z.F. 18, 538, 543
Xiao D.Q. 251
Xu C.Z. 603
Xu F. 632, 637

Yakovlev D.V. 548
Yamaguchi T. 298
Yan F. 598
Yang D. 617
Yang D.G. 560
Yang G.M. 482
Yianakopoulos G. 131
Youssef F.M.H. 344, 349, 354

Zhang Y. 477
Zhao H.J. 642
Zhao Y. 598
Zheng T. 632
Zhu Y. 637

SUBJECT INDEX

Numbers refer to first page of paper or abstract containing subject term.

absorption current 175, 308
accelerometers 214
ac conductivity 627
ac poling 525
acoustic sensor 663
acoustic wave method 536
acrylic acid doping 323
acrylic doping 313
acrylonitrile-methylacrylate copolymer 384
air filter 515, 549
aluminium-hydroxy-nontronite 266
aluminium porous oxide 548
amorphous phase 452
amorphous silicon 113
antistatic agent 440
application of PVDF 251
azo dye doping 647

bakelite 354
β-irradiation ageing 425
bimorphs 155, 214
bioelectret 462, 637
biological dielectric 520
biomaterials 632
biomedical application 374
biomedical sensors 234
block copolymer 281
blocking electrode 246, 303
bone 462
borosilicate glass 531
butadiene-styrene copolymer 510

cable manufacture 663
calcified tissue 462
capacitors (two-layered) 292
carbon-fluoro polymers 582
carp scale 632
CDF_2:Y crystal 108
cellulose 276
ceramic (PCM) 617

ceramic-polymer composite 261, 617
charge centroid 482, 487
charge decay 52, 389, 560
charge distribution 1, 7
charge location 23
charge pair production 170
charge relaxation 424
charge storage 37, 47, 642
charge transfer complex 323
charge transport 37, 394
charge transport model 409
charge trapping 52, 104
chemical relaxation 57
clearance distance 354
cold drawing 131
composite 182, 261, 414, 477, 525, 617
contact electrification 565
contact, metal-polymer 98
corona charging 142, 313, 409, 482, 493, 515, 538, 560, 668
corona charging method 87
corona triode 87, 404
creepage distance 354
cross-linked polyethylene or XLPE 118
crystalline orientation 291
crystallinity 47
crystallinity enhancement 642
crystallite size 47
Curie transition 175, 291
current-voltage characteristics 113
cyano vinyl acceptor 647

dc conduction 472
dc conductivity 175
defect induced mechanisms 160
density of states 113
desorption current 165, 313, 493
dielectric behaviour 175, 261
dielectric dispersion spectrum 576
dielectric properties 617, 627
dielectric relaxation 241, 339, 441
dielectric response 607
dielectric study 266, 271, 276
differential scanning calorimetry or DSC 457
diffusion coefficient 576
dipolar chromophores 647

dipolar reorientation 266
disordered polymer 394
DNA 271
doped polystyrene 308
doped PVDF 399
dosimeter 603, 662
dosimetry 328
double layer composite 477
dust counter 251
dysprosium oxide 607

electret 18, 23, 52, 137, 142, 165, 209, 286, 328
389, 414, 419, 435, 487, 493, 499, 504, 515
526, 538, 543, 549, 565, 587, 603, 612, 617
electret applications 209
electret condenser microphone 213
electret materials 582
electret microphone 213, 593
electrical breakdown 98
electrical conduction 323, 440
electrical conductivity 292, 414
electrical trees 92
electric charge distribution 536
electric field effect 292, 520
electrode effect 344, 570
electromechanical properties 154
electron beam charging 170
electron beam deposition 18
electron beam irradiation 1, 75, 364
electron beam methods 37, 137
electron beam poling 80
electron-electron interaction 108
electro-optical behaviour 334
electrostatic precipitator 549
epoxy resin 441

fabrication 593
Fermi level 113
ferroelectric 334, 384
ferroelectric copolymer 298
ferroelectric polymers 182, 251
field distribution 292
fission fragments 170
flashover strength 344
fluoropolymer corona electrets 446

gamma irradiation 499
glass fibre/polymer composite 414
glass transition 510

high energy storage 292
high frequency application 447
hopping conduction 108
hydrophone 223
hysteresis behaviour 384

infra-red absorption 622
infra-red array sensors 214
infra-red detection 251, 399
infra-red spectrum analysis 92, 632
insulator 571
insulator conductor interface 7
interfaces 7, 462, 499, 504
interfacial polarization 576
iodine doping 318
ionic conductivity 531
ionization chamber 328
ionization distribution 504
irradiated polyethylene 536
irradiation 1, 75, 364, 499, 509
isothermal charge decay 493
isothermal polarization 98

kapton 37, 75
$KTaO_3$ 424

large surface sensors 214
laser induced pressure pulse 75
laser radiation 399
latex 457
lead zirconate or PZT 182, 261, 525
leakage current 344
liquid crystal 334
liquid crystal display 334
liquid dielectrics 537
liquid-liquid transition temperature 369
local order 452
luminescence stimulated by temperature changes 652

magnetic field effect 520
marine electrical insulation 354
market situation 214

mass analyser 251
mathematical model 98, 104, 292, 394, 435, 571
memory effect 160
metal polymer contact 98
mica electrets 592
micromachining 213, 593
microphone 213, 593
microstructure 457
MIM sandwich 607
modelling 98, 104, 292, 394, 435, 509, 559, 571, 581
moisture effect 441
Monte-Carlo method 571
MOS FET 587
multi-element transducer 379
mylar 75, 593
mylar PETP 37

negative charging 364
n-isopropylcarbazole 652
non-linear optical effect 647
non-linear piezo electricity 204, 430
nylon 5,7 256

optical fibre absorption loss 251
optically active doping 199
opto-ferroelectric memory 298

personal identification number (PIN) 229
personnel monitoring 662
phase transition 160, 467, 510
phillosilicates 592
photolithography 582
photoplastic devices 241
photo-stimulated current (PSC) 142
piezoelectric cable 663
piezoelectric coefficient 13, 204
piezoelectric coefficient e_{31} 598
piezoelectricity 155, 182, 199, 256, 379, 384, 617
piezoelectric membrane 229
piezoelectric polymer 209, 223, 234
piezoelectric pressure step 13
pig bone 637
plasma etching 582
plasma treatment 642
p-n junction 504

polarization 241, 419, 452, 554
polarization behaviour 318
polarization distribution 13, 18, 28, 98
polarization growth 359
polarization reversal 359
poling of multilayer films 598
polyamides 256
polyampholyte 57
polycarbonate 65, 131, 452, 565
polycarbonate-polypropylene composite 147
polyester 281
polyethylene 7, 23, 47, 98, 339
polyethylene adipate 281
polyethylene-PVC blend 147

polyethylene terephthalate or PETP 118, 286, 409, 425
543, 554, 612
polyfluoroethylene propylene or FEP 170, 349, 477
polyimide 472
polymer blend 147, 182, 303, 384, 627, 668
polymer insulation 349
polymethyl methacrylate or PMMA 147, 199, 344, 349
354, 419, 477, 647
polymethyl methacrylate-poly vinyl acetate blend 147
polyoctenamer 369
polypropylene 47, 65, 92, 246, 313, 318, 440
499, 515, 538, 543, 549, 642
polypyridinium 57
polystyrene 52, 65, 118, 308, 323, 344, 354, 570
polystyrene-polymethyl methacrylate blend 303
polytetrafluoroethylene or PTFE 603
polytetrafluoroethylene copolymer 668
poly (trans 1-octenylene) 369
polyurethane 281
polyvinylacetate or PVA 147
polyvinylchloride or PVC 344, 354
polyvinylidene fluoride or PVDF 13, 28, 37, 70, 194
199, 204, 214, 223, 229, 234, 251, 359, 374
379, 399, 404, 430, 447, 598, 617, 657, 663
polyvinylidene fluoride-lead zirconate composite 525
polyvinylidene fluoride-PCM composite 617
polyvinylidene fluoride-VDCN copolymer 182

pressure pulse method 37, 80, 477
pressure sensor 587
pressure wave propagation 1, 7

protonic charge carrier 266
PVB 419
pyroelectric behaviour 261
pyroelectric current 28
pyroelectric detector 374
pyroelectric device 399
pyroelectricity 182, 199
pyroelectric luminescence 652
pyroelectric polymer 209
PZT-polypropylene composite 261
PZT-PVDF composite 262, 525
PZT-VDF-TrFE composite 261

quasi-gaussian trap distribution 571

radiation dose 603
radiation induced polarization 509
refractive index 537
relaxation processes 286
remnant polarization 298, 359, 467
resinic esters 241

secondary emission 364
second cross-over point 364
second harmonic component 204
second order response 430
sensor 657
sensor array 374
shockwaves 223
signature verification 229
silicon 137, 213, 593
silicon dioxide or SiO_2 137, 165, 593
silicon micromachining 213, 593
Si-SiO_2 interface 137
smectic layer 334
solution grown polystyrene 308
sorbed water 276
space charge 70, 99, 104, 246, 308, 554, 612
space charge distribution 75, 435, 477, 537
space charge evolution 394
space charge limited current or SCLC 113
spatial distribution 113
$SrTiO_3$ 424
stochastic hopping 394

structural changes 194
substrate influence 652
surface charge 155, 404, 560
surface charge density 565
surface contamination 389
surface deterioration 349
surface flashover 349
surface potential decay 543
surface traps 487
surface treatment 165
surface TSDC 441

tactile sensor 234
teflon 209
teflon FEP 1, 18, 37, 142, 155, 364, 389, 404
482, 487, 493, 543, 560, 582, 587
tefzel 668
temperature distribution 18
thermal ageing 425
thermally stimulated conductivity (TSC) 118
thermally stimulated current 559
thermally stimulated depolarization 424
thermally stimulated discharge current or TSDC 57
65, 70, 92, 98, 118, 131, 147, 241, 246
256, 266, 271, 276, 281, 286, 303, 313, 318
339, 369, 389, 409, 414, 419, 425, 452, 457
467, 472, 482, 487, 510, 515, 526, 531, 538
543, 554, 570, 571, 598, 612, 637, 668
thermally stimulated infra-red spectroscopy 92
thermally stimulated luminescence (TSL) 118
thermally stimulated polarisation current 131, 531
thermal neutron detectors 170
thermal sampling 339
thermal step technique 23
thermal wave 28
thermodynamic model 154
thermodynamic properties 291
thermoelectret 526
thin film capacitor 607
time domain simulation 447
touch trigger probe 657
trapped charge 303
trapping levels 446
tunnel mechanism of relaxation 581

ultrasonic transducer 379, 447
ultrasound sensors 214

VDF-Tr.FE copolymer 80, 160, 175, 182, 298, 467
very thin film 80
VF_2TrFE copolymer 291
vibrating grid 87
vinyl acetate 622, 627
vinyl alcohol terpolymer 622
vinyl chloride 622, 627

water 271
water content 266
wax 435
Wigner-glass state 108
windowing polarization 65

x-ray study 632
x-ray texture method 194

ytterbium oxide 607

zeolites 576
zirconia 526